University of Southampton

Faculty of Natural and Environmental Sciences

School of Chemistry

Bioinspired, Heterogeneous Amino Acid Complexes For Benign Oxidation Catalysis.

By

Joanna Dzierżak

Thesis for the degree of Doctor of Philosophy

September 2011

DECLARATION OF AUTHORSHIP

I, Joanna Dzierżak, declare that the thesis entitled

Bioinspired, heterogeneous amino acid complexes for the benign oxidation catalysis.

The work presented in the thesis is both my own, and has been generated by me as the result of my own original research. I confirm that:

- This work was done wholly or mainly while in candidature for a research degree at this University;
- Where any part of this thesis has previously been submitted for a degree or any other qualification at this University or any other institution, this has been clearly stated;
- Where I have consulted the published work of others, this is always clearly attributed;
- Where I have quoted from the work of others, the source is always given. With the exception of such quotations, this thesis is entirely my own work;
- I have acknowledged all main sources of help;
- Where the thesis is based on work done by myself jointly with others, I have made clear exactly what was done by others and what I have contributed myself;
- Parts of this work have been published as:
    1. J. Dzierzak, R. Raja and M. Lefenfeld US Pat. Appl. No: US. 033510-018099, 2009.
    2. J. Dzierzak, M. Lefenfeld and R. Raja, *Top. Catal.*, 2009, 52, 1669-1676.
    3. J. Dzierzak, E. Bottinelli, G. Berlier, E. Gianotti, E. Stulz, R. M. Kowalczyk and R. Raja, *Chem. Commun.*, 2010, 46, 2805–2807.
    4. D. Xuereb, J. Dzierzak, R. Raja, ChemInform Abstract: *Biomimetic Single-Site Heterogeneous Catalysts: Design Strategies and Catalytic Potential*, 2011, 44.

Signed: ……..

Date:……

UNIVERSITY OF SOUTHAMPTON
FACULTY OF NATURAL AND ENVIRONMENTAL SCIENCES
SCHOOL OF CHEMISTRY

Joanna Dzierżak

Bioinspired, Heterogeneous Amino Acid Complexes For Benign Oxidation Catalysis.

Abstract

Metalloenzymes catalyse the most fundamental reactions in organic chemistry from oxidation of hydrocarbons to complex C-C bond forming reactions with exceptional selectivity. Mimicking the active site of a metalloenzyme by immobilising well-defined amino acids containing catalytically active transition metal centres based on transition-metals on a robust inorganic framework, affords powerful catalysts that can be utilised in oxidation reactions. Porous aluminosilicates, mesoporous silicas and polymers offer suitable supports for single-site bio-derived catalysts. Dispersion of catalytically active centers within porous solids with high surface area improves site-isolation which is essential in catalytic processes. These materials can be created from a range of methodologies and the different strategies used for immobilisation can greatly affect the nature of the active catalyst. The routes by which these catalysts are immobilised have given the potential to derivatize inorganic porous hosts and organic polymer structures with amino acids for complexation to metal centres. These bio-derivatized frameworks offer advantages over the homogeneous counterparts in terms of easy separation, recover and recyclability and can carry out selective oxidation reactions with great effectiveness.

Herein, heterogenous bioinspired complexes of two amino acids; proline and valine with a series of transition metals (Fe, Cu) were synthesised and immobilised within zeolite cages, mesoporous silica MCM-41 and polystyrene. The preparation methods allowed the synthesis of materials with varying loadings of immobilized active sites. The structural information obtained by spectral and elemental analysis suggested tetrahedral geometry for iron complexes and distorted square planar geometry for copper complexes. Both amino acids coordinated to metal ions through the nitrogen atom of amino group and oxygen atom of carboxylate group *via* dissociation of the acidic proton as bidentate N,O-donors.

The resulting biomimetic complexes were employed as catalysts for oxidation of cyclohexane, cyclohexene, benzyl alcohol and dimethyl sulfide, using molecular dioxygen (O_2), *tert*-butyl hydroperoxide (TBHP) and acetylperoxyborate (APB) as oxidants. The observed trends in catalytic activity showed that the metal loading and separation of the active sites played key role in the selective oxidation reactions. By decreasing the loading of metal active centres, their spatial separation increased which strongly enhanced the activity of catalysts. The decrease in metal active site content resulted in significant increase in TON and TOF. The product selectivity was dependent on the nature of oxidant, hydrophobicity/hydrophilicity of the support, loading of metal active centres and the metal/substrate ratio.

TABLE OF CONTENTS

List of Figures.

List of Schemes.

List of Tables.

Abbreviations.

APB acetylperoxyborate
ARG arginine
BET Brunauer-Emmett-Teller Analysis
BPMEN [*N*,*N*-dimethyl-*N*,*N*-bis(2-pyridylmethyl)-1,2-diaminoethane]
BQEN=N,N'-dimethyl-N,N'-bis(8-quinolyl) ethane-1,2-diamine
CBZ benzylcarboxy carbamate
CHP cumene hydroperoxide
DCC *N,N'*-dicyclohexylcarbodiimide
DEADH$_2$ = diethylhydrazino dicarboxylate)
DIC *N,N'*-diisopropylcarbodiimide
DMF Dimethylformamide
DMSO Dimethyl sulfoxide
DR UV-Vis Diffuse Reflectance UV-Visible spectroscopy
EBHP ethyl benzene hydroperoxide
EPR Electron paramagnetic resonance
EtOAc Ethyl acetate
EtOH Ethanol
EXAFS Extended X-ray Absorption Fine Structure
FAD flavin adenine dinucleotide
FID Flame Ionisation Detector
FMOC 9-fluorenylmethyloxycarbonyl
FTIR Fourier Transform Infrared Spectroscopy
GC Gas chromatography
GLU Glutamic acid
GO Galactose oxidase
HAP Hydroxyapatite
HOBt 1-hydroxy-benzotriazole
HOAt 1-hydroxy-7-aza-benzotriazole
HRP Horseradish peroxidise
ICP Inductively Coupled Plasma Spectrometry
LMCT Ligand-to-metal charge transfer
LYS Lysine
MAS NMR Solid-state magic-angle spinning nuclear magnetic resonance
MCM-41 Mobil Composition of Matter (mesoporous molecular sieve)
MeOH Methanol
MLCT Metal to ligand charge transfer
MLCT Metal to ligand charge transfer
MMOB Methane monooxygenase Regulatory protein
MMOH Methane monooxygenase hydroxylase
MMOR Methane monooxygenase reductase
M-PC Metallophthalocyanine
M-POR Metalloporphyrin
MS Mass Spectrometry
N$_4$Py N,N-bis(2-pyridylmethyl)-N-bis(2-pyridyl)methylamine)
PC Phtalocyanine
PDMS Polydimethylsiloxane

PHEN 1,10-phenanthroline; $DEADH_2$ = diethylhydrazino dicarboxylate
PHIO Iodosylbenzene
pMMO Particulate methane monooxygenase
Por Porphyrin
PRO Proline
P450 Cytochrome P450
RF Response Factor
SCXRD Single Crystal X-ray diffraction
sMMO soluble methane monooxygenase
SPPS solid phase peptide synthesis
SSHC single-site heterogeneous catalyst
TBHP *tert*- butyl hydroperoxide
T-BOC *tert*-butyloxycarbonyl
TDCPP Tetra(4-carboxyphenyl)porphyrin
TEMPO 2,2',6,6'-tetramethylpiperidine-N-oxyl
TEOS tetraethoxy silane
TGA Thermogravimetric analysis
THF Tetrahydrofuran
TMOS Tetramethoxy silane
TMP Tetramesitylporphyrin
TOF Turnover frequency
TON Turnover number
TPA Tris(2-pyridylmethyl)amine
TPAP/NMO Tetra-N-propylammonium perruthenate/ N-methyl-morpholine-N-oxide
TROC Trichloroethyl carbamate
USY Ultra Stable Zeolite Y
Val Valine
XRD X-ray diffraction

Acknowledgements.

Foremost, I would like to express my thanks and sincere gratitude to my supervisor, Dr Robert Raja for providing me with the opportunity to conduct this research, and for his support, motivation and invaluable advice throughout the course of the project. His guidance and stimulating suggestions helped me in the time during research and completing this thesis. I am indebted to him for allowing me the opportunity to present my work at number of conferences.

My special thanks go to my advisor Dr Eugen Stulz, his assistance and support have been crucial to the development of this project. I am very appreciative for his challenging and insightful comments concerning my quarterly reports and this thesis. Without his expertise this research project would not have been successful.

I would like to express my thanks to all members of the Raja research group; especially James Paterson for his sincerity and advice during the thesis writing. My thanks go to Jon Blaine, David Xuereb, Matthew Potter, Becky Leithall, Mary Cholerton and Sarah Gaskel who have all contributed along the way.

I acknowledge, gratefully Dr Gloria Berlier, Dr Emanuela Bottinelli, Dr Enrica Gianottii for their expertise and valuable direction with catalysts characterization. I am very appreciative of Dr Radoslaw Kowalczyk for his assistance with the EPR experiments. My thanks go to Dr Mark Light for his work on SCXRD.

Finaly I would like to thank my parents and my sister who have been ever supportive throughout my PhD.

1. INTRODUCTION.

1.1. Single-Site Heterogeneous Catalysis.

Catalysis is an important strategic field of chemistry due to its implication in many fields including industry, energy, environment and life sciences. Whether it is homogeneous, heterogeneous or enzymatic, catalysis is primarily a molecular phenomenon as it involves the chemical transformation of one molecule into another.[1, 2] It offers many advantages to economical and environmental problems in pharmaceuticals, petrochemicals, agrochemicals, polymers and basic chemicals production.[3, 4]

Catalysis is divided into two groups: homogeneous, where the catalyst is in the same phase as the reaction mixture, and heterogeneous, where the catalyst is in a different phase than the reaction mixture.[5] Heterogeneous catalysis has a fundamental role in the development of sustainable and green industrial processes. The strengths of heterogeneous systems such as easy recovery, separation and reusability in purpose to reduce the cost of production and to facilitate environmentally benign processes, making heterogeneous catalysis very attractive objectives for industrial catalytic technologies.[6-8]

Biocatalysis often uses enzymes that are highly active and selective under mild conditions such as ambient temperature, atmospheric pressure and neutral pH.[9] However, industrial scale application of enzymes is limited due to lack of stability in more extreme conditions such as harsher temperatures, pressures and pH, high cost of operation, cofactor requirements and organic solvents as may be required.[10, 11]

A single-site heterogeneous catalyst (SSHC) is a solid with well-defined catalytically active sites, spatially separated from each other and chemical surroundings.[12] The single-sites are typically located within solid supports and display general features: (I) consist of individual ions, atoms, complexes or clusters that are well isolated from one another; (II) have identical energy of interaction between the active site itself and a reactant; and (III) are structurally well defined and characterized. The dispersion and the degree of site-isolation are essential in catalytic processes, for yielding the desired products selectively and efficiently. Heterogeneous systems have great advantages in terms of easy separation, recovery and recyclability.[13, 14]

The host matrices, where single-sites are dispersed, can have inorganic, organic or composite nature. Inorganic matrices are typically solid oxides such as silicates, aluminosilicates or aluminophosphates, that exhibit high porosity and large surface area. Organic host matrices have a carbon-based backbone and are constituted of polymers with different functionalities that are able to bind covalently the active site. Composite

matrices are composed of combinations of inorganic and organic constituents, in variable proportions and morphologies, e.g. mesoporous hybrid frameworks.[15]

1.2. Bioinspired single-site heterogeneous catalysts.

Catalytic oxidation reactions play a key role in many areas that benefit the chemical industry, ranging from pharmaceuticals to large scale commodity chemicals.[16] Oxidation catalysis is one of the most dynamic, challenging and fruitful areas of catalytic chemistry with the design of catalytically active structures and the control of their reactivity being crucial in achieving high catalytic performance with good selectivity. Work in the last few decades shows impressive progress in terms of catalyst design for oxidation reactions. There is therefore a great need for such processes, especially for the preparation of various alcohols, ketones, aldehydes, acids and phenols.[17-19] Reactions of this type, like oxidation of cyclohexane to cyclohexanol and cyclohexanone (the so-called ol-one mixture or K-A oil), benzene to phenol and methane to methanol are included into the top 10 challenges of modern chemistry.[20]

Increasing restrictions on industrial oxidation technologies demand the use of sustainable and environmentally friendly oxidants. Molecular oxygen is particularly attractive due to low costs and its ready availability allowing economically viable processes. Selective oxidation with molecular oxygen has received much attention recently but it is still difficult to activate molecular oxygen with commercially available catalysts. The uncatalyzed reactions of O_2 with organic substrates are thermodynamically favourable but kinetically slow because they are spin-forbidden and the one-electron reduction potential of O_2 is unfavourable.[21]

At the same time, natural metalloenzymes easily perform these transformations in a single step by simply adding one oxygen atom to the starting substrate molecule. Attempts to understand and reproduce this unique ability of oxygenase metalloenzymes are hampered by the difficulties in creating artificial systems that are highly active for the activation of molecular oxygen.[22]

Nature oxidizes substrates into products with extreme selectivity that is accomplished through a well-defined geometry of active centres. Metalloenzyme mimics have long held the fascination of synthetic chemists, and both structural and functional enzyme mimics have been rationally developed through the interaction of transition-metal complexes containing suitably designed organic ligands, natural amino acids or by the utilisation of de-novo designed artificial proteins. [23] Bio-inspired catalysts offer an alternative for conventional biological and chemical processes and have many advantages over natural

metalloenzyme systems, allowing development of more robust catalysts at relatively low cost. Such catalysts are pH and thermally more stable, may expand the scope of possible substrates and increase the scale of production. Moreover, their stability and selectivity may be improved by chemical modifications of the active sites by altering the immobilisation procedures.[24] Developing strategies for anchoring active entities on stable inorganic or organic frameworks can lead to the creation of highly active and selective catalysts that can facilitate highly selective transformations. Through the immobilisation of active sites within solid host materials recovery and reusability issues can be improved for continuous processing. [25]

1.3. Metalloenzymes.

Metalloenzymes are biocatalysts that rely on transition metals for their catalytic activity. A metalloenzyme is usually a huge protein that contains a small metal complex in the active site. The metal ion is coordinated by a few amino acids from the protein scaffold that stabilizes and isolates active metal centre as well as providing a specific binding pocket for a substrate (Figure 1.1.).[26] Proteins coordinate to metal ions with nitrogen, oxygen and sulphur containing ligands. Metal active centres possess a well-defined coordination when surrounded by proteins amino acids that give a precise shape to the cavity in which it is situated. [27] The peptide chain is made up of small building blocks of amino acids, which are composed of an acidic carboxyl group (–COOH), a basic amino group ($–NH_2$), a hydrogen atom and a characteristic side chain (–R). Amino acid side chains such as the imidazole group of histidine, the phenol ring of tyrosine, the carboxylate group of aspartate and glutamate, amino group of lysine and arginine, the mercapto group of methionine and the thiol group of cysteine serve as the metal binding sites in proteins.

Metalloenzymes that activate molecular oxygen possess great potential as catalysts for specific oxidation reactions and as guides for the development of efficient catalysts.[28] Iron and copper ions are the most commonly occurring metal centres in biological oxidation systems and also play important roles in heterogeneous and homogeneous catalysis, mainly due to their inherent electronic properties and accessible redox potentials.

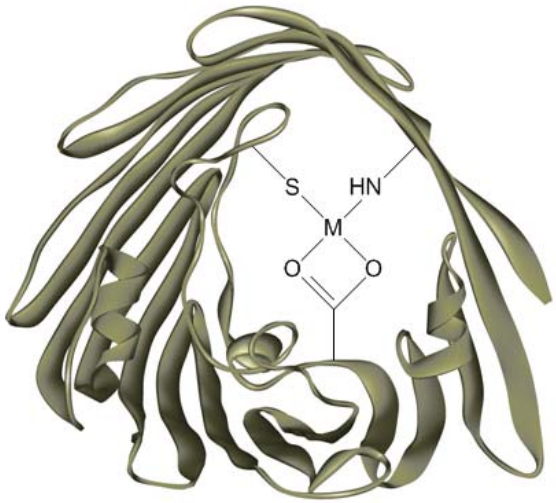

Figure 1.1. Schematic representation of metalloenzyme active site.

1.3.1. O_2 activation by Fe and Cu metalloenzymes.

Dioxygen reduction (oxidase activity) and activation for incorporation into organic substrates (oxygenase activity) are catalyzed by iron heme enzymes, non-heme iron and copper enzymes.[29, 30] Oxidases couple one-, two- or four electron oxidation of the substrate to two- or four electron reduction of dioxygen to hydroperoxide or water. Oxygenases can incorporate either one (monooxygenases) or two (dioxygenases) atoms of oxygen into an organic substrate. In monooxygenase systems, the non-incorporated oxygen atom is reduced to water by an additional two-electron reductant or by the substrate itself.

Transition-metal ions Fe and Cu are ideal catalysts for O_2 oxidation reactions as they readily react with O_2 to afford metal-containing active oxidants, such as iron-superoxo (Fe^{III}-O_2^{-}), iron-peroxo (Fe^{III}-O_2^{2-}),iron-oxo (Fe^{IV}=O and Fe^{V}=O) and copper superoxo (Cu^{II}-O_2) or copper peroxo [$(Cu^{II})_2O_2$] species. Mechanistic pathways of O_2 activation by metalloenzymes are determined by the electronic and geometric properties of the metal ion and by the environment of the surrounding protein. [31, 32]

Oxidations with dioxygen are thermodynamically favoured, but are slow in the absence of a catalyst. The direct oxidation of organic substrates by O_2 is rare due to high energy barrier for electron transfer from the organic substrate to oxidant. For molecular oxygen, this high energy barrier is nature's way of protecting organic compounds from destructive oxidation. Dioxygen in its ground state is a spin-polarized triplet and as such is inert toward substrate oxidation. The singlet or doublet (radical) states are much more reactive.[33] Metal catalysts promote the spin-forbidden transition from triplet to singlet or

doublet state. Dioxygen is activated from its abundant triplet ground state to reactive singlet or doublet (radical) species by oxidase and oxygenase metalloenzymes. By cleaving the O-O bond these enzymes can generate species of even greater reactivity. In biological systems, O_2 is reductively activated and the dioxygen moiety undergoes a partial reduction toward a superoxide or a peroxide (Scheme 1.1.). The source of the activating electrons can involve transition metal located in the active site of the metalloenzyme, organic cofactor (e.g. flavin, pterin), second redox-active metal or organic substrate itself.[34]

$$O_2 + 1e^- \longrightarrow O_2^- \quad \text{(superoxide)}$$

$$O_2 + 2e^- \longrightarrow O_2^{2-} \quad \text{(peroxide)}$$

Scheme 1.1. Reductive activation of O_2 to superoxide and peroxide.

The mechanism of O_2 activation by iron enzymes is presented in Scheme 1.2. and involves initial formation of Fe^{II}–O_2 species (A) that can be converted to end-on hydroperoxide Fe^{III}–OOH (B) upon electron addition or to side-on peroxide Fe^{III}–O_2 (E). These two intermediates in metalloenzyme catalysed reactions can activate both oxygen atoms of O_2 favouring dioxygenase chemistry where both oxygen atoms are incorporated into a substrate molecule. By adding a proton, side-on peroxide becomes more reactive. Protonation converts side-on peroxide (E) to more reactive end-on hydroperoxide (B). End-on hydroperoxide can undergo heterolytic cleavage that results in high-valent Fe^{V}=O species formation (C). The O–O bond could also be cleaved homolytically affording lower oxidized Fe^{IV}=O intermediate (D). These intermediates are key active species employed in iron-catalyzed oxidation chemistry.[35-37]

The reaction between the reduced form of Cu^{I} and O_2 can produce a Cu^{II}-superoxo species (Scheme 1.3. A) or a Cu^{III}-peroxo species (B). Addition of another electron producess a copper^{II}-peroxo intermediate (C). This intermediate can be further protonated and give a Cu^{II}-hydroperoxo complex (D). Donation of hydrogen atom to the Cu^{II}-superoxo (A) and Cu^{III}-peroxo (B) species can also lead to the Cu^{II}-hydroperoxo intermediate (D). A Cu^{II}-hydroperoxo species (D) was suggested to be the key reactive intermediate in enzymatic copper based oxidation reactions. Recent studies, however, indicated that Cu^{II}-superoxo species is more likely to be the reactive oxidant for the C–H bond activation of the organic substrates. [38-40]

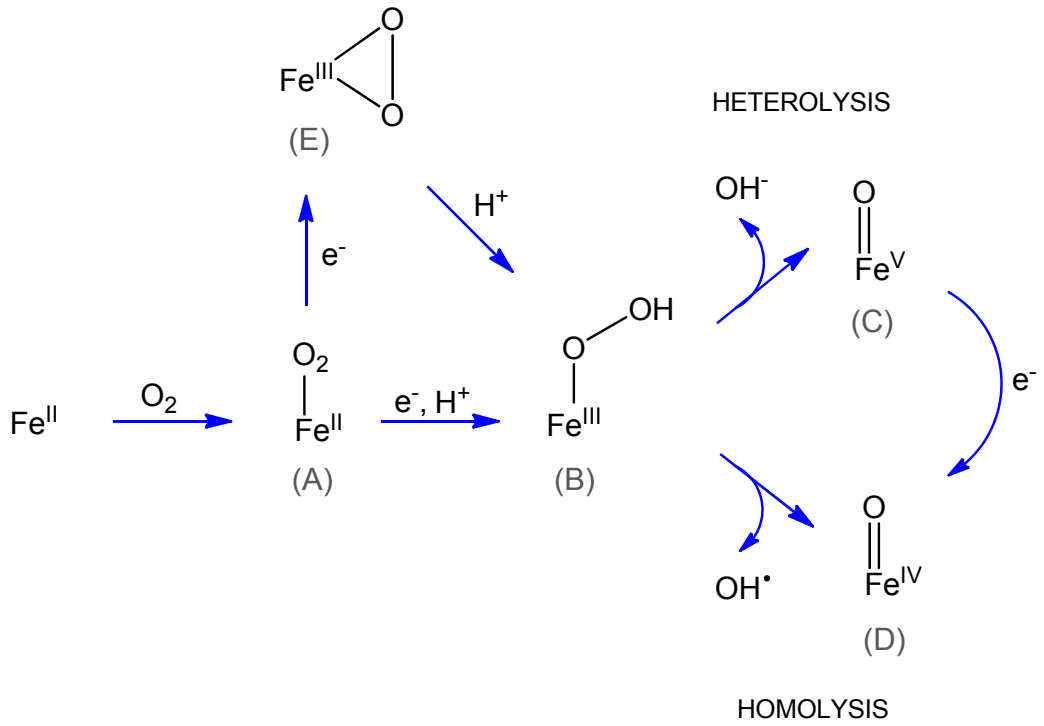

Scheme 1.2. Proposed mechanistic pathways for iron in metalloenzymatic oxidation reactions.

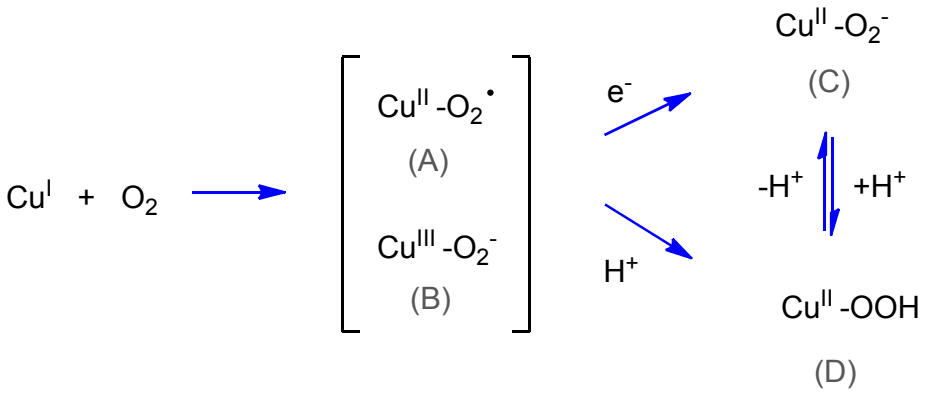

Scheme 1.3. Dioxygen activation at the mononuclear copper active centres.

In the coupled binuclear copper enzymes like tyrosinase the oxygen intermediate is fundamentally different from the high-valent iron-oxo species. In oxy-tyrosinase the active species is the side-on μ-η^2:η^2-peroxo complex that has extremely weak O-O bond which is cleaved and one oxygen atom is transferred to the substrate molecule and the second oxygen atom is used to produce water (Scheme 1.4.).[41]

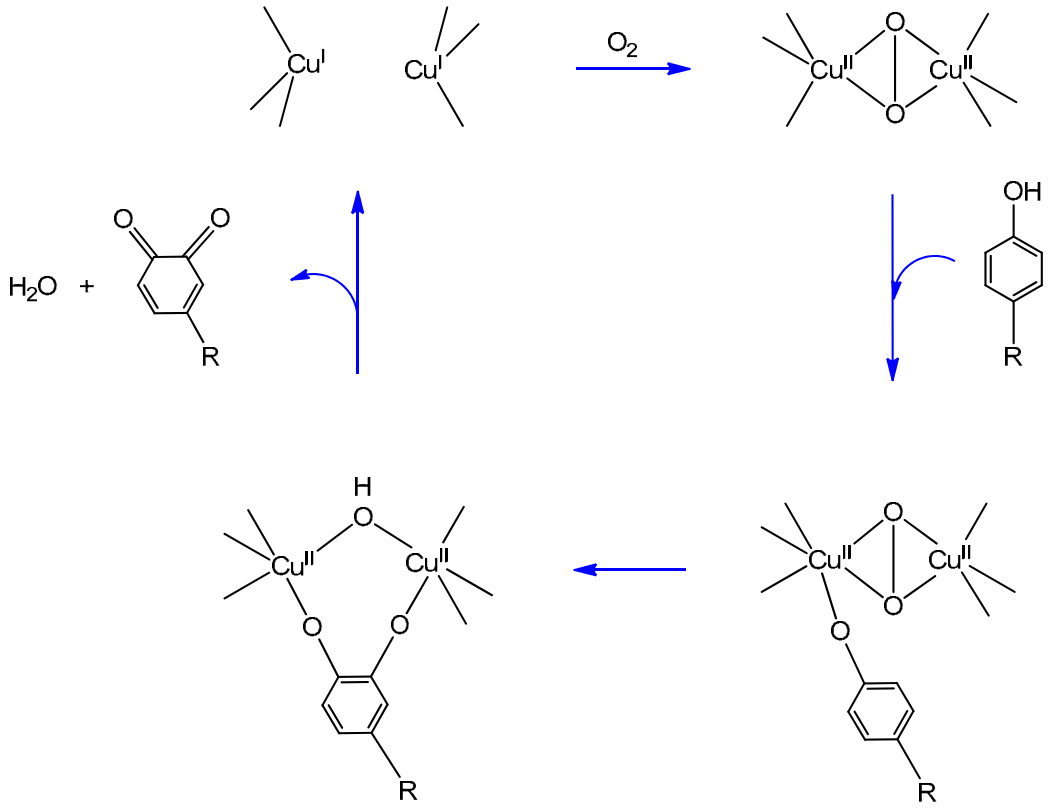

Scheme 1.4. Dioxygen activation at the coupled binuclear copper site in tyrosinase active centre.

1.3.2. Iron enzymes.

Metalloenzymes containing iron active sites comprise a large group of dioxygen activating enzymes that possess the capability for functionalizing a wide-range of organic substrates with high efficiency and selectivity.

Iron containing enzymes can be classified depending on the structure of the active site as:

- Heme enzymes: Cytochrome P450.[42]
- Mononuclear non-heme enzymes: Rieske dioxygenase, Bleomycin, Intradiol dioxygenase, Lipoxygenase.[43, 44]
- Dinuclear non-heme enzymes: Methane monooxygenase.[45]

Cytochromes P450 constitute a large family of cysteine thiolate-ligated heme monooxygenase enzymes that are present in all forms of life and play a key role in the transfer of an oxygen atom from dioxygen into a wide variety of biological substrates, with the second oxygen atom being reduced by two electrons to a water molecule. P450 inserts one of its oxygen atoms from molecular dioxygen into a substrate, and reduces the

second oxygen to a water molecule utilizing two electrons that are provided by NAD(P)H *via* a reductase protein (Scheme 1.5.). P450 are called monooxygenases as they insert only one of the two oxygen atoms present in O_2 into substrate.[46, 47]

$$S + O_2 + 2e^- + H \xrightarrow{P450} SO + H_2O$$

Scheme 1.5. Oxidative transformation catalysed by P450 (S = substrate).

O_2 activating P450 enzymes play a critical role in the biological hydroxylation of saturated carbon-hydrogen bonds, epoxidation of double bonds, oxidation of heteroatoms (N-, O-, S-oxidation), aromatisation and dealkylation reactions. The cytochrome P450 containing haem in the active site that consists of porphyrin (organic, ring-shaped compound) with an iron atom bound at its centre. The iron porphyrin is strongly linked to the protein backbone through coordination of a sulphur atom of a cysteine ligand (Figure 1.2.). Haem forms the active site of many proteins that fulfil a diverse range of biological functions, including metabolic oxidation reactions and the transportation of gases, such as oxygen. The iron atom acts as a source or sink of electrons for redox reactions, and it is the binding site for dioxygen. In some enzymes, the porphyrin ring also acts as an electron source.[48, 49]

The catalytic cycle of P450 (Figure 1.3.) is triggered when the substrate molecule enters the active site (pocket, not the metal centre) and displaces the axial water molecule. After this step an electron is transferred from the reductase protein. This results in reduction of the Fe^{III} centre to the ferrous Fe^{II} intermediate. Then one electron from Fe^{II} center and one electron from the triplet oxygen pair create an Fe^{III}-oxygen complex (A). This intermediate with an unpaired electron on the terminal oxygen atom consists of η^1- superoxide ion coordinated to the Fe^{III} centre. The second reduction step is the rate-determining step and generates the negatively charged Fe^{III}-peroxo complex (B). This intermediate can be protonated to generate Fe^{III}-hydroperoxo complex (C). A second protonation step produces the active oxidant species which is high-valent Fe^{V}-oxo (D) and a water molecule (after protonation of the terminal oxygen atom of the Fe^{III}-OOH entity). Iron of high-valent Fe-oxo species has formally four electrons and is hence an Fe^{IV} intermediate. However, a third unpaired electron of this intermediate is largely on the porphyrin moiety that appears as radical-cationic species $Por^{\bullet+}$. The active high-valent iron intermediate contains two oxidation equivalents higher than the resting state and is described either as $Por^{\bullet+}$- Fe^{IV}- oxo or as Fe^{V}-oxo.[50-53]

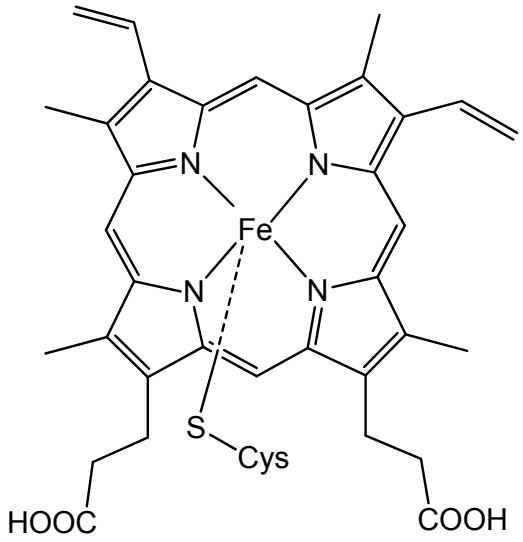

Figure 1.2. Structure of protoporphyrin IX, found in proteins including haemoglobin and myoglobin, is the most common haem in nature. Haem occurs in the active sites of many proteins and enzymes, and consists of a porphyrin structure with an iron atom in the centre[46].

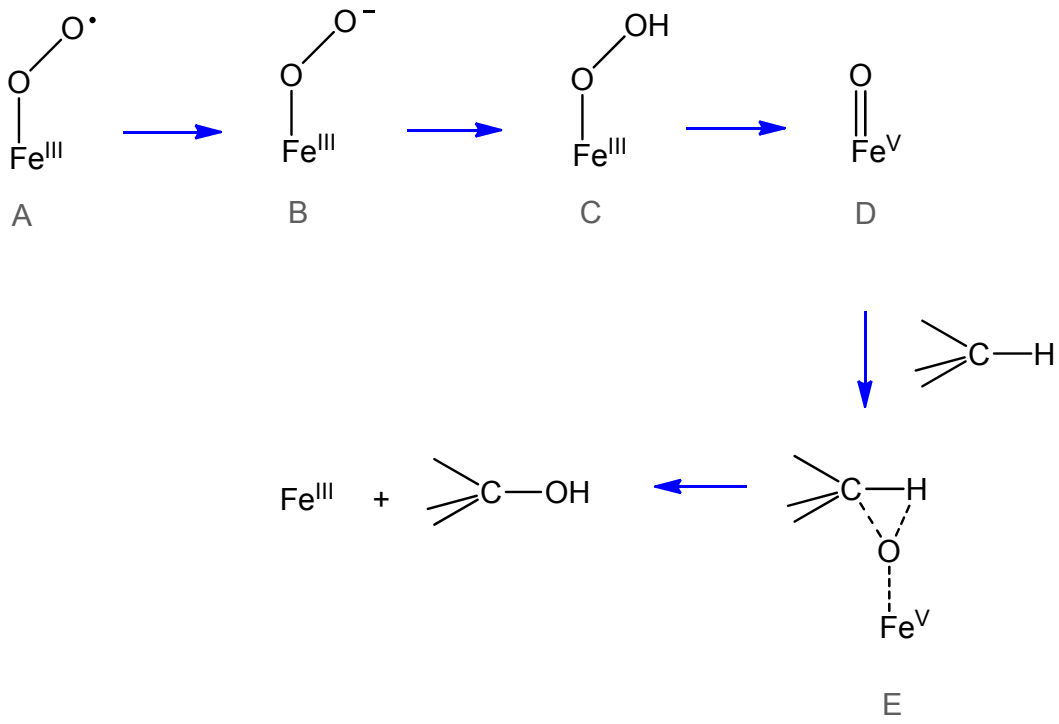

Figure 1.3. Representation of iron intermediates in catalytic cycles of cytochrome P450: η^1- superoxo (A), Fe ^{III}-peroxo (B), Fe ^{III}-hydroperoxo (C), Fe ^{V}-oxo (D).[53]

Mononuclear non-heme iron enzymes comprise of a large collection of dioxygen activating enzymes that are very different from their heme counterparts due to electronic and geometric differences arising from ligand environment. Non-heme metalloenzymes overcome the barriers involved in dioxygen reactions by substrate activation (oxidized metal centre induces radical character), or dioxygen activation (reduced metal site through two-electron reduction) (Scheme 1.6.) .[54] Non-heme iron enzymes catalyse oxidative transformations either by involving high-spin ferrous (Fe^{II}) ions or by the utilization of high-spin ferric (Fe^{III}) active centres. The Fe^{III} site is usually utilized to activate substrates for reactions with dioxygen and include intradiol dioxygenases and lipoxygenases.[55] The Fe^{II} site activates oxygen by direct binding to O_2, resulting in iron-oxygen intermediates that react with the substrate and include Rieske dioxygenases, pterin-dependent hydroxylases or extradiol dioxygenases.[56, 57]

Substrate activation. Intradiol dioxygenases and lipoxygenases are the enzymes that utilize the mechanisms involving substrate activation by their oxidized Fe^{III} active site (Scheme 1.7., A). In the first step the catecholate substrate binds to the $iron^{III}$ centre, displacing the hydroxide and the axial tyrosine residue (B).This leads to the reduction of the metal and formation of a substrate radical (C), which is susceptible to O_2 attack. Addition of oxygen to the activated radical species, produce a peroxy radical intermediate (D). In the mechanism of intradiol dioxygenase, the substrate molecule coordinates in a bidentate mode covalently, directly to the Fe^{III} centre (B). Such interactions could possibly lead to donation of electron density from substrate to iron, that results in formation of a substrate radical and partial reduction of iron. The coordinated substrate is activated and attacked directly by O_2 and in result a peroxo-substrate intermediate is generated (E). This intermediate undergoes rearrangement and the oxygen atom is inserted into the C-C bond producing anhydride (F) which is converted into the ring-opened muconic acid product (G). Intradiol dioxygenase mechanism is presented in Scheme 1.7. [58, 59]

Dioxygen activation. A majority of metalloenzymes, however, utilise dioxygen activation by their reduced Fe^{II}-active sites (Scheme 1.8., A). In the first step catecholate substrate binds to Fe^{II}-active site displacing two water molecules (B). In the mechanism of extradiol dioxygenase, the O_2 coordinates to Fe^{II}-centre, which results in the formation of Fe^{III}–superoxide (C). Higher Lewis acidity of Fe^{III} favours deprotonation of the diol substrate. The substrate semiquinone radical (D) undergoes reaction with superoxide and produces an alkyl peroxo complex (E). Then the oxygen atom is inserted resulting in a lactone ring formation, which is hydrolyzed to afford the muconic semialdehyde product (F). [56, 60] Extradiol dioxygenase mechanism is presented in Scheme 1.8.

Substrate activation

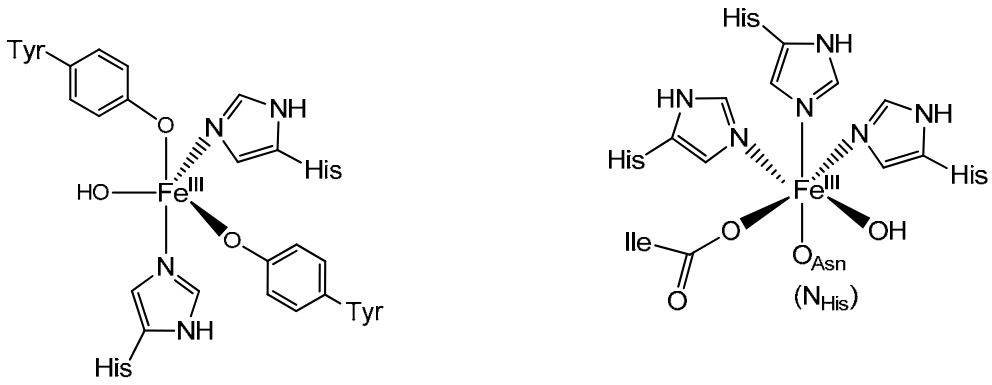

A B

O_2 activation

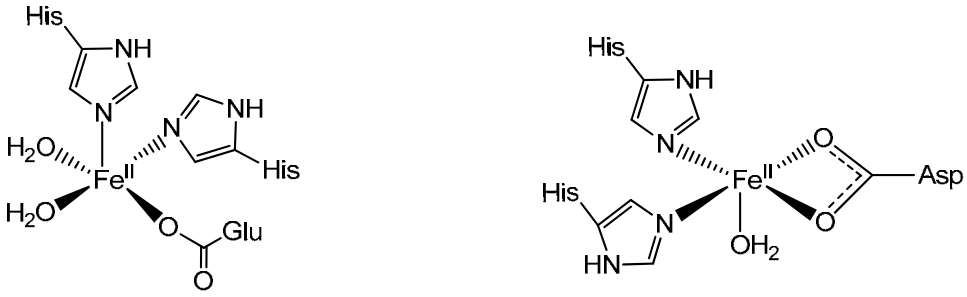

C D

Scheme 1.6. Representation of non-heme iron active sites for substrate activation: intradiol dioxygenases (A), lipoxygenases (B) and O_2 activation: extradiol dioxygenases (C), cis-dihydroxylating dioxygenases (D).[56]

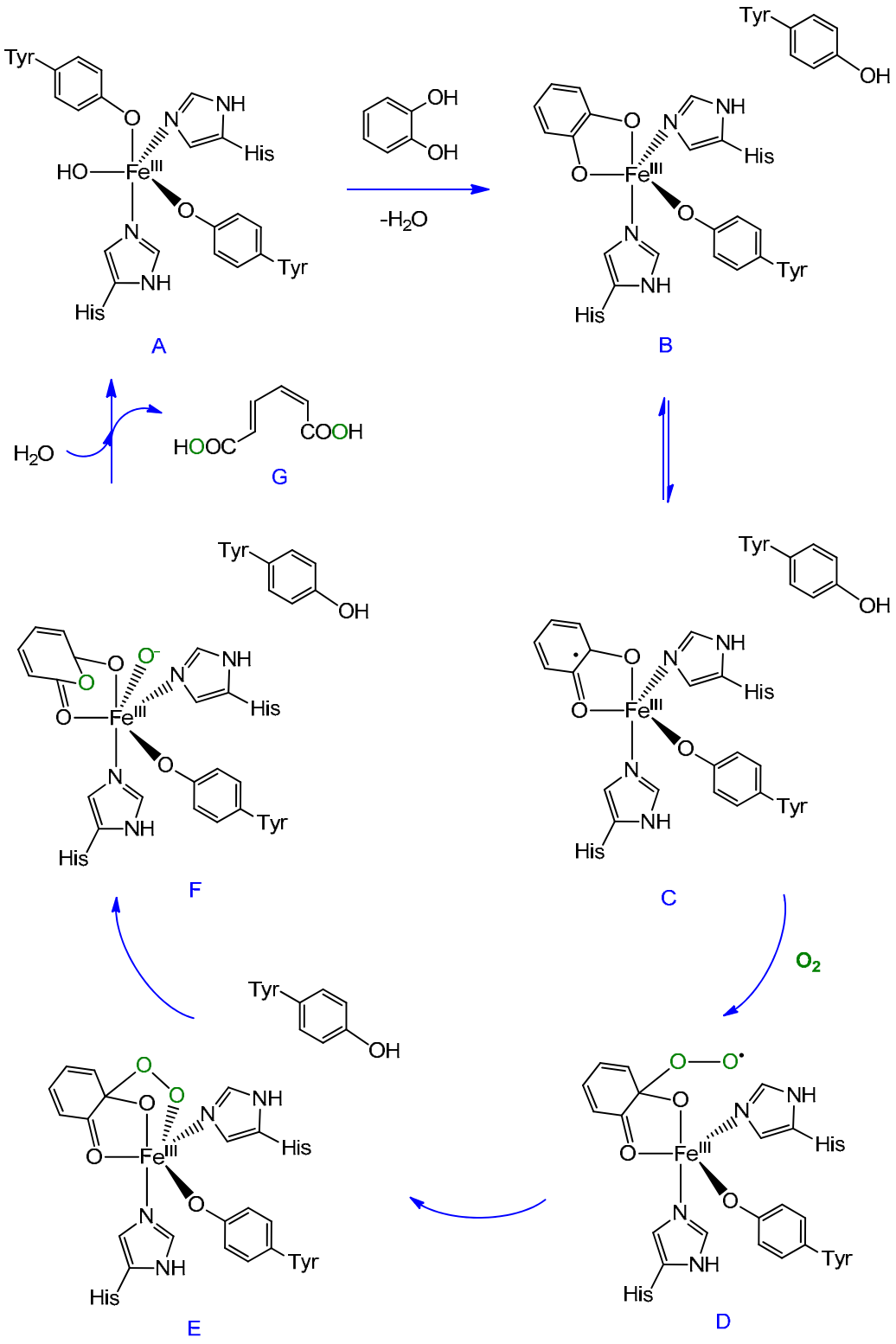

Scheme 1.7. Mechanism proposed for intradiol dioxygenase.[58]

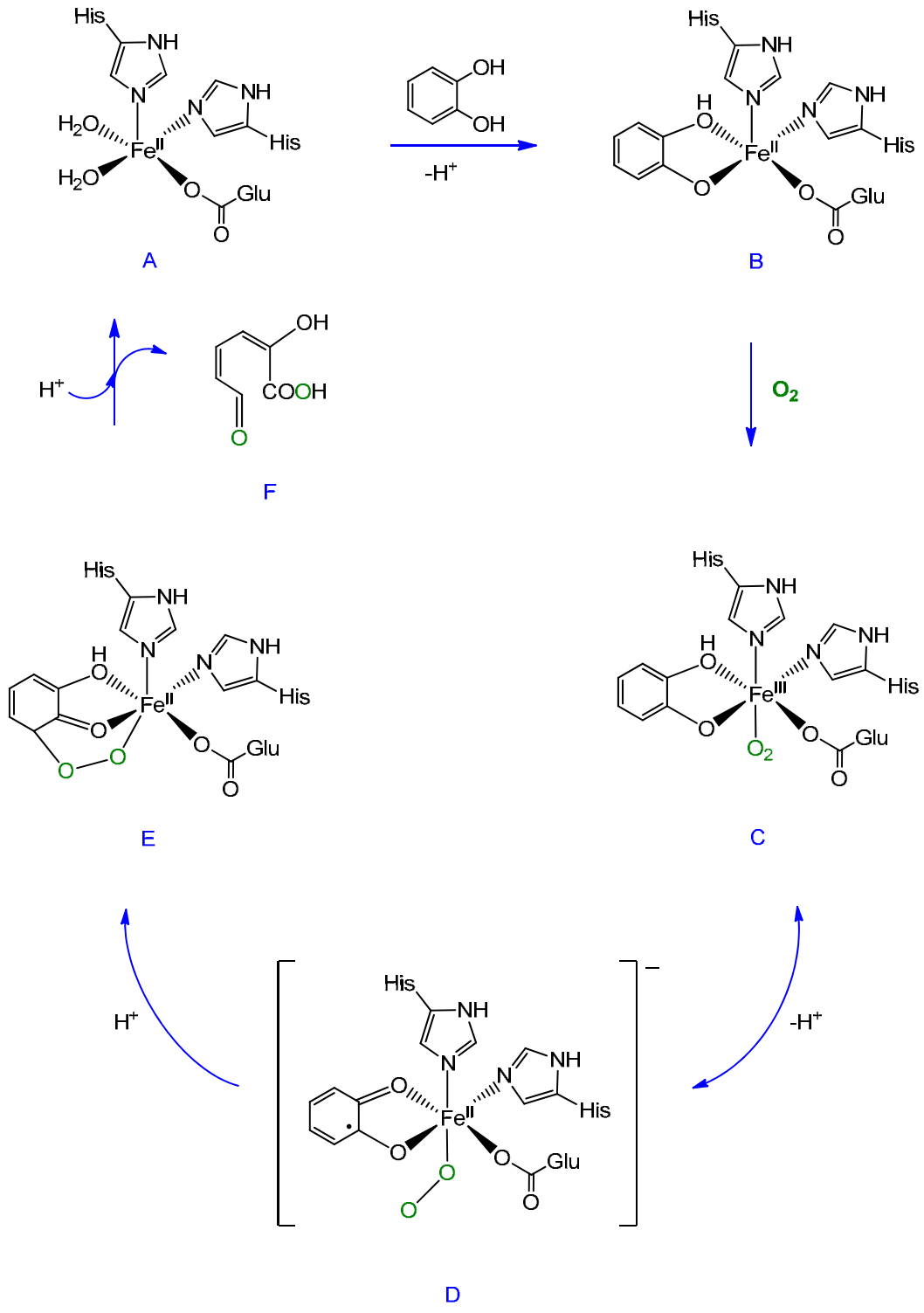

Scheme 1.8. Mechanism proposed for extradiol dioxygenase.[56]

Binuclear iron enzymes involved in O_2 activation primarily exist in two oxidation states: the fully reduced bi-ferrous $[Fe^{II}]_2$ and the oxidized bi-ferric $[Fe^{III}]_2$ form. A particular example of a di-iron containing enzymes is soluble methane monooxygenase (sMMO) which consists of a carboxylate-bridged dinuclear iron centre (Figure 1.4.) that is capable

of dioxygen activation, producing active species of much superior activity than other monooxygenases.[35] In addition to hydroxylation of alkanes and aromatics, MMO exhibits a unique ability to convert even methane, which is known to be the most inert hydrocarbon (C-H bond energy, 104 kcal/mol), into methanol using dioxygen as the oxidant (Scheme 1.9.). One oxygen atom is reduced to water, and the second is incorporated into substrate molecule, yielding the alcohol.[61]

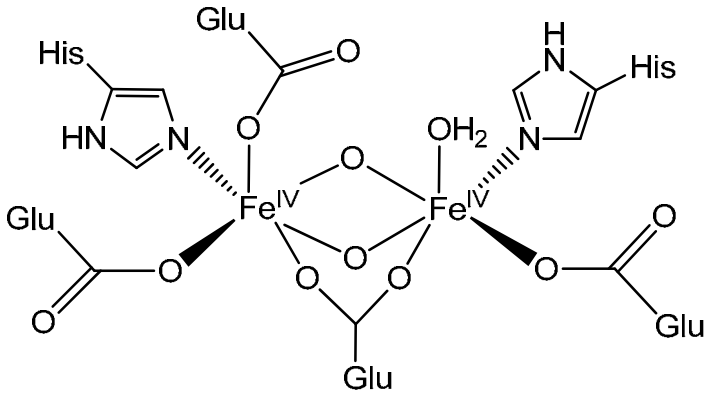

Figure 1.4. Structure of active O_2-derived intermediate of methane monooxigenase. The active site consists of two iron atoms that are coordinated by 2 histidine and 4 glutamic acid residues, one of which forms carboxylate bridge and a terminal water molecule.[35]

$$CH_4 + O_2 + NADH + H^+ \xrightarrow{MMO} CH_3OH + H_2O + NAD^+$$

Scheme 1.9. Selective conversion of methane to methanol by reductive activation of dioxygen by methane monooxygenase system.

The sMMO system requires three proteins to complete its catalytic cycle: MMOH, MMOB and MMOR. MMOH is methane monooxygenase hydroxylase that contains dinuclear iron centre where dioxygen activation and methane hydroxylation occur. MMOB is a regulatory protein forming specific complexes with the hydroxylase that affect the structure and reactivity of the diiron site.[62] Methane monooxygenase reductase MMOR (NADH-binding reductase) which is an iron-sulfur flavoprotein shuttles electrons from NADH through its flavin adenine dinucleotide (FAD) and [2Fe-2S] cofactors to the hydroxylase active site.[63] Regulatory protein MMOB binds weakly to the hydroxylase stabilizing intermediates required for dioxygen activation. In the presence of MMOB, $MMOH_{red}$ binds and reductively activates dioxygen through $MMOH_{superoxo}$ and $MMOH_{peroxo}$ adducts. The $MMOH_{peroxo}$ intermediate is then converted to strongly oxidizing $MMOH_Q$ which is the intermediate that hydroxylates methane, leaving MMOH in the resting diiron^{III} form ($MMOH_{ox}$). The MMOR which is an ironsulfur flavoprotein

employs two electrons derived from NADH to return $MMOH_{ox}$ to its reduced state $MMOH_{red}$ completing the catalytic cycle. It was proposed that activation of methane proceeds by conversion of $MMOH_Q$ from diiron high-valent Fe^{IV} to $Fe^{III}Fe^{IV}O^{\bullet}$ state. The oxygen radical form of $MMOH_Q$ abstracts hydrogen atom from CH_4. The reaction then proceeds by a radical rebound mechanism, where a methyl radical first recoils away from the oxo group of $MMOH_Q$ and then rebounds to form the new C–O bond of the product.[64, 65] Mechanistic proposal for the catalytic cycle of sMMO is presented in Scheme 1.10.

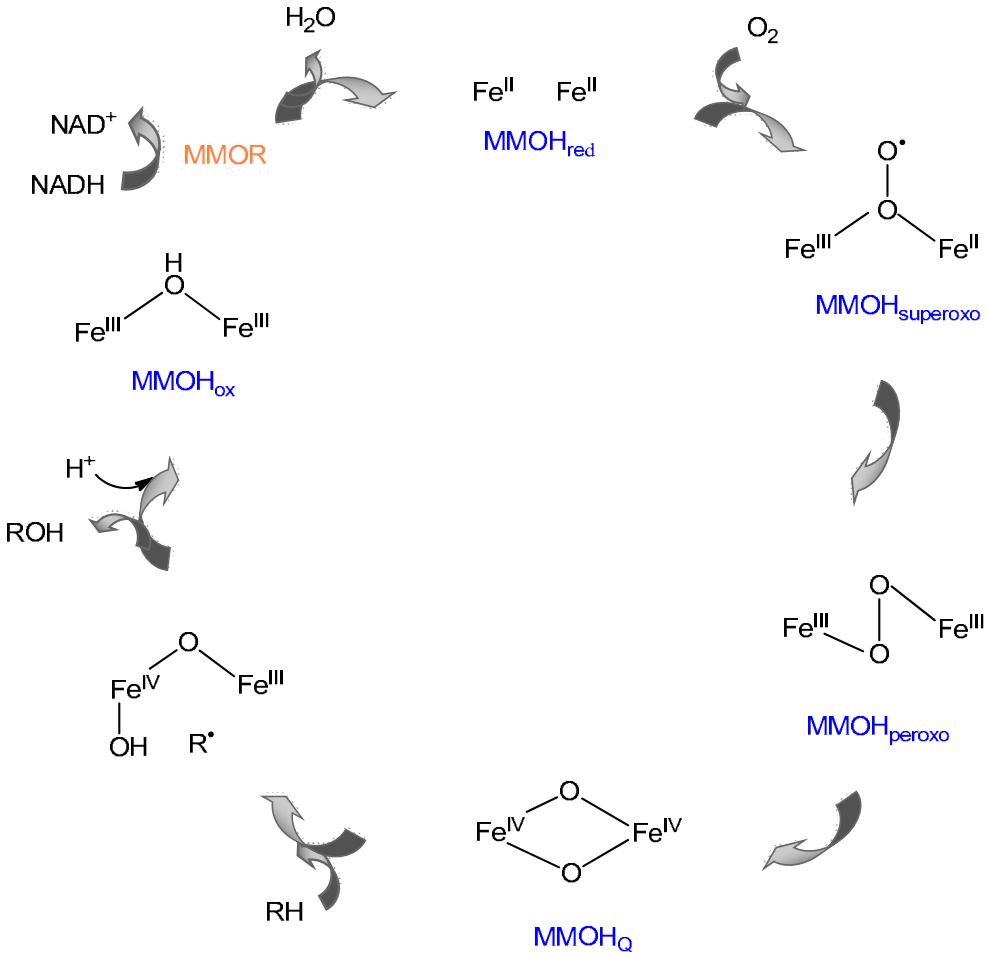

Scheme 1.10. Mechanistic proposal for the catalytic cycle of sMMO.

1.3.3. Copper enzymes.

Copper active sites also play a major role in biological dioxygen activation systems. Copper-containing enzymes include monoooxygenases, dioxygenases, and oxidases. Active sites of copper metalloenzymes contain one or more copper ions and some contain additional metal ions such as iron or zinc, and some of the enzymes contain multiple copper centres with distinct functions. Copper enzymes are involved in hydroxylation

reactions (particulate methane monooxygenases pMMO, tyrosinase), reversible dioxygen binding (hymocyanin), two-electron reduction of O_2 to peroxide coupled with oxidation of organic molecules (galactose oxidase GO, amine oxidase, catechol oxidase) and four-electron reduction to water coupled with substrate oxidation (ascorbate oxidase, laccase).[66]

Copper containing enzymes can be classified depending on the structure of the active site as:[67]

- Mononuclear copper centre: Amine oxidase, Galactose oxidase.[68]
- Non-coupled dinuclear copper centre (there is no bridge between copper centres): Dopamine β-hydroxylase.[69]
- Coupled dinuclear copper centre (coupling refers to magnetic interactions between the copper centers): Tyrosinase, Catechol oxidase, Hemocyanin.[70]
- Trinuclear copper centre: Laccase, Ascorbate oxidase.[71]
- Polymetallic centre: Superoxide dismutase (SOD), Cytochrome c oxidase.[72]

The majority of biological Cu sites serve as a one electron shuttle, alternating between Cu^{I} and Cu^{II}. The Cu^{III} oxidation state is generally considered to be inaccessible because of the highly positive Cu^{III}/Cu^{II} redox potentials that result from ligation of amino acid side chains like imidazole and phenolate ions. However, interconversion between Cu^{II}/O_2 and Cu^{III}/O_2 species has been observed for many synthetic systems (μ-η2:η2 peroxo dicopper^{II} and bis(μ-oxo)dicopper^{III}. Bis(μ-oxo)dicopper^{III} complexes have been characterized in synthetic models, but not in biological systems. Cu^{II} or Cu^{III} can be ligated to O_2-derived ligands such as superoxide (1e-), peroxide (2e-) or oxide (4e-) ions.

Cu/O_2 species formed by the reaction of Cu^{I} complexes with O_2 are divided into four groups: $Cu:O_2$ 1:1, $Cu:O_2$ 2:1, $Cu:O_2$ 3:1, $Cu:O_2$ 4:1.[73, 74] The Cu/O_2 cores structures are shown in Table 1.1.

$Cu:O_2$ 1:1. Two different structural types of $Cu:O_2$ 1:1 are observed: end-on O_2 of Cu^{II}- superoxo species (η^1-superoxo) and Cu^{II}- hydroperoxo (η^1-hydroperoxo) and side-on O_2 in the Cu^{II}- superoxo (η^2-superoxo) and the Cu^{III}-peroxo (η^2-peroxo).

$Cu:O_2$ 2:1. There are five structures of Cu/O_2 2:1 complexes: end-on peroxodicopper^{II} (trans-μ-*1,2-pe*roxo and η^1-peroxo), side-on peroxodicopper^{II} (μ-η^2:η^2-peroxo and μ-*1,1*-hydroperoxo), and bis(oxo)dicopper^{III} (bis μ-oxo).

Cu:O2 3:1. The 3:1 species bis(μ_3-oxo)tricopper^{II,II,III} (bis μ_3- oxo), results from the 4e- reduction of O_2 by three Cu^{I} centres. O_2 connect the three Cu centres in a $Cu^{III}Cu^{II}Cu^{II}$ cluster. This results from ability of Cu^{III} and Cu^{II} ions to adopt a square planar geometry.

Cu:O2 4:1. The tetranuclear peroxide structural types *cis*-μ_4-η^2:η^2-peroxo and *trans*-μ_4-η^2:η^2-peroxo are currently unknown in biological systems and only exist as synthetic complexes.

Table 1.1. Cu/O_2 species formed by reaction of a Cu^I with O_2.[66]

	Cu:O_2 ratio			
	1:1	2:1	3:1	4:1
Cu^{II}	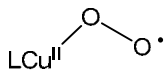 η^1-superoxo	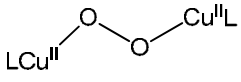 trans-μ-*1,2-p*eroxo		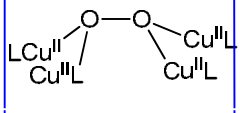 *cis*-μ_4-η^2:η^2-peroxo
	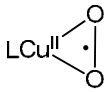 η^2-superoxo	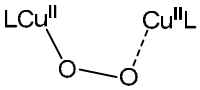 η^1-peroxo		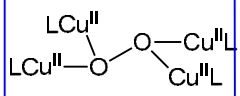 *trans*-μ_4-η^2:η^2-peroxo
	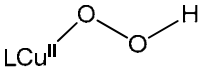 η^1-hydroperoxo	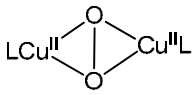 μ-η^2:η^2-peroxo		
		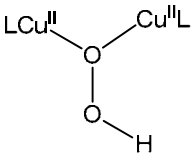 μ-*1,1*-hydroperoxo		
Cu^{III}	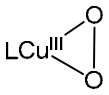 η^2-peroxo	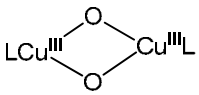 bis μ-oxo	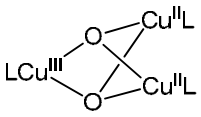 bis μ_3- oxo	

Galactose oxidase (GO) is a member of the mononuclear copper enzymes that highly efficiently catalyze two-electron oxidation of a broad variety of primary alcohols and even polyalcohols are converted, in a highly regio and stereoselective way, into the corresponding aldehydes. This enzyme is capable of catalytic oxidations in water, making direct use of the molecular oxygen from the air.[75]

The galactose oxidase active centre contains a copper ion coordinated by two nitrogen and two oxygen donor atoms originating from two histidine and two tyrosine residues, respectively. The mononuclear Cu centre is also bound by the water molecule to form a distorted five-coordinate metal complex (Figure 1.5.).

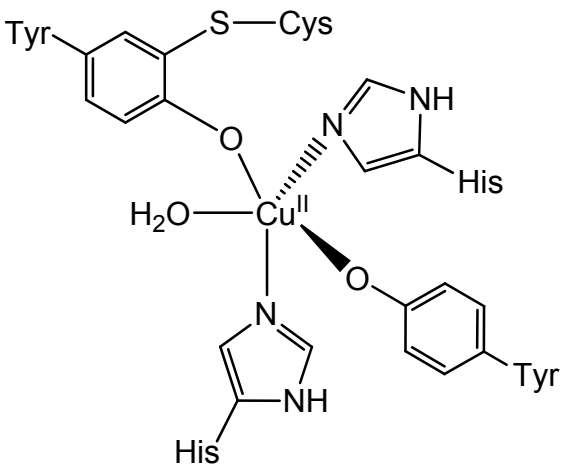

Figure 1.5. Galactose oxidase active site.

Galactose oxidase applies a tyrosyl radical unit to perform a two-electron redox reaction (Scheme 1.11.). The inactive form of galactose oxidase contains tyrosinate ligand covalently linked to a mercapto side chain of cysteine (A). In the active form of the enzyme, this ligand exists as a one-electron oxidized tyrosyl radical (B). As a first step of the catalytic process the alcohol binds to the copper centre of active form of the enzyme (C). This is followed by alcoholate formation through deprotonation of the substrate by the axial tyrosinate ligand. In the next step the hydrogen atom is abstracted from the substrate by the tyrosyl radical (D) and the copper centre is reduced to Cu^{I} (E) by single-electron transfer from the ketyl radical. The weakly bound formed aldehyde is replaced by dioxygen (F) and the catalytic cycle is closed by recovering the initial copper oxidation state under reduction of O_2 to H_2O_2 (step G to B). Hydrogen atom abstraction is the rate-limiting step for substrates that are difficult to oxidize.[68, 76, 77]

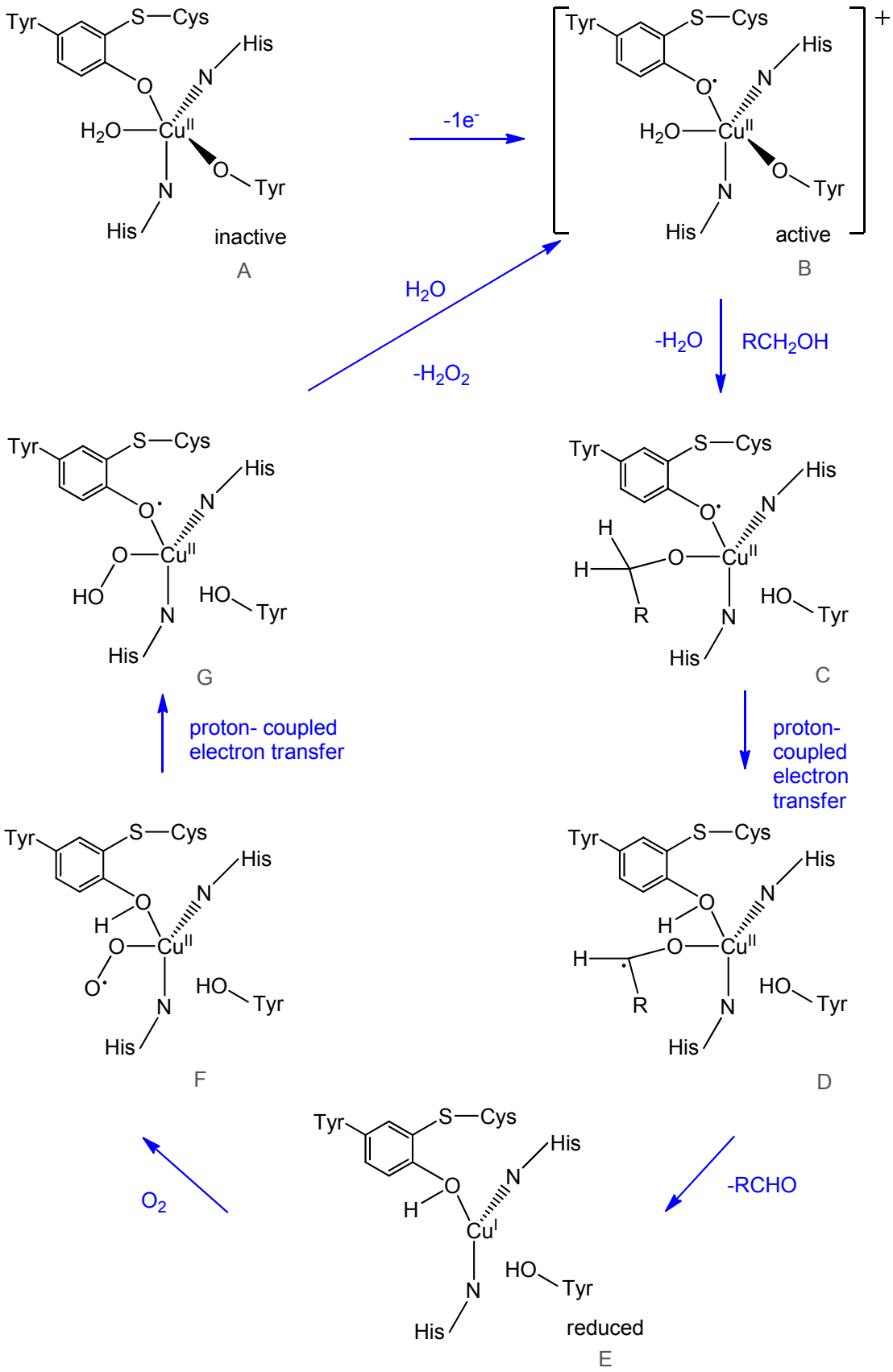

Scheme 1.11. Proposed mechanism for alcohol oxidation by galactose oxidase. During the catalyzed cycle, the enzyme alters between three different forms: active, inactive and fully reduced form.

Coupled dinuclear copper enzymes (type-3 copper centres) serve either as oxygenase/oxidase enzymes or as dioxygen transport proteins. This group includes the closely related tyrosinase, catechol oxidase and hemocyanin which is an oxygen transport protein. All these proteins have a dinuclear copper center that possess similar structural-functional relationships and similar spectroscopic behaviour.[38] Both copper atoms forming the metal centre are coordinated by three imidazole nitrogen atoms from histidine (Figure 1.6.).

Both, tyrosinase and catechol oxidase, can oxidize catechol to quinone, but only tyrosinase can hydroxylate phenol. Catechol oxidase (CO), known as *o*-diphenol oxidase, catalyzes exclusively the oxidation of catechols (i.e., *o*-diphenols) to the corresponding *o*-quinones (catecholase activity, Scheme 1.12.).[78] In contrast to CO, tyrosinase (TYR) shows additional monooxygenase activity (cresolase activity). This enables the enzyme to also transform monophenols (i.e. tyrosine or cresol) as substrates.

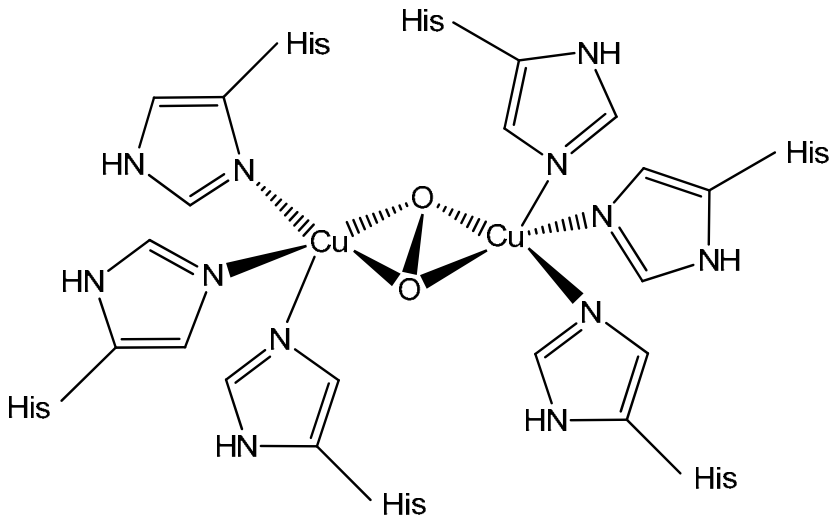

Figure 1.6. Dioxygen-binding mode of type-3 dinuclear copper enzymes.

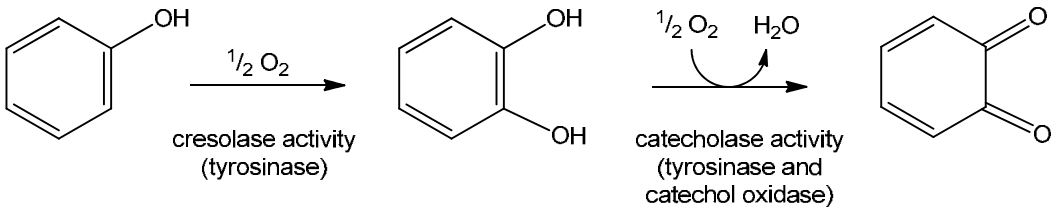

Scheme 1.12. Reaction pathway of tyrosinase and catechol oxidase.

In the mechanism of cresolase activity, monophenol substrate binds to the *oxy* state of enzyme (Scheme 1.13., A).[79] In the *oxy* state dioxygen is most likely bound in the peroxide oxidation state as μ-η^2:η^2-peroxo (O_2^{2-} localized between the two Cu atoms). When bonded to the dicopper active site (*oxy* state), the monophenol (B) is monooxygenated to *o*-diphenol and the *met* state of the enzyme is formed (C). In the *met* state both copper ions are in the +2 oxidation state. Each of them is coordinated by three histidine residues. In the *met* state Cu ions are also bridged by another ligand, most likely a hydroxide ion. The formed diphenol subsequently binds to dicopper *met* state in a bidentate binding mode (D). In this stage the diphenol is oxidized to quinone which leads to the reduced state *(deoxy* state), of the dinuclear copper centre (E). In the *deoxy* state both copper atoms are in the +1 oxidation state. Reoxidation of the reduced state to the *oxy* state occurs by attack of dioxygen and closes the catalytic cycle. The catalytic cycle of catecholase is shown in Scheme 1.13.

The mechanism of catecholase activity can start from the *oxy* or *met* states. A diphenol substrate binds to the *oxy* (Scheme 1.14., A) state in a bidentate binding mode (B) followed by the oxidation of the substrate to the first quinone, and the *met* state of the active site is formed (C). Then a second diphenol substrate binds to the *met* state (D), followed by the formation of second quinone molecule and the reduced state of the enzyme *deoxy* state (E). Binding of dioxygen to the *deoxy* state centre leads to the *oxy* state again and closes the catalytic cycle.[80] The mechanism of catecholase activity is shown in Scheme 1.14.

Particulate methane monooxygenase (pMMO) is an integral membrane copper-containing enzyme that is similar to diiron sMMO and converts methane to methanol. Whereas diiron sMMO is selective towards alkanes, alkenes, aromatics, and halogenated hydrocarbons, the pMMO is more selective toward alkanes and alkenes substrates that have five carbons or less. There are three metal sites in pMMO: mononuclear copper centre, dinuclear copper centre and zinc centre. The dinuclear copper site is the most likely candidate for O_2 binding and activation. A dinuclear copper center is coordinated by three histidine residues through imidazole nitrogen, together with the amino-terminal nitrogen of one histidine (Figure 1.7.). It is likely that exogenous ligands are also present at this site. However, due to difficulties in isolation of membrane pMMO, the detailed structure, mechanism and actual reaction sites for the methane hydroxylation are still under investigation.[81, 82]

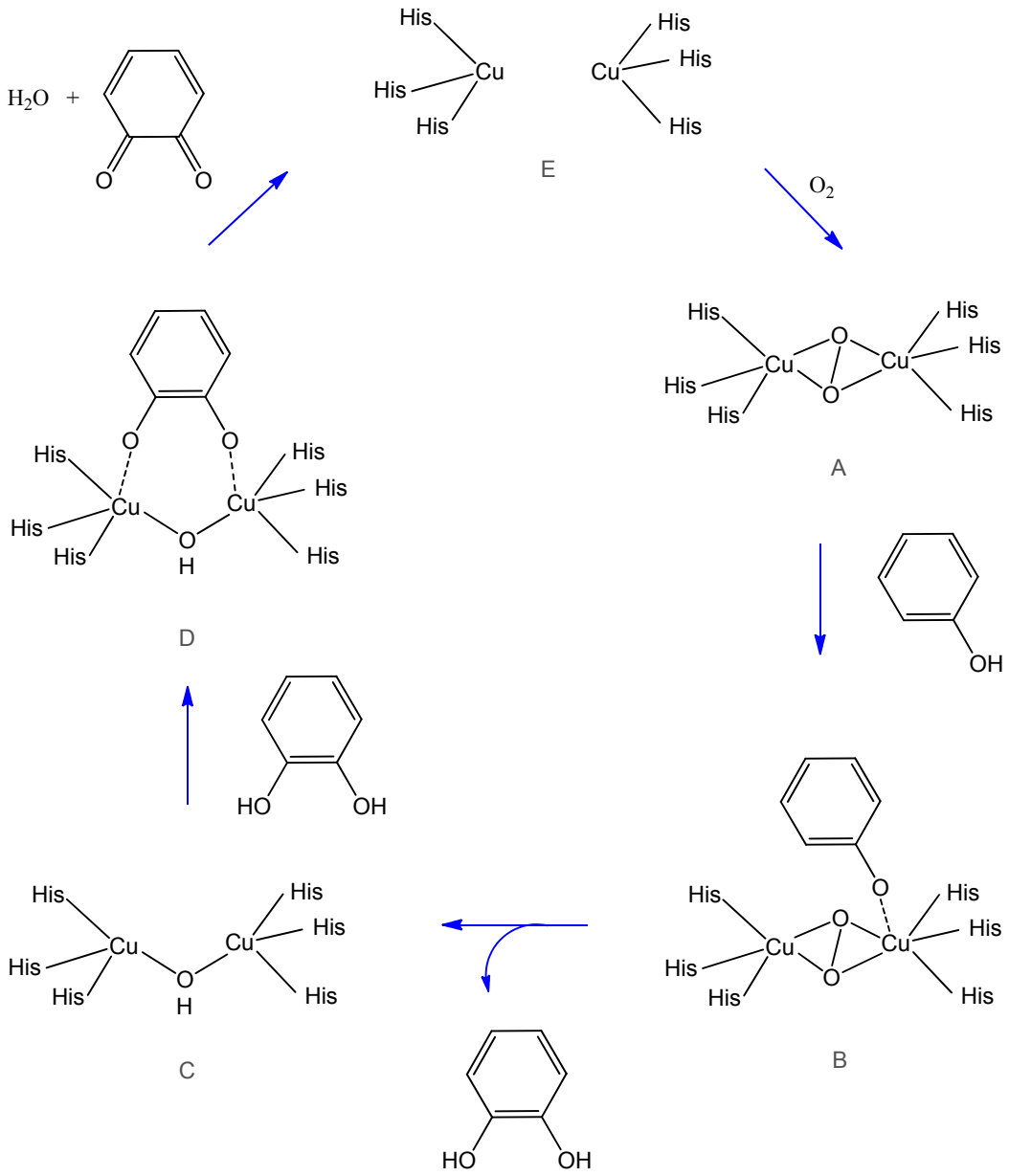

Scheme 1.13. Proposed mechanism of cresolase activity: *oxy* state A, *oxy* binding mode B, *met* state C, *met* bidentate binding mode D, *deoxy* state E.[83]

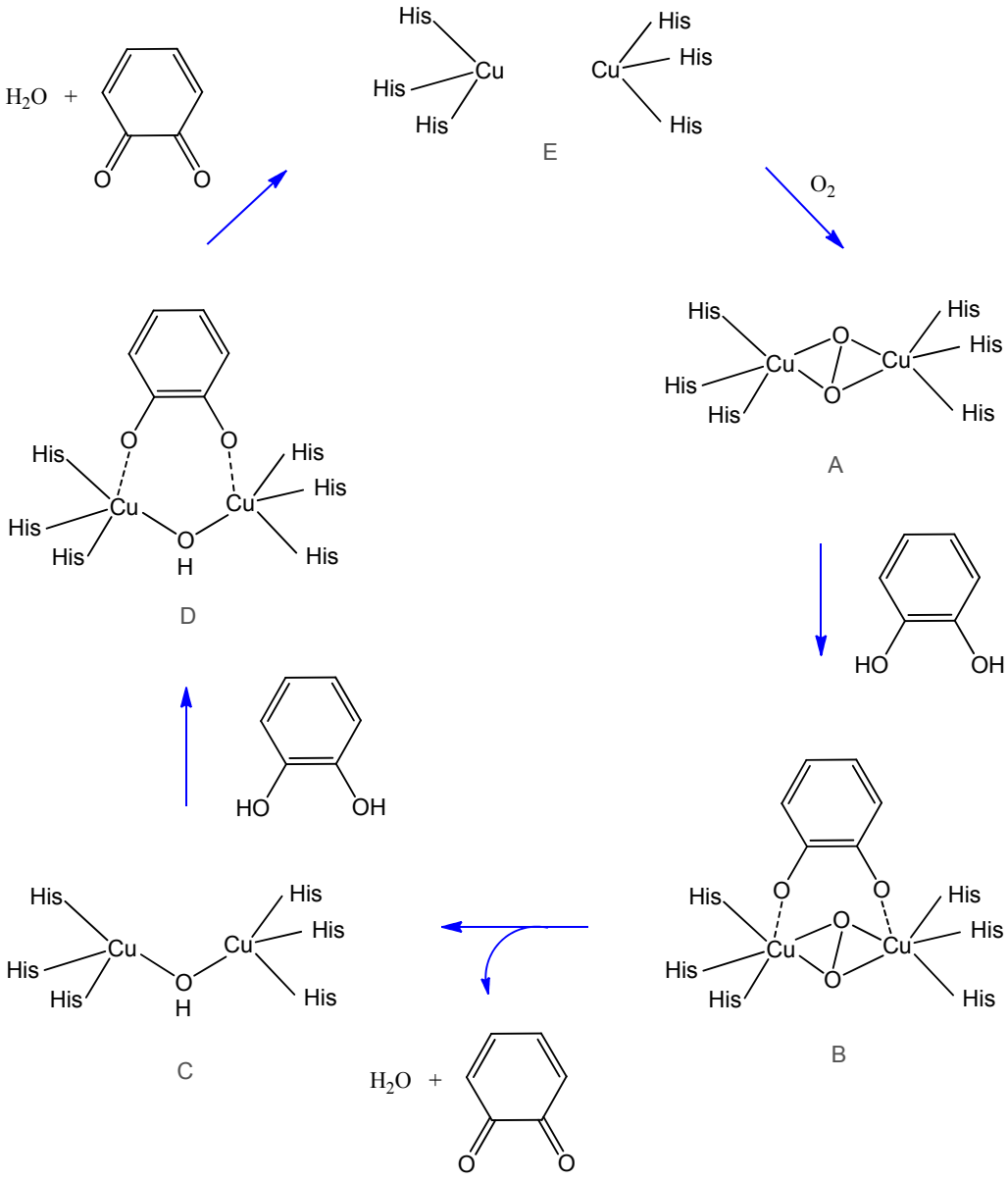

Scheme 1.14. Proposed mechanism of catecholase activity: *oxy* state A, *oxy* bidentate binding mode B, *met* state C, *met* bidentate binding mode D, *deoxy* state E.[84]

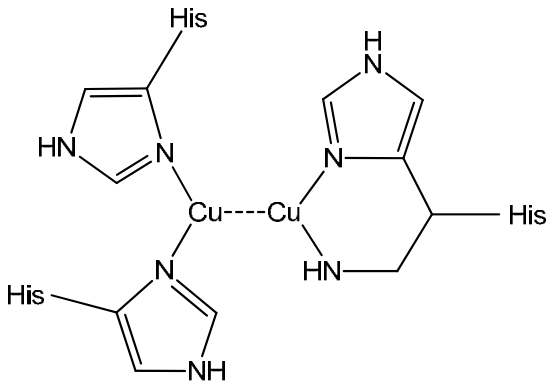

Figure 1.7. Proposed structure of dicopper active site of particulate methane monooxygense (pMMO).[85]

1.4. Strategies for immobilisation of active sites onto solid supports.

The heterogenization of transition metal complexes onto solid supports has been widely investigated for the purpose of designing selective heterogeneous catalysts for clean catalytic transformations. Different methods can be used to immobilize the catalytically active complexes onto solid supports (Figure 1.8.).[86] Single sites can be added to solid support by *post-synthesis* (covalently or non- covalently), or *via* direct synthesis techniques.[87, 88] In the case of post-synthesis methods the active centre is added directly to the support by the formation of a covalent bond, or after modification with a tether (side functional group) if necessary.[89] Active centres can also be immobilized onto a supports by non-covalent interactions, such as hydrogen bonds, weak van-der-Waals interactions or by mechanical trapping (encapsulation). [90]

Encapsulation of catalytically active species within the pores of host solids can be achieved post-synthetically (e.g. ion-exchange followed by flexible-ligand methods) [91] or indirect synthesis (e.g. zeolite synthesis methods).[92] In the case of direct synthesis, the precursor of the catalytically active species is dispersed in the reaction mixture of the final material and the single-sites are introduced during the synthesis step.

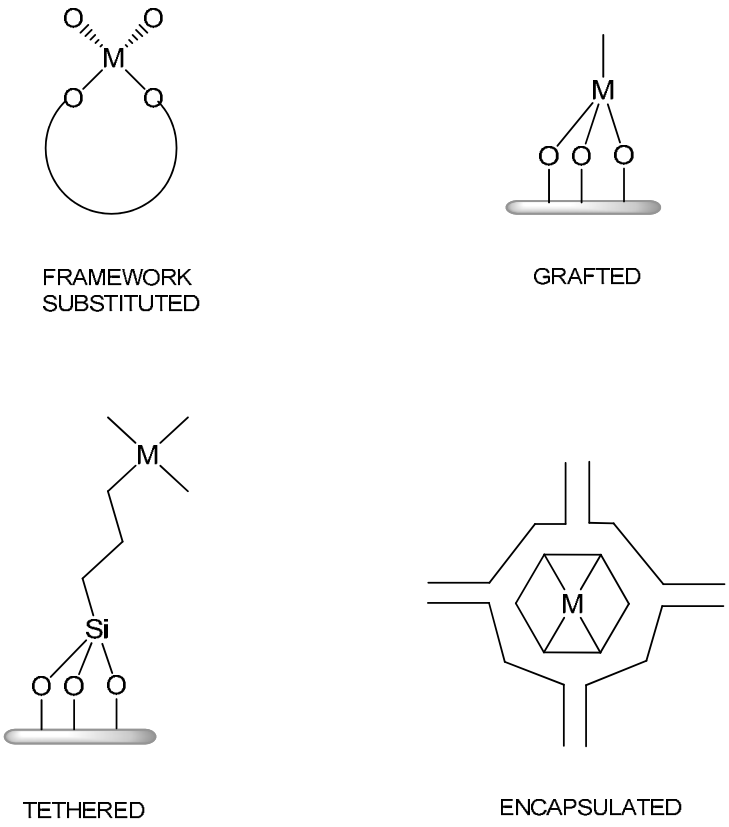

Figure 1.8. Schematic representation of strategies for heterogenization of a metal centre (M).[25]

1.4.1. Transition metal complexes immobilized within zeolites.

Zeolites are crystalline aluminosilicates with a three-dimensionally connected pore structure. The zeolite framework consists exclusively of corner-sharing AlO_4 and SiO_4 tetrahedra. The primary building units are single TO_4 tetrahedra, where the T atom is an aluminium or silicon atom. Each T atom is tetrahedrally bonded to four oxygen atoms forming a bridge to neighbouring T atoms. Silicon surrounded by four oxygen atoms (essentially SiO_2) has no charge. Aluminium has 3^+ charge, thus AlO_2 has a net negative charge. The charge balance between Si and Al results in an overall net negative charge on the zeolitic framework. The presence of aluminium produces this negative charge and is balanced by non-framework cations that can be readily exchanged.[93, 94]

Zeolites facilitate as catalysts for chemical reactions which take place within their internal cavities. They are thermally stable, chemically robust and easy to separate from the reaction products. Zeolites can incorporate and immobilize various active sites within their structure in the channels and cages. Careful combination of metal complexes immobilized as active sites in an inorganic matrix can result in catalysts that can mimic the functional aspects of enzyme activity.[95] Zeolites are ideal supports and by judicious choice of the active site novel single-site heterogeneous catalysts can be designed. Such zeolite encapsulated active centres present many advantages. Zeolites have well organized pores and channels, which readily serve as supporting hosts for various molecules. In such systems zeolites can serve as a substitute for the protein mantle of natural enzymes and provide a controlled steric environment, where the catalysis ensues. These heterogeneous catalysts are resistant to harsh reaction conditions, more stable at high temperatures, facilitate separation of products from reactants and aid catalyst recyclability.

Several general routes are known for preparation of metal complexes inside zeolites (Figure 1.9.):

- ***Ion exchange:*** The ion-exchange strategy involves the exposure of a sodium-ion charge balanced zeolite to a solution containing other cations, facilitating an exchange of the sodium ions. This method has been used for encapsulating metal–amino acid complexes inside a zeolite structure (for details see section 16).[96, 97]

- ***Flexible ligand method:*** The flexible-ligand method involves the synthesis of metal complexes in the zeolite cavity by coordination of the ligand with the exchanged metal cations. Complexes with previously exchanged metal ions are able to diffuse freely through the zeolite pores. This approach is well suited for the

encapsulation of metal–salen complexes as the salen ligand offers the flexibility to move throughout the channels.[98, 99]

- ***Ship in the bottle:*** The ship-in-bottle method involves assembling the final active metal complex inside the pores of the host by reacting smaller precursors to afford the larger complex that becomes sterically entrapped inside the cages. This route was employed for encapsulating metal–phthalocyanine or metal–porphyrin complexes within the zeolite.[100, 101]

- ***Zeolite synthesis method*:** The zeolite synthesis method follows a templated synthesis approach. Preformed transition-metal complexes are included in the zeolite synthesis mixture and the zeolite is formed around the metal complex, using it as a sort of template. Metal complexes of phthalocyanines, porphyrins and amino acids provide examples of such entrapped catalysts.[102, 103]

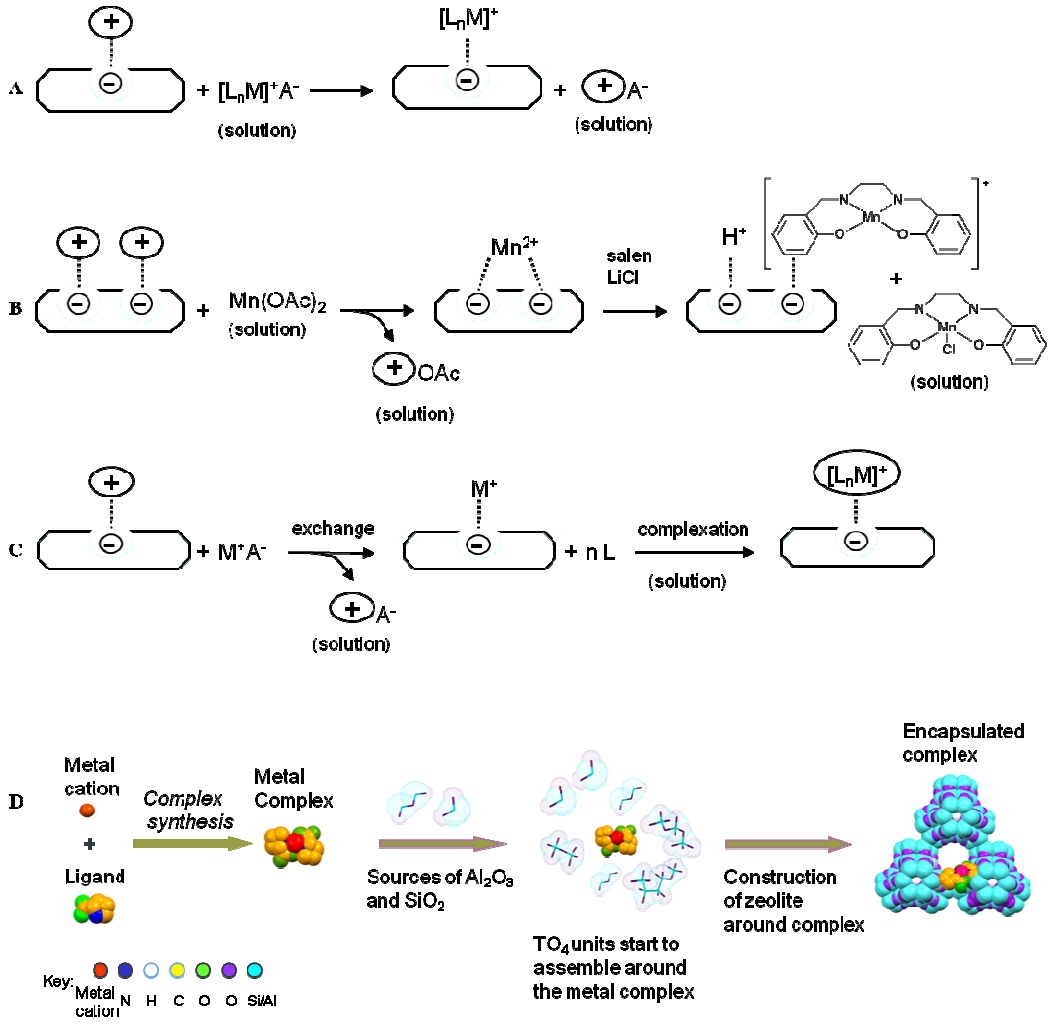

Figure 1.9. Methods for encapsulating metal complexes within zeolites: Ion exchange (A), flexible ligand (B), 'ship in a bottle' (C) and zeolite synthesis methods (D).[104]

Many attempts have been made to simulate the functions of natural metalloenzymes by immobilising catalytically active coordination complexes in the network of zeolite porous solids.[105] The encapsulation approach has many advantages which combines specific characteristics of the support, like pore diameter, cavity size, well-organised nanopores and nanochannels and electrostatic potential with the electronic and stereochemical properties of the complex. The zeolite matrix replaces the protein portion of natural enzymes and can readily serve as suitable hosts for supporting active entities thereby providing a controlled steric environment for enclosed transition-metal-complexes.[106] Such heterogeneous catalysts can be used in organic media for the highly selective oxidation transformation of hydrophobic substrates. However, the immobilization of transition-metal complexes within solid supports can sometimes result in a decrease in catalyst activity due to additional mass-transfer restrictions (sorption and diffusion).

Phthalocyanine, synthetic porphyrin and salen metal complexes encapsulated within zeolites have been widely studied as biomimetic catalysts and have revealed promising oxidation potential. Many attempts have been made to immobilize these complexes on solid supports such as silica, zeolites, activated carbon, alumina and polymers.[107] The first approach of immobilizing phthalocyanine metal complex within zeolite Y was reported by Romanovsky *et al.* and involved the formation of zeolite Y entrapped metal phthalocyanine *via* template condensation of four dicyanobenzene molecules around the intrazeolite metal species (Figure 1.10.).[108] Metallophthalocyanines have also been immobilised onto zeolites embedded in polydimethylsiloxane membranes,[109] activated carbon black,[110] and MCM-41 by sol–gel synthesis. Metallosalenes, metallophthalocyanines and metalloporphyrines have also been covalently grafted onto silicas and organic copolymers.[111]

Metallophthalocyanine (MPc) complexes are attractive potential oxidation catalysts because of their rather cheap and facile large scale preparation and chemical and thermal stability. Their macrocyclic structure is similar to that of porphyrin ligands which are widely used in nature in the active sites of oxygenase enzymes, but phthalocyanines are more stable to degradation and more readily available than porphyrins.[112] Metallophtalocyanine complexes encapsulated in zeolites have been widely investigated in oxidation of hydrocarbons. Iron phthalocyanine was employed as a catalyst for selective cyclohexane oxidation with PhIO and cyclohexanol was obtained as sole product.[112] Zeolite encapsulated perfluorinated Co-phthalocyanine and Cu-phthalocyanine incorporated inside zeolite Y were found to be more active in cyclohexane oxidation than the unsupported complexes (Table1.2.).[113]

A similar trend was observed with $RuF_{16}PcX$ catalyst where homogeneous $RuF_{16}Pc$ catalyst afforded TON of 250 in cyclohexane oxidation with TBHP, while in presence of heterogeneous $RuF_{16}PcX$ TON increased to 3000.[114]

The $RuF_{16}PcX$ heterogeneous catalyst that contained less metal complex was > 10 times more active than homogeneous analogue. This increase in TON was attributed to the site-isolation effect. Homogeneous complex showed rapid dimerization and formation of catalytically inactive oxo dimers of the form $PcF_{16}Ru\text{-}O\text{-}RuF_{16}Pc$. Encapsulation of $RuF_{16}Pc$ complexes within the supercages of Zeolite NaX precluded dimerization and clearly enhanced catalytic activity.

Synthetic metalloporphyrins have been studied as cytochrome P-450 models and are found to be efficient catalysts for alkene epoxidation and alkane oxidation. The use of homogeneous metalloporphyrin systems has many draw-backs due to porphyrin ring oxidative self-degradation and aggregation. Oxidation of hydrophobic substrates by water-soluble cationic metalloporphyrins is difficult as the catalytically active species remains dissolved in the aqueous phase. To overcome these difficulties metalloporphyrins have been encapsulated within zeolite frameworks that stabilize the porphyrin ring. This approach was described for the first time by Nakamura *et al*. and involved $iron^{III}$ and $manganese^{III}$ 5,10,15,20-tetramethylporphyrin complexes synthesised within the cages of NaY.[92, 115] These materials showed catalytic activity in the oxidation of cyclohexane with hydrogen peroxide. Supporting metalloporphyrins onto a rigid solid host provided the site-isolation of the active centres and prevented the formation of less reactive dimers (oxo metalloporphyrin dimers). The complex synthesized within supercages is too large to pass through the channels which retard dimerisation and deactivation and favourably influence the catalytic activity.[116]

The chemical modification of metalloporphyrin microenvironment for the improvement of the catalytic efficiency has been achieved by the introduction of electron-withdrawing substituents into the porphyrino ring to restrict the formation of unreactive oxo-dimers and hence improve the activity and stability of metalloporphyrins (eg. porphyrin substituted with NO_2 groups (Figure 1.12. top).[117, 118]

Metallophtalocyanine and metalloporphyrin complexes are presented in Figure 1.13.

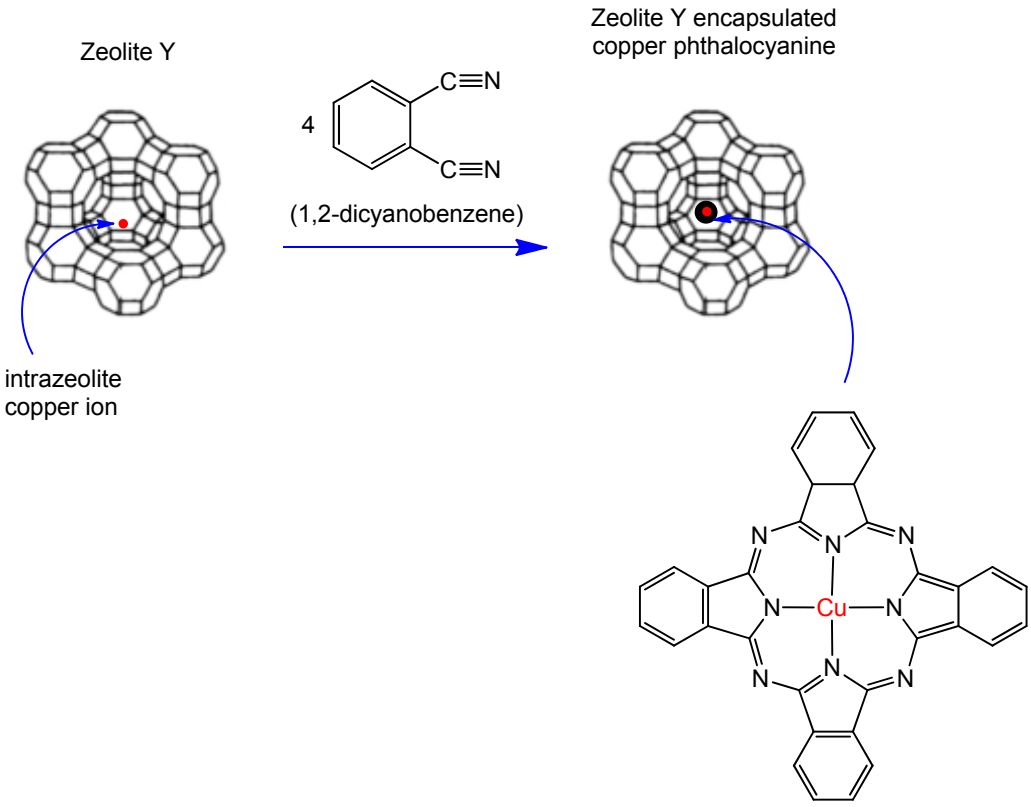

Figure 1.10. Schemetic representation of synthesis of zeolite Y encapsulated copper phtalocyanine.

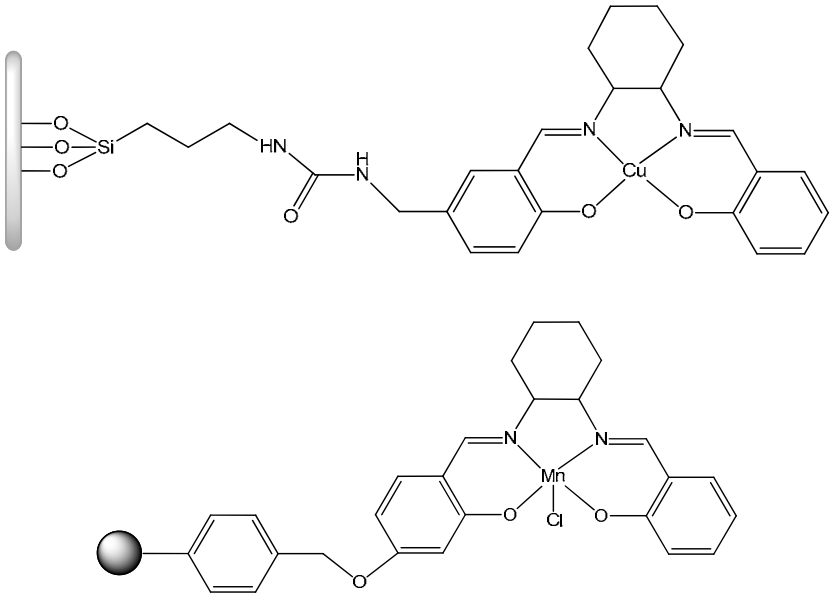

Figure 1.11. Schematic representation of copper salen bound to silica *via* ureapropyl linkage (top) and polymer-supported manganese salen (bottom).

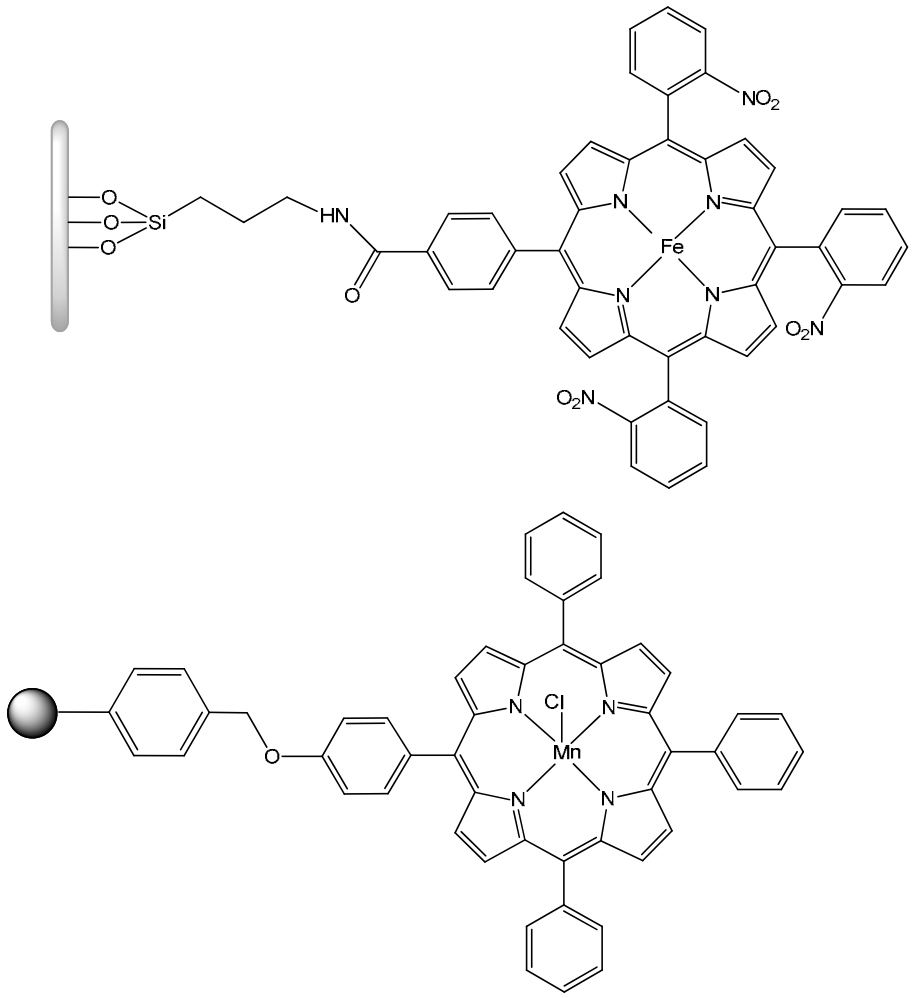

Figure 1.12. Representation of iron porphyrin bound to silica *via* an aminopropyl linkage (top) and polymer-supported manganese porphyrin (bottom).

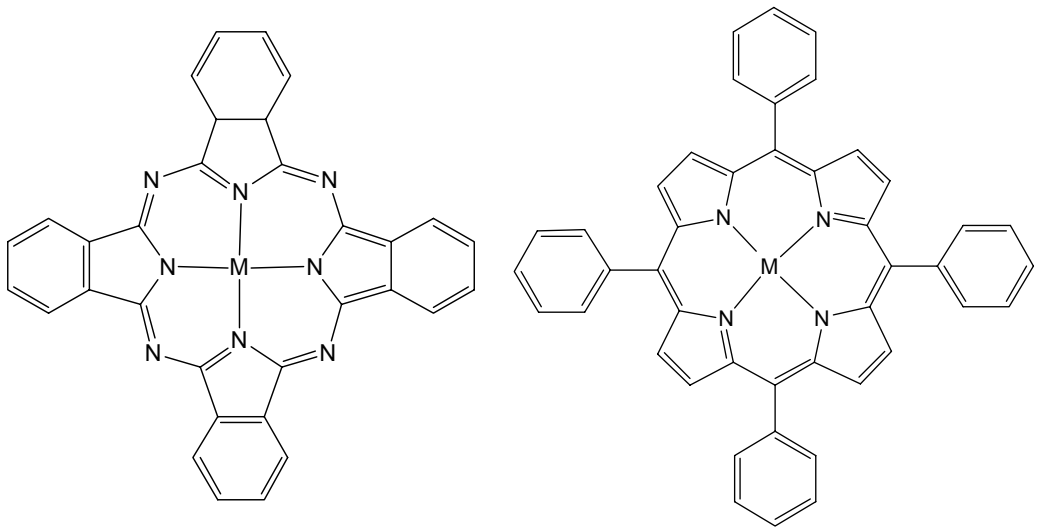

Figure 1.13. Representation of metallophtalocyanine (tetrabenzophthalocyanine) complex (left) and metalloporphyrin (tetraphenyl porphyrin) complex (right).

Another well studied zeolite encapsulated system involves the tetradentate salen ligand (*N,N'*-bis(salicylaldehyde)ethylenediimine) that possesses two oxygen and two nitrogen atoms and can form stable complexes with transition metal ions (Figure 1.14.). The salen ligand is able to diffuse freely through the zeolite pores where upon complexation with previously exchanged metal-ions it becomes too large and rigid to escape the cage. Due to the desired flexibility of salen, the flexible ligand method was adapted for encapsulation of a large variety of Co, Mn, Fe, Cu, Rh, Pd, Ni salen complexes within faujasite supercages.[119] These complexes proved to be active and selective catalysts for hydrogenation and oxidation of alkanes, alkenes and alcohols.[120] MnsalenX showed high activity for the oxidation of styrene and *p*-xylene whereas chiral MnsalenY was reported as an effective heterogeneous enantioselective catalyst for the epoxidation of alkenes.[99, 119, 121] CusalenY showed high activity in phenol oxidation. FesalenY and MnsalenY complexes were used in the oxidation of cyclohexane (Table 1.3).[122] The substituted copper salens that contain electron withdrawing groups like -Cl, -Br or $-NO_2$ showed higher activity than their nonsubstituted analogues in oxidation reactions with H_2O_2 and TBHP. Substitution of the aromatic hydrogen atoms of the salen ligand by electron withdrawing groups like -Cl, -Br and $-NO_2$ has two major effects: (I) retention of the copper complexes in the zeolite cavities is enhanced (due to the larger size of the substituents) and (II) the electronic properties of the encapsulated complex are modified.[123, 124]

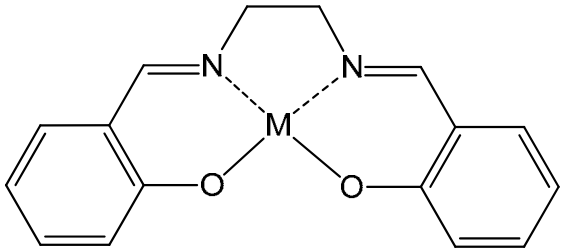

Figure 1.14. Representation of the parent metallosalen complex.

Table 1.2. Catalytic performances of metallophtalocyanine and metalloporphyrin based catalysts in oxidation reactions. PhIO (iodosylbenzene) has been often chosen as oxygen source in oxidation reactions with metalloporphyrin because it has been successfully used with P-450 to support the proposed $Por^{\bullet+}$- Fe^{IV}=O formation as an active species in cytochromes P-450.[92]

Catalyst	*Substrate*	*Oxidant*	*Conversion (%)*	*Selectivity (%)*	*Ref.*
CuPc	cyclohexane	TBHP	1.1	cyclohexanol (70) cyclohexanone (30)	125
CuPcY	cyclohexane	TBHP	26	cyclohexanol (50) cyclohexanone (50)	113
	cyclohexane	H_2O_2	7	cyclohexanol (44) cyclohexanone (56)	113
$CoF_{16}Pc$	cyclohexane	H_2O_2	0.82	cyclohexanol (46) cyclohexanone (54)	113
$CoF_{16}PcY$	cyclohexane	H_2O_2	0.91	cyclohexanol (58) cyclohexanone (42)	113
$CoF_{16}Pc$	cyclohexane	TBHP	5.0	cyclohexanol (55) cyclohexanone (55)	113
$CoF_{16}PcY$	cyclohexane	TBHP	1.0	cyclohexanol (50) cyclohexanone (50)	113
$RuF_{16}Pc$	cyclohexane	TBHP	8	cyclohexanol (33) cyclohexanone (67)	114
$RuF_{16}PcX$	cyclohexane	TBHP	70	cyclohexanol (1.6) cyclohexanone (98.4)	114
$FePorCl_4$	cyclohexane	PhIO	15	cyclohexanol (99)	126
$FePorCl_4Y$	cyclohexane	PhIO	25	cyclohexanol (99)	126
FePor	(*Z*)-cyclooctene	PhIO	50	(*Z*)-cyclooctene epoxide (99)	92
FePorX	(*Z*)-cyclooctene	PhIO	86	(*Z*)-cyclooctene epoxide (99)	92

Key: Pc = phtalocyanine, Por = porphyrin.

Table 1.3. Catalytic performances of metallosalen based catalysts in oxidation reactions.

Catalyst	*Substrate*	*Oxidant*	*Conversion (%)*	*Selectivity (%)*	*Ref.*
CuSal	cyclohexane	H_2O_2	6.1	cyclohexanol (43) cyclohexanone (57)	[127]
	cyclohexene	O_2	33.6	2-cyclohexen-1-ol (55) 2-cyclohexen-1-one (41)	[128]
CuSalY	cyclohexane	H_2O_2	4.0	cyclohexanol (26) cyclohexanone (74)	[127]
CuSal	styrene	O_2	84.2	styrene oxide (62.4)	[129]
CuSalSBA	styrene	O_2	47.3	styrene oxide (49.4)	[129]
FeSalY	cyclohexane	TBHP	1.9	cyclohexanol (23) cyclohexanone (77)	[122]
FeSal	styrene	O_2	83.1	styrene oxide (51.2)	[129]
FeSalSBA	styrene	O_2	80.9	styrene oxide (59.7)	[129]
CoSal	styrene	O_2	85.9	styrene oxide (54.4)	[129]
CoSalSBA	styrene	O_2	49.2	styrene oxide (72.4)	[129]
MnSal	styrene	O_2	78.8	benzaldehyde(52.0) styrene oxide(32.5)	[119]
MnSal X	styrene	O_2	54.8	benzaldehyde(66.7) styrene oxide(27.7)	[119]
MnSalY	cyclohexane	TBHP	7.9	cyclohexanol (33) cyclohexanone (67))	[122]

Key: Sal- salen,

1.4.1.1. Amino acid complexes immobilised in zeolite.

Amino acids being building blocks of natural metalloenzymes have also been employed as ligands affording suitable transition metal complexes for oxidation reactions. Amino acid–transition-metal complexes can perform as isolated active sites when encapsulated in inorganic host materials such as aluminosilicates or covalently bonded to mesoporous silica frameworks and polymers. These supports may serve as substitutes for the protein

scaffold and may create an environment that is analogous to natural enzymes, therefore presenting an alternative method to conventional biological and chemical processes.

The first stable and catalytically active example of a zeolite immobilized transition metal complex containing amino acid ligands is Cu^{II}-histidine synthesized by the ion exchange method.[130] The strategy involves ion-exchanging a sodium-enriched zeolite Y (NaY) with a solution of Cu^{II}-histidine at pH 7.3. The capability of the copper complex to undergo ion-exchange is dependent on its charge and stability, which are both influenced by the pH of the reaction media. At low pH values of around 2, only 0.83 % of the Cu^{II} is coordinated to the histidine ligand. On increasing the pH to 3, Cu^{II} forms mono-histidine complexes and within a pH range 6–10 bis complexes are formed. Bis complexes are formed by coordination of nitrogen atom from the imidazole and the nitrogen atom from the amine group, carboxylate oxygens can also coordinate to the metal.[131]

A histidine molecule contains three coordination sites: the amino nitrogen, N_{am}, the imidazole nitrogen, N_{im}, and the carboxylate oxygen, and it can behave as a mono-, bi-, and tridentate ligand. Structures of possible histidine complexes are presented in Figure 1.16. In solution, at pH range 6–10 two histidine ligands coordinate to the Cu^{II} ion in a square-planar geometry.[132] However, in a confined space in the cages of the zeolite where the complex is encapsulated by the ion-exchange method, a framework oxygen atom replaces the oxygen atom from carboxy group of histidine (Figure 1.15.).[133 134]

Similar procedure of encapsulation within zeolite Y was also employed for Cu^{II} complexes with lysine and arginine at pH 10. The key parameters controlling the ion exchange process are the type of amino acid and the pH. Both lysine and arginine at pH 10 coordinated to the Cu^{II} centre in a square planar geometry by ligation of two lysine/arginine molecules *via* two N and two O atoms.[96]

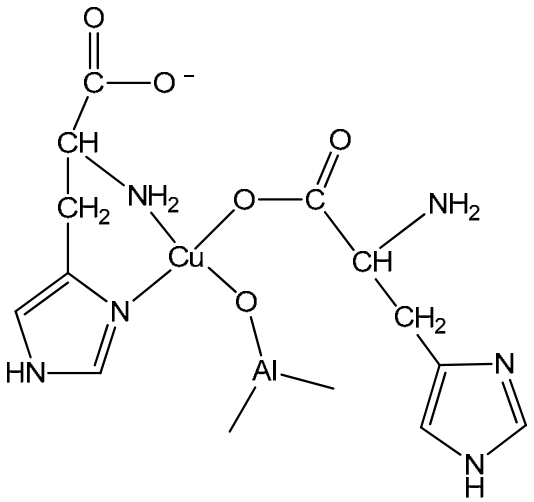

Figure 1.15. The structure of Cu^{II}-histidine complexes encapsulated in the zeolite Y with $N_{am}(1)N_{im}(1)$ $O_{COO}(2)$ Oframework coordination.[133]

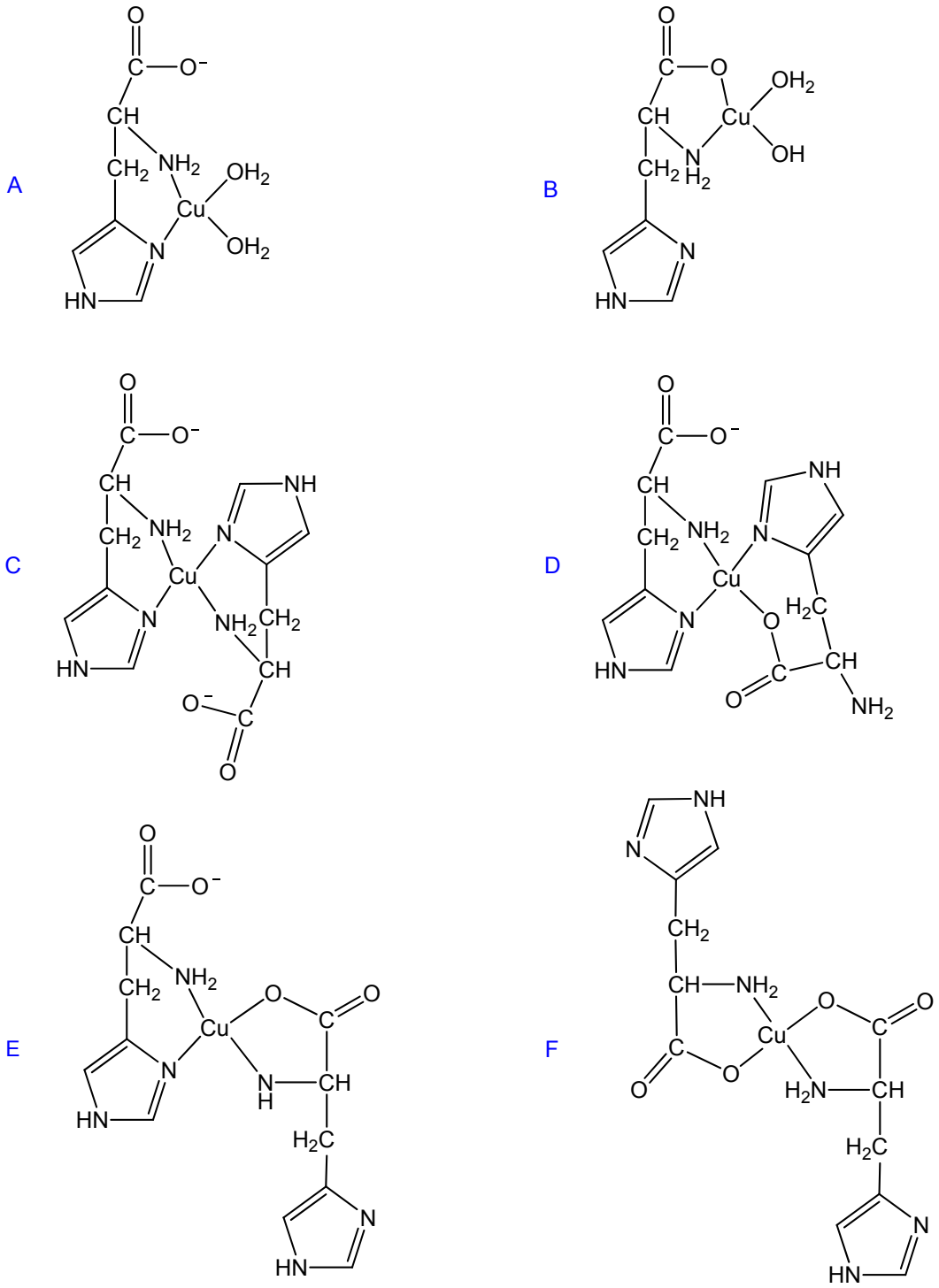

Figure 1.16. Possible structures of Cu-histidine complexes: mono complex with $N_{am}N_{im}O_wO_w$ (A) and $N_{am}O_{COO}O_wO_w$ (B) coordination and bis-complexes with $N_{am}(1)N_{im}(1)N_{am}(2)N_{im}(2)$ (C),$N_{am}(1)N_{im}(1)N_{im}(2)O_{COO}(2)$ (D), $N_{am}(1)N_{im}(1)N_{am}(2)O_{COO}(2)$ (E), $N_{am}(1)O_{COO}(1)N_{am}(2)O_{COO}(2)$ (F) coordination.[131]

Cu^{II}-histidine complexes encapsulated in Zeolite Y proved to be active catalysts for the oxidation of alcohols, alkanes and alkenes with *tert*-butyl hydroperoxide. The catalytic performance of Cu^{II}-histidine-Y is presented in Table 1.4. In the epoxidation of cyclohexene, 1,2-cyclohexanediol was obtained as the major reaction product (TON of 3230), probably formed from the hydrolysis of cyclohexene oxide on acid sites of zeolite Y. A minor allylic oxidation to 2-cyclohexene-1-one and 2-cyclohexene-1-ol was also observed. Much lower TON (450) was observed in oxidation of cyclohexane toward cyclohexanol and cyclohexanone. Benzyl alcohol was oxidized to benzaldehyde and benzoic acid in a ratio of 2:1. 1-Pentanol was oxidized to pentanoic acid with 100% selectivity.[96]

Table 1.4. Catalytic performance of Cu^{II}-histidine complex encapsulated in Zeolite Y.[96]

Substrate	***TON***	***Selectivity (mol%)***
cyclohexane	450	cyclohexanol (50) cyclohexanone (50)
benzyl alcohol	2421	benzaldehyde (66) benzoic acid (33)
1-pentanol	1425	pentanoic acid (100)
cyclohexene	3230	1,2-cyclohexanediol (89) cyclohexene oxide (9) 2-cyclohexene-1-one (1.7) 2-cyclohexene-1-ol (0.3)

The catalytic activity of Cu^{II}-lysine and Cu^{II}-arginine complexes encapsulated in Zeolite Y in cycloxexene oxidation was much lower than this obtained by Cu^{II}-histidine. The lower activity was explained by the fact that coordination geometries of the encapsulated complexes of NNOO Cu^{II}-lysine and Cu^{II}-arginine were probably less stable than in Cu^{II}-histidine system (Table 1.5.).[96]

Table 1.5. Catalytic performance of Cu^{II}-lysine and Cu^{II}-arginine complexes encapsulated in Zeolite Y in cycloxexene oxidation.[96]

Catalyst	***TON***	***Selectivity (mol%)***
Cu^{II}-lysine	735	1,2-cyclohexanediol (84) cyclohexene oxide (10) 2-cyclohexene-1-one (4.5) 2-cyclohexene-1-ol (1.5)
Cu^{II}-arginine	669	1,2-cyclohexanediol (85) cyclohexene oxide (8) 2-cyclohexene-1-one (5) 2-cyclohexene-1-ol (2)

1.4.2. Metal amino acid complexes immobilized on silica.

MCM-41 (Mobil Composition of Matter) is a mesoporous molecular sieve with hexagonally packed channels, uniform pore size distribution ranging from micropores to mesopores, high surface area (> 600m^2g^{-1}), high capacity of adsorption and high thermal stability.[135] These properties make it suitable for a wide variety of applications, especially where the mechanical, thermal and chemical stabilities are required, e.g. in oil refining and in petrochemistry, catalysis, optics, conductors, and electronic devices.[136]

Chemical modification of mesoporous silica with organic and inorganic entities generates matrices that can host a wide variety of guest molecules and can be applied in modern heterogeneous catalysis.[137, 138] The mesoporous silica surface contains a large number of silanol (Si-OH) and siloxane (Si-O-Si) groups which enable silica functionalization. Modification of silica can occur *via* reaction of a particular entity with silanol (reaction with hydroxyl groups) or siloxane (nucleophilic substitution at Si atom) groups.

There are three main routes in which silica can be functionalized with organic moieties: [139-142]

- ***Grafting:*** Modification of silica surface functions (silanol or siloxane groups) with organosilanes or organic molecules. The tethering is achieved by covalently attaching the organosilane to a surface silicon atom through the silicon (surface)-oxygen-silicon (external)-carbon bond in the organosilanes (Scheme 1.15.). Such modifications can use trialkoxysilanes (e.g. methoxy- and ethoxy- silanes) which react with silanol groups, liberating the corresponding alcohol, or by employing chlorosilanes to react with silanol groups liberating HCl. A disadvantage of trialkoxysilanes is their potential for polymerisation on silica surface due to the presence of three alkoxy groups.The availability of the silanol groups can determine whether the grafted silicon atom is tethered *via* one, two, or three silicon-oxygen bonds.

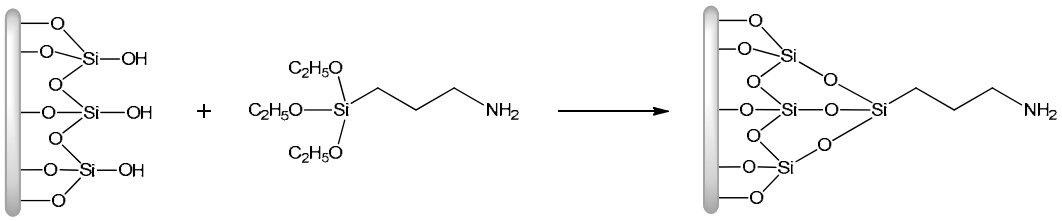

Scheme 1.15. Grafting of 3-aminopropyl-(triethoxy)silane onto silica surface (silicon atom is tethered *via* three silicon-oxygen bonds).

❖ ***Chlorination and subsequent displacement:*** Chlorination is a less frequently used methodology but gives the alternative route for Si-O-Si bonds, as a direct, very strong Si-C bond is formed. The Si-Cl functions are reacted with Grignard reagent or organolithium species to displace Cl and form strong Si-C surface bond (Scheme 1.16.). This method suffers from the involvement of hazardous reagents, chlorinating agents (thionyl chloride or carbon tetrachloride). An advantage of this method is the formation of thermal and chemically robust Si-C surface bonds and precluding surface bound oligomer formation.

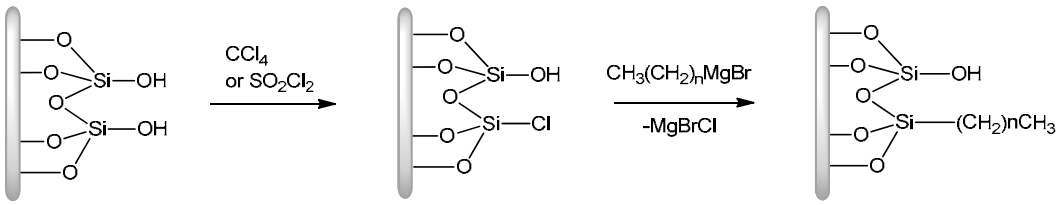

Scheme 1.16. Chlorination of silica surface and modification with Grignard reagent.

❖ ***Templated sol-gel:*** This method uses the "one-pot" co-hydrolysis and co-condensation of silica precursor (typically a tetraalkyl orthosilicate, also called orthosilicic acid esters, Figure 1.17.) with other organosilicate precursor (e.g. trialkoxy(organo)silane (e.g. 3-aminopropyl-(trimethoxy)silane, or 3-chloropropyl-(trimethoxy)silane) (Figure 1.18.). By incorporation of the organosilane into the synthesis mixture, more uniform dispersion throughout the solid is produced. General representation of co-condensation of organosilanes and trialkoxysilanes in sol-gel synthesis is shown in Scheme 1.17.

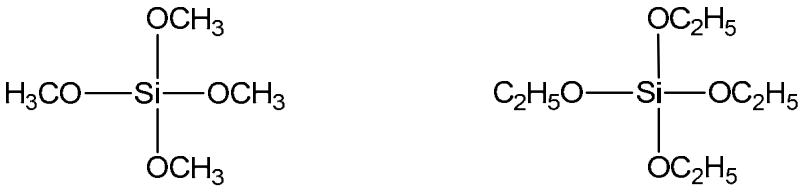

A B

Figure 1.17. Representation of tetraalkyl orthosilicates: tetramethoxy silaneTMOS (A) and tetraethoxy silaneTEOS (B).

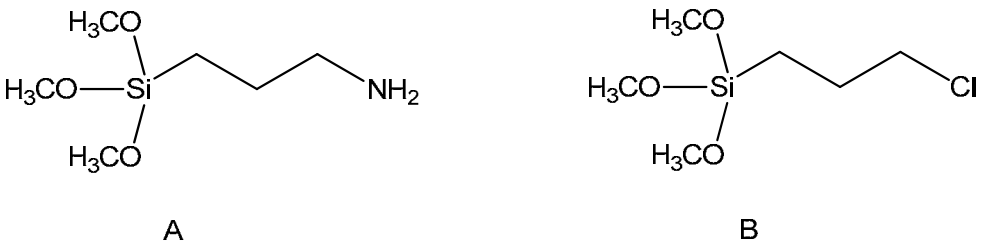

Figure 1.18. Representation of trialkoxy(organo)silanes: 3-aminopropyl-(trimethoxy)-silane (A) and 3-chloropropyl-(trimethoxy)silane (B).

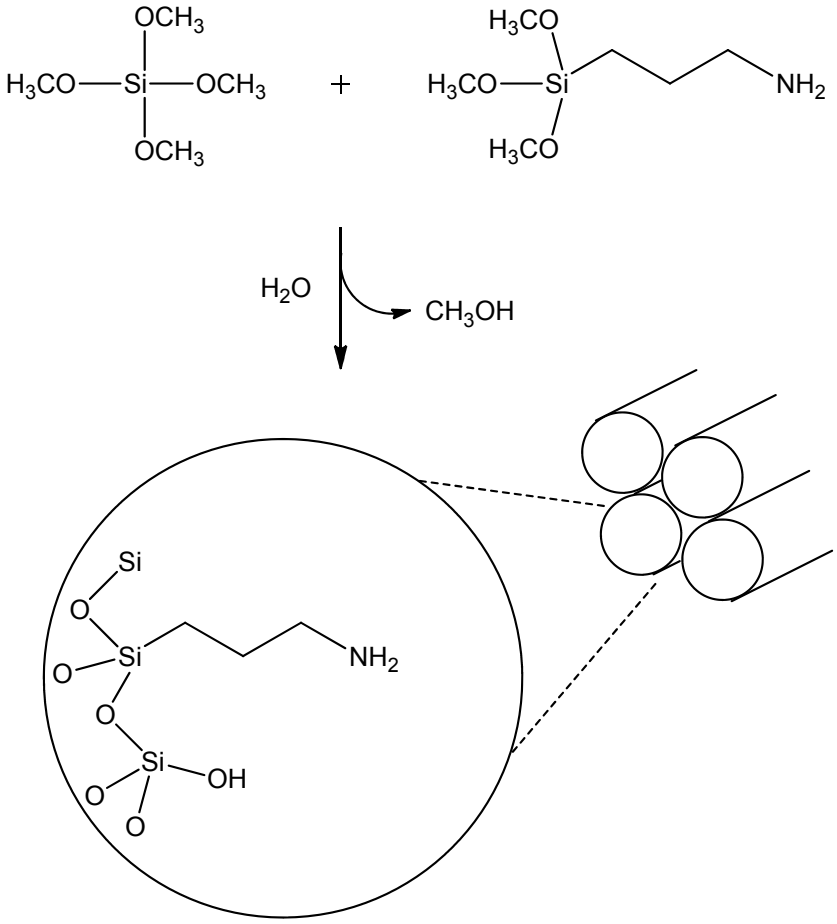

Scheme 1.17. General representation of co-condensation of organosilanes and trialkoxysilanes (3-aminopropyl-(trimethoxy)silane) in sol-gel synthesis.

1.4.2.1. Silica supported amino acids.

Amino acids used for catalysis must have the amino and carboxylate groups accessible for metal ion coordination and to fulfil the requirements of the well-defined catalytic sites and mechanism for each particular catalysed reaction.[143] Therefore amino acids are immobilised by reacting the modified functionalities present on the side chain with a linker that can be covalently attached to the silica surface. There are numerous

strategies for covalent amino acids immobilisation onto mesoporous silica employing grafting methodology through silylation.[144, 145]

Generally, the protected amino acid is reacted with a linker and the isolated product is attached to the silica surface under reflux conditions and purified *via* soxhlet extraction and numerous washings. The amino acid is deprotected (e.g. Fmoc cleavage with piperidine) to leave an accessible amino acid derivatized silica framework ready for metal ion coordination (Scheme1.18.).[146]

- **MCM-41 supported proline *via* isocyanate silane linker.**

In this route amine functionalised protected amino acid (Scheme 1.19. B) reacts with an isocyanate silane [(3-isocyanatopropyl) triethoxysilane] linker (A) producing a stable urea linkage (C). The isolated product is attached to the silica surface under reflux conditions and purified *via* soxhlet extraction (D). The amino acid is deprotected to leave an accessible amino acid derivatized silica framework ready for catalysis (E). The amino acid side chain can, if necessary, be converted into amine functionality, which is capable of nucleophilic attack to an isocyanate derivatized silane that can then be covalently anchored to a silanol group of porous silica. The amine functionality is usually obtained by treatment of a derivatised amino acid side chain with sodium azide, which can be reduced to the amine with e.g. palladium on carbon catalysts.[146]

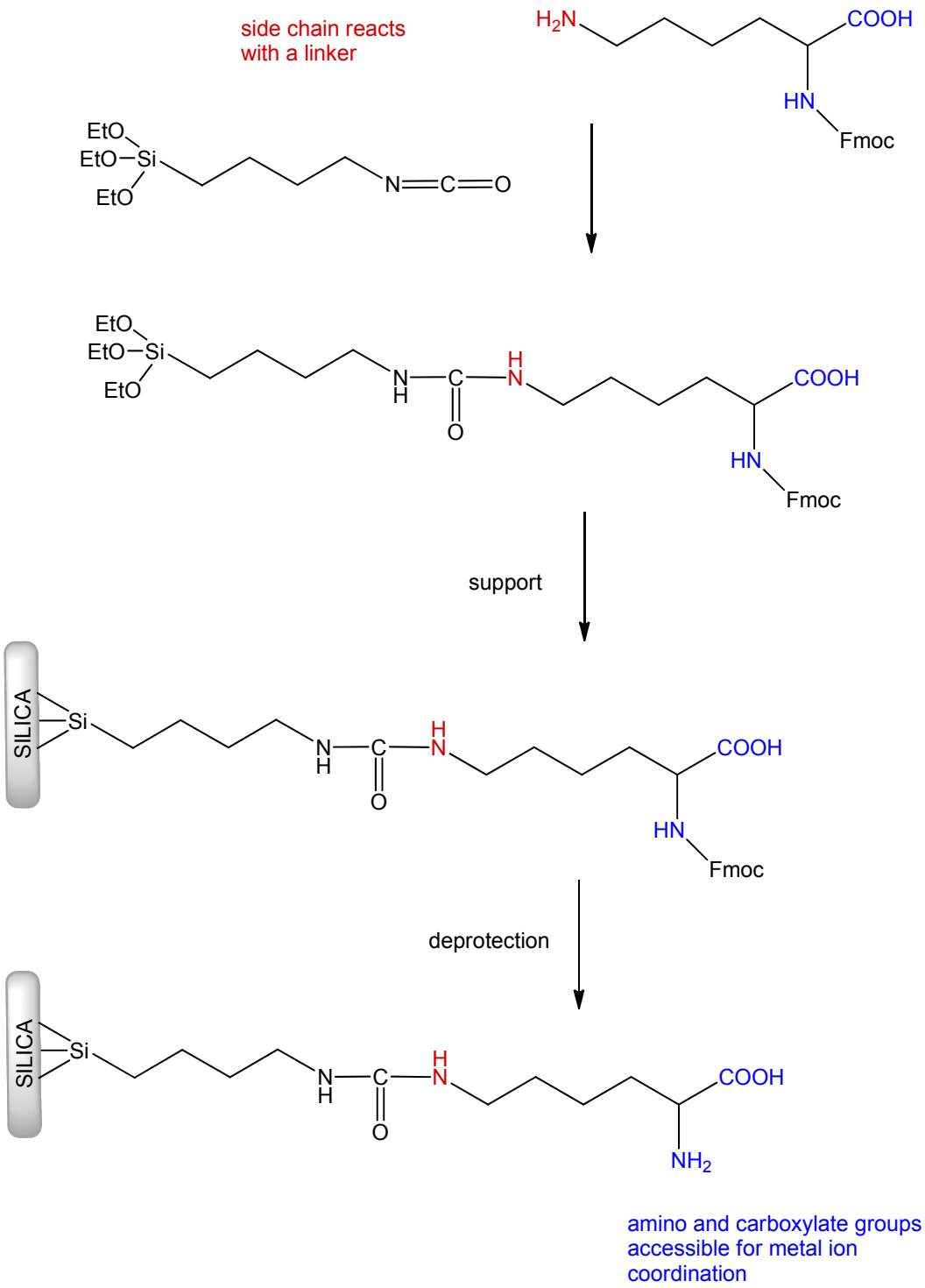

Scheme 1.18. General route of immobilisation of the amino acid on silica. Protected amino acid, in this case Fmoc-Lys-OH reacts with a linker (eg. isocyanate silane). The isolated product is attached to the silica surface followed by Fmoc cleavage (amino group deprotection) leaving amino acid functionalized silica ready for metal ion coordination.

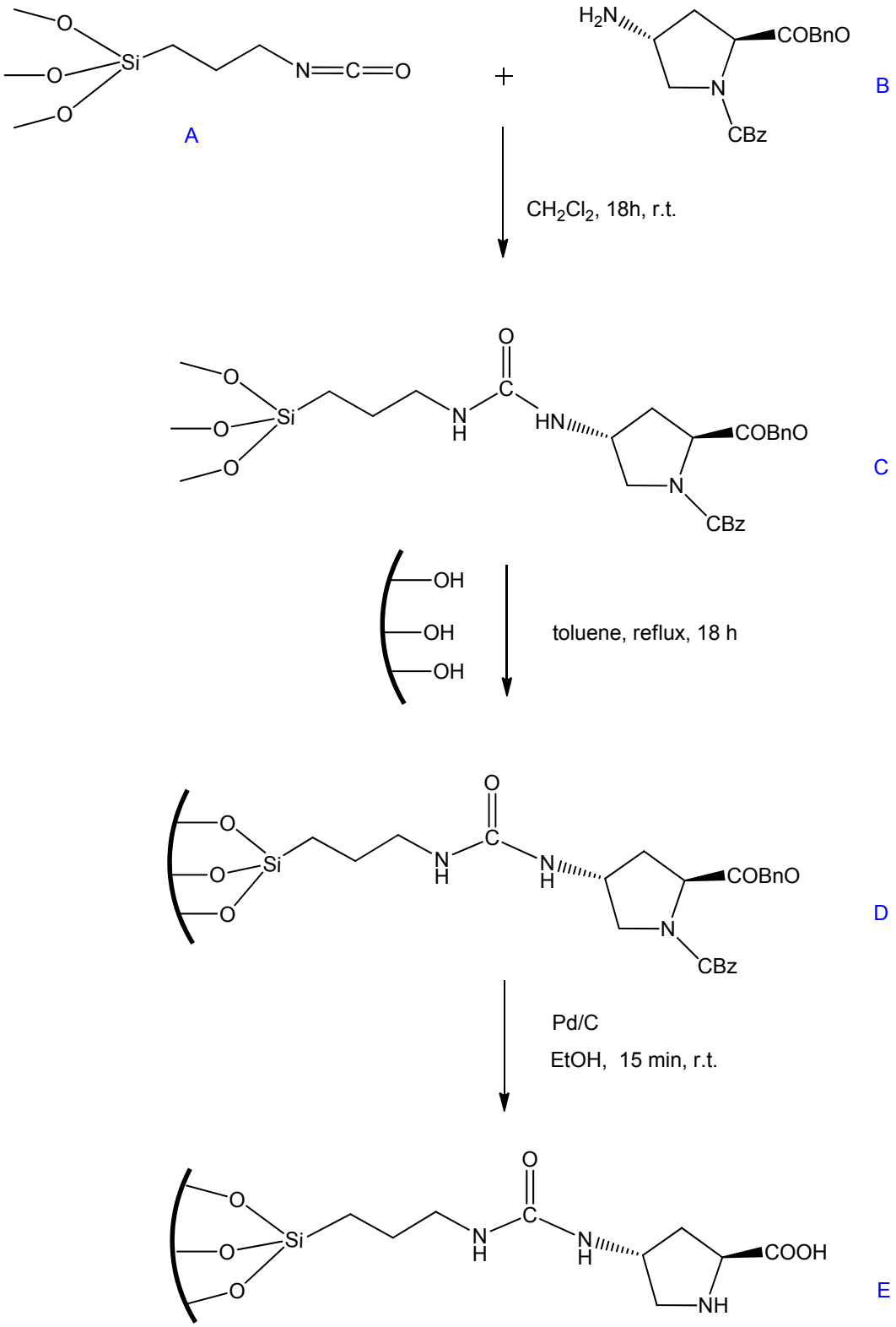

Scheme 1.19. General representation of main synthetic steps in supporting of proline onto MCM-41 *via* isocyanate silane linker.

- **MCM-41 supported amino acids using solid phase peptide synthesis.**

The use of primary amine functional groups such as 3-aminopropyl allows the attachment of single amino acids and peptides to amino functionalized silica supports by solid phase peptide synthesis (SPPS) methodology (Scheme 1.20.).[147] The hydrophobic character inside the pores of silica can be adjusted by co-functionalization with other species, e.g. methyl groups. Amino acids can be covalently anchored onto the support by the formation of very stable amide bonds with surface bound amine groups. Amine functionalized materials can be prepared by post synthetic grafting of 3-aminopropyl-trimethoxysilane on a silica surface, or by co-condensation of 3-aminopropyl-trimethoxysilane with a silica precursor.[148] However, materials with only the 3-aminopropyl moieties show a poor hydrothermal stability. The reason for this is basicity of the functional groups and the fast hydrolysis of the silica in the presence of an amine. Silica surfaces that are functionalized with a mixture of methyl groups and 3-aminopropyl groups are more stable.[149] The hydrothermal stability improves by decreasing the amount of 3-aminopropyl bound to the silica surface. This is due to a decreasing basic character inside the pores and also because the silica is protected from hydrolysis when hydrophobic methyl groups are present together with 3-aminopropyl groups.[150]

Solid phase peptide synthesis (SPPS), developed by R. B. Merrifield *et al*, was a major breakthrough allowing the chemical synthesis of peptides and small proteins that are bound to an insoluble support and any unreacted reagents left at the end of the synthetic step can be removed by a simple washing procedure.[151] SPPS comprises of repeated cycles of coupling and deprotection of successive amino acids. Unlike ribosome protein synthesis, SPPS proceeds in a C→N terminal fashion. The free N-terminal amine of a solid-phase attached peptide is coupled to a single N-protected amino acid. This unit is then deprotected, revealing a new N-terminal amine to which a further amino acid is attached.

There are two major protecting groups used in solid phase peptide synthesis, which are Fmoc (9-fluorenylmethyloxycarbonyl), base labile alpha-amino protecting group and t-Boc (*tert*-butyloxycarbonyl), acid labile protecting group.[152, 153] Each involves different protection, deprotection and cleavage steps. To remove Fmoc from peptide chain, basic conditions are used (usually piperidine in DMF) and to remove the t-Boc, acidic conditions are used (usually trifluoroacetic acid). The carboxyl group is activated before coupling to another amino acid, this make the reaction proceed at faster rate.

Carbodiimides; *N,N'*-dicyclohexylcarbodiimide (DCC) and *N,N'*-diisopropylcarbodiimide (DIC) are used as activating groups forming with a carboxylic acid a highly reactive O-acyl-urea. Carbodiimides however are very reactive and they can cause racemisation of an amino acid. To solve this problem triazoles (e.g. 1-hydroxy-benzotriazole (HOBt) and 1-hydroxy-7-aza-benzotriazole (HOAt)), that react with O-acyl-urea to form an active ester which is less reactive and less in danger of racemisation, are employed (Figure 1.19).[153, 154]

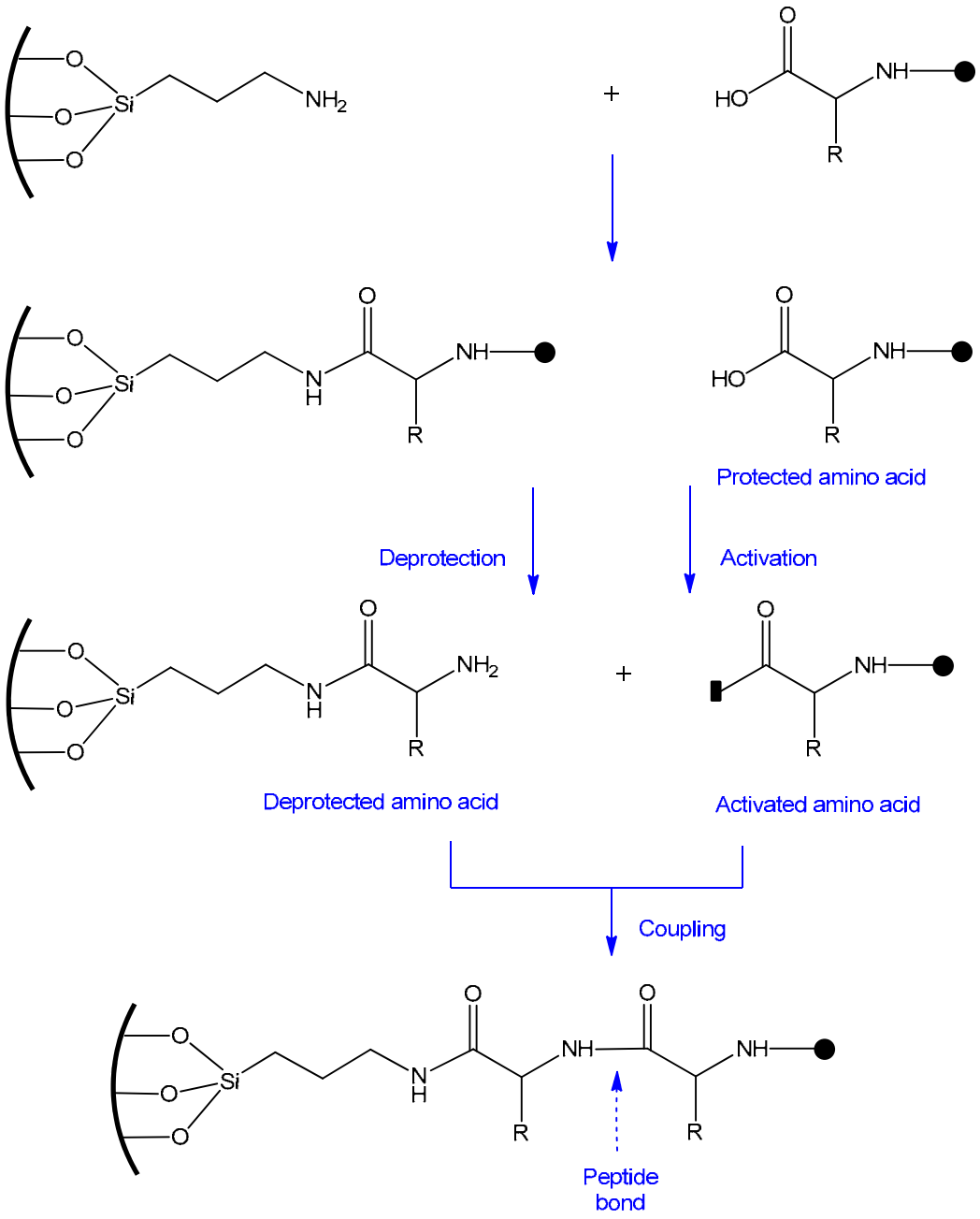

Scheme 1.20. General representation of main steps in solid phase peptide synthesis.

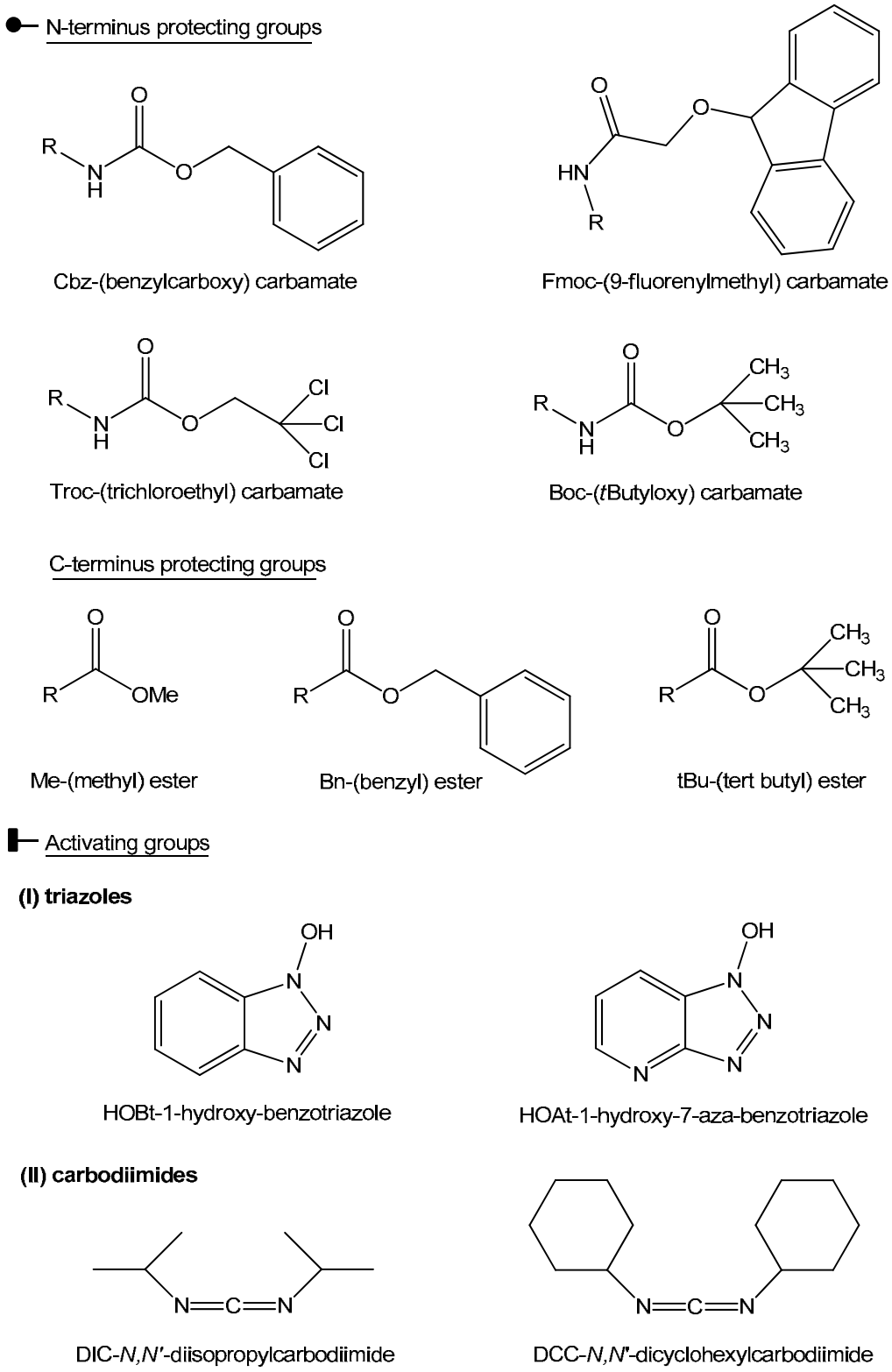

Figure 1.19. Examples of activating and C-, N- terminus protecting groups in SPPS.

A number of amino acids and short peptide complexes with iron and copper have been immobilized onto mesoporous silica *via* SPPS and these have shown promising trends in the oxidation of hydrocarbons.[155, 156] Histidine and glutamic acid complexes with iron were covalently bound by SPPS to the amino groups on the surface of silica. The terminal carboxylate group of both amino acids was converted to an amide upon binding to the amino groups of silica and only the imidazole ring and free amine group of histidine and carboxylic acid group of glutamic acid contributed to the complexation of iron. In this case the histidine acts as a tridentate ligand, forming 1:1 complex with iron *via* N_{am}, N_{im} and the lone pair of the C=O group of the amide. The amine group of glutamic acid was not involved in iron complexation and only the carboxylate group of the carboxylic acid side chain coordinated to the metal centre. Proposed structures of these complexes are shown in Figure 1.20.

The histidine and glutamic acid based complexes have been tested as catalysts for cyclohexane oxidation under mild reaction conditions with hydrogen peroxide as oxidant. Catalytic activity of those catalysts showed to be dependent on the type of amino acid and the surface density of immobilized complexes. Immobilized catalysts containing histidine were selective towards cyclohexanone formation (65 mol%) and the TOF values decreased rapidly with decreasing density of immobilized amino acids. Glutamic acid immobilized materials, on the other hand, exhibited the opposite behaviour. The highest TOF was obtained for the catalyst with the lowest concentration of the immobilized glutamic acid complex. These materials exhibited a selectivity of 74 mol% towards cyclohexanone formation. The chemical environment of the active site, the nature of the ligands and the proximity between the two active sites plays the major role influencing the catalytic activity of these complexes. Higher concentration of immobilized histidine on the surface was advantageous for the catalytic activity, whereas it was the opposite with immobilized glutamic acid (activity decreased with increased number of surface glutamic acid molecules).[157]

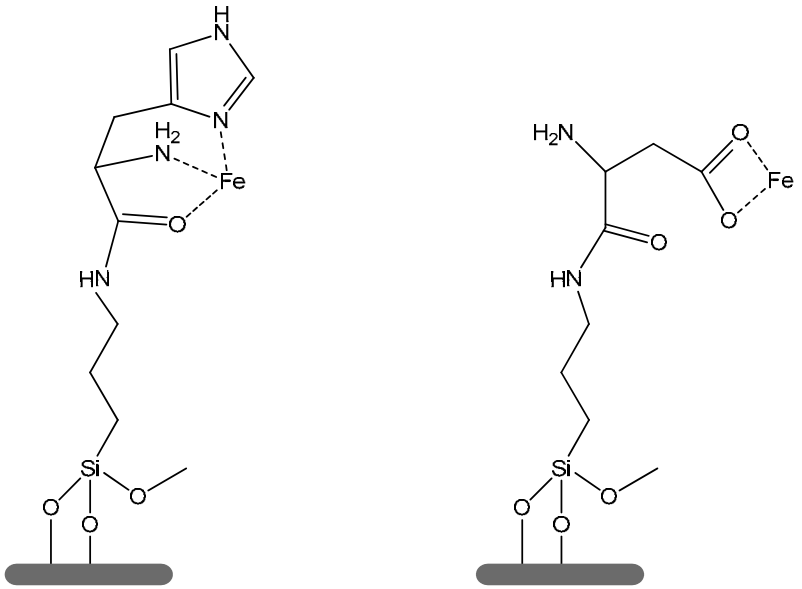

A B

Figure 1.20. Model of iron complexation by histidine (A) and glutamic acid (B) on amino functionalized silica.[157]

1.4.3. Metal amino acid complexes immobilized on polystyrene.

There are numerous strategies for covalent amino acid immobilisation onto insoluble polymers.[158] New developments involve 1,3-dipolar cycloaddition of an azide functionalised resin and an *O*-propargyl hydroxy amino acid (click chemistry); the direct attachment of amino acid to chloromethylated polystyrene resin were reported.[159] A more recent method employed the synthesis of a styrene amino acid derivative and links to mercaptomethyl polymer through sulphur *via* a radical reaction.

- **Azidomethyl polystyrene supported proline.**

Huisgen 1,3-dipolar cycloaddition is the process that unites two unsaturated reactants and provides fast access to a variety of five-membered heterocycles.[160] The cycloaddition of alkynes and azides gives triazoles (Scheme 1.21.) that are the most crucial functional groups for click chemistry due to their unique stability toward H_2O, O_2, and the majority of organic synthetic conditions. Azides are also a very reliable means to introducing a nitrogen substituent through the reaction: -RH→[R-N_3] →R-NH_2.

The mechanistic proposal for catalytic cycloaddition reaction is shown in Scheme 1.22. and proceeds *via* copper^{I} acetylide formation followed by six-membered copper-

containing intermediate formation.[161] This reaction yields a thermally and hydrolytically stable triazole connection. A number of copper salts can be used as catalyst for this reaction. Copper^{II} sources such as $CuSO_4*5H_2O$ can be employed and prepared in situ by reduction to copper^{I} by such reductants as ascorbic acid and/or sodium ascorbate. Copper^{I} salts like CuI, $CuOTf*C_6H_6$ can be used directly in the absence of reducing agents. It should be noted that in the absence of a copper catalyst the reaction proceeds only under thermal activation which produces a mixture of 1,4- and 1,5-disubstituted triazole regioisomers. The copper catalysed variation yields the 1,4-regioisomer selectively under ambient conditions even in water; ruthenium based catalysts have been developed to selectively form the 1,5-regioisomer.[161, 162]

The click chemistry technique proved to be effective for anchoring of *O*-propargyl functionalised proline to azide substituted Merrifield resin *via* the 1,2,3-triazole moiety catalysed by copper^{I} salts. The pathway for azidomethyl polymer supported proline synthesis is presented in Scheme 1.23.

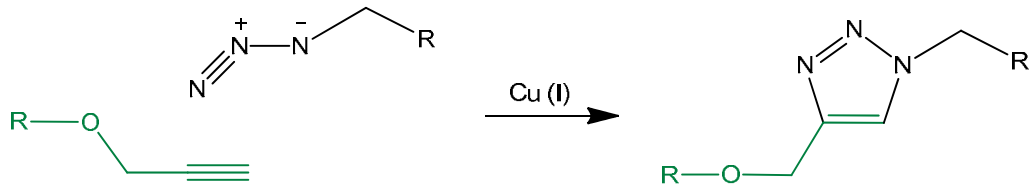

Scheme 1.21. 1,3-dipolar cycloaddition of alkynes and azides.

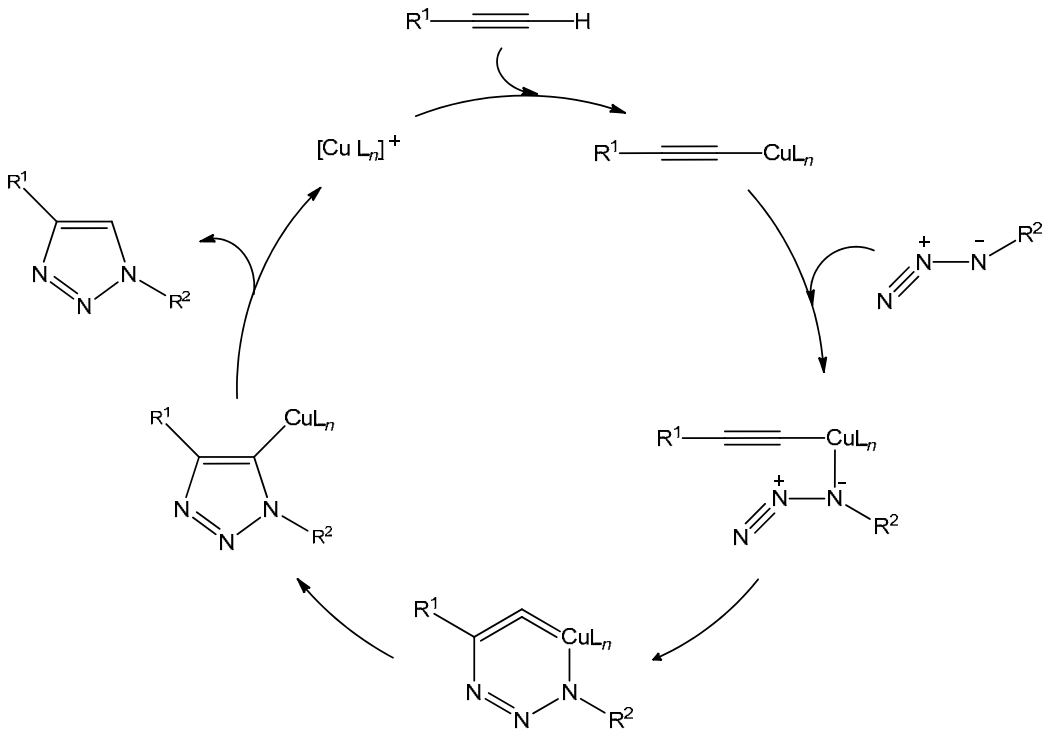

Scheme 1.22. Proposed catalytic cycle for 1,3-dipolar cycloaddition catalysed by Cu (I).

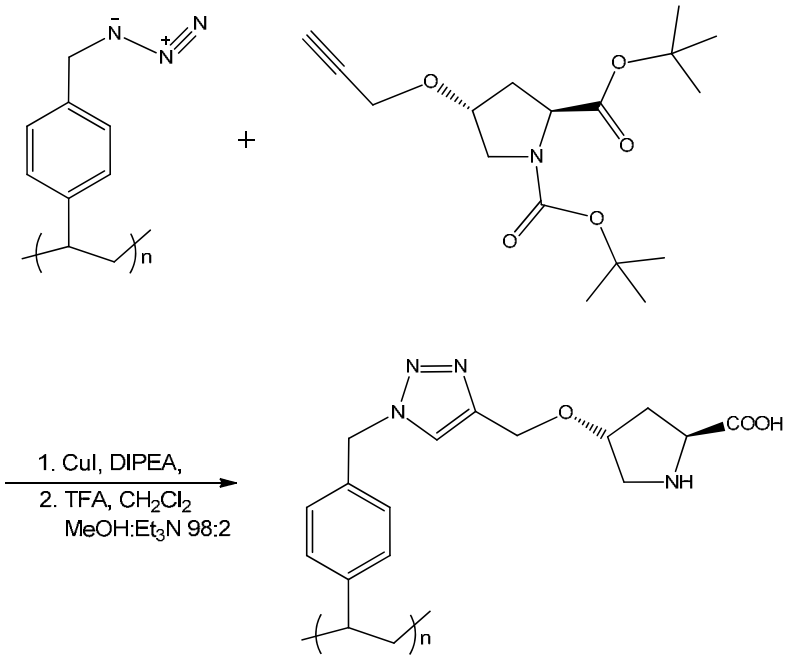

Scheme 1.23. Schematic synthetic pathway to polymer supported proline *via* azidomethyl derivatisation of the solid support.

- **Mercaptomethyl polymer supported proline.**

The hydroxyl group of hydroxyproline can be easily functionalised with styrene. This styrene derivative of proline can be covalently immobilised onto mercaptomethyl polymer (Scheme 1.24.). The anchorage of proline is accomplished in two steps; synthesis of the styrene derivative of hydroxy-proline and reaction between the mercapto-polystyrene and styrene functionalised proline.[163]

The proline catalysts immobilised onto the solid support showed high activity in the asymmetric aldol reaction between a range of ketones and arylaldehydes and α-selenenylation reactions.[164-166]

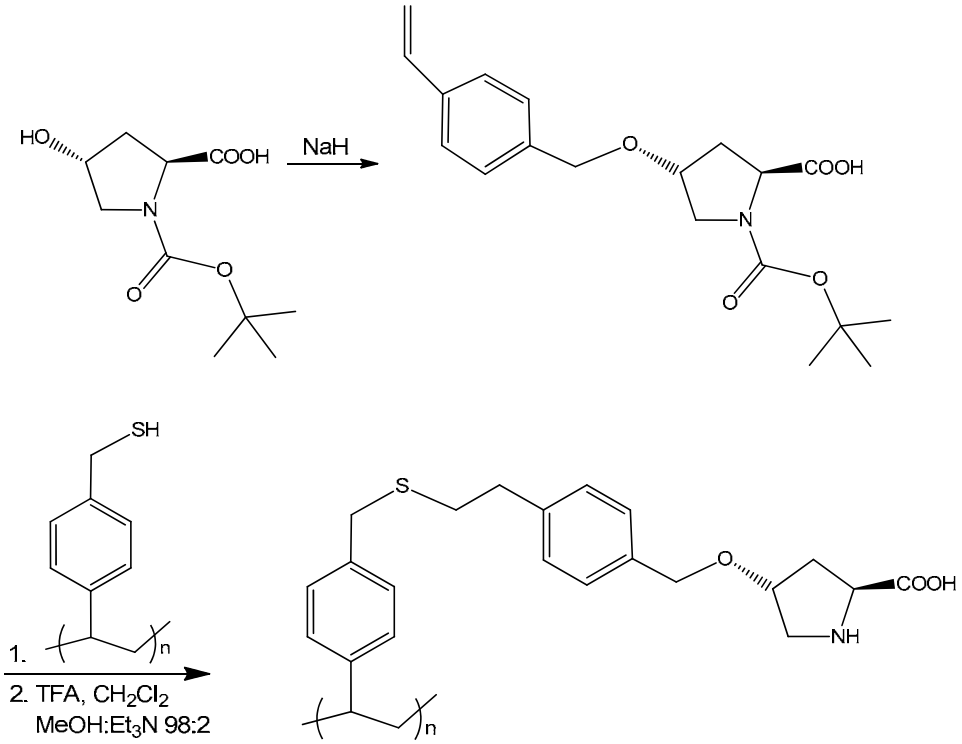

Scheme 1.24. Schematic synthetic pathway to polymer supported proline *via* mercaptomethyl coupling to styrene-proline.

- **Polystyrene supported valine.**

The direct single-step attachment of valine to chloromethylated polystyrene was accomplished by employing pyridine as a base under reflux conditions in the aqueous methanol media (Scheme 1.25.). In this method, the reaction of amino acid with a stoichiometric amount of pyridine leads to the desired grafting by facilitating elimination of HCl as the pyridine hydrochloride salt (pyridinium chloride).[167, 168]

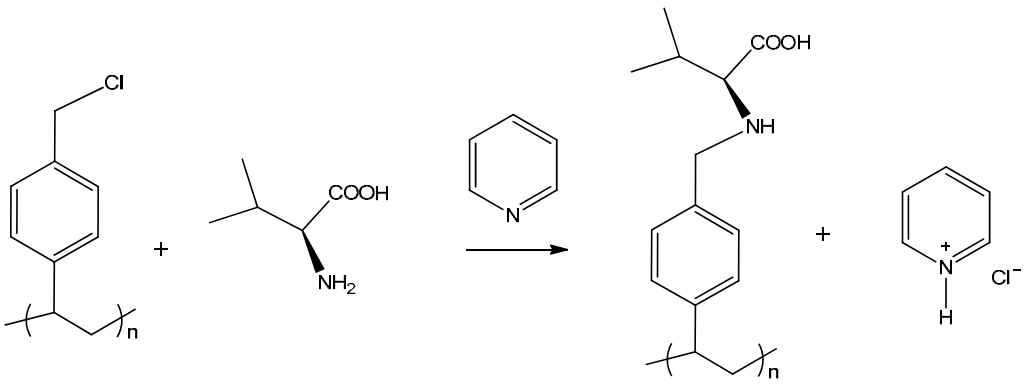

Scheme 1.25. Schematic pathway for synthesis of polystyrene supported valine.

1.5. An overview on amino acid ligands and their complexes with transition metals.

1.5.1. Amino acid ligands properties.

Amino acids are highly functional molecules that are protein constituents. An amino acid is composed of a basic amino functional group ($-NH_2$), an acidic carboxyl functional group (-COOH), a hydrogen atom and a characteristic side chain (-R) giving a general formula R-CH-(NH_2)-COOH (Figure 1.21.). Twenty different amino acids are naturally incorporated into polypeptides and are called proteinogenic or standard amino acids; these are encoded by the universal genetic code. The characteristic side chain can be acidic, basic, hydrophilic or hydrophobic. All amino acids apart from glycine are chiral; the standard chirality is *(S)*; the exception is cysteine which is *(R)*. Cysteine has a sulfur atom at the second position in its side-chain, which has a larger atomic mass than the groups bounded to the first carbon, which is attached to the α-carbon in the other standard amino acids. *S* and *R* stereoisomers are presended in Figure 1.22.

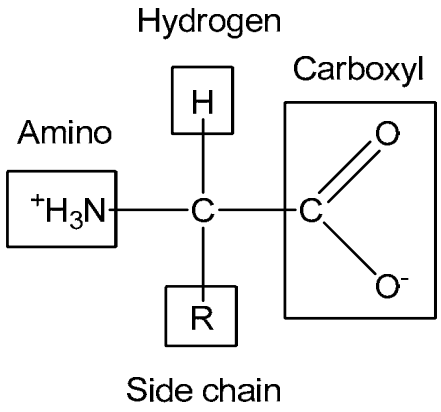

Figure 1.21. Generalized structure of a typical amino acid.

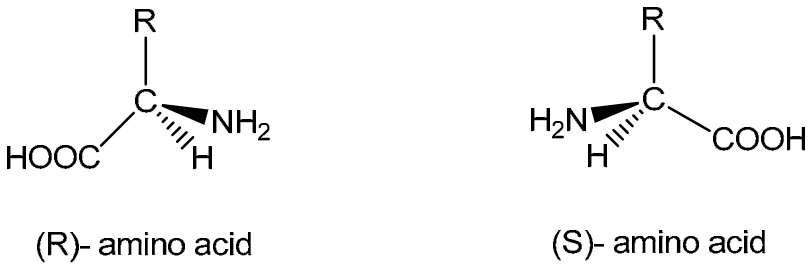

Figure 1.22. Representation of *S* and *R* stereoisomers.

At high pH the carboxyl group tends to be dissociated, giving the molecule a negative charge. At low pH the amino group is protonated therefore giving the molecule a net positive charge. At the isoelectric point the amino acid in solution has a net charge of zero and therefore contains positively and negatively charged substituents in equal quantities, this state is called a zwitterion (Figure 1.23.).[169, 170]

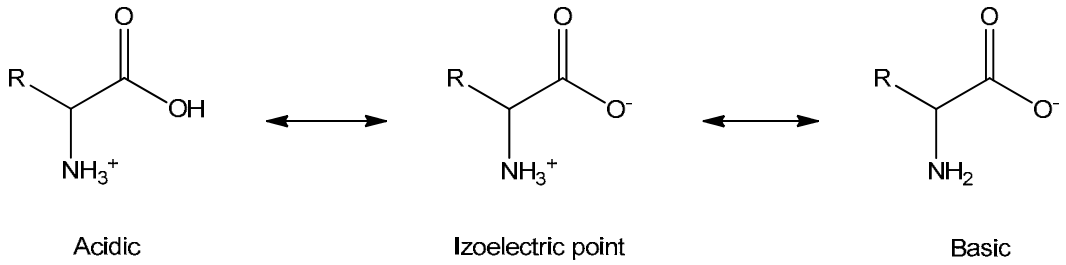

Figure 1.23. Amino acid dissociation at equilibrium.

1.5.2. Amino acid complexes with transition metals.

Amino acids are good metal-complexing agents, forming chelate rings through the amino and carboxylate groups *via* dissociation of the acidic proton as a bidentate N,O-donor (Figure 1.24.). A side chain, e.g. phenol ring of tyrosine, imidazole group of histidine, mercapto group of cysteine or carboxylato groups of aspartate and glutamate, can also be involved as a metal binding site.[171]

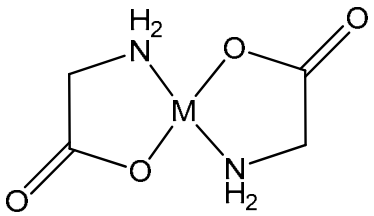

Figure 1.24. General structural formula proposed for amino acid complex.

1.5.3. Proline.

l-Proline [(*S*)-Pyrrolidine-2-carboxylic acid] is unique among the amino acids because the α-amino group (NH) is secondary. The side chain is bonded to the nitrogen of the α-amino group, as well as the α-carbon atom. Proline is sometimes called an imino (NH) acid rather than an amino (NH_2) acid because of the bond to nitrogen. Proline is a neutral and non-polar amino acid. The NH group starts to deprotonate around pH 8, and forms

a strong complex with the metal at pH 10 (Figure 1.25.). *l*-Proline can occur in several pH dependent states of protonation. At low pH *l*-proline exists in a cationic form, at high pH in an anionic form and as a zwitterion at the isoelectric point (Figure 1.26.). Because proline lacks hydrogens on the amide group, it cannot act as a hydrogen bond donor, but only as a hydrogen bond acceptor. The imino (NH) group is fixed rigidly in the pyrrolidine ring, limiting the mobility of the N-H bond with respect to the carboxyl group. This rigidity is one of the factors that determine the important role played by proline in the folding of proteins where steric effects arising from the proline side chains help to determine the stabilities and positions of the protein folds.[172-174]

l-Proline and its metal complexes are prominent catalysts. A number of heterogeneous proline-based catalysts have been reported. *l*-Proline and its chiral complexes with zinc have shown to act as enantioselective catalysts for aldol reactions, selenenylation of aldehydes, synthesis of bromoesters, and benzimidazole.[175-178]

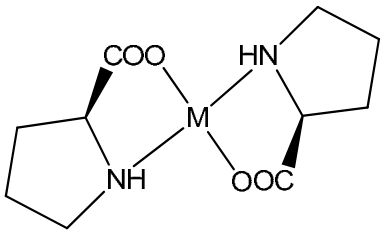

Figure 1.25. Bis-proline metal complex.

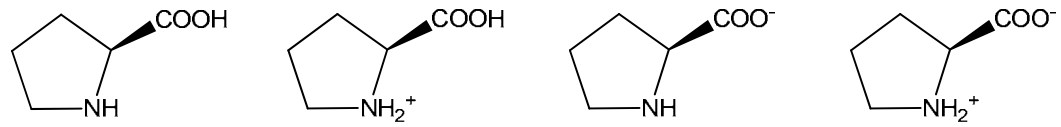

Figure 1.26. Structural formulae of *l*-proline.

1.5.4. Valine.

l-Valine [*(S)*-2-Amino-3-methylbutanoic acid] is a non-polar amino acid with an aliphatic side chain. *l*-valine is hydrophobic and is usually found in the interior of proteins. At high pH the carboxyl group of *l*-valine is dissociated, at low pH the amino group is protonated, and at the isoelectric point the *l*-valine has a net charge of zero (zwitterion), Figure 1.27. *l*-Valine coordinates to the metal ion through the amino and carboxylato groups forming a five-membered chelate ring (Figure 1.28.).

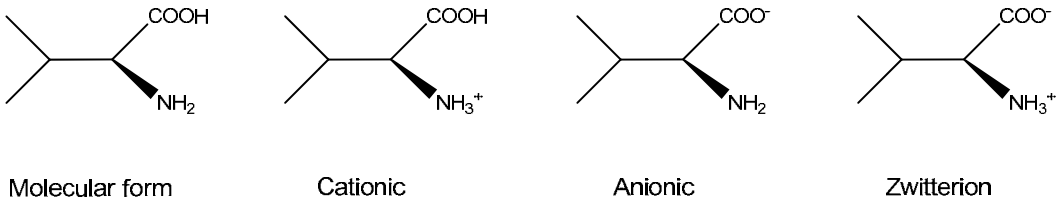

Figure 1.27. Structural formulae of valine.

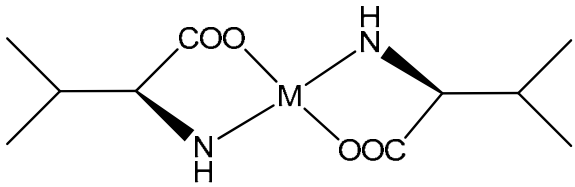

Figure 1.28. Bis-valine metal complex.

2. INTRODUCTION TO TECHNIQUES.

2.1. Fourier Transform Infrared Spectroscopy (FTIR).

Infrared spectroscopy is one of the most common techniques used for compound identification and structural elucidation. The infrared portion of the electromagnetic spectrum is usually divided into three regions: the near (14000 – 4000 cm^{-1}), mid (4000 – 400 cm^{-1}) and far (400 – 10 cm^{-1}) infrared. Infrared spectroscopy exploits the fact that molecules absorb specific frequencies that are characteristic for their structure. Absorption of IR is restricted to compounds with small energy differences in the possible vibrational and rotational states. For a molecule to absorb IR, the vibrations or rotations within a molecule must cause a net change in the dipole moment of the molecule. The alternating electrical field of the radiation (electromagnetic radiation consists of an oscillating electrical field and an oscillating magnetic field, perpendicular to each other) interacts with fluctuations in the dipole moment of the molecule. If the frequency of the radiation matches the vibrational frequency of the molecule then radiation will be absorbed, causing a change in the amplitude of molecular vibration. The positions of atoms in molecules are not fixed; they are subject to a number of different vibrations. Molecular vibrations can be divided into two main categories: stretching (change in inter-atomic distance along bond axis) and bending (change in angle between two bonds) (Figure 2.1.).

The IR spectrum is obtained by detecting changes in transmittance (or absorption) intensity as a function of frequency.

Infrared spectroscopy is a simple and reliable technique widely used in both organic and inorganic chemistry, in research and industry. In this study FTIR was used to elucidate the nature of amino acid complexes with transition metals and the structural integrity of the homogeneous and heterogeneous (encapsulated/immobilized) amino acid complexes. In particular, IR spectroscopy is used to detect characteristic signals arising from the carbonyl or carboxyl groups and amino groups in order to differentiate the binding modes of amino acids to transition metals.

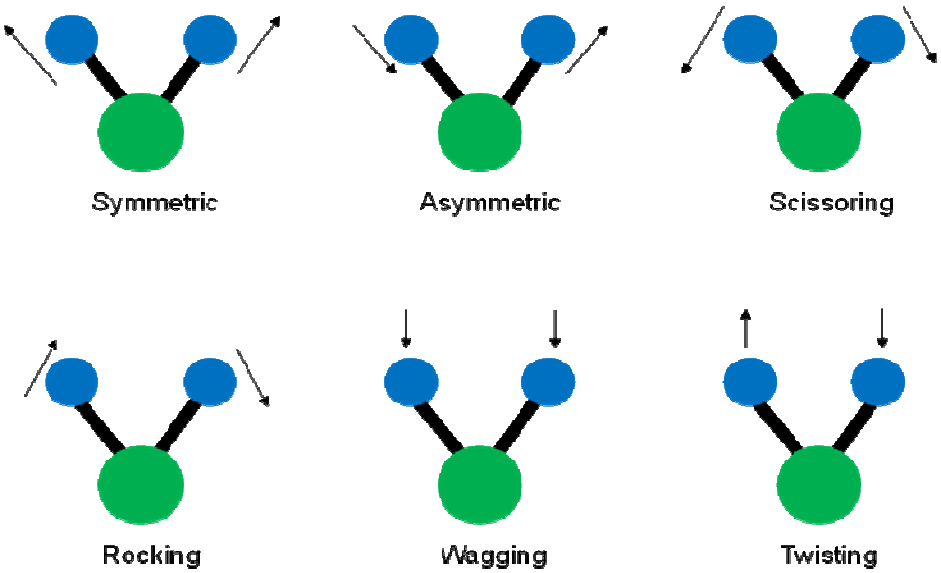

Figure 2.1. Representation of stretching (symmetric and antisymmetric) and bending (scissoring, rocking, wagging and twisting) vibrations.

2.2. Diffuse Reflectance UV-Visible Spectroscopy (DR UV-Vis).

UV-Vis spectroscopy uses the ultraviolet and visible radiation and identifies electron excitation to an excited electronic level (electronic transitions), oxidation state, molecular structure and functional groups.

When molecules are exposed to light having an energy that matches a possible electronic transition within the molecule, some of the light energy is absorbed as the electron is promoted to a higher energy orbital. A spectrometer records the wavelengths at which absorption occurs, together with the degree of absorption at each wavelength. The part of the beam that is scattered within a sample and returned to the surface is considered to be diffuse reflection. DR UV-Vis instead of measuring the transmitted light measures the reflected light (Figure 2.2.).

UV-vis spectra of transition metal complexes originate from charge transfer (LMCT ligand-to-metal charge transfer, or *vice versa* as in MLCT) and electronic d-d transitions. LMCT involves a shift in electron density from ligand towards the metal centre. For a complex to demonstrate charge-transfer behaviour one of its components must have electron donating properties and another component must be able to accept electrons. Absorption of radiation then involves the transfer of an electron from the donor to an orbital associated with the acceptor. Metal centred d-d transitions involve the excitation of electrons within the d orbitals of the metals, where the d orbitals have different energies according to the ligand field splitting; this is determined by the ligand (strong

field or weak field ligand) and the nature of the geometry around the metal centre (tetrahedral, octahedral etc.).

Kubelka-Munk conversion is applied to a diffuse reflectance spectrum to compensate the differences between the raw diffuse reflectance spectra and its transmission equivalent producing a linear relationship of concentration against observed intensity. The Kubelka-Munk equation is expressed as follows:

$$F(R) = \frac{(1-R)^2}{2R} = \frac{k}{s}$$

where R is the reflectance of the sampled layer (mostly the reflectance relative to a standard is measured not the absolute reflectance), k is the molar absorption coefficient and s is the scattering coefficient.

The Kubelka-Munk equation creates a linear relationship for spectral intensity relative to sample concentration.

In this study DR UV-Vis spectroscopy was used to elucidate the nature of Fe and Cu species (oxidation state and coordination) of homogeneous and heterogeneous amino acid complexes.

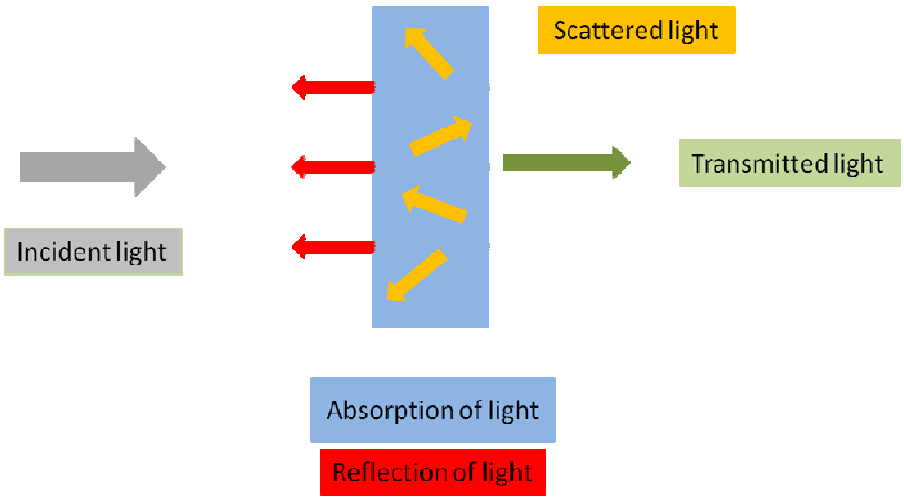

Figure 2.2. Interaction of light with a sample.

2.3. Electron Paramagnetic Resonance Spectroscopy (EPR).

Electron paramagnetic resonance (EPR) spectroscopy, which is also called electron spin resonance (ESR) spectroscopy, is a resonant absorption of microwave radiation by chemical species that have one or more unpaired electrons (paramagnetic species), such as organic and inorganic free radicals, transition metal ions, and systems with conducting electrons. The basic physical concepts of EPR are analogous to those of NMR, but it is the electron spin that is excited instead of spins of atomic nuclei. Because most stable molecules have all their electrons paired, the EPR technique is less widely used than NMR. When a molecule with unpaired electron is placed in strong magnetic field, the spin of the unpaired electron can align in two different ways creating two spin states. The alignment can either be along the direction to the applied magnetic field which corresponds to the lower energy state (ms = 1/2) or opposite to the direction to the magnetic field (ms = +1/2) (Figure 2.3.). The two alignments have different energies and the energy difference is given by:

$$\Delta E = h\nu = g_e \mu B B_0$$

Where h is Planck's constant ($6.626*10^{-34}$ J s^{-1}), ν is the frequency of radiation, g is the g-factor, μB is the Bohr Magneton ($9.274*10^{-24}$ J T^{-1}) and B is the strength of magnetic field.

The g-factor called the Landé splitting energy is a unitless measurement of the intrinsic magnetic moment of the electron and its value for a free electron is 2.0023. The g-factor decreases as B increases.

An EPR spectrum is the absorption of microwave frequency radiation plotted against the magnetic field intensity.

In this study EPR spectroscopy was used to elucidate Fe^{III}-Proline complex geometry (in neat and encapsulated in zeolite X form).

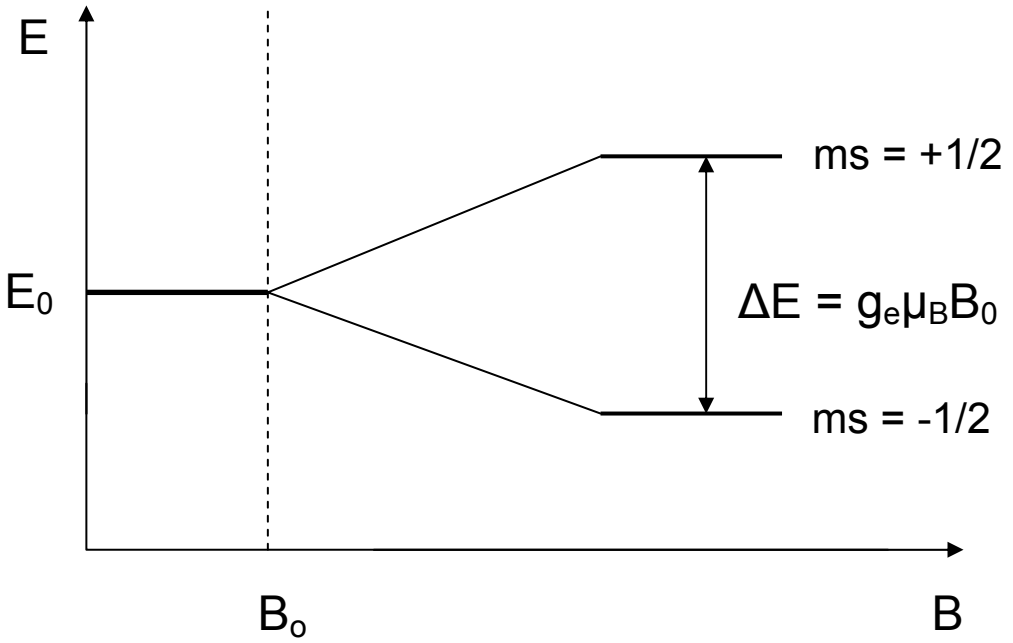

Figure 2.3. Splitting of electron energy levels in the presence of external magnetic field.

2.4. X-ray Diffraction (XRD).

X-ray diffraction is a versatile, non-destructive technique that reveals detailed information about the chemical composition and crystallographic structure. X-ray diffraction is based on constructive interference of monochromatic X-rays and a crystalline sample. X-rays are generated by a cathode ray tube, filtered to produce monochromatic radiation, and directed toward the sample. The interaction of the incident rays with the sample produces constructive interference and a diffracted ray when conditions satisfy Bragg's Law that relates the wavelength of electromagnetic radiation to the diffraction angle and the lattice spacing in a crystalline sample **(**Figure 2.4.**)**. To satisfy Bragg's Law, θ must change as d changes e.g., θ decreases as d increases. Bragg's Law equation is presented below:

$$2d\sin\theta = n\lambda$$

where: d is the distance between the planes in the atomic lattice, θ is the angle between the incident ray and the scattering planes, λ is the wavelength of the incident X-ray beam, n is an integer.

A diffraction pattern records the X-ray intensity as a function of 2 θ angle. Diffracted X-rays are detected, processed and counted. Conversion of the diffraction peaks to d-spacings allows identification of materials (each material has a unique d-spacing).

In this study X-ray diffraction was used for the structural analysis of the zeolite (X and LTA) and MCM-41 framework. Phase purity and relative crystallinity were indicated with subsequent Rietveld refinement using the CelRef 258 that are presented in Appendix.

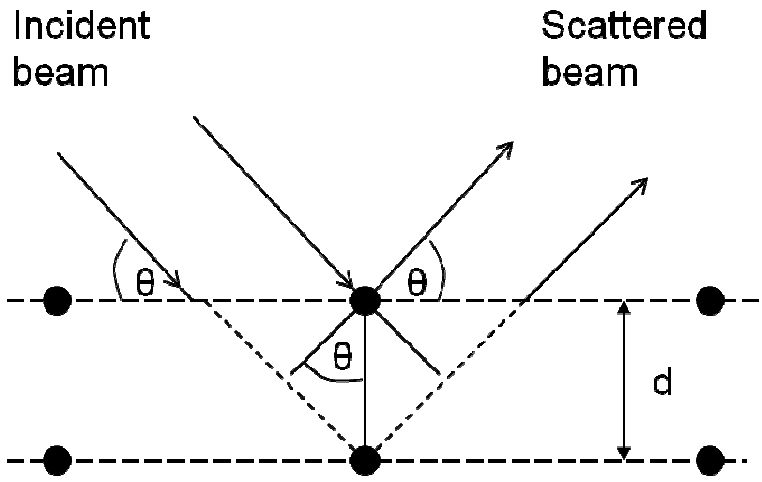

Figure 2.4. Bragg condition (two beams with identical wavelength approach a solid and are scattered off two different atoms. The lower beam traverses an extra length of $2d\sin\theta$. Constructive interference occurs when this length is equal to an integer multiple of the wavelength of the radiation).

2.5. Brunauer-Emmett-Teller Analysis (BET).

Gas sorption (adsorption and desorption) at the surface of solid powders is the most popular method used for determining the surface area as well as the pore size distribution. Brunauer-Emmett-Teller (BET) and Langmuir techniques use the adsorption of gas molecules which are either modeled as a monolayer (Langmuir) or multilayer (BET) of gas.[179] Langmuir adsorption model is applicable under the conditions of low pressure and high temperature and assumes that: (I) all the adsorption sites are equivalent; (II) adsorbed molecules do not interact; (III) adsorption occurs through the same mechanism; (IV) a monolayer is formed at the maximum adsorption. BET model is an extension of the Langmuir theory but assumes that infinite layers of gas molecules can be physisorbed onto the surface with no interactions between the layers. In a gas sorption experiment, the material is heated and degassed by vacuum to remove adsorbed molecules. Then, inert gas (e.g. nitrogen, krypton, argon) is introduced and adsorbed. The sample material is placed in a vacuum chamber at a constant low temperature, usually at the temperature of liquid nitrogen (-195.6 °C), and subjected to a wide range of pressures, to generate

adsorption and desorption isotherms. Different amounts of gas molecules are adsorbed or desorbed at different doses of the gas. The BET method is widely used for a determination of surface areas of solids by physical adsorption of gas molecules. The total surface area of the material can be determined using the BET equation for multilayer adsorption:

$$\frac{1}{v[(P_0/P)-1]} = \frac{c-1}{v_m c}\left(\frac{P}{P_0}\right) + \frac{1}{v_m c}$$

where: P = adsorption pressure (equilibrium pressure), Po = saturation pressure, v= adsorbed gas quantity, v_m = monolayer adsorbed gas quantity, c = BET onstant.

2.6. Mass Spectrometry (MS).

Mass spectrometry is used in order to measure the relative molecular mass of individual molecules. In this technique the sample molecules are first converted into ions, for which various techniques are available. In the case of electrospray ionisation, which is one of the most commonly used techniques, a vaporised sample passes into the ionisation chamber where it is bombarded with a high energy beam of electrons generated by the heated metal coil. These collisions remove electrons from the sample particles to produce positively charged sample molecules (ions). In a protic carrier solvent the sample molecules can also be protonated. The ions are then accelerated and a magnetic field deflects the ion beam according to the relative ion mass. The amount of deflection depends on the mass of the ion (lighter ions are deflected more than heavier ones) and the charge of the ion (ions with 2 or more positive charges are deflected more than those with one positive charge). These two factors are combined into the mass/charge ratio m/z (sometimes m/e). Most of the ions formed in a mass spectrometer have a single charge, so the m/z value is equivalent to mass itself. The m/z values can be expressed as:

$$m/z = (MW + nH^+)/n$$

where: m/z = the mass-to-charge ratio, MW = the molecular mass of the sample, n = the integer number of charges on the ions, H = the mass of a proton = 1.008 Da.

By varying the strength of the magnetic field, ions of different mass can be focused progressively on a detector. Ion stream passing through the detector produces a current

which is proportional to the number of ions arriving. The mass of each ion detected is related to the size of the magnetic field used to bring it to the detector. The mass analyzer sorts the ions according to m/z and the detector records the abundance of each m/z. There are many types of detectors; the most common are the photomultiplier, the electron multiplier and the micro-channel plate detectors.

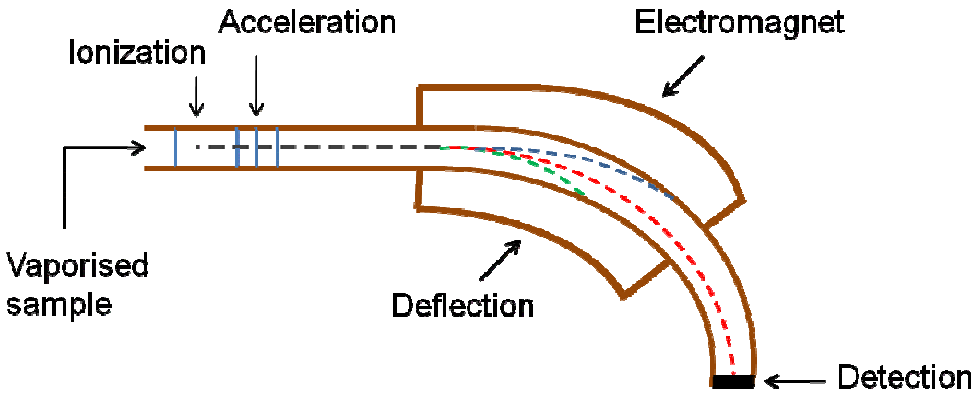

Figure 2.5. Diagram of a mass spectrometer.

2.7. Gas Chromatography (GC).

Gas chromatography is used for separation of volatile components of a sample and determination of the amount of each component present. This technique involves a sample being first injected and vaporized. Once in the gas phase, the sample is carried onto the chromatographic column by the carrier gas. The carrier gas (mobile phase) must be chemically inert. Commonly used gases include nitrogen, helium, argon, and carbon dioxide). The sample is then transported through the column by the flow of an inert gas and the components of the sample are separated on the column. The column itself contains a liquid stationary phase which is adsorbed onto the surface of an inert solid. Components that interact more strongly with the stationary phase move through the column more slowly. The rate at which compounds move through the column depends on the nature of the interactions between the compound and the stationary phase. The rate is also affected by column temperature and carrier gas flow rate. Components in the sample exit the column and flow past the detector. The choice of detector is determined by the general class of compounds being analyzed and required sensitivity. Flame ionization detectors (FID) that are the most widely used detectors for organic samples. FID uses an air/hydrogen flame

to pyrolyze the effluent sample. The pyrolysis of the compounds in the flame creates ions. A voltage is applied across the flame and the resulting flow of ions is detected as a current. The FID detector is mass sensitive rather than concentration sensitive; this gives the advantage that changes in mobile phase flow rate do not affect the detector's response (however FID destroys the sample). There are many detector types which are used in gas chromatography (Table 2.1.).

Table 2.1. Types of detectors.

Detector	**Type**	**Selectivity**
Flame ionization (FID)	Mass flow	Most organic compounds
Thermal conductivity (TCD)	Concentration	Universal
Electron capture (ECD)	Concentration	Halides, nitrates, nitriles, peroxides, anhydrides, organometallics
Nitrogen-phosphorus	Mass flow	Nitrogen, phosphorus
Flame photometric (FPD)	Mass flow	Sulphur, phosphorus, tin, boron, arsenic, germanium, selenium, chromium
Photo-ionization (PID)	Concentration	Aliphatics, aromatics, ketones, esters, aldehydes, amines, heterocyclics, organo-sulphurs, organometallics
Hall electrolytic conductivity	Mass flow	Halide, nitrogen, nitrosamine, sulphur

3. RESULTS AND DISCUSSION.

3.1. Synthesis, characterisation and catalytic potential of Fe^{III}-Proline and Fe^{III}-Proline-X complexes.

3.1.1. Synthesis of neat Fe^{III}-Proline complex and its encapsulation in zeolite X.

Fe^{III}-Proline. Fe^{III}-Proline complex was prepared according to the procedure reported in literature for Zn^{II}-Proline complex synthesis.[175] This procedure required amino acid treatment with a base to obtain ionization conditions, as amino acids coordinate to the metal ion *via* the charged carboxylate group. Triethylamine (Et_3N) was used as a base to deprotonate proline (COO^-, NH_2). This procedure involves reaction of 2 equivalents of proline with 1 equivalent of iron (II) acetate to form a five-membered chelate ring, with metal:proline ratio of 1:2. The synthesis was carried out in methanol as proline is soluble in methanol. The synthetic route is shown in section 6.2.1.

Fe^{III}-Proline-X. Fe^{III}-Proline was encapsulated within Zeolite X using zeolite synthesis method in which zeolite was synthesised in the presence of the preformed Fe^{III}-Proline metal complexes.[125] This technique assured building of zeolite cages around the complex (synthesis details are given in section 6.3.1.).

3.1.2. Characterization of Fe^{III}-Proline and Fe^{III}-Proline-X complexes.

3.1.2.1. FTIR spectroscopy.

Neat and encapsulated Fe^{III}-Proline materials were characterized by IR spectroscopy and analyzed in comparison to the spectra of the free ligand and crosschecked with literature data.[180, 181] IR spectrum of Fe^{III}-Proline complex shows changes in the band positions and their profiles, as compared to those of the free proline ligand. Proline molecule is in its anionic form with the δ_{NH}^{+} vibration missing when is chelated to the metal but with strong vibrations associated with the ν_{COO-} and the ν_{NH2} groups. The bands around 3050 cm^{-1} identify the ν_{NH2}^{+} symmetric stretching and 1556 cm^{-1} band reflecting δ_{NH}^{+} scissoring confirming the protonation of the amino group of free proline ligand. As expected this band disappeared in the spectrum of the complex, while the ν_{NH} was shifted

to 3210 cm^{-1}, which suggest coordination through NH group. The absence of any peak around 1550 cm^{-1}, the δ_{NH2}^{+} scissors region support the viewpoint that the proline coordinates in its anionic form. Also ν_{NH2}^{+} bending mode at 1376 cm^{-1} of proline spectrum was not observed (or very weakly) in the complex spectrum due to deprotonation of NH_2^{+} group to NH.

The neutral molecular form of proline has vibrations specifically due to the stretches of the C=O group at around 1790 cm^{-1}. Because the COO^{-} group is present in the zwitterions and the complex, the C=O group stretches were not observed. This result strongly indicated that the carboxylic group was not protonated in the Fe^{III}-Proline complex, otherwise, a strong band at about 1790 cm^{-1} should have been observed. The carboxylate group (COO^{-}) has two characteristic bands. The carboxylate ion group absorbs strongly near 1600 cm^{-1} and more weakly near 1400 cm^{-1} because of antisymmetric ($\nu_{as\ COO^{-}}$) and symmetric ($\nu_{s\ COO^{-}}$) stretching modes respectively. In the Fe^{III}-Proline complex, the band at 1660 cm^{-1} is assigned to $\nu_{as\ COO^{-}}$ and the band at 1400 cm^{-1} is assigned to $\nu_{s\ COO^{-}}$. CH stretching vibrations are observed in the spectral range of 3000-2800 cm^{-1}. There are three methylene groups in the five membered pyrrolidine ring which were expected to give bands near 2900 cm^{-1}. The NH stretching band of the free ligand at 3050 cm^{-1} is broadened and shifted to higher frequency (3210 cm^{-1}) after the reaction with the iron precursor. This could possibly indicate electron donation of the amine group to the iron. The carboxylate stretching band at 1607 cm^{-1} ($\nu_{as}\ COO^{-}$) was shifted to lower wavenumber at 1662 cm^{-1} and $\nu_s\ COO^{-}$ bands at and 1448 cm^{-1} to 1455 cm^{-1}. A summary and comparison of the main frequencies of proline, Fe^{III}-Proline and Cu^{II}-Proline complexes are presented in the Table 3.1.1. FTIR spectra of proline and Fe^{III}-Proline are shown in Figure 3.1.1. and 3.1.2.

Table 3.1.1. IR absorption (cm^{-1}) of main groups of proline, Fe^{III}-Proline and Cu^{II}-Proline complexes.

Assignment	**Proline** [180]	**Fe^{III}-Proline**	**Cu^{II}-Proline** [180]
ν_{NH2}^{+}	3050	-	-
ν_{NH}	-	3210	3196
δ_{NH2}^{+}	1556	-	-
ν_{CH}	2982	2975	2978
	2925	2910	2970
	2810	2869	2877
$\nu_{as\ COO^{-}}$	1607	1662	1628
$\nu s\ _{COO^{-}}$	1448	1455	1450

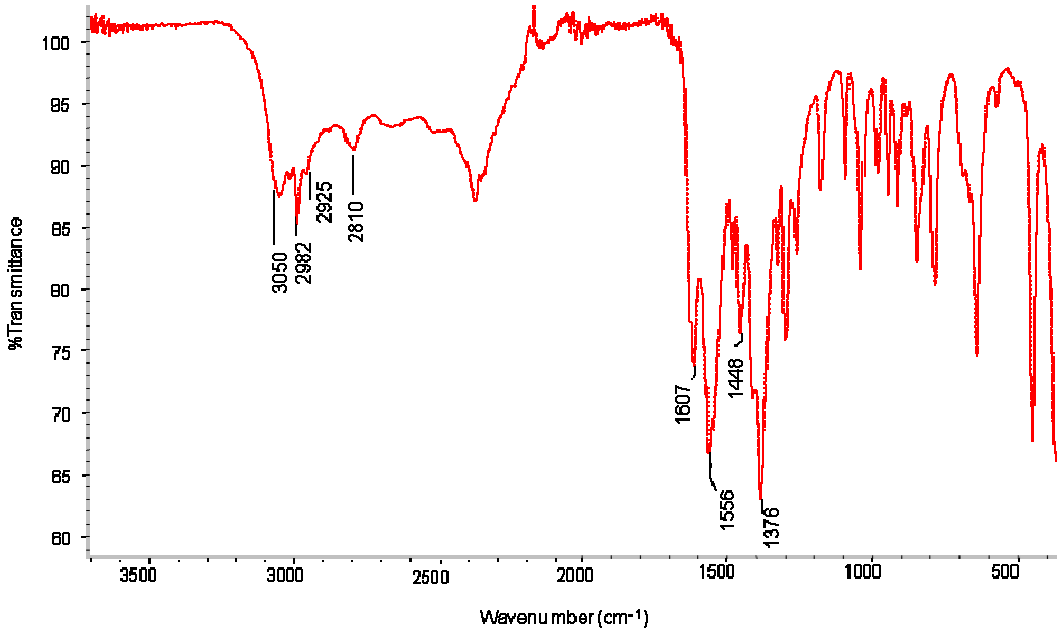

Figure 3.1.1. FTIR spectrum of proline.

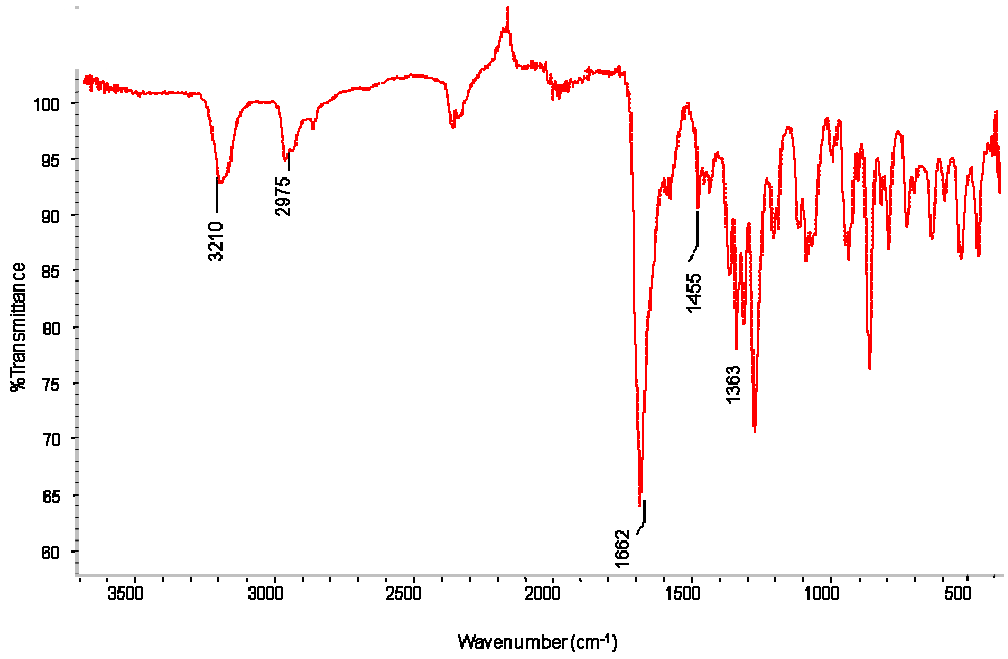

Figure 3.1.2. FTIR spectrum of Fe^{III}-Proline.

The FTIR spectrum of Fe^{III}-Proline encapsulated within zeolite X (Figure 3.1.3.), along with the assignments for the various bands) provided spectroscopic information on the nature and structural integrity of the encapsulated amino acid complexes. The most revealing signals are those related to the carboxyl and the amino groups, since they distinctly change in the molecular, cationic, anionic and zwitterionic forms.[182] The presence of a strong band at 1662 cm^{-1} for Fe^{III}-Proline-X and neat Fe^{III}-Proline coupled with the

absence of signal around 1790 cm^{-1}, which is typical of the COOH species, confirm that the carboxyl group is deprotonated. The carboxylate ions can be characterised by an antisymmetric ($\nu_{as\ COO^-}$) and a symmetric stretching mode ($\nu_{a\ COO^-}$) around 1650 and 1400 cm^{-1}, respectively. However, only the high frequency component is observed, strongly suggesting that the carboxylate group is involved in the binding to the metal ion. As for the amino group, the ν_{NH} bands of neutral NH_2 groups can be seen at 3285 cm^{-1} for Fe^{III}-Proline-X and at 3210 cm^{-1} for neat Fe^{III}-Proline (weak bending NH vibration can be observed at 1375 and 1363 cm^1 respectively). In Fe^{III}-Proline -X, these bands can be readily superimposed to a broad signal in the 3700 – 2800 cm^{-1} interval, which can be attributed to the hydrogen bonding between proline and zeolite. Some bands related to ν_{OH} modes of unperturbed isolated Si-OH (3740 cm^{-1}) and slightly perturbed water molecules (3700 – 3500 cm^{-1} range) are also seen in the encapsulated system (corresponding δ_{OH} expected around 1630 cm^{-1}, superimposed to the ν_{as} COO^-). The IR spectrum of zeolite X showed only weak IR modes in the ν_{OH} region at 3686 and 3650 cm^{-1}, assigned to a small amount of Al-OH and Brønsted Si(OH)Al groups, respectively. In both samples, the absence of the δNH_3^+ vibration at 1550 cm^{-1} is conspicuous, which confirms that the amino group is not protonated and can play a role in complexing the iron sites. Since the main differences between the spectra of neat and encapsulated Fe^{III}-Proline involve N-H vibrations, it is possible that this group is also interacting with the zeolite surface, probably acting as acceptor in hydrogen bonding interactions.

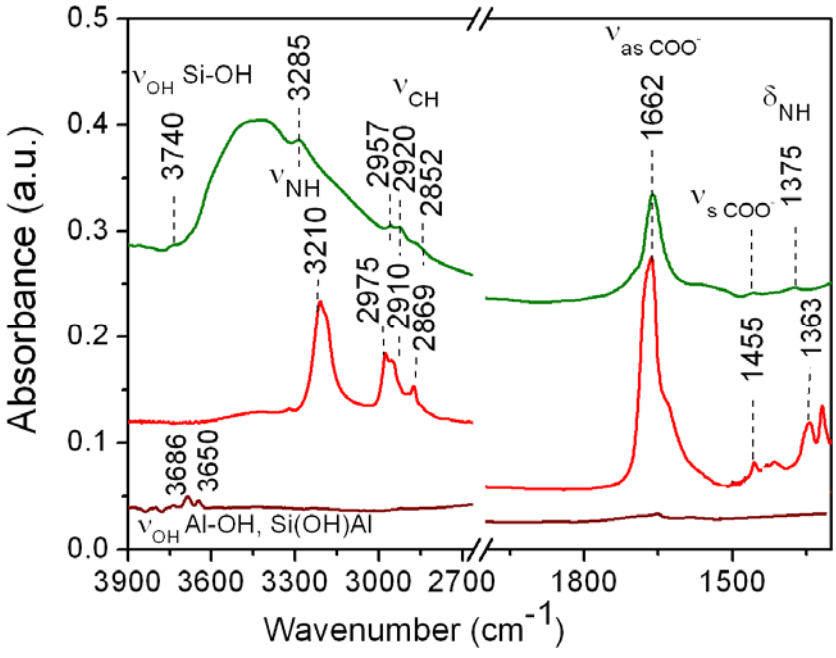

Figure 3.1.3. IR spectra of Fe^{III}-Proline (red), Fe^{III}-Proline-X (green), Zeolite X (brown). Spectra were arbitrarily normalized and vertically shifted for easier comparison.

Table 3.1.2. Summary of FTIR characterisation of Fe^{III}-Proline materials (absorption in cm^{-1}).

Assign -ment	Fe^{III}- Proline	Fe^{III}- Proline -X	Characterisation
ν_{NH}	3210	3285	Shifted ν_{NH} when compared to proline ligand suggests deprotonation of amino group and coordination to Fe through NH.
ν_{CH}	2975 2910 2869	2970 2910 2869	ν_{CH} stretching observed in similar spectral range for both Fe^{III}-Proline and Fe^{III}-Proline -X.
$\nu_{as\ COO^-}$ $\nu_{s\ COO^-}$	1662 1455	1662 1455	Shifted $\nu_{as\ C\ OO^-}$ and $\nu_{s\ C\ OO^-}$ when compared to proline ligand confirms carboxyl group involvement in Fe binding, absence of band at around 1790 cm^{-1} confirms carboxyl group deprotonation.

3.1.2.2. DR UV-Vis spectroscopy.

DR UV-Vis spectroscopy was used to elucidate the nature of Fe species of neat and encapsulated complex within zeolite X (Figure 3.1.4.). The neat Fe^{III}-Proline complex shows two strong absorption bands at 45400 and 37600 cm^{-1} that can be assigned to ligand to metal charge transfer transitions (LMCT) involving Fe^{III} sites in tetrahedral or octahedral coordination sphere (Figure 3.1.4., left). In addition, the weak and broad band at 20800 cm^{-1}, in the d-d transition range (Figure 3.1.4., right), confirms the presence of Fe^{III} ions (d^5 configuration).[183] In order to accurately assign the coordination geometry of the Fe^{III} centres, DR UV-Vis data was combined with EPR (Figure 3.1.5.), The encapsulated analogue in zeolite X showed bands in the same range as the neat complex, whilst the feature at 37600 cm^{-1} was less pronounced (due to the low loading of the Fe^{III}-Proline complex); the band at 45400 cm^{-1} is more predominant. This component at higher wavenumber (45400 cm^{-1}) can be assigned to well-dispersed and isolated Fe^{III} sites. From this result it can be inferred that zeolite synthesis method employed for the encapsulation of Fe^{III}-Proline in zeolite X, facilitates the site-isolation of the Fe^{III} centres. It is clearly evident (see results on catalytic oxidation, Table 3.1.5. and 3.1.8.) that these isolated Fe^{III} active centres play a major role in enhancing the catalytic turnovers in the oxidation of cyclohexane and benzyl alcohol.

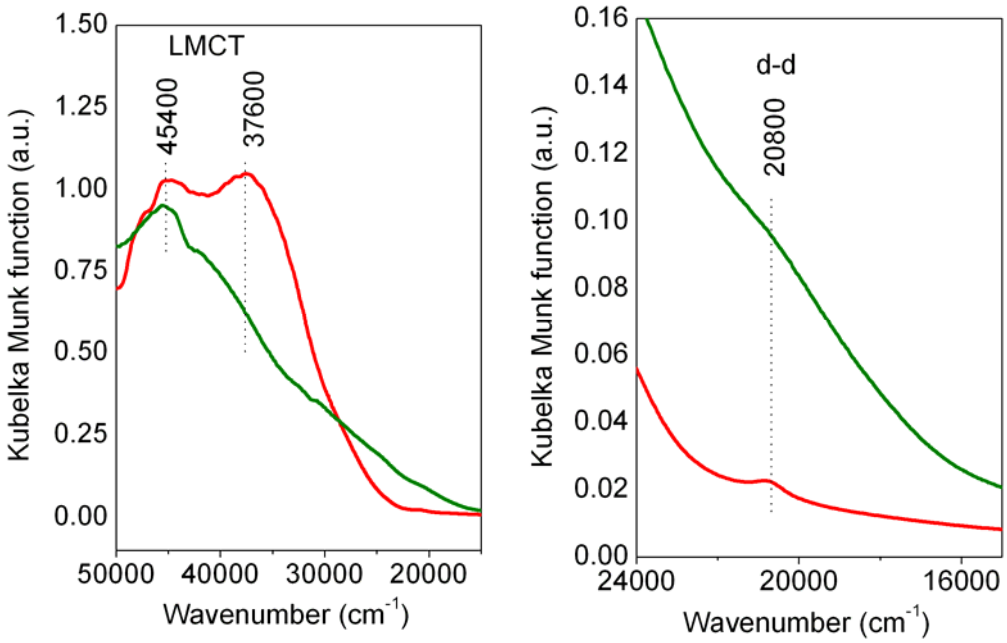

Figure 3.1.4. DR UV-Vis spectra of Fe^{III}-Proline (red) and Fe^{III}-Proline-X (green). Spectra were arbitrarily normalized for easier comparison, LMCT (left) and d-d (right).

Table 3.1.3. Summary of DRUV-Vis characterisation of Fe^{III}-Proline materials (absorption in cm^{-1}).

Assignment	**Fe^{III}-Proline**	**Fe^{III}-Proline - X**
LMCT	45400 37600	45400 37600
d-d	20800	20800

3.1.2.3. EPR spectroscopy.

The Electron Paramagnetic Resonance (EPR) spectrum of the powder of neat Fe^{III}-Proline consisted of a single broad line centred at $g \sim 2.0$ without a resolved hyperfine structure. Dysonian shape of the resonance line and temperature dependence (line width increase with decreasing temperature) that was observed is characteristic of strongly interacting Fe^{III} paramagnetic ions. A similar resonance dominated the EPR spectrum of the Fe^{III}-Proline incorporated in zeolite X. In addition, a narrow signal centred at $g = 4.26$ was observed, which is characteristic of isolated Fe^{III} ions in tetrahedral coordination (Figure 3.1.5.).[184] It is highly likely that such signals originated from strongly interacting Fe^{III}-Proline centres located near the extremities of the cages of zeolite X. Similar EPR spectra were recorded for Fe^{III} exchanged zeolite Y, where a broad resonance line at $g = 2$ was present together

with a narrow signal at g = 4.26. The detailed Fe^{III}-Proline complex geometry, on the basis of the paramagnetic ion coordination, could not be proposed due to the absence of the sufficiently resolved hyperfine structure.[102]

It is evident that these isolated Fe^{III} active centres play a major role in enhancing the catalytic turnovers in the oxidation reactions (see results on catalytic oxidation, Table 3.1.5. and 3.1.8.).

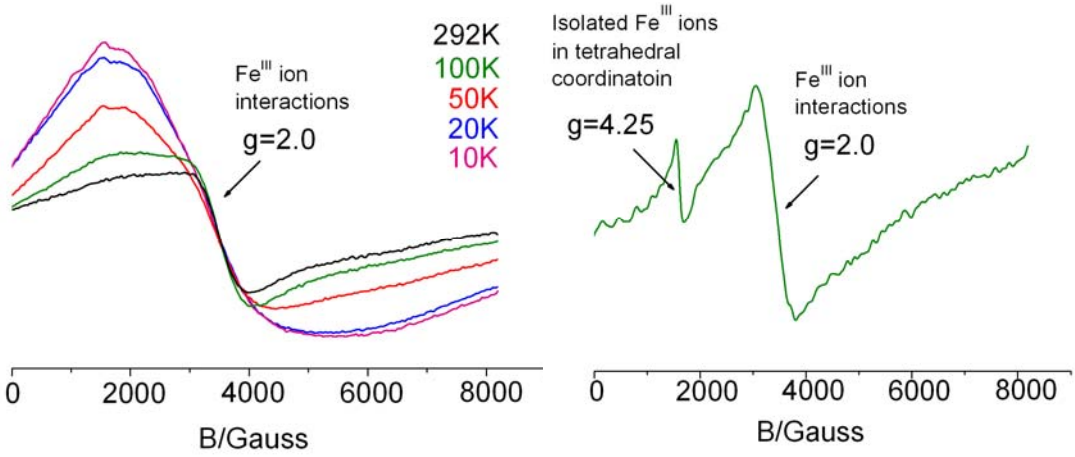

Figure 3.1.5. X-band (9.4 GHz) EPR spectrum of Fe^{III}-Proline -X (left) at 100K and EPR spectra of neat Fe^{III}-Proline recorded at different temperature range (right).

3.1.2.4. XRD analysis.

XRD patterns (Figure 3.1.6.) of Fe^{III}-Proline encapsulated within zeolite X were in good agreement with patterns reported for the neat zeolites.[185] The presence of well-resolved peaks with no phase impurities indicates that the faujasitic architecture was structurally unaltered after the encapsulation procedure. The absence of additional structural reflections due to the neat Fe^{III}-Proline complex revealed its dispersion predominantly within the internal cages, not on the external surface.

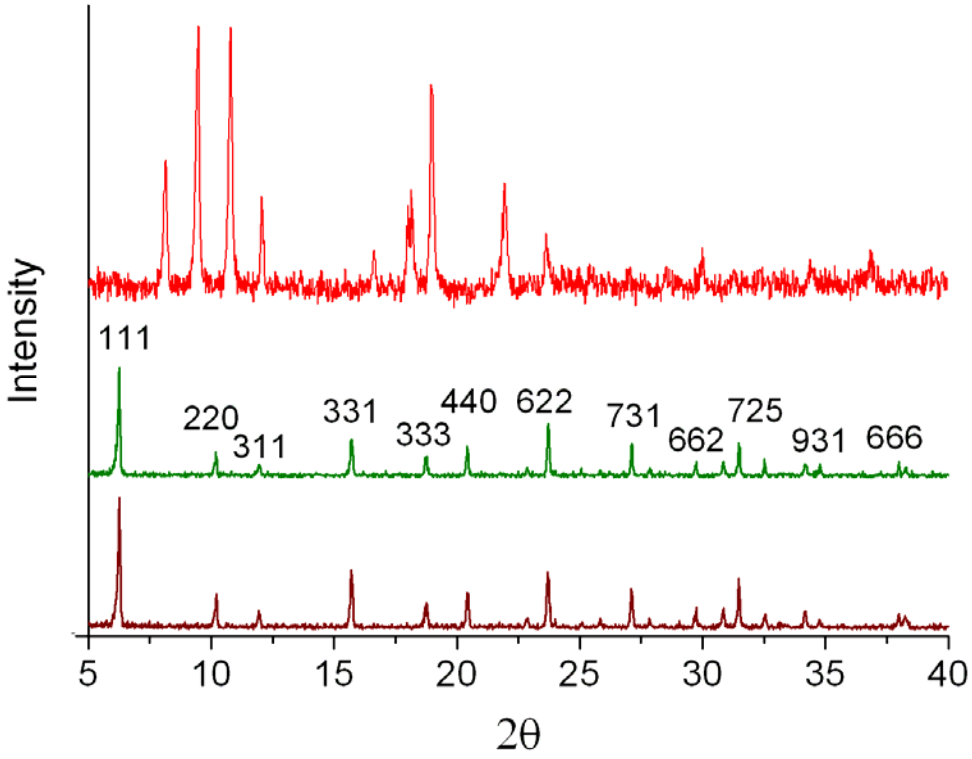

Figure 3.1.6. Powder XRD patterns of Fe^{III}-Proline (red) Fe^{III}-Proline-X (green) and Zeolite X (brown). Scan rate 12°min., step size 0.02°.

3.1.2.5. BET analysis.

N_2 adsorption measurement of Fe^{III}-Proline-X and neat Zeolite X was performed in a liquid nitrogen temperature. Samples were first dehydrated and degassed overnight in vacuum at 80°C.

Fe^{III}-Proline-X exhibited lower external surface area compared with pure Zeolite X. The supported catalyst showed the external surface area of 85 m^2/g while pure Zeolite X showed the external surface area of 660 m^2/g. The lowering of the surface area indicates the presence of the Fe^{III}-Proline complex within the micropores of Zeolite X.[186]

Table 3.1.4. Summary of BET characterisation of Fe^{III}-Proline-X catalyst.

Material	BET surface area m^2/g	Micropore Volume cm^3/g
Zeolite X	660	0.30
Fe^{III}-Proline-X	85	0.05

3.1.3. Cyclohexane oxidation with Fe^{III}-Proline and Fe^{III}-Proline-X complexes.

3.1.3.1. Introduction to cyclohexane oxidation with iron catalysts.

Catalytic, selective oxidation of hydrocarbons is amongst the most important process in the chemical industry. Oxidation of cyclohexane is one of the most important processes for the production of polymers such as Nylon-6 and Nylon-6,6 and polyamide fibers. Cyclohexanone and cyclohexanol (K/A oil) are valuable products of cyclohexane oxidation.[18] Industrial cyclohexane oxidation involves a system that uses homogeneous cobalt (II) salts, such as a cobalt (II) carboxylate, corrosive acids and temperatures above 425 K.[187] The subsequent oxidation to adipic acid uses nitric acid as an oxidant and two moles of nitrous oxide is produced per mole of adipic acid (Scheme 3.1.1.). In the DuPont process of manufacturing Nylon-6 and Nylon-6,6, cyclohexane is oxidized to a mixture of cyclohexanol and cyclohexanone. The conversion of cyclohexane is kept under 5% to avoid over-oxidation. Unreacted cyclohexane is then extracted and recycled.[188] Due to the great market demands for valuable cyclohexane oxidation products together with increasing environmental requirements for more efficient and green processes, catalytic systems that operate under mild condition preferably employing molecular oxygen as oxidant are highly desirable.

Many studies involving iron and its role in chemical and biological oxidation reactions stem from studies of Fenton's reagent which is a mixture of hydrogen peroxide and ferrous salts.[189, 190] The history of Fenton chemistry dates to 1894, when Henry J. Fenton reported that H_2O_2 could be activated by Fe^{II} salts to oxidize tartaric acid. In 1934 Haber and Weiss proposed that the active oxidant generated by the Fenton reaction is the hydroxyl radical ($HO^{\bullet}$). The mechanism proposed by Haber and Weiss is now referred to as the "classical" or "free radical" Fenton chain reaction and it involves $HO^{\bullet}$ radical formation as the key step. The Fenton's reagent oxidation of organic compounds proceeds *via* initial one-electron reduction of hydrogen peroxide to yield free hydroxyl radicals and Fe^{III} (Scheme 3.1.2., 1). Fe^{III} is then reduced by H_2O_2 and hydroperoxyl radicals $HOO^{\bullet}$ are formed (2). Hydroxyl radicals $HO^{\bullet}$ then subsequently abstract hydrogen atom from substrate molecule to form substrate radical $R^{\bullet}$ (3). The oxidation products, alcohol (R-OH) and ketone (R=O) can then be formed by two pathways: by autoxidation of substrate radicals $R^{\bullet}$ by O_2 (5 and 6) or a metal-based pathway where substrate radicals $R^{\bullet}$ react with Fe^{III}-OH complexes to form alcohol and Fe^{II} (7). O_2 originates from the parallel decomposition of H_2O_2 (4).

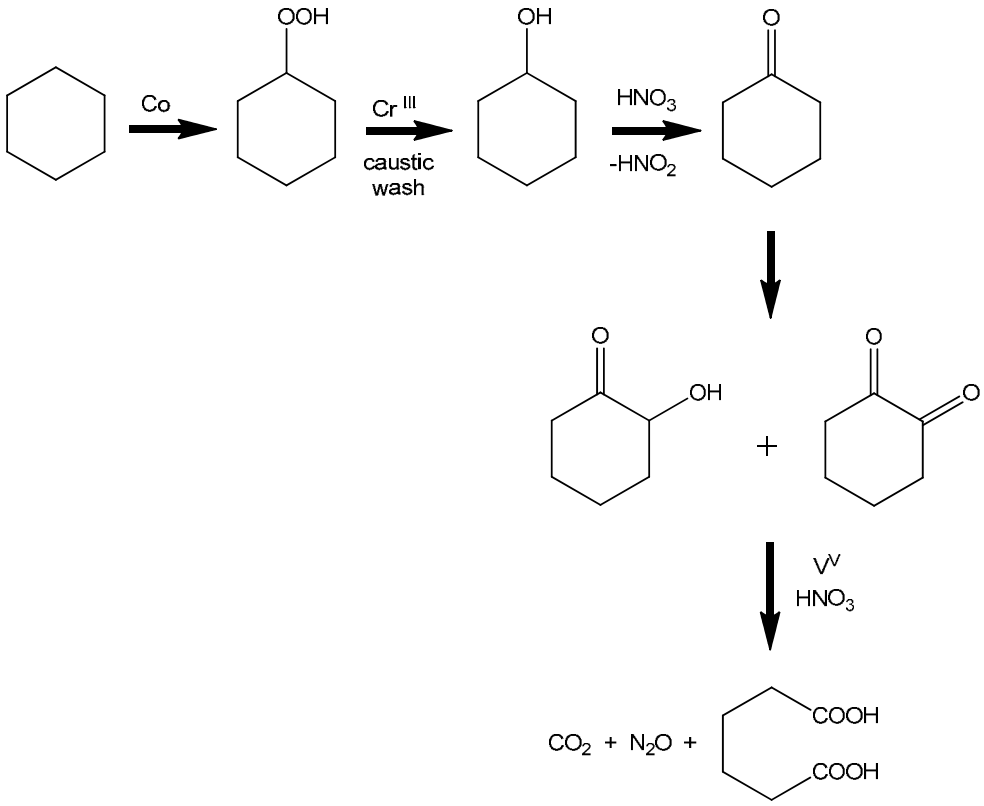

Scheme 3.1.1. Conventional method of cyclohexane oxidation. Two moles of nitrous oxide is produced for one mol of adipic acid.

$$Fe^{II} + H_2O_2 \longrightarrow Fe^{III} + OH^- + HO^\bullet \quad (1)$$

$$Fe^{III} + H_2O_2 \longrightarrow Fe^{II} + H^+ + HOO^\bullet \quad (2)$$

$$RH + HO^\bullet \longrightarrow R^\bullet + H_2O \quad (3)$$

$$Fe^{III} + H_2O_2 + HO^\bullet \longrightarrow Fe^{II} + O_2 + H_2O + H^+ \quad (4)$$

$$R^\bullet + O_2 \longrightarrow ROO^\bullet \quad (5)$$

$$2\,ROO^\bullet \longrightarrow R\text{-}OH + R{=}O + O_2 \quad (6)$$

$$R^\bullet + Fe^{III}\text{-}OH \longrightarrow R\text{-}OH + Fe^{II} \quad (7)$$

Scheme 3.1.2. Fenton mechanism of catalytic generation of hydoxyl radicals by Fe^{II} ions and schematic organic substrate oxidation (RH).

A non-radical pathway and formation of ferryl intermediate (high valent Fe^{IV}=O) which is then the active species in Fenton-like reactions was also proposed as a resulting intermediate in the reaction between H_2O_2 and Fe^{II}.[191] The possible hydroxyl radical and ferryl ion pathways for the Fenton's reagent mechanism is shown in Scheme 3.1.3.

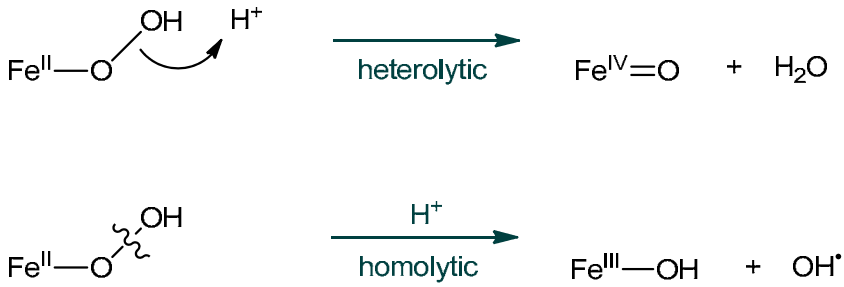

Scheme 3.1.3. Homolytic and heterolytic cleavage of hydrogen peroxide with ferrous ion Fe^{II}.

Many variants of the Fenton reaction have been explored for homogeneous and heterogeneous oxidation processes, including complexes of iron with organic ligands, solid iron oxides and iron species immobilized on solid supports.[192] Iron based zeolites (Fe-ZSM-5, Fe-Beta Fe-silicalite and Fe-TS-1) have been studied as Fenton-type catalysts in various oxidation reactions. In cyclohexene epoxidation reactions with H_2O_2 and zeolites Fe-ZSM-5, Fe-Beta the $HO^{\bullet}$ radical was not a reactive species and ferryl intermediate Fe^{IV}=O was proposed to be an active oxidant.

The Fenton system is widely used in industry for cleaning wastewater from cyan-containing compounds as well as phenols and organic solvents. Fe-ZSM-5 showed high activity for total oxidation of phenols to carbon dioxide and water in aqueous solutions.[193]

Nature utilizes metalloenzymes as catalysts in selective hydrocarbon oxidation. Iron-containing metalloenzymes such as heme cytochrome P450 and the nonheme methane monooxygenase activate dioxygen and play an important role in these essential hydrocarbon transformations. However due do fragile nature of biological catalytic systems it is difficult to adapt them to harsher industrial conditions. For this reasons development of bioinspired, robust, inorganic catalysts have recently attracted great attention.

The hydrogen abstraction–oxygen rebound mechanism was proposed for hydroxylation reactions catalysed by cytochrome P450 (Scheme 3.1.4.). In this pathway, the iron-oxo species ($Por^{+\bullet}$-Fe^{IV}=O) react by hydrogen atom abstraction from the substrate molecule to give a radical substrate intermediate. This carbon-centred radical then reacts with the iron hydroxide species in the substitution reaction, called the 'oxygen-rebound' step.[46]

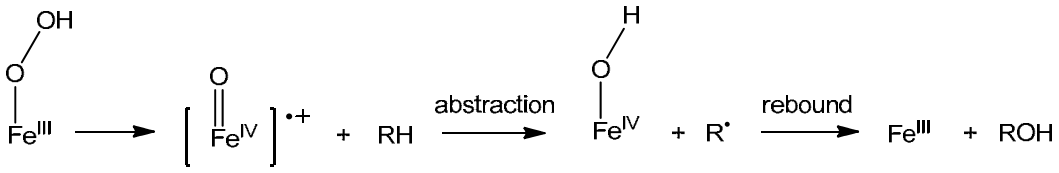

Scheme 3.1.4. Oxygen rebound mechanism of hydrocarbon hydroxylation catalyzed by cytochrome P450.

Nonheme diiron methane monooxygenase (MMO) generates two reactive intermediates in oxidation transformations. A peroxo species, (μ-1,2-peroxo)diiron^{III} was proposed to be analogous to the Fe^{III}-OOH intermediate of P450. Diiron^{IV} species, $Fe_2(\mu\text{-}O)_2$ corresponds to porphyrin cation radicals $[(Por^{\bullet})Fe^{IV}=O]^+$ in cytochrome P450 (Figure 3.1.7.).[194]

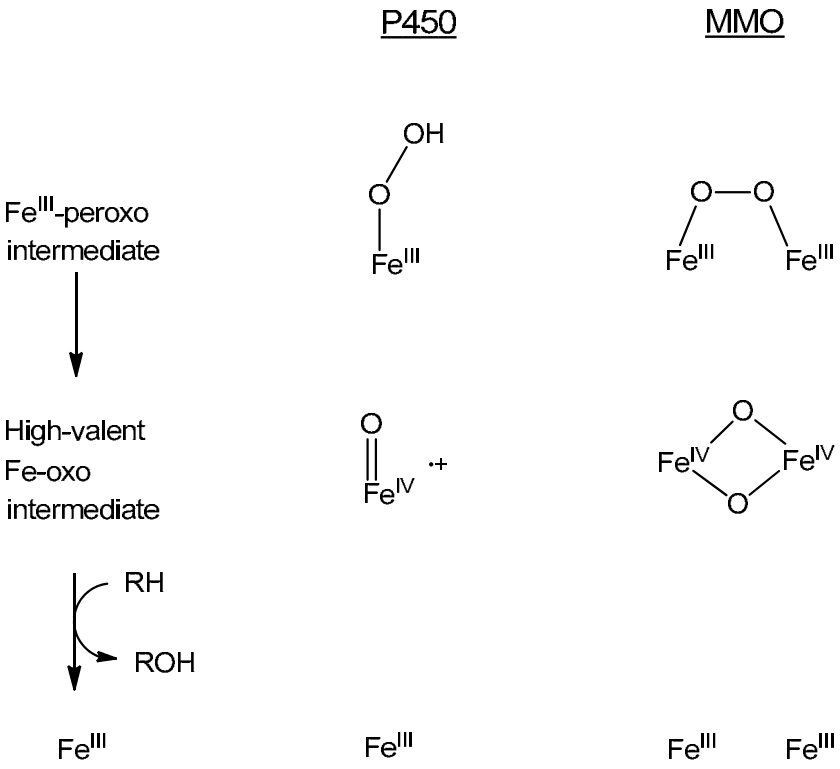

Figure 3.1.7. Comparison of the reactive intermediates of P450 and MMO.

Spectroscopic studies on biomimetic iron systems like Fe(TPA) (TPA = tris (2-pyridyl-methyl) amine), Fe(bpmen), Fe(N_4Py) and $Fe_2O(bpy)_4$ also suggested the formation of the iron^{III} hydroperoxo intermediate (Fe^{III}-OOR) by the reaction of the iron complexes with peroxide.[195] Fe^{III}-OOR intermediates can decompose in different pathways and generate different active oxidants such as HO$^{\bullet}$ or RO$^{\bullet}$, or metal based oxidants such as Fe^{III}-OOH, Fe^{IV}=O, Fe^{V}=O species (Figure 3.1.8.). The Fe-O bond of the peroxide intermediates can

undergo homolysis and form Fe^{II} and $ROO^{\bullet}$ radicals. The $ROO^{\bullet}$ radical can generate a more powerful oxidant such as an $RO^{\bullet}$ radical, which can attack the cyclohexane C-H bond. Fe-OOR species may also undergo O-O bond homolysis to form Fe^{IV}=O and $RO^{\bullet}$ radicals and both can attack the substrate molecule. The O-O bond heterolysis of the Fe-OOR intermediate is also possible and leads to Fe^{V}=O species formation. The Fe-OOR intermediate can also directly attack organic substrates. Transformations catalyzed by P450 and MMO involve the generation of active and selective metal-oxo species. $HO^{\bullet}$ and $RO^{\bullet}$ radicals are undesirable as they initiate non-selective radical chain autoxidation reactions in the presence of dioxygen.[196, 197]

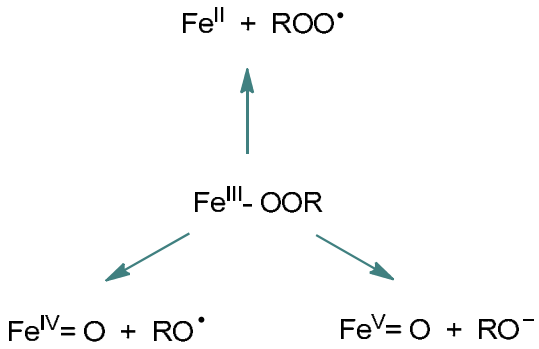

Figure 3.1.8. Proposed pathways of iron^{III} hydroperoxo (Fe^{III}-OOR) decomposition.

Fe^{III}/TBHP based catalytic systems can oxidize alkanes *via* a mechanism that involves alkoxyl radicals or via metal based intermediates. Fe^{III}/TBHP systems may undergo heterolysis resulting in high valent iron-oxo species formation (Fe^{IV}=O) (Scheme 3.1.5) or may undergo homolysis that results in *tert*-butylperoxy radicals formation (Scheme 3.1.6.).

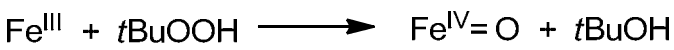

Scheme 3.1.5. Heterolytic Fe^{IV}=O species formation.

The Haber-Weiss decomposition of *t*BuOOH (*tert*- butyl hydroperoxide) occurs in the first stage of the homolytic reaction (Scheme 3.1.6.). This results in reduction of Fe^{III} to Fe^{II} and *tert*-butylperoxy radical formation (*t*BuOO$^{\bullet}$) (1). Fe^{II} is oxidized by TBHP generating *t*BuO$^{\bullet}$ (2) that undergoes rapid hydrogen atom abstraction from TBHP at a much faster rate that than hydrogen atom abstraction from the substrate molecule. At this stage more stable *tert*-BuOO$^{\bullet}$ radicals are formed (3). During Haber–Weiss decomposition of *t*BuOOH, O_2 is formed *via* bimolecular decomposition of *tert*-BuOO$^{\bullet}$ (4). The *tert*-butylperoxy radicals abstract a hydrogen atom from the cyclohexane

molecule forming the cyclohexyl radical (5). This substrate alkyl radical can be trapped by O_2 to form an alkylperoxy species (6). Alkylperoxy radicals can abstract a hydrogen atom from the cyclohexane molecule forming a cyclohexane hydroperoxo species and cyclohexyl radicals (7). Cyclohexane hydroperoxo intermediates decompose to alcohol and ketone (8a and 8b). Alkylperoxy radicals can also decompose to alcohol and ketone *via* Russel termination step (9).[198-200]

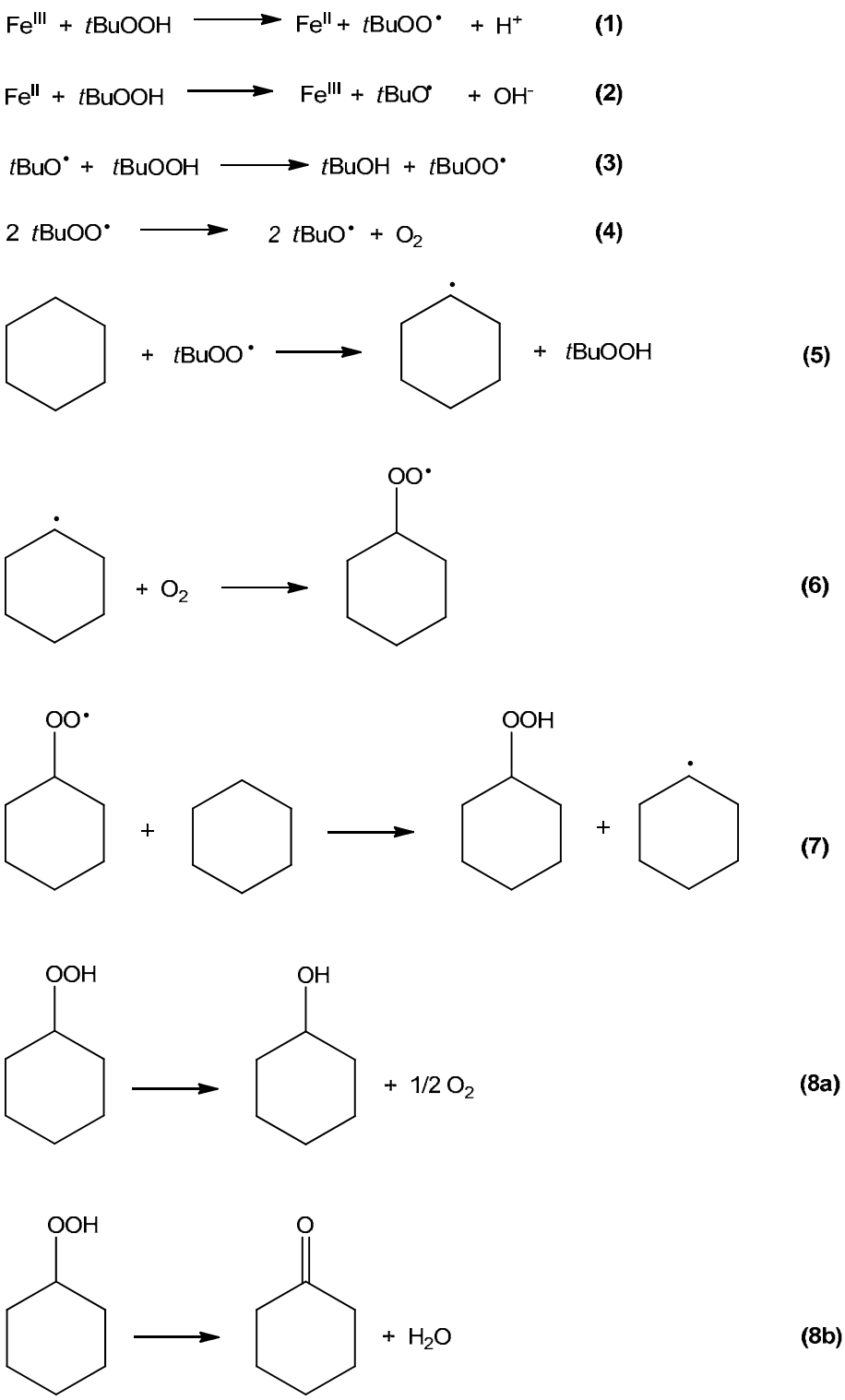

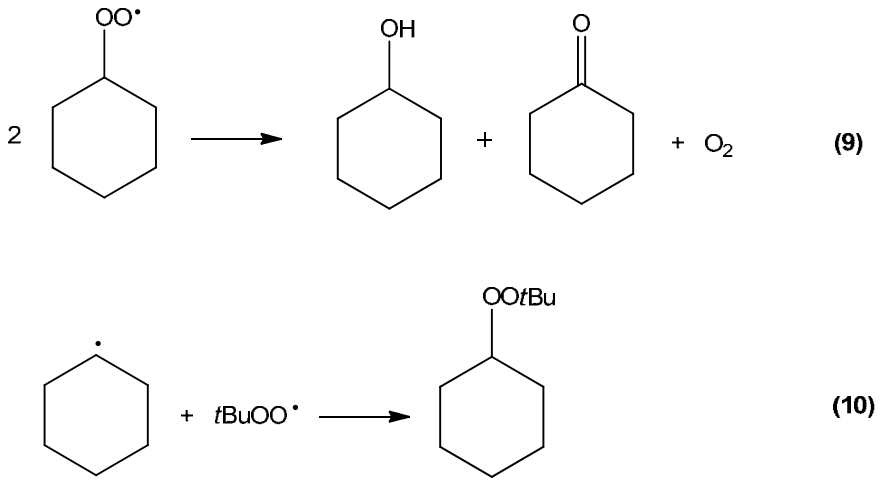

Scheme 3.1.6. Model mechanism of cyclohexane oxidation.

3.1.3.2. Cyclohexane oxidation with Fe^{III}-Proline catalysts.

The catalytic activity of the neat Fe^{III}-Proline and encapsulated Fe^{III}-Proline-X complexes was evaluated in the oxidation of cyclohexane with air and TBHP as oxidants. The results are summarised in Table 3.1.5. A control experiment in the absence of catalyst gave conversions of 4.8 mol% with TBHP and 2.1 mol% in the presence of air, confirming that the presence of Fe^{III}-Proline complex was essential to obtain catalytic oxidation.

Table 3.1.5. Results on selective oxidation of cyclohexane with Fe^{III}-Proline catalysts. For reaction conditions see section 6.10.1.

Cat	Metal load.	Oxid.	Substrate: Metal ratio	Oxidant: Substrate ratio	TON	TOF (h^{-1})	Conv. mol %	Selectivity mol %	
								ol	one
Neat	16.9	AIR	242	1.65	27	27	14.3	>99	
Neat	16.9	TBHP	242	1	143	143	66.1	>99	
X	0.49	AIR	1670	1.65	105	105	7.8		>99
X	0.49	TBHP	1670	1	1161	1161	70.0	>99	
Blanc	-	AIR	-	1.65	-	-	2.1	>99	
Blanc	-	TBHP	-	1	-	-	4.8	>99	

T=371, K air 3.0 MPa, acetonitrile 35 g, reaction time=1h, ol-cyclohexanol, one-cyclohexanone, TON (turn over number)- molar ratio of converted substrate to catalyst, TON = (%conv) x (mol(substrat)) / mol (catalyst), TOF (turn over frequency)- TON per hour, TOF = TON / time(h).

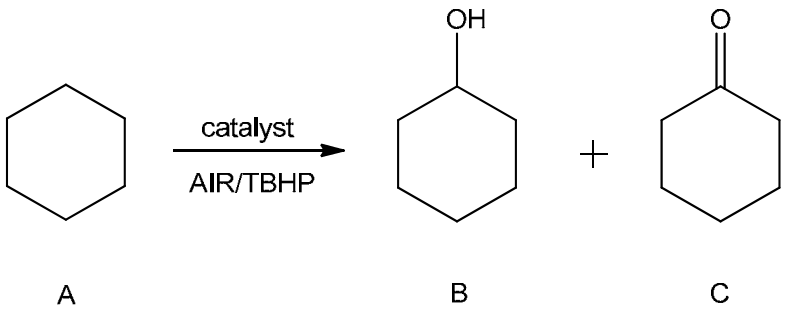

Scheme 3.1.7. Schematic representation of product formation in cyclohexane (A) oxidation to cyclohexanol (B) and cyclohexanone (C) with homogeneous and heterogeneous Fe^{III}-Proline catalysts.

Both neat and encapsulated Fe^{III}-Proline complexes showed higher activities with TBHP employed as the oxidant. Neat complex reached a conversion of 66.1 mol% and the heterogeneous catalyst afforded a conversion of 70.0 mol% in the presence of TBHP. In the presence of air the Fe^{III}-Proline-X catalyst exhibited a conversions of 7.8 mol% and its homogeneous analogue reached a substrate conversion of 14.3 mol%. The homogeneous Fe^{III}-Proline complex was selective to cyclohexanol (>99 mol %), with both oxidants. Heterogeneous Fe^{III}-Proline-X catalyst revealed interesting changes in product selectivity depended on oxidant type. In the presence of TBHP, this catalyst, similar to the homogeneous complex, was selective towards cyclohexanol, but when air was used Fe^{III}-Proline-X showed preference for cyclohexanone formation (99. 5 mol %).

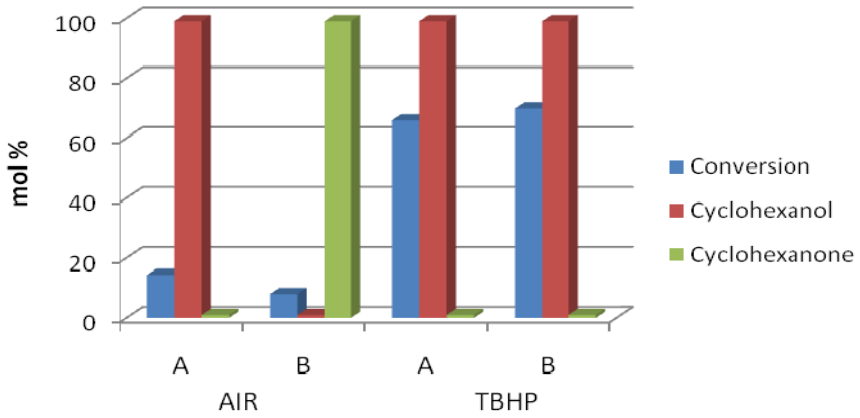

Figure 3.1.9. Representation of changes in conversion and selectivity in cyclohexane oxidation with Fe^{III}-Proline (A) and Fe^{III}-Proline-X (B) in presence of air and TBHP.

In the presence of *tert*-butyl hydroperoxide, the heterogeneous Fe^{III}-Proline-X catalyst showed an *eight-fold* increase in activity (TON and TOF of 1161) when compared with its homogeneous analogue that obtained TON and TOF of 143. When air was used, heterogeneous Fe^{III}-Proline-X catalyst afforded a *four-fold* increase in activity (TON and TOF of 105) while the homogeneous analogue showed TON and TOF of 27. These results strongly suggested that the isolated active sites that were generated during the encapsulation procedure and were responsible for the increase in catalytic activities. The hydrophobicity/hydrophilicity of the host (zeolite) together with the nature of oxidant seemed to be responsible for the changes in product selectivity.

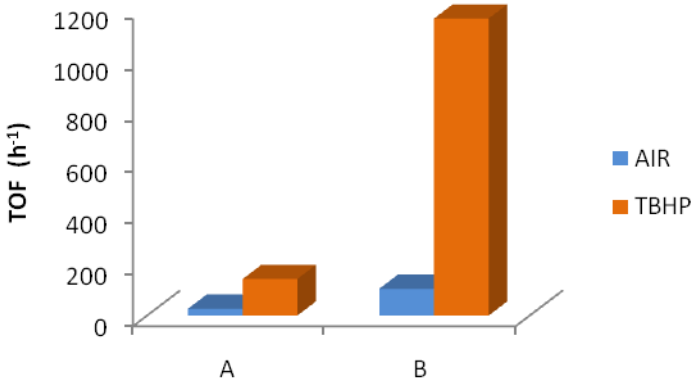

Figure 3.1.10. Comparison of turnover frequency (TOF=TON, reaction time 1h) in the oxidation of cyclohexane using homogeneous Fe^{III}-Proline (A) and heterogeneous Fe^{III}-Proline -X (B) catalysts.

The changes in selectivity suggest involvement of two competing mechanisms; a radical chain and metal-based oxidation. Radical chain pathway would have produced a mixture of both alcohol and ketone and not only a single product. Cyclohexanol was reported as the only observed product of the reaction catalysed by the Fe(TPA) catalyst in the presence of TBHP (10 equiv) that was added to reaction mixture *via* syringe pump (under argon).[200] In the virtual absence of O_2, only *t*BuOO$^{\bullet}$ radicals can trap cyclohexyl radicals. Different iron species could be produced at this stage: Fe^{III}-OH, Fe^{IV}-OH or Fe^{IV}=O and OH. The reaction mechanism proposed for this system is based on initial metal-peroxo intermediate formation (Scheme 3.1.8.). Cyclohexanone could be a major product formed due to decomposition (essentially dehydration) of the cyclohexane hydroperoxo intermediate.[201]

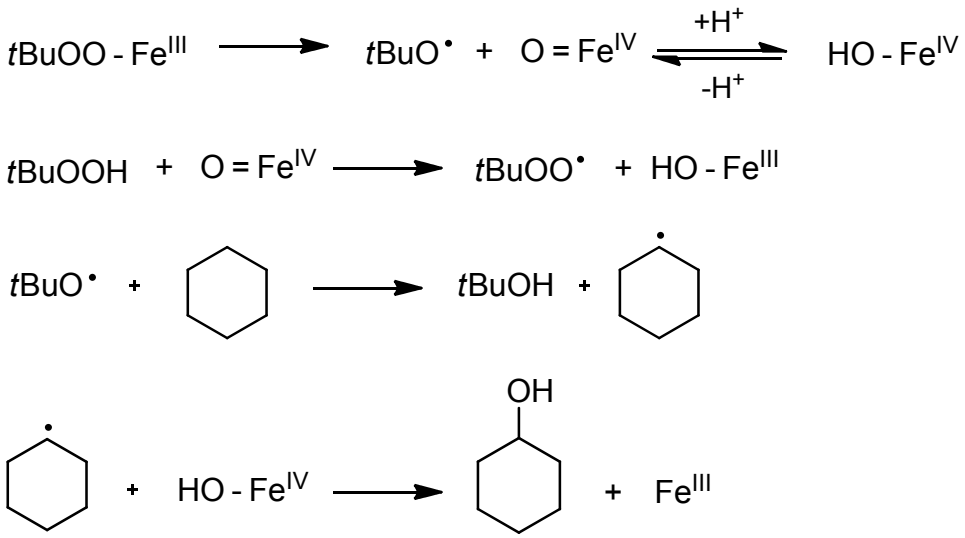

Scheme 3.1.8. Proposed metal-oxo based mechanism of cyclohexane oxidation.

3.1.4. Benzyl alcohol oxidation with Fe^{III}-Proline and Fe^{III}-Proline.

3.1.4.1. Introduction to benzyl alcohol oxidation with iron catalysts.

Selective oxidation of alcohols to the corresponding carbonyl compounds (aldehydes or acids) is an important step in the synthesis of fine chemicals and intermediates, and plays a fundamental role in organic synthesis.[202, 203] Aldehydes are valuable components for the perfume industry. Many aldehydes occur naturally in plants oils and fruits e.g. benzaldehyde (rose, peach, apricot), n-hexenal (eucalyptus oils), n-octyl aldehyde (lemon oil, lemongrass oil).

Traditional, industrial methods of alcohol transformation involve the use of stoichiometric amounts of chromate, permanganate or TPAP/NMO (tetra-N-propylammonium perruthenate/ N-methyl-morpholine-N-oxide) oxygen donors. However these reagents are expensive, environmentally unfriendly, generate equal amounts of metal waste and have serious toxicity issues associated with them.[204] Developing green, efficient and selective catalysts for alcohol oxidation that ideally utilize molecular oxygen as oxidant are of paramount importance from economic and environmental viewpoints. Such green processes produce water as the only waste product (Scheme 3.1.9.).[205]

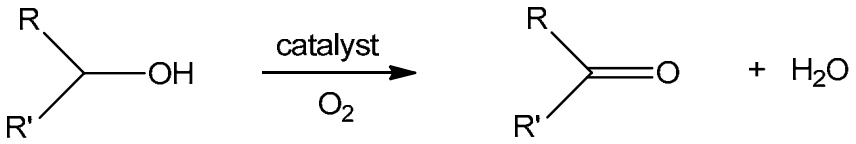

Scheme 3.1.9. Catalytic oxidation of alcohols with molecular oxygen.

Many heterogeneous and homogeneous catalysts were investigated for alcohol oxidation with various oxidants. The oxidation of benzyl alcohol has been intensively investigated using a range of titania-supported Au (Au/TiO_2) and Pd (Pd/TiO_2) catalysts. The TiO_2-supported Au-Pd catalysts were studied for the oxidation of benzyl alcohol at 373 K with O_2 as oxidant in the absence of a solvent.[206, 207] The Au-Pd/TiO_2 catalysts have shown high activity and selectivity to benzaldehyde with the only byproduct being benzyl benzoate. In contrast, Pd/TiO_2 also produced toluene and benzene as byproducts, and the Au/TiO_2 catalyst produced a significant amount of an acetal product. These by-products are likely to be the outcome of side reactions due to hydrogenolysis (toluene formation), decarbonylation (benzene) and esterification reaction (benzyl benzoate) (Scheme 3.1.10.). TiO_2-supported Au-Pd nanocrystals gave significantly enhanced activity for alcohol oxidation when compared with monometallic supported Au and Pd. In fact the Au-Pd nanocrystal catalysts give enhanced TOF by a factor of 25 (Table 3.1.6.).[17] The introduction of Au to Pd/TiO_2 improved selectivity probably due to the changes in electronic structure and particle size. It has also been shown that Au can isolate Pd sites within bimetallic systems. Au-Pd nanocrystals supported on Al_2O_3 and Fe_2O_3 were also effective in benzyl alcohol oxidation reactions.[208] TiO_2-supported Au-Pd catalysts exhibited higher selectivity towards benzaldehyde formation. It was proposed that the more acidic nature of the Al_2O_3 and Fe_2O_3 supports led to enhanced byproduct formation. Pd supported on hydroxyapatite (PdHAP-0) is the most active solid catalyst reported for selective oxidation of benzyl alcohol with molecular oxygen, exhibiting turnover number of 236000 and a TOF of 9800 h^{-1}.[209]

Supported gold nanoparticles also showed to be very effective catalysts for the oxidation of alcohols. Magnesium oxide (MgO) and aluminium oxide (Al_2O_3) supported gold catalysts proved to be highly active in benzyl alcohol oxidation to benzaldehyde with TBHP under solvent-free conditions. Gold nanoparticles deposited on nanocrystalline ceria (Au/CeO_2) gave a highly active and selective catalyst for the oxidation of alcohols into the corresponding aldehydes with high turnover numbers and frequencies (12500 h^{-1}).[210] The performance of these catalysts was strongly influenced by the method of preparation, metal loading, particle size, particle–support interactions, reaction temperature and calcination temperature.

Table 3.1.6. Comparison of catalytic performance of heterogeneous catalysts in selective oxidation of benzyl alcohol.[17]

Catalyst	Oxidant	Conversion (mol%)	Selectivity to benzaldehyde (mol%)
Au/TiO_2	O_2	15	63.9
Pd/TiO_2	O_2	60	54.4
$Au\text{-}Pd/TiO_2$	O_2	74.5	91.6
$Au\text{-}Pd/Al_2O_3$	O_2	83.3	86.6
$Au\text{-}Pd/Fe_2O_3$	O_2	63.4	66.4
$Au\text{-}Pd/SiO_2$	O_2	35.7	88.0
Au/Al_2O_3	TBHP	75.5	65.2
Au/MgO	TBHP	99	72.5

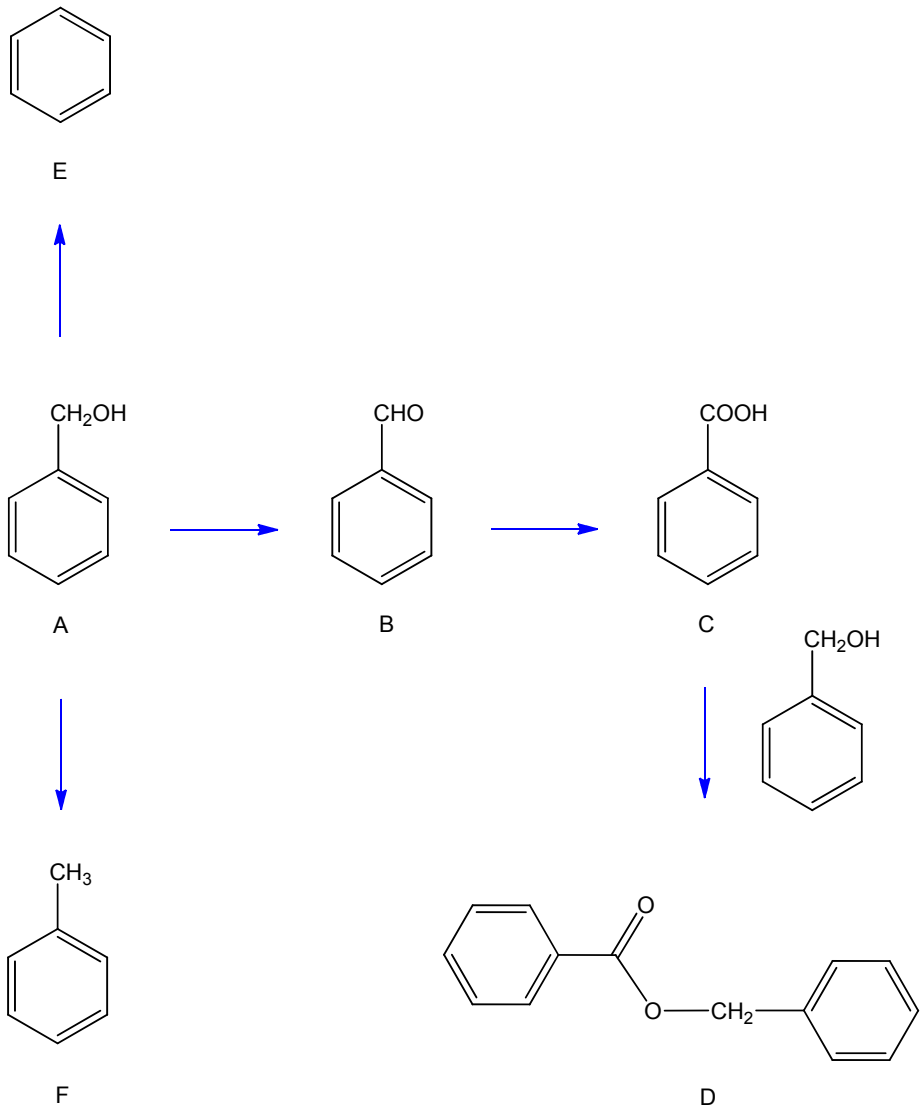

Scheme 3.1.10. General reaction pathway of by-products formation in benzyl alcohol transformation reactions: benzyl alcohol (A); benzaldehyde (B), benzoic acid (C), benzyl benzoate (D) benzene (E) toluene (F).[211]

The aerobic alcohol oxidation pathway that involves β-hydride elimination was proposed for many catalytic systems.[212, 213] β-Hydride elimination is the rate determining step and this pathway involves dehydrogenation of the alcohol *via* β-hydride elimination from the metal alkoxide to form a metal hydride. In this mechanism alcohol binds to metal, forming hydrogen-bonded-alcohol intermediate. In the next step, an intramolecular deprotonation of a metal-bound alcohol occurs and the metal-alkoxide is formed. This species undergoes β-hydride elimination to form the product and metal hydride species. The hydridometal is reoxidized by molecular oxygen, probably via insertion into the M–H bond, to reform the active catalyst and produce hydrogen peroxide. Alternatively, the metal alkoxide species can abstract a proton and release the reduced form of the catalyst, either directly or *via* the intermediacy of a hydridometal species. Both reaction pathways are presented in Figure 3.1.11. and 3.1.12.

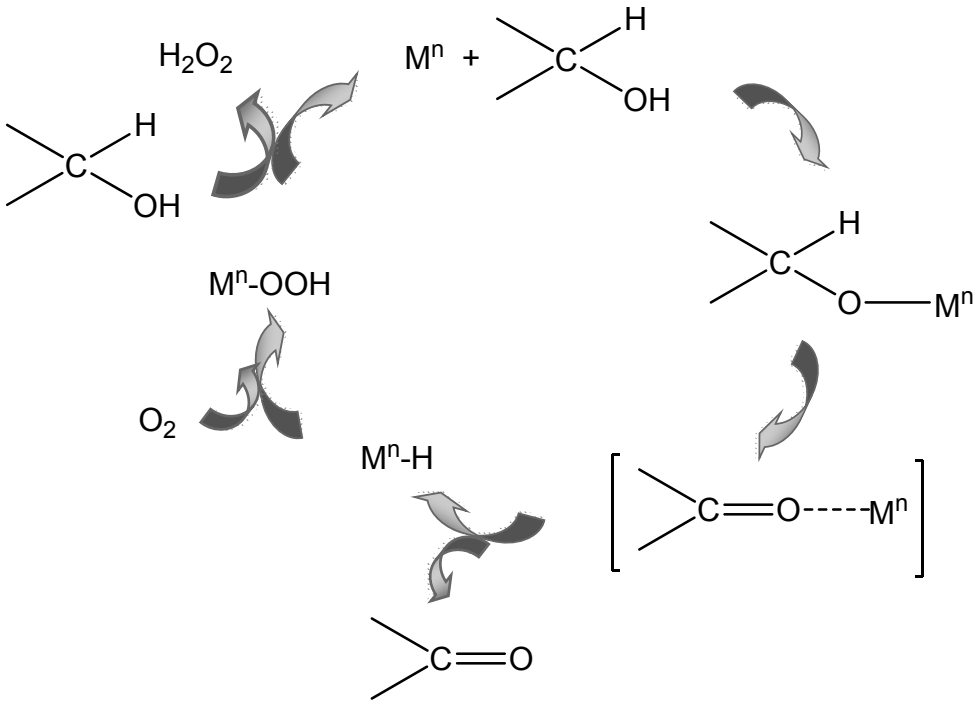

Figure 3.1.11. Hydridometal pathway for alcohol oxidation *via* metal hydride species.[212]

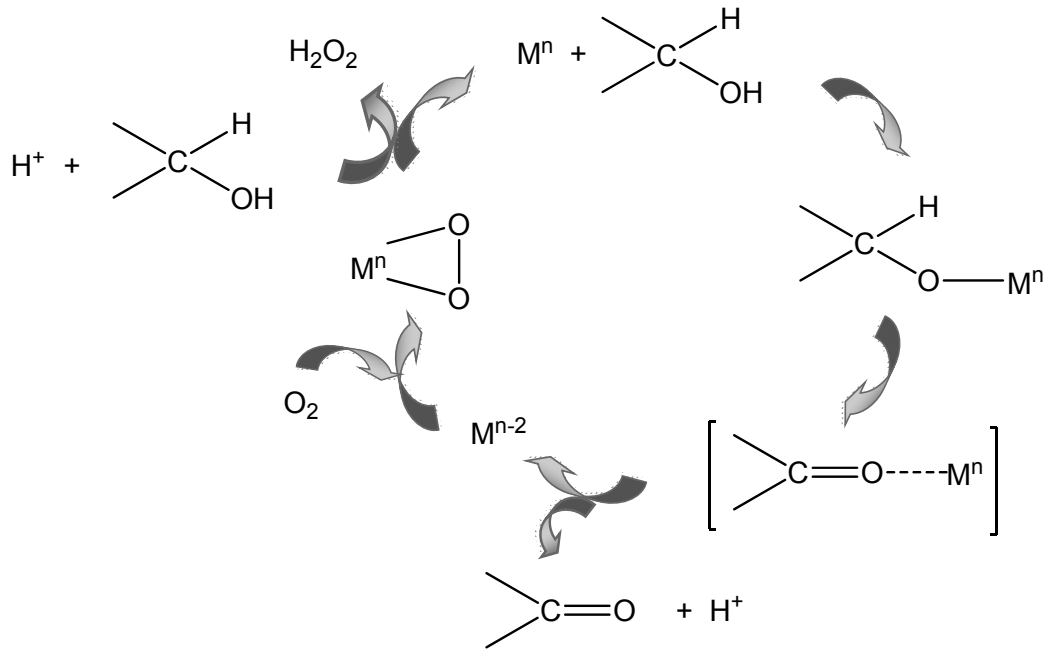

Figure 3.1.12. Hydridometal pathways for alcohol oxidation *via* path that release proton.[212]

Iron is abundantly available and plays a crucial role in many biological systems. In comparison with other transition metals extensively used, iron-based catalysts are inexpensive, environmentally benign, and relatively non-toxic. In the past decades, various iron salts have been applied in homogeneous catalysis and different catalytically active iron complexes were reported.[214] In heterogeneous catalysis, iron oxides have been frequently used as catalysts and supports in bulk industrial processes.[215]

The Fe-phenanthroline complex supported within silica MCM-41 was found to be more active in benzyl alcohol oxidation than the unsupported complexes (Table 3.1.7.).[216] In fact the homogeneous catalyst obtained TON of 80 in benzyl alcohol oxidation with TBHP while in the presence of heterogeneous Fe-phenanthroline TON increased to 1041. Benzaldehyde was the only product observed with both neat and encapsulated complexes. Nanoparticles of iron oxides (Fe_2O_3) also showed high activities and selectivity in benzyl alcohol oxidation with hydrogen peroxide under mild reaction conditions.[215] Benzoic acid and benzyl benzoate were observed as side products (~3 mol%). Alcohols can also be smoothly oxidized to the corresponding aldehydes in the presence of Fe complexes containing triphenylphosphine ligand (Figure 3.1.13.) using H_2O_2 as oxidant. Benzyl alcohol was effectively and selectively oxidized to benzaldehyde with a high conversion of 80.1 mol%. [217]

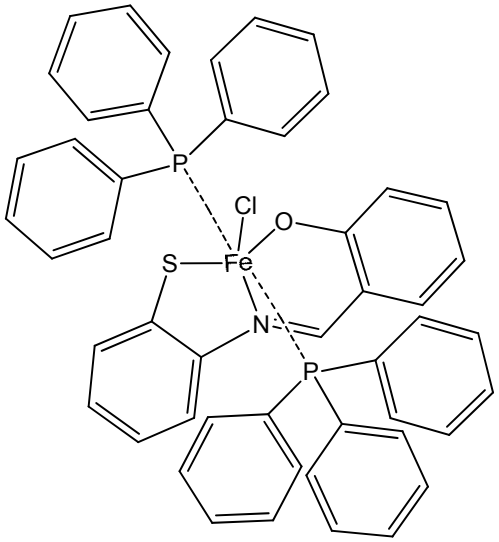

Figure 3.1.13. Representation of Fe-triphenylphosphine-*N*-(2-mercaptophenyl) salicyl-ideneimine complex.

Coordination polymers {with the formula of $[Fe(fcz)_2Cl_2]_2CH_3OH]n$, where fcz = 1-(2,4-difluorophenyl)-1,1-bis[(1*H*-1,2,4-triazol-l-yl)methyl]ethanol} containing iron ions also revealed promising catalytic activities in the oxidation of benzyl alcohol with H_2O_2 as the oxidant in aqueous medium.[218] This catalyst showed almost 100% selectivity towards benzaldehyde formation. Coordination polymers offer a variety of molecular structures and electronic properties that can be obtained by changing the metal ions, ligands, anions and coordination modes. Such diversity gives the opportunity to tune the electronic properties of the molecules that can result in enhanced catalytic activity as the success of metal complexes in catalysis is largely dependent on their structure and electronic properties. Every fcz ligand (Figure 3.1.14.) binds with two Fe^{II} ions, and each Fe^{II} ion is located at the centre of an elongated octahedron.

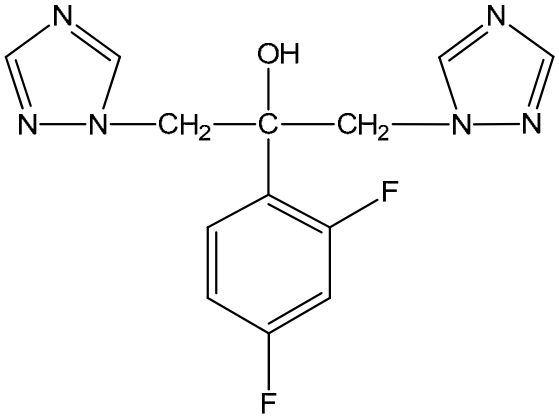

Figure 3.1.14. Representation of 1-(2,4-difluorophenyl)-1,1-bis[(1*H*-1,2,4-triazol-l-yl)methyl] ethanol) ligand.

Table 3.1.7. Catalytic performances of iron based catalysts in benzyl alcohol oxidation reactions.

Catalyst	Oxidant	Conversion (mol%)	Selectivity to benzaldehyde (mol%)	Ref.
Fe-phenanthroline	TBHP	7.1	99	[216]
Fe-phenanthroline-MCM-41	TBHP	35.0	99	
Nano Fe_2O_3	H_2O_2	33.0	97	[215]
Fe-triphenylphosphine-*N*-(2-mercaptophenyl) salicylidene –imine	H_2O_2	80.1	99	[217]
Fe coordination polymer	H_2O_2	87	99	[218]

Oxidation of organic substrates catalysed by heme and non-heme iron monooxygenases involves high-valent iron–oxo species that are the key intermediates. Oxidation reactions with oxoiron^{IV} porphyrin cation radicals like $[(tdcpp)^{\bullet+}Fe^{IV}=O]^{+}$ and $[(tmp)^{\bullet+}Fe^{IV}=O]^{+}$ and mononuclear non-heme oxoiron^{IV} complexes such as $[(tpa)Fe^{IV}=O]^{2+}$ (tpa=tris (2-pyridylmethyl)amine) and $[(N_4Py)Fe^{IV}=O]^{2+}$ (N_4Py=N,N-bis(2-pyridylmethyl)-N-bis(2-pyridyl)methylamine) were studied in detail in benzyl alcohol oxidation reactions (Figure 3.1.15.).[219] Heme and non-heme oxoiron intermediates activate alcohols by hydrogen atom abstraction. C-H bond cleavage is the rate-determining step.

The synthetic iron porphyrin model complexes were shown to catalyse efficiently alcohol oxidation to the carbonyl compounds *via* high-valent iron-oxo porphyrin intermediate $Por^{\bullet+}$- $Fe^{IV}=O$.[220]

The proposed oxidation mechanism (Scheme 3.1.11.), involves a common *gem*-diol intermediate formation and its dehydration to the carbonyl product. Pathway A utilizes direct insertion from the iron-oxo species into the C–H bond. Pathway B involves stepwise oxidation of the alcohol to hydroxy carbinyl radical *via* hydrogen-atom abstraction, followed by oxygen rebound.[221]

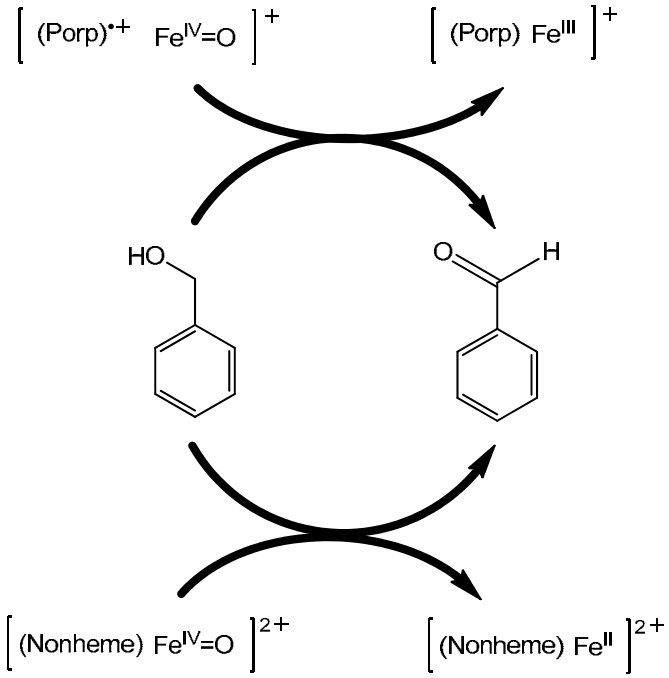

Figure 3.1.15. Oxidation of benzyl alcohol by heme and non-heme high-valent iron–oxo complexes.

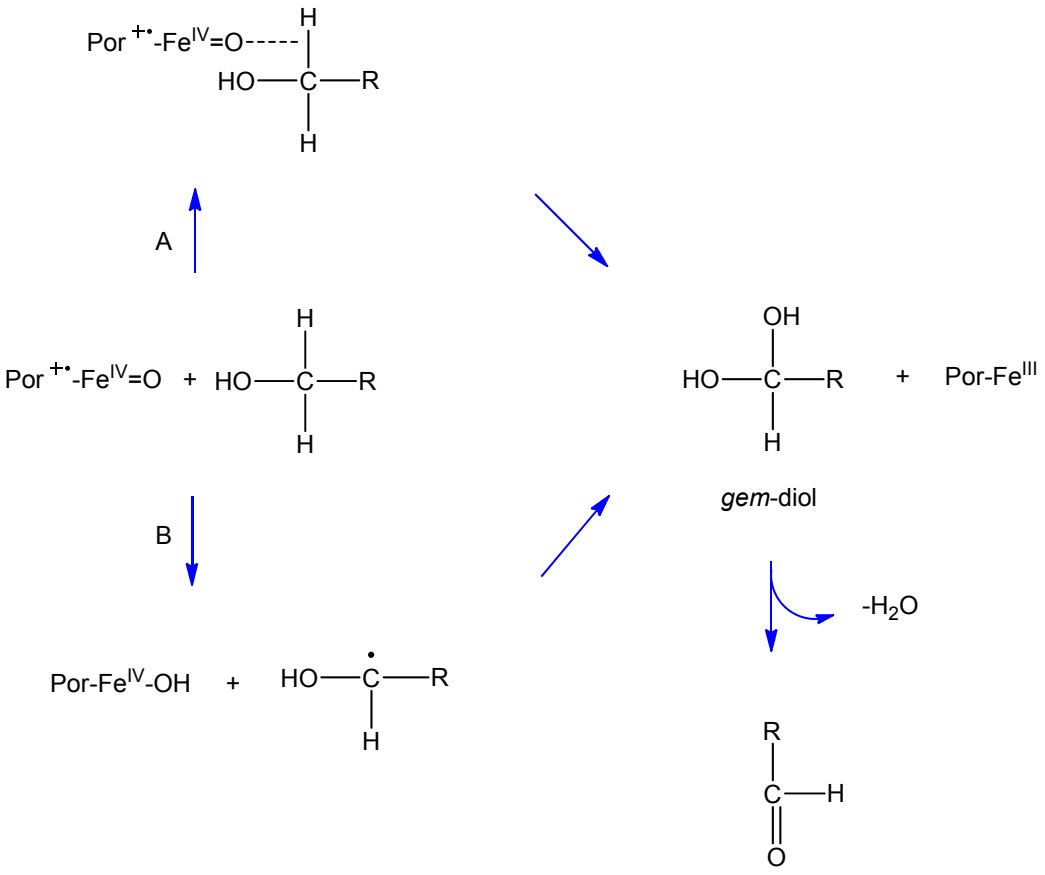

Scheme 3.1.11. Proposed mechanism for alcohol oxidation by the high-valent iron-oxo species $Por^{\bullet+}$- Fe^{IV}=O of synthetic Fe-porphyrin complex.[221]

In oxygenation of organic substrates catalysed by non-heme iron enzymes, iron^{IV} oxo intermediates were proposed as active oxidants. Iron^{III} hydroperoxo, iron^{III} alkylperoxo and iron^{V} oxo species were also proposed and investigated as active intermediates in oxidation reactions. Spectroscopic studies together with reactivity in oxidation reactions over mononuclear non-heme iron $[(TPA)Fe^{IV}=O]^{2+}$ and $[(TPA)Fe^{III}\text{-}OO\textit{t}Bu]^{2+}$ complexes showed that the iron^{III} alkylperoxo intermediate was not capable of oxygenating organic substrates and that a high-valent iron^{IV} oxo intermediate $[(TPA)Fe^{IV}=O]^{2+}$ generated through O-O bond homolysis of the Fe^{III}-OOR species was the active oxidant (Figure 3.1.16.). These results were also strongly supported by computational calculations, which showed that the energy barrier for O-O bond activation of Fe^{III}-OOR species was lower than that for direct oxygen-atom transfer from the intermediate to organic substrates.[222]

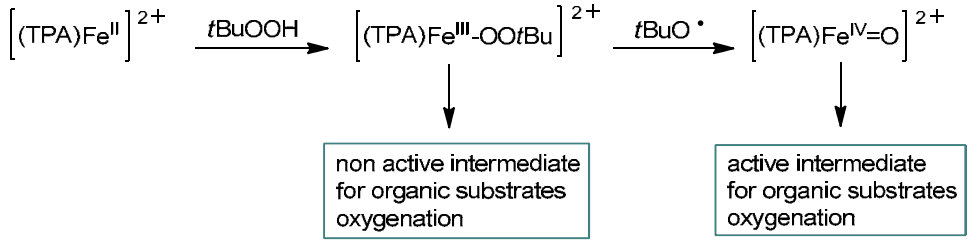

Figure 3.1.16. Iron^{III} alkylperoxo and active iron^{IV} oxo intermediates.[222]

Non-heme iron^{IV} oxo species proved to be capable of oxygenating organic substrates, such as alcohols, alkanes, alkenes and sulfides.[223, 224] This intermediate was characterized spectroscopically and its crystal structure was also reported. An iron^{V} oxo species was also proposed as the active oxidant for organic substrates oxidation. Recently the non-heme iron complex $[Fe^{II}(bqen)]^{2+}$ (bqen=N,N'-dimethyl-N,N'-bis(8-quinolyl) ethane-1,2-diamine) was reported.[225] This complex showed a high reactivity in alcohol and alkane oxidation with peracetic acid (CH_3CO_3H). Reactivity studies revealed that oxidation occurs by a hydrogen-atom abstraction mechanism but the active intermediate was different from the iron^{IV} oxo species, and an iron^{V} oxo intermediate was proposed to be the active oxidant. In the first step of this mechanism $[Fe^{II}(bqen)]^{2+}$ was oxidized by peracetic acid to $[Fe^{III}(bqen)]^{3+}$. Then in the reaction of $[Fe^{III}(bqen)]^{3+}$ with CH_3CO_3H, $[Fe^{III}(bqen)(OO(C=O)CH3)]^{2+}$ was generated. The heterolytic cleavage of O-O bond produced $[Fe^{V}=O(bqen)]^{3+}$. However this intermediate is unstable and undergoes one-electron reduction that leads to $[Fe^{IV}=O(bqen)]^{2+}$ formation. Other iron oxo species, like $[FeI^{V}(OH)_2(bqen)]^{2+}$ and $[FeI^{V}(O)(bqen)]^{2+}$ could also be plausible active intermediates.
The reactivity of iron (V) oxo intermediate $[Fe^{V}=O(bqen)]^{3+}$ was greater than that of iron^{IV} oxo intermediate $[Fe^{IV}=O(bqen)]^{2+}$ and the observed product distribution was also

different with these two intermediates. $[Fe^{V}=O(bqen)]^{3+}$ preferred the aromatic ring hydroxylation in the oxidation of benzyl alcohol, and $[Fe^{IV}=O(bqen)]^{2+}$ did not hydroxylate the aromatic ring of benzyl alcohol but oxidized benzyl alcohol to benzaldehyde (Scheme 3.1.12.).

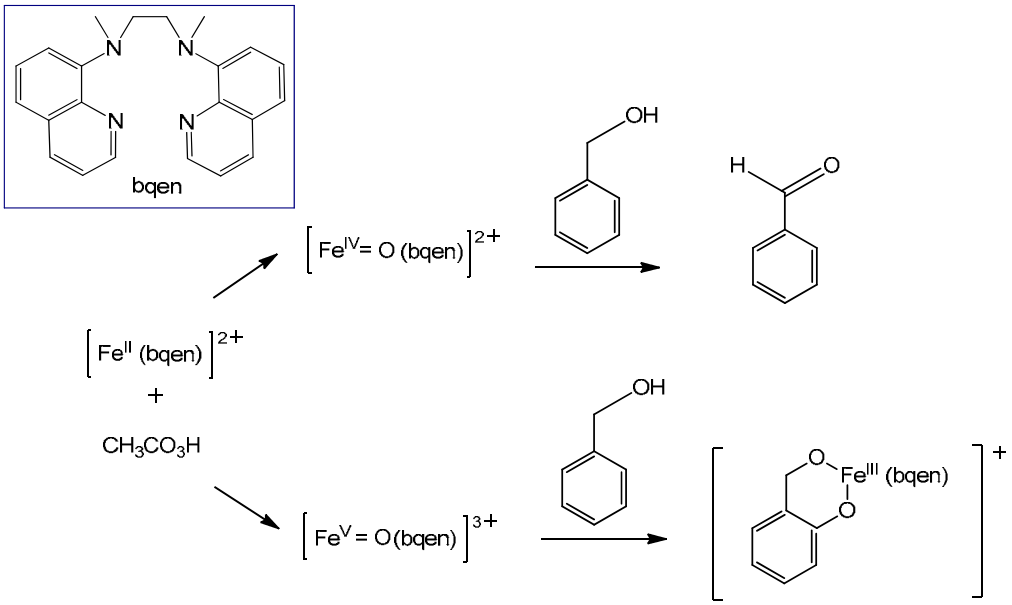

Scheme 3.1.12. Proposed reaction mechanisms of $[Fe^{II}(bqen)]^{2+}$.[225]

The mechanisms for alcohol oxidation by heme and non-heme oxoiron^{IV} intermediates, in which the oxidation of alcohol occurs *via* α-CH hydrogen atom abstraction followed by electron transfer, is shown in Figure 3.1.17. (pathway A). Benzaldehyde can be also formed by hydride transfer (Figure 3.1.17., pathway B).[219]

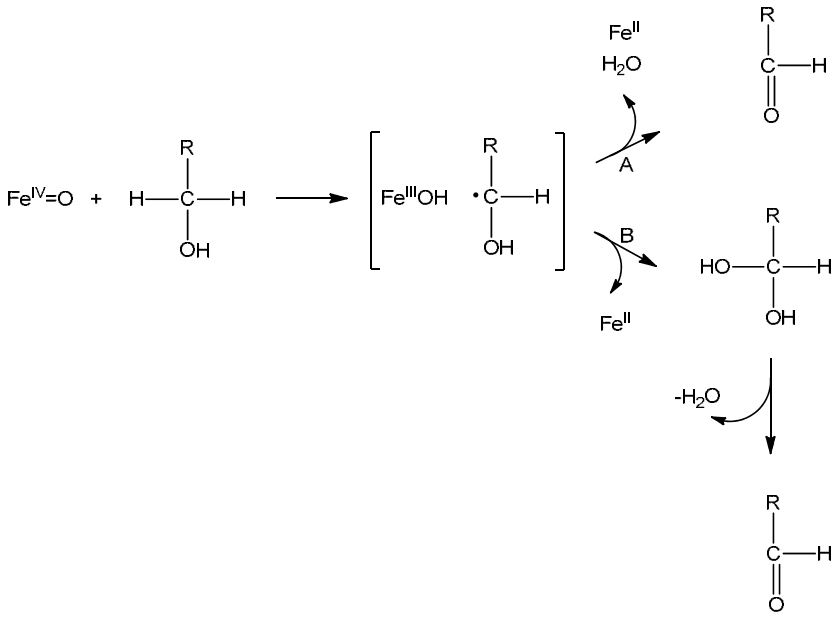

Figure 3.1.17. Proposed mechanism of benzyl alcohol oxidation with high-valent iron–oxo complexes.[219]

3.1.4. 2. Benzyl alcohol oxidation with Fe^{III}-Proline catalysts.

In order to exemplify further the role of isolated active sites, the activity of the neat Fe^{III}-Proline and encapsulated Fe^{III}-Proline-X complexes was evaluated in the oxidation of benzyl alcohol using air and TBHP as oxidants.

The results are summarized in Table 3.1.8. Fe^{III}-Proline based catalysts were >99mol% selective to benzaldehyde. A control experiment in the absence of catalyst gave conversions of 10.9 mol% with TBHP, and 6.5 mol% in the presence of air.

Table 3.1.8. Results on selective oxidation of benzyl alcohol with Fe^{III}-Proline catalysts. For reaction conditions see section 6.10.2.

Cat	Metal load.	Oxid.	Substrate: Metal ratio	Oxidant: Substrate ratio	TON	TOF (h^{-1})	Conv. mol %	Select. mol % bald.
Neat	16.9	AIR	581	1.65	319	53	54.3	>99
Neat	16.9	TBHP	581	1	386	64	65.1	>99
X	0.49	AIR	581	1.65	351	58	60.4	>99
X	0.49	TBHP	581	1	551	92	94.9	>99
Blanc	-	AIR	-	1.65	-	-	6.5	>99
Blanc	-	TBHP	-	1	-	-	10.9	>99

T=371 K, air 3.0 MPa, DMSO 35g, reaction time=6h, bald=benzaldehyde.

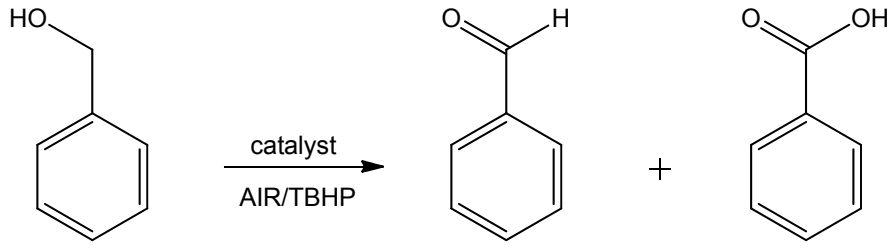

Scheme 3.1.13. Schematic representation of product formation in benzyl alcohol (A) oxidation to benzaldehyde (B) and benzoic acid (C).

Homogeneous Fe^{III}-Proline and heterogeneous Fe^{III}-Proline-X catalysts showed to be more efficient with TBHP as an oxidant affording conversions of 65.1 mol% and 94.9 mol%, respectively. When air was used these catalysts reached conversions of 54.3 mol% and 60.4 mol%. Heterogenisation of Fe^{III}-Proline complex within zeolite X resulted in increased

values of TON and TOF with both oxidants. In fact, TON and TOF increased from 386 and 64 h^{-1} for neat Fe^{III}-Proline to 551 and 92 h^{-1} for Fe^{III}-Proline-X with TBHP. When air was employed, TON and TOF increased from 319 and 53 h^{-1} (neat Fe^{III}-Proline) to 351 and 58 h^{-1} (Fe^{III}-Proline-X). A comparison of TON and TOF is presented in Figure 3.1.18.

These results further highlight the role of the isolated active centres in the encapsulated, heterogeneous analogue and suggests that these sites are the loci where the catalysis ensues. It is clear that both higher conversions and TONs/TOFs can be achieved by encapsulation of homogeneous Fe^{III}-Proline catalyst within zeolite X cages. The selectivity to benzaldehyde was always >99 mol% and appeared to be independent from both the nature of oxidant and support. However a small quantities of benzoic acid could also be adsorbed on the catalyst.

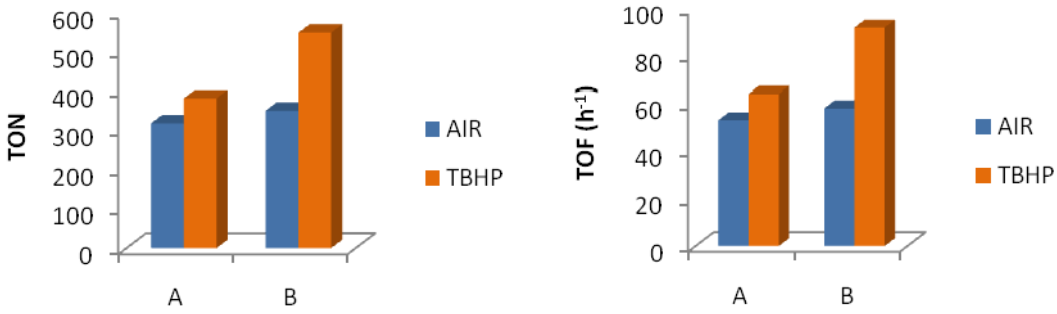

Figure 3.1.18. Comparison of TOF (right) and TON (left) in the oxidation of benzyl alcohol using homogeneous Fe^{III}-Proline (A) and heterogeneous Fe^{III}-Proline-X (B) catalysts with air and TBHP.

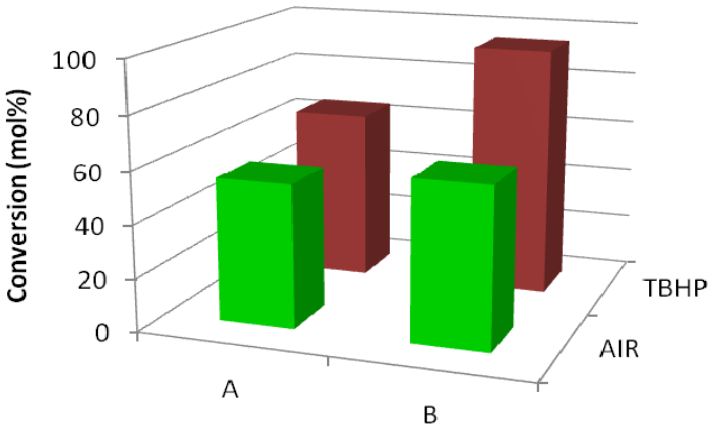

Figure 3.1.19. Comparison of conversions in benzyl alcohol oxidation using Fe^{III}-Proline (A) and Fe^{III}-Proline -X (B) with air and TBHP.

Catalyst recycling. To investigate catalyst reusability, benzyl alcohol oxidation with air was studied with Fe^{III}-Proline-X catalyst. At the end of the first run, the catalyst was separated by filtration, washed with DMSO and acetonitrile and dried in air at 80 °C. The catalyst was then retested for benzyl alcohol oxidation and preliminary results on catalyst recycling seem to be reasonable, however detailed studies involving higher numbers of recycling cycles and characterization of the reused catalysts are required. The high selectivity to benzaldehyde was unaffected. Comparison of TON and selectivity using fresh and reused catalysts is presented in Figure 3.1.20.

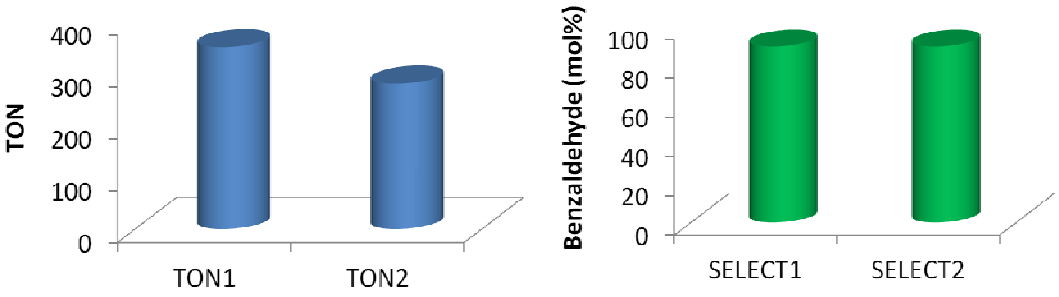

Figure 3.1.20. Comparison of turnover number (TON) and selectivity (SELECT) in the oxidation of benzyl alcohol using Fe^{III}-Proline-X with air, t=4h, TON1, SELCT1 catalysed by fresh catalyst, TON2, SELCT2 catalysed by reused catalyst.

Summary.

A natural amino acid proline complex with iron was synthesized and encapsulated within the cages of Zeolite X. These materials were characterized by IR, DRUV-Vis, EPR, XRD, ICP, elemental CHN analysis and N_2 BET analysis for the purposes of structure and integrity determination. The resulting materials were employed as catalysts for the selective oxidation of cyclohexane and benzyl alcohol using air and *tert*-butyl hydroperoxide as the oxidants. The heterogeneous Fe^{III}-Proline-X catalyst obtained significantly higher TON and TOF when compared with homogeneous Fe^{III}-Proline analogue. This indicates good separation of the active iron sites which is the key factor leading to enhanced catalytic activities of heterogeneous Fe^{III}-Proline-X catalyst.

3.2. Synthesis, characterisation and catalytic potential of Cu^{II}-Valine, Cu^{II}-Valine-LTA, Cu^{II}-Valine-MCM-41 and Cu^{II}-Valine-Polystyrene.

3.2.1. Synthesis of neat Cu^{II}-Valine complex and its encapsulation in zeolite LTA.

Cu^{II}-Valine. The Cu^{II}-Valine complex was prepared following the procedure described by Szabó-Plánka that employs NaOH as a base to obtain the deprotonated form of valine (COO^-, NH_2), which is then ready to coordinate to copper ion.[226] This procedure involves reaction of 2 eq. of valine with 1 eq. of copper sulfate pentahydrate to form a five-membered chelate ring, with a metal:valine ratio of 1:2. This synthesis was carried out in water as valine is soluble in water (the synthetic route is shown in section 6.2.2.).

Cu^{II}-Valine-LTA. Encapsulation of Cu^{II}-Valine within zeolitic framework was performed using the zeolite synthesis method, in which the zeolite was synthesised in the presence of preformed Cu^{II}-Valine metal complexes.[125] This synthesis was carried out under the same conditions and using the same gel composition as described for Fe^{III}-Proline encapsulation within Zeolite X (section 6.3.2.). However, the XRD pattern revealed Zeolite LTA formation instead of zeolite X around the Cu^{II}-Valine complex. Zeolite LTA formation could be explained by the fact that valine is more linear than proline (due to rigid pyrrolidine ring). Cu^{II}-Valine as more linear complex could be located between the two neighbouring sodalite cages of Zeolite LTA and this could stop further zeolite crystallization and large cavity FAU formation (sodalite cages are also the building blocks of Zeolite X). Fe^{III}-Proline complex, being more rigid, prefers to be located in the larger cage as FAU cage rather than in interconnecting cavity. The pore diameter of Zeolite LTA is defined by an 8 membered oxygen ring and its diameter is 4.2 Å, while the Zeolite X pore diameter is much larger at 7.4Å, and the aperture is defined by a 12 membered oxygen ring (Figure 3.2.1.).[227, 228] Formation of Zeolite LTA around a Cu^{II}-Valine complex disabled this material as catalyst in oxidation of target molecules due to the pore size not being large enough for substrate/product molecules to enter/exit. For these reasons the Cu^{II}-Valine complex was heterogenized by immobilization on MCM-41 and polystyrene supports.

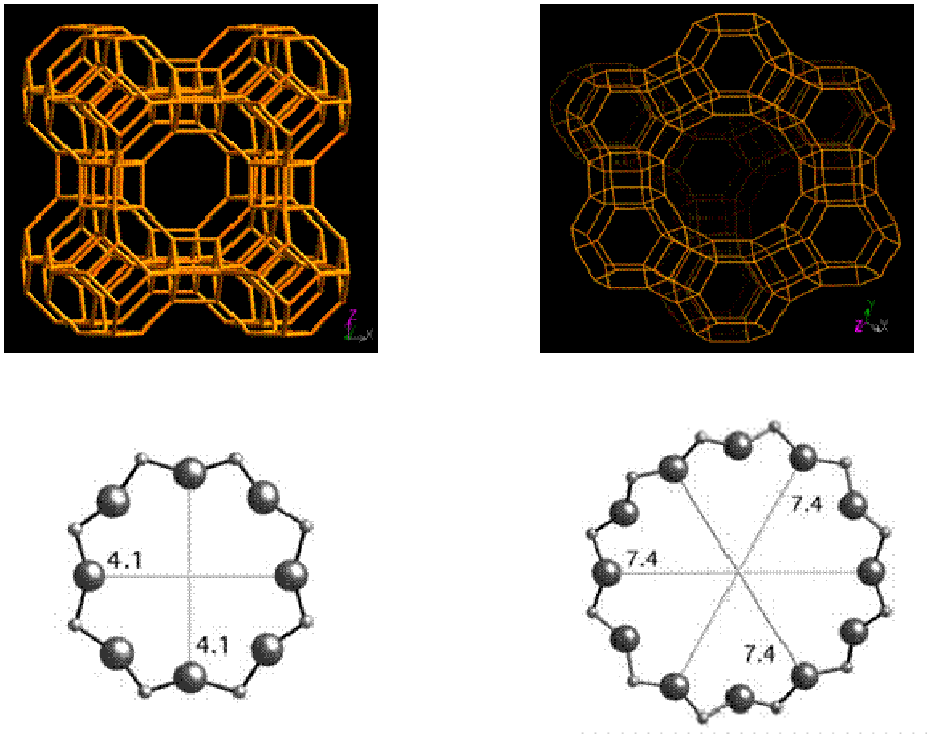

Figure 3.2.1. Comparison of Zeolite LTA (left) with 8-ring view and Zeolite X (right) with 12-ring view.

3.2.2. Synthesis of MCM-41 and Polystyrene immobilized Cu^{II}-Valine complex.

MCM-41 functionalisation. Prior to functionalisation with the valine ligand, the surface of silica was first functionalized with a mixture of chloropropyl and methyl groups (Scheme 3.2.1.). [150, 229] The presence of methyl groups not only enhances the hydrophobicity of the silica but also enhances its hydrothermal stability, when compared with materials functionalized with chloropropyl groups alone.[149] This grafting methodology with an adjustable amount of active chloropropyl species on the surface allowed the control of the chloropropyl groups loading. This is important for application of these materials as supports for the immobilization of metal complexes and applications where a defined chemical environment on the surface is more important than the high number of functional groups, which is usually the case in heterogeneous catalysis.

Before the functionalization procedure the MCM-41 was treated in water, followed by azeotropic distillation in toluene. Next both silanes were added to the support dispersion in toluene. The solid material was filtered and redispersed in fresh toluene for the final refluxing. The initial water treatment was performed to generate silanol groups on the silica surface by hydrolyzing siloxane groups on the surface of the calcined MCM-41. Azeotropic distillation was performed to remove excess water. A small amount of water

should remain in the pores to hydrolyze the alkoxysilanes. If azeotropic distillation is not performed then too much water is left in the mesopores and this can cause an oligomerization of the silanes and pore blocking. Both silanes were added to silica after the azeotropic distillation and intermediate filtration was performed to remove unreacted silanes. The final refluxing step was considered to strengthen further the already bound silane species by condensation of unreacted –OH or $–OCH_3$ groups. If the intermediate filtration was omitted, H_2O which is formed during the condensation of –OH groups would cause an oligomerization of unreacted silanes and cause pore blocking.

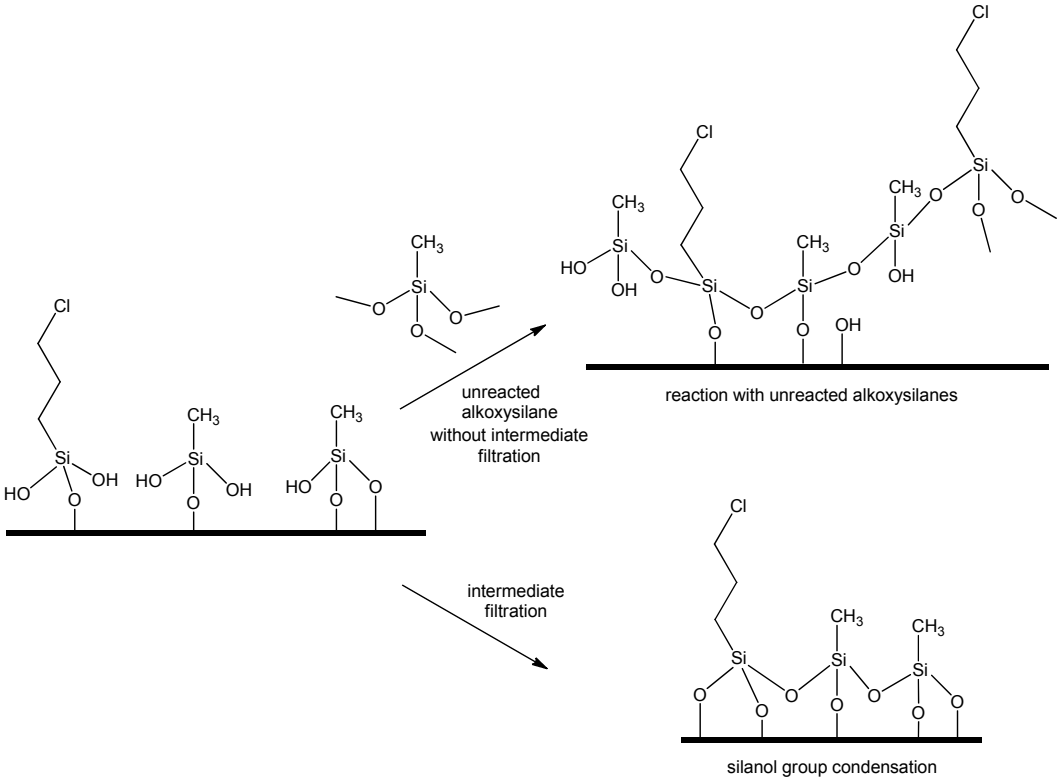

Scheme 3.2.1. Role of filtration and redispersion in fresh toluene for functionalizing the silica surface with alkoxysilanes.[150]

MCM-41 functionalisation with Cu^{II}-Valine. Valine was immobilised on chloropropyl and methyl functionalised MCM-41 in a direct single-step reaction.[168] This procedure employed pyridine as a base under reflux conditions in aqueous ethanol media. The reaction of the amino acid with stoichiometric amounts of pyridine in an aqueous medium leads to desired grafting by facilitating elimination of HCl as the pyridine hydrochloride salt. The procedure for Cu^{II}-Valine complex formation employed NaOH as a base to obtain the deprotonated form of valine (COO^-, NH_2) that was then ready to coordinate to copper ion (the synthetic route is shown in section 6.7.).

Polystyrene functionalisation with Cu^{II}-Valine. The Cu^{II}-Valine complex was immobilised on chloromethylated polystyrene employing the same strategy as for Cu^{II}-Valine immobilization on MCM-41 (the synthetic route is shown in section 6.8.).

3.2.3. Characterization of Cu^{II}-Valine, Cu^{II}-Valine-LTA, Cu^{II}-Valine -MCM-41, Cu^{II}-Valine-Polystyrene.

3.2.3.1. Single crystal X-ray diffraction (SCXRD).

The single crystal X-ray diffraction structure confirmed formation of a chelate ring through the amino and carboxylate groups of valine and the square planar coordination of the central copper ion (Figure 3.2.2.). A carboxyl O-atom and the amino N-atom from each valine ligand coordinate to the metal centre in a *trans* square planar arrangement. The crystal structure also revealed long range interactions between Cu and two distant oxygen atoms from neighboring valine molecules. Recently reported crystal structures of Cu^{II}-Asparagine and Cu^{II}-Glutamine showed similar square planar coordination and long range interactions with amide O-atoms from neighbouring amino acid molecules.[226] Bond lengths and angles of the Cu^{II}-Valine complex are listed in Table 3.2.1.

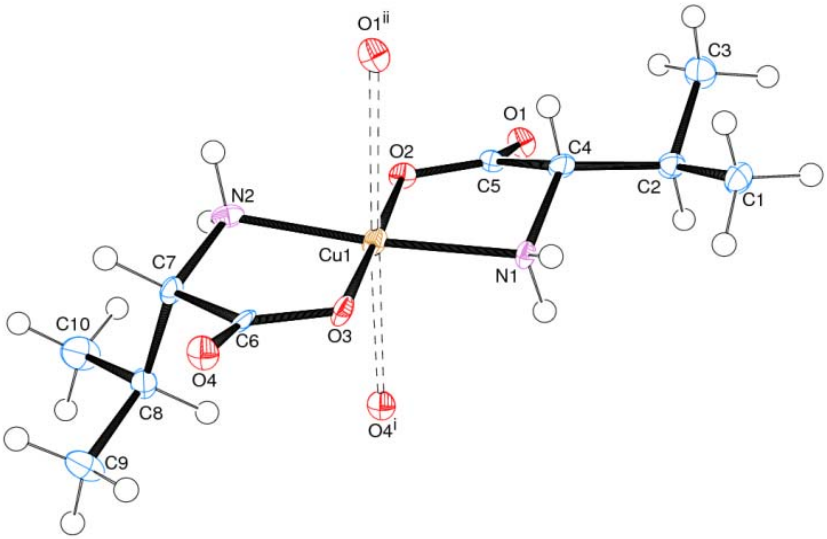

Figure 3.2.2. Crystal structure of Cu^{II}-Valine complex. Thermal ellipsoids are drawn at 50% probability level. Symmetry codes: (i) x-1, y, z ; (ii) x+1, y, z.

Table 3.2.1. Bond lengths [Å] and angles [deg] of Cu^{II}-Valine complex.

Bond lengths [Å].		Bond angles [deg].	
Cu(1)-O(3)	1.930(5)	O(3)-Cu(1)-O(2)	178.5(2)
Cu(1)-O(2)	1.948(4)	O(3)-Cu(1)-N(2)	83.4(2)
Cu(1)-N(2)	1.984(5)	O(2)-Cu(1)-N(2)	95.98(19)
Cu(1)-N(1)	2.010(5)	O(3)-Cu(1)-N(1)	96.73(18)
O(1)-C(5)	1.250(8)	O(2)-Cu(1)-N(1)	83.7(2)
O(2)-C(5)	1.292(7)	N(2)-Cu(1)-N(1)	174.5(2)
O(3)-C(6)	1.282(7)	C(5)-O(2)-Cu(1)	113.3(4)
O(4)-C(6)	1.224(8)	C(6)-O(3)-Cu(1)	116.9(4)
N(1)-C(4)	1.498(7)	C(4)-N(1)-Cu(1)	104.9(3)
N(2)-C(7)	1.470(7)	C(7)-N(2)-Cu(1)	109.1(3)
C(1)-C(2)	1.538(5)	C(4)-C(2)-C(3)	111.8(3)
C(2)-C(4)	1.527(6)	C(4)-C(2)-C(1)	109.7(3)
C(2)-C(3)	1.528(5)	C(3)-C(2)-C(1)	108.4(3)
C(4)-C(5)	1.540(8)	N(1)-C(4)-C(2)	115.2(4)
C(6)-C(7)	1.552(8)	N(1)-C(4)-C(5)	103.7(5)
C(7)-C(8)	1.536(6)	C(2)-C(4)-C(5)	117.2(5)
C(8)-C(9)	1.529(5)	O(1)-C(5)-O(2)	122.9(6)
C(8)-C(10)	1.533(5)	O(1)-C(5)-C(4)	121.5(5)
		O(2)-C(5)-C(4)	115.6(5)
		O(4)-C(6)-O(3)	124.6(6)
		O(4)-C(6)-C(7)	120.8(5)
		O(3)-C(6)-C(7)	114.6(6)
		N(2)-C(7)-C(8)	113.0(4)
		N(2)-C(7)-C(6)	107.3(5)
		C(8)-C(7)-C(6)	110.5(4)
		C(9)-C(8)-C(10)	108.3(3)
		C(9)-C(8)-C(7)	112.0(4)
		C(10)-C(8)-C(7)	111.0(3)

3.2.3.2. FTIR characterization of Cu^{II}-Valine and Cu^{II}-Valine-LTA.

The obtained Cu^{II}-Valine complex was characterized by IR spectroscopy and analyzed in comparison with the spectra of the free ligand and cross-checked with literature data.[226, 230, 231] The IR spectrum of the Cu^{II}-Valine complex showed changes in the positions and the profiles of some bands, as compared with those of the free valine ligand (Table 3.2.2.).The NH_2 stretching bands of valine were observed at 3050 cm^{-1}. As it was expected, these bands were shifted in the spectrum of the Cu^{II}-Valine complex which suggests coordination through the NH_2 group. The peaks at 3267 and 3156 cm^{-1} can be assigned as $\nu_{as\ NH}$ and $\nu_{s\ NH}$ modes.

In general, the neutral molecular form of a carboxylic acid has vibrations specifically due to the stretches of the carbonyl C=O group around 1790 cm^{-1} and does not exhibit vibrations due to the carboxylate COO^- group. This result indicates that the carboxylic group was not protonated in the complex, otherwise, a strong band at about 1790 cm^{-1} should have been observed. The carboxylate ion group absorbs strongly near 1600 cm^{-1} and more weakly near 1400 cm^{-1} because of the antisymmetric and symmetric stretching modes, respectively. For the valine ligand $\nu_{as\ COO^-}$ and $\nu_{s\ COO^-}$ are observed at 1563 cm^{-1} and 1407 cm^{-1}, respectively. In the Cu^{II}-Valine complex the peak at 1613 cm^{-1} is assigned to COO^- antisymmetric stretching and the peak at 1370 cm^{-1} is assigned to COO^- symmetric stretching. The antisymmetric carboxylate COO^- stretching band usually overlaps due to the NH_2 scissoring vibrations. The bands at 2982 cm^{-1}, 2876 cm^{-1} and 2776 cm^{-1} are assigned to the C-H stretching.

The FTIR spectrum of Cu^{II}-Valine encapsulated within zeolite LTA (Figure. 3.2.3., along with the assignments for the various bands) provides spectroscopic information on the nature and structural integrity of the encapsulated amino acid ligand. Most revealing signals were those related to the carboxyl and the amino groups, since they distinctly change in the molecular, cationic, anionic and zwitterionic forms. The presence of a strong band at 1633 cm^{-1} for Cu^{II}-Valine-A and 1644 cm^{-1} for neat Cu^{II}-Valine, coupled with the absence of signal around 1790 cm^{-1}, which is typical of the COOH species, confirm that the carboxyl group is deprotonated. The carboxylate ions can be characterized by an antisymmetric ($\nu_{as\ COO^-}$) and a symmetric stretching mode ($\nu_{s\ COO^-}$), around 1650 and 1400 cm^{-1}, respectively. However, in this case, only the high frequency component is observed, strongly suggesting that the carboxylate group is involved in the binding to the metal ion.

The main differences between the spectra of neat and encapsulated Cu^{II}-Valine involve N-H vibrations, which suggests that this group is also interacting with the zeolite surface, probably acting as acceptor in hydrogen bonding interactions. In Cu^{II}-Valine-LTA, these bands can readily be superimposed to a broad signal in the 3700 – 2800 cm^{-1} interval, which can be attributed to the hydrogen bonding between valine and zeolite. Recent IR studies showed that amines strongly interact with the surface *via* hydrogen bonding or *via* the formation of ion-pair complexes Si-O$^{\cdots}NH_3^+$-R.[150] Two broad N-H stretching bands above 3000 cm^{-1}, and a very broad and intense feature between 3000 and 2000 cm^{-1}, is caused by stretching vibrations of H-bonded NH_2 and NH_3^+ groups. Some bands related to ν_{O-H} modes of unperturbed isolated Si-OH (3743 cm^{-1}) and slightly perturbed water molecules (3700 – 3500 cm^{-1} range) are also seen in the encapsulated system (corresponding δ_{O-H} expected around 1630 cm^{-1}, superimposed to the $\nu_{as\ COO^-}$). The IR spectrum of zeolite LTA is shown for comparison in Figure 3.2.4., revealing only weak IR modes in the ν_{O-H} region at 3686 and 3650 cm^{-1}, assigned to a small amount of defective Al-OH and Brønsted Si(OH)Al groups, respectively.[232]

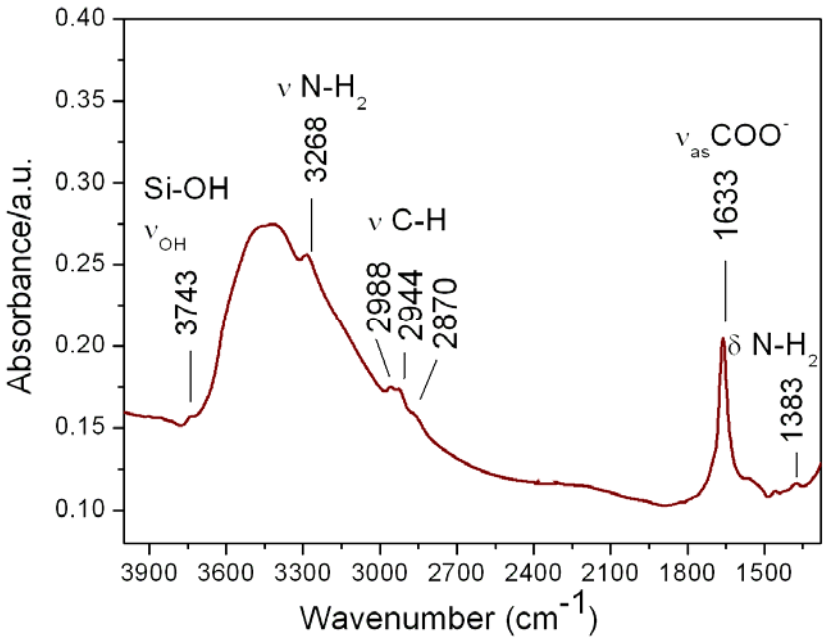

Figure 3.2.3. FT-IR spectrum of Cu^{II}-Valine-LTA showing the presence of a strong band at 1633 cm^{-1}, confirming deprotonation of carboxyl group (COO^-) and band at 3268 cm^{-1} due to NH_2 vibrations.

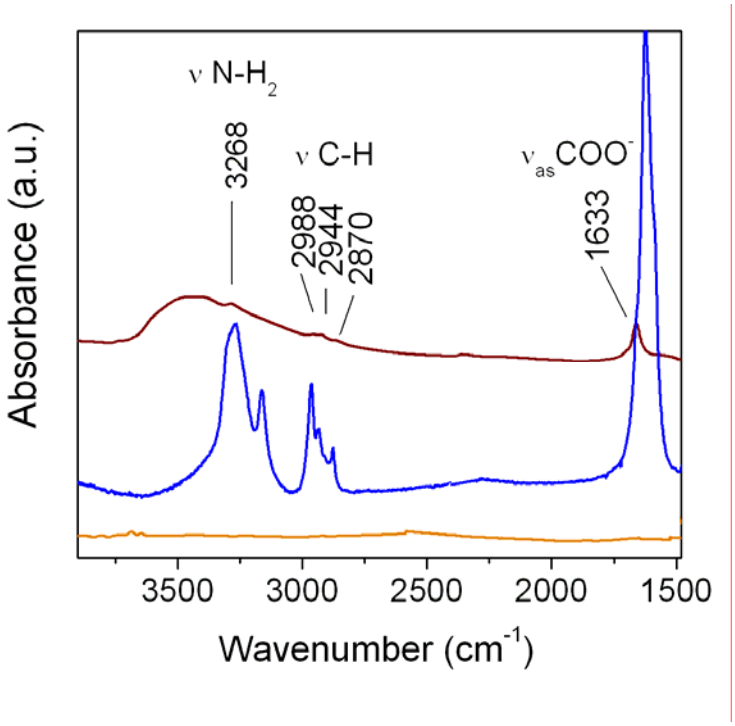

Figure 3.2.4. Comparison of FTIR spectra of Cu^{II}-Valine-LTA (brown), Cu^{II}-Valine (blue), Zeolite LTA (orange) outgassed at 343K. The assignments of the vibrations are indicated in this figure.

3.2.3.3. XRD analysis.

XRD patterns Cu^{II}-Valine-LTA revealed Zeolite LTA formation around the Cu^{II}-Valine complex. Patterns of Cu^{II}-Valine encapsulated within zeolite LTA (Figure 3.2.5.) are in good agreement with patterns reported for the neat zeolite LTA.[233] The presence of well-resolved peaks with no phase impurities indicates that the correct architecture is structurally unaltered after the encapsulation procedure. The absence of additional structural reflections due to the neat Cu^{II}-Valine complex revealed its dispersion predominantly within the internal cages, not on the external surface.

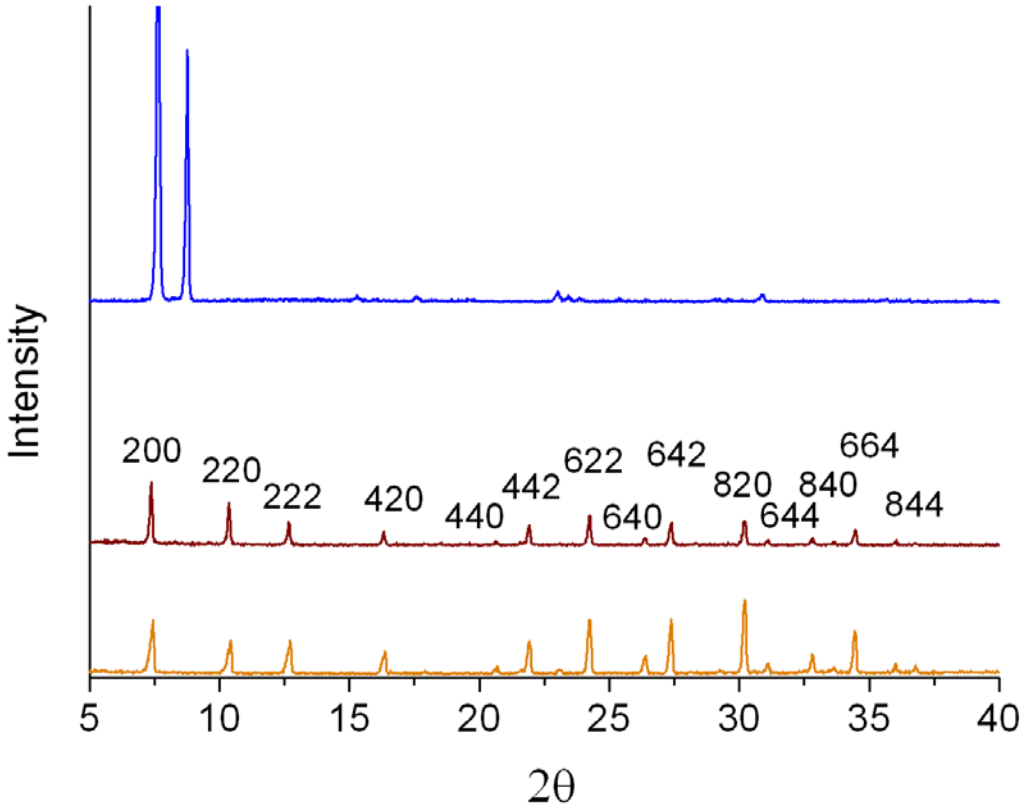

Figure 3.2.5. Comparison of XRD patterns of Cu^{II}-Valine (blue), Cu^{II}-Valine-LTA (brown), Zeolite LTA (orange). Scan rate 12°min., step size 0.02°.

XRD patterns of neat MCM-41 confirmed hexagonal order and a high crystallinity of silica MCM-41 which is indicated by the presence of *d*100, *d*110, and *d*200 reflections (Figure 3.2.6.). The XRD of MCM-41 displays a *d*100 spacing of =4.8 nm, which is similar to that reported in literature for other MCM-41 prepared with hexadecyl-trimethylammonium bromide (CTAB) and the 'silicate surfactant lyotropic liquid crystal' method (*d*100 spacing of =4.9 nm).[234, 235] XRD patterns of MCM-41 exhibit strong *d*100 reflection and several low-order weak reflections that are associated with hexagonal symmetry of the lattice and are usually observed in mesoporous material such as HMS, MCM-41 and FSM. Cu^{II}-Valine -MCM-41 materials revealed the broadening of the peaks of the *d*100 reflection probably due to reduction of the order of silanol Si-OH groups and the decrease of the crystallite mosaic size. The decrease in the intensity of the 100 reflection peak may be assigned to the partial structure deformation of the ordered hexagonal phase, or the flexibility of the silica framework resulting from the strain of the incorporated metal complexes.[236 135, 237]

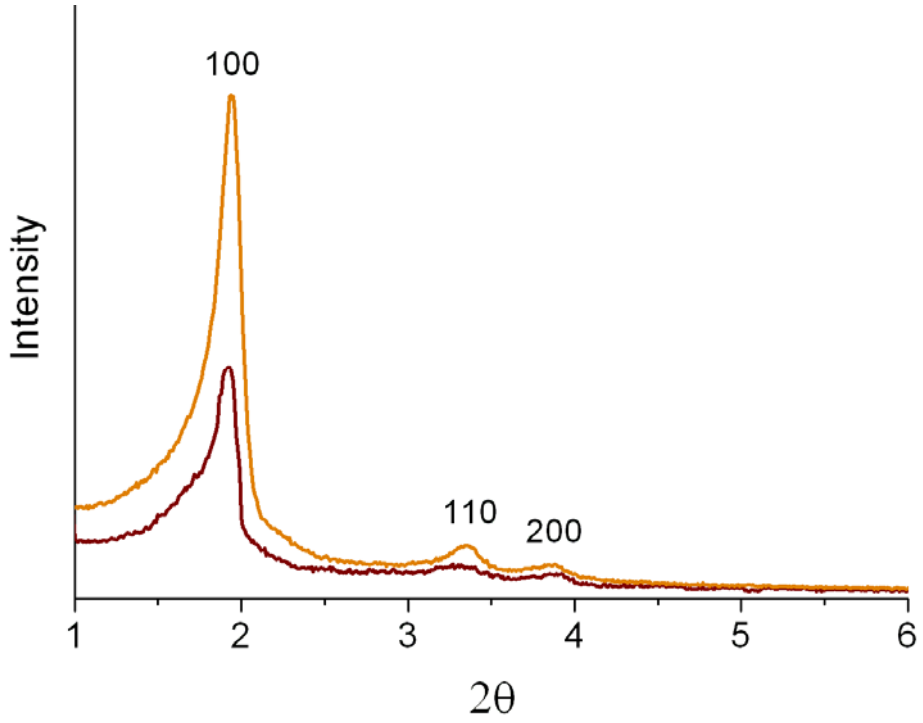

Figure 3.2.6. Comparison of XRD patterns of Cu^{II}-Valine-MCM-41 (brown) and MCM-41 (orange).

3.2.3.4. FTIR characterization of Cu^{II}-Valine-MCM-41 and Cu^{II}-Valine-Polystyrene.

The structural features of immobilized Cu^{II}-Valine complexes was investigated by IR spectroscopy and compared with that of neat Cu^{II}-Valine complex.[238, 239] For the neat Cu^{II}-Valine complex, the typical C-H stretching (ν) modes of valine were seen at 2964 ($\nu_{as\ CH}$), 2919 ($\nu_{\ CH}$) and 2862 cm^{-1} ($\nu_{s\ CH}$). The presence of strong bands at 3267 and 3156 cm^{-1} can be assigned as $\nu_{as\ NH}$ and $\nu_{s\ NH}$ modes, respectively, and the corresponding bending (δ) mode at 1584 cm^{-1} was also observed. Bands in the COOH region at around 1800 cm^{-1} were not observed, confirming deprotonation of the carboxylic acid group. This is in agreement with the presence of bands at 1623 and 1375 cm^{-1} in the low energy range, assigned to ν_{as} and ν_s modes, of carboxylate ions interacting with the metal ions.

As for the Cu^{II}-Valine -MCM-41 complex, the $\nu_{\ N-H}$ and $\nu_{\ C-H}$ modes of valine are very weak, being superimposed to a strong and broad adsorption due to hydrogen bonded Si-OH species. However, in the low energy region the bands due to the valine carboxylate (ν_{as} and ν_s at 1635 and 1375 cm^{-1}) and amino groups ($\delta_{\ NH}$ at 1595 cm^{-1}) are evident, superimposed to the overtones and combination modes of the silica support. The shift with respect to the neat complex suggests an influence of the support (probably through surface Si-OH groups)

on the ligand-metal interaction. This was probably due to strong interactions with the silica surface *via* hydrogen bonding or *via* the formation of ion-pair complexes Si-O$^{\cdots}$NH$_3^+$-R. These two broad N-H stretching bands above 3000 cm^{-1}, and a very broad and intense feature between 3000 and 2000 cm^{-1}, was caused by stretching vibrations of H-bonded NH_2 and NH_3^+ groups (assignment is shown in Figure 3.2.7.).

The IR spectrum of the Cu^{II}-Valine-Polystyrene was complicated by the intense vibrational modes of the polystyrene matrix: the typical aromatic and aliphatic $\nu_{C\text{-}H}$ modes (3100 – 3000 and 3000 – 2800 cm^{-1} ranges, respectively), the corresponding $\delta_{C\text{-}H}$ overtones, ν aromatic ring and fingerprint modes in the low energy range (detailed assignment is shown in Figure 3.2.8.). Additional bands were clearly seen at 3572 and 3310 cm^{-1} ($\nu_{O\text{-}H}$ and $\nu_{N\text{-}H}$, respectively, superimposed to a broad absorption due to hydrogen bonding) and 1630 cm^{-1} assigned to $\nu_{as\ COO^-}$. The $\nu_{O\text{-}H}$ modes could be assigned to the carboxylic group of a protonated unreacted valine molecule. The $\nu_{N\text{-}H}$ band at 3310 cm^{-1} could be related to a valine molecule covalently bonded to the matrix, while that at 1630 cm^{-1} (ν_{asCOO^-}) testifies of a carboxylate group interacting with the copper metal ion.

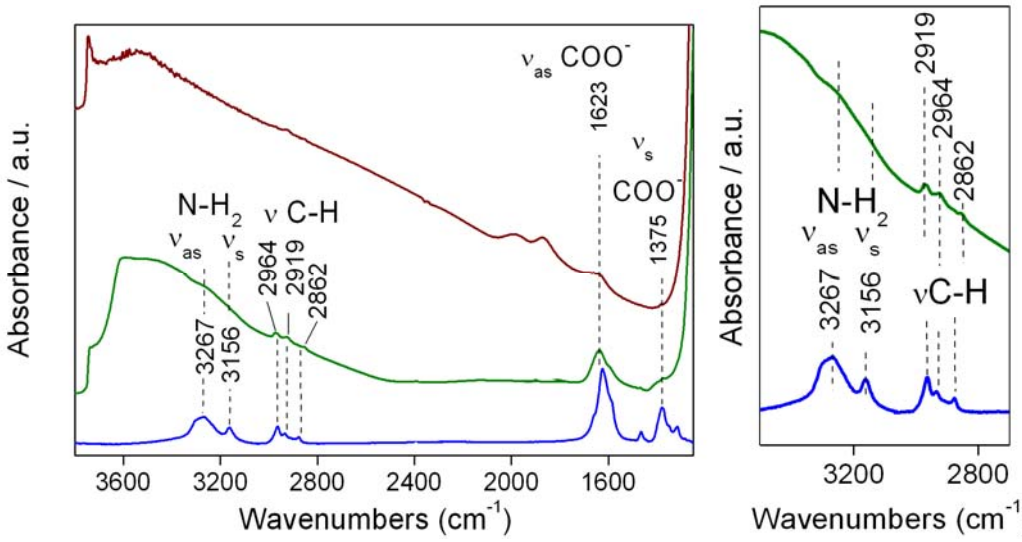

Figure 3.2.7. FTIR spectra of Cu^{II}-Valine (blue), Cu^{II}-Valine -MCM-41 (green), MCM-41 (brown) (left) and NH_2 and CH region of Cu^{II}-Valine (blue), Cu^{II}-Valine-MCM-41 (green) for easier comparison (right). Spectra were arbitrarily normalized and vertically shifted for easier comparison.

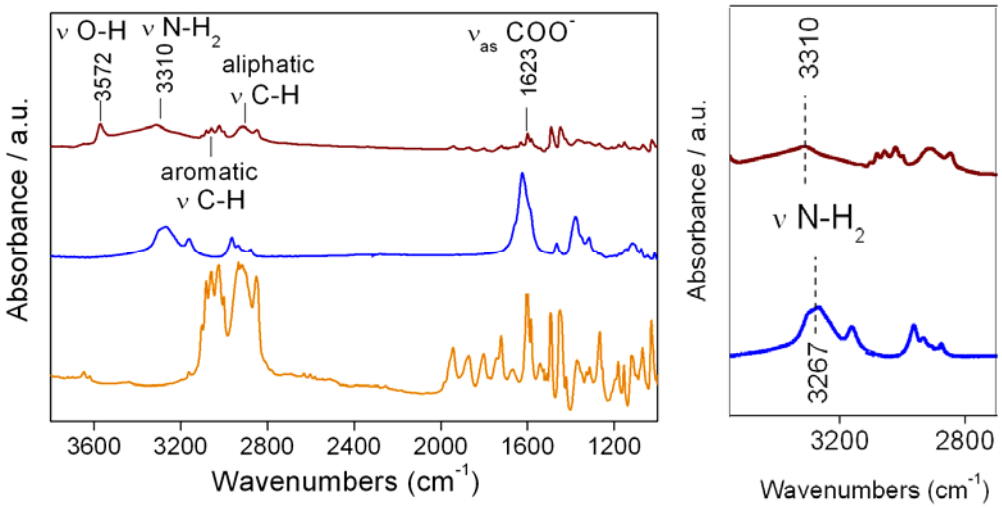

Figure 3.2.8. Comparison of IR spectra of Cu^{II}-Valine (blue), Cu^{II}-Valine-Polystyrene (brown), Polystyrene (orange) on the left and NH_2 region of Cu^{II}-Valine (blue), Cu^{II}-Valine-Polystyrene (brown) for easier comparison (right). Spectra were arbitrarily normalized and vertically shifted for easier comparison.

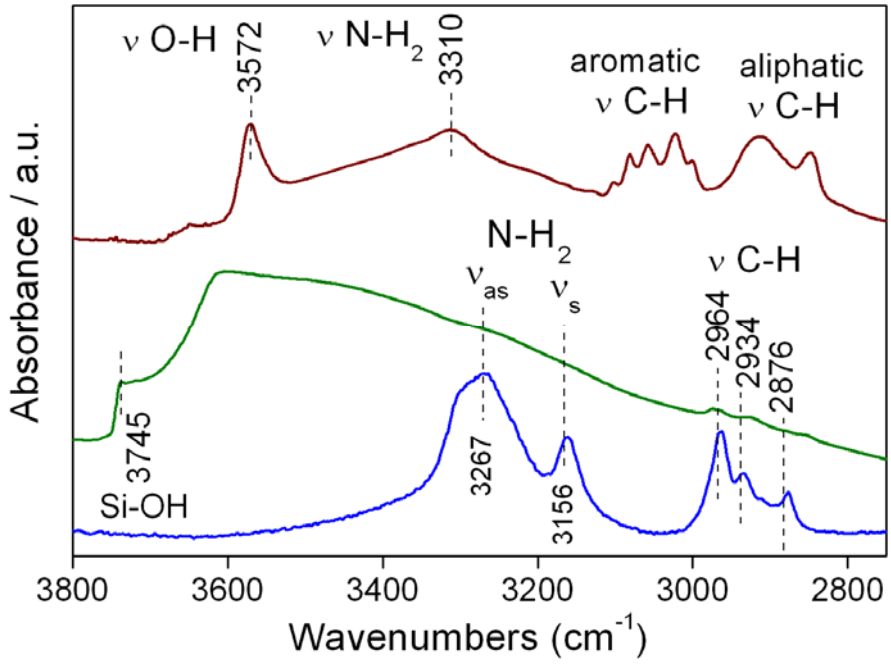

Figure 3.2.9. Comparison of IR spectra of Cu^{II}-Valine (blue), Cu^{II}-Valine-MCM-41 (green), Cu^{II}-Valine-Polystyrene (brown) in the low energy range (3800 – 2800 cm^{-1}). Spectra were arbitrarily normalized and vertically shifted for easier comparison.

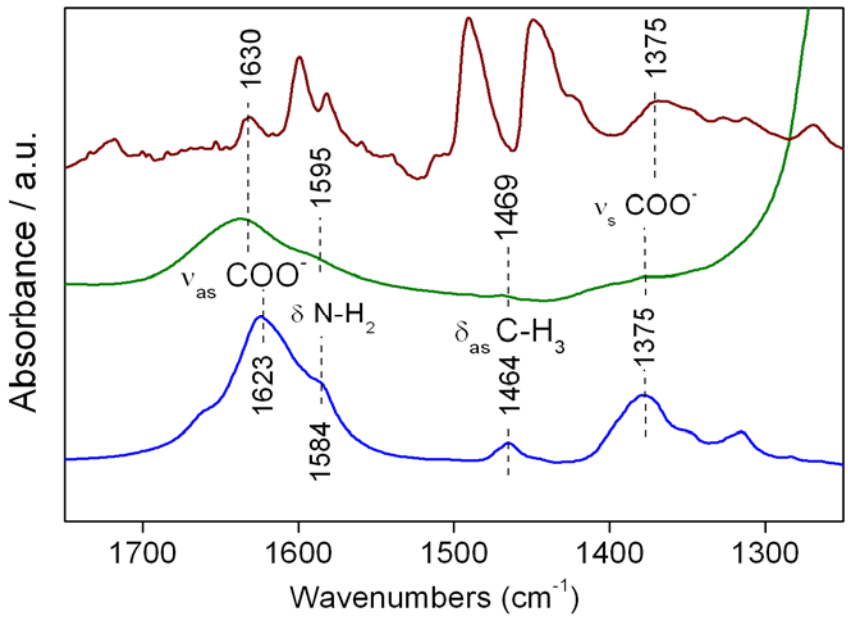

Figure 3.2.10. Comparison of IR spectra of Cu^{II}-Valine (blue), Cu^{II}-Valine-MCM-41 (green), Cu^{II}-Valine-Polystyrene (brown) in the high energy range (1750 – 1250 cm^{-1}). Spectra were arbitrarily normalized and vertically shifted for easier comparison.

Table 3.2.2. Summary of FTIR characterisation of Cu^{II}-Valine catalysts (absorption in cm^{-1}).[230, 239]

Assign-ment	Valine	Cu^{II}-Valine	Cu^{II}-Valine-LTA	Cu^{II}-Valine MCM-41	Cu^{II}-Valine-Polyst.	Characterisation
NH_2 ν_{as} NH_2 ν_s NH_2 δ	3148 3070 1500	3267 3156 1584	3268 - -	- - 1595	3310 - -	Shifted NH_2 ν when compared to valine ligand suggest deprotonation of amino group and coordination to Cu through NH_2.
CH ν	2933 2869 2623	2964 2919 2862	2988 2944 2870	2964 2919 2861	- - -	ν_{CH} of Cu^{II}-Valine in polystyrene supported material is overlapped by aromatic and aliphatic ν_{CH} modes of polystyrene matrix
COO^- ν_{as}	1661	1619	1633	1635	1630	Shifted $\nu_{as\ C\ OO^-}$ and $\nu_{s\ C\ OO^-}$ when compared to valine ligand confirms carboxyl group involvement in Cu binding, absence of band at around 1800 cm^{-1} confirms carboxyl group deprotonation.
COO^- ν_s	1470	1402	1383	1375	1375	

DR UV-Vis spectroscopy.

DR UV-Vis spectroscopy was used to elucidate the local structure of the Cu species. In the spectrum of the Cu^{II}-Valine complex an intense absorption centred at 40000 cm^{-1} and a band at 16000 cm^{-1}, were assigned to ligand to metal charge transfer (LMCT) and d-d transitions of Cu^{II} ions, respectively (Figure 3.2.11.). Similar spectra were reported for Cu^{II}-amino acid complexes, and explained by square planar coordination of the central ion.[131] This was in agreement with the Cu^{II}-Valine crystal structure shown in Figure 3.2.2., involving a chelated $Cu^{II}(N_2O_2)$ core. Two d-d bands were expected on the basis of the ligand field theory, corresponding to $^2B_{1g} \rightarrow {}^2A_{1g}$ and $^2B_{1g} \rightarrow {}^2E_g$ transitions. The presence of a single band could be explained as the result of a symmetry distortion, due to the presence of two distant oxygen atoms from neighbouring valine molecules along the z-axis. In Cu^{II}-Valine -MCM-41 a new component of LMCT band was formed between 27000 and 32000 cm^{-1}, while the d-d transitions increase in intensity and are red-shifted to 13500 cm^{-1}.[156, 157] This indicates an octahedral coordination of Cu^{II} ions, involving chemically heterogeneous ligands and suggests that the two coordinative vacancies of the $Cu^{II}(N_2O_2)$ core are occupied by ligands from the support: oxygen atoms from surface silanols and/or chlorine atoms from polymer matrix. As for Cu^{II}-Valine-Polystyrene, the intensity of the absorbance in the visible region (30000 – 10000 cm^{-1}) dramatically increased with respect to the high energy one. In this case a major contribution to the bands above 30000 cm^{-1} was related to the π-π^* transition of the polystyrene matrix, while the intense bands with maxima at 21600 and 15500 cm^{-1} can be related to the cupric ions. The nature of these absorption bands was not clear: two d-d components in the same range could be explained as transitions of Cu^{II} square planar complexes, but the high intensity is more compatible with LMCT transitions. It was tentatively proposed that these are related to Cu^{II} ions interacting with valine molecules and aromatic moieties from the polystyrene matrix. The hypothesis that the band at 21700 cm^{-1} could be related to a LMCT transition involving highly dispersed Cu-oxo species does not seem likely due to the hydrophobic character of the polystyrene matrix.[240]

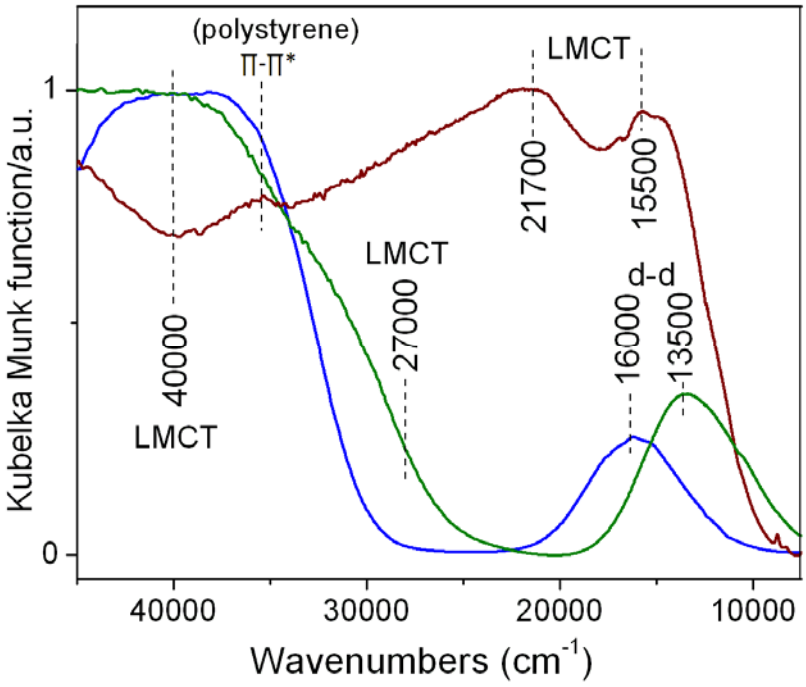

Figure 3.2.11. DR UV-Vis spectra of Cu^{II}-Valine (blue), Cu^{II}-Valine-MCM-41 (green), and Cu^{II}-Valine-Polystyrene (brown). Spectra were arbitrarily normalized to 1 for easier comparison.

Table 3.2.3. Summary of DRUV-Vis characterisation of Cu^{II}-Valine catalysts (absorption in cm^{-1}). Detailed explanation in text above.

Assignment	**Cu^{II}-Valine**	**Cu^{II}-Valine-MCM-41**	**Cu^{II}-Valine-Polyst.**
LMCT	40000	40000 27000	21700 15500
d-d	16000	13500	-

3.2.3.5. BET analysis.

N_2 adsorption measurement of Cu^{II}-Valine-MCM-41 and neat MCM-41 were performed at liquid nitrogen temperature. Samples were first dehydrated and degassed overnight in vacuum at 80°C.

Cu^{II}-Valine-MCM-41 exhibited lower external surface area compared with pure MCM-41 silica. The supported catalyst with low loading of active sites showed the external surface area of 562 m^2/g and supported catalyst with high active centres loading showed the external surface area of 250 m^2/g while pure MCM-41 showed the external surface area

of 1250 m^2/g. The lowering of the surface area indicates the presence of the Cu^{II}-Valine complex within the mesopores of MCM-41.[156, 241]

Table 3.2.4. Summary of BET characterisation of Cu^{II}-Valine-MCM-41 catalysts.

Material	BET surface area m^2/g
MCM-41	1250
Cu^{II}-Valine-MCM-41 (Cu 0.42%wt.)	562
Cu^{II}-Valine-MCM-41 (Cu 9.22%wt.)	250

3.2.4. Benzyl alcohol oxidation with neat Cu^{II}-Valine and heterogeneous Cu^{II}-Valine-MCM-41 and Cu^{II}-Valine-Polystyrene complexes.

3.2.4.1. Introduction to alcohol oxidation with Cu.

For general introduction to alcohol oxidation see section 3.1.4.

A typical example of aerobic oxidation of alcohols with a biological Cu^{II} complex is the chemistry of galactose oxidase (GO) which is a Cu^{II}- metalloprotein that selectively oxidizes primary alcohols to aldehydes with oxygen, forming 1 equiv. of hydrogen peroxide. The mechanism of alcohol oxidation by GO involves H-abstraction from the α-carbon atom of the alkoxide by the tyrosyl radicals. Cu^{I} species formed through one-electron oxidation are re-oxidized by oxygen that regenerates the Cu^{II}-tyrosyl form of the enzyme and produce H_2O_2 (for details see section 1.3.3.).

A large number of copper complexes have been studied widely in aerobic alcohol oxidation.[242] Recent examples of 'green' benzylic alcohol oxidations catalyzed by copper complexes include CuCl(Phen–$DEADH_2$) (Phen = 1,10-phenanthroline; $DEADH_2$ = diethylhydrazino dicarboxylate),[243] Cu^{II}BSP (BSP = salen-type ligand with a binaphthyl backbone and thioether functions),[244] Cu^{II}-histidine, Cu^{II}-arginine, Cu^{II}-lysine,[96] Cu^{II}-triethanolamine,[245] and Cu–TEMPO catalytic systems[246]. Alcohol oxidations using Cu^{II}–complexes were proposed to proceed *via* a H-atom abstraction mechanism with Cu^{II}-superoxo as active species. Computational calculations and experimental data support a superoxo species as the most likely reactive species in H-atom abstraction reaction due to low reaction barrier (15 kcal/mol). The C-H bond of the substrate is cleaved by Cu/O_2 active species *via* an H-atom abstraction which is the rate determining step. This

mechanism results in direct formation of aldehyde and produces water as the only by-product (Figure 3.2.12.). Cu(II)-superoxo species are produced by dioxygen binding to a Cu centre (for details of Cu/O_2 active species see section 1.3.3.)[247, 248]

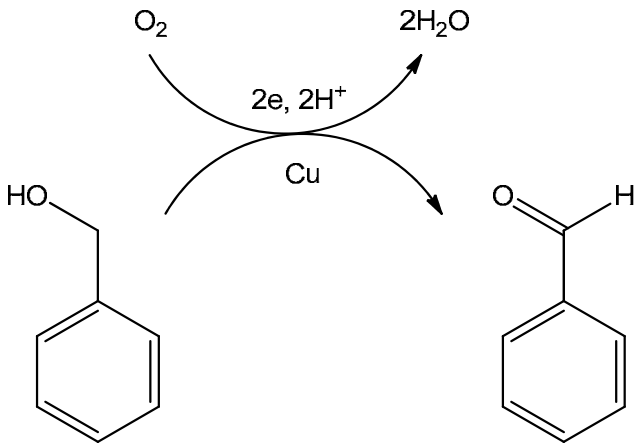

Figure 3.2.12. Direct formation of benzaldehyde and water as byproduct in aerobic copper oxidation of benzyl alcohol.[209]

The mechanism for oxidation of alcohols to the corresponding carbonyl compounds has been studied in great detail with the combination of Cu complexes with stable nitroxyl radical, TEMPO (2,2',6,6'-tetramethylpiperidine-N-oxyl). Nitroxyl radicals are well-established and applied on industrial and laboratory scale in oxidation processes.[249, 250] Copper-centred oxidative dehydrogenation of the alcohol mechanism was proposed for this system. Reaction of $copper^{I}$ with TEMPO affords a piperidinyloxyl $copper^{II}$ complex (Figure 3.2.13., A). Reaction of this complex with an alcohol affords the alkoxy $copper^{II}$ complex and TEMPOH (B). The second molecule of TEMPO coordinates to alkoxy $copper^{II}$ and abstracts hydrogen from the alkoxy ligand (C). In the next step, hydrogen of the alkoxide ligand is intramolecularly transferred to TEMPO generating a ketyl radical and TEMPOH (D). Subsequently, one-electron transfer from the ketyl group to Cu^{II} affords Cu^{I} and the carbonyl product. TEMPOH is re-oxidized to TEMPO by oxygen. The resulting Cu^{I} is rapidly re-oxidized by TEMPO to afford Cu^{II} and TEMPOH.

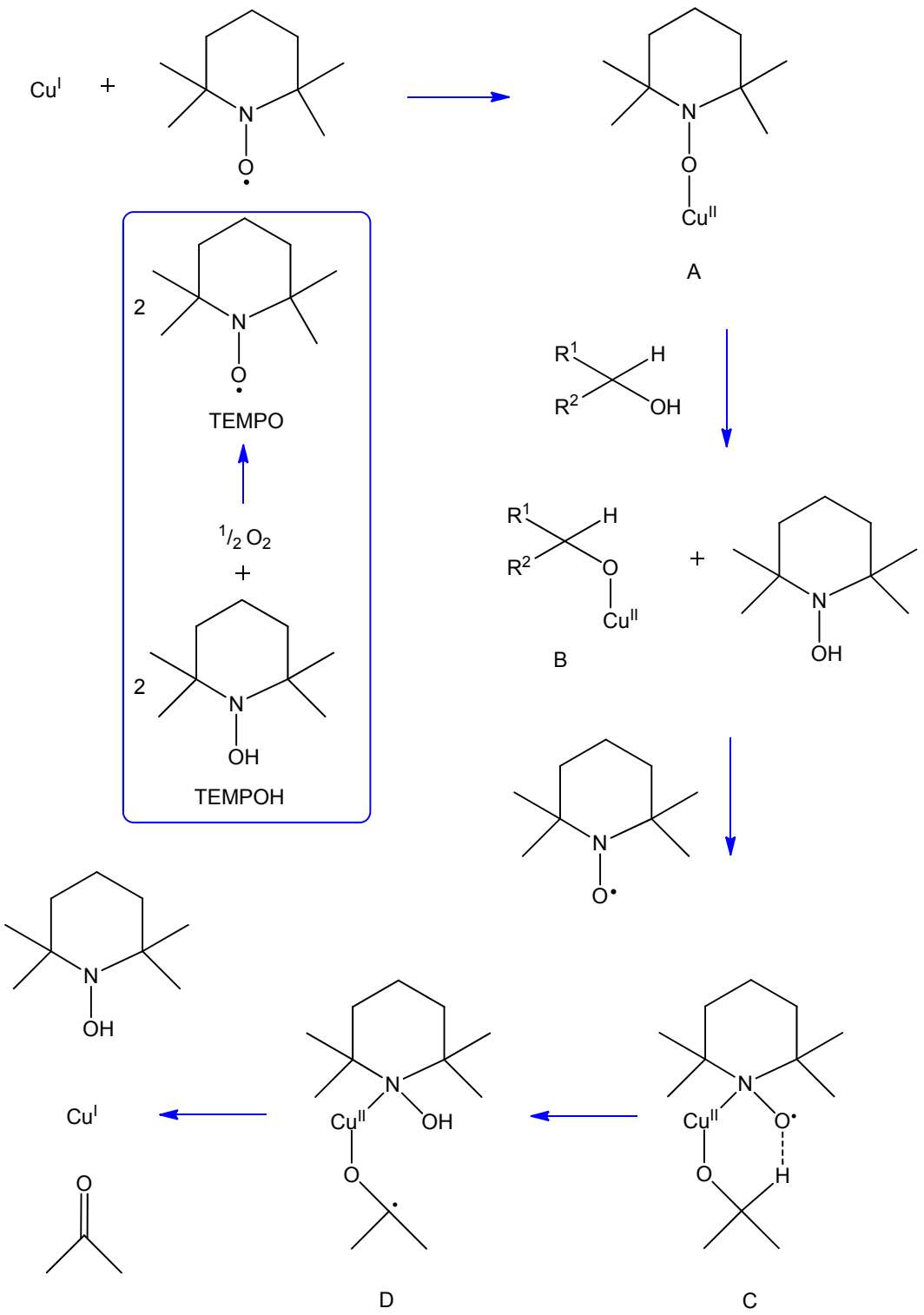

Figure 3.2.13. Schematic representation of alcohol oxidation by Cu/TEMPO system. The active Cu^{II}-species is generated *via* a one-electron oxidation of Cu^{I} by TEMPO. Alkoxy replacement, followed by coordination of a second molecule of TEMPO and intramolecular β-hydrogen abstraction affords the desired carbonyl compound, Cu^{I} and TEMPOH. Finally TEMPO is regenerated by rapid air oxidation of TEMPOH.

The mechanism of benzyl alcohol oxidation with Cu/TBHP, as proposed by Kochi, involves in the initial step Haber-Weiss decomposition of *t*BuOOH where *tert*-butyl radicals are formed in Cu^{II}/Cu^{I} redox reactions (*t*BuOO$^{\bullet}$) (Figure 3.2.14., A).[251] Cu^{I} is re-oxidized by TBHP generating *t*BuO$^{\bullet}$ (B) that undergoes rapid hydrogen atom abstraction from TBHP (*tert*- butyl hydroperoxide) at the rate that is much faster than hydrogen atom abstraction from the substrate molecule. At this stage more stable *tert*-BuOO$^{\bullet}$ radicals are formed (C). During Haber–Weiss decomposition of *t*BuOOH, O_2 is formed *via* bimolecular decomposition of *tert*-BuOO$^{\bullet}$ (D). In the presence of O_2 highly reactive copper superoxo species can be generated (E). This Cu-superoxo intermediate is capable of H-atom abstraction from the substrate molecule (F). Cleavage of the benzylic C–H bond (H-atom abstraction) to produce aldehyde was proposed to be the rate-determining step. The model mechanism of the alcohol oxidation is shown in Figure 3.2.14.

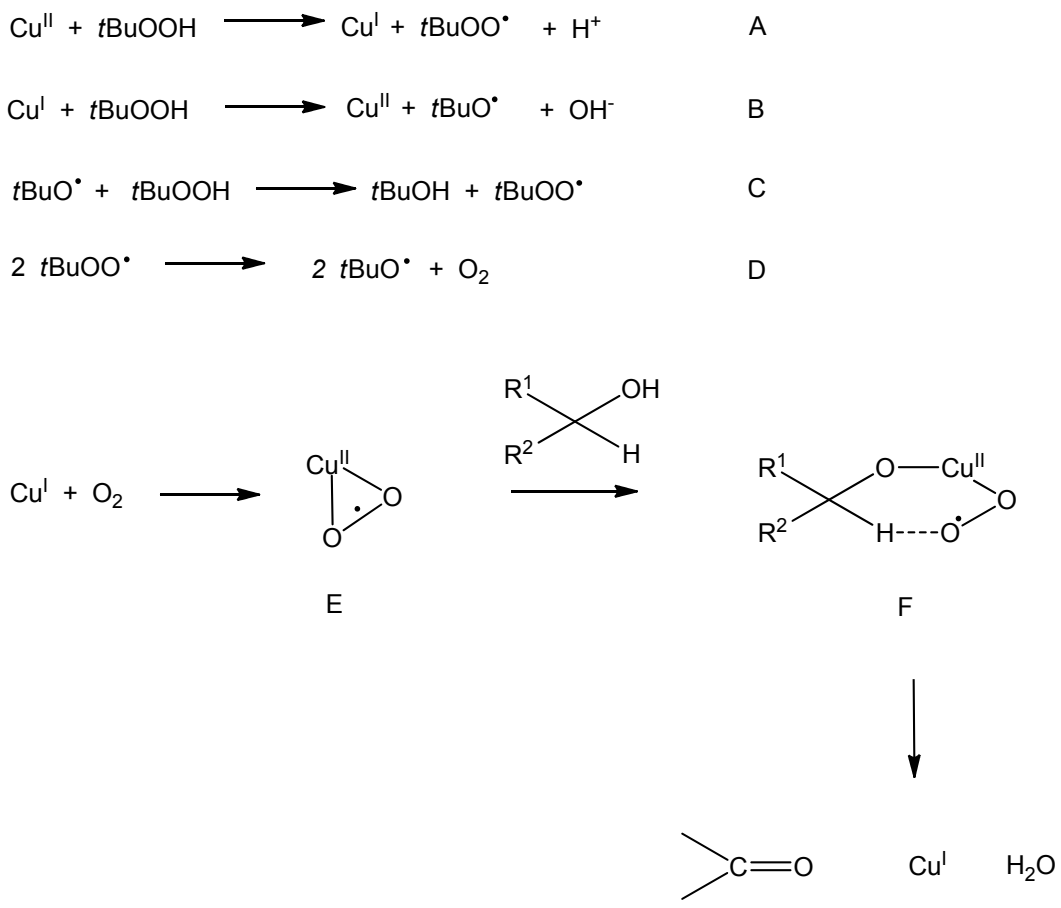

Figure 3.2.14. Model mechanism of alcohol oxidation with copper.

3.2.4.2. Benzyl alcohol oxidation with Cu^{II}-Valine based catalysts.

For closer evaluation of the role of isolated active sites and their influence on catalytic activity, benzyl alcohol oxidation was studied with neat Cu^{II}-Valine complex and its heterogeneous analogues immobilised within MCM-41 and on Polystyrene supports.

Cu^{II}-Valine-A was not catalytically tested in oxidation reactions due to formation of zeolite LTA around the complex that disabled this material as catalyst in the oxidation of target molecules due to not large enough pore sizes for substrate/product molecules to enter/exit (see section 3.2.1.for details). All Cu^{II}-Valine based catalysts were selective to form benzaldehyde (the results are summarized in Table 3.2.5.). A control experiment in the absence of catalyst gave conversions of 10.9 mol% with TBHP, and 6.5 mol% in the presence of air (see Table 3.1.8.).

Table 3.2.5. Results on selective oxidation of benzyl alcohol with Cu^{II}-Valine based catalysts. For reaction conditions see section 6.10.5.

Cat.	Metal load.	Oxid.	Mmol of metal	Cat. (g)	Subst: Metal ratio	Oxid: Subst. ratio	TON	TOF (h^{-1})	Conv. mol %	Select. mol % bald.
Neat	22.4	AIR	0.027	0.008	581	1.6	113	19	19.4	>99
Neat	22.4	TBHP	0.027	0.008	581	1	256	43	44.2	>99
MCM	0.42	AIR	0.004	0.06	1864	1.65	311	52	16.7	>99
MCM	0.42	TBHP	0.004	0.06	1864	1	396	65	21.8	>99
Polyst	0.018	AIR	0.0003	0.1	1174	1.65	147	25	12.9	>99
Polyst	0.018	TBHP	0.0003	0.1	1174	1	272	45	26.9	>99

T=371 K, air 3.0 MPa, DMSO 35g, reaction time=6h, bald=benzaldehyde.

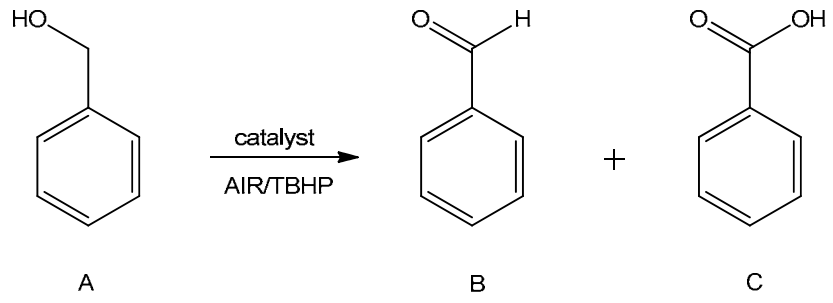

Scheme 3.2.2. Schematic representation of product formation in benzyl alcohol (A) oxidation to benzaldehyde (B) and benzoic acid (C).

From the data presented above it is clear that those heterogeneous catalysts which posses well isolated active sites displayed higher activities than their neat, homogeneous analogue. In fact, TON and TOF increased from 113 and 19 h^{-1} (neat complex) to 311 and 52 h^{-1} (Cu^{II}-Valine-MCM-41) and 147 and 25 h^{-1} (Cu^{II}-Valine-Polystyrene) in the presence of air as oxidant. When TBHP was employed, a significant increase in TON and TOF was also observed. While neat Cu^{II}-Valine complex afforded TON of 256 and TOF of 43 h^{-1}, Cu^{II}-Valine-MCM-41 obtained much higher TON and TOF of 396 and 65 h^{-1} and Cu^{II}-Valine-Polystyrene afforded TON and TOF of 272 and 45 h^{-1}, respectively. A comparison of TON and TOF using homogeneous and heterogeneous materials is shown in Figure 3.2.15.

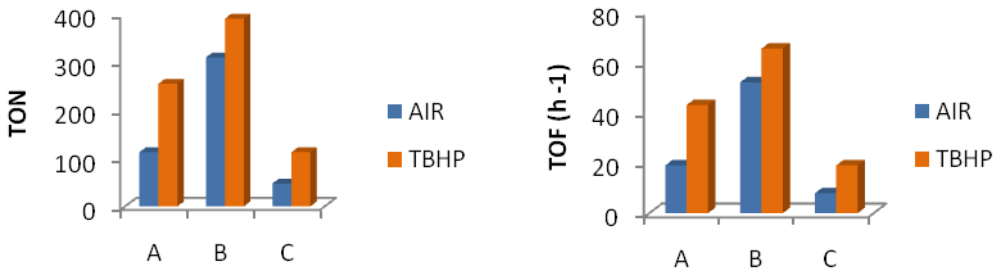

Figure 3.2.15. Comparison of TON (left) and TOF (right) using Cu^{II}-Valine (A), Cu^{II}-Valine -MCM-41, (Cu 0.42%wt.) (B), Cu^{II}-Valine -Polystyrene, (Cu 0.018 %wt.) (C) with air and TBHP.

Influence of oxidant on reaction conversions. In reactions with TBHP the number of moles of oxidant was equal to the number of moles of substrate. In reactions with air, O_2 was used in excess and the substrate:O_2 ratio was equal to 1:1.6 (for experimental details section 6.10.5.). The conversions of benzyl alcohol using Cu^{II}-Valine complexes showed to be dependent on oxidant type. Conversions were higher when TBHP was used and lower in reactions with air as oxidant. Neat Cu^{II}-Valine catalyst obtained higher conversions of 44.2 mol% with TBHP, and conversions of 19.4 mol% when air was used. Cu^{II}-Valine -MCM-41 produced conversions of 16.7 mol% and 21.8 mol% with air and TBHP, respectively. Cu^{II}-Valine-Polystyrene catalyst also produced higher conversion with TBHP (26.9 mol%) than with air (12.9 mol%). Comparison of reaction conversions using homogeneous and heterogeneous catalysts is shown in Figure 3.2.16.

The type of oxidant was an important factor that influenced the reaction yields, and peroxide (*tert*- butyl hydroperoxide, TBHP) showed to be more efficient than air in benzyl alcohol oxidation reactions with Cu^{II}-Valine based catalysts. Aerobic conditions

are less effective as molecular oxygen is very difficult to activate when compared to highly reactive peroxide species (for details see section 1.3.1.).

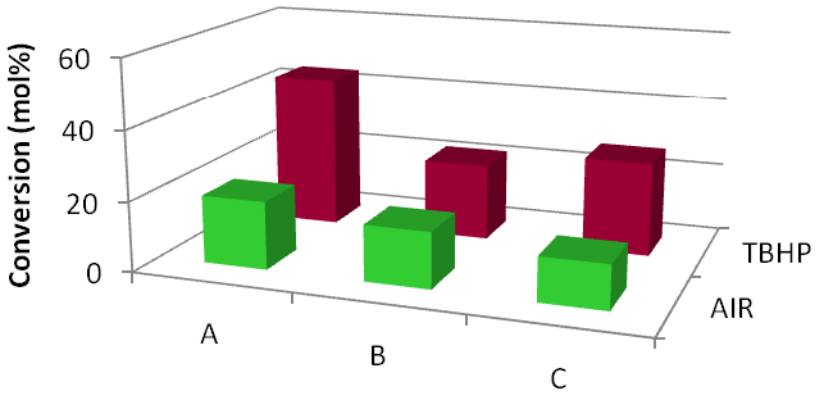

Figure 3.2.16. Comparison of reaction conversions in benzyl alcohol oxidation reactions using Cu^{II}-Valine (A), Cu^{II}-Valine-MCM-41, Cu 0.42%wt. (B), Cu^{II}-Valine-Polystyrene, Cu 0.018 %wt.(C) with air and TBHP.

Influence of active site loading on catalytic activity. The increase in copper content of heterogeneous Cu^{II}-Valine catalysts resulted in increased substrate conversions, but decreased TON and TOF. Cu^{II}-Valine-MCM-41 catalyst, when air was used as the oxidant, afforded conversions of 21.8 mol% for Cu rich and 16.7 mol% for Cu low content catalysts. However, by increasing the loading of metal sites the TON and TOF decreased from 311 and 52 h^{-1} (Cu^{II}-Valine -MCM-41, Cu 0.42%wt.) to 48 and 8 h^{-1} (Cu^{II}-Valine -MCM-41, Cu 9.22%wt.). When TBHP was employed Cu^{II}-Valine-MCM-41 catalysts with higher metal loading afforded higher conversion (52.1%), than the analogous material with low metal content (21.0 mol%), but TON and TOF significantly decreased. In fact, Cu^{II}-Valine-MCM-41 (Cu 0.42%wt.) obtained a TON and TOF of 392 and 65 h^{-1}, that decreased to 113 and 19 h^{-1} when Cu^{II}-Valine-MCM-41 high metal loading (Cu 9.22%wt.) was employed. Similar trends were observed when polystyrene supported Cu^{II}-Valine catalysts were employed for the oxidation of benzyl alcohol. In the presence of air, Cu rich Cu^{II}-Valine-Polystyrene (Cu 8.79 %wt.) afforded conversions of 22.8 mol% and the analogous Cu^{II}-Valine-Polystyrene with low loading of metal sites (Cu 0.018 %wt.) obtained conversion of 12.9 mol%. By increasing the metal content, TON and TOF decreased from 147 and 25h^{-1} (Cu^{II}-Valine-Polystyrene, Cu 0.018 %wt.) to 52 and 9 h^{-1} (Cu^{II}-Valine-Polystyrene, Cu 8.79 %wt.), in the presence of air. In reactions with TBHP, Cu^{II}-Valine-Polystyrene (Cu 8.79 %wt.) afforded higher conversion (48 mol%) than its low copper content analogue (26.9 mol%). Cu^{II}-Valine-Polystyrene (Cu 8.79 %wt.) catalyst exhibited TON and TOF of 110 and 18 h^{-1} and by

decreasing metal sites loading to Cu 0.018 %wt., TON and TOF increased to 272 and 45 h^{-1}. A comparison of results on selective oxidation of benzyl alcohol with low and high metal loading Cu^{II}-Valine materials is shown in Table 3.2.6.

Table 3.2.6. Results on selective oxidation of benzyl alcohol with low and high metal loading Cu^{II}-Valine catalysts. For reaction conditions see section 6.10.5.

Cat.	Metal load.	Oxid.	Mmol of metal	Cat. (g)	Subst: Metal ratio	Oxid: Subst. ratio	TON	TOF (h^{-1})	Conv. mol %	Select. mol % bald.
Neat	22.4	O_2	0.027	0.008	581	1.6	113	19	19.4	>99
Neat	22.4	TBHP	0.027	0.008	581	1	256	43	44.2	>99
MCM	9.22	O_2	0.072	0.05	218	1.65	48	8	21.8	>99
MCM	0.42	O_2	0.004	0.06	1864	1.65	311	52	16.7	>99
MCM	9.22	TBHP	0.072	0.05	218	1	113	19	52.1	>99
MCM	0.42	TBHP	0.004	0.06	1864	1	392	65	21.0	>99
Polyst	8.79	O_2	0.069	0.05	228	1.65	52	9	22.8	>99
Polyst	0.018	O_2	0.0003	0.1	1174	1.65	147	25	12.9	>99
Polyst	8.79	TBHP	0.069	0.05	228	1	110	18	48.1	>99
Polyst	0.018	TBHP	0.0003	0.1	1174	1	272	45	26.9	>99

T=371 K, air 3.0 MPa, DMSO 35g, reaction time=6h, bald=benzaldehyde.

It is clear from the results obtained that greater dispersion of the metal active sites plays a key role in the catalytic benzyl alcohol oxidation reactions. By decreasing the active site loading the active site isolation increased, which strongly enhanced the TON's and TOF's of catalysts. The decrease in copper content, which resulted in drastic changes of TON and TOF, clearly indicates that good isolation of the active sites is crucial to obtain high catalytic activities.

This decrease in TON and TOF with increasing catalyst loading could be explained in terms of cluster formation and accumulation of support-bound dimers or oxo- and hydroxo- bridged metal species which could have lower activity than the corresponding well-isolated and more accessible single sites.[91, 252] Formation of inactive oxo and peroxo dimeric and other polymeric species could be avoided by employing the heterogeneous catalysts with reduced number and well-dispersed metal active sites. Site isolation

resulted in higher turnover numbers and frequencies of single-site heterogeneous Cu^{II}-Valine catalysts.

Similar trends were reported in the literature for oxidation reactions with neat and zeolite X encapsulated Mn-salen complexes.[119] TOF values for styrene oxidation enhanced after encapsulation probably resulted from the isolation of the Mn sites in the zeolite cavities. Conversion of styrene however decreased upon encapsulation suggesting diffusional resistance encountered by the substrate styrene molecules in reaching the active sites located inside the supercages of zeolite crystals.

The lower activity for styrene oxidation in the case of heterogeneous catalysts when compared with homogeneous was also observed for Co-salen complexes supported onto aminopropyl functionalized SBA-15.[129] This result was ascribed to the presence of the bulky organometallic complexes and the linker moieties in the channels that could lead to diffusion limitation. Despite of lower conversions, heterogeneous catalyst revealed higher turnover frequency than the corresponding homogeneous complex (Table 3.2.7.).

Table 3.2.7. Comparison of catalytic performance of homogeneous and heterogeneous salen complexes in styrene oxidation reactions.

Catalyst	***Conv. (%)***	***TOF (h^{-1})***	***Ref.***
Mn-salen	78.8	28	[119]
Mn-salen-X	54.8	761	
Co-salen	85.9	69	[129]
Co-salen-SBA-15	77.5	194	

The selectivity to benzaldehyde appeared to be independent on the metal content, Cu/substrate ratio, type of oxidant, nature of support and reaction time. Benzaldehyde was obtained in high yields with both oxidants under any given conditions. Reaction control and aldehyde oxidation to carboxylic acid largely depend on the concentration of oxidants e.g. oxidation of cinnamaldehyde to corresponding carboxylic acid requires a three fold oxidant excess (TBHP or H_2O_2).[253]

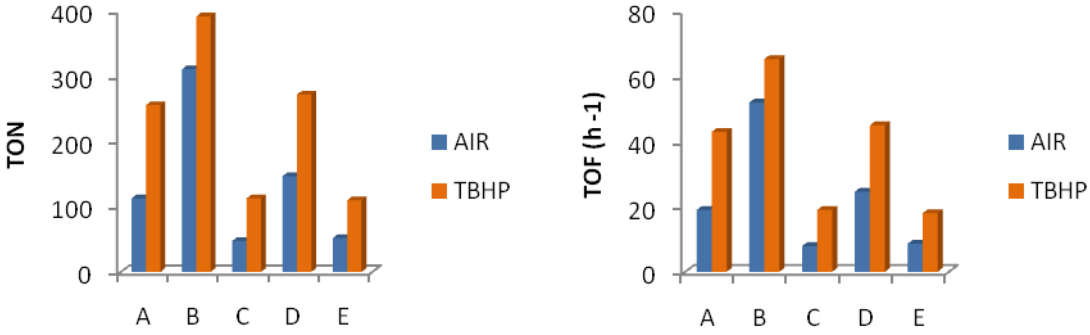

Figure 3.2.17. Comparison of TON (left) and TOF (right) in benzyl alcohol oxidation reactions using Cu^{II}-Valine (A), Cu^{II}-Valine-MCM-41 (Cu 0.42%wt.) (B), Cu^{II}-Valine-MCM-41 (9.22%wt.) (C), Cu^{II}-Valine-Polystyrene (Cu 0.018 %wt.) (D), Cu^{II}-Valine-Polystyrene (8.79 %wt.) (E) with air and TBHP.

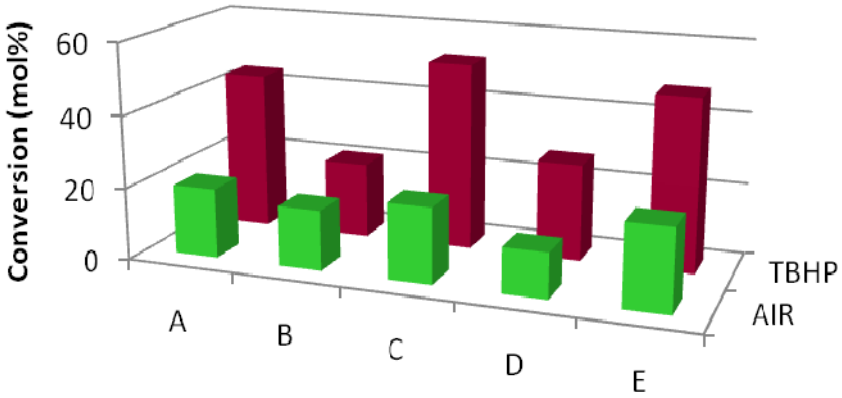

Figure 3.2.18. Comparison of conversions in benzyl alcohol oxidation reactions using Cu^{II}-Valine (A), Cu^{II}-Valine-MCM-41, Cu 0.42%wt. (B), Cu^{II}-Valine-MCM-41 (9.22%wt.) (C), Cu^{II}-Valine-Polystyrene (Cu 0.018 %wt.) (D), Cu^{II}-Valine-Polystyrene (8.79 %wt.) (E), with air and TBHP.

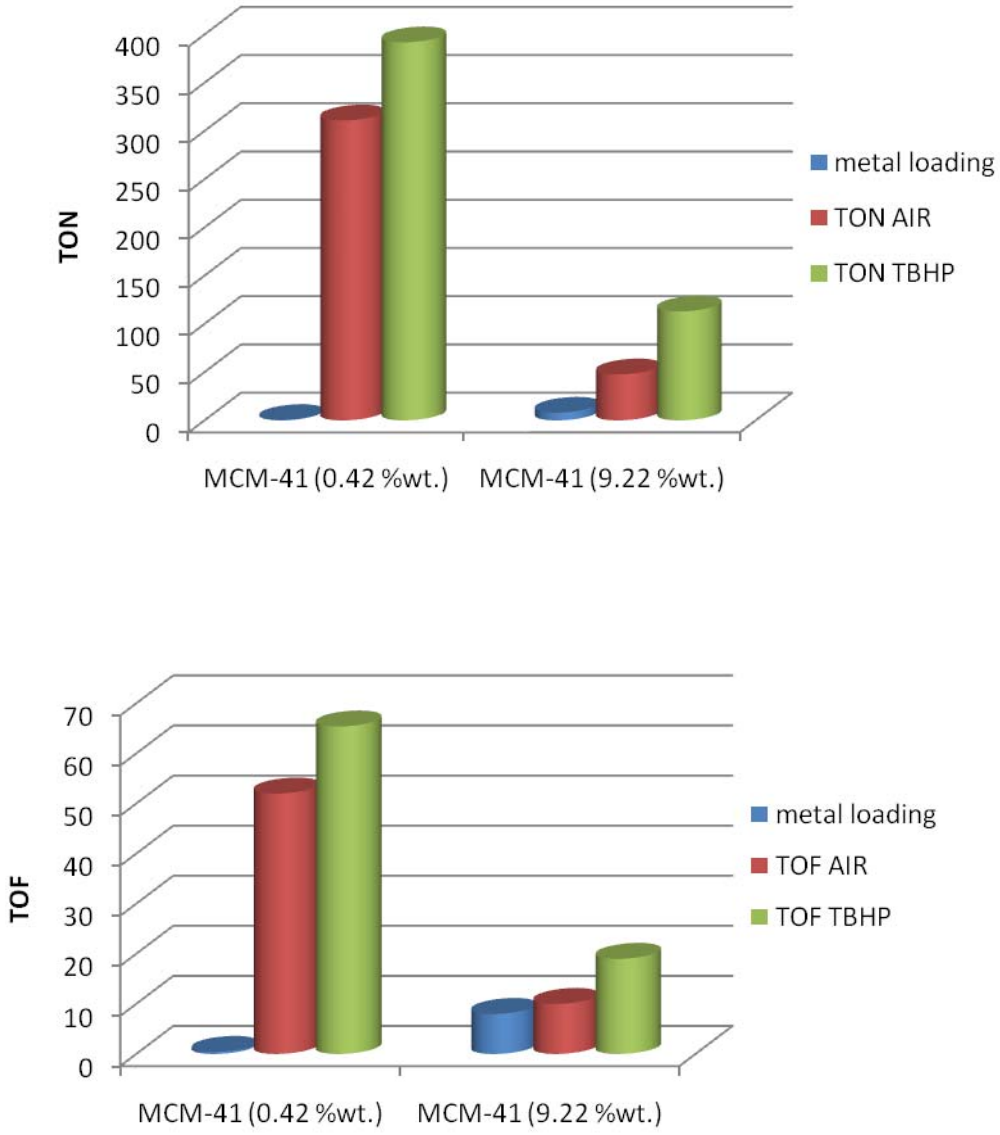

Figure 3.2.19. Comparison of TON (upper) and TOF (bottom) in benzyl alcohol oxidation reactions using Cu^{II}-Valine-MCM-41 (Cu 0.42%wt.) and Cu^{II}-Valine-MCM-41 (9.22%wt.).

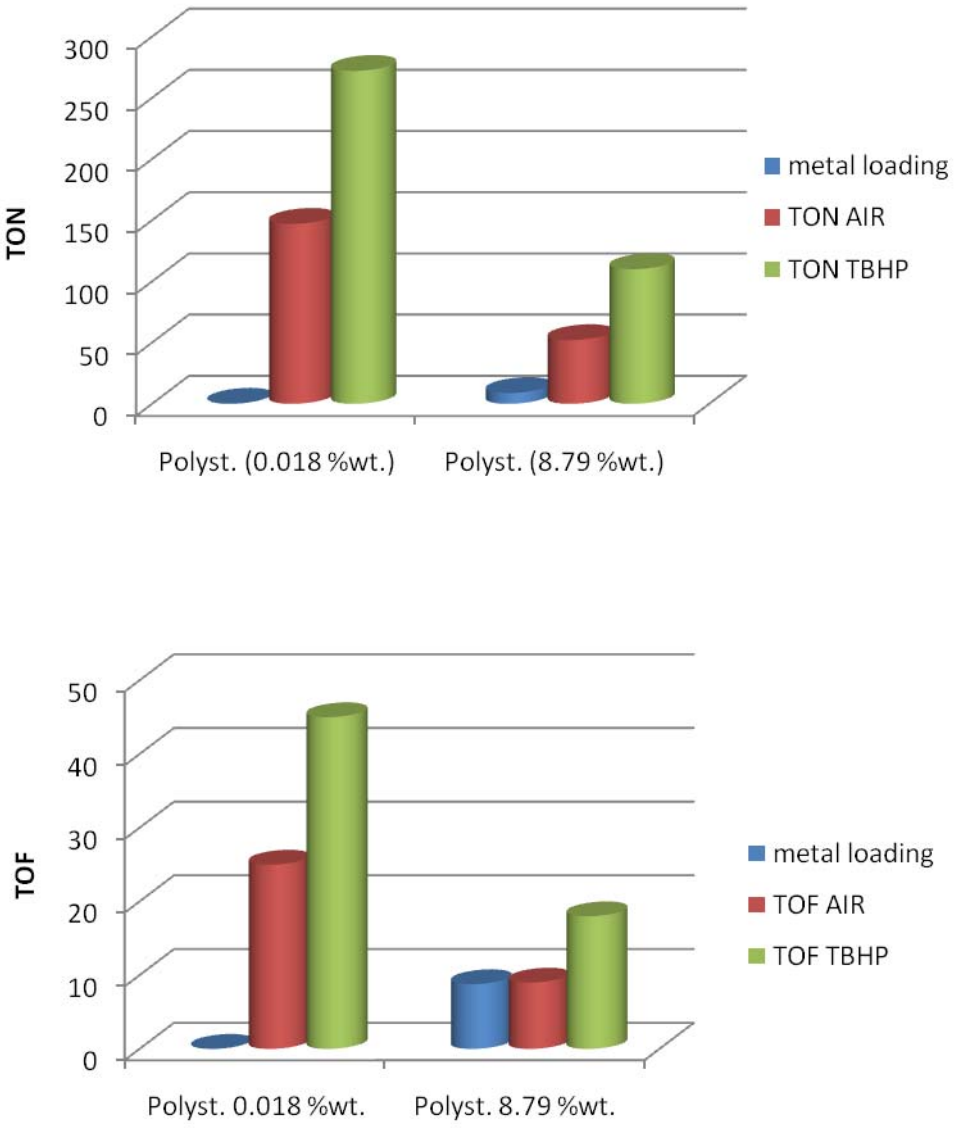

Figure 3.2.20. Comparison of TON (upper) and TOF (bottom) in benzyl alcohol oxidation reactions using Cu^{II}-Valine-Polystyrene (Cu 0.018 %wt.) and Cu^{II}-Valine-Polystyrene (8.79 %wt.).

3.2.5. Cyclohexene oxidation with neat Cu^{II}-Valine and heterogeneous Cu^{II}-Valine-MCM-41 and Cu^{II}-Valine-Polystyrene complexes.

3.2.5.1. Introduction to cyclohexene oxidation.

Catalytic oxidation of alkenes that are derived directly from crude oil fractions is a key industrial reaction for production of a wide variety of chemicals such as plastics, resins, and synthetic rubbers.[254] Conventional oxidation of alkenes to epoxides commonly uses organic peroxides such as peracids or dioxiranes, without the use of catalyst. However, peracids are expensive, hazardous to handle, non-stereoselective and create undesirable waste products.[255] Frequently, the carboxylic acid formed from the peracid during epoxidation reacts with the acid-sensitive epoxides to give α-hydroxyesters as the major product.[256] In order to overcome these limitations metal-catalyzed olefin oxidations has attracted increased attention due to the possibility of performing efficient, selective transformations with green oxidizing agents including molecular oxygen. Among oxidants O_2, TBHP and H_2O_2 were widely investigated in olefin epoxidation with metal catalysts.[257]

Oxidation of alkenes can result either in either allylic oxidation or oxidation of the C=C bond.[258, 259] Epoxides that are the products of C=C bond oxidation are very useful and versatile synthetic compounds and are convenient building blocks for the synthesis of many commodity and fine chemicals.[260] On the other hand, allylic C-H bond oxidation of olefins forms α,β-unsaturated ketones which play a crucial role in synthetic organic chemistry and provide useful intermediates in pharmaceuticals, pesticides and natural products synthesis. Since allylic oxidation preserves the C=C bond of the olefin, this route allows further functionalisation of the molecules, and the Michael system is particularly attractive for cycloaddition reactions. Compounds possessing α,β-unsaturated ketone cores are used as intermediates in the synthesis of nitrogen-containing heterocycles that are selective cannabinoid receptor antagonists and novel antibacterial agents. α,β- unsaturated ketones have also been used as precursors in the synthesis of isophosphinoline compounds, ipriflavones and optically active phenylpropylene oxides.[261]

Selective oxidation of alkenes using heterogeneous catalysts and clean oxidants under mild conditions still continues to be a challenge.[262] Currently there are four commercial epoxidation technologies available: the Arco process using *tert*-butyl hydroperoxide (TBHP) and Mo catalyst, the Shell process using ethyl benzene hydroperoxide (EBHP)

and TiO_2/SiO_2, the Sumitomo process using cumene hydroperoxide (CHP) and Ti–zeolite, and the BASF process using hydrogen peroxide and TS-1.[263, 264]

R= $(CH_3)_3C$-, $PhCH(CH_3)$-, $PhC(CH_3)_2$-, H-

Catalyst: A) homogeneous Mo(VI) and TBHP - ARCO

B) heterogeneous TiO_2/SiO_2 and EBHP – Shell

C) heterogeneous Ti–zeolite and CHP – Sumitomo

D) heterogeneous TS-1 and H_2O_2 – BASF

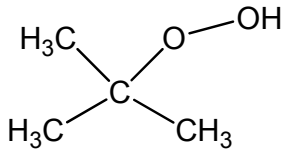

A

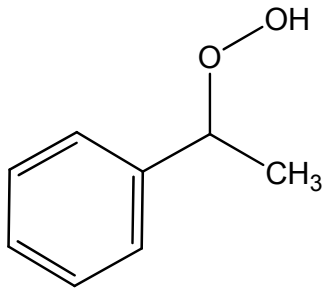

B

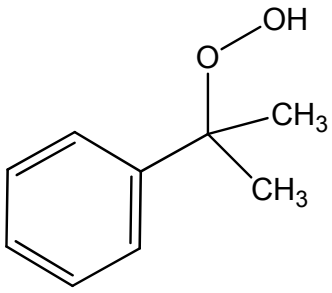

C

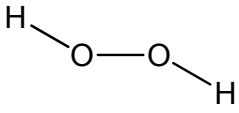

D

Figure 3.2.21. Industrial processes for the epoxidation of propylene and representation of oxidants employed: *tert*-butyl hydroperoxide (TBHP) (A), ethyl benzene hydroperoxide (EBHP) (B), cumene hydroperoxide (CHP) (C) and hydrogen peroxide (H_2O_2) (D).

The development of metal-catalyzed oxidations encouraged further attempts to develop selective and commercially attractive catalysts. Many different solid catalysts such as supported oxides, mixed oxides, framework substituted redox molecular sieve silicates, zeolites, aluminophosphates, layered type materials, heterogenized homogeneous catalysts, mixed metal exchanged zeolites and resins, chiral ligands, tethered or grafted complexes, and encapsulated complexes have been used in liquid phase epoxidation of olefins.[265] Metal complexes with nitrogen containing ligands (e.g. phthalocyanines, porphyrins, salens) have been widely studied as model compounds for mimicking the catalytic properties of metalloenzymes.[266]

A typical example of aerobic oxidation of alcohols with Cu^{II} complexes is the biomimetic chemistry of particulate methane monooxygenase (pMMO) which is a copper metalloprotein that selectively oxidizes methane to methanol (see section 1.33.). A number of $copper^{II}$ based complexes immobilized in microporous and mesoporous host materials have been developed and used as catalysts for olefin oxidations with environmentally benign oxidants. Cu^{II} systems with salen ligands, Cu^{II} bipyridine, 2,2'-methylenebis[(4S)-4-phenyl-2-oxazoline (Figure 3.2.22., A) and 2,6-bis[(4S)-isopropyl-2-oxazolin-2-yl]-pyridine (Figure 3.2.22., B) ligands were also studied.[128, 265, 267] Cu^{II} complexes with amino acids like histidine, arginine and lysine were also used for olefin oxidation.[96]

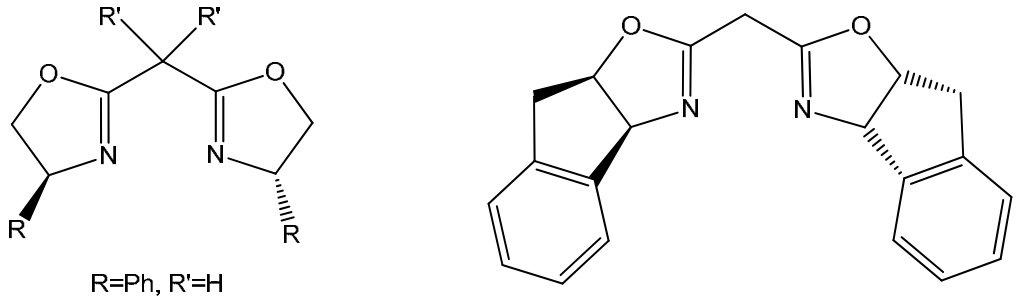

Figure 3.2.22. Representation of 2,2'- methylenebis[(4S)-4-phenyl-2-oxazoline (A) and 2,6-bis[(4S)-isopropyl-2-oxazolin-2-yl]-pyridine (B) ligands.

For many olefin oxidation systems, mechanisms related to oxidation with organic peracids have been proposed. Peracids are commonly used epoxidizing agents.[268, 269] Peracids posses an extra oxygen atom between the carbonyl group and acidic hydrogen (electrophilic oxygen). Attack at this position by a nucleophile displaces the carboxylate, which is a good leaving group. The "Butterfly mechanism" proposed by Bartlett involves nucleophilic attack of the π-electrons of double bond at the terminal electrophilic oxygen

atom of the hydroperoxide group where the proton is transferred intramolecularly to the carbonyl oxygen (C=O). As result a stable three-membered epoxide ring is formed (Scheme 3.2.3.).

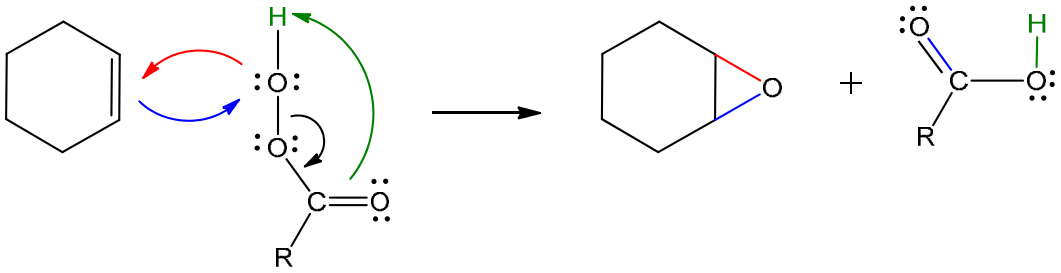

Scheme 3.2.3. Epoxidation of cyclohexene with peracid.

3.2.5.2. Cyclohexene oxidation with Cu^{II}-Valine catalysts.

The role of isolated Cu^{II}-Valine active sites was investigated in cyclohexene oxidation with air, TBHP and APB. Cu^{II}-Valine based catalysts showed high activities in oxidation of cyclohexene, exhibiting different behavior depending on the oxidant type, nature of the support and metal site loading. The conversion of cyclohexene was much higher when air and APB were employed and very low when TBHP was used as the oxidant. Control experiment in the absence of catalyst gave conversions of 2.0 mol% with TBHP, 6.8 mol% with APB and 4.5 mol% in the presence of air. The results of cyclohexene oxidation catalyzed by Cu^{II}-Valine catalysts are listed in Table 3.2.8.

Heterogeneous Cu^{II}-Valine catalysts with well isolated active sites when employed with air and APB proved to be much more active than their corresponding homogeneous analogue. Reactions with TBHP afforded very low conversions, TON and TOF. In the presence of air, TON and TOF increased from 258 and 43 h^{-1} (neat Cu^{II}-Valine complex) to 281 and 47 h^{-1} (Cu^{II}-Valine-MCM-41) and to 432 and 72 h^{-1} (Cu^{II}-Valine-Polystyrene). A similar increase in activities was observed with APB as oxidant, the neat Cu^{II}-Valine complex afforded TON of 189 and TOF of 32 h^{-1}; Cu^{II}-Valine-MCM-41 obtained higher TON and TOF of 729 and 121 h^{-1}; and Cu^{II}-Valine-Polystyrene afforded an even higher TON and TOF of 1808 and 301 h^{-1}, respectively. A comparison of TON and TOF using homogeneous and heterogeneous materials is shown in Figure 3.2.23.

Table 3.2.8. Results on selective oxidation of cyclohexene with Cu^{II}-Valine catalysts. For reaction conditions see section 6.10.6.

Cat.	Metal load.	Oxid.	Mmol of metal	Cat. (g)	Subst: Metal ratio	Oxid: Subst. ratio	TON	TOF (h^{-1})	Conv. mol %	Select. mol %	
										oxide	enone
Neat	22.4	AIR	0.027	0.008	581	1.65	258	43	44.4	25.0	75.0
Neat	22.4	TBHP	0.027	0.008	581	1	101	17	17.5	17.0	83.0
Neat	22.4	APB	0.027	0.008	581	1	189	32	32.5	>98	>2
MCM	0.42	AIR	0.002	0.03	1595	1.65	281	47	17.6	6.4	93.6
MCM	0.42	TBHP	0.002	0.03	1595	1	67	11	4.2	30.0	70.0
MCM	0.42	APB	0.002	0.03	1595	1	729	121	45.7	74.4	25.6
Polyst	0.018	AIR	0.0003	0.12	2398	1.65	432	72	18.0	8.3	91.7
Polyst	0.018	TBHP	0.0003	0.12	2398	1	92	15	3.9	15.4	84.6
Polyst	0.018	APB	0.0003	0.12	2398	1	1808	301	75.4	31.8	68.2
Blanc		AIR	-	-	-	1.65	-	-	4.5	9.3	90.7
Blanc		TBHP	-	-	-	1	-	-	2.0	18.5	81.3
Blanc		APB	-	-	-	1	-	-	6.8	>98	<2

T=371 K, air 3.0 MPa, acetonitrile 35g (reactions with air and TBHP) and acetonitrile 25g, water 10g (reactions with APB), reaction time=6h, oxide=cyclohexene oxide, enone=2-cyclohexene-1-one.

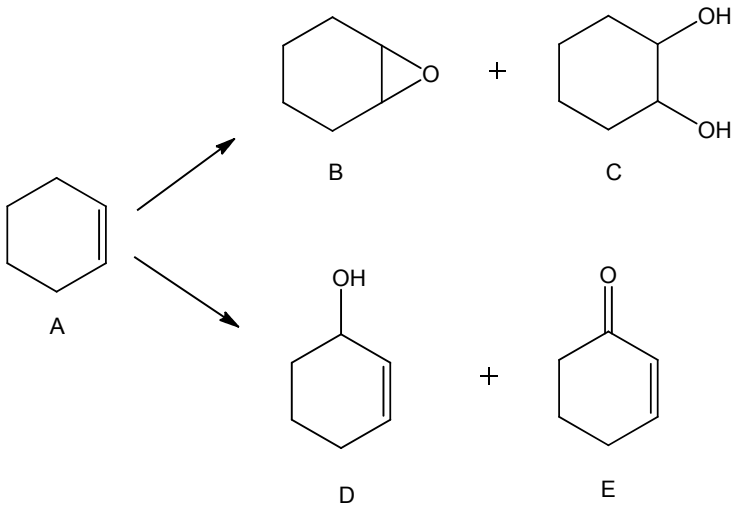

Scheme 3.2.4. Schematic representation of product formation in cyclohexene oxidation: cyclohexene (A), cyclohexene oxide (B), 1,2 cyclohexane diol (C), 2-cyclohexene-1-ol (D), 2-cyclohexene-1-one (E).

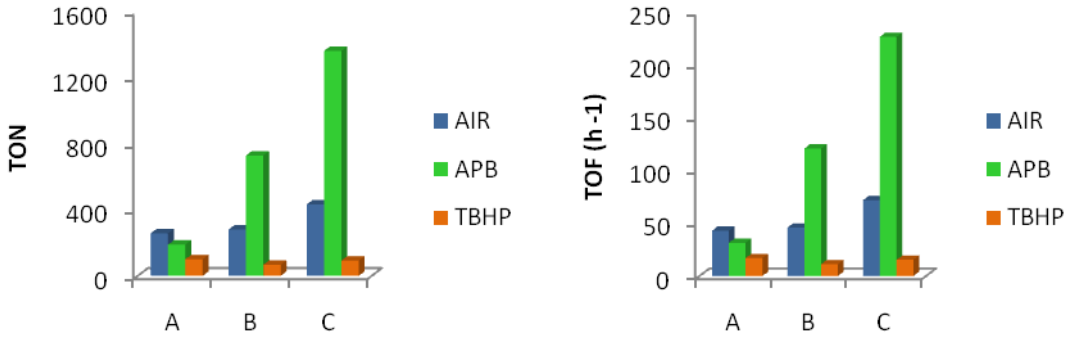

Figure 3.2.23. Comparison of TON (left) and TOF (right) in cyclohexene oxidation reactions using Cu^{II}-Valine (A), Cu^{II}-Valine-MCM-41(Cu 0.42%wt.) (B), Cu^{II}-Valine-Polystyrene (Cu 0.018 %wt.) (C), with air APB and TBHP.

Influence of oxidant on reaction conversions. Conversions of cyclohexene using the Cu^{II}-Valine catalysts showed to be strongly dependent on the nature of the oxidant. Homogeneous catalysts showed the highest conversion of 44.4 mol% in the presence of air, 32.5 mol% with APB, and much lower with TBHP (17.5 mol%). On the other hand, both heterogeneous catalysts Cu^{II}-Valine-MCM-41 and Cu^{II}-Valine-Polystyrene obtained the highest conversions with APB as oxidant (45.7 mol% and 75.4 mol%, respectively) and lower when air was used (17.6 mol% and 18.0 mol%, respectively). In the presence of TBHP the obtained conversions were very low (4.2 mol% and 3.9 mol%), revealing that TBHP was not the optional choice of oxidant for this catalytic system. The comparison of reaction conversions using homogeneous and heterogeneous catalysts is shown in Figure 3.2.24.

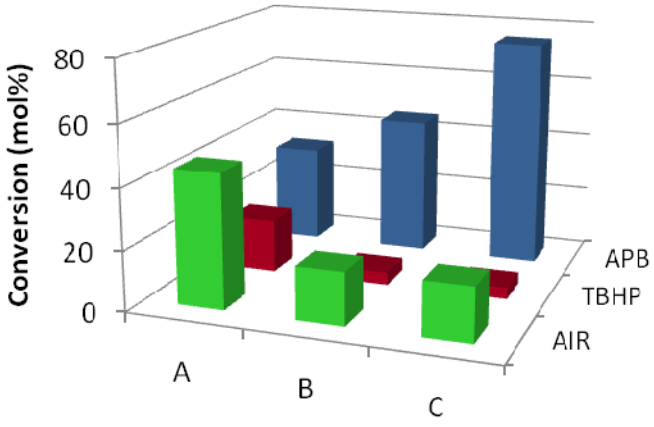

Figure 3.2.24. Comparison of reaction conversions in cyclohexene oxidation reactions using Cu^{II}-Valine (A), Cu^{II}-Valine-MCM-41 (Cu .42%wt.) (B), Cu^{II}-Valine-Polystyrene (Cu 0.018 %wt.) (C), with air, APB and TBHP.

Low reaction conversions with TBHP as oxidant could be explained by autoretardation and catalyst deactivation. Autoretardation in olefin epoxidation reactions in presence of TBHP has been reported in literature and this was attributed to the formation of *tert*-butanol during the epoxidation process.[270] There are two potential reasons for strong catalyst deactivation by *tert*-butanol. The first could be steric effects like steric hindrance to the coordination of the alcohol in the metal active site.[271] The second reason could be the hydrophobic/hydrophilic effects that could hold the alcohol within MCM-41 pores or polystyrene matrix. It was also shown that olefin epoxidation reactions can be inhibited by addition of tert-butanol to the reaction mixture. The hydrophobic support could also hold cyclohexene within its matrix hindering the less hydrophobic oxidant to access and react with the active site to form active oxidant (for details see section 3.2.6.2.).[272]

It has been shown that water seriously retards epoxidation reactions and the application of organic peroxides, like *tert*-butyl hydroperoxide (TBHP) which is employed as a water solution of TBHP (70 wt %) can negatively affect the reaction conversions.[273, 274] The presence of water obstructs the active sites of the catalyst and thereby sterically prevents the alkene to react with the metal site. This obstructing effect occurs at the time when the catalyst has formed an active complex with peroxide, and the water coordinates around this peroxo complex preventing the alkene from coming close enough to the active site to react. This effect has been observed with Ti catalysts where water reacted with the titanium site forming catalytically inactive Ti-OH complexes.[270] Epoxidation performance of supported Cu catalyst was also influenced by the nature of TBHP (anhydrous or aqueous) and catalyst deactivation was caused by the presence of water. The CuO-MCM-41 showed better activity with anhydrous TBHP. Polar solvents, particularly alcohols and water, retard the epoxidation by competing with the hydroperoxide and alkene substrate for coordination sites on the metal. The use of anhydrous solution of TBHP in organic solvents like toluene was reported to increase reaction yields.[275, 276] Water also reduces selectivity by reacting with the epoxide to form the corresponding diol. However in the case of Cu^{II}-Valine catalysts diols were not observed when 70 wt% TBHP in water was employed.

Heterogeneous Cu^{II}-Valine catalysts were more affected by presence of aqueous TBHP as oxidant in epoxidation reactions, showing reduced conversions, TONs and TOFs than homogeneous catalysts (Table 3.2.9.). Such decrease in activity of MCM-41 and polystyrene supported catalysts is probably due to a double effect of water retardation and the support that could hold *tert*-butyl alcohol within MCM-41 pores and polystyrene matrix, thus limiting the accessibility of the active sites to the substrate. A further detailed investigation would be required to evaluate the influence of TBHP and interactions between Cu active centres and aqueous and anhydrous TBHP.

Table 3.2.9. Summary of the results in cyclohexene oxidation over Cu^{II}-Valine, Cu^{II}-Valine-MCM-41 and Cu^{II}-Valine-Polystyrene catalysts with air as oxidant.

Catalyst metal loading	***Selectivity to 2-cyclohexene-1-one (mol%)***	***Conversion (mol%)***	***TON***
Cu^{II}-Valine 22.4 % wt	75.0	44.4	258
Cu^{II}-Valine-MCM-41 0.42%wt	93.6	17.6	281
Cu^{II}-Valine-MCM-41 9.22%wt.	70.2	68.4	149
Cu^{II}-Valine-Polystyrene 0.018 %wt	91.7	18.0	432
Cu^{II}-Valine-Polystyrene 8.79 %wt	80.6	62.5	142

Table 3.2.10. Summary of results in cyclohexene oxidation over Cu^{II}-Valine, Cu^{II}-Valine-MCM-41 and Cu^{II}-Valine-Polystyrene catalysts with APB as oxidant.

Catalyst metal loading	***Selectivity to cyclohexene oxide (mol%)***	***Conversion (mol%)***	***TON***
Cu^{II}-Valine 22.4 % wt	98.0	32.5	189
Cu^{II}-Valine-MCM-41 0.42%wt	74.4	45.7	729
Cu^{II}-Valine-MCM-41 9.22%wt.	93.5	76.5	166
Cu^{II}-Valine-Polystyrene 0.018 %wt	41.8	56.6	1362
Cu^{II}-Valine-Polystyrene 8.79 %wt	69.4	74.0	168

Influence of the active site loading on catalytic activity. The decrease in metal content of heterogeneous Cu^{II}-Valine-MCM-41 and Cu^{II}-Valine-Polystyrene catalysts resulted in decreased substrate conversions, but significant increase in TON and TOF with all oxidants. In the presence of air, the Cu^{II}-Valine-MCM-41 catalyst with high metal sites content (Cu 9.22%wt.) afforded conversion of 68.4 mol%, while its low metal content analogue (Cu 0.42%wt.) obtained conversion of 17.6 mol%. However, by decreasing metal sites loading the TON and TOF appreciably increased from 149 and 24 h^{-1} (Cu^{II}-Valine-MCM-41, Cu 9.22%wt.) to 281 and 47 h^{-1} (Cu^{II}-Valine-MCM-41 Cu 0.42%wt.). Increasing metal loading of Cu^{II}-Valine-MCM-41 materials resulted in increased conversions from 45.7 mol%, (Cu^{II}-Valine-MCM-41 Cu 0.42%wt.) to

(Cu^{II}-Valine-MCM-41, Cu 9.22%wt.) 76.5 mol%, but catalysts with low copper loading produced much higher TON and TOF than catalysts with high copper content, when APB as oxidant was used. In fact, catalysts with high loading of metal sites afforded TON and TOF of 166 and 28 h^{-1} but the catalysts with low concentration of metal sites content exhibited a much greater turnover number and turnover frequency of 729 and 121 h^{-1}.
Similar trends were observed when the Cu^{II}-Valine-Polystyrene catalyst was used with air. Cu^{II}-Valine -Polystyrene (Cu 8.79%wt.) afforded conversion of 62.5 mol%, and TON and TOF values of 142 and 24 h^{-1}, respectively. Cu^{II}-Valine-Polystyrene with low metal sites loading (Cu 0.018 %wt.) obtained lower conversion of 18.0 mol%, but exhibited very high TON and TOF of 432 and 72 h^{-1}, respectively. In the presence of APB, the Cu^{II}-Valine-Polystyrene catalysts with low and high metal content afforded similar conversions of ~74 mol% but catalysts with low metal content exhibited much greater turnover number and turnover frequency (1808 and 301 h^{-1}) than Cu^{II}-Valine - Polystyrene with higher metal sites loading (168 and 28 h^{-1}).

The contrasting increase in catalytic TON and TOF in the case of heterogeneous MCM-41 and polystyrene with low metal loading catalysts most likely arises from increased active site dispersion and microenvironmental changes in the solid support allowing a larger percentage of bound Cu^{II} to become more accessible for catalysis.[277] Relatively lower TON and TOF in the case of heterogeneous catalysts with high metal loading can be attributed to the slower diffusion of substrate olefins and oxidants into the solid support matrix in which the active sites are located due to higher density of the immobilised complexes.[278] This decrease in activity with increasing degree of catalyst loading could be also explained in terms of accumulation of dimers or clusters and/or support-bound dimers or clusters which could have much lower activity than the corresponding single sites.

Table 3.2.11. Results on selective oxidation of cyclohexene with low and high metal loading Cu^{II}-Valine catalysts. For reaction conditions see section 6.10.6.

Cat.	Metal load.	Oxid.	Mmol of metal	Cat. (g)	Subst: Metal ratio	Oxid: Subst. ratio	TON	TOF (h^{-1})	Conv. mol %	Select. mol %	
										oxide	enone
Neat	22.4	AIR	0.027	0.008	581	1.65	258	43	44.4	25.0	75.0
Neat	22.4	TBHP	0.027	0.008	581	1	101	17	17.5	17.0	83.0
Neat	22.4	APB	0.027	0.008	581	1	189	31	32.5	>98	
MCM	9.22	AIR	0.072	0.05	218	1.65	149	24	68.4	49.0	70.2
MCM	0.42	AIR	0.002	0.03	1595	1.65	281	47	17.6	6.4	93.6
MCM	9.22	TBHP	0.072	0.05	218	1	30	5	13.9	34.8	65.2
MCM	0.42	TBHP	0.002	0.03	1595	1	67	11	4.2	30.0	70.0
MCM	9.22	APB	0.072	0.05	218	1	166	28	76.5	93.5	6.5
MCM	0.42	APB	0.002	0.03	1595	1	729	121	45.7	74.4	25.6
Polyst	8.79	AIR	0.069	0.05	228	1.65	142	24	62.5	19.4	80.6
Polyst	0.018	AIR	0.0003	0.12	2398	1.65	432	72	18.0	8.3	91.7
Polyst	8.79	TBHP	0.069	0.05	228	1	30	5	13.3	5.2	94.8
Polyst	0.018	TBHP	0.0003	0.12	2398	1	92	15	3.9	15.4	84.6
Polyst	8.79	APB	0.069	0.05	228	1	168	28	74	69.4	30.6
Polyst	0.018	APB	0.0003	0.12	2398	1	1362	227	56.6	31.8	68.2

T=371 K, air 3.0 MPa, acetonitrile 35g (reactions with air and TBHP) and acetonitrile 25g, water 10g (reactions with APB), reaction time=6h, oxide=cyclohexene oxide, enone=2-cyclohexene-1-one.

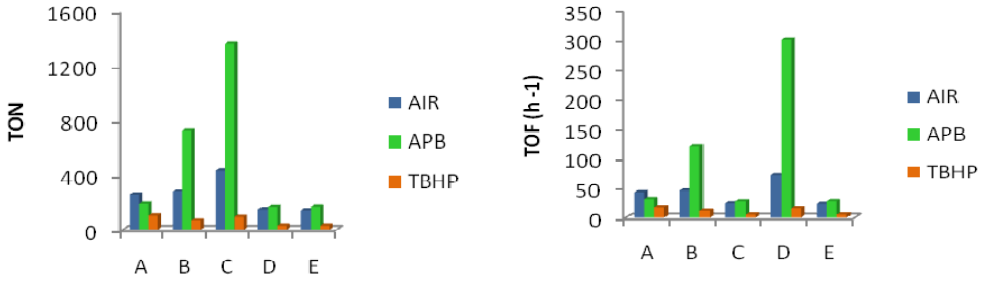

Figure 3.2.25. Comparison of TON (left) and TOF (right) in cyclohexene oxidation reactions using Cu^{II}-Valine (A), Cu^{II}-Valine-MCM-41 (Cu 0.42%wt.) (B), Cu^{II}-Valine-MCM-41 (9.22%wt.) (C), Cu^{II}-Valine-Polystyrene (Cu 0.018 %wt.) (D), Cu^{II}-Valine-Polystyrene (8.79 %wt.) (E) with air, APB and TBHP.

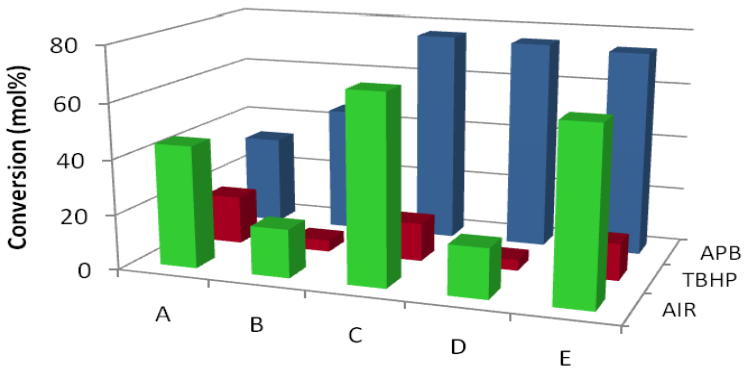

Figure 3.2.26. Comparison of conversions in cyclohexene oxidation reactions using Cu Cu^{II}-Valine (A), Cu^{II}-Valine-MCM-41, Cu 0.42%wt. (B), Cu^{II}-Valine-MCM-41, 9.22%wt. (C), Cu^{II}-Valine-Polystyrene, Cu 0.018 %wt.(D), Cu^{II}-Valine-Polystyrene, 8.79 %wt. (E) with air, APB and TBHP.

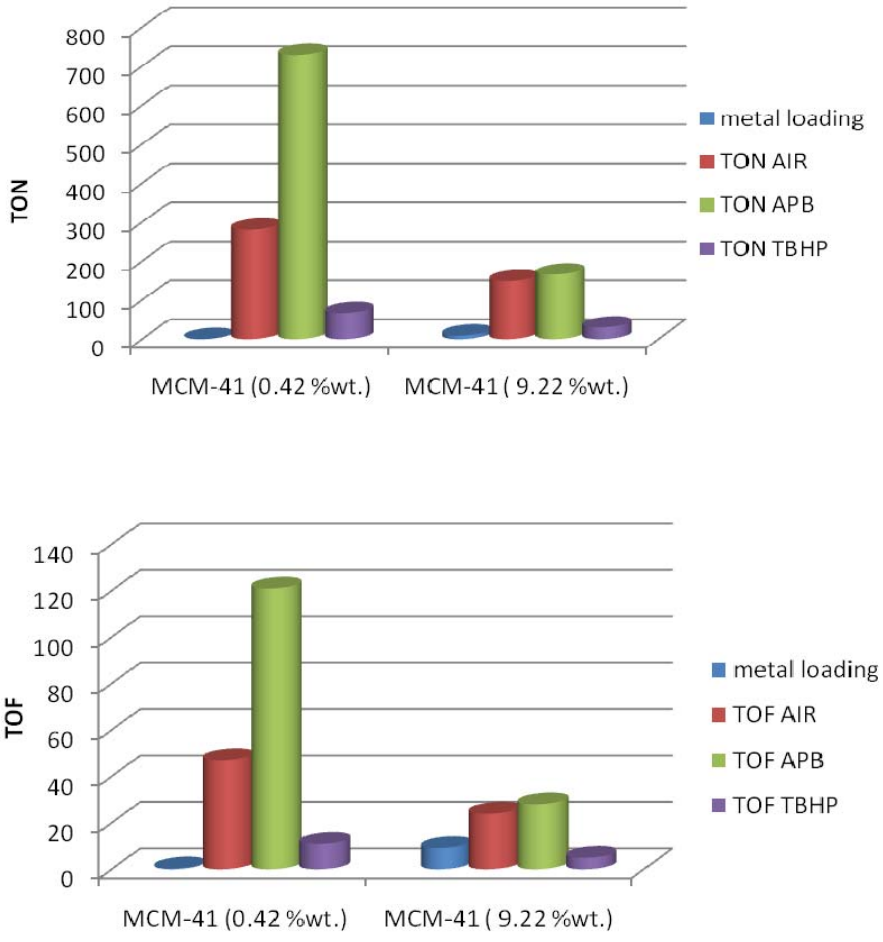

Figure 3.2.27. Comparison of TON (upper) and TOF (bottom) in cyclohexene oxidation reactions using Cu^{II}-Valine-MCM-41 (Cu 0.42%wt.) and Cu^{II}-Valine-MCM-41 (9.22%wt.).

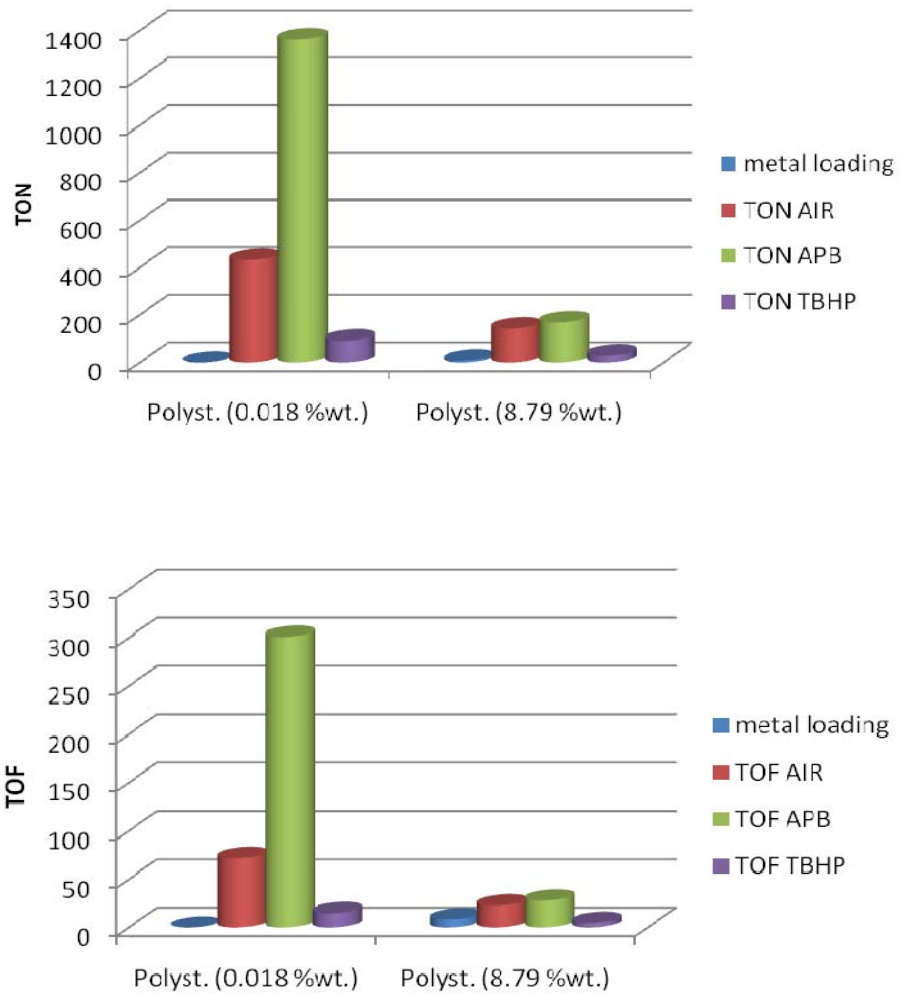

Figure 3.2.28. Comparison of TON (upper) and TOF (bottom) in cyclohexene oxidation reactions using Cu^{II}-Valine-Polystyrene (Cu 0.018 %wt.) and Cu^{II}-Valine-Polystyrene (8.79 %wt.).

Influence of oxidant and solid support on reaction selectivities. The type of oxidant was a key factor that influenced the selectivity and conversion in cyclohexene oxidation reactions with Cu^{II}-Valine catalysts. In the presence of air higher selectivity towards 2-cyclohexene-1-one was observed and when APB was used higher selectivity towards cyclohexene epoxide was observed. Homogeneous Cu^{II}-Valine catalyst was >98 mol% selective towards cyclohexene epoxide with APB, but in the presence of air the selectivity changed and 2-cyclohexene-1-one was formed with a selectivity of 75.0 mol%. Heterogeneous catalysts showed to be selective to the epoxide with APB. In fact, when Cu^{II}-Valine-MCM-41 (0.42%wt.) was used with APB, selectivity towards cyclohexene oxide dropped to 74.4 mol % (when compared with >98 mol% with neat Cu^{II}-Valine) and 2-cyclohexene-1-one was also formed. In the presence of Cu^{II}-Valine-Polystyrene

(0.018%wt.) selectivity towards cyclohexene oxide dropped further to 69.4 mol %, when APB was used. This indicates that hydrophobicity of the support plays an important role in selectivity changes (increased selectivity towards enone formation). Furthermore, when air was used as the oxidant with homogeneous Cu^{II}-Valine complex, the selectivity to 2-cyclohexene-1-one was 75 mol% but MCM-41 and polystyrene immobilized analogues exhibited higher selectivity to 2-cyclohexene-1-one formation (93.6 mol% and 91.7 mol% respectively)**.** This suggest that the type of oxidant and the nature of the solid support (strongly hydrophobic polystyrene and less hydrophobic methyl functionalized MCM-41) strongly influence the selectivity and increased the selectivity towards enone formation.

Influence of copper sites loading on reaction selectivity. In the presence of air, both heterogeneous catalysts with low copper site loading exhibited higher selectivity to the enone than the homogeneous Cu^{II}-Valine complex. By decreasing the metal loading of heterogeneous catalysts, a significant increase in selectivity towards 2-cyclohexene-1-one was observed with both oxidants. Decreasing the copper loading of Cu^{II}-Valine-MCM-41 resulted in the increased selectivity to enone from 6.5 mol% (9.22%wt.) to 25.6 mol% (0.42%wt) with APB and from 70.2 mol% (9.22%wt.) to 93.6 mol% (0.42%wt) with air. Cu^{II}-Valine-Polystyrene catalysts revealed even more dramatic changes in selectivity towards 2-cyclohexene-1-one, in fact the selectivity increased from 30.6 mol% (8.79 %wt.) to 68.2 mol% (0.018 %wt.) with APB. In the presence of air, the increase of selectivity towards enone was less significant, changing from 80.6 mol% to 91.7 mol% for high and low copper content Cu^{II}-Valine-Polystyrene catalysts, respectively.

Selectivity to 2-cyclohexene-1-one/ cyclohexene epoxide appeared to be strongly dependent on oxidant type, the nature of support, active site loading and substrate/metal ratio. In particular, the lower substrate/metal ratio, the higher selectivity towards 2-cyclohexene-1-one was observed with both oxidants; air and APB. Selectivity was not changing with reaction time.

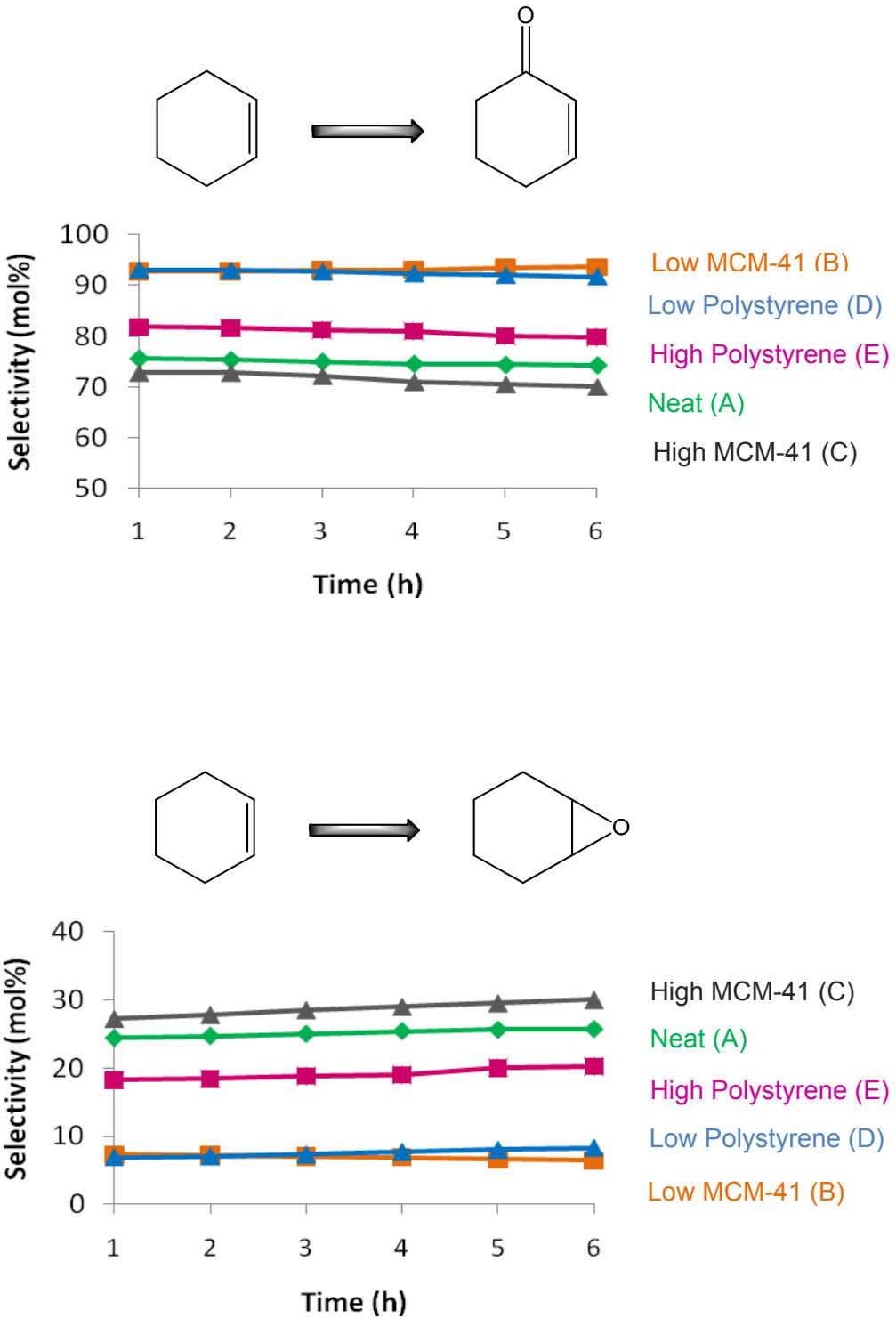

Figure 3.2.29. Origin of product selectivity in cyclohexene oxidation: 2-cyclohexene-1-one (top) and cyclohexene oxide (bottom) using Cu^{II}-Valine (A), Cu^{II}-Valine-MCM-41, Cu 0.42%wt. (B), Cu^{II}-Valine-MCM-41, 9.22%wt. (C), Cu^{II}-Valine-Polystyrene, Cu 0.018 %wt.(D), Cu^{II}-Valine-Polystyrene, 8.79 %wt. (E) with air.

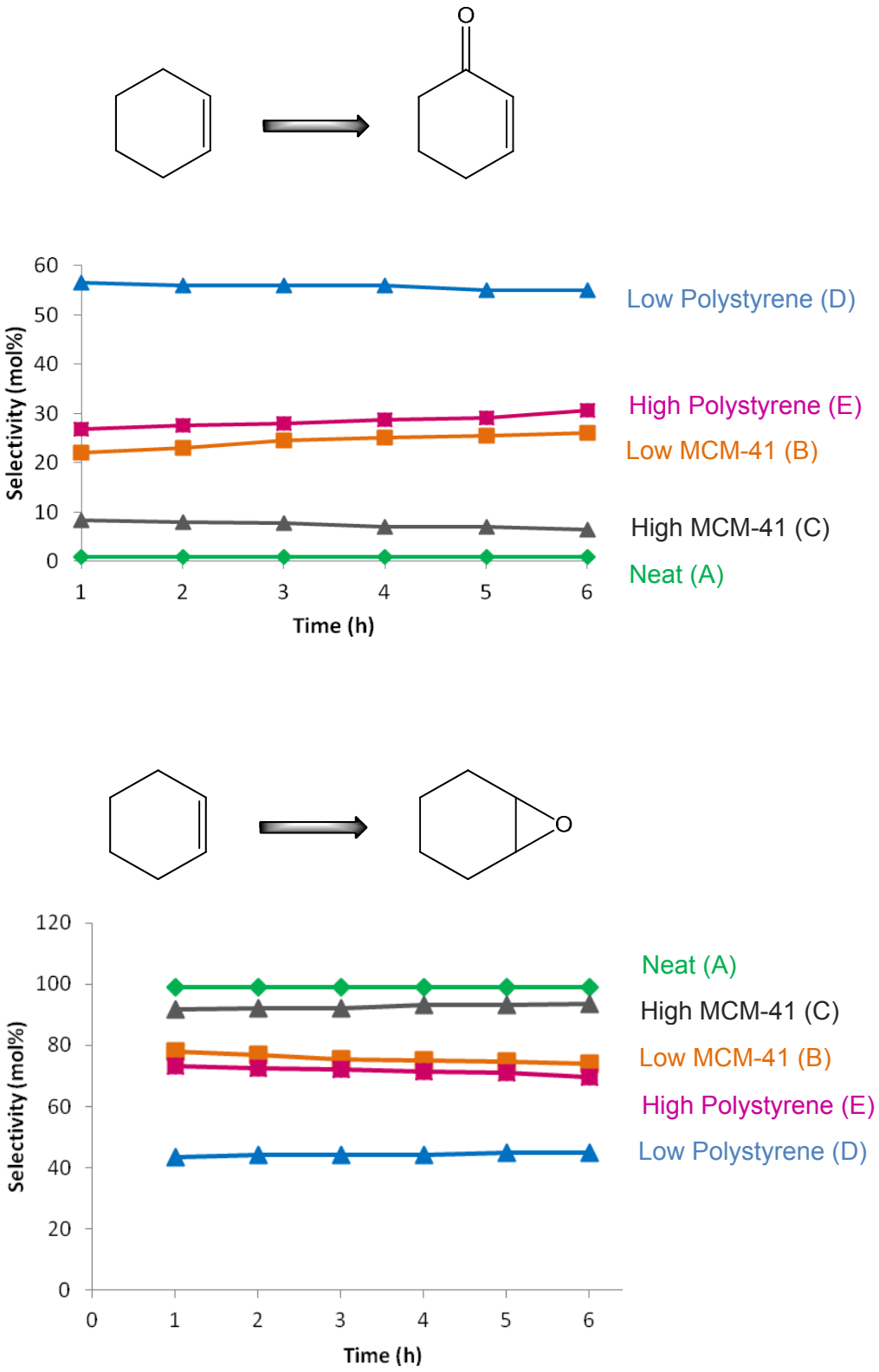

Figure 3.2.30. Origin of product selectivity in cyclohexene oxidation: 2-cyclohexene-1-one (top) and cyclohexene oxide (bottom) using Cu^{II}-Valine (A), Cu^{II}-Valine-MCM-41, Cu 0.42%wt. (B), Cu^{II}-Valine-MCM-41, 9.22%wt. (C), Cu^{II}-Valine-Polystyrene, Cu 0.018 %wt.(D), Cu^{II}-Valine-Polystyrene, 8.79 %wt. (E) with APB.

The changes in selectivity could be explained by interactions between Cu active sites and the solid support. Such metal-support interactions could influence the electronic properties of the Cu centres and affect the selectivity. In fact the SCXRD and DR UV-Vis studies of homogeneous Cu^{II}-Valine catalyst revealed square planar coordination of the central Cu ion that weakly interacts with two distant oxygen atoms from neighbouring valine molecules. In analogous heterogeneous Cu^{II}-Valine catalysts, distant oxygen atoms from neighbouring valine molecule are replaced by oxygen atoms from surface silanols of MCM-41 and chlorine atoms of chloromethylated polymer matrix. Therefore such changes in selectivity can be explained by differences in steric, geometric and electronic effects in the mechanistic pathways that lead to different product formation.[279]

It was reported that the type of organo-functional groups of the support influence the electronic and steric properties of the active metal site which resulted in selectivity changes.[280, 281] Mn(Salen)Cl complex supported on SBA-15 molecular sieves functionalized with propylamine and propylthiol groups revealed selectivity changes in the oxidation of limonene with air as oxidant. This yielded the 1,2-limonene epoxide with 99 mol% chemo- and regioselectivity while the neat complex afforded selectivity of 74 mol% (Table 3.2.12.). It was suggested that the higher electron density of immobilised manganese active sites is responsible for the changes in selectivity.

Table 3.2.12. Results on selective oxidation of limonene to 1,2-limonene epoxide over neat and immobilized Mn(Salen)Cl complexes.[281]

Catalyst	***TOF (h^{-1})***	***Selectivity (mol%)***
Mn(Salen)Cl	7.0	74
SBA-15-NH_2-Mn(Salen)Cl	35.4	89
SBA-15 -SH-Mn(Salen)Cl	59.0	99

The changes in selectivity could be also explained by increasing or decreasing the extent of interactions between metal sites and between metal centres with the support, formation of clusters or oxo- and hydroxo- bridged metal complexes. The electronic effects together with the occurrence of mixed sites might significantly influence the selectivity and activity of the catalyst. Electronic effects influence intermediate compound formation that must be stable enough to be formed but not too stable since it must decompose to yield the products. The key point of the electronic effect lies in the interaction between the d-band orbitals of the metal sites with the molecular orbitals of reactants, transition states and products. The presence of the mixed- active sites where both components participate

in the catalytic transformation can also influence the reaction selectivity, e.g. presence of clusters or oxo- and hydroxo- bridged metal complexes next to an isolated active site.
The effect of metal sites structure and dispersion on catalyst reactivity and selectivity was studied with metal oxides such as ZnO, TiO_2, V_2O_5, SiO_2 or Al_2O_3supported Co and Ru catalysts. Ethane oxidation reactions with silica supported vanadium oxide exhibited large changes in selectivity (ethylene vs. carbon dioxide production) that was dependent on the metal oxide dispersion. In the case of a catalyst with high dispersion of V_2O_5 (0.3%) the main product observed was carbon dioxide. For the 3.5% and higher concentration of metal oxide this behaviour was entirely reversed, with ethylene being the dominant product, indicating that catalyst structure affected the various reaction pathways available. The formation of metal clusters, bridged species, poorly dispersed active sites and metal-support interactions were proposed to affect the selectivity.
Significant changes in selectivity were also reported for Al_2O_3 supported Ru catalysts where high dispersion of the metal sites, caused the selectivity in CO hydrogenation to subsequently increase towards C_1 hydrocarbon production in Fischer-Tropsch synthesis. This result was explained by changes in metal-support interactions that influenced the electronic properties of the Ru particles and affected the selectivity.

The selectivity could also be affected by the formation of clusters or oxo- and hydroxo-bridged metal complexes. An increase in transition metal loading favours formation of surface bound metal clusters. Differences in oxygen bonding strength in isolated sites and clusters can be responsible for changes in selectivity. It was suggested that the strength of oxygen bonding in metal oxide determines distribution of ammonia oxidation products with Cu^{II} containing hydrotalcite catalyst (double layered hydroxide with the general formula $[Mg_6Al_2\{CO_3\}\{OH\}_{16}*4H_2O]$.[282] The higher copper content, the lower the selectivity towards N_2 formation was observed. An increase in Cu loading favoured formation of surface clusters which have a lower oxygen bonding strength as compared with isolated Cu sites. The highest selectivity towards nitrogen was found for the catalysts with the lowest Cu content. An increase in transition metal loading resulted in a decrease of the selectivity to nitrogen and an increase of the selectivity to nitric oxide.

Allylic oxidation vs. epoxidation of cyclohexene.[283-285] The key step in the mechanism of olefin oxidation catalyzed by copper is reduction of Cu^{II} to Cu^{I}. This reduction in the oxidation state decomposes TBHP to *t*BuOO$^{\bullet}$ radical (*tert*-butylperoxy radical) and a proton (Scheme 3.2.5., 1). Then, Cu^{I} is oxidized by TBHP generating *t*BuO$^{\bullet}$ radical and closing the Cu^{II}/Cu^{I} redox cycle (2). *t*BuO$^{\bullet}$ (*tert*-butoxy) radical undergoes rapid hydrogen atom abstraction from TBHP (*tert*- butyl hydroperoxide) at a rate that is much

faster than hydrogen atom abstraction from the alkene, to form the more stable *tert*-BuOO$^{\bullet}$ radical (3). The *tert*-butylperoxy radical undergoes selective hydrogen atom abstraction from the hydrocarbon allylic position forming an allyl radical (4). Capture of the allyl radical by the *tert*-BuOO$^{\bullet}$ radical forms an allylic *tert*-butylperoxide (5) which undergoes rapid reaction with the *tert*-butylperoxy radical forming an α,β-enone (6). The proposed mechanism for allylic oxidation of cyclohexene is presented in Scheme 3.2.5.

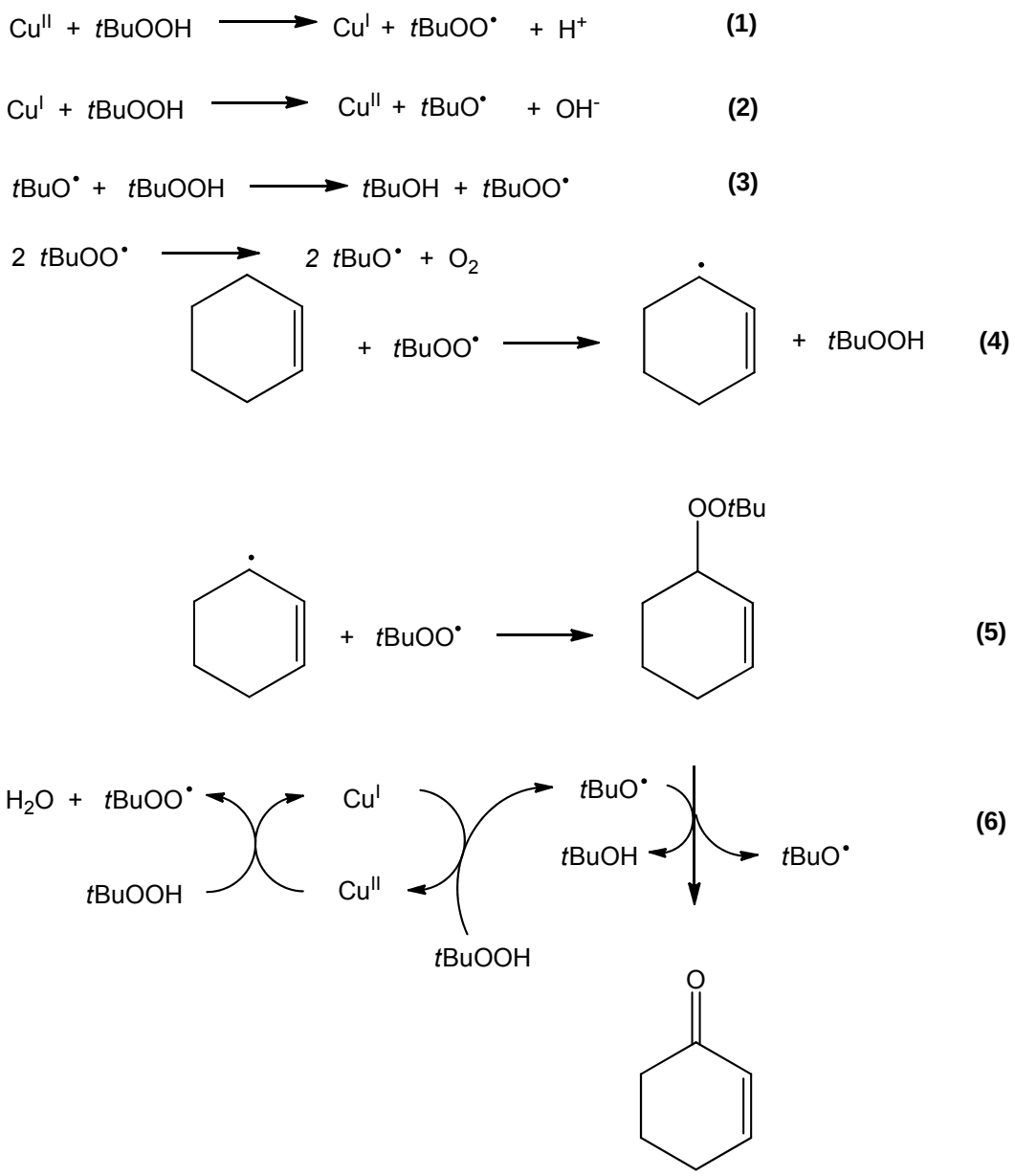

Scheme 3.2.5. Mechanistic proposal of allylic oxidation of cyclohexene with TBHP.

In the presence of O_2, the allylic radicals formed by *tert*-BuOO$^{\bullet}$ free radical induced allylic H-atom abstraction are intercepted by O_2 to form an intermediate allylperoxy radical.[286-289] This intermediate radical either abstracts a hydrogen atom from the allylic

position of another hydrocarbon to form allylic hydroperoxide (Scheme 3.2.6., 5a), or undergoes direct conversion to ketone (6a). This direct conversion explains the absence of alcohols in allylic oxidation reactions with TBHP and O_2 (Table 3.2.11.). The selectivity in the conversion of the allylperoxy radical to ketone in competition with hydrogen atom abstraction from hydrocarbon substrate is the core feature of allylic oxidations (Scheme 3.2.6.) and has been also reported for Rh_2(caprolactamate)$_4$ catalyst.[290]

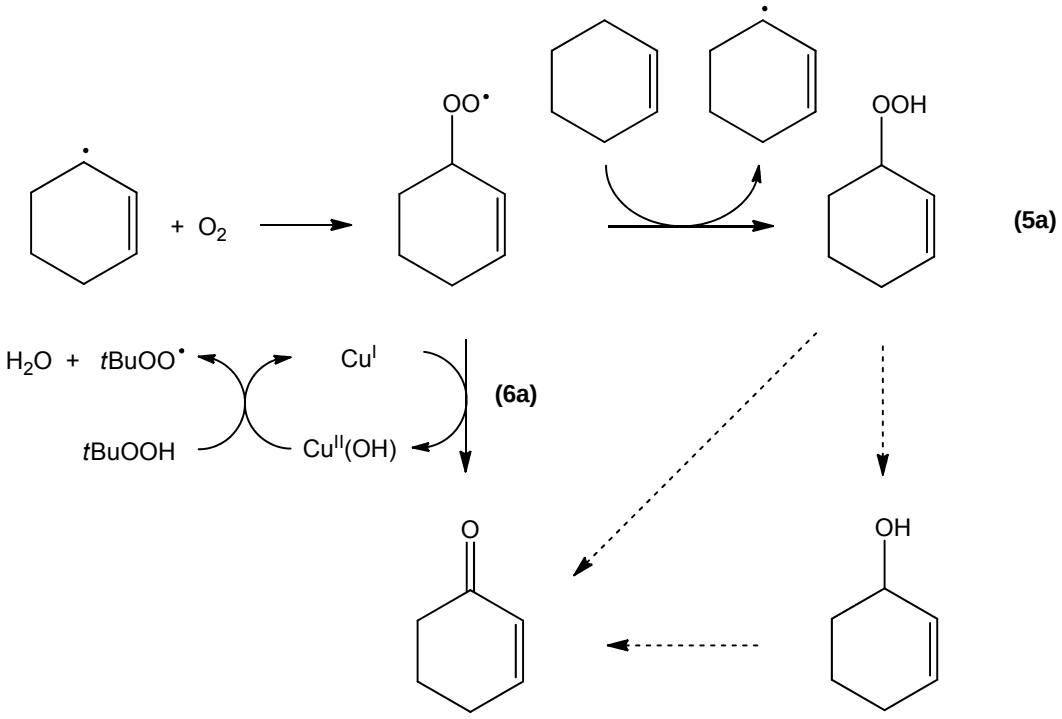

Scheme 3.2.6. Mechanistic proposal of allylic oxidation of cyclohexene with O_2.

Ligand transfer oxidation of the allylic radical was also proposed to be involved in allylic cyclohexene oxidation (Scheme 3.2.7.).[284] Ligand transfer of metal bonded *tert*-butyl peroxide to the carbon-centered radical results in allylic *tert*-butylperoxide formation that undergoes rapid decomposition yielding α,β-enone formation.

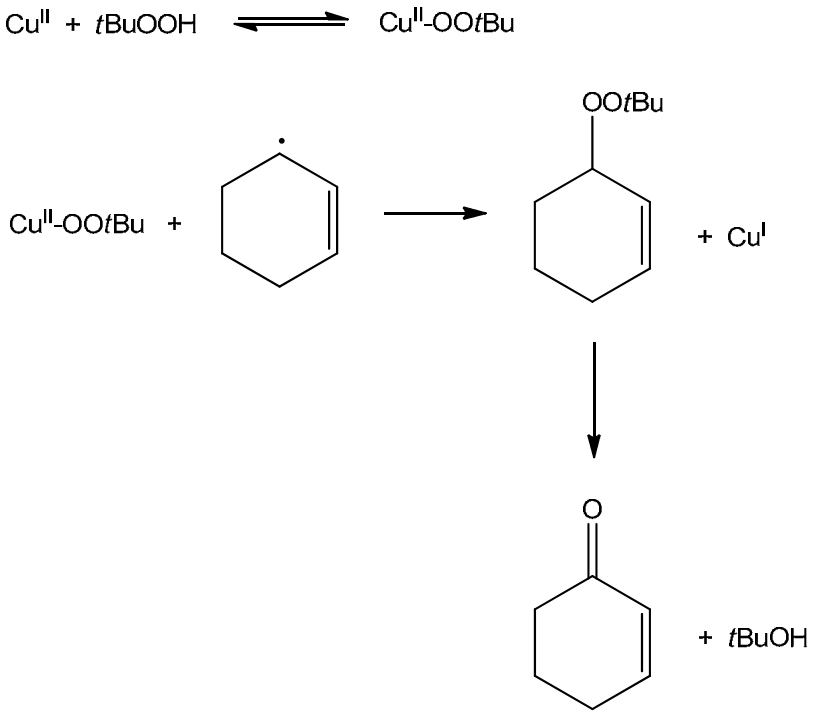

Scheme 3.2.7. Mechanistic proposal of allylic oxidation of cyclohexene *via.* ligand transfer with TBHP.

High selectivity of air and TBHP towards allylic oxidations of unsaturated hydrocarbons and steroids was reported in literature with various catalysts. Cu^{II}-Valine based catalysts also exhibited high selectivity towards α,β-unsaturated enone with air and TBHP as oxidants. Selectivity towards allylic C-H bond activation can be explained by the ability of *tert*-butylperoxy radicals (t-Bu-$OO^{\bullet}$) to abstract a hydrogen atom from the site that has the lowest carbon-hydrogen dissociation energy (372 kJ/mol).

Allylic C-H bonds show enhanced reactivity as they are about 15% weaker than C-H bonds in ordinary sp^3 carbon centres.[291, 292] The *tert*-butylperoxy radical is the most likely hydrogen abstraction agent, but there is also the possibility of involvement of metal-oxo species. Interestingly, both homogeneous and heterogeneous catalysts produced 2-cyclohexene-1-one and cyclohexene oxide (~18-28 mol%), but formation of 2-cyclohexene-1-ol was not observed (Table 3.2.11.). The fact that 2-cyclohexene-1-ol was not produced has also recently been reported with a Rh_2(caprolactamate)$_4$ catalyst and may be explained by the ability of cyclohexene peroxy radicals to undergo oxidation of the metal leading to direct formation of α,β-enone (2-cyclohexene-1-one). This explains the absence of alcohols in allylic oxidation reactions with TBHP and O_2.[293]

Small amounts of cyclohexene oxide formation with air and TBHP can be explained by the fact of free radical chain process involvement and cyclization of β-alkyl peroxy carbon radicals that yield epoxide formation.[294] Such radical formation of cyclohexene

oxide with TBHP as oxidant has been reported for (*Z*)-stilbene oxidation to stilbene oxide with $Pd(OAc)_2$ (Pd (II) acetate) catalyst. [295] Additional support for the radical epoxidation pathway was also derived from the styrene oxidation with TBHP in the presence of $Pd(OAc)_2$ catalyst that produced styrene oxide with selectivity of 5%. The balance between allylic oxidation and epoxidation depends on the olefin structure, steric effects and relative stabilities of the allylic radicals resulting from hydrogen atom abstraction and radicals resulting from addition of *tert* -butylperoxy radicals (*t*BuOO•) to C=C double bond. The comparison of epoxidation and allylic oxidation mechanisms is the summarised in Scheme 3.2.8.

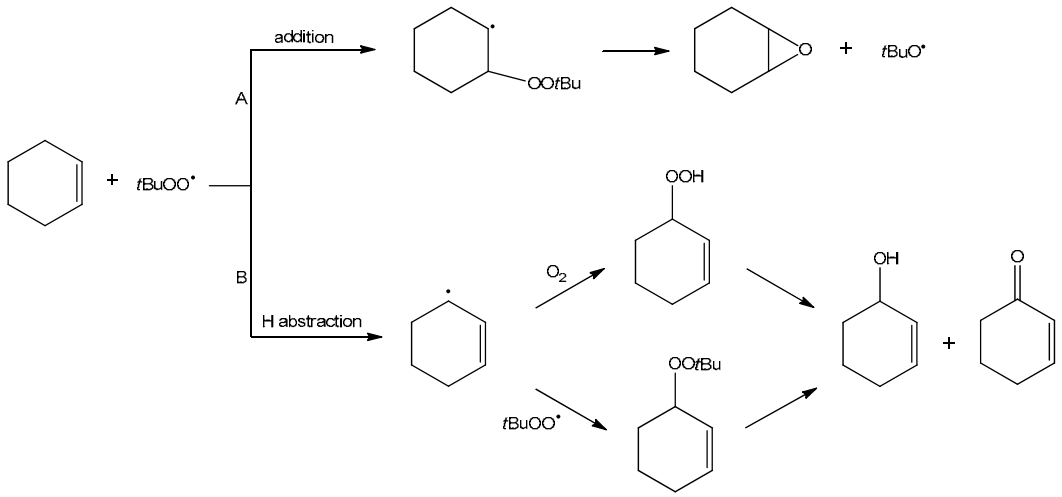

Scheme 3.2.8. Comparison of radical epoxidation (A) and allylic oxidation (B) mechanisms.

APB (acetylperoxyborate) has been reported in the literature to be a selective oxidant for alkene epoxidation reactions with single-site aluminophosphate catalysts.[296] Cu^{II}-perchlorophthalocyanine encapsulated within MCM-41 also exhibited higher yield of epoxide formation when a peracid was used as oxidant compared with TBHP which favoured abstraction over addition resulting in lower epoxide yields.[255] In this study, APB also proved to be a selective oxidant towards epoxide formation with Cu^{II}-Valine catalysts. This solid oxidant source, when being dissolved in water, liberates peracetic acid that is a selective epoxidizing agent. Peracids are known to be effective oxidants for C=C double bond oxidation resulting in high yields of epoxide formation (for more details see section 3.2.5.1. and Scheme 3.2.3.).

Catalyst recycling. To investigate catalyst reusability, cyclohexene oxidation with air was studied with low metal loading Cu^{II}-Valine-MCM-41 (Cu 0.42%wt.) and Cu^{II}-Valine-Polystyrene (Cu 0.018 %wt.) catalysts. At the end of the first run, the catalysts were

separated by filtration, washed with acetonitrile and dried in air at 80°C. Preliminary results on catalyst recycling seem to be reasonable, however detailed studies involving larger number of recycling steps and characterization of reused catalysts are required. The high selectivity to 2-cyclohexene-1-one was unaffected with both catalysts. Comparison of TON and selectivity using fresh and reused catalysts is presented in Figure 3.2.31. for Cu^{II}-Valine-MCM-41 (Cu 0.42%wt.) and Figure 3.2.32. for Cu^{II}-Valine-Polystyrene (Cu 0.018 %wt.).

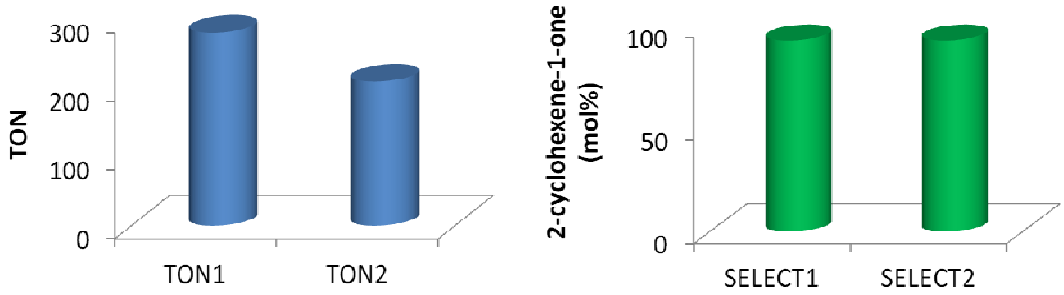

Figure 3.2.31. Comparison of turnover number (TON) and selectivity (SELECT) in the oxidation of cyclohexene using Cu^{II}-Valine-MCM-41 with air, t=4h, TON1, SELCT1 catalysed by fresh catalyst, TON2, SELCT2 catalysed by reused catalyst.

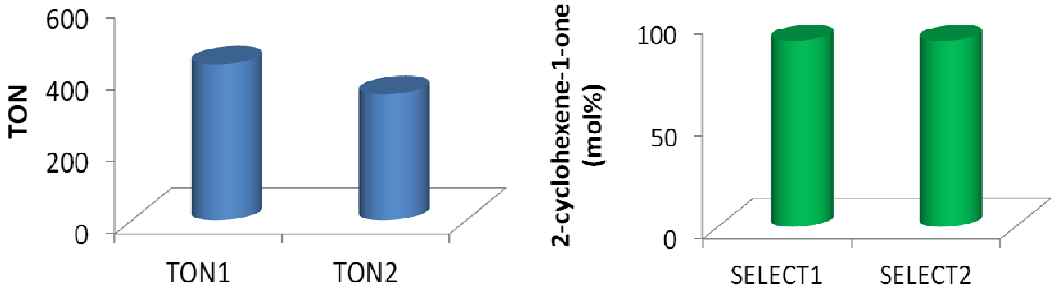

Figure 3.2.32. Comparison of turnover number (TON) and selectivity (SELECT) in the oxidation of cyclohexene using Cu^{II}-Valine-Polystyrene with air, t=4h, TON1, SELCT1 catalysed by fresh catalyst, TON2, SELCT2 catalysed by reused catalyst.

3.2.6. Dimethyl sulfide oxidation with neat Cu^{II}-Valine and heterogeneous Cu^{II}-Valine-MCM-41 and Cu^{II}-Valine-Polystyrene complexes.

3.2.6.1. Introduction to sulfide oxidation.

Sulfide oxidation is a very important reaction in synthetic transformations and has attracted wide interest as valuable synthetic reagents can be generated through this oxidation process. In particular sulfoxides are valuable intermediates for the production of a wide range of biologically and chemically active molecules including antibacterial (sulfonamides), antifungal and cardiotonic agents, anti-atherosclerotic, antihypertensive, psychotonics, and anti-ulcer (proton pump inhibitor) therapeutics.[297, 298]

Preferably transformation of sulfide to sulfoxide should proceed with high selectivity, avoiding overoxidation to sulfones. Sulfones are also important intermediates in organic synthesis; but again quantitative conversions and high sulfone selectivity is needed. Organic sulfoxides play an important role in biomedicine due to similarities of sulphur centres in many bioactive molecules, also playing key roles in the activation of enzymes. Many insecticides that contain a sulfoxide group are commercially manufactured by oxidizing sulfides with H_2O_2. Sulfoxides are also very useful building blocks as chiral auxiliaries in organic synthesis.[299] Examples of bioactive molecules that contain sulfoxide or sulfone groups are presented in Figure 3.2.33.

Stoichiometric oxidation of sulfides to sulfoxides can be accomplished with reagents like HNO_3, $KMnO_4$, MnO_2, but cleaner methods based on catalytic oxidation using molecular oxygen, aqueous hydrogen peroxide, or tertbutyl hydroperoxide are preferred.[300] Various tungsten based catalysts for the oxidation of aromatic and aliphatic sulfides using 30% H_2O_2 were reported as selective catalysts for sulfoxide transformations.[301] Oxorhenium dithiolates in the presence of TBHP also showed activity towards selective oxidation of sulfides.[302] Liquid-phase oxidation of sulfides with heterogeneous titanium silicates TS-1 and TS-2 with H_2O_2 were demonstrated, however bulky sulfides were not oxidised due to limited access to the Ti active sites.[303, 304] Ti-zeoliteβ catalysts also allowed the oxidation of sulfides.[305] Several efficient systems for catalytic sulfide oxidation based on V, Mo, Co, Cu and Fe metal ions were also reported.[306]

Table 3.2.13. Comparison of catalytic performance of heterogeneous and homogeneous catalysts in selective oxidation of sulfide to sulfoxide.

Catalyst	***Substrate***	***Oxidant***	***Conv. (%)***	***Sulfoxide Selectivity (%)***	***Ref.***
Ammonium Tungstate-MCM-41	dimethyl sulfide	H_2O_2	99	99	[301]
MeReO-(dithiolate)PPh_3	dimethyl sulfide	TBHP	99	99	[302]
Ti TS-2	dimethyl sulfide	H_2O_2	100	97	[303]
	diethyl sulfide	H_2O_2	100	85	
	methyl phenyl sulfide	H_2O_2	98	78	
Ti-zeoliteβ	diethyl sulfide	H_2O_2	99	99.5	[305]
	methyl phenyl sulfide	H_2O_2	77.2	92.8	
Cu-TACN	ethyl phenyl sulfide	H_2O_2	99	92	[307]
Mn-TACN	diphenyl sulfide	H_2O_2	99	50	[308]
	ethyl phenyl sulfide	H_2O_2	32	25	
	2-chloroethyl-phenyl sulfide	H_2O_2	99	1	
Mo(O_2)-L-MCM-41	methyl phenyl sulfide	H_2O_2	99	99	[309]
V(O)L-MCM-41	methyl phenyl sulfide	H_2O_2	99	99	[309]

TACN = 1,4,7-tris(carbamoylethyl)-1,4,7-triazacyclononane, L=[(2S,4S)-N-(3-triethoxy silyl)-propylaminocarbonyl-4-hydroxy-4-phenyl-2-(1,1-diphenylmethyl)-pyrrolidinyl-methanol], Por = porphyrin.

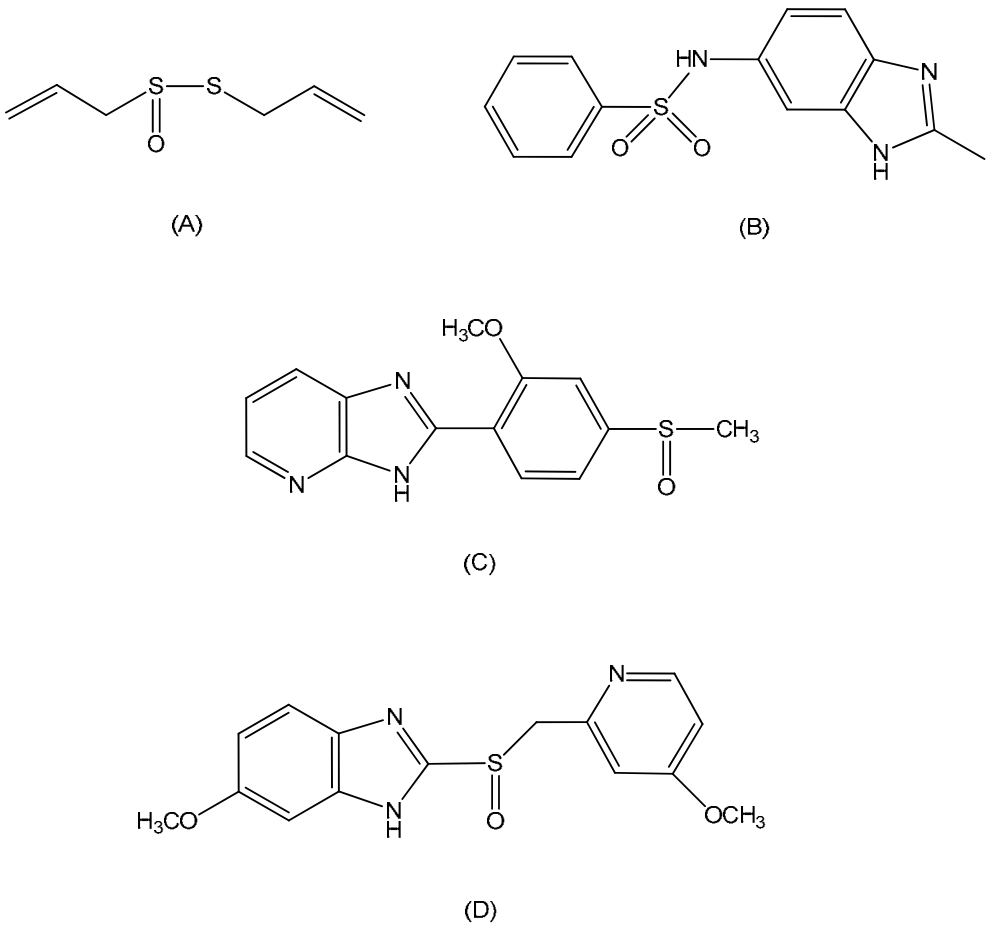

Figure 3.2.33. Representation of biologically active sulfur containing molecules: allicin - antimicrobial agent (A) benzimidazolyl-benzenesulfonamide-antibacterial activity against *Staphylococcus aureus* and *Bacillus subtilis*. (B), Sulmazole - cardiotonic agent (C), Omeprazole - proton pump inhibitor (D).

Heterogeneous Cu and Mn complexes with *N*,*N*-bis[(*S*)-prolyl]ethylenediamine ligand (Figure 3.2.34.) were reported as selective catalysts for sulfides oxidation using iodosylbenzene (PhIO) as oxidant, yielding sulfoxides as the main or sole products.[310] These complexes were immobilised through covalent bonding of triethoxysilyl groups to zeolite USY (ultrastable Y) and MCM-41. In the case of Cu based catalyst the TOF of USY and MCM-41 immobilized complexes was higher than the corresponding homogeneous complexes but conversion was lower (Table 3.2.14.). It was proposed that the lower conversions obtained with heterogeneous catalysts, compared to the homogeneous counterpart, could originate from restrictions imposed on the diffusion of substrates and products through the pores of the solid support. In the case of Mn catalysts the heterogeneous analogues displayed higher conversions than homogeneous catalysts (Table 3.2.15.). This was explained by possible termination of the catalytic cycle that could occur due to two factors: formation of Mn–O–Mn species, that have poor catalytic

activity, or due to the oxidative degradation of metal complexes. Heterogenisation of this complex within solid porous supports improved the stability of the metal complex under the reaction conditions preventing the catalytic species from dimerization or aggregation.

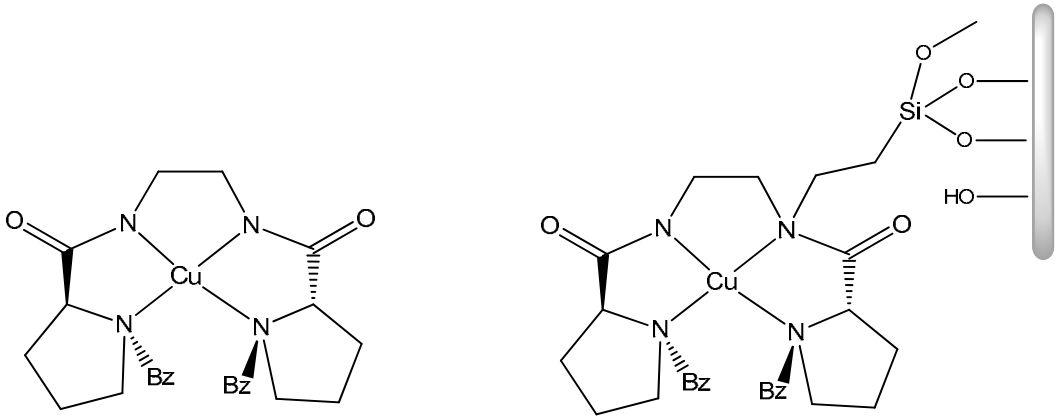

Figure 3.2.34. Representation of homogeneous (left) and heterogeneous MCM-41 anchored (right) Cu-*N*,*N*'-bis[(*S*)-prolyl]ethylenediamine complex.

Table 3.2.14. Results of methyl phenyl sulfide oxidation with Cu-*N*,*N*'-bis[(*S*)-prolyl]-ethylenediamine complex.

Catalyst	Conversion (%)	TOF
Cu homogeneous	86	103
Cu-USY	67	225
Cu-MCM41	83	250

Table 3.2.15. Results of methyl phenyl sulfide oxidation with Mn-*N*,*N*'-bis[(*S*)-prolyl]-ethylenediamine complex.

Catalyst	Conversion (%)	TOF
Mn homogeneous	76	163
Mn-USY	92	311
Mn-MCM41	78	274

Similar studies were performed with homogeneous and USY or MCM-41 heterogenised molybdenum and vanadium based catalysts.[309] In methyl phenyl sulfide oxidation reactions the immobilised complexes were more active than the corresponding homogeneous counterparts. Molybdenium heterogeneous MCM-41 catalysts were more active than USY analogues. This fact was explained as a possible consequence of the easier diffusion of the sulfide through the pores of MCM-41 (35 Å) than in the cavities and channels of zeolite USY (12–15Å). However, in the case of heterogenised vanadium catalysts the activity of USY-heterogenised catalyst was similar to that of the MCM-41 analogue. It was suggested that, due to the high affinity of vanadium to coordinate to free silanol groups from the surface of the support, some of the metal catalytic active centres were no longer available for the reactants. Thus, in the case of MCM-41, where the content of silanol groups (Si-OH) is higher, a higher number of active centres could coordinate resulting in lose of catalytic activity.

Organic sulfides are oxidized by nucleophilic attack of the sulfur atom on the oxygen.[311] Due to high nucleophilicity of the sulfur atom, sulfides (thioethers) are much more reactive than hydrocarbon compounds (alkenes, alkanes or aromatic) in oxidation reactions. In the first step of sulfide oxidation reaction, the sulfur atom attacks the terminal oxygen of the peroxide group. Cleavage of the peroxide O-O bond results in the formation of an alkoxy anion and a sulfoxide which is protonated at the oxygen atom. Proton exchange yields formation of sulfoxide and the alcohol (corresponding to the peroxide formation in alkene oxidation, Scheme 3.2.9.).
Ti zeolites and Ti-MCM-41catalysts with H_2O_2 have been widely studied for applications in selective sulfoxidation reactions. The active catalytic species in the oxidation reactions with hydrogen peroxide over Ti-containing molecular sieves is a complex containing a peroxo (Scheme 3.2.10., A) or a hydroperoxo ligand (Scheme 3.2.11., A).[305] The nucleophilic attack of the sulfur atom on an oxygen atom of such complexes (Scheme 3.2.10., B and Scheme 3.2.11., B) leads to the sulfoxide formation.

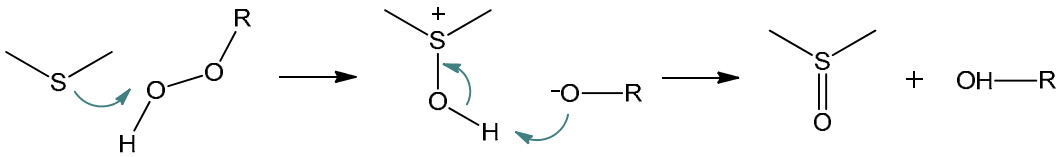

Scheme 3.2.9. Mechanism of sulfide oxidation with peroxide.

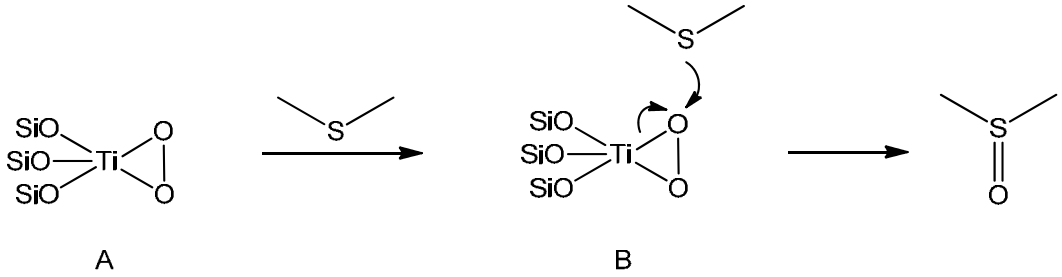

Scheme 3.2.10. Proposed mechanism of sulfide oxidation with H_2O_2 catalyzed by Ti-containing zeolites *via* peroxo active species (A).

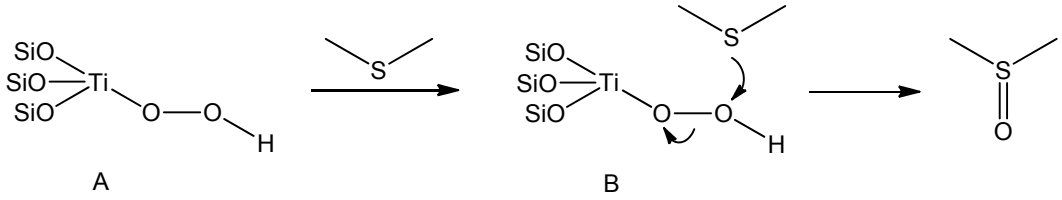

Scheme 3.2.11. Proposed mechanism of sulfide oxidation with H_2O_2 catalyzed by Ti-containing zeolites *via* hydroperoxo active species (A).

Cu^{II} complexes with triaza macrocyclic ligands such as 1,4,7-tris(carbamoylethyl)-1,4,7-triazacyclononane (Figure 3.2.35.) and Cu^{II} salts ($CuBr_2$, $CuCl_2$ *$2H_2O$, $Cu(OAc)_2$ *H_2O) were explored and showed potential towards selective sulfide transformations.[307] It was proposed that oxidation of organosulfur compounds with these copper catalysts occurs by transfer of the oxygen atom from the active Cu-oxo species to the sulfur atom of substrate that leads to product formation. Such a mechanism was proposed to proceed *via* an active oxidant–substrate complex and it has been suggested that the Cu^{II}/Cu^{III} redox couple is involved in the key step. In the first step, this mechanism involves the formation of the active oxidant species *via* copper *tert*-butylperoxide species (Cu-OO*t*Bu). Copper *tert*-butylperoxide undergoes O-O cleavage that results in the formation of a reactive Cu-oxo species (Cu^{III}=O). This active species form a complex with the substrate and facilitates oxygen atom transfer to the substrate and selective oxidation of sulfides to sulfoxides. A proposed mechanism for sulfide oxidation with Cu^{II}/TBHP is shown below (Scheme 3.2.12.).

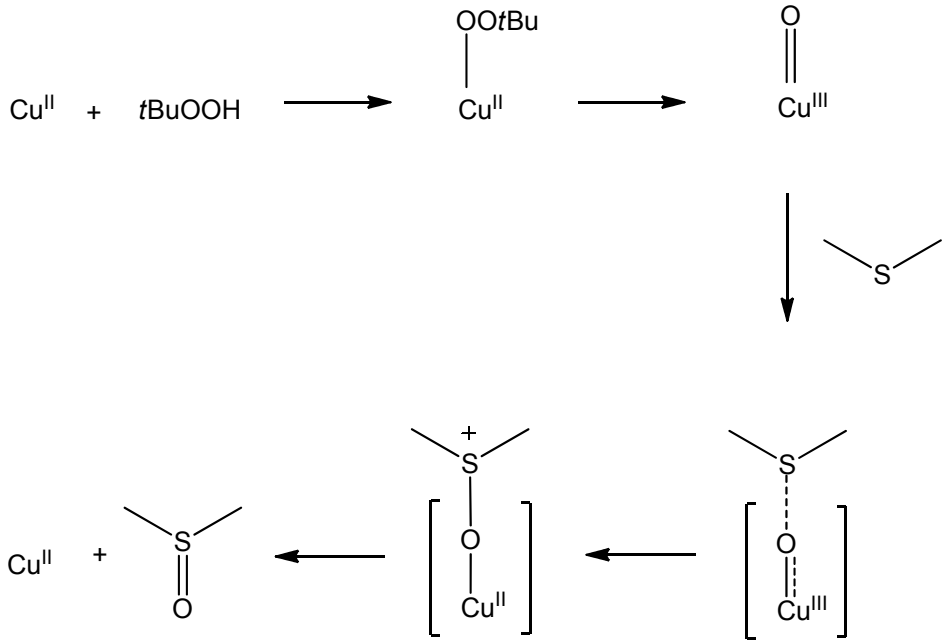

Scheme 3.2.12. Proposed mechanism of sulfide oxidation with Cu^{II}.

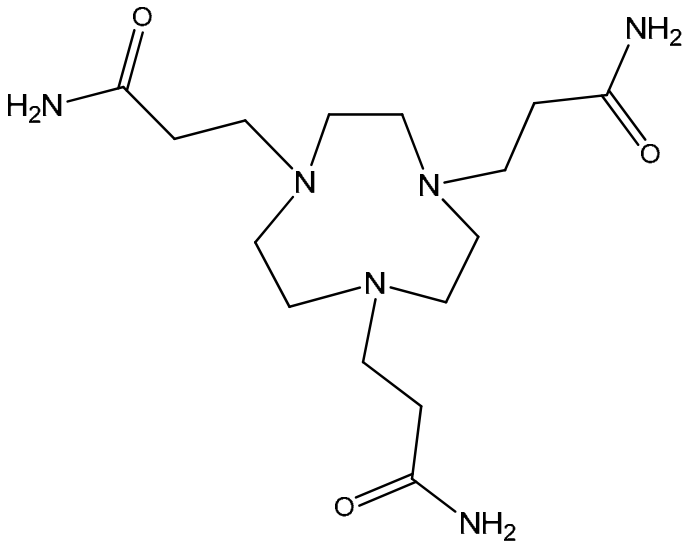

Figure 3.2.35. Representation of 1,4,7-tris(carbamoylethyl)-1,4,7-triazacyclononane ligand. [1]

Bis(μ-oxo)dicopper^{III} complexes with bidentate (*N*-ethyl-*N*-[2-(2-pyridyl)ethyl]-α,α-dideuteriobenzylamine) ligands have also been reported as catalysts for sulfide oxidation to the corresponding sulfoxides.[312] Since bis(μ-oxo)dicopper^{III} species were considered as possible active oxygen intermediates of copper monooxygenases, direct oxygen atom transfer *via* formation of a binary complex between the substrate and the metal−oxo species has been proposed for this catalytic system (Scheme 3.2.13.).

[1] This name is ambiguous and the molecule may have different names such as *N,N,N*-tris(propanamide)-1,4,7-triazacyclononane or Hexahydro-1H-1,4,7-Triazonine-1,4,7-tripropanamide (CAS).

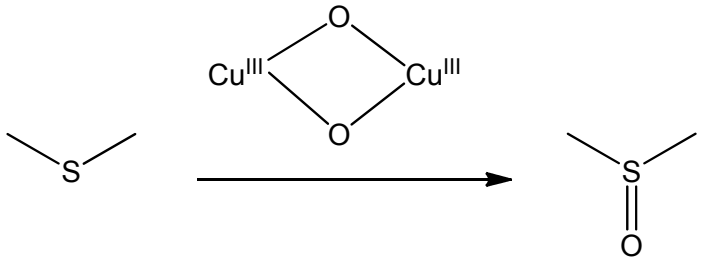

Scheme 3.2.13. Schematic model of sulfide oxidation with bis(μ-oxo) dicopper^{III} complexes.

3.2.6.2. Dimethyl sulfide oxidation with Cu^{II}-Valine catalysts.

The reactivity of Cu^{II}-Valine based catalysts and the role of isolated active sites was tested towards the selective oxidation of dimethyl sulfide. Cu^{II}-Valine catalysts displayed a high propensity for dimethyl sulfoxide formation, and dimethyl sulfone was not produced. All Cu^{II}-Valine based catalysts were >99mol% selective to dimethyl sulfoxide. Control experiments in the absence of catalyst gave conversions of 11.0 mol% with TBHP, and 5.1 mol% in the presence of air. The results on selective oxidation of dimethyl sulfide with Cu^{II}-Valine catalysts are listed in Table 3.2.16.

Table 3.2.16. Results on catalytic, selective oxidation of dimethyl sulfide with Cu^{II}-Valine catalysts. For reaction conditions see section 6.10.7.

Cat.	Metal load.	Oxid.	Mmol of metal	Cat. (g)	Subst: Metal ratio	Oxid: Substr. ratio	TON	TOF (h^{-1})	Conv. mol %	Select. mol % soxide.
Neat	22.4	AIR	0.027	0.008	581	1.65	274	46	47.2	>99
Neat	22.4	TBHP	0.027	0.008	581	1	483	81	83.1	>99
MCM	0.42	AIR	0.004	0.06	1865	1.65	1113	185	59.7	>99
MCM	0.42	TBHP	0.004	0.06	1865	1	1596	266	85.6	>99
Polyst	0.018	AIR	0.0003	0.12	1892	1.65	1258	209	66.4	>99
Polyst	0.018	TBHP	0.0003	0.12	1892	1	1560	260	82.5	>99
Blanc	-	AIR	-	-	-	1.65			5.1	>99
Blanc	-	TBHP	-	-	-	1			11.0	>99

T=371 K, air 3.0 MPa, acetonitrile 35g, reaction time=6h, soxide-dimethyl sulfoxide.

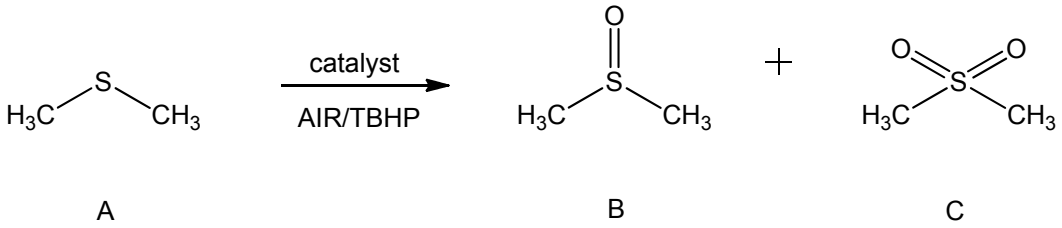

Scheme 3.2.14. Schematic representation of product formation in dimethyl sulfide (A) oxidation to dimethyl sulfoxide (B) and dimethyl sulfone (C).

Heterogeneous MCM-41(Cu 0.42%wt.) and polystyrene supported Cu^{II}-Valine catalysts (Cu 0.018 %wt.) with well-isolated active sites showed to be much more active than their homogeneous analogues in the presence of both oxidants used in this study (air and TBHP). In fact, in the presence of air, TON and TOF increased from 274 and 46 h^{-1} (neat Cu^{II}-Valine) to 1113 and 185 h^{-1} (Cu^{II}-Valine-MCM-41) and to 1113 and 209 h^{-1} (Cu^{II}-Valine-Polystyrene). When TBHP was used, both heterogeneous catalysts showed a *three-fold* increase in activity (TON of 1596 and 1560, TOF of 266 h^{-1} and 260 h^{-1} for Cu^{II}-Valine-MCM-41 and Cu^{II}-Valine-Polystyrene, respectively), while the homogeneous analogue afforded TON and TOF of 483 and 81 h^{-1}. This large increase in activity strongly suggests that the isolated active sites generated during immobilisation of the homogeneous Cu^{II}-Valine complex within solid host matrices were responsible for significant changes in catalyst activity.

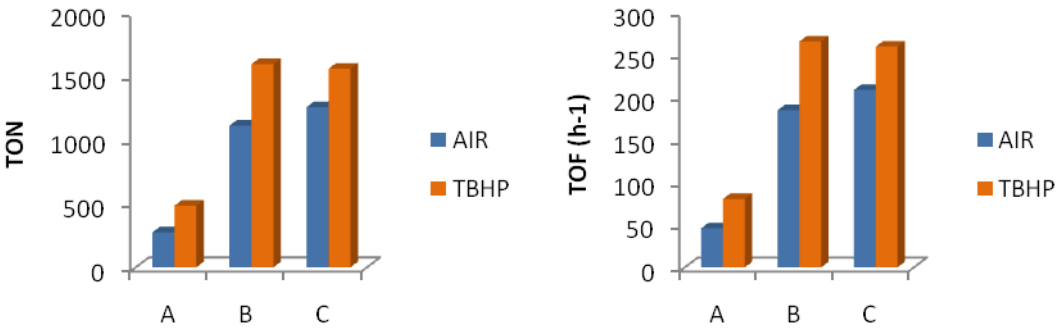

Figure 3.2.36. Comparison of TON (left) and TOF (right) in dimethyl sulfide oxidation reactions using Cu^{II}-Valine (A), Cu^{II}-Valine-MCM-41 (Cu 0.42%wt.) (B), Cu^{II}-Valine-Polystyrene (Cu 0.018 %wt.)(C), with air and TBHP.

Influence of oxidant on reaction conversions. Conversions of dimethyl sulfide, in reactions with homogeneous Cu^{II}-Valine complex, were found to be strongly dependant on oxidant nature. The neat Cu^{II}-Valine catalyst produced much higher conversion with

TBHP (83.1 mol%) than with air (47.2 mol%), under the given reaction conditions. In the case of heterogeneous catalysts, reaction conversions were less dependent on oxidant type. Cu^{II}-Valine-MCM-41 exhibited higher conversion of 85.6mol% in the presence of TBHP, and 59.7mol% with air as the oxidant. In the reaction employing Cu^{II}-Valine-Polystyrene, air afforded 66.4 mol% and TBHP afforded conversion of 82.5 mol%. Comparison of reaction conversions using homogeneous and heterogeneous catalysts is shown in Figure 3.2.37.

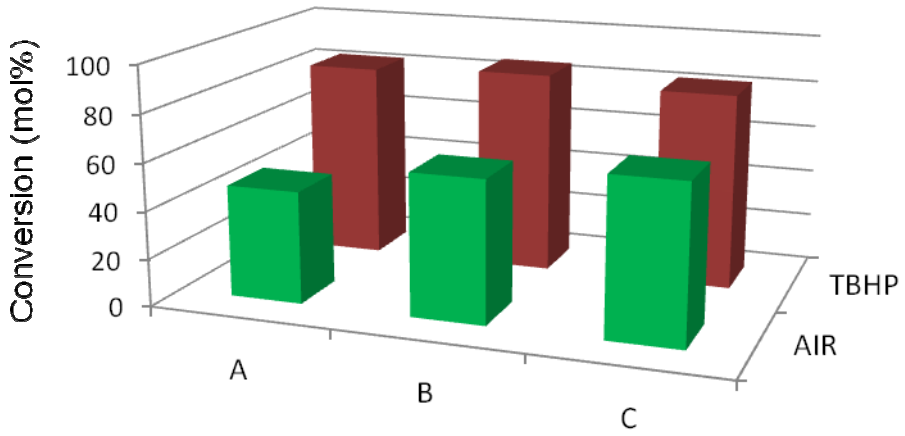

Figure 3.2.37. Comparison of reaction conversions in dimethyl sulfide oxidation reactions using Cu^{II}-Valine (A), Cu^{II}-Valine-MCM-41 (Cu 0.42%wt.) (B), Cu^{II}-Valine-Polystyrene (Cu 0.018 %wt.) (C), with air and TBHP.

In dimethyl sulfide oxidation reactions in presence of TBHP autoretardation was not observed. These effects could be explained by hydrophobic/hydrophilic interactions of the solid support with the oxidant, substrates and products and by competition between oxidant and substrates to access the active site.[313]

When comparing the hydrophobicity of cyclohexene, benzyl alcohol and dimethyl sulfide, cyclohexene is the most hydrophobic (log P = 2.38). A comparison of log P values is presented in Table 3.2.17. Log P (partition coefficient) is a measure of how hydrophilic or hydrophobic a chemical compound is. Partition coefficient is defined as the ratio of a chemical compound concentration in the octanol phase to its concentration in the aqueous phase of a two-phase octanol/water system. The higher the partition coefficient ,the higher the hydrophobicity of the compound.

The more hydrophobic cyclohexene, which posseses a higher affinity for hydrophobic supports than *t*BuOH, may restrict active site accessibility for the oxidant that could result in lower catalyst activity. Hydrophobic supports could hold cyclohexene within its matrix hindering the less hydrophobic oxidant its ability to access and react with the active site to form the active oxidant. Cyclohexene oxidation products cyclohexene oxide and

2-cyclohexene-1-one are less hydrophobic, their interactions with the support should be weaker and their diffusion should be more effective.

The hydrophobicity of benzyl alcohol on the other hand is very similar to that of *t*BuOOH and both, reagent and oxidant, have a similar affinity to the support. Dimethyl sulfide is slightly less hydrophobic than *t*BuOH, which means that the oxidant has a slightly higher affinity for the support and may reach the active site quicker to form the active oxidant. Dimethyl sulfoxide which is the product of dimethyl sulfide oxidation has amphiphilic properties due to its hydrophilic sulfoxide group and two hydrophobic methyl groups and its diffusion from the support should be more effective.

The activity of heterogeneous Cu^{II}-Valine catalysts seemed to be restricted by the preferential sorption/desorption of oxidant, reagents and reaction products, e.g. high sorption of peroxide on solid support induces excessive peroxide decomposition and low efficiencies. On the other hand high sorption of substrate onto solid support could create a barrier against oxidant (TBHP) and block access or slower diffusion of peroxide to the active site.

Table 3.2.17. Comparison of log P values.

Compound	***Log P***
Cyclohexene	2.38
Cyclohexene oxide	0.95
2-cyclohexene-1-one	0.75
Benzyl alcohol	1.02
Benzaldehyde	1.78
Dimethyl sulfide	0.81
Dimethyl sulfoxide	-1.49
*t*BuOOH	1.05
*t*BuOH	0.6

Such sorption/desorption and decomposition effects were reported in the literature for polydimethylsiloxane (PDMS) embeded FePcY catalyst.[314] This catalyst consisted of a highly hydrophobic PDMS-polymer combined with a hydrophilic zeolite Y. This hydrophobic membrane adsorbed cyclohexane preferentially and created a barrier against polar compounds. The membrane was saturated with cyclohexane at the start of the reaction and the peroxide diffused slowly into the membrane and then into the zeolite and to the active complex. These diffusion effects were suggested to be responsible for relatively slow product formation. It was also proposed that deactivation of this catalyst could occur due to sorption of the hydrophilic compounds formed during the reaction onto zeolite that have not completely desorbed from the zeolite during reaction. Especially adsorption of large amounts of water onto hydrophilic zeolite Y deactivated

the catalyst. Removal of water molecules from the zeolite enhanced catalyst activity as reagents could reach the active sites more easily.

The affinities of reagents and products to the membrane were determined by measuring the sorption of the compounds in the membrane. The measurements clearly showed predominant cyclohexane sorption (most hydrophobic compound). Cyclohexanone, the ketone, being more hydrophobic was adsorbed much more effective than the alcohol, cyclohexanol. Water sorption was intermediate and mainly associated with the sorption in the zeolite. Sorption of *tert*-butyl hydroperoxide was difficult to measure because its partial decomposition when adsorbed onto the catalyst.

Influence of the active site loading on catalytic activity. The decrease in copper sites loading resulted in increased dimethyl sulfide conversions as well as TON and TOF with both oxidants; air and TBHP. In the presence of air, the Cu^{II}-Valine-MCM-41 catalyst with high metal content (Cu 9.22%wt.) afforded conversion of 50.7 mol%, while its low metal content analogue (Cu 0.42%wt.) obtained higher conversion of 59.7 mol%. By decreasing metal site loading, the TON and TOF significantly increased from 112 and 19 h^{-1} (Cu^{II}-Valine-MCM-41, Cu 9.22%wt.) to 1113 and 185 h^{-1} (Cu^{II}-Valine-MCM-41 Cu 0.42%wt.). When TBHP was used, Cu^{II}-Valine-MCM-41 with high metal site content afforded lower conversion (71.3 mol%) than its low metal content analogue, which obtained the highest dimethyl sulfide conversion of all Cu^{II}-Valine based catalysts (85.6 mol%). Cu^{II}-Valine-MCM-41, (Cu 0.42%wt.) obtained TON and TOF of 1596 and 266 h^{-1}, that decreased to 158 and 26 h^{-1} when Cu^{II}-Valine-MCM-41 catalyst with high metal loading (Cu 9.22%wt.) was employed.

Similar trends were observed when polystyrene supported Cu^{II}-Valine catalysts were used with both oxidants. In presence of air, Cu rich Cu^{II}-Valine-Polystyrene (Cu 8.79 %wt.) afforded a conversion of 41.8mol% and its analogue with low loading of metal sites (Cu 0.018 %wt.) obtained much higher conversion of 75.4 mol%. By decreasing the metal content TON and TOF increased from 97 and 16 h^{-1} (Cu^{II}-Valine-Polystyrene, Cu 8.79 %wt.) to 1472 and 238 h^{-1} (Cu^{II}-Valine-Polystyrene, Cu 0.018 %wt.)), in presence of air.

In reactions with TBHP, Cu^{II}-Valine-Polystyrene (Cu 0.018 %wt.) afforded higher conversion (82.5 mol%) than its high copper content analogue (71.8 mol%). With decreased loading of metal sites the activity also increased. In fact, Cu^{II}-Valine-MCM-41 catalyst with high metal content (Cu 9.22%wt.) obtained TON and TOF of 167 and 28 h^{-1} that increased to 1560 and 220 h^{-1} when Cu^{II}-Valine-MCM-41 with low metal loading (Cu 0.42%wt.) was employed with TBHP.

Table 3.2.18. Results on selective oxidation of dimethyl sulfide with low and high metal loading Cu^{II}-Valine catalysts. For reaction conditions see section 6.10.7.

Cat.	Metal load.	Oxid.	Mmol of metal	Cat. (g)	Subst: Metal ratio	Oxid: Subst. ratio	TON	TOF (h^{-1})	Conv. mol %	Select. mol % soxide.
Neat	22.4	AIR	0.027	0.008	581	1.65	274	46	47.2	>99
Neat	22.4	TBHP	0.027	0.008	581	1	483	81	83.1	>99
MCM	9.22	AIR	0.072	0.05	221	1.65	112	19	50.7	>99
MCM	0.42	AIR	0.004	0.06	1865	1.65	1113	185	59.7	>99
MCM	9.22	TBHP	0.072	0.05	221	1	158	26	71.3	>99
MCM	0.42	TBHP	0.004	0.06	1865	1	1596	266	85.6	>99
Polyst	8.79	AIR	0.069	0.05	232	1.65	97	16	41.8	>99
Polyst	0.018	AIR	0.0003	0.12	1892	1.65	1258	209	66.4	>99
Polyst	8.79	TBHP	0.069	0.05	232	1	167	28	71.8	>99
Polyst	0.018	TBHP	0.0003	0.12	1892	1	1560	260	82.5	>99

T=371 K, air 3.0 MPa, acetonitrile 35g, reaction time=6h, soxide-dimethyl sulfoxide.

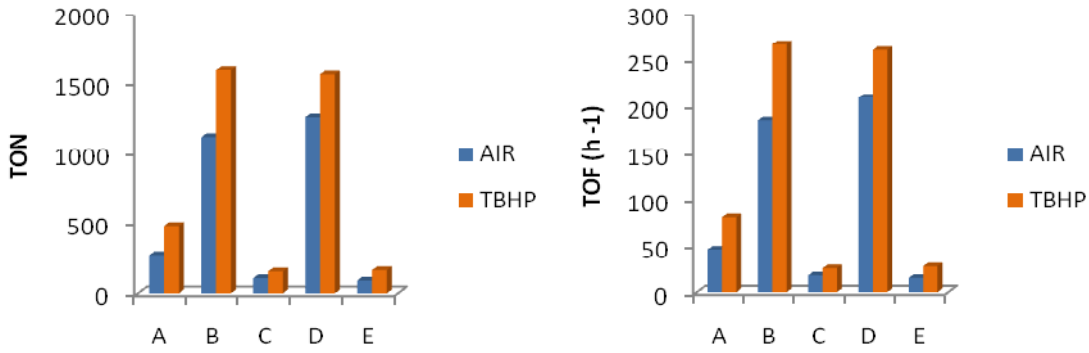

Figure 3.2.38. Comparison of TON (left) and TOF (right) in dimethyl sulfide oxidation reactions using Cu^{II}-Valine (A), Cu^{II}-Valine -MCM-41 (Cu 0.42%wt.) (B), Cu^{II}-Valine -MCM-41 (9.22%wt.) (C), Cu^{II}-Valine-Polystyrene (Cu 0.018 %wt.) (D), Cu^{II}-Valine-Polystyrene (8.79 %wt.) (E) with air and TBHP.

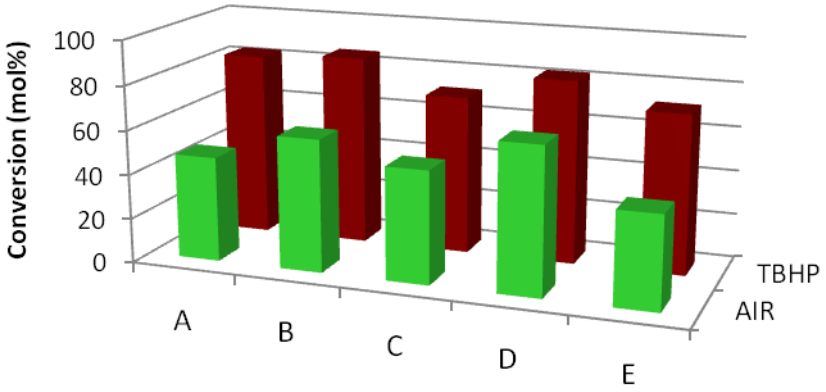

Figure 3.2.39. Comparison of conversions in dimethyl sulfide oxidation reactions using Cu^{II}-Valine (A), Cu^{II}-Valine-MCM-41 (Cu 0.42%wt.) (B), Cu^{II}-Valine-MCM-41 (9.22%wt.) (C), Cu^{II}-Valine-Polystyrene (Cu 0.018 %wt.) (D), Cu^{II}-Valine-Polystyrene (8.79 %wt.) (E) with air and TBHP.

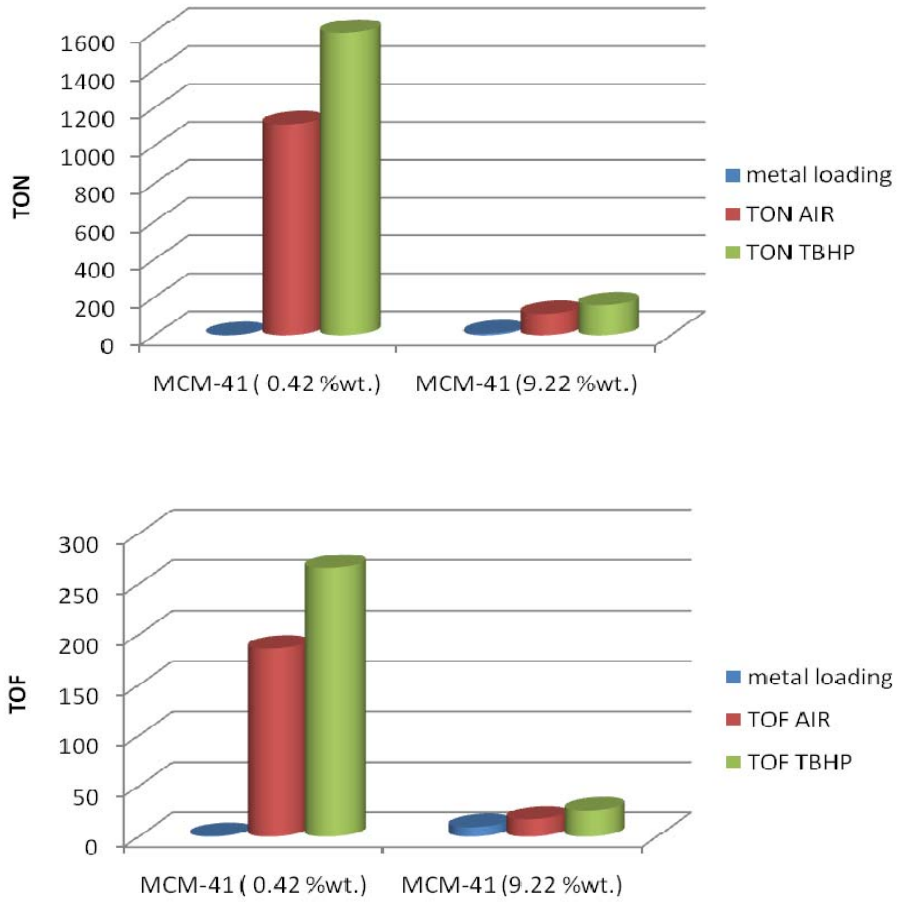

Figure 3.2.40. Comparison of TON (upper) and TOF (bottom) in dimethyl sulfide oxidation reactions using Cu^{II}-Valine-MCM-41 (Cu 0.42%wt.) and Cu^{II}-Valine-MCM-41 (9.22%wt.).

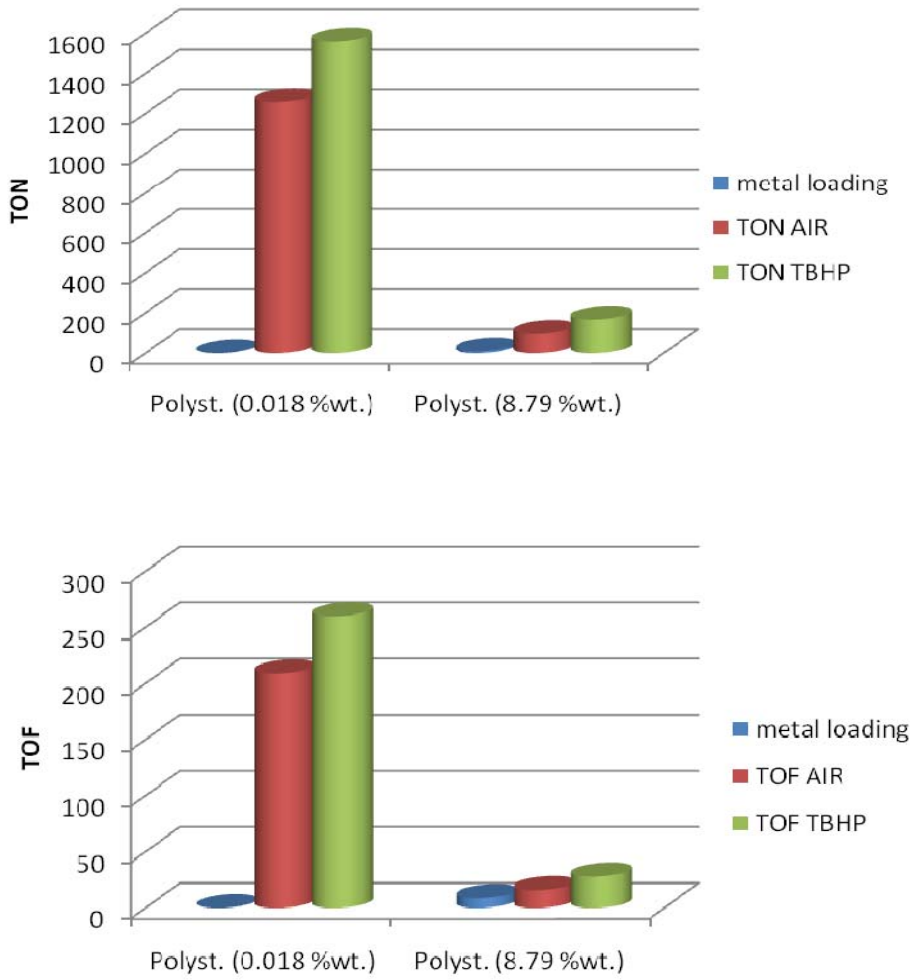

Figure 3.2.41. Comparison of TON (upper) and TOF (bottom) in dimethyl sulfide oxidation reactions using Cu^{II}-Valine -Polystyrene (Cu 0.018 %wt.) and Cu^{II}-Valine -Polystyrene (8.79 %wt.).

In dimethyl sulfide oxidation reactions with the heterogeneous catalysts it was found that higher metal loading produced lower reaction conversions than those with lower metal loading. This result could be a consequence of high density and poor dispersion of the active sites of heterogeneous high metal loading catalysts and could be associated with the slower diffusion of substrate and oxidant towards the active sites. This decrease in activity with increasing catalyst loading could also be explained in terms of cluster formation and accumulation of support-bound dimers which could have lower activity than the corresponding well-isolated and more accessible single sites.

High selectivity towards dimethyl sulfoxide formation with homogeneous and heterogeneous Cu^{II}-Valine catalysts can be explained by the fact that the reaction rate of sulfide oxidation to sulfoxide is faster than that for sulfoxide oxidation to sulfone.

Sulfides are more electron-rich and more nucleophilic than sulfoxides which results in higher reactivity.[315, 316]

Organic sulfides follow an electrophilic oxidation mechanism.[317] Thus the reaction proceeds through an electrophilic attack of the oxygen of the oxidant at the electron-rich sulfur centre of the substrate. Oxygen attack at the sulfide was postulated to be the rate-determining step.

The majority of oxidative metal-oxo species can attack through an electrophilic path in their catalytic cycle. In this process formation of sulfoxides is faster than sulfones, since sulfides are more electron-rich than sulfoxides. This can explain high sulfoxide selectivities. Based on literature reports for sulfoxidation reactions, the plausible oxidation path *via* Cu-oxo species is presented at Scheme 3.2.15.

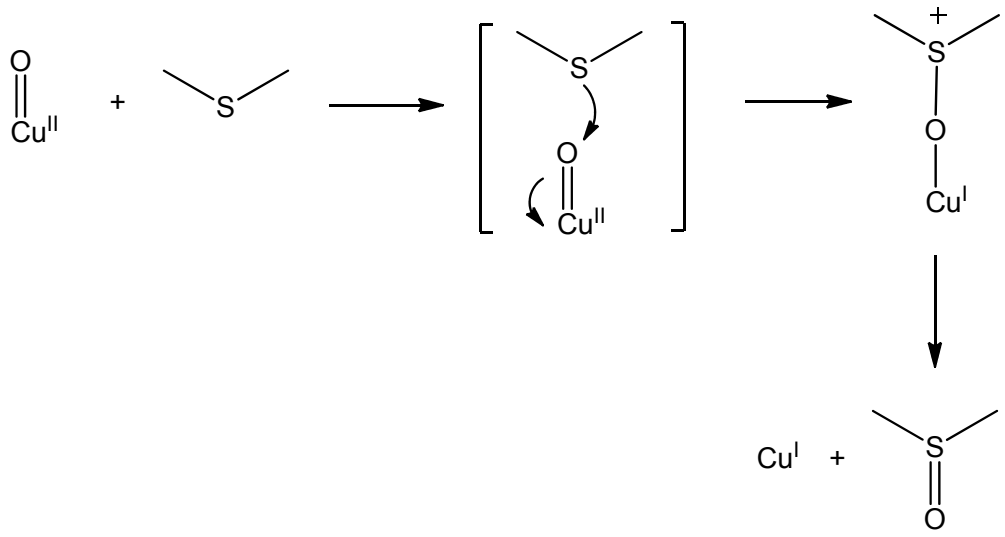

Scheme 3.2.15. Mechanistic proposal of sulfide oxidation of *via* attack of the oxygen at the sulfur center of the substrate.

Summary.

Cu^{II}-Valine complexes were successfully immobilized on MCM-41 and polystyrene supports.

Prior to functionalisation with the valine ligand, the silica surface was functionalized with methyl groups that enhanced the MCM-41 hydrophobicity and hydrothermal stability. Valine was grafted onto chloropropyl functionalised MCM-41 and chloromethylated polystyrene in the reaction that employed pyridine as a base under reflux condition.

The obtained materials were characterized by IR, DRUV-Vis, ICP and BET techniques. The immobilized amino acid formed stable complexes with copper. These heterogeneous

catalysts exhibited promising activity in the oxidation of such substrates as: benzyl alcohol, cyclohexene and dimethyl sulfide with various oxidants. Heterogeneous Cu^{II}-Valine-MCM-41 and Cu^{II}-Valine-Polystyrene catalysts obtained significantly higher TON and TOF when compared with homogeneous Cu^{II}-Valine analogue, indicating that good separation of the active metal sites was a key factor that enhanced the catalytic activities. Immobilization within a solid support matrix resulted in the active sites isolation that leads to higher turnover numbers and frequencies. The selectivities were modified by the geometric, steric and electronic effects exerted by the solid supports. Employed synthetic methodology resulted in formation of bioinspired, efficient and selective catalysts for oxidation reactions.

3.3. Synthesis, characterization and catalytic potential of Fe^{III}-Proline-MCM-41 and Fe^{III}-Proline-Polystyrene complexes.

3.3.1. Synthesis of MCM-41 and Polystyrene immobilized Fe^{III}-Proline complexes.

MCM-41 functionalization with Fe^{III}-Proline. MCM-41 was functionalized by chloromethylation reactions followed by azidation. The silica surface was first functionalized with a mixture of chloropropyl and methyl groups (the synthetic details are discussed in section 3.2.2. and 6.4.2.). The organo-chloro functionalized silica that contained a C-Cl end functional group was then used for immobilization of the azido moiety onto silica surface. Additional functionalisation with methyl groups was carried out to enhance the hydrophobicity and hydrothermal stability of the MCM-41support.[150] The lowering of the surface area from 1250 m^2/g (pure MCM-41) to 811 m^2/g was observed after introduction of chloropropyl and methyl groups indicated their presence within the mesopores of MCM-41.

Prior to further functionalization with proline, chloropropyl moieties of MCM-41 were first modified with azido groups, using the same methodology as with polystyrene functionalisation with azido groups which is discussed below. Functionalisation of MCM-41 and polystyrene with azido groups was confirmed by FTIR spectroscopy. The azido group (N_3) adsorption bands were observed at 2099 cm^{-1} in MCM-41 materials and at 2095 cm^{-1} in polystyrene. The synthetic details are given in section 6.4.3. and 6.4.4.

Polystyrene functionalization with Fe^{III}-Proline. The hydroxy group of 3-hydroxyproline was first functionalized with a propargyl group in order to generate the alkyne, that in the next step was involved in a cycloaddition reaction with the azido substituted polystyrene and MCM-41supports.[159] The click chemistry strategy that was employed facilitates the fusion of alkynes and azides (unsaturated reactants) and provides access to often very stable five-membered heterocycles. The click chemistry technique was employed for the purpose of anchoring of the *O*-propargyl functionalised proline to the azide substituted Merrifield resin *via* the 1,2,3-triazole moiety (Scheme 3.3.1.). This reaction is catalysed by copper (I) salts (mechanism is described in section 1.4.3.). Azides are the most crucial functional groups for click chemistry due to their stability toward H_2O, O_2 and the majority of organic synthesis conditions. Such Cu^I catalysed synthesis of triazoles resulted in formation of thermally and hydrolytically stable 1,2,3-triazole moiety in high yields and regioselectivity.

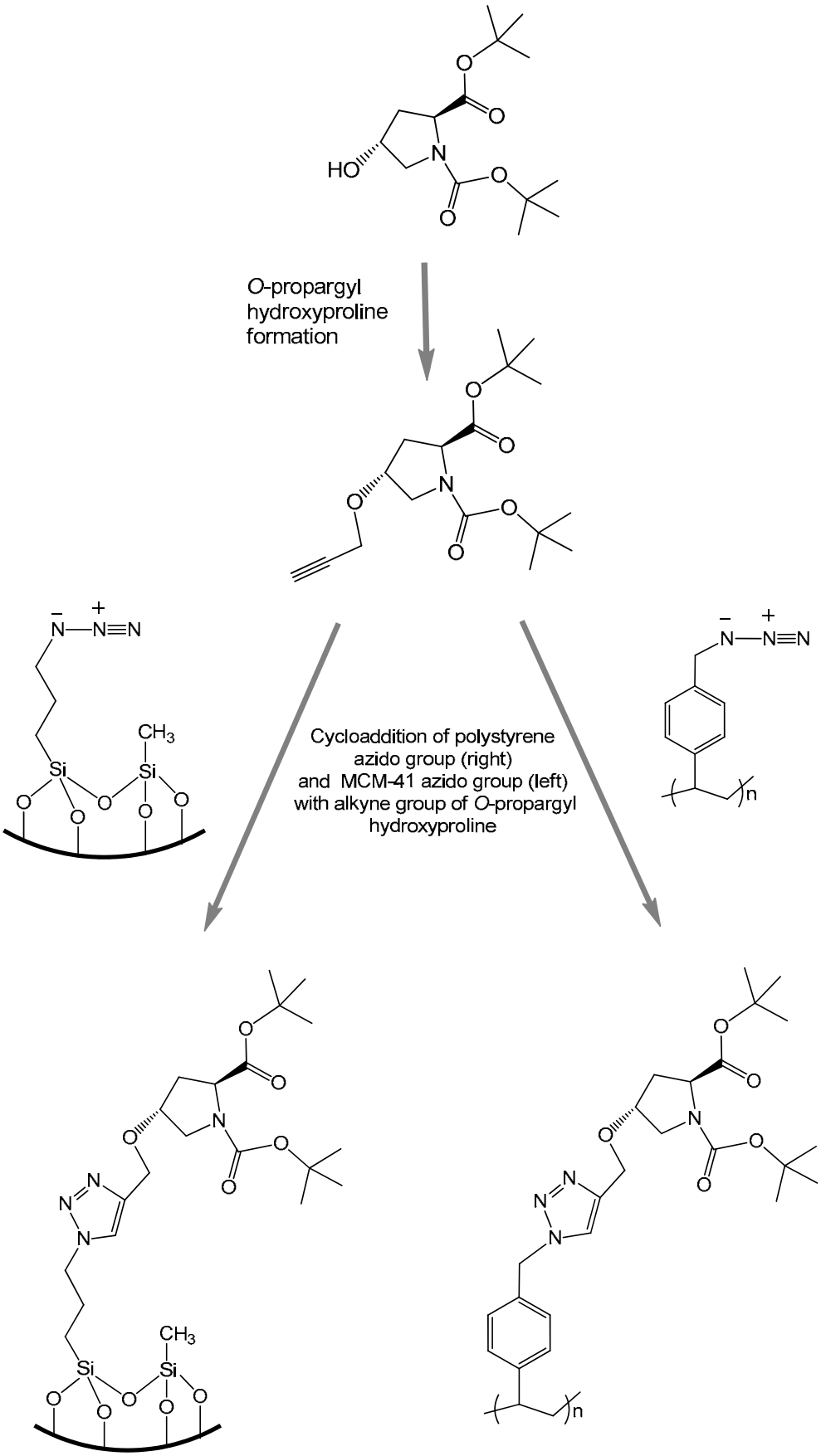

Scheme 3.3.1. Schematic representation of cycloaddition of azido group with alkyne group of O-propargyl hydroxyproline.

By employing the click chemistry methodology, 3-hydroxyproline could be anchored to polystyrene and the MCM-41 solid supports with minimal perturbation of its catalytic *α*-amino acid moiety which remained free and available for further complexation with the metal and further catalytic reactions. The anchoring of the amino acid to solid supports *via* cycloaddition also eliminated the negative effects on the reactivity of amino acid as the 1,2,3-triazole moiety is rather inert.

3.2.1. Characterization of Fe^{III}-Proline-MCM-41 and Fe^{III}-Proline -Polystyrene.

3.2.1.1. FTIR spectroscopy.

There are several literature reports of the characterization of histidine and glutamic acid complexes with Fe immobilized onto MCM-41 using FTIR spectroscopy.[156, 157] In the case of the histidine complex, the ν_{NH} stretching band was observed at 3100 cm^{-1}. This band was broadened most likely due to hydrogen bonding. The spectra of immobilized glutamic acid also showed the bands due to stretching vibrations of the amine group at around 3100 cm^{-1} (ν_{NH}). The carboxylate group of the side chain at around 1600 cm^{-1} was slightly shifted to lower wavenumbers after complexation with iron. This indicated that the carboxylate group of the carboxylic acid side chain was involved in the complexation of the iron cations.

FTIR spectroscopy was also employed to check the nature and structural integrity of amino acid complexes immobilized within MCM-41 and polystyrene matrices. In the high energy range, the spectrum of the Fe^{III}-Proline complex was characterized by clear bands at 3210 cm^{-1} (ν_{NH}) and at 3000-2800 cm^{-1} interval which are related to ν_{CH} stretching modes. At low frequency, the most noticeable band of Fe^{III}-Proline is the carboxylic group ($\nu_{as\ COO^-}$) at 1662 cm^{-1}, with minor features due to the NH and CH bending modes (δ_{NH}, δ_{CH}) (Table 3.3.1.). These spectral features indicate that the amino acid in the complex is in its anionic form which is involved in the complexation to the Fe metal centre through COO^- and NH groups. The high energy region the spectrum of Fe^{III}-Proline MCM-41 shows a broad adsorption due to hydrogen bonding with surface Si-OH, close to a weak band at 3745 cm^{-1} due to free Si-OH and to complex bands in the 3000 - 2800 cm^{-1} region, related to ν_{CH} modes. The latter region is more complex, suggesting the superposition of ν_{CH} modes of the proline molecules and organic chains employed to functionalize the silica surface. In the same range, the spectrum of Fe^{III}-Proline-Polystyrene only shows the ν_{CH} modes (aromatic and aliphatic) due to the polystyrene

matrix, probably because of the very low loading of Fe^{III}-Proline. The low energy region provided a clear indication on the structural and compositional integrity of Fe^{III}-Proline. Neat, MCM-41 and polystyrene supported complexes showed bands at 1662 and 1645 cm^{-1} confirming the presence of the carboxylic moiety.

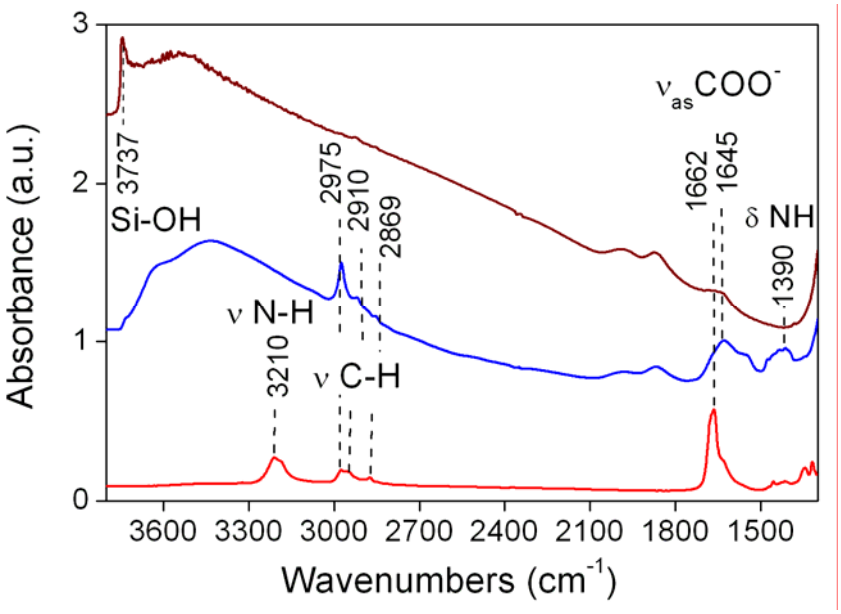

Figure 3.3.1. IR spectra of Fe^{III}-Proline (red), Fe^{III}-Proline-MCM-41 (blue) and MCM-41 (brown). Spectra were arbitrarily normalized and vertically shifted for easier comparison.

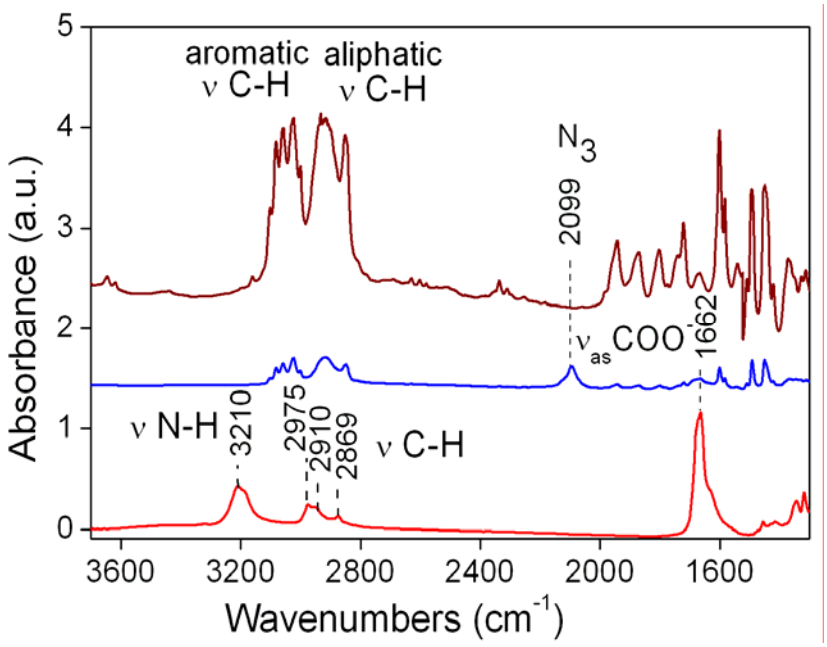

Figure 3.3.2. Comparison of IR spectra of Fe^{III}-Proline (red), Fe^{III}-Proline -Polystyrene (blue) and Polystyrene (brown). Spectra were arbitrarily normalized and vertically shifted for easier comparison.

Table 3.3.1. Summary of FTIR characterisation of Fe^{III}-Proline catalysts (absorption in cm^{-1}).

Assign-ment	Proline	Fe^{III}-Proline	Fe^{III}-Proline-X	Fe^{III}-Proline-MCM-41	Fe^{III}-Proline-Polyst.	Characterisation
ν_{NH} δ_{NH}	3050	3210 1375	3285 1380	- -1395	- -	Shifted ν_{NH} when compared to proline ligand suggests deprotonation of amino group and coordination to Fe through NH.
ν_{CH}	2955 2935 2920	2975 2910 2869	2970 2910 2869	2975 2910 2869	- - -	ν_{CH} of Fe^{2+}-Proline in polystyrene supported material is overlapped by aromatic and aliphatic ν_{CH} modes of polystyrene matrix.
$\nu_{as\ COO^-}$ $\nu s_{\ COO^-}$	1620 1400	1662 1375	1662 1345	1645 -	1662 -	Shifted $\nu_{as\ C\ OO^-}$ and $\nu_{s\ C\ OO^-}$ when compared to proline ligand confirms carboxyl group involvement in Fe binding, absence of band at around 1800 cm^{-1} confirms carboxyl group deprotonation.

3.2.1.2. DR UV-Vis spectroscopy.

DRUV-Vis spectroscopy was also reported in the literature as a characterization technique for histidine and glutamic acid complexes with iron immobilized onto MCM-41.[156, 157] The comparison of the DRUV-Vis spectra before and after iron treatment showed that two bands at 44000 and 37000 cm^{-1} appeared after the treatment with iron. Both were ligand-to-metal charge transitions indicating the formation of complexes between iron and amino acid. These materials showed strong absorption bands below 30000 cm^{-1} that were assigned to clustered iron species.

DRUV-Vis spectroscopy was employed to get information on the oxidation state and coordination of the metal centre of Fe^{III}-Proline-MCM-41 and Fe^{III}-Proline-Polystyrene materials. The UV-Vis spectrum of neat Fe^{III}-Proline complex is presented for comparison, showing two strong absorptions at 45400 and 37600 cm^{-1} (Figure 3.3.3.), that can be explained in terms of ligand to metal charge transitions (LMCT) involving isolated Fe sites in tetrahedral coordination. After immobilization of the Fe^{III}-Proline complex within polystyrene and MCM-41 the absorption onset was shifted to lower frequency in both samples. This can be interpreted as a change in the coordination state of iron ions, as

a consequence of the interaction with the matrix. Noticeably, the components at 22000 and 18000 cm^{-1} in the spectrum of Fe^{III}-Proline-Polystyrene are similar with the reported literature spectrum of ferrocene suggesting an interaction between the metal centre and an aromatic group of the polystyrene support.[318] In addition, the weak and broad band at around 20800 cm^{-1}, in the d-d transition, suggested the presence of small amount of iron aggregates.

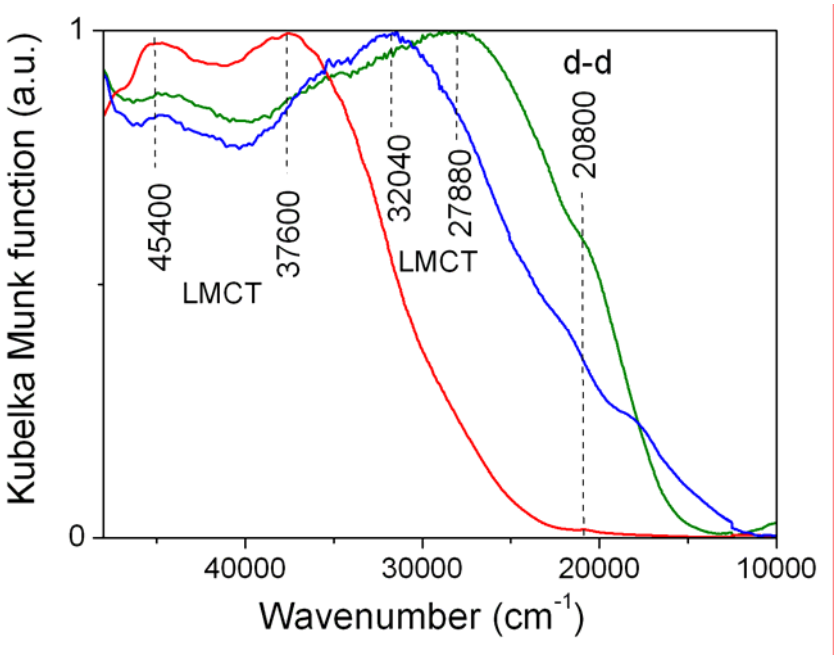

Figure 3.3.3. DR UV-Vis spectra of Fe^{III}-Proline (red), Fe^{III}-Proline-MCM-41 (blue) and Fe^{III}-Proline-Polystyrene (green). Spectra were arbitrarily normalized for easier comparison.

Table 3.3.2. Summary of DRUV-Vis characterisation of Fe^{III}-Proline catalysts (absorption in cm^{-1}).

Assign -ment	**Fe^{III}-Proline**	**Fe^{III}-Proline-X**	**Fe^{III}-Proline-MCM-41**	**Fe^{III}-Proline - Polyst.**
LMCT	45400 37600	45400 37600	45400 32040	45400 27880
d-d	20800	20800	20800	20800

3.2.1.3. XRD analysis.

The XRD characterization of neat MCM-41 is described in section 3.2.3.3. The XRD patterns of Fe^{III}-Proline -MCM-41 are similar to Cu^{II}-Valine-MCM-41 materials and revealed the broadening of the peaks of the *d*100 reflection after complex immobilization probably due to the reduction of the order of silanol Si-OH groups and the decrease of the crystallite mosaic size. The decrease in the intensity of the 100 reflection peak could be assigned to the partial structure deformation of the ordered hexagonal phase, or the flexibility of the silica framework resulting from the strain of the incorporated Fe^{III}-Proline complexes.

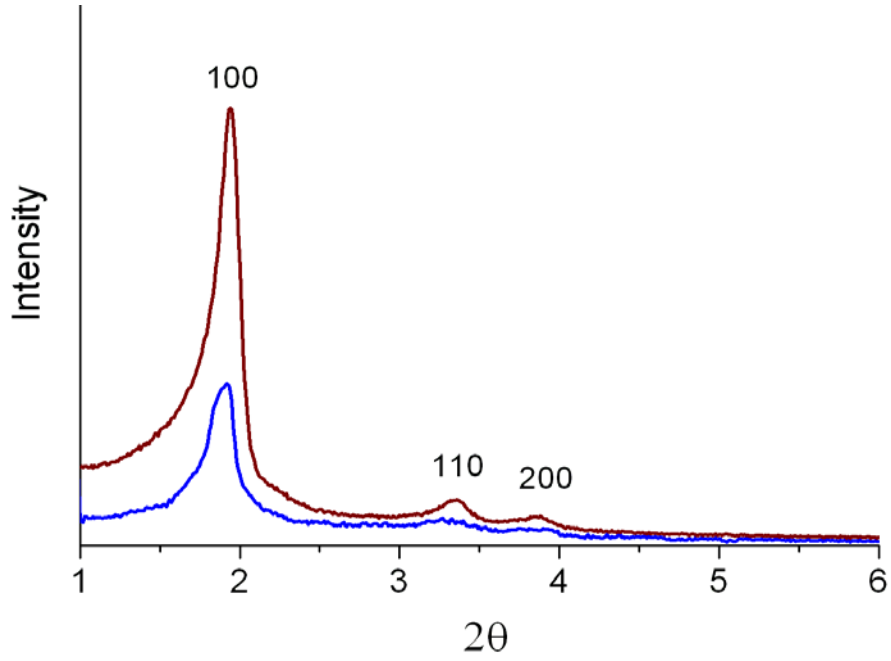

Figure 3.3.4. Comparison of XRD patterns of Fe^{III}-Proline-MCM-41 (blue) and MCM-41 (brown).

3.2.1.4. BET analysis.

N_2 adsorption measurement of Fe^{III}-Proline-MCM-41 and neat MCM-41 was performed at liquid nitrogen temperature. Samples were first dehydrated and degassed overnight in vacuum at 80°C.

Fe^{III}-Proline-MCM-41 exhibited a lower external surface area compared to pure MCM-41 silica. The supported catalyst with low active sites loading showed an external surface area of 381 m^2/g, and supported catalyst with high active centres loading showed an external surface area of 213 m^2/g, while pure MCM-41 showed an external surface area

of 1250 m^2/g. The lowering of the surface area indicates the presence of the Fe^{III}-Proline complex within the mesopores of MCM-41.

Table 3.3.3. Summary of BET characterisation of Fe^{III}-Proline-MCM-41 catalysts.

Material	BET surface area m^2/g
MCM-41	1250
Fe^{III}-Proline-MCM-41 (Fe 2.07 %wt.)	381
Fe^{III}-Proline-MCM-41 (Fe 8.73 %wt)	213

3.2.2. Benzyl alcohol oxidation with Fe^{III}-Proline-MCM-41 and Fe^{III}-Proline-Polystyrene complexes.

Alcohol transformations are of paramount importance in laboratory-scale organic synthesis and in the industrial manufacturing processes.[319] For a general introduction to alcohol oxidation and alcohol oxidation catalyzed by iron catalysts see section 3.1.4.1.

Primary alcohols (R-CH_2-OH) like benzyl alcohol can be oxidized either to aldehydes (R-CHO) or to carboxylic acids (R-CO_2H). Secondary alcohols (R^1R^2CH-OH) terminates at the ketone (R^1R^2C=O) stage. Tertiary alcohols ($R^1R^2R^3$C-OH) are resistant to oxidation because they have no hydrogen atoms attached to the oxygen bearing carbon. In oxidation reactions of primary and secondary alcohols a hydrogen atom from the -OH group and hydrogen from the carbon atom (benzylic C-H) attached to the –OH group are removed which is required in order to form the carbon-oxygen double bond.[206] Schematic representation of primary, secondary and tertiary alcohols is shown in Figure 3.3.5. A comparison of oxidation products of primary and secondary alcohols is presented in Figure3.3.6.

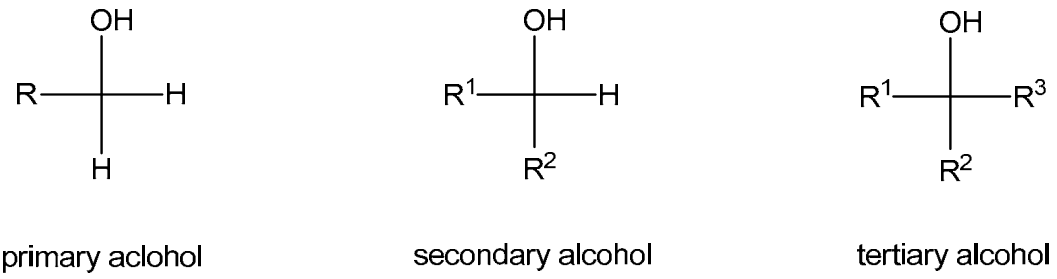

Figure 3.3.5. Representation of primary, secondary and tertiary alcohols.

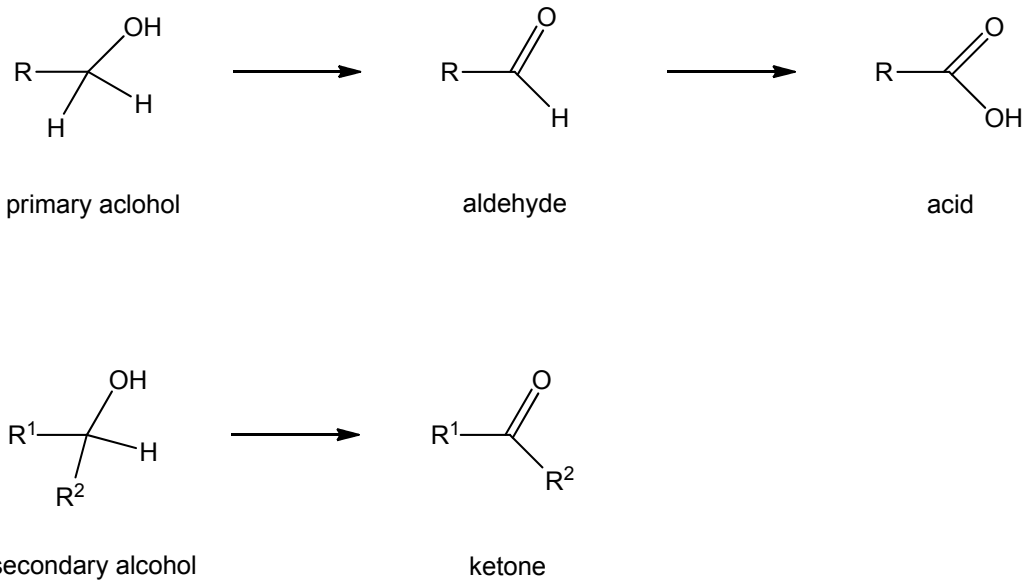

Figure 3.3.6. Oxidation products of primary and secondary alcohols.

Primary alcohols can be oxidised to either aldehydes or carboxylic acids depending on the reaction conditions. In the case of the formation of carboxylic acids, the alcohol is first oxidised to an aldehyde which is then oxidised further to the acid. An excess of oxidant is required to carry out the second stage of the reaction (oxidation of aldehyde to acid). The direct oxidation of primary alcohols (Scheme 4.3.2., A) to carboxylic acids (D) usually proceeds *via* the corresponding aldehyde (B), which is transformed *via* an aldehyde hydrate (R-CH(OH)$_2$) (C) by reaction with water before it can be further oxidized to the carboxylic acid. For mechanistic details of alcohol oxidation see section 3.1.4.1. It is possible to interrupt the oxidation of a primary alcohol at the aldehyde level by performing the reaction in absence of water, so that no aldehyde hydrate can be formed.

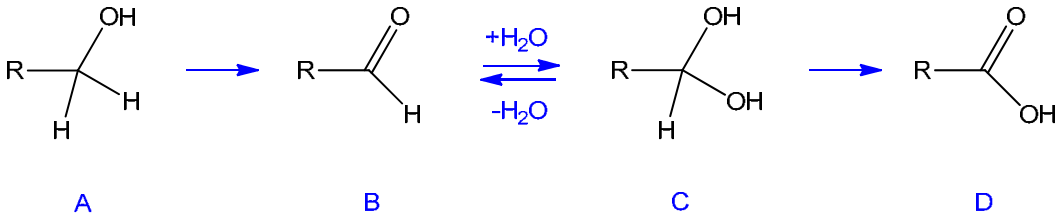

Scheme 3.3.2. Pathway of primary alcohols oxidation.

Benzylic and allylic alcohols are more reactive than aliphatic alcohols.[320] The enhanced reactivity of the benzylic positions is attributed to the low bond dissociation energy for benzylic C-H bonds (377 kJ/mole). Specifically, the bond $C_6H_5CH_2$-H is about 15% weaker than other kinds of C-H bonds, e.g. methyl C-H bond (H_3C-H) 439 kJ/mole, ethyl C-H (C_2H_5-H) bond 423 kJ/mole, phenyl C-H bond (C_6H_5-H) 473 kJ/mole. The allylic

C-H bond akin to benzylic bonds also show enhanced reactivity due to lower bond dissociation energy (372 kJ/mole) when compared with other C-H bonds.

3.2.2.1. Benzyl alcohol oxidation with Fe^{III}-Proline catalysts.

The role of isolated active sites and their influence on catalytic activity was studied for the oxidation of benzyl alcohol with the neat Fe^{III}-Proline complex and its heterogeneous analogues immobilised within MCM-41 and polystyrene supports and the results are summarized in Table 3.3.4. Fe^{III}-Proline based catalysts were >99mol% selective to benzaldehyde. Control experiments in the absence of catalyst gave conversions of 10.9 mol% with TBHP, and 6.5 mol% in the presence of air (see Table 3.1.8.).

Table 3.3.4. Results on selective oxidation of benzyl alcohol with Fe^{III}-Proline catalysts. For reaction conditions see section 6.10.2.

Cat.	Metal load.	Oxid.	Mmol of metal	Cat. (g)	Subst: Metal ratio	Oxid: Subst. ratio	TON	TOF (h^{-1})	Conv. mol %	Select. mol % bald.
Neat	16.9	AIR	0.027	0.009	581	1.65	319	53	54.3	>99
Neat	16.9	TBHP	0.027	0.009	581	1	386	64	65.1	>99
MCM	8.73	AIR	0.078	0.05	201	1.65	106	18	43.9	>99
MCM	2.07	AIR	0.011	0.03	1025	1.65	542	90	52.9	>99
MCM	8.73	TBHP	0.078	0.05	201	1	157	26	77.8	>99
MCM	2.07	TBHP	0.011	0.03	1025	1	993	165	96.8	>99
Polyst	0.05	AIR	0.0004	0.05	35213	1.65	5374	895	15	>99
Polyst	0.05	TBHP	0.0004	0.05	35213	1	7602	1267	22	>99

T=371 K, air 3.0 MPa, DMSO 35g, reaction time=6h, bald-benzaldehyde.

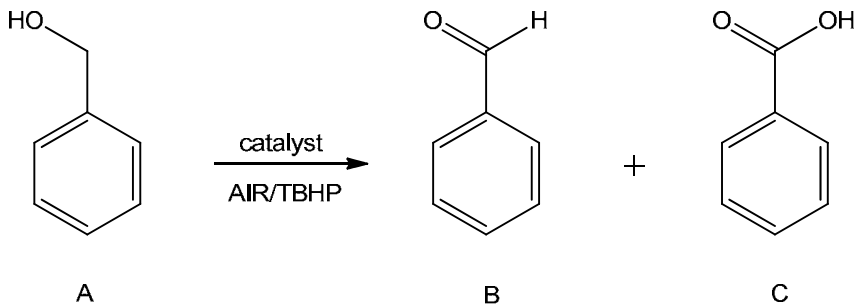

Scheme 3.3.3. Schematic representation of product formation in benzyl alcohol (A) oxidation to benzaldehyde (B) and benzoic acid (C).

The catalytic results (Table 3.3.4.) proved that heterogeneous catalysts that posses well isolated active sites, displayed higher activities than their neat, homogeneous analogue. In the presence of air, TON and TOF increased from 319 and 53 h^{-1} for neat complex to 542 and 90 h^{-1} (Fe^{III}-Proline -MCM-41, Fe 2.07%wt.) and 5374 and 895 h^{-1} (Fe^{III}-Proline-Polystyrene, Fe 0.05%wt.). When TBHP was employed as the oxidant a significant increase in TON and TOF was also observed. While neat Fe^{III}-Proline complex afforded TON of 386 and TOF of 64 h^{-1}, Fe^{III}-Proline -MCM-41 obtained higher TON and TOF of 993 and 165 h^{-1} and Fe^{III}-Proline-Polystyrene afforded TON and TOF of 7602 and 1267 h^{-1}, respectively.

The increase in iron content of heterogeneous Fe^{III}-Proline-MCM-41catalysts resulted in decreased TON and TOF when compared with Fe^{III}-Proline-MCM-41catalysts with low Fe loading (Fe 2.07%wt.). By increasing loading of metal sites the TON and TOF decreased from 542 and 90 h^{-1} (Fe^{III}-Proline-MCM-41, Fe 2.07%wt.) to 106 and 18 h^{-1} (Fe^{III}-Proline-MCM-41, Fe 8.73%wt.) with air as oxidant. When TBHP was employed Fe^{III}-Proline-MCM-41 catalysts with lower metal loading also exhibited higher activity. In fact, Fe^{III}-Proline-MCM-41, (Fe 2.07%wt.) produced a TON and a TOF of 993 and 165 h^{-1}, these decreased to 157 and 26 h^{-1} when Fe^{III}-Proline-MCM-41 with high metal loading (Fe 8.73%wt.) was employed. Comparison of TON and TOF using homogeneous and heterogeneous materials is shown in Figure 3.3.7.

The Fe^{III}-Proline-Polystyrene catalyst afforded much higher TON and TOF than Fe^{III}-Proline-MCM-41 manly due to the fact that metal loading of polystyrene supported catalyst (Fe 0.05 %wt.) was 40 times lower than the low loading of Fe^{III}-Proline-MCM-41, (Fe 2.02 %wt.) and 174 times lower than the metal loading of Fe^{III}-Proline-MCM-41 (Fe 8.73 %wt.). However, conversions produced by Fe^{III}-Proline-Polystyrene were much lower than those produced by Fe^{III}-Proline-MCM-41 catalysts most likely because the number of active iron sites responsible for substrate conversion was very low (Fe 0.05 %wt.).

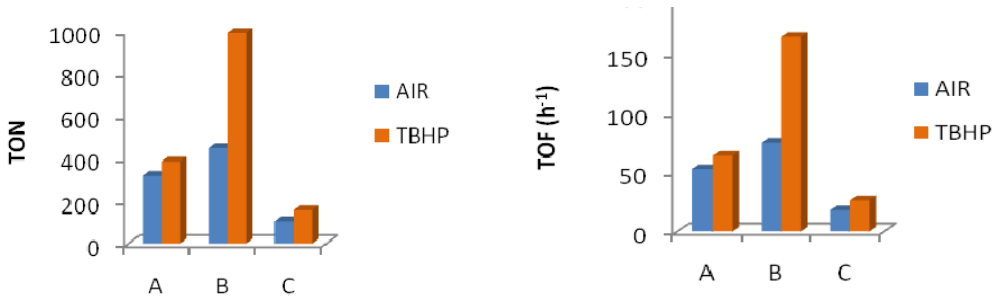

Figure 3.3.7. Comparison of TON (left) and TOF (right) using Fe^{III}-Proline (A), Fe^{III}-Proline-MCM-41, (Fe 2.02%wt.) (B), Fe^{III}-Proline-MCM-41(Fe 8.73%wt.) (C) with air and TBHP.

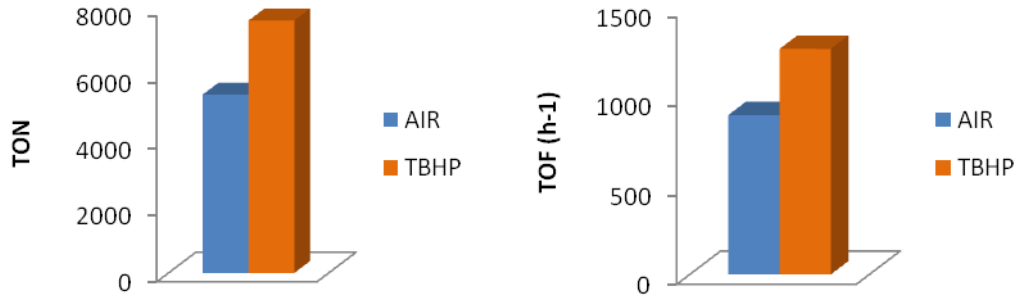

Figure 3.3.8. Comparison of TON (left) and TOF (right) using Fe^{III}-Proline-Polystyrene, (Fe 0.05 %wt.) with air and TBHP.

From these results it can also be concluded that the choice of support affects the TON and TOF of Fe^{III}-Proline heterogeneous catalysts, providing clear evidence that the chemical nature of the support also has an important influence on catalytic performance. Higher TON and TOF obtained by the polystyrene supported catalyst could be attributed to the factors such as the metal ion interactions with the support, localization of the catalytic sites within the solid support and less significant diffusion limits than in the case of Fe^{III}-Proline immobilized within porous MCM-41. Relatively lower TON and TOF in the case of heterogeneous MCM-41 supported catalysts can be attributed to the slower diffusion of the substrate and oxidant into the pores of silica. Diffusion within pores could be even slower due to the high density of the immobilised metal complexes. In the case of polystyrene supported catalyst, high TON and TOF may be attributed to the predominant localization of the active sites in the accessible region of the polymer matrices (not in the pores as for MCM-41) and faster diffusion due to the lower density of the immobilised iron complexes.

These results also suggest that the activity of the immobilized catalyst can be sufficiently improved to overcome the decrease in the activity caused by the steric hindrance of the support by employing polystyrene instead porous MCM-41. In this case the support not only served as carrier for catalytic metal sites facilitating their separation but also contributed to the catalytic activity by support effects. It can be hypothesized that the nature of the metal-support interactions and related support-induced changes in electronic properties of the metal influenced the catalytic properties of Fe^{III}-Proline.

The iron cation of heterogeneous Fe^{III}-Proline-MCM-41 catalysts could interact with the oxygen atoms from surface silanols of MCM-41. In the analogues Fe^{III}-Proline-Polystyrene catalyst, oxygen atoms could be replaced by chlorine atoms from chloromethylated polymer matrix. Resulting differences in steric, geometric and electronic effects due to interactions with oxygen and chlorine additional ligands could be

responsible for the changes in the catalytic activity of MCM-41 and polymer supported Fe^{III}-Proline catalyst in benzyl alcohol oxidation reactions.

In the literature it was also reported that changes in catalytic activities are a result of support interactions with metal centres.[321] The evaluation of the metal-support interaction has been investigated with vanadium oxide based catalysts where the vanadium oxide phase was deposited on the surface of different oxide supports such as SiO_2, Al_2O_3, TiO_2 and ZrO_2. In these catalysts the ratio of polymerized to isolated supported vanadium oxide species increased with increasing vanadium oxide loading. As a consequence, the surface concentration of bridging V-O-V bonds increased with increasing vanadium oxide loading. The TOF of these catalysts, proved to be independent of the vanadium oxide loading. This suggests that the oxygen associated with the V-O-V bond did not critically participate in the oxidation process. However changes in the support composition dramatically influenced the TOF of the corresponding supported vanadium oxide catalysts, strongly suggesting that the oxygen in the V-O- support bond was critical for this catalytic oxidation reaction (Table 3.3.5.). Monomeric, polymeric and support bonded vanadium species are shown in Figure 3.3.9. The observed trend in TOF suggested that by a careful choice of the support the catalytic performances can be tuned and that metal oxide-support effect had a significant impact on the properties of the supported vanadium species. The activity of the supported metal catalysts was significantly affected by the properties of the support oxide material. This is generally known as the metal oxide-support effect, although its exact origin and mechanism of operation is still unclear. The fundamental basis lies in the variability in geometric and electronic structure of the surface vanadium oxide species. However the metal oxide-support effect in the hydrated state, dehydrated state as well under reaction conditions is not well understood both at a molecular and electronic level. Up to now, no consistent model can describe, in a quantitative manner, the role of the structure/composition of support oxides and the presence of specific promoter elements on the electronic structure of the supported vanadium catalysts.

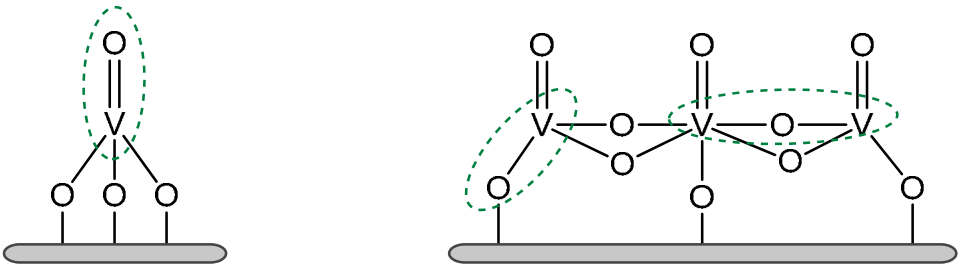

Figure 3.3.9. Three possible V–O bonds involved in the selective oxidation reactions: monomeric VO_4 species (A) and polymeric VO_4 species characterized by V=O, V–O–V and V–O–support bonds (B).[321]

Table 3.3.5. Catalytic performances in the oxidation of methanol to formaldehyde with supported vanadium oxide catalysts.

Catalyst	***TOF (s^{-1})***
V/SiO_2	$3*10^{-3}$
V/Al_2O_3	$7*10^{-2}$
V/TiO_2	1.1
V/ZrO_2	1.8

Influence of oxidant on reaction conversions. Conversions of benzyl alcohol oxidation catalyzed by Fe^{III}-Proline materials were higher when TBHP was used and lower in reactions with air as the oxidant. The neat Fe^{III}-Proline catalyst obtained a higher conversion of 65.1 mol% with TBHP, than with air which produced a conversion of 54.3 mol%. Fe^{III}-Proline-MCM-41(2.07 %wt.) reached conversion of 52.9 mol% and 96.8 mol% with air and TBHP, respectively. Fe^{III}-Proline-Polystyrene (0.05%wt.) catalyst also reached higher conversion with TBHP (21.6 mol%) than with air (15.3 mol%).

By increasing the iron active sites loading of MCM-41 supported Fe^{III}-Proline complexes conversions of benzyl alcohol decreased with both oxidants (air and TBHP). In fact Fe^{III}-Proline-MCM-41 catalyst with high metal content (8.73 %wt.) exhibited conversion of 43.9 mol% with air and 77.8 mol% with TBHP. The analogous low iron content Fe^{III}-Proline catalyst (2.07 %wt.) afforded conversion of 52.9 mol% in the presence of air, and 96.8 mol% with TBHP as oxidant. Comparison of reaction conversions using homogeneous and heterogeneous materials is shown in Figure 3.3.10.

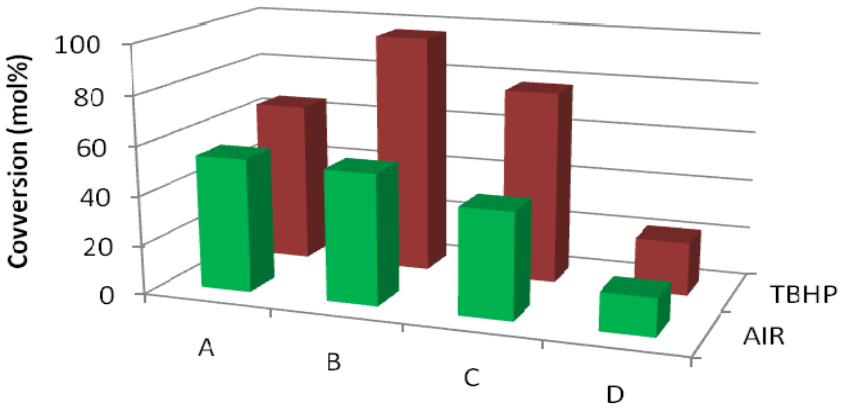

Figure 3.3.10. Comparison of conversions in benzyl alcohol oxidation using Fe^{III}-Proline (A), Fe^{III}-Proline-MCM-41, (Fe 2.02%wt.) (B), Fe^{III}-Proline-MCM-41(Fe 8.73%wt.) (C), Fe^{III}-Proline-Polystyrene, (Fe 0.05 %wt.) (D), with air and TBHP.

The results strongly suggest that the metal loading and greater dispersion of active sites (as evidenced in the lower metal content) play a key role in the benzyl alcohol oxidation reactions with Fe^{III}-Proline complexes. By decreasing the active site loading, one can hypothesize that active site separation increased which strongly enhanced the activity of the catalysts. The decrease in iron content resulted in a drastic increase of TON and TOF in all reactions, clearly indicating that enhanced isolation of the active sites was crucial for obtaining high catalytic activities.

As O_2 is very difficult to activate (for details see section 1.3.1) when compared with active peroxides (TBHP), the oxidation of benzyl alcohol was less efficient than with TBHP.

The selectivity towards benzaldehyde was similar to the case of Cu^{II}-Valine catalysts and appeared to be independent of the metal content, Fe/substrate ratio, type of oxidant, nature of support and reaction time. Benzaldehyde was obtained in high yields with both oxidants under given conditions. Benzyl alcohol can be oxidised to either benzaldehyde or benzoic acid depending on the reaction conditions. Benzyl alcohol is first oxidised to benzaldehyde which is then oxidised further to benzoic acid. However an excess of oxidant is required to carry out the second stage of the reaction (aldehyde oxidation to acid) (section 3.2.4.2.).

In benzyl alcohol oxidation reactions catalyzed by homogeneous and heterogeneous complexes of Fe^{III}-Proline and Cu^{II}-Valine in presence of TBHP as oxidant the molar ratio of oxidant to substrate was 1:1. As the oxidant was not used in excess the oxidation

of benzaldehyde to benzoic acid was not observed. In reactions with air small excess of oxidant was employed. In fact molar ratio of oxidant to substrate equaled 1.6:1.
However the excess of O_2 did not produce benzoic acid and this result can be explained by the absence of water in the reaction system that disabled aldehyde hydrate formation which is the intermediate between aldehyde and acid (section 3.2.2.).

Comparison of catalytic performance of Fe^{III}-Proline complexes encapsulated within microporous zeolite X and mezoporous silica MCM-41. Heterogeneous Fe^{III}-Proline-MCM-41 catalysts proved to be more active than Fe^{III}-Proline-X. In the presence of air Fe^{III}-Proline-MCM-41 produced higher TON and TOF of 542 and TOF of 90 h^{-1} while the zeolite X encapsulated analogue afforded TON of 351 and TOF of 58 h^{-1}. When TBHP was employed as oxidant a significant increase in TON and TOF was also observed. While Fe^{III}-Proline-X complex reached TON of 551 and TOF of 92 h^{-1}, Fe^{III}-Proline-MCM-41 obtained higher TON and TOF of 993 and 165 h^{-1} (Table 3.3.6.).

Table 3.3.6. Comparison of catalytic performance of Fe^{III}-Proline-X and Fe^{III}-Proline-MCM-41 in selective oxidation of benzyl alcohol. For reaction conditions see section 6.10.2.

Catalyst	Metal load.	Oxid.	Subst: Metal ratio	Oxid: Subst. ratio	TON	TOF (h^{-1})	Conv. mol %	Select. mol % bald.
Fe^{III}-Proline-X	0.49	AIR	581	1.65	351	58	60.4	>99
Fe^{III}-Proline-MCM-41	2.07	AIR	1025	1.65	542	90	52.9	>99
Fe^{III}-Proline-X	0.49	TBHP	581	1	551	92	94.9	>99
Fe^{III}-Proline-MCM-41	2.07	TBHP	1025	1	993	165	96.8	>99

T=371 K, air 3.0 MPa, DMSO 35g, reaction time=6h, bald-benzaldehyde.

The reason for the higher activity of Fe^{III}-Proline -MCM-41 as an oxidation catalyst could lie in the diffusion limits through the micropores of zeolite and mesopores of MCM-41. The structure of Zeolite X consists of 13 Å cavities interconnected tetrahedrally through smaller apertures of 7.4 Å diameter. On the other hand mesoporous silica MCM-41 consists of long range ordered mesopores of 30 Å of diameter. The structure and dimensions of microporous and mesoporous support materials could result in easier diffusion of the substrates and products through the larger pores of MCM-41 than in the cavities and channels of zeolite X. It is also possible that the Fe^{III}-Proline complex is

more stable when bound to MCM-41 than when mechanically entrapped in zeolite X cages.

These results suggest that the catalytic activity of Fe^{III}-Proline can be tuned and influenced by the dimension of the porous host materials and by immobilization methodology that could result in formation of more stable catalysts.

Similar results were observed with $CoF_{16}PcY$ and $CoF_{16}PcMCM$-41 catalysts (Pc= phthalocyanine), and it was found that $CoF_{16}Pc$ complex immobilized within MCM-41 was more active than $CoF_{16}Pc$ complex encapsulated in zeolite Y.[113] This was explained as a consequence of the easier diffusion of the substrates and products through the larger pores of MCM-41 (30 Å) than in the cavities and channels of zeolite X (7.4–13 Å). It was also claimed that phthalocyanine complexes were more stable when incorporated inside mesoporous MCM-41 with respect to zeolite X and this may reflect differences between the planar (MCM-41) and the bent distorted (zeolite X) conformation of the complexes depending on the dimensions of the pores.

The other explanation of higher activity of MCM-41 immobilized Fe^{III}-Proline complexes could arise from the fact that the organic linker introduced during immobilization (1,2,3-triazole moiety attached to chloropropyl group) provided sufficient mobility of the reactive centre and in contrast to the zeolite encapsulated catalyst, diminished undesired steric effects of the matrix over the accessibility of the reactive centre.[301]

The Fe^{III}-Proline complex could be additionally stabilized when immobilized within silica by hydrogen bonding interaction between hydroxyl groups of silica and carbonyl and/or amino groups of proline.

The hydrophobic/hydrophilic effect of the support could also influence the catalytic activity of Fe^{III}-Proline complexes. The hydrophobicity of the MCM-41 surface was tailored by grafting methyl groups that enhance the hydrophobicity of silica (section 3.2.2.). It can be hypothesized that the iron complex immobilized in the channels of the mesoporous host with enhanced hydrophobic properties, showed preferred accessibility to the substrate. The better the affinity of the support surface to the substrate, the more substrate species come into contact with the immobilized active centres. MCM-41 being more hydrophobic than the zeolite X surface probably favoured the accessibility of immobilized Fe^{III}-Proline complexes to the substrate molecules.[273]

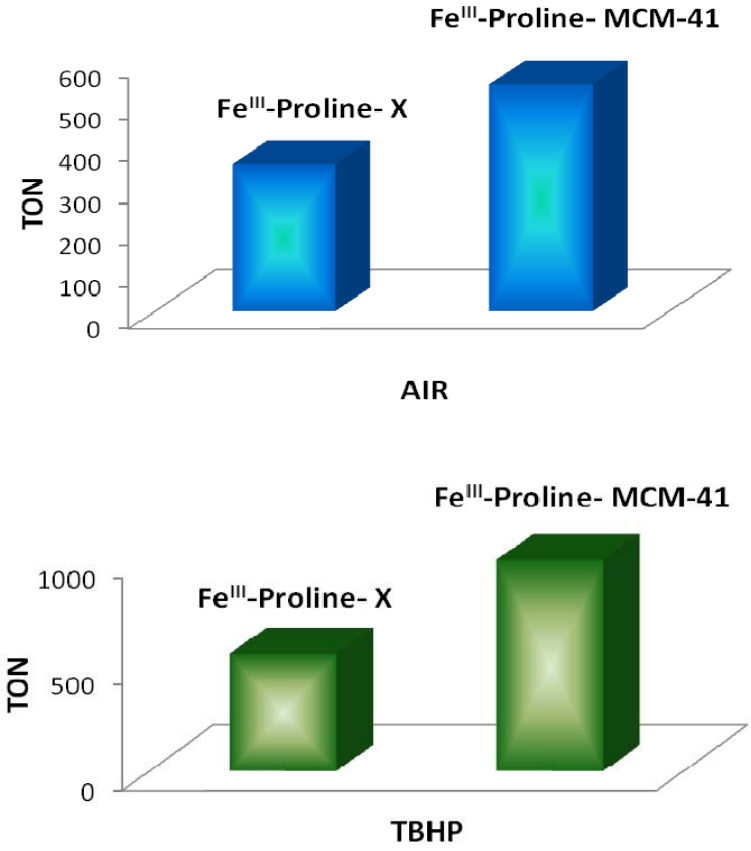

Figure 3.3.11. Comparison of catalytic performance of Fe^{III}-Proline-X and Fe^{III}-Proline-MCM-41 in selective oxidation of benzyl alcohol with air (upper) and TBHP (bottom).

3.3.4. Cyclohexene oxidation with Fe^{III}-Proline-MCM-41 and Fe^{III}-Proline-Polystyrene complexes.

3.3.4.1. Introduction to cyclohexene oxidation with iron catalysts.

Olefin epoxidation and allylic oxidations are two competing processes. Epoxides are formed when electrophilic attack at the double bond of the cyclic olefin occurs. Allylic oxidation products are usually formed when hydrogen abstraction is the dominant reaction (the details of epoxidation and allylic oxidation are explained on page 165). In contrast to epoxidation, allylic oxidation retains the olefinic functionality allowing further transformations. Allylic oxidation reactions involve a free-radical mechanism and mainly occur in the presence of low-oxidation state transition-metal species. Epoxidation is generally associated with oxometallic species of high oxidation state metals. In the

oxidation of cyclic olefins, epoxidation and allylic oxidations are often competitive and both processes can occur simultaneously. The selectivity also depends on the nature of olefin substrate used and stability of the intermediate allylic radical. Table 3.3.7. presents recent literature data on allylic oxidation of cyclohexene.

Table 3.3.7. Comparison of literature data on allylic oxidation of cyclohexene.

Catalyst	*Oxidant*	*Conv. (%)*	*2-cyclohexene-1-one Selectivity (%)*	*2-cyclohexene-1-ol Selectivity (%)*	*Ref.*
Co-SD-MCM-41	H_2O_2	41	99	-	[322]
Cu-SD-MCM-41	H_2O_2	43	55	45	
Cu-DA-PS	O_2	52	41	33	[323]
Ru/CeO_2	TBHP	38	50	40	[324]
Co/CeO_2	TBHP	36	51	36	
Cr-MCM-41	O_2	52	71	11	[325]
Cr-Y	O2	35	90	-	[326]

SD=salicylaldimine, Cu-DA-PS =Cu-2,4-dihydroxyacetophetone supported on chloromethylated polystyrene.

Olefin transformations are catalyzed by both heme (e.g. cytochrome P450) and non-heme iron enzymes (e.g. methane monooxygenase).[327]

Key intermediates in the heme mechanism of dioxygen activation are (porphyrin) Fe^{III}–OOH and (porphyrin radical)Fe^{IV}=O species, that are implicated in alkane hydroxylation and olefin epoxidation reactions. Parallel mechanism of non-heme iron enzymes follow the heme paradigm, Fe^{III}–OOH and high-valent iron-oxo Fe^{IV}=O intermediates. These active species have also been observed for methane monooxygenase (MMO). (Schematic representation of olefin epoxidation with non-heme Fe^{IV}=O complexes is shown in Figure 3.3.12.). Fe^{V}=O active species in the oxygen activation reactions were also postulated for non-heme iron enzymes and synthetic iron complexes.

A number of heme and nonheme iron complexes have been identified and proved to catalyze efficiently the olefin oxidation reactions. Such bioinspired catalysts typically contain a mononuclear iron centre coordinated to synthetic porphyrins or ligands such as TPA [tris-(2-pyridylmethyl) amine] and BPMEN [*N*,*N*-dimethyl-*N*,*N*-bis(2-pyridylmethyl)-1,2-diaminoethane] (Figure 3.3.13.).[328]

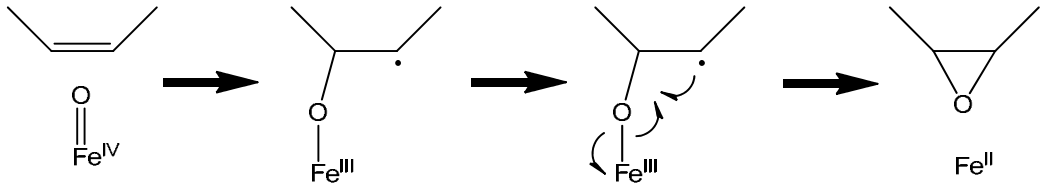

Figure 3.3.12. Schematic representation of epoxidation with Fe^{IV}=O active species.

The mechanistic pathway of olefin oxidation was investigated in great detail using Fe(BPMEN) complexes. Two possible mechanisms were proposed: one path involved initial cleavage of the O-OH bond followed by attack of the olefin (Figure 3.3.14.), The other path proceeded by direct attack of active Fe^{III}-OOH species on olefin double C-C bond (Figure 3.3.15.). When water was present in the reaction medium, it was proposed that olefin oxidation with Fe(BPMEN) occurs via Fe^{V}=O species (Fe^{III}-OOH species were not formed when water was present). The HO-Fe^{V}=O oxidant was proposed to form via O-O bond cleavage of Fe^{III}-OOH intermediate leading to epoxide and diol formation. Addition of oxygen to the double bond presumably produces a radical species that is short lived and rapidly reacts with the coordinated OH to form the diol (Figure 3.3.16.).

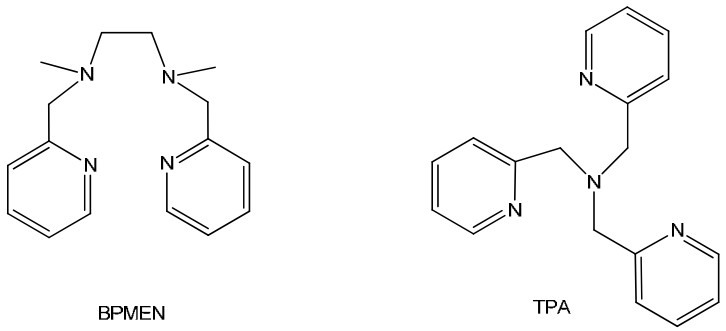

Figure 3.3.13. Representation of BPMEN and TPA ligands.

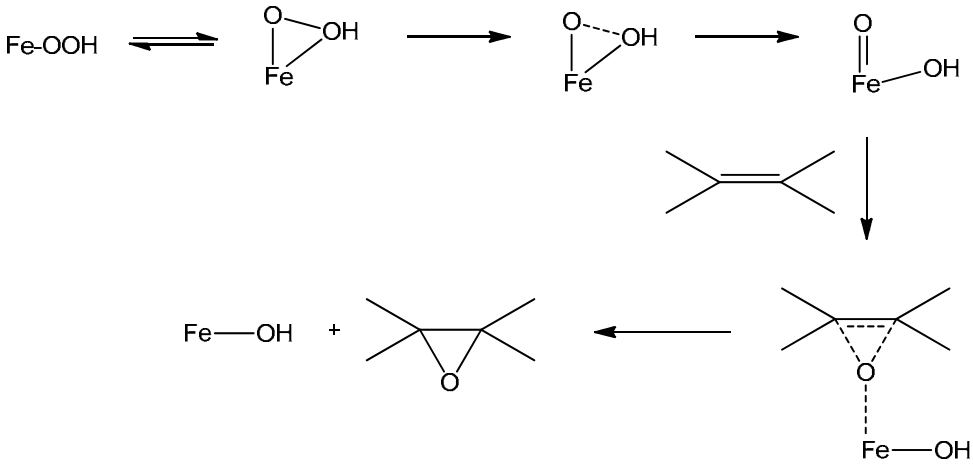

Figure 3.3.14. Proposed schematic representation of epoxidation via O-O bond cleavage mechanisms catalyzed by the Fe (BPMEN) complex.

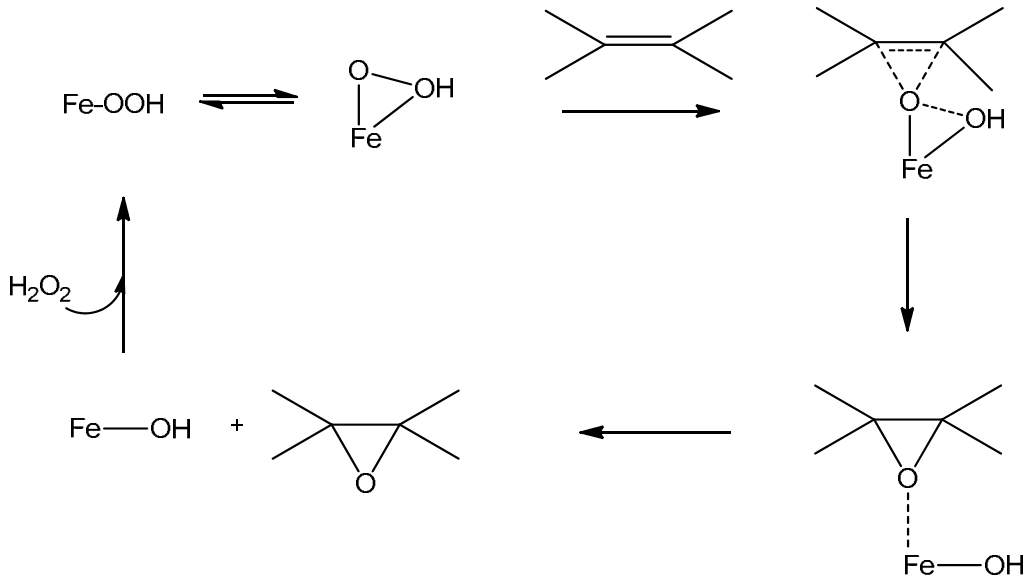

Figure 3.3.15. Proposed schematic representation of direct epoxidation mechanisms catalyzed by the Fe (BPMEN) complex.

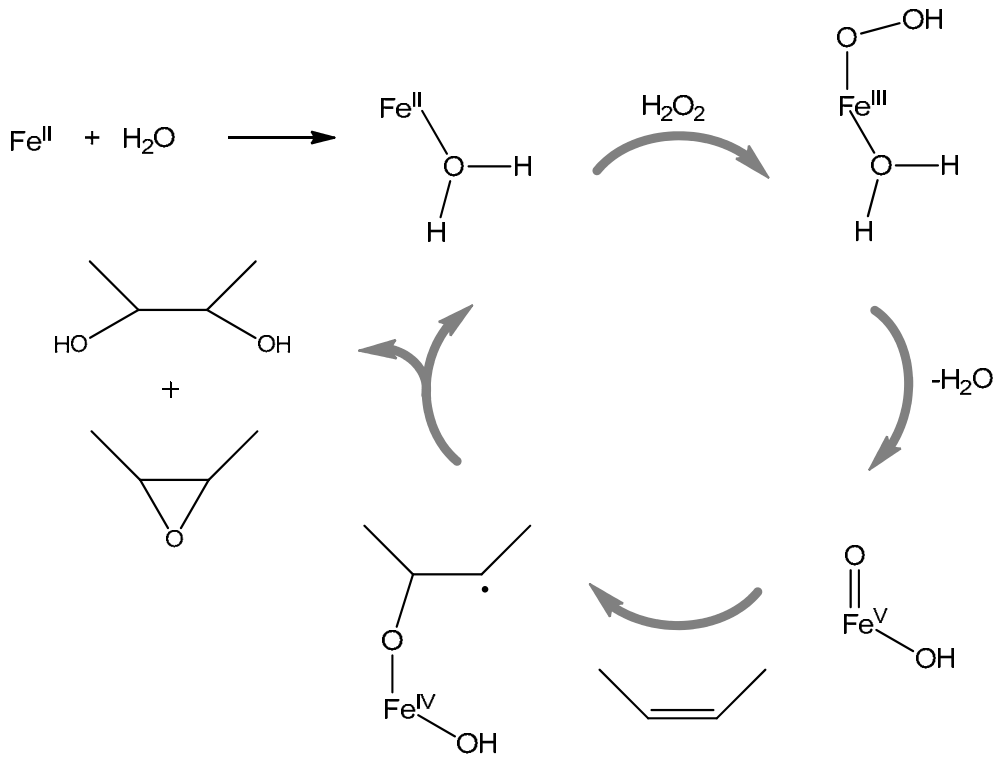

Figure 3.3.16. Schematic representation of epoxidation mechanisms catalyzed by the Fe (BPMEN) complex in presence of water.

3.3.4.2. Cyclohexene oxidation with Fe^{III}-Proline catalysts.

The role of isolated Fe^{III}-Proline active sites was investigated in cyclohexene oxidation with air, TBHP and APB. Fe^{III}-Proline based catalysts displayed different catalytic behaviours depending on the type of oxidant, nature of the support and loading of metal sites. The trends discussed here were analogous to that of Cu^{II}-Valine systems described in section 3.2.5.2. The conversion of cyclohexene was higher with air and APB and very low when TBHP was employed as the oxidant. Control experiment in the absence of catalyst gave conversions of 2.0 mol% with TBHP, 6.8 mol% with APB and 4.5 mol% in the presence of air (see Table 3.2.8.). The results of cyclohexene oxidation catalyzed by Fe^{III}-Proline materials are listed in Table 3.3.8.

Table 3.3.8. Results on selective oxidation of cyclohexene with Fe^{III}-Proline based catalysts. For reaction conditions see section 6.10.3.

Cat.	Metal load.	Oxid.	Mmol of metal	Cat. (g)	Subst: Metal ratio	Oxid: Subst. ratio	TON	TOF (h^{-1})	Conv. mol %	Select. mol %	
										oxide	enone
Neat	16.9	AIR	0.027	0.009	581	1.65	395	66	68.0	31.0	69.0
Neat	16.9	TBHP	0.027	0.009	581	1	115	19	19.9	3.2	96.8
Neat	16.9	APB	0.027	0.009	581	1	283	47	48.7	99.7	0.03
MCM	8.73	AIR	0.078	0.05	180	1.65	119	20	66.1	24.2	75.8
MCM	2.07	AIR	0.011	0.03	1010	1.65	550	92	61.8	5.4	94.6
MCM	8.73	TBHP	0.078	0.05	180	1	~1	~1	1.6	11.1	88.9
MCM	2.07	TBHP	0.011	0.03	1010	1	25	4.1	2.5	2.8	97.2
MCM	8.73	APB	0.078	0.05	180	1	99	16	48.7	89.5	10.5
MCM	2.07	APB	0.011	0.03	1010	1	412	69	46.3	84.2	15.8
Polyst	0.05	AIR	0.0004	0.05	35370	1.65	23832	3972	79.0	12.5	87.5
Polyst	0.05	TBHP	0.0004	0.05	35370	1	2629	438	7.4	1.8	98.2
Polyst	0.05	APB	0.0004	0.05	35370	1	16507	2751	49.5	85.0	15.0

T=371 K, air 3.0 MPa, acetonitrile 35g (reactions with air and TBHP) and acetonitrile 25g, water 10g (reactions with APB), reaction time=6h, oxide=cyclohexene oxide, enone=2-cyclohexene-1-one.

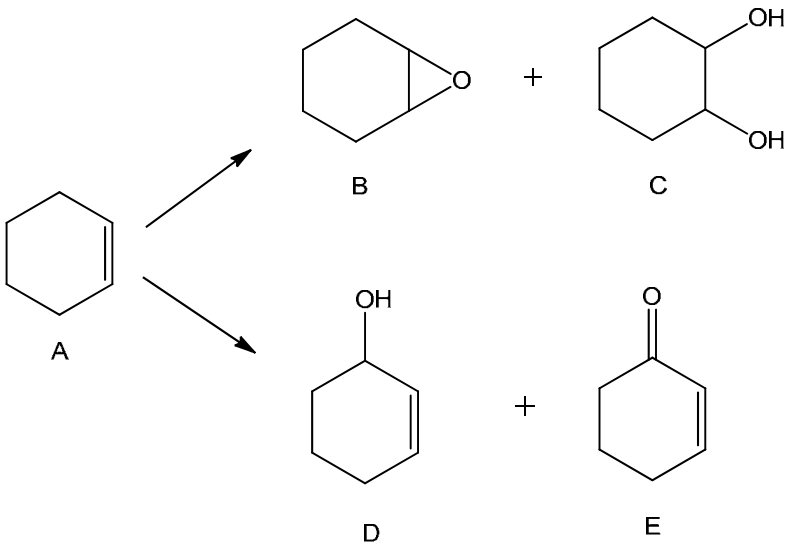

Scheme 3.3.4. Schematic representation of product formation in cyclohexene oxidation: cyclohexene (A), cyclohexene oxide (B), 1,2 cyclohexane diol (C), 2-cyclohexene-1-ol (D), 2-cyclohexene-1-one (E).

Heterogeneous Fe^{III}-Proline catalysts with low metal loading and isolated active sites proved to be more active than their corresponding homogeneous analogues, when employed with air and APB as oxidants. Reactions with TBHP afforded very low TON, TOF and conversions. In the presence of air and APB Fe^{III}-Proline-Polystyrene afforded the highest TON and TOF of all catalysts studied in this research. In the presence of air this catalyst reached TON of 23832 and TOF of 3972 h^{-1}. The analogous homogeneous Fe^{III}-Proline catalyst afforded a TON of 395 and TOF of 66 h^{-1} with air. Increase in TON and TOF when compared to neat complex was also observed when the Fe^{III}-Proline-MCM-41 catalyst was used. In fact the TON increased to 550 and TOF reached 92 h^{-1}. When APB was employed as oxidant increase in activities was also observed. Heterogeneous Fe^{III}-Proline-Polystyrene and Fe^{III}-Proline-MCM-41 obtained TON of 16507 and 412 and TOF of 2751 h^{-1} and 69 h^{-1} respectively, while homogeneous Fe^{III}-Proline complex reached a TON of 283 and TOF of 47 h^{-1} under the same reaction conditions. A comparison of TON and TOF using homogeneous and heterogeneous materials is shown in Figure 3.3.17.

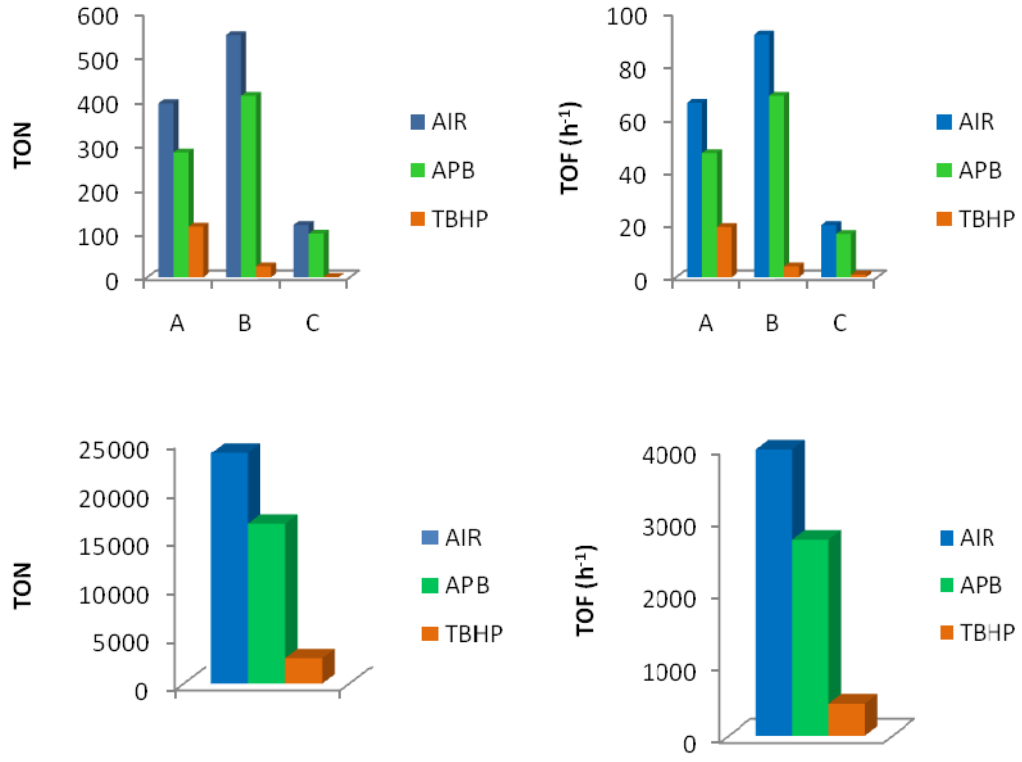

Figure 3.3.17. Comparison of TON (left) and TOF (right) using Fe^{III}-Proline (A), F Fe^{III}-Proline-MCM-41, (Fe 2.07 %wt.) (B) and Fe^{III}-Proline-MCM-41 (Fe 8.73 %wt.) (C), with air, APB and TBHP. For a better visualization bottom charts show TON (left) and TOF (right) using Fe^{III}-Proline-Polystyrene (Fe 0.05 %wt.).

It is worth noting that Fe^{III}-Proline-MCM-41 complexes with low (Fe 2.07 %wt.) and high (Fe 8.73 %wt.) metal loading produced similar conversions with all oxidants. This was unlike in the case of Cu^{II}-Valine catalysts that produced lower conversions when low metal loading was used. These comparable conversions with low and high metal content Fe^{III}-Proline-MCM-41 catalysts could be explained in terms of the density of the immobilised complexes and the effects related to diffusion of substrates and products. In fact, the metal content of high loading Fe^{III}-Proline-MCM-41 (Fe 8.73 %wt.) is only four times higher than the one with low metal loading (Fe 2.07 %wt.). While in the case of Cu^{II}-Valine-MCM-41, the metal content of Cu^{II}-Valine-MCM-41 (Cu 9.22%wt.) is 22 times higher than the one with low metal loading (Cu 0.42 %wt.). This result suggests that the relatively similar active centres density of Fe^{III}-Proline-MCM-41 catalysts with high and low metal loading could allow similar velocity of diffusion of substrates and products into the solid support matrix in which the active sites are located. That may explain similar conversions in cyclohexene oxidation produced by Fe^{III}-Proline-MCM-41 catalysts. On the other side, a significant increase in TON and TOF was observed with

decreasing degree of catalyst loading. It can be hypothesized that such a decrease in metal site loading enhanced their dispersion and isolation and also disabled the accumulation of iron dimers or clusters and/or support-bound dimers which could have much lower activity than the corresponding single sites. In contrast a 22 fold increase in the metal loading of Cu^{II}-Valine-MCM-41 catalysts resulted in a significant increase in conversions but decrease in TON and TOF (for details see section 3.2.5.2.).

Comparable conversions produced by MCM-41 and polystyrene supported Fe^{III}-Proline complexes, i.e. 46.3 mol% and 49.5 mol% respectively (with APB), suggest that hydrophobic/hydrophilic effects of the support were not critical for the catalytic properties of these catalysts in cyclohexene oxidation reactions. Similar behaviour was observed with Cu^{II}-Valine complexes immobilized within MCM-41 and polystyrene supports eg. 17.6 mol% and 18.0 mol% conversion was observed for MCM-41 and polystyrene supported Cu^{II}-Valine complexes respectively, with air (Figure 3.3.18.).

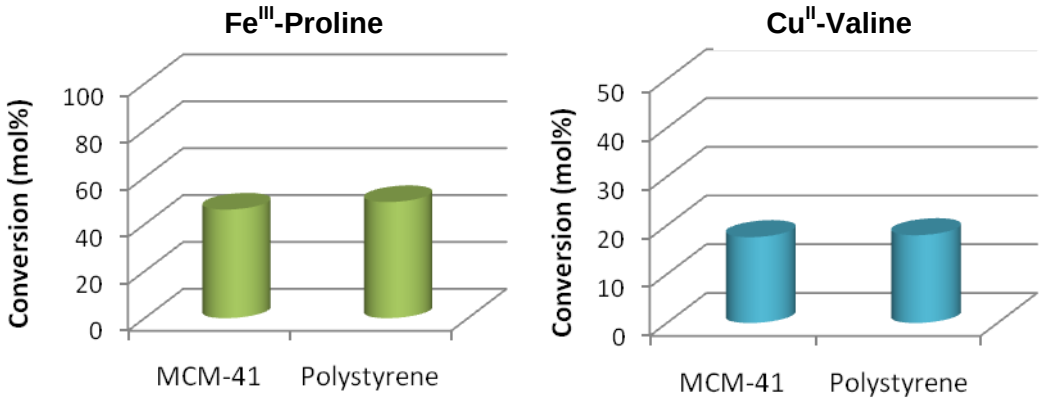

Figure 3.3.18. Comparison of effects of hydrophobic polymeric support and less hydrophobic MCM-41 support on reaction conversions in cyclohexene oxidation catalyzed by heterogeneous Fe^{III}-Proline (left, APB) and Cu^{II}-Valine (right, AIR).

Obtained results indicated that separation of the metal active sites is a key factor for efficient catalytic oxidation reactions. Active site separation was obtained by immobilization of the neat metal complex within MCM-41 and polymer solid host materials. Such heterogeneous catalysts displayed enhanced activity when compared with their homogeneous analogues. The enhanced activity of heterogeneous complexes could be attributed to dispersion and isolation of the catalyst complexes on the mesopores of MCM-41 and polymeric matrix which allowed to avoid the dimerization and polymerization of metal species.

Influence of the active site loading on catalytic activity. The increase in metal content of the heterogeneous Fe^{III}-Proline-MCM-41 catalyst resulted in a significant decrease in TON and TOF with air and APB. Fe^{III}-Proline-MCM-41 catalyst with low metal loading (Fe 2.07 %wt.) exhibited greater catalytic activity, affording more than a four fold increase in turnover number and turnover frequency compared with the corresponding high-metal content analogue (Fe 8.73 %wt.). In the presence of air, TON and TOF decreased from 550 and 92 h^{-1} for Fe^{III}-Proline-MCM-41 (Fe 2.07 %wt.) to 119 and 20 h^{-1} for Fe^{III}-Proline-MCM-41 (Fe 8.73 %wt.). A similar trend was also observed when APB was employed as oxidant. In fact, Fe^{III}-Proline-MCM-41catalyst with high loading of the metal sites (Fe 8.73 %wt.) afforded TON and TOF of 99 and 16 h^{-1} while catalyst with low metal sites content exhibited greater turnover number and turnover frequency of 412 and 69 h^{-1}.

The decrease in iron content of Fe^{III}-Proline-MCM-41 materials resulted in a drastic increase in TON and TOF and clearly indicates that good-isolation of the metal active sites was crucial to obtain high catalytic activities.

Literature data reports that pore size, density of active sites and diffusion rates of liquid reactants are the main parameters affecting the accessibility of the metal centre and as a result govern catalytic activities.[148, 329] Increasing population of active sites can lead to restricted mass transfer because of increasing steric hindrance that can retard the chemical reaction.

A study on cyclohexene oxidation with MCM-41 supported Ti revealed that turnover frequencies (TOF) decreased as the titanium content increased (Table 3.3.9.).[330] It was suggested that catalysts with low loadings of titanium possess the highest number of isolated active sites and that the more isolated sites appeared to be more active in oxidation reactions. In fact TOF increased from 634 for Ti-MCM-41 (1.42 wt%) to 651 for catalyst with 1.32 wt% of Ti loading. The TOF of the samples derived from supporting of Ti onto SBA-15 also decreased as the Ti coverage increased. These results again indicated that catalysts with low loadings of titanium possessed the highest number of the most active sites. TOF of 258 was afforded by Ti-SBA (1.77 wt%) while for catalyst with 1.36 wt% of Ti loading TOF increased to 643. It was also concluded that the high surface area of SBA-15 and MCM-41, allowed greater dispersion of the Ti centers and therefore a higher concentration of isolated Ti species. At low Ti loadings, the possibility of dimerization/oligomerization is relatively low, therefore active sites are better isolated and catalysts are most active. The characterization data of these materials indicated that the best catalysts possess the highest number of isolated, tetrahedral Ti centres. It was suggested that materials with low metal loading contained a higher number

of isolated, tetrahedral Ti^{IV} sites, and samples with higher metal loading contained also a small amount of oligomerized Ti^{IV} species. It should be noted, however, that in these examples the differences in metal loading is much smaller compared to Fe^{III}-Proline and Cu^{II}-Valine catalysts.

Table 3.3.9. Comparison of catalytic performance of Ti catalysts in cyclohexene oxidation reactions.[330]

Catalyst	***Metal loading wt. %***	***Oxidant***	***TOF***
Ti-SBA-15	1.77	CHP	258
	1.41	CHP	384
	1.34	CHP	643
Ti-MCM-41	1.42	CHP	634
	1.32	CHP	651

Catalytic activity of Ru^{II} phosphine complexes supported on aluminated mesoporous silica was also strongly dependent on the loading of the active sites.[331] It was suggested that the catalytically active zone was limited to the area where an efficient transport of substrates and products in and out of the support matrix could occur. The catalytic activity depended primarily on the surface density of ruthenium phosphine complexes. The decrease in reaction rates at higher metal loading suggested that an increasing density of active sites has its limits. High density of metal sites could lead to overcrowding of active species and could hinder the access to the sites located especially deeper within the pore network. It was also assumed that the decrease in activity observed for higher loading of active sites was due to the increasing pore blockage caused by the accumulation of complexes. As a result, the number of catalytically active, isolated sites was effectively reduced, leading to a decrease in the reaction rates. Catalytic activity was affected by the accessibility of active sites and diffusion rates of the reactants. Increasing the population of grafted metal sites led to restricted mass transfer rates due to increasing steric hindrance. In view of the diffusional limitations encountered by liquid phase reaction it was suggested that the optimum catalytic performance required such loading of isolated sites that could prevent the excessive diffusional constraints.

Influence of oxidant on reaction conversions. Conversions of cyclohexene catalyzed by Fe^{III}-Proline have been shown to be strongly dependent on the nature of oxidant, exhibiting similarities to reactions catalyzed by Cu^{II}-Valine materials. Homogeneous catalyst displayed conversions of 68.0 mol% in presence of air, 48.7 mol% with APB, and much lower conversions when TBHP was used (19.9 mol%). Both heterogeneous catalysts Fe^{III}-Proline-MCM-41 and Fe^{III}-Proline-Polystyrene with a low loading of active centres also afforded high conversions with air as oxidant (61.8 mol% and 79.0 mol%, respectively) and lower when APB was used (46.3 mol% and 49.5 mol%, respectively) and very low conversions with TBHP, which were 2.5 mol% and 7.4 mol% for MCM-41 and polystyrene immobilized catalysts, respectively. A similar trend was observed when the Fe^{III}-Proline-MCM-41 catalyst that possessed high metal content (Fe 8.73 %wt.), was employed. In the presence of air this catalyst exhibited conversion of 66.1 mol% while when APB was employed this catalyst reached conversions of 62.5 mol% and 1.6 mol% with TBHP. In the presence of TBHP all Fe^{III}-Proline catalysts obtained very low conversions (Table 3.3.8.).

Low reaction conversions with TBHP could be explained by autoretardation and probable catalyst deactivation. The observed lack of catalytic activity when TBHP is used as the oxidant could be attributed to the presence of water, which is known to severely inhibit the epoxidation reactions. Another reason could be retardation of the catalysis by increasing quantities of the alcohol co-products (*tert*-butanol) in the reaction mixture that can hinder the formation of the active oxidant (for more details see section 3.2.5.2.). A comparison of reaction conversions using homogeneous and heterogeneous catalysts is shown in Figure 3.3.19.

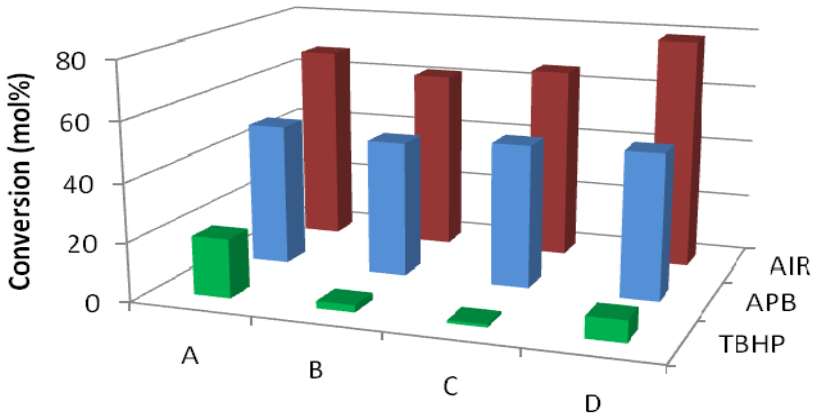

Figure 3.3.19. Comparison of conversions in cyclohexene oxidation using Fe^{III}-Proline (A), Fe^{III}-Proline -MCM-41 (Fe 2.07 %wt.) (B), Fe^{III}-Proline -MCM-41 (Fe 8.73 %wt.) (C) and Fe^{III}-Proline -Polystyrene (Fe 0.05 %wt.) (D), with air, APB and TBHP.

Influence of oxidant and solid support on product selectivities. The type of oxidant clearly was a key factor that influenced the selectivity and conversion in cyclohexene oxidation reactions with Fe^{III}-Proline catalysts. In the presence of air, high selectivity towards 2-cyclohexene-1-one was observed while, when APB was employed high selectivity towards cyclohexene epoxide was observed. The homogeneous Fe^{III}-Proline catalyst was 69.0 mol% selective towards 2-cyclohexene-1-one in the presence of air. The selectivity changed in the presence of APB, and as expected, cyclohexene epoxide was formed with selectivity of >99.0 mol%. Heterogeneous catalysts showed to be less selective to epoxide formation with APB, and a significant amount of 2-cyclohexene-1-one was also produced. In fact, when Fe^{III}-Proline-MCM-41 (Fe 2.07 %wt.) was used with APB, selectivity towards cyclohexene oxide dropped to 84.2 mol % (when compared with >99 mol% with neat Fe^{III}-Proline) and 2-cyclohexene-1-one was formed with selectivity of 15.8 mol%. In the presence of Fe^{III}-Proline-Polystyrene (Fe 0.05%wt.) selectivity towards cyclohexene oxide dropped to 85.0 mol %. This indicates that hydrophobicity of the support plays an important role in the observed selectivity changes (increased selectivity towards enone formation). Furthermore, in the presence of air, and as seen for Cu^{II}-Valine catalysts, selectivity towards 2-cyclohexene-1-one increased to 94.6 mol% and 87.5 mol% with MCM-41 (Fe 2.07 %wt.) and polystyrene (Fe 0.05%wt.) immobilized catalysts respectively (while neat Fe^{III}-Proline exhibited selectivity of 69.0 mol% to 2-cyclohexene-1-one). The direct conversion of cyclohexene to 2-cyclohexene-1-one in presence of O_2 is explained in section 3.2.5.2.

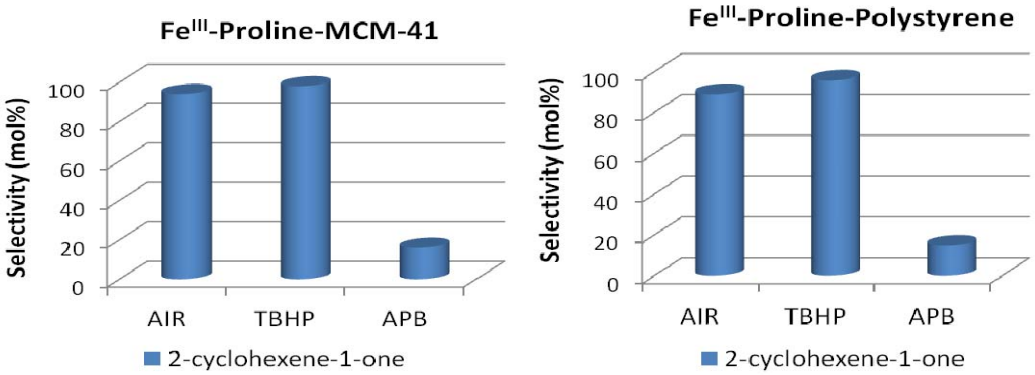

Figure 3.3.20. Comparison of selectivity towards 2-cyclohexene-1-one in cyclohexene oxidation reactions catalysed by Fe^{III}-Proline –MCM-41 (Fe 2.07 %wt.) and Fe^{III}-Proline-Polystyrene (Fe 0.05%wt.) with air, TBHP and APB.

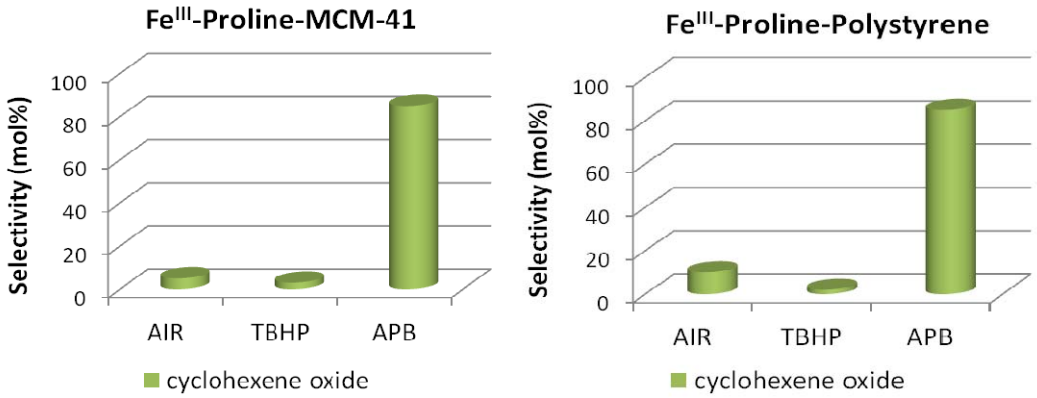

Figure 3.3.21. Comparison of selectivity towards cyclohexene oxide in cyclohexene oxidation reactions catalysed by Fe^{III}-Proline-MCM-41 (Fe 2.07 %wt.) and Fe^{III}-Proline-Polystyrene (Fe 0.05%wt.) with air, TBHP and APB.

The results obtained suggest that the type of oxidant and the nature of the solid support (hydrophobic polystyrene and less hydrophobic methyl functionalized MCM-41) strongly influenced the selectivity and increased the selectivity towards enone formation. 2-cyclohexene-1-one was produced even in the presence of peracetic acid (formed from APB decomposition) that is known to be highly selective towards epoxide products.

Influence of iron site loading on reaction selectivities. In the presence of air heterogeneous Fe^{III}-Proline-MCM-41 catalysts with low iron sites loading (Fe 2.07 %wt.) exhibited higher selectivity to the enone than its high iron content analogue (Fe 8.73 %wt.). By increasing the metal loading of heterogeneous MCM-41 supported catalysts, a significant decrease in selectivity towards 2-cyclohexene-1-one was observed with air. In fact, by increasing the iron loading of Fe^{III}-Proline -MCM-41 the selectivity towards 2-cyclohexene-1-one decreased from 94.6mol% (Fe^{III}-Proline-MCM-41 Fe, 2.07 %wt.) to 75.8 mol% (Fe^{III}-Proline -MCM-41 Fe, 8.73 %wt.). The homogeneous Fe^{III}-Proline catalyst was the less selective towards 2-cyclohexene-1-one formation, afording selectivity of 69.0 mol%.

In the presence of APB, the decrease of selectivity towards 2-cyclohexene-1-one was less significant when compare with the low and high metal loading MCM-41 immobilized catalysts. The selectivity changed from 15.8 mol% for Fe^{III}-Proline-MCM-41 (Fe 2.07 %wt.) to 10.5 mol% for high metal content analogue Fe^{III}-Proline-MCM-41 (Fe 8.73 %wt.).

Selectivity to 2-cyclohexene-1-one/cyclohexene epoxide appeared to be strongly dependent on oxidant. However, in the case of the heterogeneous catalysts the nature of support, active site loading and substrate/metal ratio had also significant influence on the product

selectivity, especially in reactions with APB producing 2-cyclohexene-1-one alongside the major cyclohexene epoxide product. With a lower substrate/metal ratio, a higher selectivity for 2-cyclohexene-1-one was observed with both oxidants, air and APB, using Fe^{III}-Proline and Cu^{II}-Valine (Figure 3.3.22.). It is interesting to note that selectivity does not change with reaction time. Evaluation of the reaction products over reaction time with homogeneous and heterogeneous Fe^{III}-Proline catalysts is shown in Figure 3.3.23. and 3.3.24.

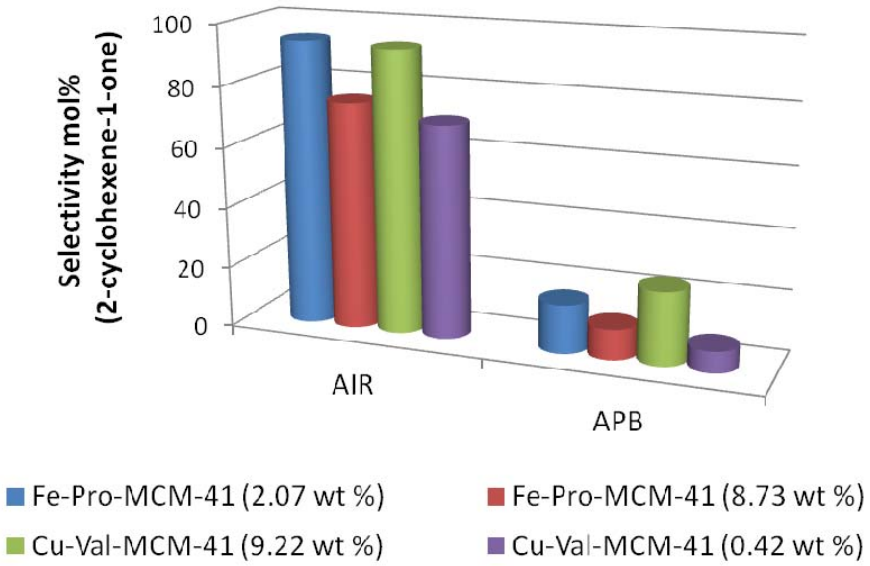

Figure 3.3.22. Comparison of selectivities to 2-cyclohexene-1-one using Fe^{III}-Proline-MCM-41 and Cu^{II}-Valine-MCM-41 with a low and high metal loading, with air and APB. The lower metal loading, the higher selectivity to 2-cyclohexene-1-one.

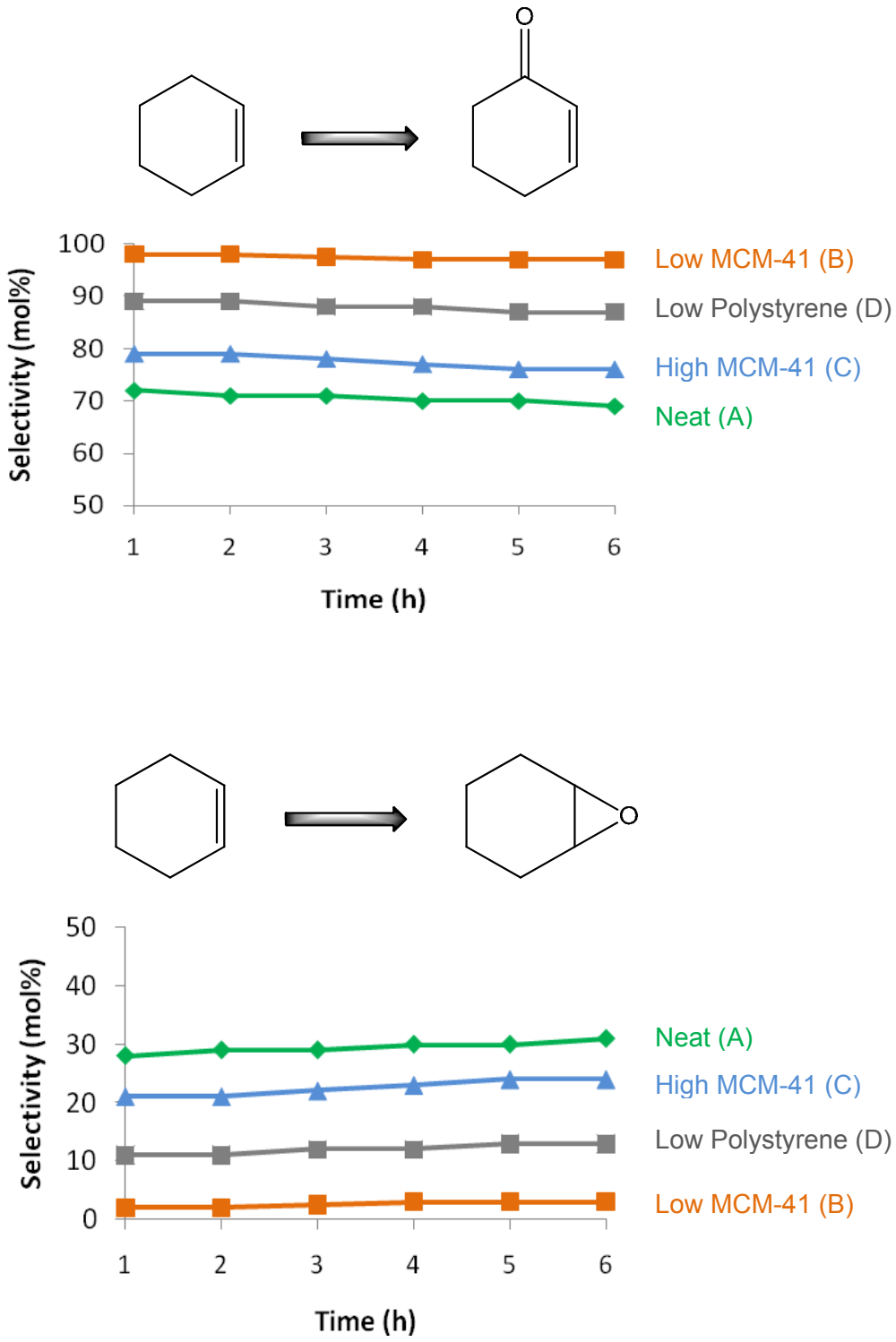

Figure 3.3.23. Distribution of products in cyclohexene oxidation: 2-cyclohexene-1-one (top) and cyclohexene oxide (bottom) using Fe^{III}-Proline (A), Fe^{III}-Proline -MCM-41, Fe 2.07 %wt. (B), Fe^{III}-Proline -MCM-41, 8.73 %wt. (C), Fe^{III}-Proline -Polystyrene, Fe 0.05 %wt.(D), with air.

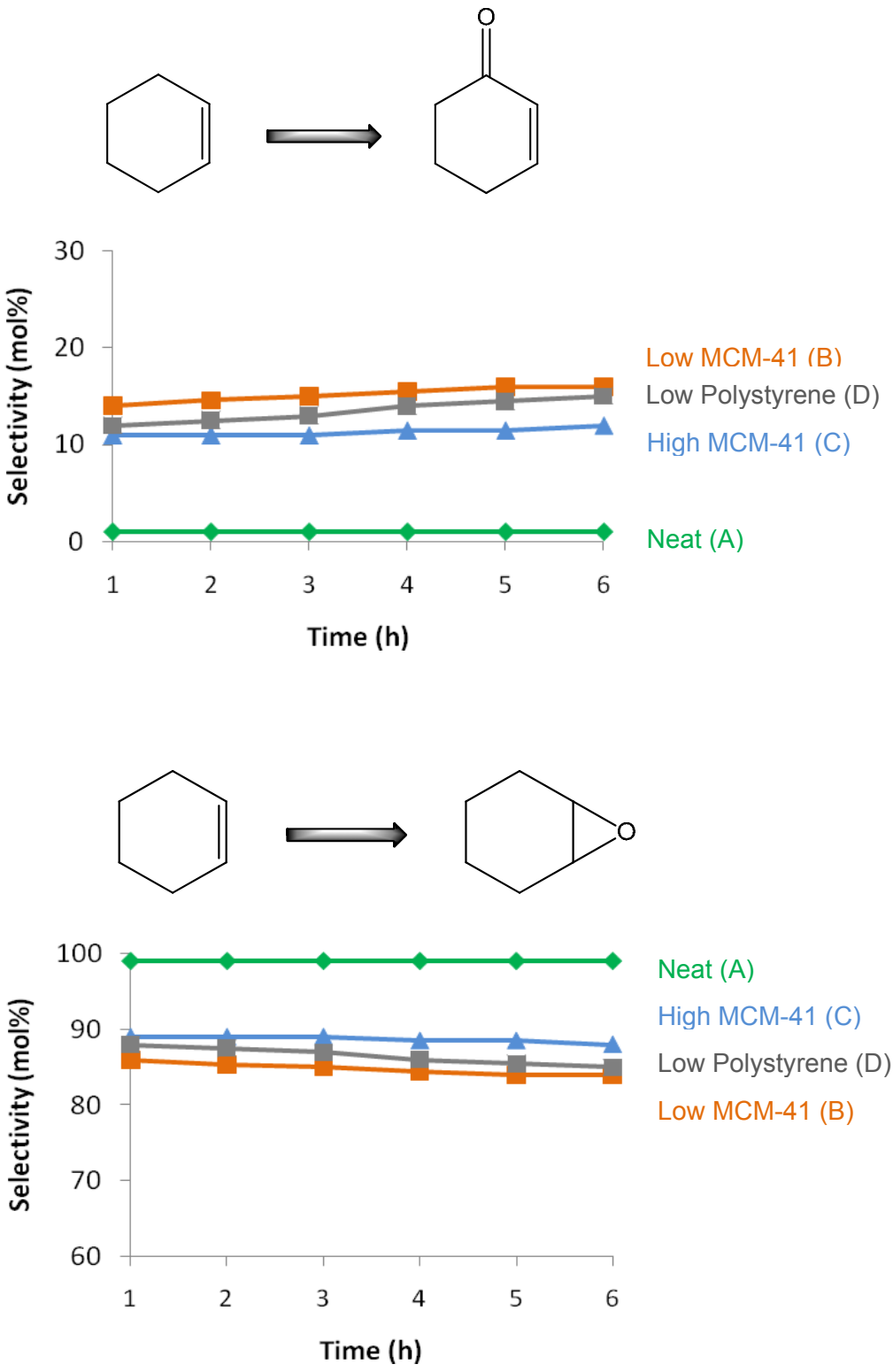

Figure 3.3.24. Distribution of products in cyclohexene oxidation: 2-cyclohexene-1-one (top) and cyclohexene oxide (bottom) using Fe^{III}-Proline (A), Fe^{III}-Proline-MCM-41, Fe 2.07 %wt. (B), Fe^{III}-Proline-MCM-41, 8.73 %wt. (C), Fe^{III}-Proline-Polystyrene, Fe 0.05 %wt.(D), with APB.

Fe^{III}-Proline catalysts exhibited high selectivity towards α,β-unsaturated enone formation in the presence of air. The key step in the mechanism of olefin oxidation catalyzed by iron is the reduction of Fe^{III} to Fe^{II} (Scheme 3.3.5.). The involvement of Fe^{V}=O or Fe^{IV}=O active metal-oxo species is also probable (discussed in section 3.1.3.1.). Selectivity of air and TBHP towards allylic oxidations of unsaturated hydrocarbons is also reported in the literature with various catalysts (section 3.2.5.2.). Both Fe^{III}-Proline and Cu^{II}-Valine catalytic systems exhibited a similar selectivity profile depending on the type of oxidant employed. In the presence of APB, epoxidation reactions were dominant with Fe^{III}-Proline and Cu^{II}-Valine catalysts resulting in a high yield of epoxide formation. Air and TBHP, on the other hand favoured, abstraction over addition resulting in low epoxide formation and high selectivity to the enone.

The key step in the mechanism of olefin oxidation catalyzed by iron is the reduction of Fe^{III} to Fe^{II}, which is classical Haber–Weiss decomposition of *t*BuOOH. This reduction in the oxidation state decomposes *t*BuOOH to the *t*BuOO$^{\bullet}$ radical (*tert*-butylperoxy radical) and a proton (3.3.5., 1). Then, Fe^{II} is oxidized by TBHP generating *t*BuO$^{\bullet}$ radical and giving the Fe^{III}/Fe^{II} redox chain (2). *t*BuO$^{\bullet}$ (*tert*-butoxy) radical undergoes rapid hydrogen atom abstraction from TBHP (*tert*- butyl hydroperoxide) at a much faster rate than hydrogen atom abstraction from the alkene, to form the more stable *tert*-BuOO$^{\bullet}$ radical (3). The *tert*-butylperoxy radical undergoes selective hydrogen atom abstraction from the allylic position of hydrocarbon forming the allyl radical (4). Capture of the allyl radical by *tert*-BuOO$^{\bullet}$ radical forms allylic *tert*-butylperoxide (5) which undergoes rapid reaction with the *tert*-butylperoxy radical forming α,β-enone (6). The proposed mechanism for allylic oxidation of cyclohexene is presented in Scheme 3.3.5.

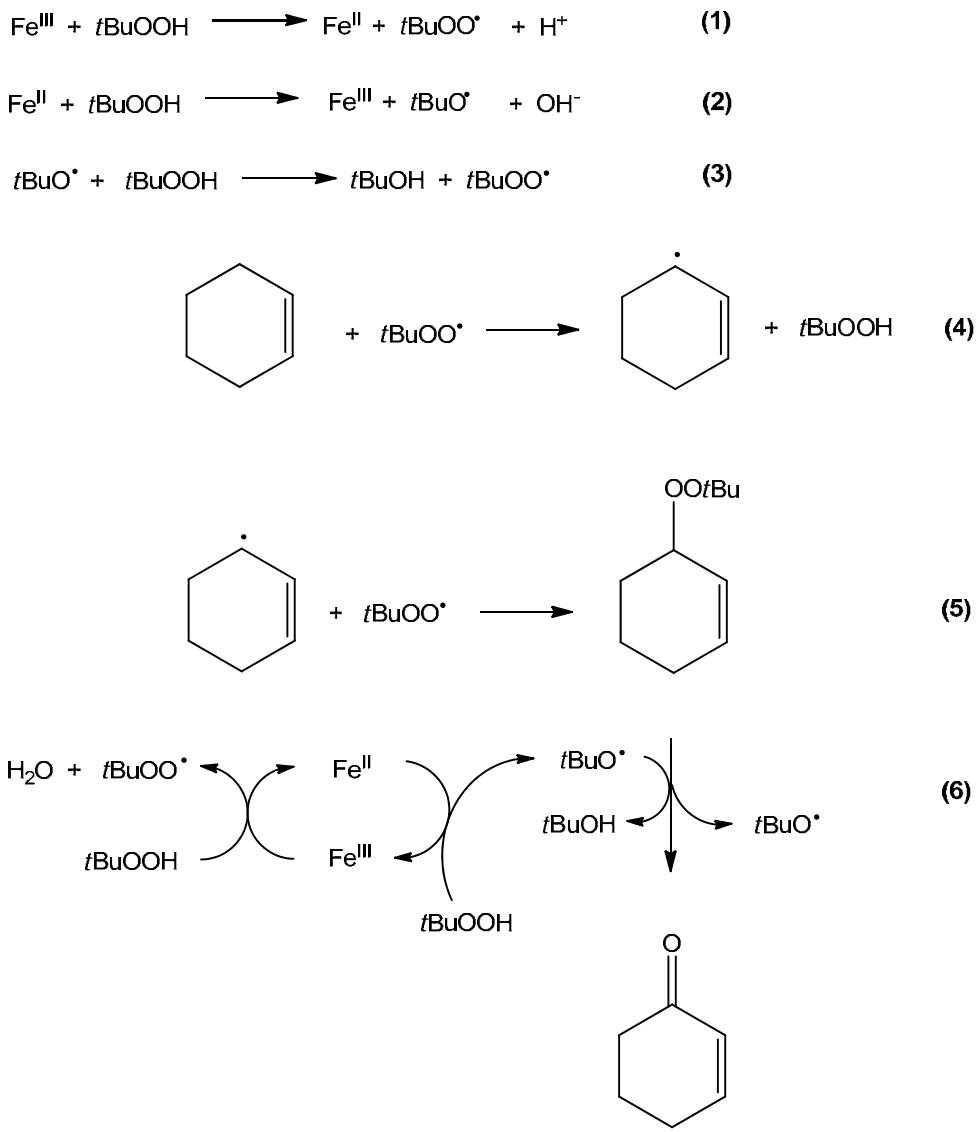

Scheme 3.3.5. Mechanistic proposal for allylic oxidation of cyclohexene with TBHP.

Catalyst recycling. To investigate catalyst reusability, cyclohexene oxidation with air was studied with low metal loading Fe^{III}-Proline-MCM-41 (Fe 2.07 %wt.) and Fe^{III}-Proline-Polystyrene (Fe 0.05 %wt.) catalysts. At the end of the first run the catalyst was separated by filtration, washed with acetonitrile and dried in air at 80°C. Preliminary results on catalyst recycling seem to be reasonable, however detailed studies involving higher number of recycling cycles and characterization of reused catalysts is required. The high selectivity to 2-cyclohexene-1-one was unaffected with both catalysts. Comparison of TON and selectivity using fresh and reused catalysts is presented in Figure 3.3.25. for Fe^{III}-Proline-MCM-41 (Fe 2.07 %wt.) and Figure 3.3.26. for Fe^{III}-Proline-Polystyrene (Fe 0.05 %wt.).

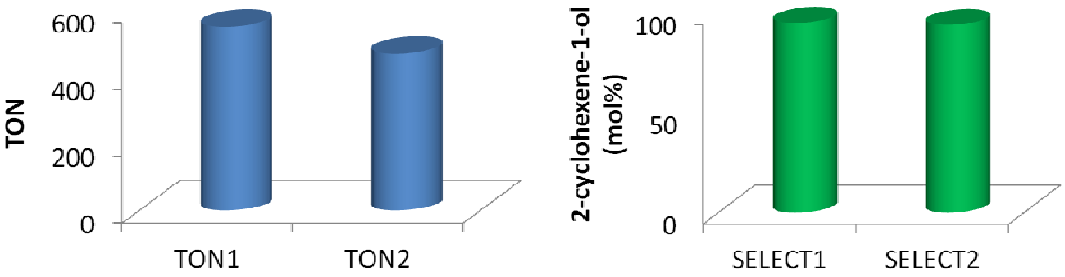

Figure 3.3.25. Comparison of turnover number (TON) and selectivity (SELECT) in the oxidation of cyclohexene using Fe^{III}-Proline-MCM-41 with air, t=4h, TON1, SELCT1 catalysed by fresh catalyst, TON2, SELCT2 catalysed by reused catalyst.

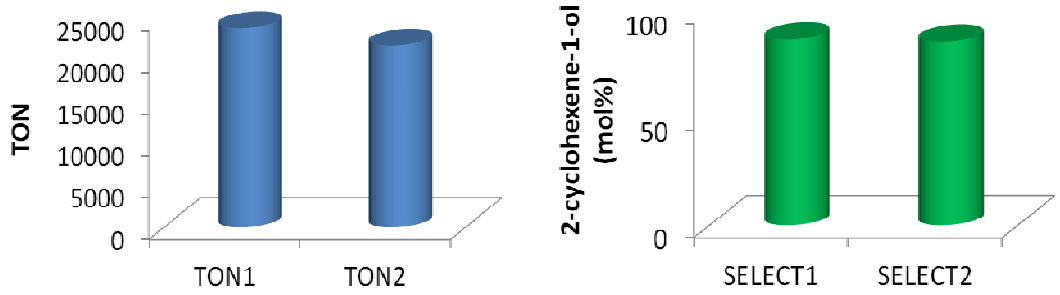

Figure 3.3.26. Comparison of turnover number (TON) and selectivity (SELECT) in the oxidation of cyclohexene using Fe^{III}-Proline- Polystyrene with air, t=4h, TON1, SELCT1 catalysed by fresh catalyst, TON2, SELCT2 catalysed by reused catalyst.

3.3.5. Dimethyl sulfide oxidation with Fe^{III}-Proline-MCM-41 and Fe^{III}-Proline-Polystyrene complexes.

3.3.5.1. Introduction to sulfide oxidation with iron.

Selective oxidation of sulfides to the corresponding sulfoxides is particularly interesting due to the importance of sulfoxides as synthetic intermediates in organic synthesis (section 3.2.6.1.). Oxidation of organic sulfides catalyzed by high-valent intermediates of iron heme enzymes like peroxidases, catalases, and cytochrome P450 have been widely investigated. Synthetic metalloporphyrins like Fe^{III} and Mn^{III} tetraarylporphyrins and salen complexes have been also studied and reported as efficient catalysts for selective sulfide oxidation (Table 3.3.10.).

Table 3.3.10. Comparison of catalytic performance of diffrent catalysts in dimethyl sulfide oxidation reactions.

Catalyst	***Substrate***	***Oxidant***	***Conv. (%)***	***Sulfoxide Selectivity (%)***	***Ref.***
MnPor	methyl phenyl sulfide	H_2O_2	100	86	[332]
	diphenyl sulfide	H_2O_2	100	91	
$FePorF_{20}$	methyl phenyl sulfide	H_2O_2	96	94	[333]
	diphenyl sulfide	H_2O_2	92	95	
	dibuthyl sulfide	H_2O_2	90	93	
FeSalen	methyl phenyl sulfide	H_2O_2	88	99	[334]

It was suggested that the active species in sulfoxidation reactions catalyzed by peroxidases such as HRP (horseradish peroxidase) is initiated by the transfer of one electron from the sulfide to the iron^{IV} oxo porphyrin radical cation [Por$^{\bullet+}$-Fe^{IV}=O].[335] This intermediate is reduced by one-electron transfer from the substrate molecules to form Por-Fe^{IV}=O. The reaction of the substrate radical cation with highly active Por-Fe^{IV}=O oxidant results in the formation of sulfoxide and reduction of Por-Fe^{IV} to Por-Fe^{III} (Scheme 3.3.6., A).

In the case of oxidation of organic sulfides by cytochrome P-450 the direct oxygen-transfer mechanism was proposed. In this pathway, oxygen is directly transferred from the metal-oxo porphyrin radical cation [Por$^{\bullet+}$-Fe^{IV}=O] to sulfide which results in sulfoxide and Por-Fe^{III} formation (Scheme 3.3.6., B).

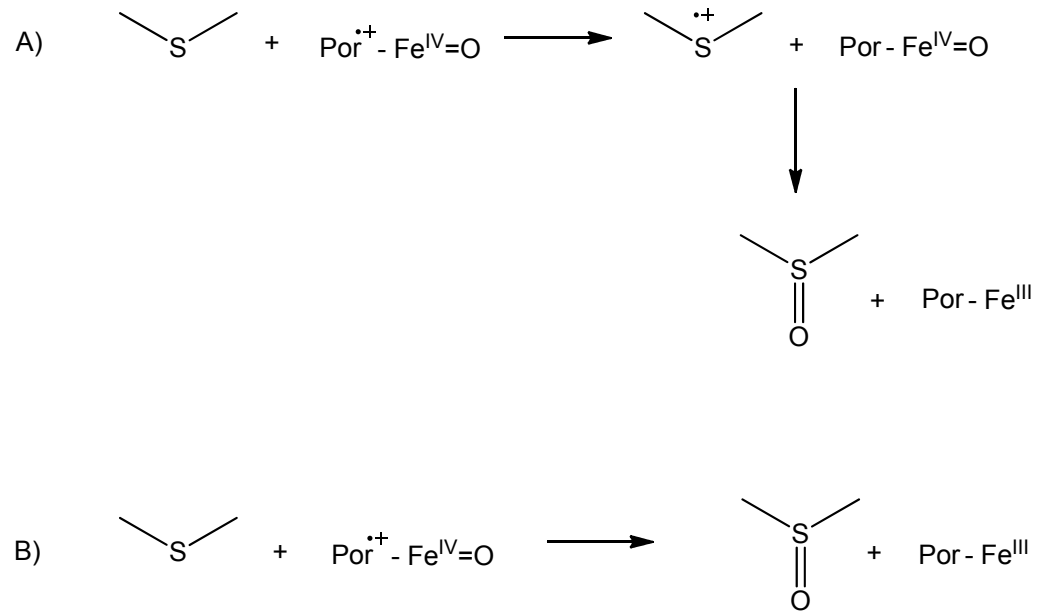

Scheme 3.3.6. Comparison of proposed selective sulfide oxidation pathways catalyzed by HRP (A) and P-450 (B).

The mechanism that involves direct oxygen atom transfer from the iron-oxo species to the sulfide was also proposed for Fe^{III}-salen complexes with H_2O_2 as oxidant. Strong binding of sulfide with the active iron-oxo species was characterized by Mossbauer, EPR and UV–Vis techniques. Mossbauer studies revealed that iron is in the 4^+ oxidation state in the active iron-oxo species. It was proposed that the oxidant, hydrogen peroxide, formed the active oxidant species with iron [$Fe^{IV\bullet+}$=O] *via* iron hydroperoxide species (Fe-OOH). Iron hydroperoxide undergoes heterolytic cleavage that results in the formation of reactive [$Fe^{IV\bullet+}$=O] species.[335] This active iron-oxo species forms a complex with the substrate and facilitates oxygen atom transfer to the substrate and selective oxidation of sulfides to sulfoxides (Scheme 3.3.7.).

An alternative mechanism that involved electron transfer from sulfide to active iron-oxo [$Fe^{IV\bullet+}$=O] species has also been proposed. In such a pathway, the electron transfer from sulfide to reactive species [$Fe^{IV\bullet+}$=O] is the rate-controlling step and leads to formation of active iron-oxo species [Fe^{IV}=O]. The reaction of sulfide radical cation with [Fe^{IV}=O] results in sulfoxide formation and produce Fe^{III}–salen (Scheme 3.3.8.).

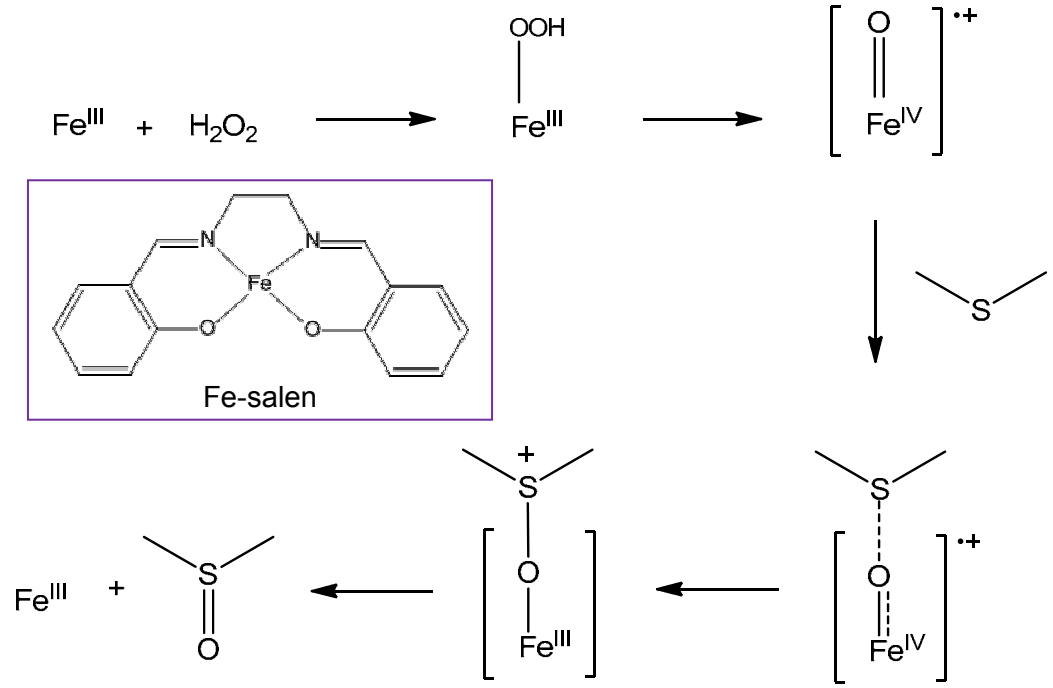

Scheme 3.3.7. Mechanistic proposal for sulfide oxidation with H_2O_2 over Fe^{III}-salen complex *via* direct oxygen transfer.

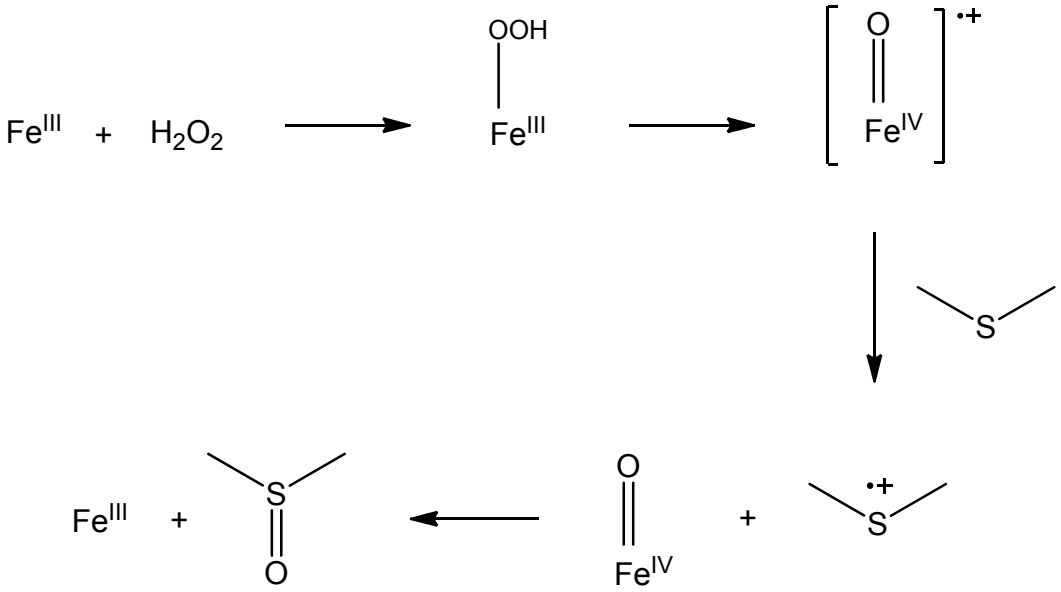

Scheme 3.3.8. Mechanistic proposal for sulfide oxidation with H_2O_2 over Fe^{III}-salen complex *via* electron transfer.

3.3.5.2. Dimethyl sulfide oxidation with Fe^{III}-Proline catalysts.

The reactivity of Fe^{III}-Proline -MCM and Fe^{III}-Proline -Polystyrene catalysts and the role of isolated active sites was tested further towards selective oxidation of dimethyl sulfide. Fe^{III}-Proline catalysts displayed a high propensity for dimethyl sulfoxide formation (>99mol % selectivity), and dimethyl sulfone was not produced. Control experiments in the absence of catalyst gave conversions of 11.0 mol% with TBHP, and 5.1 mol% in the presence of air (see Table 3.6.12.). The results on selective oxidation of dimethyl sulfide with Fe^{III}-Proline catalysts are summarized in Table 3.3.11.

Table 3.3.11. Results on catalytic, selective oxidation of dimethyl sulfide with Fe^{III}-Proline-MCM-41 and Fe^{III}-Proline-Polystyrene catalysts. For reaction conditions see section 6.10.4.

Cat.	Metal load.	Oxid.	Mmol of metal	Cat. (g)	Subst: Metal ratio	Oxid: Subst. ratio	TON	TOF (h^{-1})	Conv. mol %	Select. mol % soxide.
Neat	16.9	AIR	0.027	0.009	581	1.65	214	35	36.8	>99
Neat	16.9	TBHP	0.027	0.009	581	1	421	70	72.4	>99
MCM	8.73	AIR	0.078	0.05	201	1.65	110	18	55.0	>99
MCM	2.07	AIR	0.011	0.03	1016	1.65	328	55	32.3	>99
MCM	8.73	TBHP	0.078	0.05	201	1	124	21	61.6	>99
MCM	2.07	TBHP	0.011	0.03	1016	1	503	84	49.5	>99
Polyst	0.05	AIR	0.0004	0.05	35404	1.65	13646	2274	38.8	>99
Polyst	0.05	TBHP	0.0004	0.05	35404	1	15869	2645	44.8	>99

T=371 K, air 3.0 MPa, acetonitrile 35g, reaction time=6h, soxide-dimethyl sulfoxide.

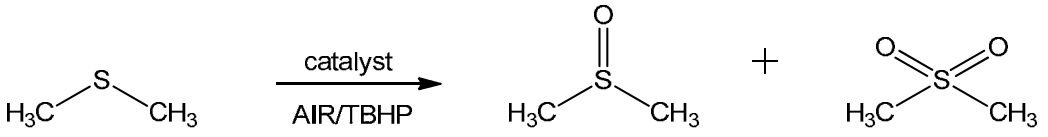

A B C

Scheme 3.3.9. Schematic representation of product formation in dimethyl sulfide (A) oxidation to dimethyl sulfoxide (B) and dimethyl sulfone (C).

Heterogeneous MCM-41 and polystyrene supported Fe^{III}-Proline catalysts with well isolated active sites proved to be more active than their homogeneous analogue, in the presence of both oxidants air and TBHP. In the presence of air, TON and TOF increased from 214 and 35 h^{-1} (neat Fe^{III}-Proline) to 328 and 55 h^{-1} for Fe^{III}-Proline–MCM-41 (Fe 2.07 %wt.) and to 13646 and 2274 h^{-1} for Fe^{III}-Proline -Polystyrene (Fe 0.05 %wt.).

When TBHP was employed, the heterogeneous catalysts also exhibited higher activity than homogeneous Fe^{III}-Proline complex. In fact, the TON and TOF increased to 503 and 83.9 h^{-1} with Fe^{III}-Proline-MCM-41(Fe 2.07 %wt.) and to 15869 and 2645 h^{-1} for Fe^{III}-Proline-Polystyrene (Fe 0.05 %wt.), while neat complex afforded TON and TOF of 421 and 70.2 h^{-1}. The increase in iron sites loading of Fe^{III}-Proline-MCM-41 catalyst resulted in increased dimethyl sulfide conversions but decreased TON and TOF with both oxidants. In fact, in the presence of air both TON and TOF decreased from 328 and 55h^{-1} for Fe^{III}-Proline-MCM-41 with low metal content (Fe 2.07 %wt.) to 110 and 18 h^{-1} with its high metal content analogue (Fe 8.73 %wt.). When TBHP was employed Fe^{III}-Proline-MCM-41 with low metal site content (Fe 2.07 %wt.) afforded TON and TOF of 503 and 84 h^{-1} and by increasing metal sites loading the TON and TOF decreased to 124 and 21 h^{-1} with Fe^{III}-Proline-MCM-41 (8.73 %wt.). Comparison of TON and TOF using homogeneous and heterogeneous catalysts is shown in Figure 3.3.27.

The increase in activity of heterogeneous Fe^{III}-Proline catalysts supported within MCM-41 and polystyrene hosts, strongly indicate that the isolated active sites generated during immobilization of homogeneous complex within solid host matrices significantly enhanced the catalytic activity.

Fe^{III}-Proline-Polystyrene catalyst afforded much higher TON and TOF than Fe^{III}-Proline-MCM-41 manly due to the fact that metal loading of polystyrene supported catalyst (Fe 0.05 %wt.) was 40 times lower than the loading of Fe^{III}-Proline-MCM-41, (Fe 2.02%wt.) and 174 times lower than metal loading of Fe^{III}-Proline-MCM-41 (Fe 8.73%wt.). However, conversions produced by Fe^{III}-Proline-Polystyrene were much lower than those produced by Fe^{III}-Proline-MCM-41 catalysts most likely because the number of active iron sites responsible for substrate conversion was much lower (Fe 0.05 %wt.). These results could suggest that the choice of support affected the TON and TOF of Fe^{III}-Proline catalysts, providing evidence that the chemical nature of the support had important influence on catalytic performance. Such drastic increase in TON and TOF of Fe^{III}-Proline-Polystyrene catalyst (Fe 0.05 wt.%) (13646 and 2274h^{-1} with air and 15869 and 2645h^{-1} with TBHP) when compare to TON and TOF obtained by MCM-41 (Fe 2.07 wt.%) supported catalyst (328 and 55 h^{-1} with air and 503 and 84 h^{-1}) could be attributed to following facts:

(I) Fe ion interactions with solid support; Fe of Fe^{III}-Proline-Polystyrene catalyst could possibly interact with chlorine atoms from chloromethylated polymer matrix, while in the case of Fe^{III}-Proline-MCM-41 catalyst this interactions could be replaced by oxygen atoms from the surface silanols of MCM-41. Such changes in microenvironment of active centre could result in changes of steric and geometric effects that could be responsible for the changes in catalytic activity between polymer and MCM-41 supported Fe^{III}-Proline catalyst in dimethyl sulfide oxidation reactions.

(II) Site isolation; greater dispersion of the active sites within polystyrene support enhanced catalytic activity of Fe^{III}-Proline catalyst. It can be hypothesized that lower loading of the metal centres improved site-isolation and prevented the formation of clusters and dimers or oxo- and hydroxo- bridged metal species which could have lower activity.

(III) Localization of the catalytic sites within solid support and diffusion limits; lower activity of MCM-41 supported catalysts could be attributed to diffusional resistance encountered by the substrate molecules in reaching the active sites located inside the channels of MCM-41, while active sites immobilized within polymeric matrix could allow larger percentage of Fe sites to become more accessible for substrate and oxidant. Higher density of MCM-41 supported Fe^{III}-Proline active sites could also block the access to metal centres that were located deeper in the silica pore.

(IV) Support hydrophobicity; hydrophobic/hydrophilic interactions of solid support with substrate and product. Polystyrene being more hydrophobic than MCM-41 could have more affinity to the substrate and sorption of dimethyl sulfide could be more effective (section 3.2.6.1.). On the other hand, free silanol groups of MCM-41 surface are known to interact strongly with residual water (TBHP 70 wt.% water solution was used as oxidant) which could block the mesoporous channels disabling the access for substrate molecules.

Similar trends were observed in benzyl alcohol oxidation reactions with Fe^{III}-Proline catalyst immobilized within MCM-41 and polystyrene matrix (section 3.2.2.1.).

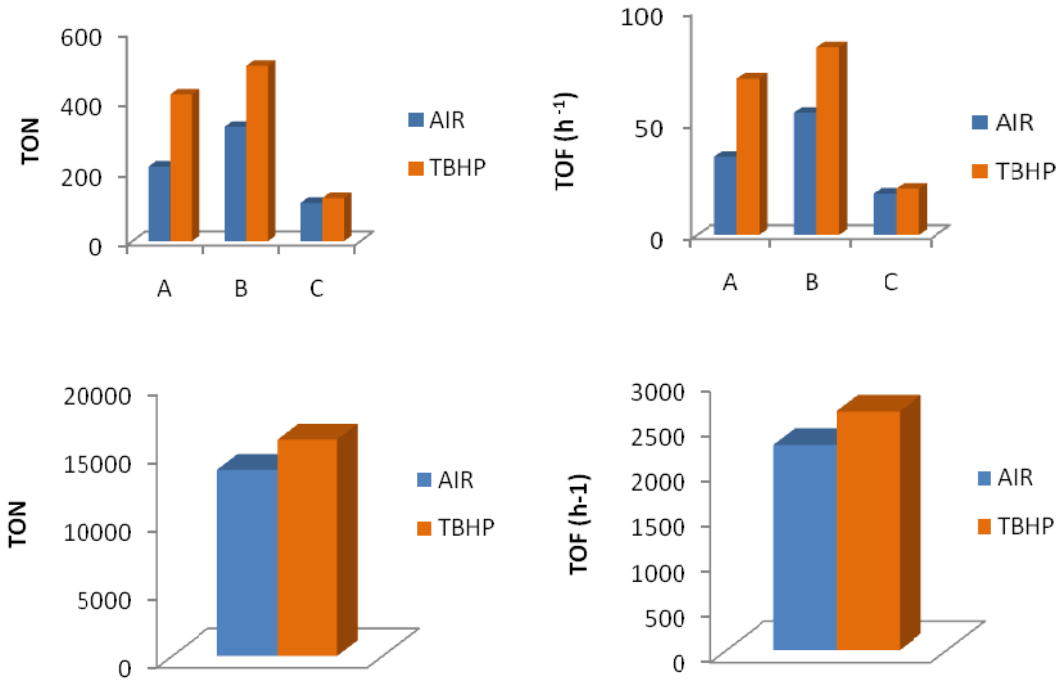

Figure 3.3.27. Comparison of TON (left) and TOF (right) using Fe^{III}-Proline (A), Fe^{III}-Proline-MCM-41, (Fe 2.07 %wt.) (B), Fe^{III}-Proline-MCM-41 (Fe 8.73 %wt.) (C), with air, APB and TBHP. For a better visualization bottom charts show TON (left) and TOF (right) using Fe^{III}-Proline-Polystyrene (Fe 0.05 %wt.).

Influence of oxidant on reaction conversions. Conversions of dimethyl sulfide, in reactions with homogeneous Fe^{III}-Proline complex, showed to be strongly dependent on oxidant nature (similar behavior was observed for Cu^{II}-Valine catalysts, section 3.2.6.2.). Neat Fe^{III}-Proline catalyst afforded higher conversion with TBHP (72.4 mol %) than with air (36.8 mol %). In case of heterogeneous catalysts, conversions were also higher in presence of TBHP. Fe^{III}-Proline-MCM-41 (Fe 2.07 %wt.) exhibited conversion of 49.5 mol% with TBHP and conversion of 32.3 mol% was reached when air was employed as oxidant. Fe^{III}-Proline-Polystyrene obtained conversion of 38.8 mol% with air and conversion of 48.8 mol% with TBHP.

The selectivity to dimethyl sulfoxide appeared to be unaffected by the metal content, Fe/substrate ratio, type of oxidant, nature of support and reaction time. Dimethyl sulfoxide was obtained in high yields with both air and TBHP under given conditions.

Dimethyl sulfide oxidation reactions, with Fe^{III}-Proline similar as with Cu^{II}-Valine catalysts, were not retarded in presence of TBHP. These results could be explained by hydrophobic/hydrophilic interactions of solid support with oxidant, substrates and products and by competition between oxidant and substrates to access the active site (for more details see section 3.2.6.2.).

Comparison of reaction conversions using homogeneous and heterogeneous catalysts is shown in Figure 3.3.28.

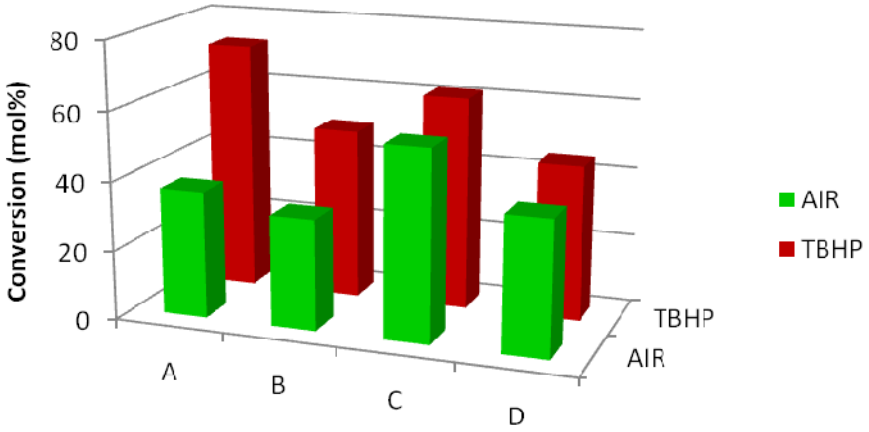

Figure 3.3.28. Comparison of conversions in dimethyl sulfide oxidation using Fe^{III}-Proline (A), Fe^{III}-Proline-MCM-41, (Fe 2.07 %wt.) (B), Fe^{III}-Proline-MCM-41 (Fe 8.73 %wt.) (C), Fe^{III}-Proline-Polystyrene (Fe 0.05 %wt.) (D), with air and TBHP.

Summary.

Fe^{III}-Proline complexes were immobilized on MCM-41 and polystyrene supports using click chemistry methodology. Hydroxyproline was first modified with a propargyl group in purpose to introduce the alkyne functionality. Both MCM-41 and polystyrene supports were functionalized with azido groups prior to further functionalisation with propargyloxyproline. The materials obtained were characterized by IR, DRUV-Vis, ICP and BET techniques. The immobilized amino acid formed stable complexes with iron. These heterogeneous catalysts exhibited promising activity in oxidation of substrates such as: benzyl alcohol, cyclohexene and dimethyl sulfide with various oxidants. Heterogeneous Fe^{III}-Proline-MCM-41 and Fe^{III}-Proline-polystyrene catalysts obtained significantly higher TON and TOF when compared to the homogeneous Fe^{III}-Proline analogue, indicating that greater separation of the active metal sites was a key factor that enhanced the catalytic activities. The employed synthetic methodology showed to have the potential for the synthesis of bioinspired, efficient and selective catalytic materials. The surface property of the MCM-41support could be tailored by grafting organic moieties (methyl groups) onto the channels of mesoporous support in which active centres were localized, thereby making impact on catalytic activity.

However, there is a lot of room for improvements and evaluation of the most effective density of the active sites, the degree of their isolation within the solid supports and influence on catalytic activity.

4. SUMMARY AND CONCLUSIONS.

Fe^{III}-Proline and Cu^{II}-Valine complexes were synthesised under basic conditions to obtain the deprotonated forms of the amino acids that can coordinate to metal ions. Complexes were formed by coordination of the amino acid to the metal ion *via* the charged carboxylate group and amino group. Formation of 2:1 ligand:metal complexes *via* the oxygen atom of carboxylate group and nitrogen atom of the amino group was confirmed by single crystal X-ray diffraction structure analysis, FTIR spectroscopy and elemental analysis.

Both homogeneous complexes were then heterogenized by encapsulation in zeolites employing the general zeolite synthesis method in which preformed transition-metal complexes were included in the zeolite synthesis mixture, and the zeolite framework was formed around the complex. Encapsulation of both Fe^{III}-Proline and Cu^{II}-Valine within zeolite was performed under the same conditions and using the same gel composition. When Fe^{III}-Proline complex was present in the gel, zeolite X was formed. However, when Cu^{II}-Valine complex was used zeolite LTA framework was obtained instead of zeolite X. These results could be explained by the fact that the valine molecule is linear while the proline side chain contains a rigid pyrrolidine ring. Cu^{II}-Valine as the more linear complex could be located between the two neighbouring sodalite cages of Zeolite LTA and this could stop further zeolite crystallization and large cavity FAU formation. Fe^{III}-Proline complex, being more rigid, prefers to be located in the larger cage of FAU rather than in interconnecting cavity. Zeolite LTA has a pore diameter of 4.2 Å which is not large enough for substrate/product molecules to enter/exit the cage and this material was not investigated as catalyst.

The encapsulation of the Fe^{III}-Proline complex into a zeolite X cavity provided enhanced activity when compared to the homogeneous Fe^{III}-Proline catalyst. Fe^{III}-Proline-X has been investigated for both cyclohexane oxidation and benzyl alcohol oxidation using either TBHP or air as oxidants. Fe^{III}-Proline complex encapsulated in the zeolite X showed an *eight-fold* increase in activity when compared with its homogeneous analogue in the presence of *tert*-butyl hydroperoxide. When air was used, the heterogeneous Fe^{III}-Proline-X catalystafforded a *four-fold* increase in activity. These results strongly suggest that the isolated active sites that were generated during encapsulation procedure were responsible for the increase in catalytic activities. The role of isolated active sites was further evaluated in the oxidation of benzyl alcohol. The heterogeneous Fe^{III}-Proline-X catalysts showed to be more efficient than its homogeneous counterpart. The turnover frequencies clearly increased when the Fe^{III}-Proline complexes were isolated from each other while dispersed within the supercages of the zeolite X.

To investigate further the role of the active sites, the influence of the nature of the support on catalytic activity, Fe^{III}-Proline and Cu^{II}-Valine complexes were covalently immobilized within meso pores of silica MCM-41 and hydrophobic polystyrene matrix.

Prior to functionalisation with proline and valine ligands, the surface of the silica was first functionalized with a mixture of chloropropyl and methyl groups. Modification with methyl groups was performed to enhance the hydrophobicity of silica surface.

Proline ligand was attached to MCM-41 and polystyrene using click chemistry methodology. Chloropropyl moieties of MCM-41 and chloromethyl moieties of polystyrene were first modified with azido groups. Then the hydroxy group of 3-hydroxyproline was functionalized with propargyl group in order to generate the alkyne, that in the next step reacted with azido substituted polystyrene and MCM-41 supports. This synthetic method allowed the α-amino acid moiety to remain free and available for further complexation with the metal ion and catalytic reactions.

Immobilized proline complexes with iron exhibited high activity and selectivity in the oxidation of cyclohexene, benzyl alcohol and dimethyl sulfide. The nature of the support, the surface density of the active sites and the type of oxidant had a significant influence on the catalytic activity and selectivity.

In benzyl alcohol oxidation reactions, homogeneous and heterogeneous Fe^{III}-Proline catalysts displayed high propensity for the benzaldehyde formation. Heterogeneous MCM-41 and polystyrene immobilized Fe^{III}-Proline catalysts that posed well isolated active sites, displayed higher activities than their neat, homogeneous analogue. The choice of support (silica or polystyrene) significantly affected the turnovers, providing evidence that the chemical nature of the support influence the catalytic performance. Polystyrene supported catalyst obtained higher TON and TOF than catalysts supported on MCM-41. This could be attributed to factors such as localization of the catalytic sites within solid support, metal ion interactions and/or metal ion interactions with the support (in case of MCM-41 oxygen atoms from surface silanols and/or chlorine atoms from chloropropyl groups, while in the case of polystyrene this could be chlorine atoms from chloromethylated matrix). Slower diffusion of reagents into the pores of MCM-41 where active sites are located could also be the reason for lower activity of silica supported Fe^{III}-Proline complexes.

Similar results were obtained in cyclohexene oxidation reactions where heterogeneous catalysts displayed enhanced activity when compared with their homogeneous analogue. The dispersion of the metal active sites within MCM-41 and polymeric matrices was a key factor that allowed to avoid the dimerization and polymerization of metal species and in result produced efficient single-site catalysts. Conversions and selectivities of cyclohexene oxidation catalyzed by heterogeneous Fe^{III}-Proline catalysts showed to be

strongly dependent on nature of oxidant. In the presence of TBHP strong auto-retardation and probable catalyst deactivation was observed. In the presence of air, high selectivity towards 2-cyclohexene-1-one was observed while, when APB was employed, cyclohexene epoxide formation was dominant. Selectivity towards allylic C-H bond activation (2-cyclohexene-1-one formation) in the presence of air and TBHP can be explained by radical mechanizm and hydrogen atom abstraction from the site that has the lowest carbon-hydrogen dissociation energy (allylic C-H bond). APB that *in situ* liberates peracetic acid that preferred double C-C bond epoxidation over allylic C-H bond oxidation. This result can be explained by the fact that peracids are effective oxidants for C=C bond oxidation that results in high yields of epoxide formation. Peracids react directly with alkenes to provide the corresponding epoxides (*via* Bartlett mechanism).

The reactivity of Fe^{III}-Proline catalysts and the role of isolated active sites were also evaluated towards the selective oxidation of dimethyl sulfide. Homogeneous and heterogeneous Fe^{III}-Proline catalysts displayed high propensity for the dimethyl sulfoxide formation. Heterogeneous Fe^{III}-Proline -MCM-41 and Fe^{III}-Proline -polystyrene catalysts displayed significantly higher TON and TOF when compared with the homogeneous Fe^{III}-Proline analogue, again suggesting that the greater separation of the active metal sites was crucial to enhance the catalytic activity.

Fe^{III}-Proline-Polystyrene catalyst afforded the highest turnovers in all investigated transformations: benzyl alcohol oxidation, cyclohexene oxidation and dimethyl sulfide oxidation. Higher TON and TOF obtained by polystyrene supported catalyst could be attributed to factors such as: metal loading, interactions of metal ions as well as iron interactions with the support, and localization of the active sites within the support. Relatively low turnovers in the case of MCM-41 supported Fe^{III}-Proline catalyst can be attributed to the slower diffusion of reagents into the pores of silica. Diffusion within pores could be even slower due to higher density of the immobilised metal complexes (when compare with the lower loading of active sites of Fe^{III}-Proline-Polystyrene). In the case of polystyrene, high turnovers may be attributed to the predominant localization of the active sites in the accessible region of the polymer matrices (not in the pores as in MCM-41) and faster diffusion due to the lower density of the immobilised iron complexes.

The activity of the immobilized Fe^{III}-Proline catalyst could be sufficiently tuned by employing polystyrene as support that not only served as a carrier for catalytic metal sites, facilitating their separation but also contributed to the catalytic activity by support effects, hypothetically inducting changes in the electronic properties of the metal that significantly influenced the catalytic properties of Fe^{III}-Proline complex.

The Cu^{II}-Valine complex has also been incorporated into inorganic (silica MCM-41) and organic (polystyrene) supports. The valine ligand was immobilised onto chloropropyl and methyl modified MCM-41 and polystyrene supports using the same methodology as for the iron catalysts. In this procedure the amino acid reacts with stoichiometric amounts of pyridine in the aqueous medium that leads to grafting of the ligand by facilitating elimination of HCl as the pyridine hydrochloride salt.

These host/guest catalysts demonstrated high activity and selectivity in the oxidation of cyclohexene, benzyl alcohol and dimethyl sulfide. For all reactions tested the heterogeneous catalysts showed higher turnovers than the corresponding homogeneous analogue.

In benzyl alcohol oxidation reactions, homogeneous and heterogeneous Cu^{II}-Valine catalysts displayed high propensity for the benzaldehyde formation. By decreasing the copper content of MCM-41 and polystyrene supported catalysts turnovers significantly increased, indicating that dispersion of the active sites was crucial to obtain high catalytic activities.

In cyclohexene oxidation reactions with Cu^{II}-Valine catalysts the type of oxidant was a key factor that influenced the product selectivity and conversions. In the presence of TBHP strong auto-retardation and probable catalyst deactivation was observed similar as for Fe^{III}-Proline catalysts. In the presence of air higher selectivity towards 2-cyclohexene-1-one was observed, and when APB was used the epoxide was formed as a predominant product. By decreasing the metal loading of heterogeneous Cu^{II}-Valine catalysts significant increase in selectivity towards 2-cyclohexene-1-one was observed with both oxidants (air and APB). Such changes in selectivity could be explained by the different extent of interactions between Cu active sites of catalysts with high and low loading of the metal. Metal-support interactions that could be stronger for catalysts with higher metal content could also influence the selectivity. Such interactions could affect the electronic, steric and geometric properties of the Cu centres and in result the mechanistic pathways that lead to changes in product distribution.

Similar trends were observed in dimethyl sulfide oxidation reactions and heterogeneous Cu^{II}-Valine catalysts with low loading of metal sites displayed higher activity than their analogues with high content of metal centres. This further strongly suggested that the isolated active sites that were generated during the immobilization procedure were responsible for the increase in catalytic activities. Both homogeneous and heterogeneous Cu^{II}-Valine catalysts displayed high propensity for dimethyl sulfoxide formation with both oxidants air and TBHP.

Fe^{III}-Proline and Cu^{II}-Valine catalyst exhibited similar catalytic behavior in terms of characteristics associated with metal sites loading. The increase in active sites loading of heterogeneous Fe^{III}-Proline and Cu^{II}-Valine catalysts negatively influenced the catalytic activity; this could be explained by:

- Formation of clusters or oxo/peroxo/hydroxo species and accumulation of support-bound dimers/polymers which could have lower activity than the corresponding isolated single-sites.
- Slower diffusion of reagents into the solid support matrix in which metal centres are located due to the high density of immobilized active sites.
- Limited accessibility of overcrowded active sites for substrate and oxidant.

Immobilization of the metal complexes resulted in greater site isolation and number of general characteristics were observed:

- Turnover numbers increased when the catalyst was immobilized (mechanically entrapped in the zeolite cavity or covalently attached to MCM-41 or polymer hosts) when compared with the homogeneous counterparts.
- Turnover numbers increased with decreasing active site loadings, pointing the effects associated with the active site density and isolation as well as pore blockage.
- The environment of the active site controls selectivities, activities and diffusion of reactants.

The results on bio-inspired oxidation reactions using supported proline and valine complexes with transition metals indicated that immobilizing these active complexes into the solid host gave the ability to mimic the oxidative function of metalloenzymes. The zeolite framework as well as matrices of mesoporous silica MCM-41 or polystyrene that can potentially model the protein portion of a metalloenzyme could prevent immobilized complexes from dimerizing and aggregating. The internal cavities and channels of host materials together with the hydrophobicity/hydrophilicity of the support control the access and transport of substrate and product molecules in an analogues way as binding pockets created by the protein scaffold in metalloenzymes. The metalloenzymatic systems in nature incorporate the active sites into a confined space defined protein structure. Immobilized onto solid supports Fe^{III}-Proline and Cu^{II}-Valine catalysts can mimic this strategy and the rigid, inorganic (zeolite, silica) or organic (polystyrene) frameworks determine the reaction environment surrounding the active centres.

5. FUTURE OUTLOOK.

1. Synthesis:

- Nature of the support, the proximity between active sites and chemical environment showed to have a significant influence on catalytic activity of Fe^{III}-Proline and Cu^{II}-Valine complexes. To evaluate the optimal density of the active sites together with optimal hydrophobicity of the support, modifications with various loadings of methyl groups is required. Methyl groups are used to modify the hydrophobicity of the support. By varying the density of methyl groups on the MCM-41 surface, the hydrophobicity can be effectively increased or decreased and the density of immobilized amino acid complexes can be adjusted.

- To examine further the effect of the support, its interactions with amino acid complexes and influence on catalytic activity, various solid host materials like SBA-15, USY, alumina (Al_2O_3), titania (TiO_2), zirconia (ZrO_2) could be also tested.
This would provide a comparison between supports with different properties and facilitate structure property relationships to be made. Supports like alumina, titania and zirconia would provide a contrast with the ordered silica used here and would open up the potential to larger pore sizes.

- To evaluate the role of the ligand and the role of the metal, complexes of proline with copper and valine with iron should be synthesized and compared against existing Fe^{III}-Proline and Cu^{II}-Valine catalysts. This would allow a direct comparison between the catalysts and their performances described in this research.

- Proline and valine complexes with different transition metals e.g. Mn, Ru, Co could be prepared for the purpose to identify the most efficient amino acid-transition metal catalyst. To continue the search of the most active and selective amino acid based catalyst for oxidation reactions other amino acid ligands and their complexes with various metal ions could be studied (there are 20 natural amino acids available to study).

2. Characterisation:

- The thermal stability of the neat and heterogeneous Fe^{III}-Proline and Cu^{II}-Valine complexes could be investigated using thermogravimetric analysis (TGA). Based on the thermal analysis and decomposition data, thermal stability and optimal temperature for

catalytic reactions could be concluded. The thermal degradation pattern for copper complexes with salen reported in literature showed the enhancement of thermal stability of a salen complex encapsulated in zeolite Y when compare with the neat complex.[336] Decomposition of the homogeneous complex occurred at 550 K while decomposition of the zeolite-encapsulated complex occurred at higher temperature of 700 K.

- Solid-state magic-angle spinning nuclear magnetic resonance (MAS NMR) is a powerful tool for studying the structure of zeolites and other heterogeneous catalysts.[337] ^{27}Al MAS NMR could be used to discriminate between framework and non-framework aluminum species. Species with different structures or different environments have a different chemical shift in the ^{27}Al MAS NMR spectra. There are two main peaks expected for aluminum species: one at 54 ppm that is associated with four-coordinated framework aluminum and the other at 0 ppm which is attributed to six-coordinated non-framework aluminum. The relative proportions of framework and non-framework Al can be directly determined from the peak intensities of tetrahedral and octahedral aluminium signals. This technique could also reveal interactions between metal species and support through e.g. oxygen bridges resulting from condensation with the hydroxyls on the support.

The corresponding quantitative ^{29}Si and ^{1}H MAS NMR studies could give information about the amount of silanols and Brønsted acidic sites and if there is any decrease in Brønsted acidic sites after incorporation of metal ions (as proton could be exchanged with metal cation during synthesis).

The high-resolution solid state ^{13}C NMR could be employed for characterization (also quantitative) of the occluded amino acids within solid support. MAS NMR is used in the study of organic templates giving information of each kind of distinct carbon atom of the organic guest species. [338]

- EXAFS studies could answer the question whether iron and copper ions are complexed in the form of isolated ions and/or in the form of oxo- or hydroxo-bridged dimers/polymers. EXAFS spectra of histidine and glutamic acid complexes with iron which are reported in the literature revealed the presence of oxygen and nitrogen atoms in the first coordination shell of iron (total coordination number ~ 3).[157] The second, more distant shell was fitted by an iron neighbor (which implies the presence of an iron dimer) and also by a C/N atom of the amino acid ligand or by a sulfur atom, originating from the sulfate anion used as metal precursor (Mohr Salt (NH4)2[Fe(SO4)2]*6H2O).

EXAFS studies could supply information on the distance between the metal cations and the O and/or N atoms in the first coordination sphere and thus the changes in the local structure around the metal ions after immobilization within solid support.

3. Catalysis:

- Continuous spectroscopic studies during the catalytic cycle could be employed to examine the active oxidant species, reaction intermediates and utilize the mechanisms of oxidation reactions catalyzed by amino acid complexes with transition metals.

The role of the amino acid complexes with transition metals in oxidation reactions could be studied with combined operando DR UV–Visible monitoring of the catalyst and on-line GC or GC-MS analysis.[339] Operando spectroscopy refers to spectroscopy of a working catalyst in combination with on-line activity measurements, while *in situ* spectroscopy refers to spectroscopy of a material under specific conditions, not necessarily reaction conditions. The schematic set up for such experiment is shown in Figure.

The role of the bis(μ-oxo)dicopper core ($[Cu_2(\mu\text{-}O)_2]^{2+}$) has been studied in the decomposition of NO and N_2O by the Cu-ZSM-5 zeolite using such experimental techniques. During decomposition of NO and N_2O, a reaction temperature dependency was observed. It was shown that the intensity of the 21,500 cm^{-1} band, which was assigned to the bis(μ-oxo) dicopper species, was the highest in the 673–773 K temperature range and proportional to the N_2 yield (product). In N_2O decomposition reactions, the sharp decrease of N_2O conversion and decrease in the concentration of bis(μ-oxo) dicopper was observed upon lowering the temperature below 673 K. This experiment strongly indicated that bis(μ-oxo) dicopper core was an active site during the NO and N_2O decomposition reactions.

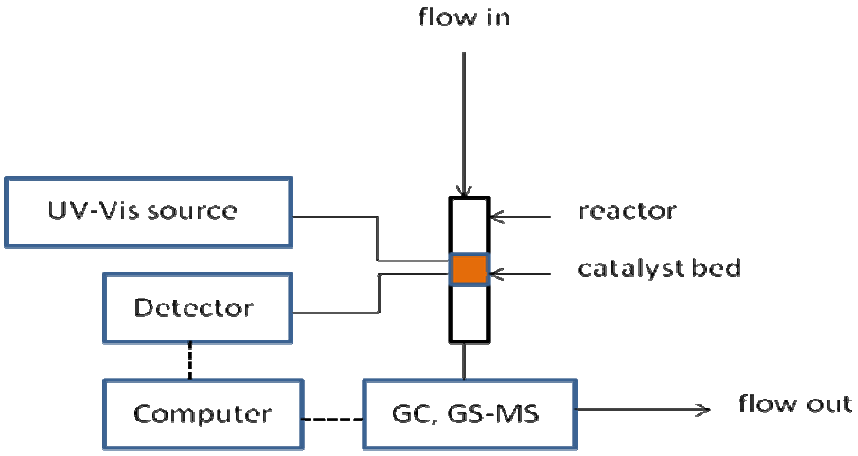

Figure 5.1. Scheme of the UV–vis spectrometer, reactor and GC/GC-MS setup.

- Kinetic studies.

Understanding of the kinetic and thermodynamic parameters is required to optimize reaction conditions and quantitatively relate the nature of the active sites to their catalytic performance. Kinetic studies are needed in order to measure the reaction rates, rate constants and reaction orders and to clarify the mechanism of catalyzed oxidation reactions. The main factors that influence the reaction rate include: the physical state of the reactants (solid, liquid, or gas), concentrations of reactants, temperature at which the reaction occurs and presence of catalysts. The activation energy could be experimentally determined through the Arrhenius equation. Investigation of different experimental conditions (reactants concentration, temperature) and its influence on the velocity and yield of reaction would give information about the reaction mechanism and transition states.

Kinetic EPR measurement could be used to obtain the value of the rate constant for e.g. hydrogen atom abstraction from substrate molecule (cyclohexane, cyclohexene, benzyl alcohol) by *tert*-butylperoxy radicals. To measure the rates of hydrogen atom abstraction from a given substrate by radicals and the rates of oxidation catalyzed by molecular oxygen, EPR spectroscopy (to monitor the decay of radical species) and a differential pressure transducer to measure the oxygen consumption in a closed system could be employed.[340]

- The influence of the different reaction parameters on reaction conversion and selectivity e.g. temperature, oxidant (H_2O_2, PhIO, CHP, EBHP), solvent, substrate to oxidant molar ratio, substrate to metal molar ratio, metal to oxidant molar ratio, reaction time. This will provide a more detailed understanding of the kinetic parameters associated with these catalysts and allow a better model to be produced to optimise catalytic reaction conditions.

- Complex recycling studies and detailed characterization of the catalyst after succeeding catalytic cycles.

- Investigation of deactivation of the catalyst in terms of: (I) agglomeration of metal sites and thermal deactivation, (II) loss in catalytic activity provoked by formation of compounds that are constituent part of a reaction mechanism, (III) strong adsorption of substrates, intermediates, products or by-products that can restrain the succession of steps involved in reaction pathway, (IV) interactions of reactants with catalytic centres that result in blockage and deactivation of the active site, (V) blockage of pores in the case of porous catalysts, (VI) poisoning of catalyst by impurities present in reaction mixture.

- Investigation of other industrially valuable oxidation reactions with Fe^{III}-Proline and Cu^{II}-Valine catalysts to widen their application and potential.

Oxidation reactions are central to numerous processes that convert bulk chemicals into highly-valuable products. However, many of the current processes employed in industry suffer from disadvantages, such as the use of aggressive oxidants, low selectivity, multiple-step reactions and the generation of excessive amounts of waste. Therefore, there is a great need for benign and selective oxidation processes that employ inexpensive and selective solid catalyst systems under relatively mild conditions and preferably with air or oxygen as oxidant. There is a pressing desire for such processes, especially for the preparation of various alcohols, ketones, aldehydes, acids and phenols. Oxidation of benzene to phenol is often included into the top 10 challenges of modern chemistry.
An interesting perspective would be to study the oxidation of benzene to phenol with Fe^{III}-Proline and Cu^{II}-Valine catalysts. Phenol is the major source of Bakelite and phenol resins, which are utilized in many commodities. The industrial production of phenol exceeds 7.2 megaton per year. Ninety-four percent of the worldwide production of phenol is obtained by a well-known three-step process, the cumene process, from benzene that is easily obtained by petroleum reforming. The cumene process is performed by first the reaction of benzene with propene on acid catalysts, second auto-oxidation of the obtained cumene to form explosive cumene hydroperoxide, and finally the decomposition of cumene hydroperoxide to phenol and acetone in sulfuric acid (Scheme 5.1.): The cumene process is however environmentally unfavorable, highly energy-consuming and produces acetone as byproduct in stoichiometric quantities. Thus, direct phenol synthesis from benzene in a one-step reaction with high benzene conversion and high phenol selectivity is of high interest.[341]

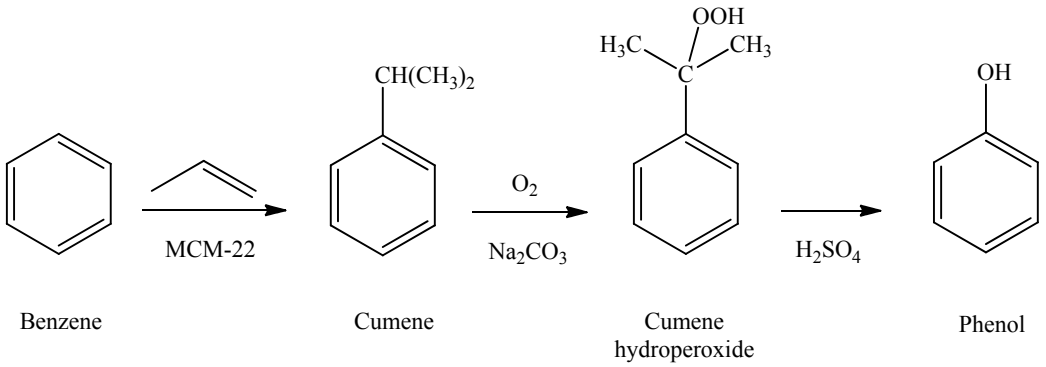

Scheme 5.1. The cumene process.

Other interesting oxidation reactions that could be studied with Fe^{III}-Proline and Cu^{II}-Valine catalysts are presented below:

Oxidation of phenol to quinone and catechol.

Hydroquinone (1,4-dihydroxy benzene) and catechol **(**1,2-dihydroxybenzene) are used for diverse applications such as polymerization inhibitors, photographic chemicals, antioxidants and flavoring agents.[342] Natural and synthetic quinones show biological and pharmacological activity (antitumoral, antimicrobacterial anti-cardiovascular). Many pigments and dyes are quinone derivatives. Reaction pathway for phenol oxidation is shown in Scheme 5.2.

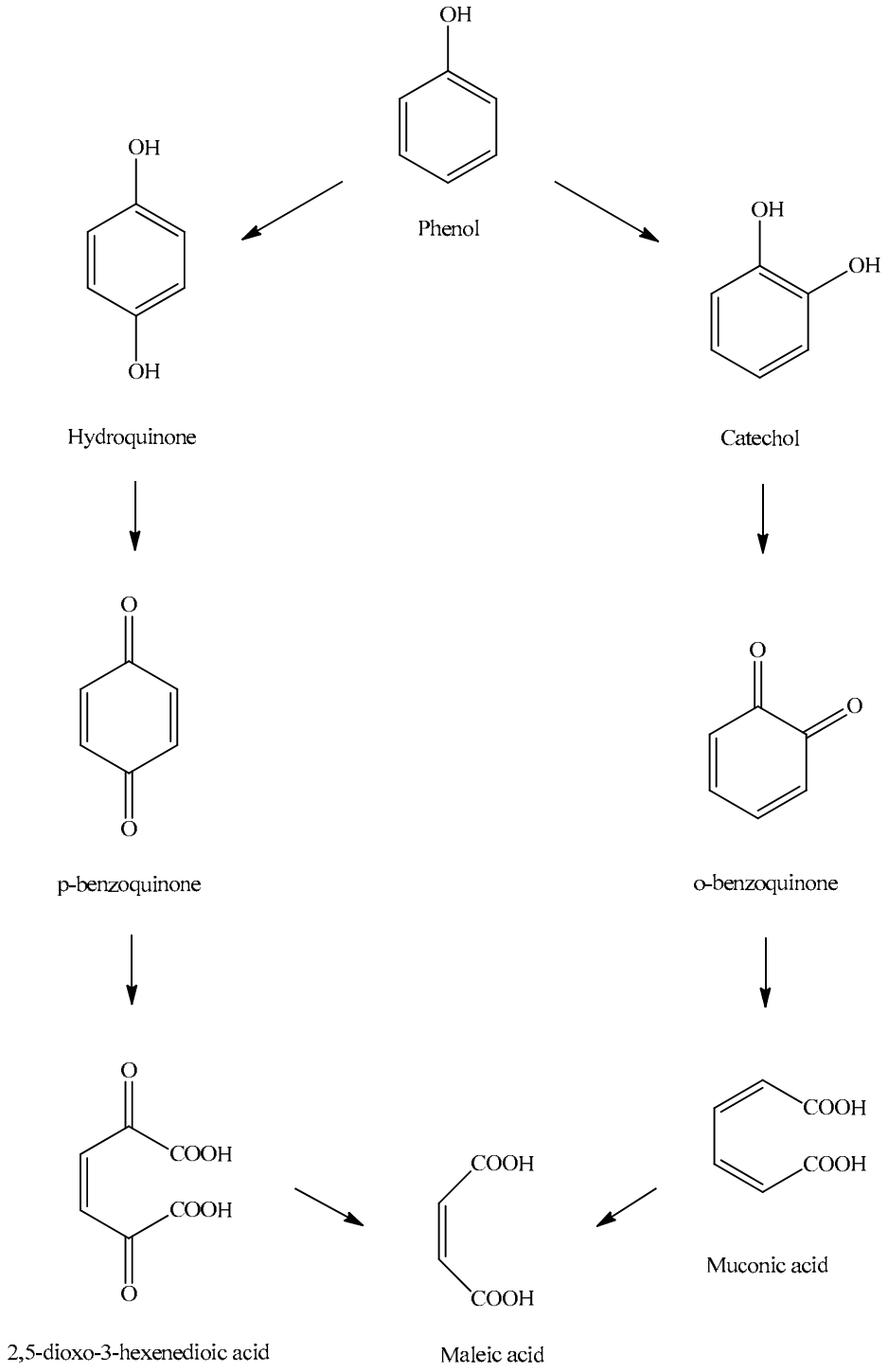

Scheme 5.2. Reaction pathway for phenol oxidation.

Epoxidation of styrene to styrene oxide.

The epoxidation of styrene has attained great attention as styrene oxide is a key intermediate in the production of many fine chemicals and pharmaceuticals.[343] In conventional process, styrene oxide is produced by epoxidation of styrene using stoichiometric amounts of peracids as the oxidants (eg. peroxybenzoic acid), Scheme 5.3. These oxidizing agents are corrosive and hazardous in nature and produce undesirable waste. Therefore, from both environmental and economic points, benign process preferably with air or molecular oxygen is highly desirable for styrene oxide production.

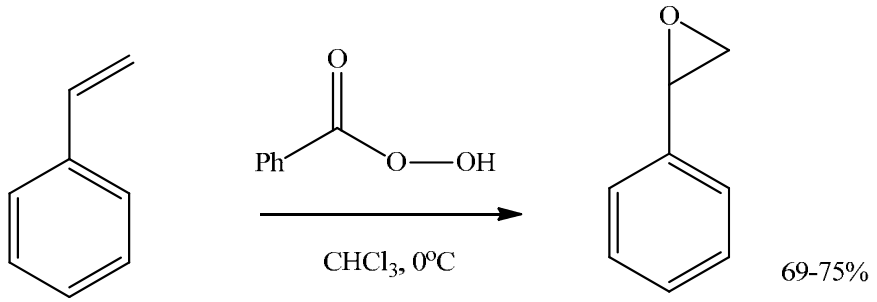

Styrene Styrene oxide

Scheme 5.3. Reaction pathway for styrene oxidation with peracid.

Oxidation of geraniol to geranial.

Geraniol (3,7-Dimethylocta-2,6-dien-1-ol) is an acyclic monoterpene alcohol. Geraniol is a mixture of the two *cis-trans* isomers: geraniol (trans-isomer) and nerol (cis-isomer).[344] The geraniol oxidation products; geranial (trans-isomer) and neral (cis-isomer), known together as citral are important intermediates for the production of perfumes (citrus effect), fragrances and pharmaceuticals. Geranial is used in the synthesis of vitamin A, and poses strong antimicrobial properties. The reaction pathway for geraniol oxidation is presented in Scheme 5.4.

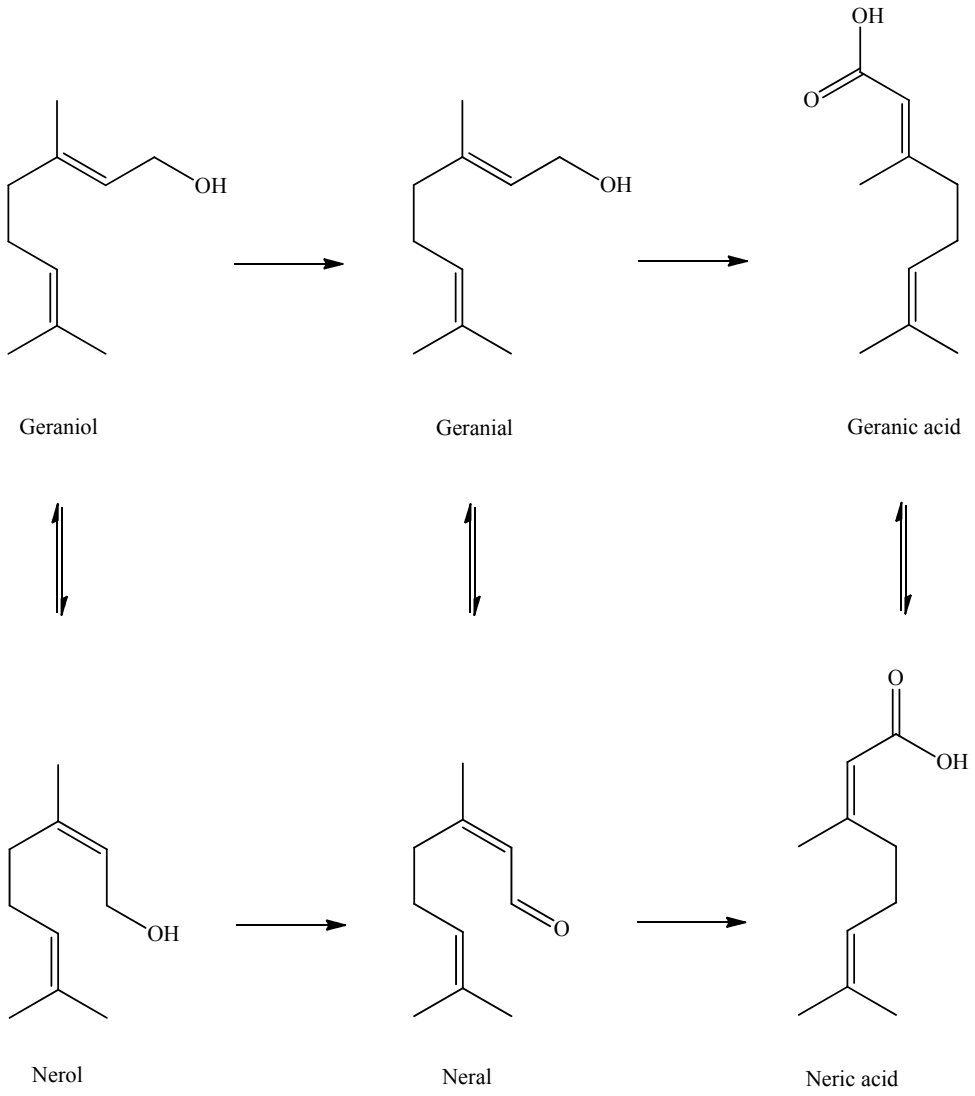

Scheme 5.4. Reaction pathway for geraniol oxidation.

6. EXPERIMENTAL.

Iron acetate (99.995%), fumed silica (99.8%), aluminum isopropoxide (99.99+%), cyclohexane (99.5%), (3-chloropropyl)trimethoxysilane, *tert*-butyl bromide, sodium azide, copper^{I} iodide (99.999%), sodium hydride, trifluoroacetic acid, cyclohexanol, cyclohexanone, benzyl alcohol (99+%), dimethyl sulphide, dimethyl sulphone, dimethyl sulphoxide, tert-Butyl hydroperoxide (TBHP) (70wt.% in water), mesitylene (98%), methanol and 1,2- dichloroethane (both analytical reagent grade) were purchased from Sigma-Aldrich. *l*-proline, *l*-valine (>95.5%), triethylamine (Et_3N) (99.5%), methyltrimethoxysilane, copper^{II} sulphate pentahydrate, (chloromethyl)polystyrene, potassium carbonate anhydrous, propargyl bromide, *N,N*-diisopropyl-ethyl amine, benzaldehyde, benzoic acid, cyclohexene oxide, 2-cyclohexene-1-one, were acquired from Fluka. Analytical grade sodium hydroxide, toluene, diethyl ether, acetonitryle, tetrahydrofuran (extra dry), ethyl acetate, hexane, dimethylformamide (extra dry), *N,N*-dimethylacetamide (extra dry) were obtained from Fisher Scientific.
All reagents were used as received.

6.1. Characterization techniques.

6.1.1. Fourier Transform Infrared Spectroscopy (FTIR).

FTIR spectra were recorded using a Nicolet 380 spectrometer in the range of 4000-400 cm^{-1}. The samples were pressed in a self-supporting pellet. Prior to the measurements the samples were outgased at 70^{o}C, under reduced pressure for 4h. The spectrum of the empty cell was used asa background.

6.1.2. Diffuse Reflectance UV-Visible Spectroscopy (DR UV-Vis).

The Diffuse reflectance UV-Vis (DRS) spectra were measured on Perkin-Elmer Lambda 900 DR UV-Vis spectrometer equipped with cylindrical solid sample (powder) holder with WinLab 900 software. $BaSO_4$ was used as reference.

6.1.3. Electron Paramagnetic Resonance Spectroscopy (EPR).

The EPR experiments were performed using Bruker EMX spectrometer consisting of an electromagnet and X-band (9.8 GHz) microwave bridge ER 041XG in conjunction with a Bruker ER 4105D double rectangular resonator with a helium-gas flow cryostat. The temperature was varied in the range from 300 K to 10 K (±1 K) by an Oxford Instruments auto-tuning temperature controller ITC503. The powdered samples were measured after vacumm treatment in quartz tube.

6.1.4. X-Ray Diffraction (XRD).

X-Ray powder diffraction (XRD) patterns were collected employing a Siemens D5000 diffractometer using Cu Kα radiation (λ=1.54056Å).

6.1.5. Brunauer-Emmett-Teller Analysis (BET).

N_2 adsorption measurements were performed at liquid nitrogen temperature. Samples were first dehydrated and outgased in vacuum at 70°C overnight. Surface area and micropore volume were determined by nitrogen adsorption-desorption isotherms using Micromeritics ASAP 2020. The surface area was calculated using the Brunauer-Emmett-Teller (BET) method and the pore size was calculated using the Barrett-Joyner-Helenda (BJH) method.

6.1.6. Mass Spectrometry (MS).

Low resolution electrospray MS were conducted on a Walters ZMD.

6.1.7. Gas Chromatography (GC).

The reaction products were analysed by GC (PerkinElmer, Clarus 400) employing Elite Wax capillary column (column length 30 m), carrier gas: He, flow rate 0.9 ml/ min, injection temperature 220^{o}C, Flame Ionisation Detector (FID).

The identity and the quantification of the products were established by using mesitylene as an internal standard using the calibration method. The identities of the products were first confirmed using authenticated standards and their individual response factors were determined using a suitable internal standard (mesitylene) by the calibration method. The

overall yields were normalized with respect to the (GC) response factors obtained as above and the conversions and selectivities were determined by the following equations:

Conv. % = [(moles of initial substrate – moles of residual substrate) / (moles of initial substrate)] x 100

Sel. % = [(moles of individual product) / (moles of total products)] x 100

For the internal standard GC method, the response factor (RF) and mol % of individual products were calculated using the following equations:

RF = (mol Product/mol Standard) × (Area Standard/Area Product)

Mol % Product = RF x Mol Standard × (Area Product/Area Standard) x 100/Mol Sample

6.2. Synthesis of amino acid complexes with Fe and Cu.

6.2.1. Synthesis of Fe^{III}-Proline complex.

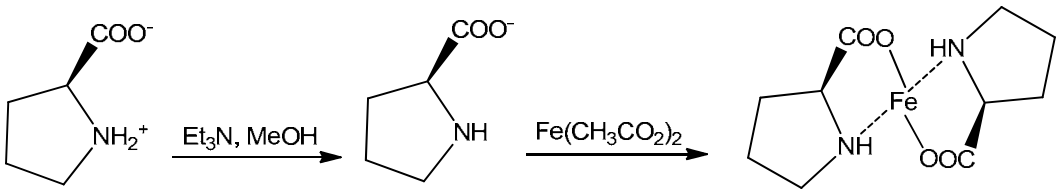

Fe^{III}-Proline: The Fe^{III}-Proline complex was prepared according to the methods described previously in the literature for Zn^{II}-Proline complex synthesis.[175] Proline (0.49g, 4,34 mmol) was dissolved in 10ml of MeOH. To this solution 0.6 ml of triethylamine (Et_3N) was added and the mixture was stirred for 0.5 h at room temperature. The addition of iron acetate (0.37g, 2.17mmol) resulted in the formation of a yellow-grey precipitate. After stirring for 1h the resulting precipitate was collected by filtration, washed with methanol and dried in the air.

Elemental analysis (wt.%): calculated for $C_{10}H_{16}N_2O_4Fe$ (Exact Mass: 284.05): C (42.28), H (5.68), N (9.86), O (22.53), found: C (42.32), H (5.71), N (9.96), O (23.45).

ICP (wt.%): calculated Fe (19.66), found: Fe (16.9).

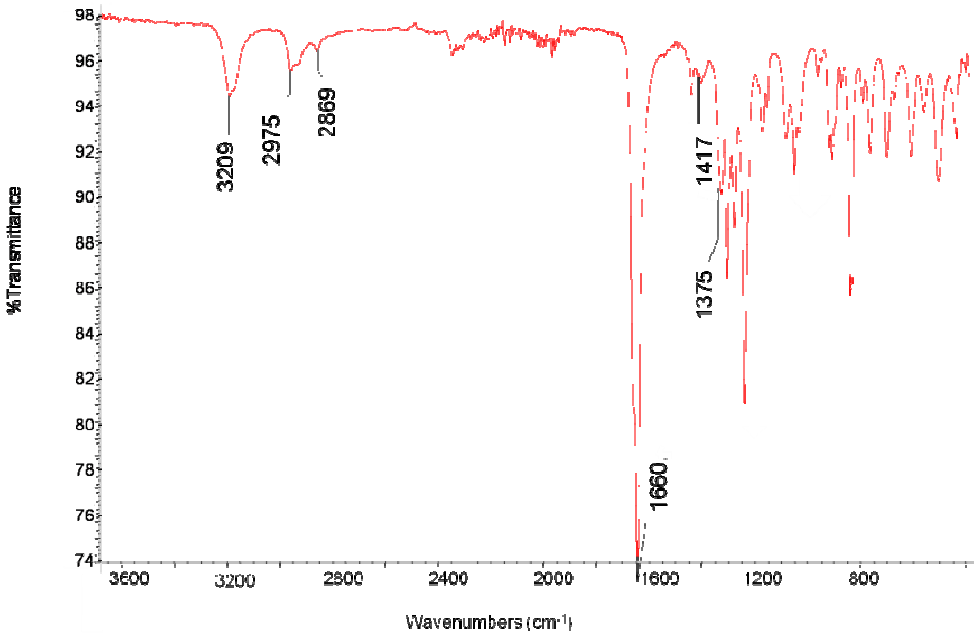

Figure 6.1. FTIR spectrum of Fe^{III}-Proline complex; ν = 3209 (NH), 2975, 2960, 2869 (CH), 1660 ($_{as}COO^-$), 1417 ($_{s}COO^-$), 1375 ($_{\delta}NH$) cm^{-1}.

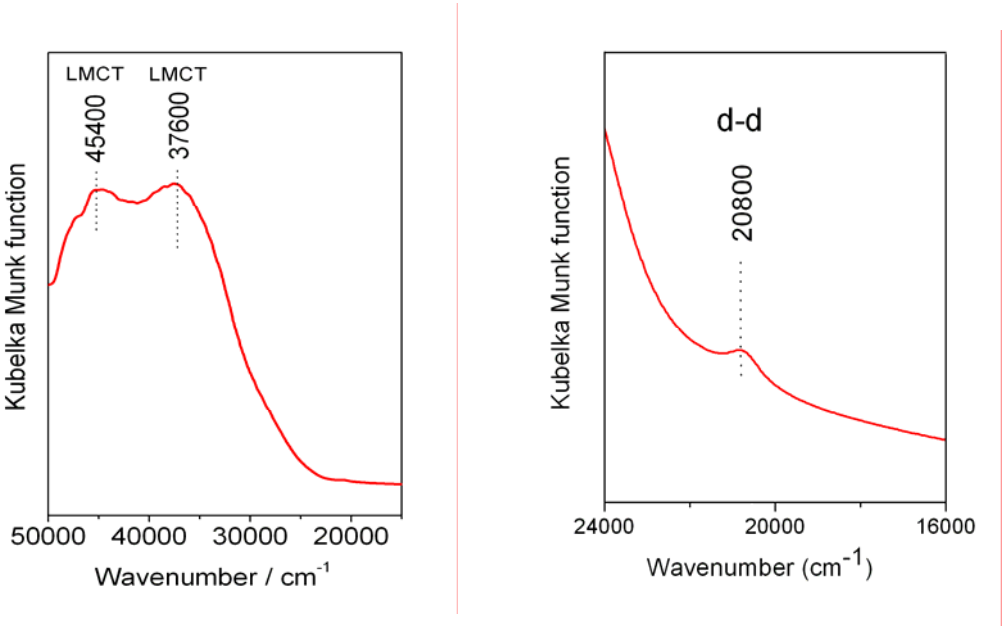

Figure 6.2. DR UV-Vis spectra of Fe^{III}-Proline; LMCT 45400, 37600 cm^{-1} (left) and d-d 20800 cm^{-1} (right).

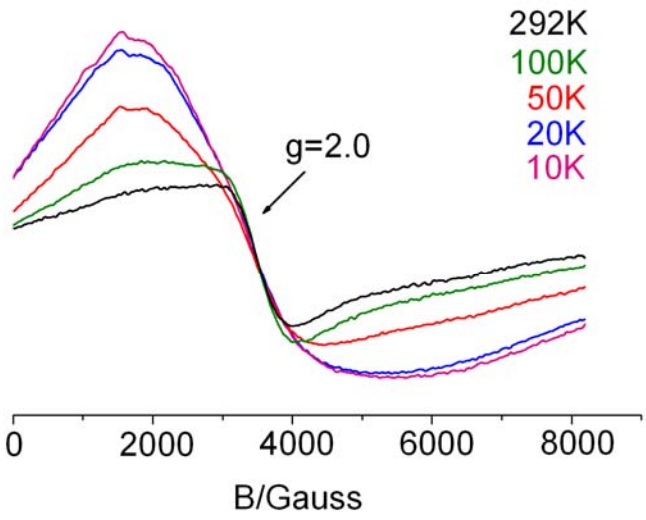

Figure 6.3. X-band (9.4 GHz) EPR spectra of Fe^{III}-Proline recorded at different temperature range, g=2 (Fe^{III}).

6.2.2. Synthesis of Cu^{II}-Valine complex.

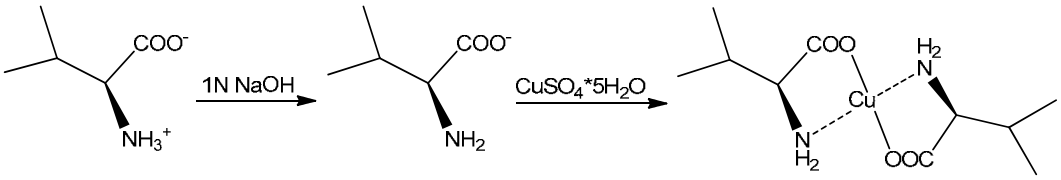

Cu^{II}-Valine: The Cu^{II}-Valine complex was prepared according to the methods described previously in the literature.[226] Valine (1,17g, 10 mmol) was dissolved in 10ml of 1N NaOH solution and slowly mixed with 25ml aqueous solution of $CuSO_4*5H_2O$ (1,245g, 5 mmol) and stirred for 0.5 h at room temperature. The blue crystalline precipitate was filtered, washed with water:acetone mixture (1:1) and dried in air. Thin blue plate crystals were obtained after one week of slow solvent evaporation (water:methanol, 5:1).

Elemental analysis (wt.%): calculated for $C_{10}H_{20}N_2O_4Cu$ (Exact Mass:295.07): C (40.60), H (6.81), N (9.47), O (21.63), found: C (40.57), H (6.79), N (9.37).

ICP (wt.%): calculated Cu (21.48), found: Cu (22.6).

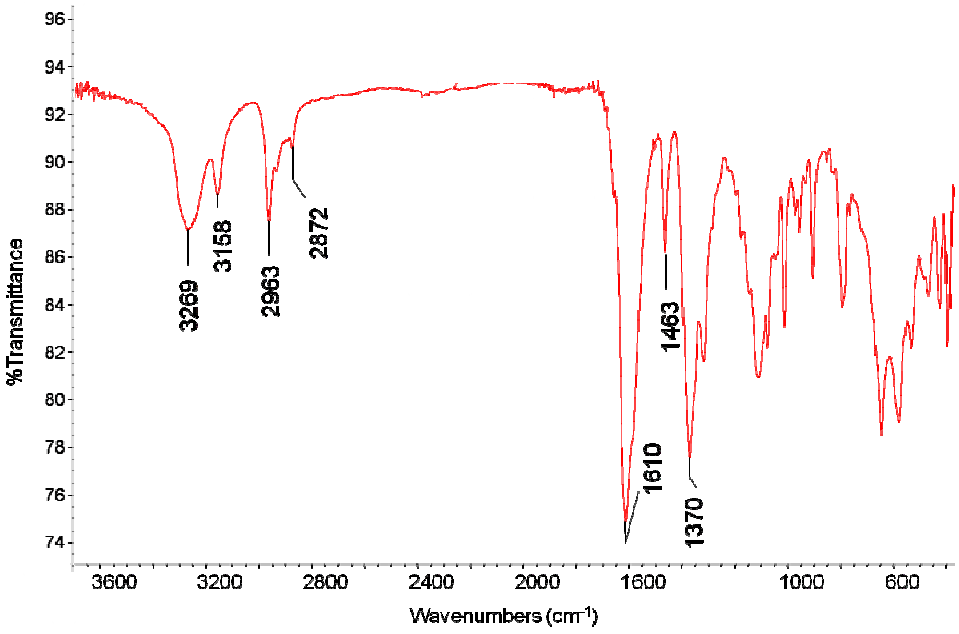

Figure 6.4. FTIR spectrum of Cu^{II}-Valine complex; ν = 3269 ($_{as}NH_2$), 3158 ($_{s}NH_2$), 2963, 2957, 2872 (CH), 1610 ($_{as}COO^-$), 1463 ($_{\delta}CH$), 1370 ($_{s}COO^-$), cm^{-1}.

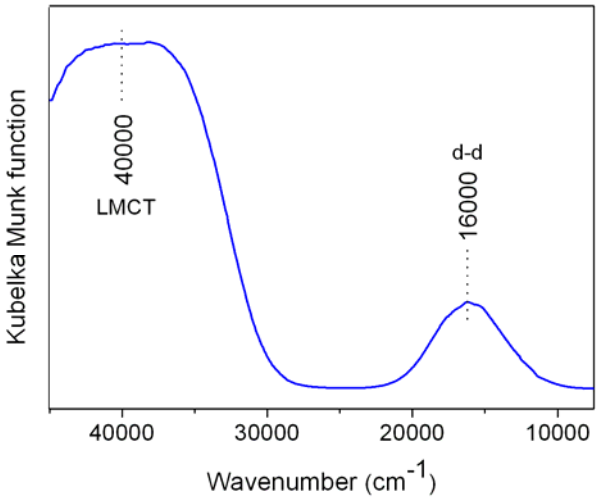

Figure 6.5. DR UV-Vis spectrum of Cu^{II}-Valine; LMCT 40000cm^{-1} (left) and d-d 16000 cm^{-1}.

SCXRD-reviled formation of Cu^{II}-Valine complex framework. Crystal structure is shown in section 3.2.3.1.

6.3. Encapsulation of amino acid complexes within zeolites.

6.3.1. Fe^{III}-Proline-X synthesis.

Fe^{III}-Proline-X: The Fe^{II}-Proline complex was encapsulated within the supercages of Zeolite-X using the '*zeolite synthesis method*'.[125] The silicate gel was prepared by stirring the 1.4 g of fumed silica, 1.06 g of NaOH, 0.1 g of Fe^{III}-Proline and 3ml of water. Addition of the aluminate solution (aluminium isopropoxide 3 g, NaOH 1.06 g and water 2 ml) resulted in a pale-orange slurry. To this mixture 12 ml of water was added. The slurry was transferred to a polypropylene bottle with stirring for 24 h at room temperature and subsequently heated at 80°C for 15 h. Complexes adsorbed on the exterior surface were removed by Soxhlet extraction technique. The resulting solid was dried at 80°C for 24h.

ICP (%), calculated: Fe (0.41), found: Fe (0.49).

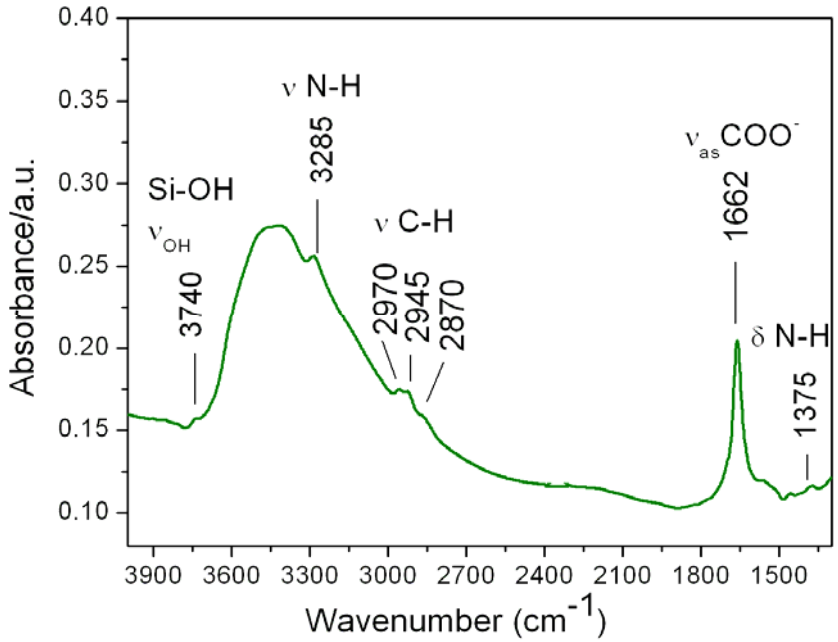

Figure 6.6. FIIR spectrum of Fe^{III}-Proline-X; ν = 3285 (NH), 2970, 2945, 2870 (CH), 1662 ($_{as}COO^-$), 1375 ($_{\delta}NH$) cm^{-1}.

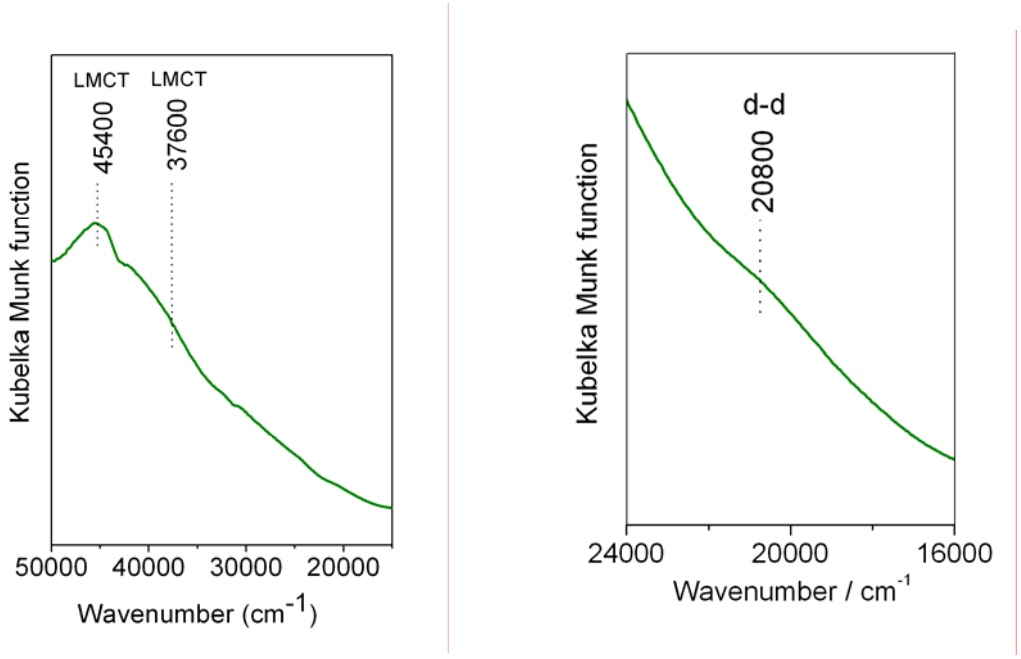

Figure 6.7. DR UV-Vis spectra of Fe^{III}-Proline-X; LMCT 45400, 37600 cm^{-1} (left) and d-d 20800 cm^{-1} (right).

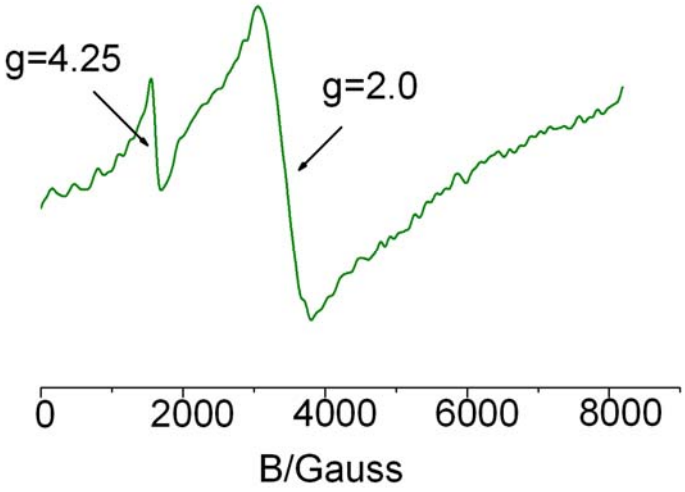

Figure 6.8. X-band (9.4 GHz) EPR spectrum of Fe^{III}-Proline-X (Fe^{III}), g=4.25, g=2 (Fe^{III}).

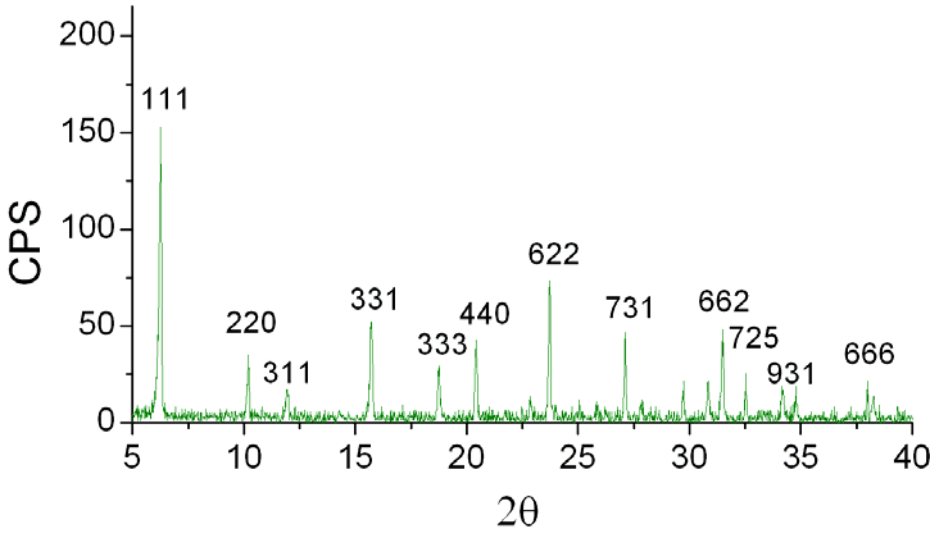

Figure 6.9. Powder XRD pattern of Fe^{III}-Proline-X. Scan rate 12°min., step size 0.02°.

BET ANALYSIS: BET surface area: 85.3 m^2/g, Langmuir surface area: 124.5 m^2/g, micropore volume: 0.04 cm^3/g, micropore area: 71.0 m^2/g.

6.3.2. Cu^{II}-Valine LTA synthesis.

Cu^{II}-Valine-LTA: The Cu^{II}-Valine complex was encapsulated within the cages of Zeolite-LTA using '*zeolite synthesis method*' methodology, the same as for Fe^{III}-Proline complex encapsulation in Zeolite-X. The silicate gel was prepared by stirring 1.4 g of fumed silica, 1.06 g of NaOH, 0.1 g of Cu^{II}-Valine and 3ml of water. Addition of the aluminate solution (aluminium isopropoxide 3 g, NaOH 1.06 g and water 2 ml) resulted in a pale-blue slurry. To this mixture 12 ml of water was added. The slurry was transferred to a polypropylene bottle with stirring for 24 h at room temperature and subsequently heated at 80°C for 15 h. Complexes adsorbed on the exterior surface were removed by Soxhlet extraction technique. The resulting solid was dried at 80°C for 24h in the air in the oven.

ICP (%), calculated: Cu (0.44), found: Cu (0.48).

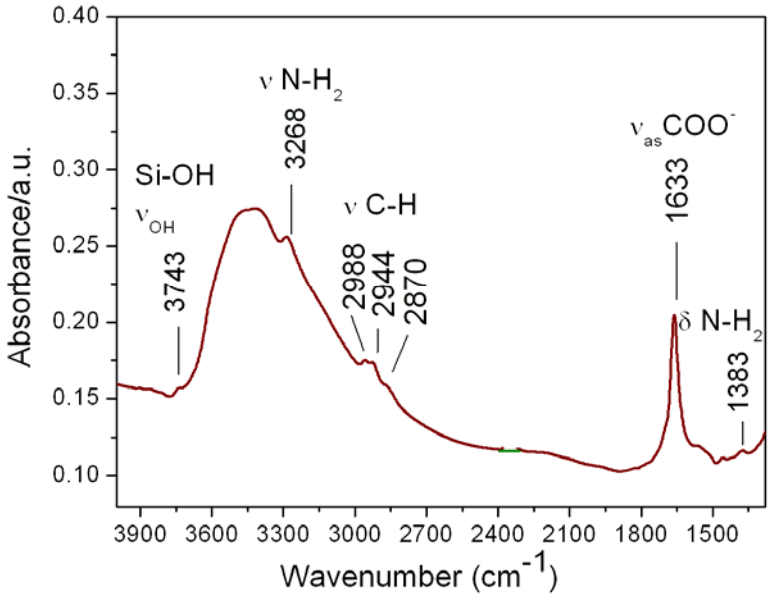

Figure 6.10. FTIR spectrum of Cu^{II}-Valine-LTA complex; ν = 3268 (NH_2), 2988, 2944, 2870 (CH), 1633 ($_{as}COO^-$), 1383 ($_{\delta}NH$) cm^{-1}.

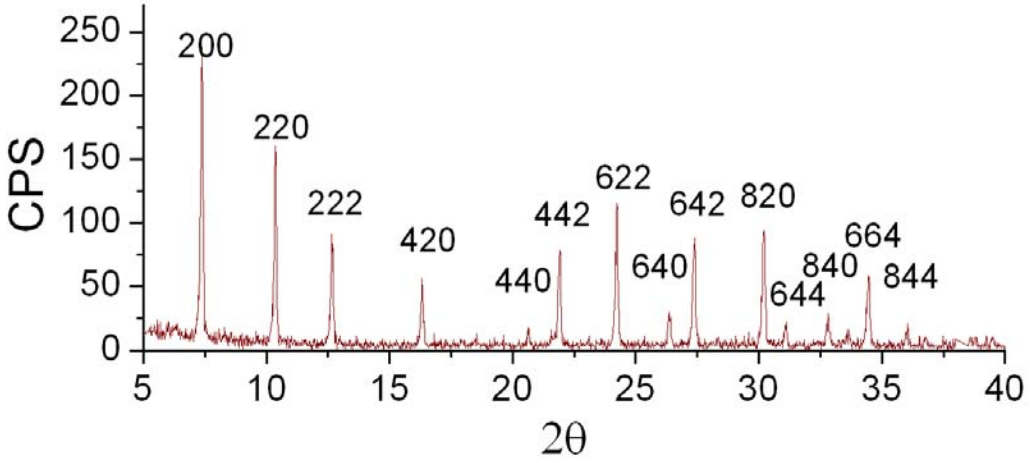

Figure 6.11. Powder XRD pattern of Cu^{II}-Valine-LTA. Scan rate 12°min., step size 0.02°.

6.4. Solid supports functionalisation.

6.4.1. Synthesis of MCM-41.

MCM-41 was prepared by a hydrothermal synthesis method described in the literature.[345] Cetyltrimethylammonium bromide (CTAB) was used as the structure directing agent and sodium silicate was used as the silica source. CTAB (4.1 g) was dissolved in distilled water (17.0 g) with vigorous stirring and heating at 80 ◦C. Sodium silicate (4.75 g) and

distilled water (10 g) were then combined with the CTAB solution. The solution was mixed and heated thoroughly for 15 min. The pH of the mixture was adjusted to 11.0 by dropwise addition of a 6N HCl solution. The reaction mixture was stirred for 30 min and then the gel was aged in stainless steel autoclave at 110°C for 5 days. The precipitated white powder was filtered, washed with distilled water and dried. The surfactant was removed from the silicate framework by calcination; at 550°C overnight under flowing of air.

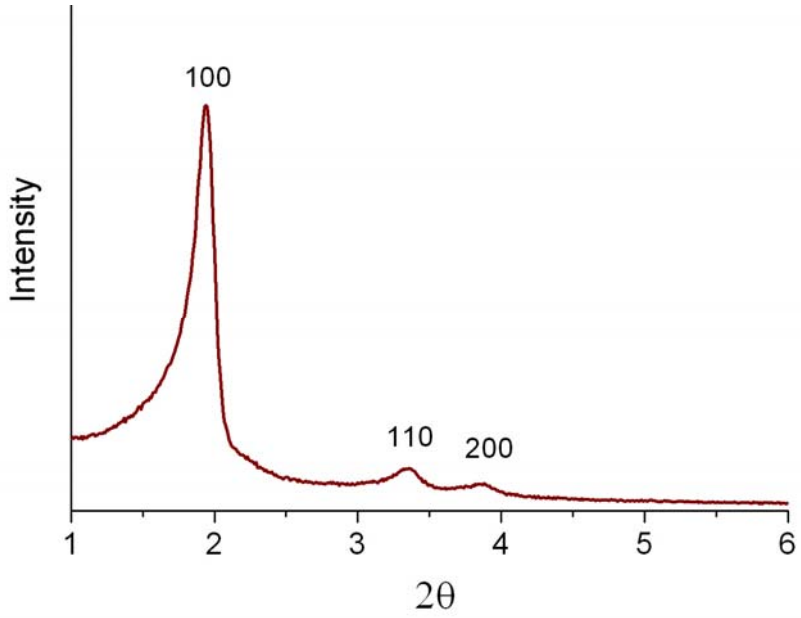

Figure 6.12. Powder XRD pattern of MCM-41. Scan rate 12°min., step size 0.02°.

6.4.2. MCM-41 functionalisation with (3-chloropropyl) trimethoxysilane and methyltrimethoxysilane groups.

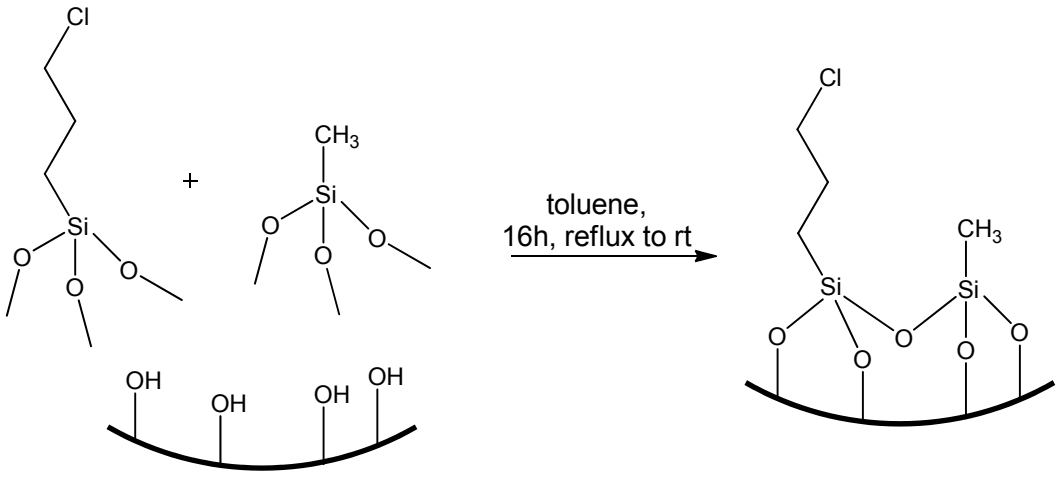

MCM-41 was functionalized with (3-chloropropyl) trimethoxysilane and methyltrimethoxysilane. Prior to functionalization silica was refluxed in water (25 ml per g of support) for 1h, then collected by filtration and washed with toluene (20 ml/g). The material was suspended in toluene (100 ml/g) and remaining water was removed by azeotropic distillation (~1 ml/g). The solid was filtered off, washed with toluene and refluxed in toluene with stirring for 1 h. After cooling to ambient temperature both silanes (3-chloropropyl) trimethoxysilane (2 mmol/g) and methyltrimethoxysilane (3 mmol/g) were added. The mixture was vigorously stirred for 4h at room temperature. The resulting solid was collected by filtration, dispersed in fresh toluene (100 ml/g) refluxed for 16 h and cooled to room temperature. The modified solid was filtered, washed with isopropanol (20 ml/g) and then washed in a Soxhlet apparatus overnight with diethyl ether and acetonitrile mixture (2:1). The functionalized material was dried overnight at 373 K in the air in the oven.[150]

6.4.3. MCM-41 modification with azido groups.

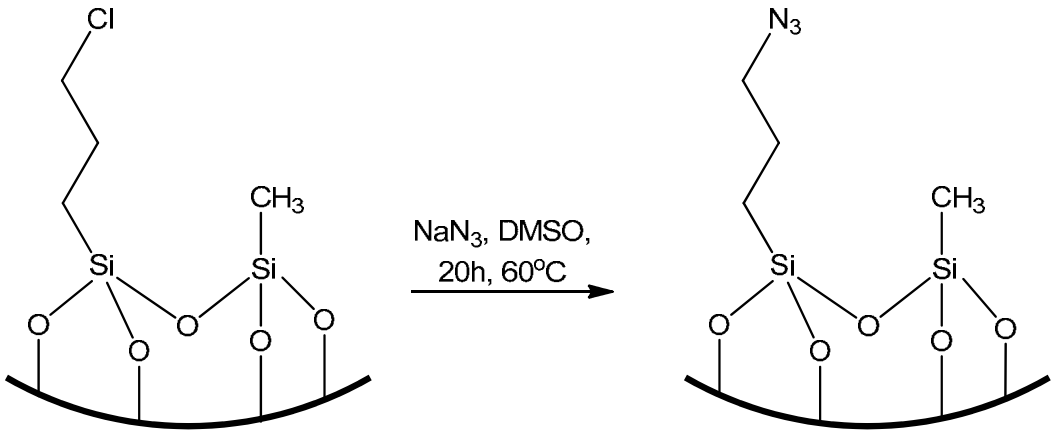

3g of MCM-41 functionalised with chloropropyl and methyl groups was dispersed in 30 ml of DMSO and sodium azide (1.5 g, 98 mmol) was added. The mixture was heated and gently stirred at 60ºC for 20 h. After cooling, the suspension was filtered and the resin was sequentially washed with THF, THF-EtOH (1:1), EtOH and THF. The modified solid was dried in vacuum at 40 ºC for 24 h.[159]

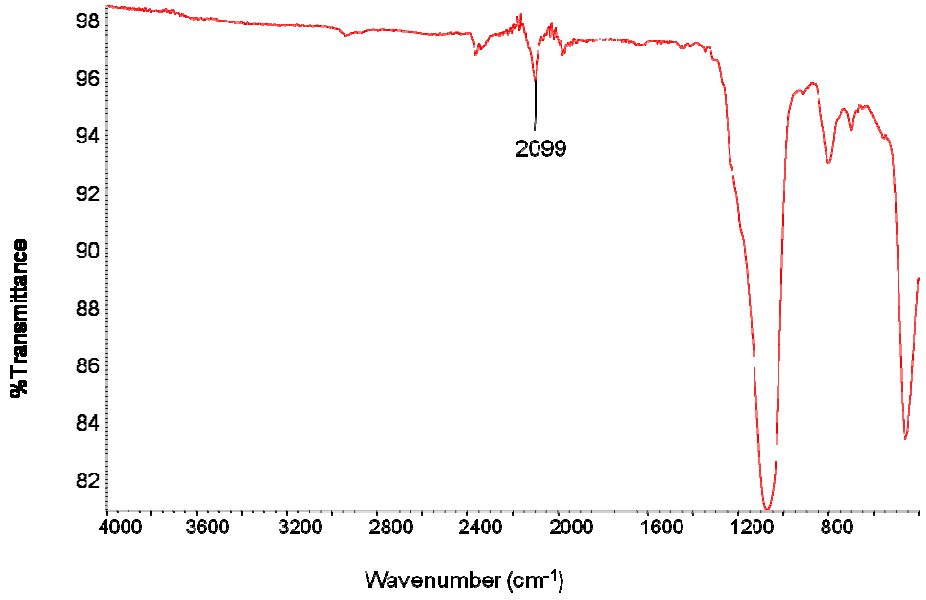

Figure 6.13. FTIR spectrum of azido modified MCM-41; ν = 2099 (N_3) cm^{-1}.

6.4.4. Merrifield polymer modification with azido groups.

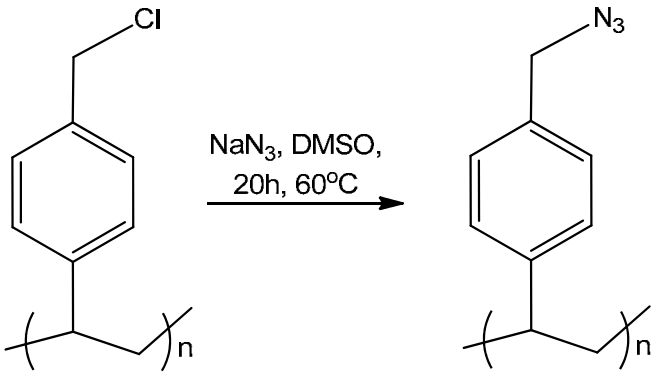

3g of (chloromethyl) polystyrene (chlorine loading ~0.8 mmol/g) was dispersed in 30 mL of DMSO and sodium azide (0.78 g, 51 mmol) was added. The mixture was heated at 60 ºC for 20 h. After cooling, the suspension was filtered and the resin was sequentially washed with THF, THF-MeOH (1:1), MeOH and THF. The modified solid was dried in vacuum at 40 ºC for 24 h.[159]

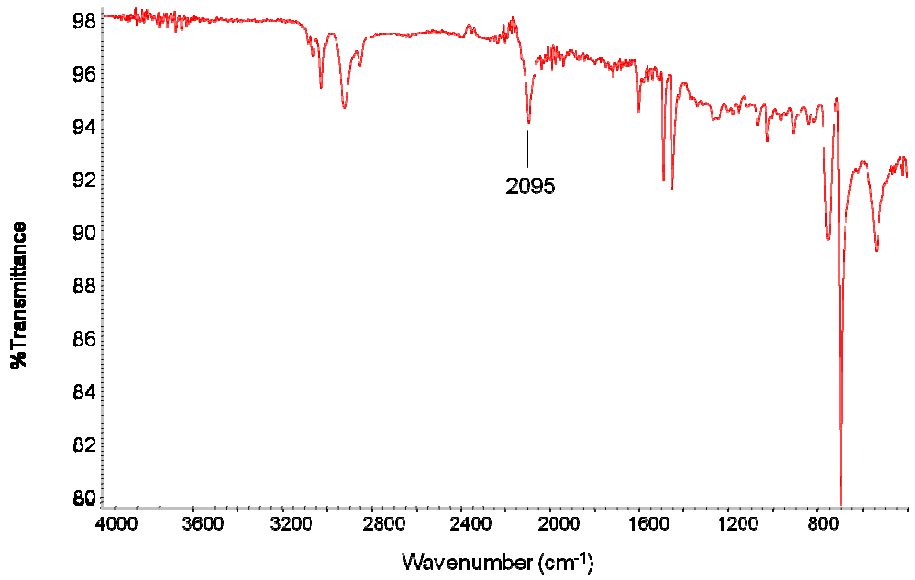

Figure 6.14. FTIR spectrum of azido modified polystyrene; ν = 2095 (N_3) cm^{-1}.

6.5. Immobilization of Fe^{III}-Proline complex on MCM-41.

6.5.1. Synthesis of low metal loading Fe^{III}-Proline-MCM-41 (Fe=2.02 wt%).

6.5.1.1. Synthesis of tert-Butyl (2S,4R)-N-Boc-4-hydroxy-prolinate.

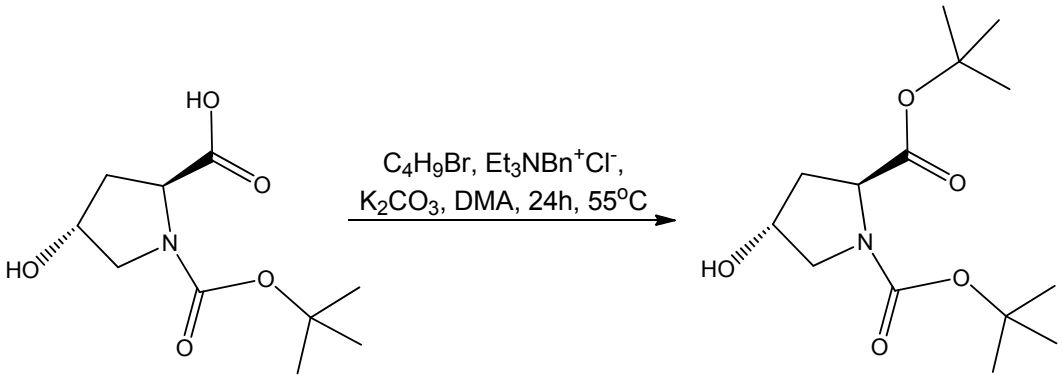

(2*S*,4*R*)-*N*-Boc-4-hydroxy-proline (8.09 g, 35.0 mmol) was treated with benzyltriethylammonium chloride (7.97 g, 35.0 mmol), K_2CO_3 (126 g, 910 mmol) and *tert*-butyl bromide (163 ml, 1.40 mol) in 175 ml of ($MeCONMe_2$) and vigorously stirred at 55 C for 24 h under N_2. After cooling to ambient temperature, water was added until a clear solution was obtained. The reaction mixture was extracted with (Et_2O). The

combined organic extracts were dried and evaporated under reduced pressure. The residue was purified by column chromatography on silica gel (EtOAc/hexane 1:1, R_f=0.31) and then recrystallized from pentane yielding final product as a white crystals.[346]

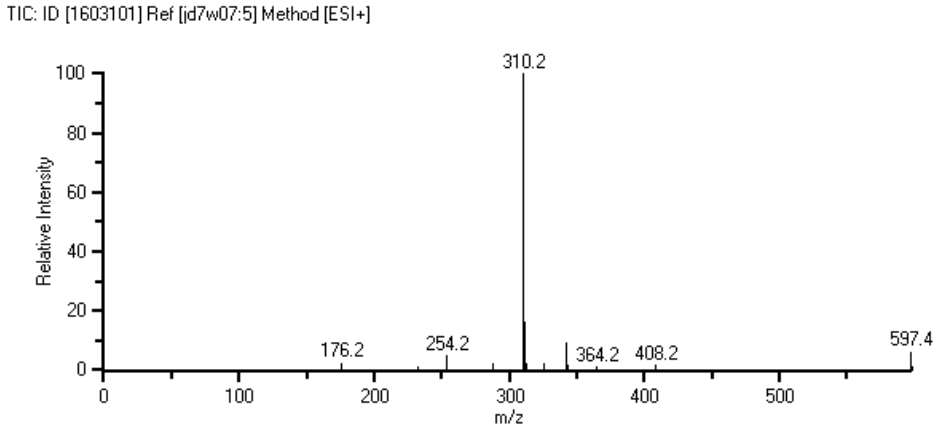

Figure 6.15. MS of tert-Butyl (2S,4R)-N-Boc-4-hydroxy-prolinate. MS(EI): m/z = calculated for $C_{14}H_{25}NO_5Na$ 310.16, found 310.2 [M+Na^+].

6.5.1.2. Synthesis of tert-Butyl (2S,4R)-N-Boc-4-propargyloxy-prolinate.

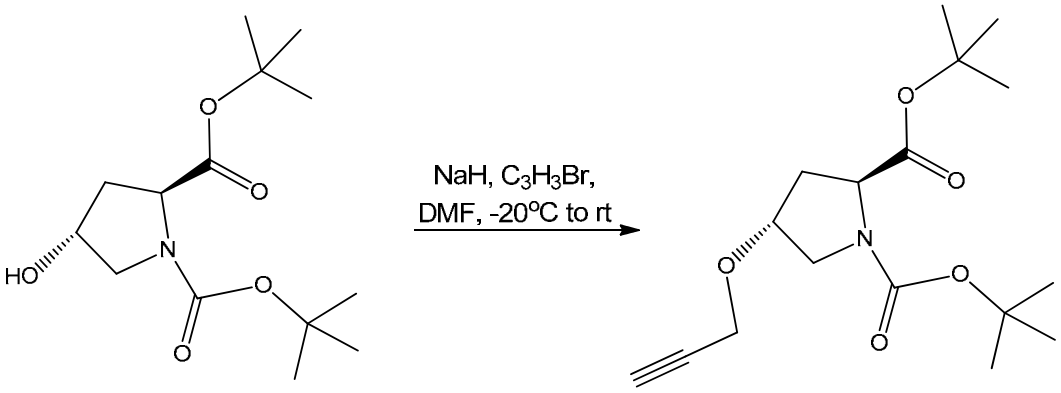

Tert-butyl (2*S*,4*R*)-*N*-Boc-4-hydroxyprolinate (0.61 g, 2.1 mmol) was dissolved in DMF (5 mL) and added to a suspension of sodium hydride (0.082 g, 3.2 mmol) in DMF (5 mL) at -20 ºC under N_2. The mixture was stirred for 40 min, then propargyl bromide (0.35 mL, 3.2 mmol) was syringed into the mixture and stirred at -20 ºC for a further 1.5 h. After cooling to room temperature, the mixture was stirred for 16 h. Methanol (2 ml) and water (10 ml) were added, and the reaction mixture was extracted with CH_2Cl_2 and washed with brine (10 ml). The combined organic extracts were dried and concentrated in vacuo. The

residue was purified by column chromatography on silica gel (EtOAc/hexane 2:8, R_f=0.26) giving final product as an oil.[346]

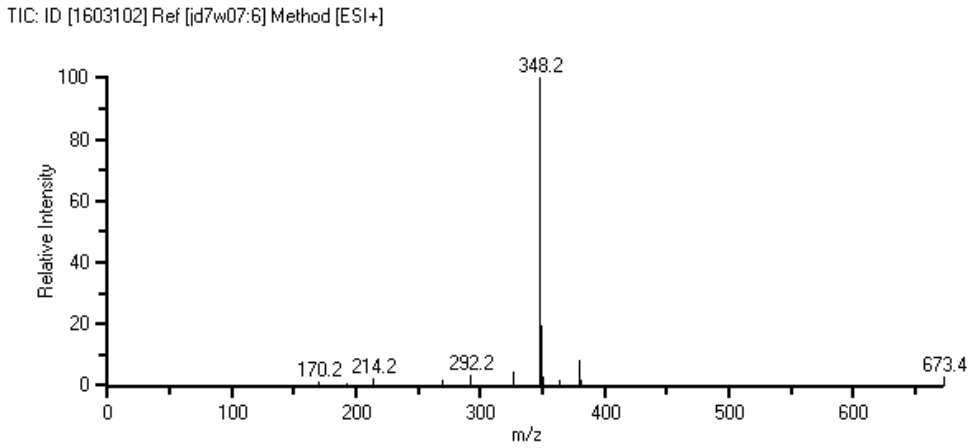

Figure 6.16. MS of tert-Butyl (2S,4R)-N-Boc-4-propargyloxy-prolinate. MS(EI): m/z = calculated for $C_{17}H_{27}NO_5Na$ 348.18, found 348.2 [M+Na^+].

6.5.1.3. Cycloaddition of tert-Butyl (2S,4R)-N-Boc-4-propargyloxyprolinate with azido functionalized MCM-41.

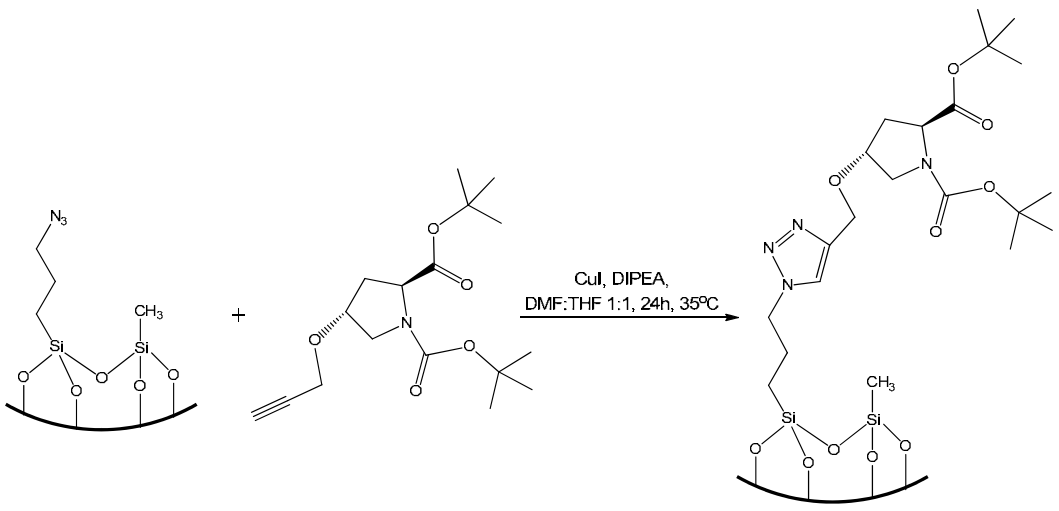

Azido functionalized MCM-41 (1g) was suspended in dry DMF:THF 1:1 (10 ml) and degassed with nitrogen for 40 min. *tert*-Butyl (2*S*,4*R*)-*N*-Boc-4-propargyloxyprolinate (0.06 g, 0.3 mmol), *N,N*diisopropyl-ethyl amine (0.52 ml, 2.95 mmol) and copper (I) iodide (0.004 g, 0.002 mmol) were added to this suspension and the mixture was gently stirred at 35 ºC for 24 h under N_2. The reaction was monitored with IR and once the signal of the azido group had completely disappeared, the solid was collected by filtration

and sequentially washed with water, DMF, THF, THF-EtOH (1:1), EtOH and THF. The modified silica was dried under vacuum at 40 ºC for 24 hours.[346]

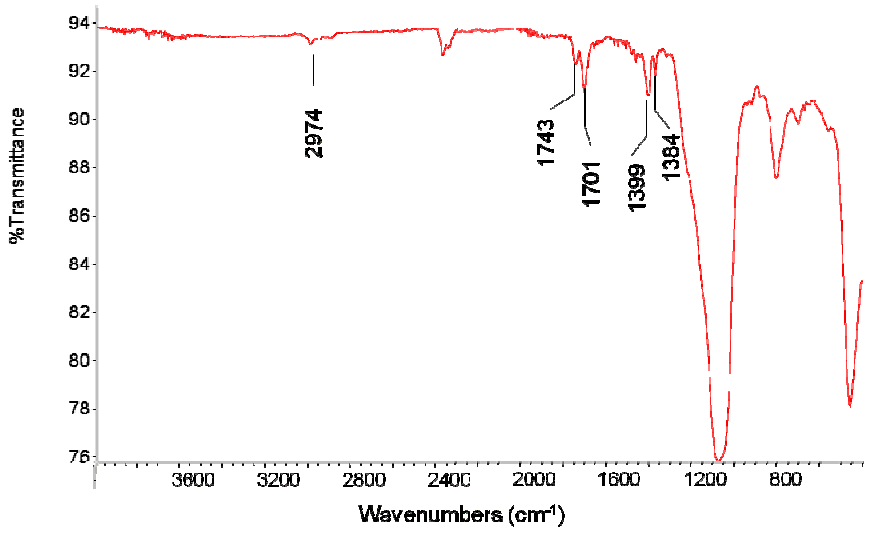

Figure 6.17. FTIR spectrum of tert-Butyl (2S,4R)-N-Boc-4-propargyloxyprolinate functionalized azido MCM-41; ν = 2974 (CH), 1743 (C=O), 1701 (C=O), 1399 (*t*Bu), 1384 (*t*Bu) cm^{-1}.

Deprotection. Functionalized MCM-41 (1 g) was dispersed in 5 ml of CH_2Cl_2, then trifluoroacetic acid (10 ml) was added and suspension was shaken for 3h. The reaction mixture was filtered and sequentially washed with THF (with 2 % of Et_3N), water, THF, THF-EtOH (1:1), EtOH and THF. The functionalised solid was dried in vacuum at 40 ºC for 24 h.

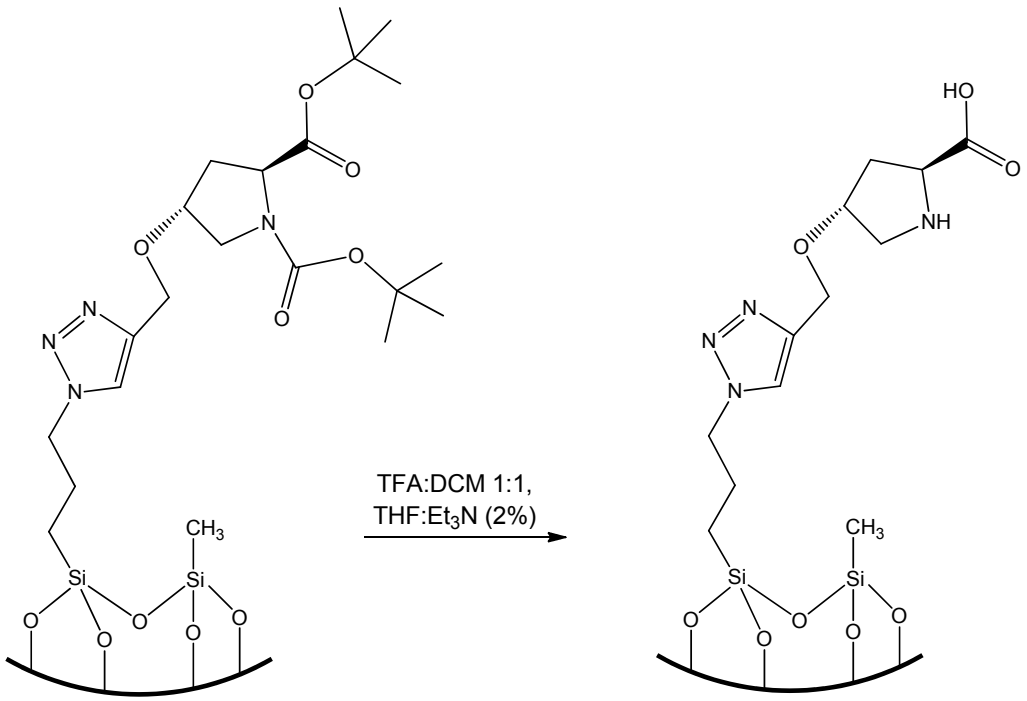

Complexation. Iron acetate (**$Fe(C_2H_3O_2)_2$**) was used as a metal source. Proline functionalized MCM-41 (g) was suspended in 10ml of EtOH:MeOH (4:1). Then 0.5 ml of triethylamine (Et_3N) was added and the mixture was shaken for 1h. Iron acetate (0.037g, 0.2 mmol) was added and the mixture was shaken for a further 1h. The resulting modified solid was collected by filtration and washed with ethanol. Proline (0.023g, 0.2 mmol) was dissolved in 10ml of EtOH:MeOH (4:1), 0.2 ml of triethylamine (Et_3N) was added and the mixture was stirred for 0.5 h. This solution was added to modified solid and suspension was shaken at room temperature for 2h. After filtration, modified MCM-41 was washed with ethanol. Drying in the air in the oven at 40°C for 8h gave the final metal complex functionalized silica.

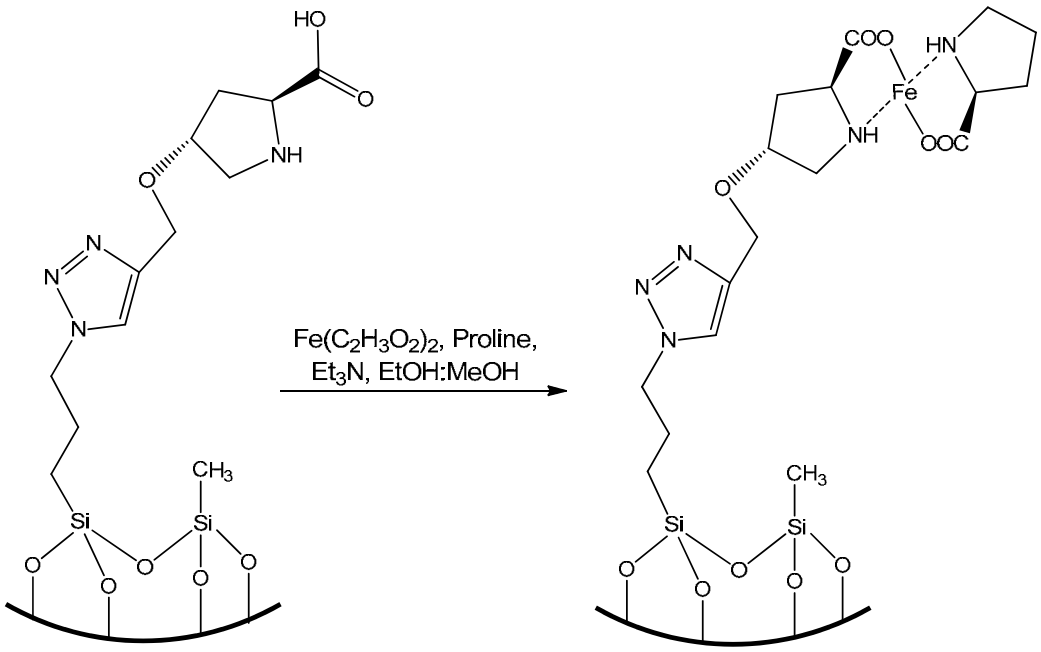

BET ANALYSIS: BET surface area: 381 m^2/g.

6.5.2. Synthesis of high metal loading Fe^{III}-Proline-MCM-41 (Fe = 8.73 wt%).

Cycloaddition of *tert*-Butyl (2*S*,4*R*)-*N*-Boc-4-propargyloxyprolinate with azido functionalized MCM-41. Azido functionalized MCM-41 (1g) was suspended in dry DMF:THF 1:1 (10 mL) and degassed with nitrogen for 40 min. *tert*-Butyl (2*S*,4*R*)-*N*-Boc-4-propargyloxyprolinate (0.32 g, 1.0 mmol), *N,N*diisopropyl-ethyl amine (1.72 ml, 9.8 mmol) and copper (I) iodide (0.012 g, 0.006 mmol) were added to this suspension and the mixture was gently stirred at 35 ºC for 24 h under N_2. The reaction was monitored with

IR and once the signal of the azido group had completely disappeared, the solid was collected by filtration and sequentially washed with water, DMF, THF, THF-EtOH (1:1), EtOH and THF. The modified silica was dried under vacuum at 40 ºC for 24 hours.

Deprotection. Functionalized MCM-41 (1 g) was dispersed in 5 ml of CH_2Cl_2, then trifluoroacetic acid (10 ml) was added and suspension was shaken for 3h. The reaction mixture was filtered and sequentially washed with THF (with 2 % of Et_3N), water, THF, THF-EtOH (1:1), EtOH and THF. The functionalised solid was dried in vacuum at 40 ºC for 24 h.

Complexation. $Fe(C_2H_3O_2)_2$ was used as a metal source. Proline functionalized MCM-41 (1g) was suspended in 10ml of EtOH:MeOH (4:1). Then 0.5 ml of triethylamine (Et_3N) was added and the mixture was shaken for 1h. Iron acetate (0.17g, 1.2 mmol) was added and the mixture was shaken for another 1h. The resulting modified solid was collected by filtration and washed with ethanol. Proline (0.12 g, 1 mmol) was dissolved in 10ml of EtOH:MeOH (4:1), 0.4 ml of triethylamine (Et_3N) was added and the mixture was stirred for 0.5 h. This solution was added to modified solid and suspension was shaken at room temperature for 2h. After filtration, modified MCM-41 was washed with ethanol and dried in air at 40^{o}C for 8h to give the final metal complex functionalized silica.

ICP (%) found: Fe (8.73).

FTIR and DRUV-Vis were recorded using materials with high Fe loading.

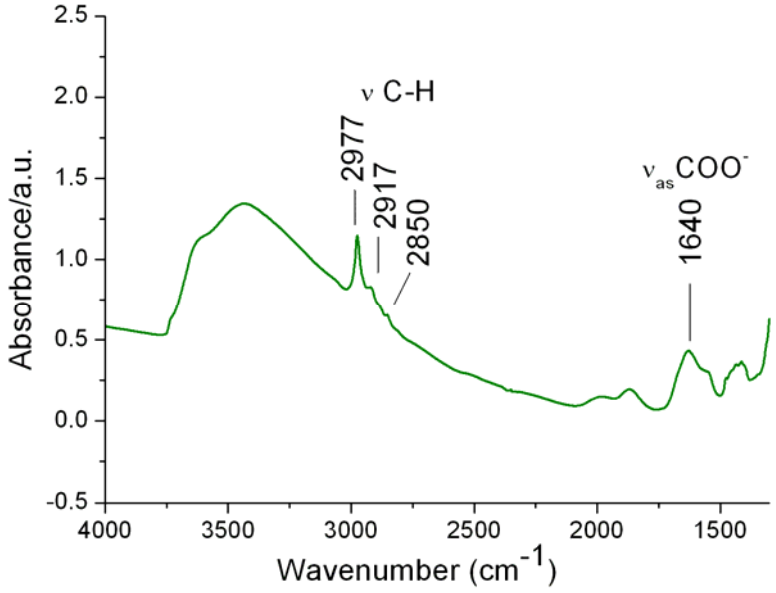

Figure 6.18. FTIR spectrum of Fe^{III}-Proline-MCM-41; ν = 2977, 2917, 2850 (CH), 1640 ($_{as}COO^{-}$) cm^{-1}.

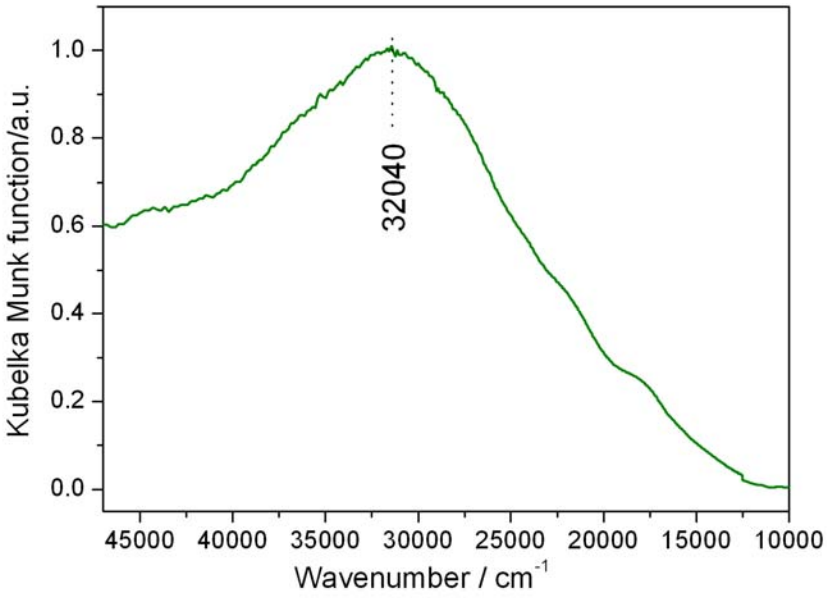

Figure 6.19. DR UV-Vis spectrum of Fe^{III}-Proline-MCM-41; LMCT 32040 cm^{-1}.

BET ANALYSIS: BET surface area: 213 m^2/g.

6.6. Immobilization of Fe^{III}-Proline complex on polystyrene.

6.6.1. Synthesis of low metal loading Fe^{III}-Proline- Polystyrene (Fe=0.05 wt%).

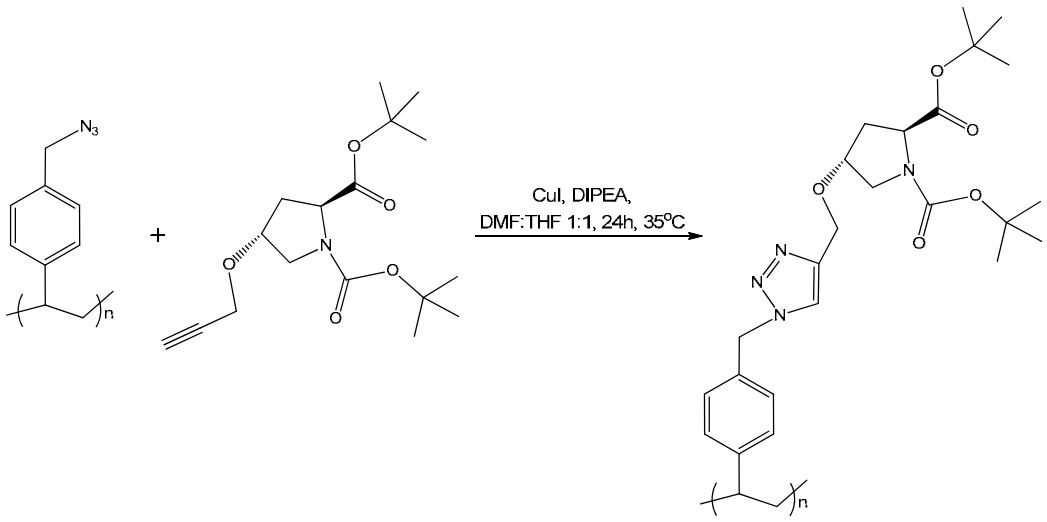

Cycloaddition of *tert*-Butyl (2*S*,4*R*)-*N*-Boc-4-propargyloxyprolinate with azido functionalized polystyrene. Azido functionalized polystyrene (1 g) was suspended in dry DMF:THF 1:1 (10 ml) and degassed with nitrogen for 40 min. *tert*-Butyl (2*S*,4*R*)-*N*-

Boc-4-propargyloxyprolinate (0.02 g, 0.1 mmol), *N,N*diisopropyl-ethyl amine (0.17 mL, 0.98 mmol) and copper (I) iodide (0.002 g, 0.001 mmol) were added to this suspension and the mixture was gently stirred at 35 ºC for 24 h under N_2. The reaction was monitored with IR and once the signal of the azido group had completely disappeared, the solid was collected by filtration and sequentially washed with water, DMF, THF, THF-MeOH (1:1), MeOH and THF. The modified resin was dried under vacuum at 40 ºC for 24 hours.

Deprotection. Modified resin (1 g) was swelled in 5 ml of CH_2Cl_2 for 10 min before trifluoroacetic acid (10 ml) was added and suspension was shaken. The evolution of the deprotection was followed by IR, when the signal of *tert*-Butyl groups disappeared, the reaction mixture was filtered and sequentially washed with THF (with 2 % of Et_3N), water, THF, THF-MeOH (1:1), MeOH and THF. The functionalised solid was dried in vacuum at 40 ºC for 24 h.

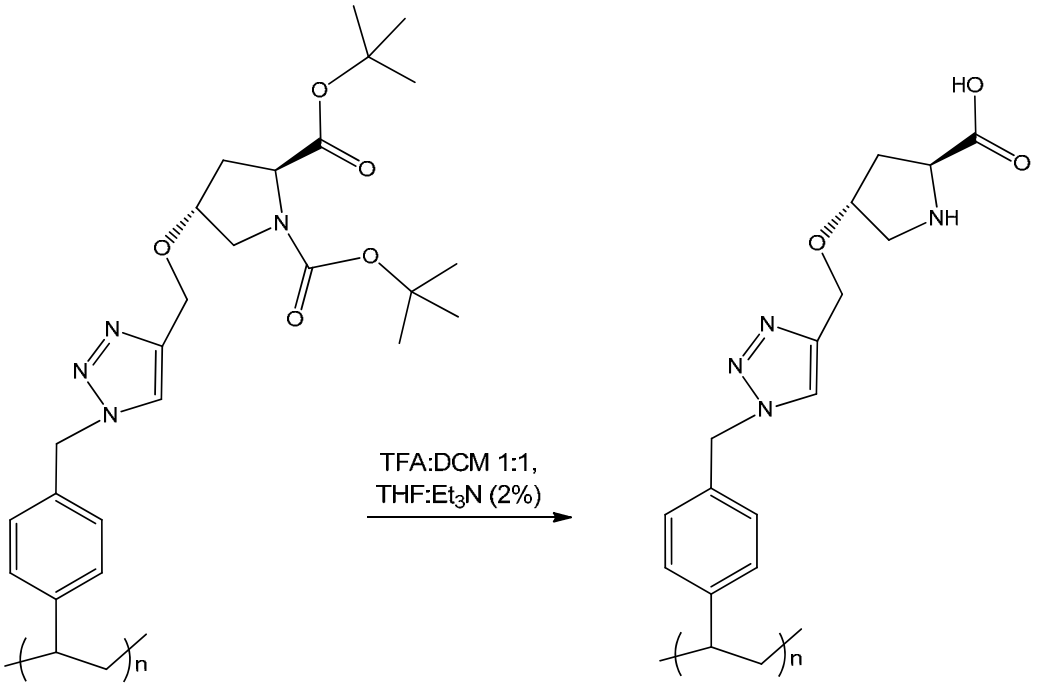

Complexation. Iron acetate **(**$Fe(C_2H_3O_2)_2$) was used as a metal source. Proline functionalized Merrifield polymer (1g) was suspended in 10ml of MeOH before 0.5 ml of triethylamine (Et_3N) was added and the mixture was shaken for 1h. Iron acetate (0.017g, 0.1 mmol) was added and the mixture was shaken for another 1h. The resulting modified solid was collected by filtration and washed with methanol. Proline (0.012g, 0.1 mmol) was dissolved in 10ml of MeOH, 0.2 ml of triethylamine (Et_3N) was added and the mixture was stirred for 0.5 h. This solution was added to modified solid and the

suspension was shaken at room temperature for 2h. After filtration, functionalized resin was washed with methanol. Drying in air at 40°C for 8h gave the final metal complex functionalized Merrifield polymer.

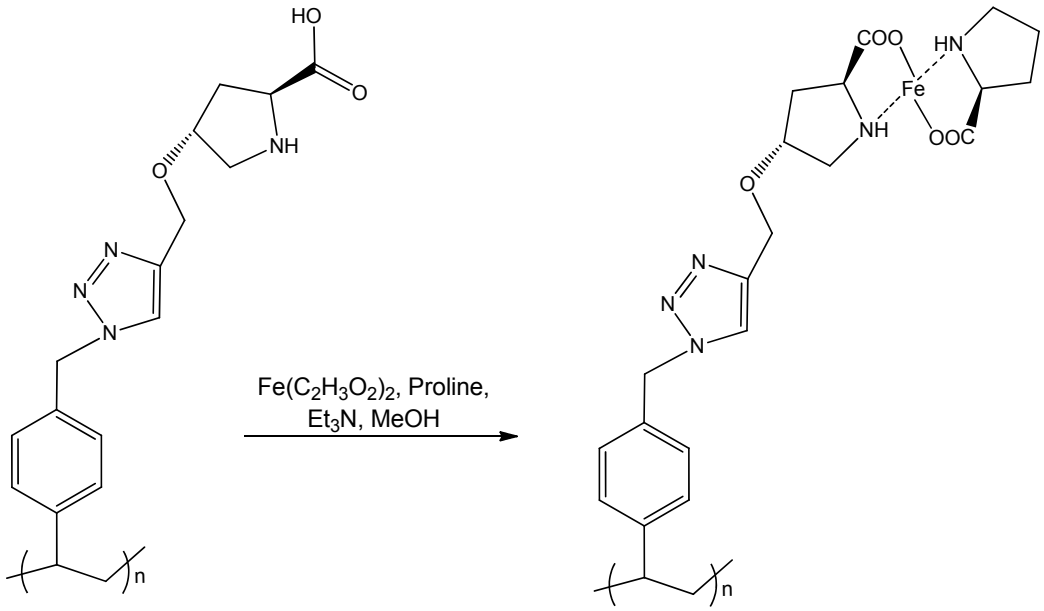

ICP (%) found: Fe (0.05).

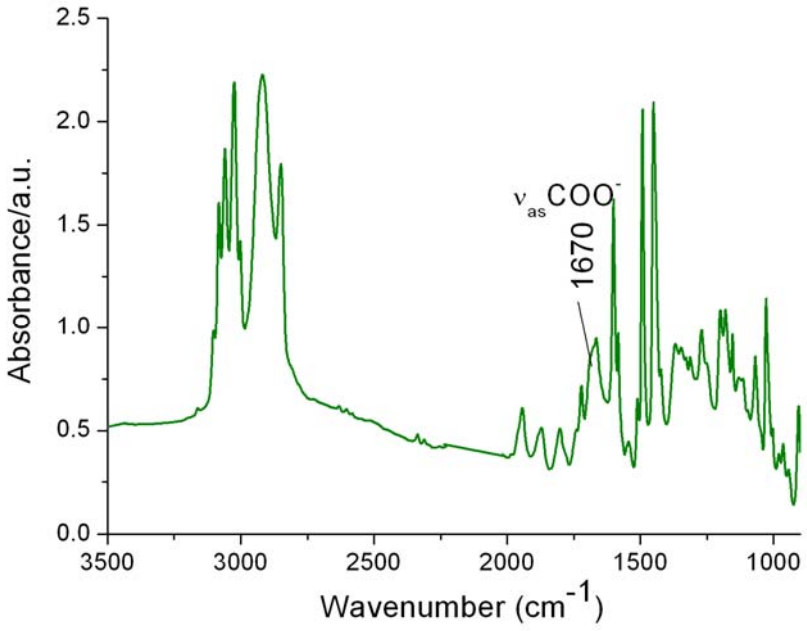

Figure 6.20. FTIR spectrum of Fe^{III}-Proline-Polystyrene; ν = 2977, 2917, 2850 (CH), 1640 ($_{as}COO^-$) cm^{-1}.

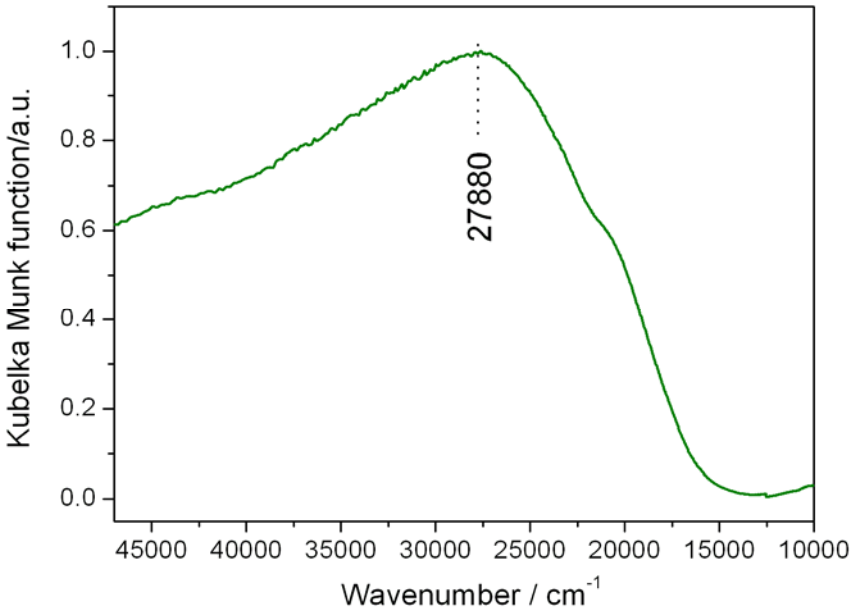

Figure 6.21. DR UV-Vis spectrum of Fe^{III}-Proline-Polystyrene; LMCT 27880 cm^{-1}.

6.7. Valine complex immobilisation on MCM-41.

6.7.1. Synthesis of low metal loading Cu^{II}-Valine-MCM-41 (Cu = 0.42 wt%).

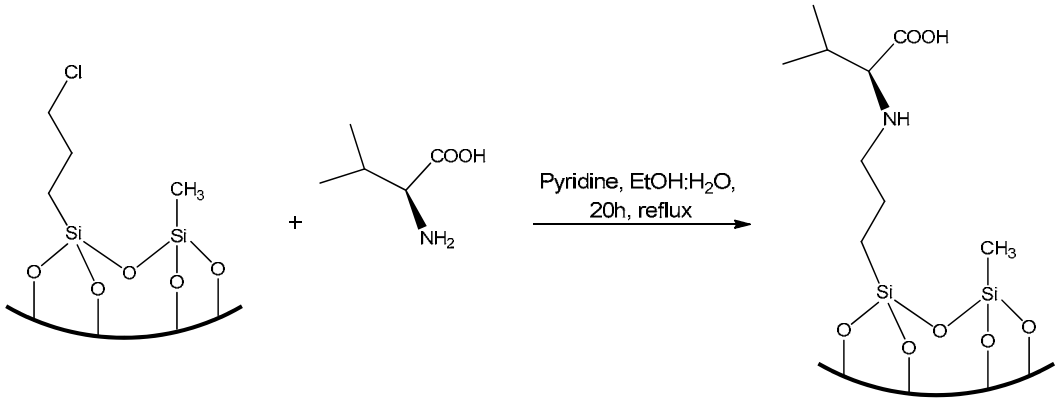

Valine immobilization on MCM-41 support: MCM-41 functionalised with chloropropyl and methyl groups (1 g) was dispersed in ethanol (5 ml) and mixed with an aqueous solution (15 ml) of valine (0.023 g, 0.2 mmol) and refluxed for 20 h in the presence of pyridine (0.22 mmol). The resulting solid was collected by filtration and washed with water followed by ethanol and dried overnight in the air at 353 K.[168]

Complexation: Copper sulfate pentahydrate ($CuSO_4*5H_2O$) was used as a metal source. 1 g of valine functionalized MCM-41 was suspended in 10 ml of 1N NaOH solution and shaken at room temperature for 1h. The aqueous solution (1 ml) of metal salt was added (0.049 g, 0.2 mmol) and the mixture was shaken for a further 1h. The resulting solid was collected by filtration and washed with ethanol. 10ml of valine (0.023 g, 0.2 mmol) solution in 1N NaOH was added and the suspension was shaken at room temperature for 2h. After filtration, the solid was washed with water:acetone mixture (2:1) and ethanol. Drying in air at 80^oC for 8h gave the final metal complex functionalized MCM-41.

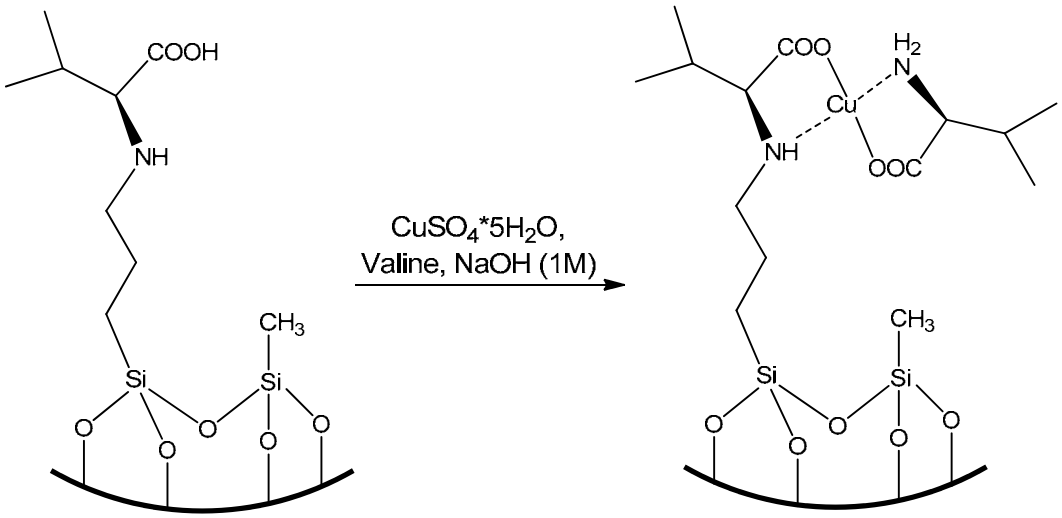

BET ANALYSIS: BET surface area: 562. 1 m^2/g.

6.7.2. Synthesis of high metal loading Cu^{II}-Valine-MCM-41 (Cu = 9.22 wt%).

Valine immobilization on MCM-41 support: MCM-41 functionalised with chloropropyl and methyl groups (1g) was dispersed in ethanol (5 ml) and mixed with an aqueous solution (15 ml) of valine (0.25 g, 2.2 mmol) and refluxed for 20 h in presence of pyridine (2.4 mmol). The resulting solid was collected by filtration and washed with water followed by ethanol and dried overnight in the air at 353 K.

Complexation: Copper sulfate pentahydrate ($CuSO_4*5H_2O$) was used as a metal source. 1g of functionalized MCM-41 was suspended in 10 ml of 1N NaOH solution and shaken at room temperature for 1h. Then the aqueous solution (10 ml) of metal salt was added (0.49 g, 2 mmol) and the mixture was shaken for 1h. The resulting solid was collected by filtration and washed with ethanol. Then, 10 ml of valine (0.25 g, 2.2 mmol) solution in

1N NaOH was added and the suspension was shaken at room temperature for 2h. After filtration, the solid was washed with water:acetone (2:1) and ethanol. Drying in the air overnight at 353 K gave the final metal complex functionalized MCM-41.

BET ANALYSIS: BET surface area: 250 m^2/g.

FTIR and DRUV-Vis were recorded using materials with high Cu loading.

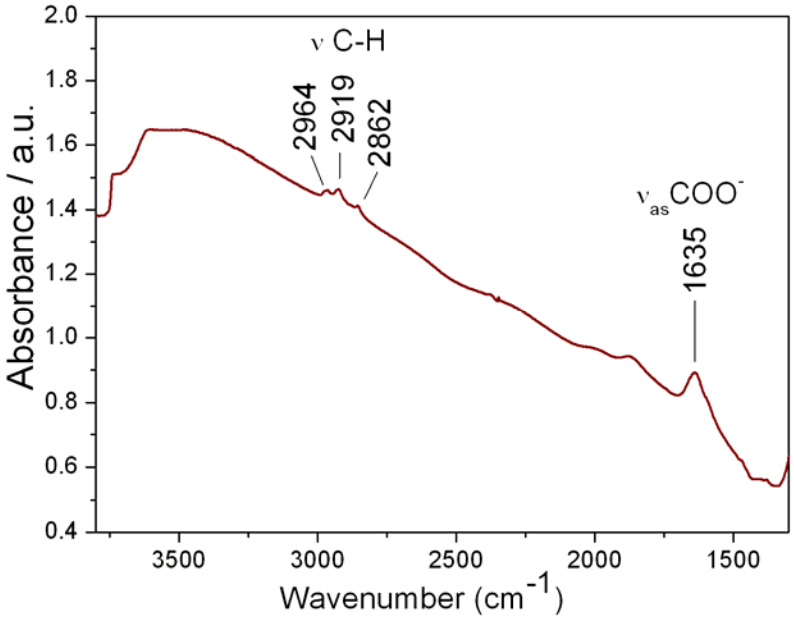

Figure 6.22. FTIR spectrum of Cu^{II}-Valine-MCM-41; ν = 2964, 2919, 2862 (CH), 1635 ($_{as}COO^-$) cm^{-1}.

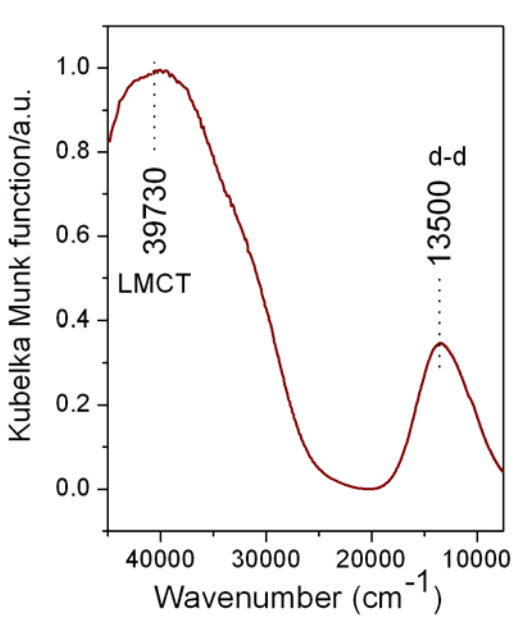

Figure 6.23. DR UV-Vis spectrum of Cu^{II}-Valine-MCM-41; LMCT 39730cm^{-1}, d-d 13500 cm^{-1}.

6.8. Cu^{II}-Valine complex immobilisation on polystyrene.

6.8.1. Synthesis of low metal loading Cu^{II}-Valine-Polystyrene (Cu =0.018 wt%).

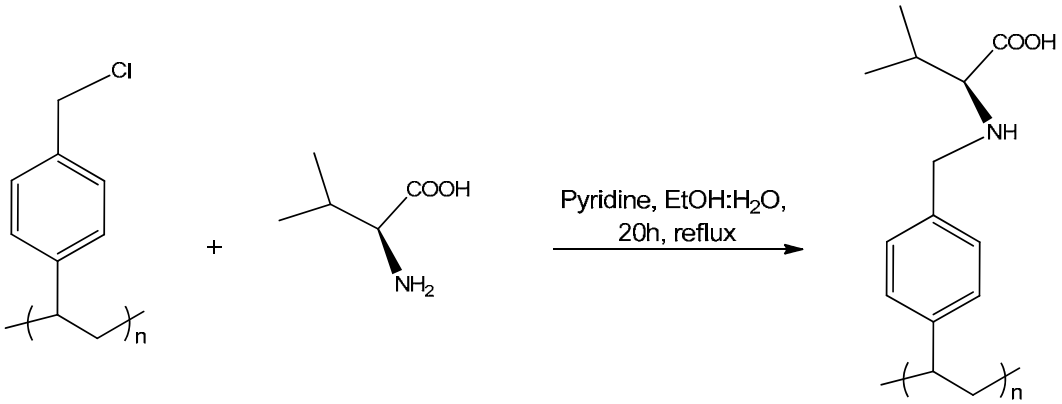

Valine immobilisation on polymer support. Merrifield polymer beads (chloromethylated styrene–divinyl benzene co-polymer, chlorine loading (~0.8 mmol/g) were pre-treated with aqueous dioxane solution (1:1) for 15 min, then washed with methanol and dried overnight in the air at 353 K. The polymer beads (1g) in methanol (5 ml) were mixed with aqueous solution (15 ml) of valine (0.012g, 0.1 mmol) and refluxed for 20 h in the presence of pyridine (0.12 mmol). The resulting solid was collected by filtration and washed with water followed by methanol and dried in air overnight at 353 K.[168]

Complexation. Copper sulfate pentahydrate ($CuSO_4*5H_2O$) was used as a metal source. 1g of valine functionalized polystyrene was suspended in 10 ml of 1N NaOH solution and shaken at room temperature for 1h. The aqueous solution (1 ml) of metal salt was added (0.0249g, 0.1 mmol) and the mixture was shaken for 1h. The resulting solid was collected by filtration and washed with methanol. Then, valine (0.012 g, 0.1 mmol) in 10 ml 1N NaOH solution was added to the previously obtained solid and the suspension was shaken at room temperature for 2h. After filtration, the solid was washed with water:acetone mixture (2:1) and methanol. Drying in air overnight at 353 K gave the final metal complex functionalized polystyrene.

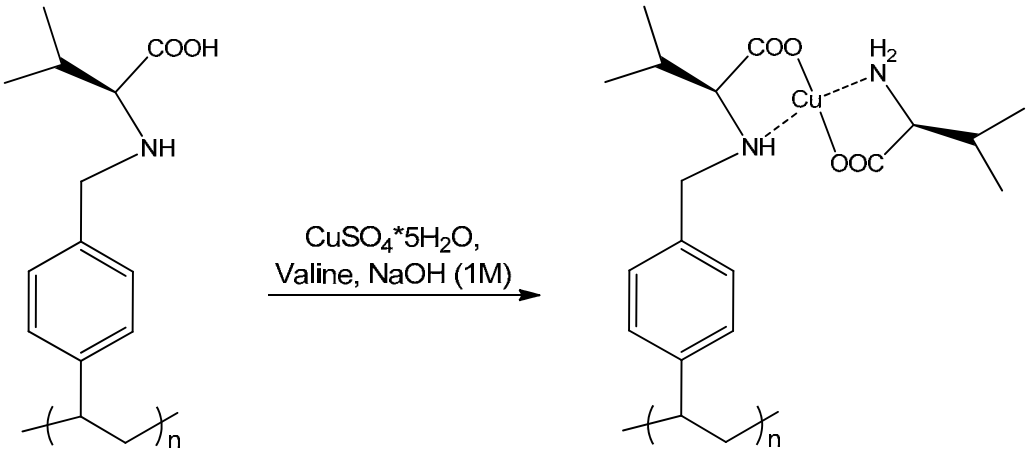

6.8.2. Synthesis of high metal loading Cu^{II}-Valine-Polystyre (Cu =8.79 wt%).

Valine immobilisation on polymer support: Merrifield polymer beads (chloromethylated styrene–divinyl benzene co-polymer, chlorine loading~0.8 mmol/g) were pre-treated with aqueous dioxane solution (1:1) for 15 min, then washed with methanol and dried under vacuum at 90 ◦C for 8 h. The polymer beads (1g) in methanol (5 ml) were mixed with aqueous solution (15ml) of valine (0.12 g, 1 mmol) and refluxed for 16 h in presence of pyridine (1.2 mmol). The resulting solid was collected by filtration and washed with water followed by methanol and dried in the air overnight at 353 K.

Complexation: Copper sulfate pentahydrate ($CuSO_4*5H_2O$) was used as a metal source. 1g of valine functionalized polystyrene was suspended in 10 ml of 1N NaOH solution and shaken at room temperature for 1h. Then the aqueous solution (5 ml) of metal salt was added (0.249 g, 1 mmol) and the mixture was shaken for 1h. The resulting solid was collected by filtration and washed with methanol. Then, valine (0.12 g, 1 mmol) in 10 ml 1N NaOH solution was added to previously obtained solid and the suspension was shaken at room temperature for 2h. After filtration, solid was washed with water:acetone mixture (2:1) and methanol. Drying in the air overnight at 353 K gave the final metal complex functionalized polystyrene.

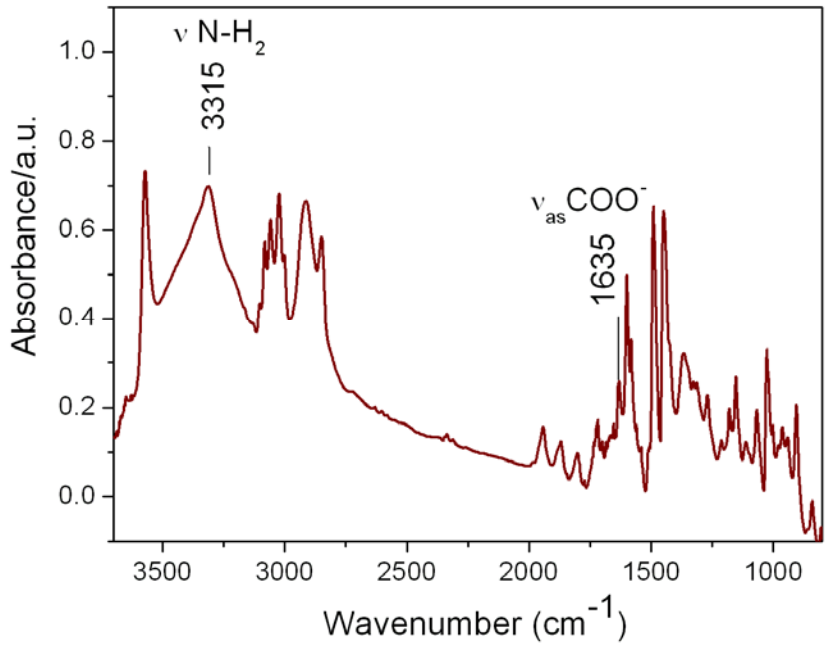

Figure 6.24. FTIR spectrum of Cu^{II}-Valine-Polystyrene; ν = 3315 (NH_2), 1635 ($_{as}COO^-$) cm^{-1}.

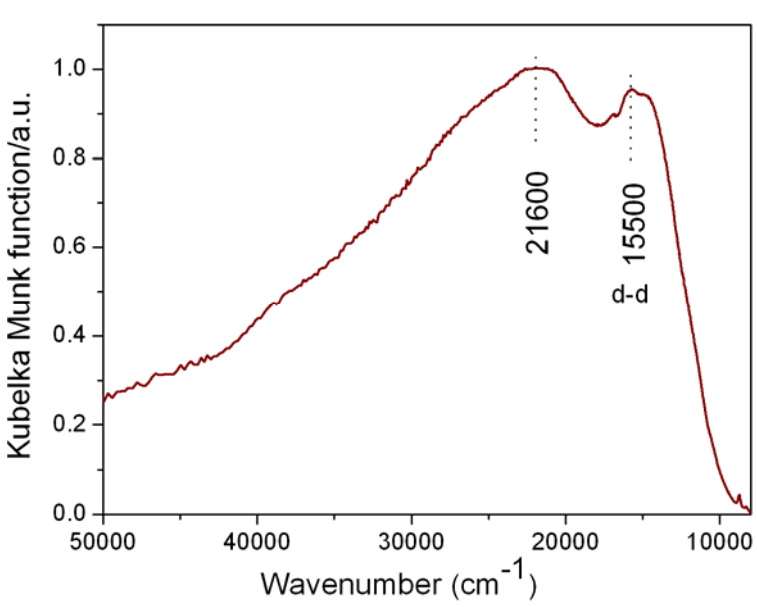

Figure 6.25. DR UV-Vis spectrum of Cu^{II}-Valine-Polystyrene; d-d 21600, 15500 cm^{-1}.

6.9. Synthesis of acetylperoxyborate (APB).

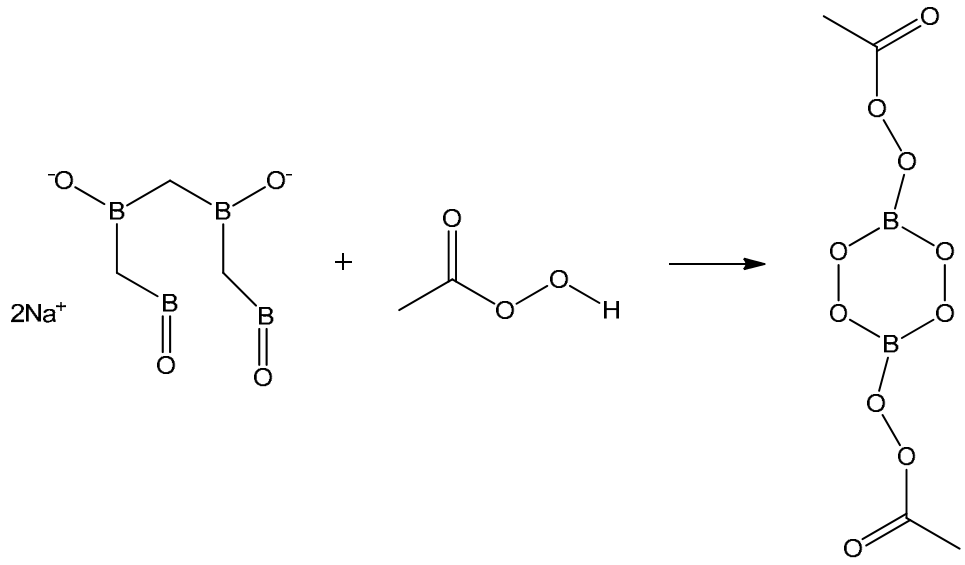

Sodium tetraborate (2.0g, 9.9mmol of Aldrich) was added to peracetic acid solution (4ml, 52.7mmol 40wt% in acetic acid, Aldrich) and stirred for 3 h at 45°C (until a homogeneous paste was formed). The resulting product was filtered, washed with ethanol and dried at 50°C overnight to obtain white powder.[296]

Titration with sodium thiosulphate was employed to determine the active oxidant content. For this purpose 0.1g of APB was added to 10ml of 0.6M potassium iodide to produce a dark red/brown solution which was titrated against 0.1M sodium thiosulphate solution. The solution colour changed from red to yellow and a few drops of starch solution were added to produce a clearer endpoint. After starch addition the colour of solution turned black. The end point was reached when the solution turned colourless. The active oxidant content was calculated using equation given below:

$$\%\ \text{oxidant} = \frac{V_{(Na_2S_2O_3)} * meg_{PAA}}{mass_{APB}}$$

Where: V $Na_2S_2O_3$ (0.1N sodium thiosulphate) – titre, meqPAA - miliequivalent of PAA (0.38 g).

6.10. Catalytic oxidation.

6.10.1. Oxidation of cyclohexane with Fe^{III}-Proline and Fe^{III}-Proline-X with air and TBHP.

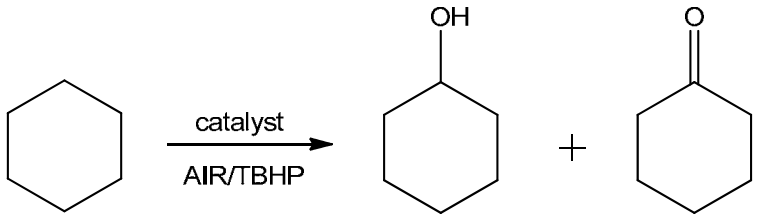

Aerobic oxidation of cyclohexane was performed in a high-pressure, stainless-steel catalytic reactor (Parr 4842), air 3.0 MPa, at T=371K. Experiments with tert-butyl hydroxyperoxide (70% wt. in water) were carried out using a glass-lined reactor at T=371K. Blank experiments, in the absence of catalysts, were running under the same conditions. Mesitylene was used as internal standard. The contents were stirred at 1000 rpm and the reactor was heated to desired temperature. The catalyst was removed by centrifugation. The products were analysed by GC (PerkinElmer, Clarus 400) employing Elite Wax capillary column (column length 30 m), carrier gas: He, flow rate 0.9 ml/ min, injection temperature 220^{o}C, Flame Ionisation Detector (FID).

Table 6.1. Reaction conditions for cyclohexane oxidation with Fe^{III} catalysts: air 3.0 MPa, T=371 K, acetonitrile 35 g, reaction time=1h.

Cat.	Oxid.	Metal loading	Cat. (g)	Mmol of metal	Substr. (g)	Mmol of subst.	Mmol of oxid.	Subst: Metal ratio	Oxid: Subst ratio
Neat	AIR	16.9	0.03	0.09	1.8	22.0	25.1	244	1.1
Neat	TBHP	16.9	0.03	0.09	1.8	22.0	22.0	244	1
X	AIR	0.49	0.15	0.013	1.8	22.0	25.1	1692	1.1
X	TBHP	0.49	0.15	0.013	1.8	22.0	22.0	1692	1
Blanc	AIR	-	-	-	1.8	22.0	25.1	-	1.1
Blanc	TBHP	-	-	-	1.8	22.0	22.0	-	1

6.10.2. Oxidation of benzyl alcohol with Fe^{III}-Proline, Fe^{III}-Proline-X, Fe^{III}-Proline-MCM-41 and Fe^{III}-Proline-Polystyrene.

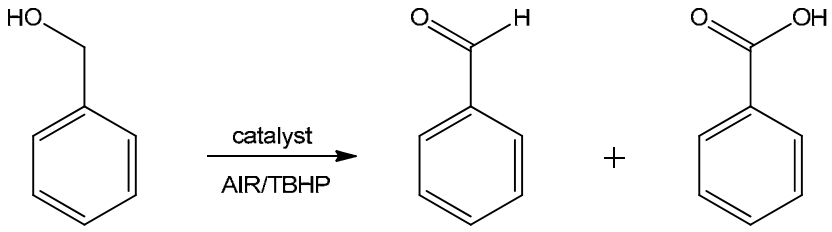

Aerobic oxidation of benzyl alcohol was performed in a high-pressure, stainless-steel catalytic reactor (Parr 4842), air 3.0, MPa T=371K. Experiments with tert-butyl hydroxyperoxide (70% wt. in water) were carried out using a glass-lined reactor at T=371K. Blanc experiments, in absence of catalysts, were running under the same conditions. Mesitylene was used as internal standard. The contents were stirred at 1000 rpm and the reactor was heated to desired temperature. The catalyst was removed by centrifugation. The products were analysed by GC (PerkinElmer, Clarus 400) employing Elite Wax capillary column (column length 30 m), carrier gas: He, flow rate 0.9 ml/ min, injection temperature 220^{o}C, Flame Ionisation Detector (FID).

Table 6.2. Reaction conditions for benzyl alcohol oxidation with Fe^{III}-catalysts: air 3.0 MPa, T=371 K, DMSO 35g, reaction time=6h.

Cat.	Oxid.	Metal loading	Cat. (g)	Mmol of metal	Substr. (g)	Mmol of subst.	Mmol of oxid.	Subst: Metal ratio	Oxid: Subst. ratio
Neat	AIR	16.9	0.009	0.027	1.70	15.7	25.1	581	1.6
Neat	TBHP	16.9	0.009	0.027	1.70	15.7	15.7	581	1
X	AIR	0.49	0.31	0.027	1.70	15.7	25.1	581	1.6
X	TBHP	0.49	0.31	0.027	1.70	15.7	15.7	581	1
MCM	AIR	8.73	0.05	0.078	1.70	15.7	25.1	201	1.6
MCM	AIR	2.07	0.03	0.011	1.23	11.4	25.1	1036	2.2
MCM	TBHP	8.73	0.05	0.078	1.70	15.7	15.7	201	1
MCM	TBHP	2.07	0.03	0.011	1.23	11.4	11.4	1036	1
Polyst	AIR	0.05	0.05	0.0004	1.70	15.7	25.1	35213	1.6
Polyst	TBHP	0.05	0.05	0.0004	1.70	15.7	15.7	35213	1
Blanc	AIR	-	-	-	1.70	15.7	25.1	-	1.6
Blanc	TBHP	-	-	-	1.70	15.7	15.7	-	1

6.10.3. Oxidation of cyclohexene with Fe^{III}-Proline, Fe^{III}-Proline-X, Fe^{III}-Proline-MCM-41 and Fe^{III}-Proline-Polystyrene.

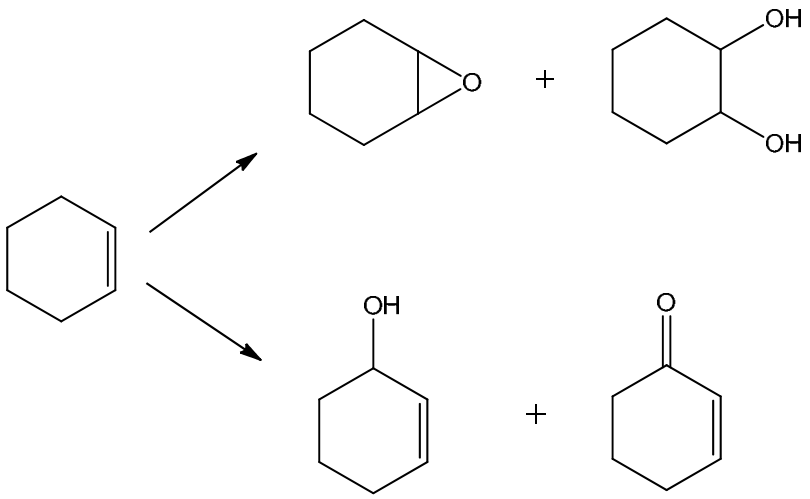

Aerobic oxidation of cyclohexene was performed in a high-pressure, stainless-steel catalytic reactor (Parr 4842), air 3.0, MPa T=371K. Experiments with tert-butyl hydroxyperoxide (70% wt. in water) and APB were carried out using a glass-lined reactor at T=371K. Blanc experiments, in absence of catalysts, were running under the same conditions. Mesitylene was used as internal standard. The contents were stirred at 1000 rpm and the reactor was heated to desired temperature. The catalyst was removed by centrifugation. The products were analysed by GC (PerkinElmer, Clarus 400) employing Elite Wax capillary column (column length 30 m), carrier gas: He, flow rate 0.9 ml/ min, injection temperature 220^{o}C, Flame Ionisation Detector (FID).

Table 6.3. Reaction conditions for cyclohexene oxidation with Fe^{III}-Proline catalysts: air 3.0 MPa, T=371 K, acetonitrile 35g (reactions with air and TBHP) and acetonitrile 25 g, water 10g (reactions with APB), reaction time=6h.

Cat.	Oxid.	Metal load.	Cat. (g)	Mmol of metal	Substr. (g)	Mmol of subst.	Mmol of oxid.	Subst: Metal ratio	Oxid: Subst. ratio
Neat	AIR	16.9	0.009	0.027	1.29	15.7	25.1	581	1.6
Neat	TBHP	16.9	0.009	0.027	1.29	15.7	15.7	581	1
Neat	APB	16.9	0.009	0.027	1.29	15.7	15.7	581	1
MCM	AIR	8.73	0.05	0.078	1.29	15.7	25.1	201	1.6
MCM	AIR	2.07	0.03	0.011	0.92	11.2	25.1	1018	2.2
MCM	TBHP	8.73	0.05	0.078	1.29	15.7	15.7	201	1
MCM	TBHP	2.07	0.03	0.011	0.92	11.2	11.2	1018	1
MCM	APB	8.73	0.05	0.078	1.29	15.7	15.7	201	1
MCM	APB	2.07	0.03	0.011	0.92	11.2	11.2	1018	1
Polyst	AIR	0.05	0.05	0.0004	1.29	15.7	25.1	35370	1.6
Polyst	TBHP	0.05	0.05	0.0004	1.29	15.7	15.7	35370	1
Polyst	APB	0.05	0.05	0.0004	1.29	15.7	15.7	35370	1
Blanc	AIR	-	-	-	1.29	15.7	25.1	-	1.6
Blanc	TBHP	-	-	-	1.29	15.7	15.7	-	1
Blanc	APB	-	-	-	1.29	15.7	15.7	-	1

6.10.4. Oxidation of dimethyl sulfide with Fe^{III}-Proline, Fe^{III}-Proline-X, Fe^{III}-Proline-MCM-41 and Fe^{III}-Proline-Polystyrene.

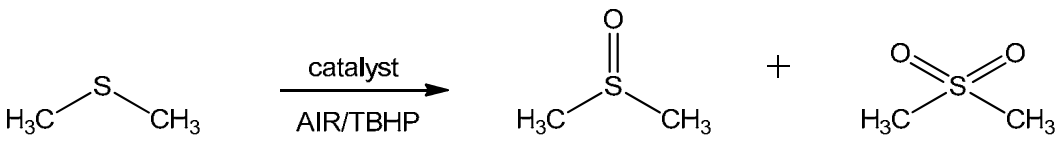

Aerobic oxidation of dimethyl sulfide was performed in a high-pressure, stainless-steel catalytic reactor (Parr 4842), air 3.0, MPa T=371K. Experiments with tert-butyl hydroxyperoxide (70% wt. in water) were carried out using a glass-lined reactor at T=371K. Blanc experiments, in absence of catalysts, were running under the same

conditions. Mesitylene was used as internal standard. The contents were stirred at 1000 rpm and the reactor was heated to desired temperature. The catalyst was removed by centrifugation. The products were analysed by GC (PerkinElmer, Clarus 400) employing Elite Wax capillary column (column length 30 m), carrier gas: He, flow rate 0.9 ml/ min, injection temperature 220^{o}C, Flame Ionisation Detector (FID).

Table 6.4. Reaction conditions for dimethyl sulfide oxidation with Fe^{III}-Proline catalysts : air 3.0 MPa, T=371 K, acetonitrile 35g, reaction time=6h.

Cat.	Oxid.	Metal load.	Cat. (g)	Mmol of metal	Subst. (g)	Mmol of subst.	Mmol of oxid.	Subst: Metal ratio	Oxid: subst ratio
Neat	AIR	16.9	0.009	0.027	0.98	15.7	25.1	581	1.6
Neat	TBHP	16.9	0.009	0.027	0.98	15.7	15.7	581	1
MCM	AIR	8.73	0.05	0.078	0.98	15.7	25.1	201	1.6
MCM	AIR	2.07	0.03	0.011	0.72	11.6	25.1	1054	2.1
MCM	TBHP	8.73	0.05	0.078	0.98	15.7	15.7	201	1
MCM	TBHP	2.07	0.03	0.011	0.72	11.6	11.6	1054	1
Polyst	AIR	0.05	0.05	0.0004	0.98	15.7	25.1	35404	1.6
Polyst	TBHP	0.05	0.05	0.0004	0.98	15.7	15.7	35404	1
Blanc	AIR	-	-	-	0.98	15.7	25.1	-	1.6
Blanc	TBHP	-	-	-	0.98	15.7	15.7	-	1

6.10.5. Oxidation of benzyl alcohol with Cu^{II}-Valine, Cu^{II}-Valine-MCM-41, Cu^{II}-Valine-Polystyrene.

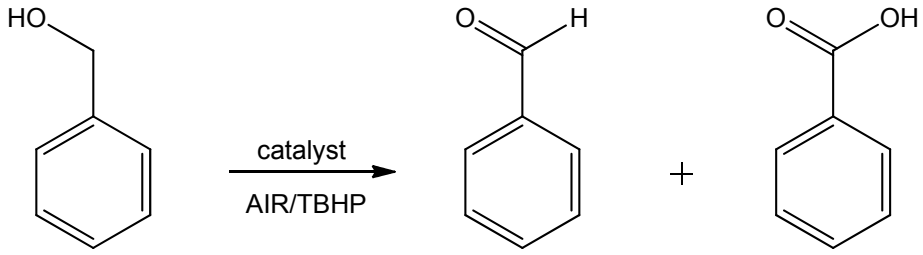

Aerobic oxidation of benzyl alcohol was performed in a high-pressure, stainless-steel catalytic reactor (Parr 4842), air 3.0, MPa T=371K. Experiments with tert-butyl hydroxyperoxide (70% wt. in water) were carried out using a glass-lined reactor at T=371K. Blanc experiments, in absence of catalysts, were running under the same

conditions. Mesitylene was used as internal standard. The contents were stirred at 1000 rpm and the reactor was heated to desired temperature. The catalyst was removed by centrifugation. The products were analysed by GC (PerkinElmer, Clarus 400) employing Elite Wax capillary column (column length 30 m), carrier gas: He, flow rate 0.9 ml/ min, injection temperature 220^{o}C, Flame Ionisation Detector (FID).

Table 6.5. Reaction conditions for benzyl alcohol oxidation with Cu^{II}-Valine catalysts: air 3.0 MPa, T=371 K, DMSO 35g, reaction time=6h.

Cat.	Oxid.	Metal load.	Cat. (g)	Mmol of metal	Subst. (g)	Mmol of subst.	Mmol of oxid.	Subst: Metal ratio	Oxid: subst. ratio
Neat	AIR	22.4	0.008	0.027	1.70	15.7	25.1	581	1.6
Neat	TBHP	22.4	0.008	0.027	1.70	15.7	15.7	581	1
MCM	AIR	9.22	0.05	0.072	1.70	15.7	25.1	218	1.6
MCM	AIR	0.42	0.06	0.004	0.80	7.40	25.1	1864	3.4
MCM	TBHP	9.22	0.05	0.072	1.70	15.7	15.7	218	1
MCM	TBHP	0.42	0.06	0.004	0.80	7.40	7.40	1864	1
Polyst	AIR	8.79	0.05	0.069	1.70	15.7	25.1	228	1.6
Polyst	AIR	0.018	0.1	0.0003	0.04	0.33	25.1	1174	76
Polyst	TBHP	8.79	0.05	0.069	1.70	15.7	15.7	228	1
Polyst	TBHP	0.018	0.1	0.0003	0.03	0.28	0.28	1174	1

6.10.6. Oxidation of cyclohexene with Cu^{II}-Valine, Cu^{II}-Valine-MCM-41, Cu^{II}-Valine-Polystyrene.

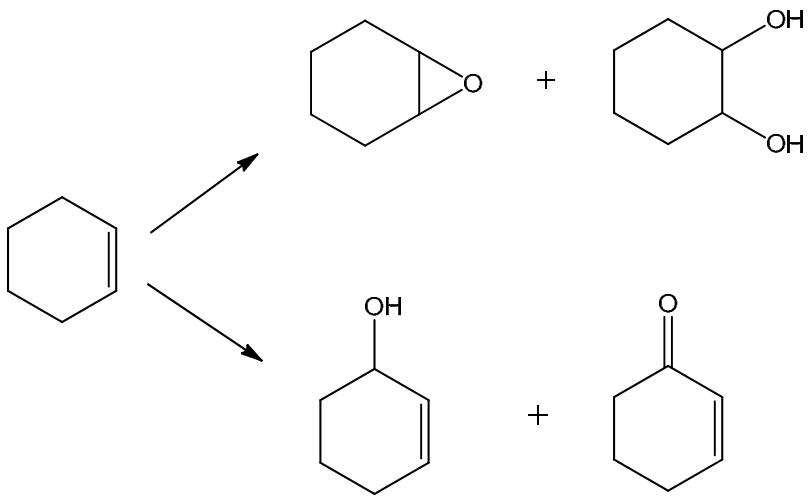

Aerobic oxidation of cyclohexene was performed in a high-pressure, stainless-steel catalytic reactor (Parr 4842), air 3.0, MPa T=371K. Experiments with tert-butyl hydroxyperoxide (70% wt. in water) and APB were carried out using a glass-lined reactor at T=371K. Blanc experiments, in absence of catalysts, were running under the same conditions. Mesitylene was used as internal standard. The contents were stirred at 1000 rpm and the reactor was heated to desired temperature. The catalyst was removed by centrifugation. The products were analysed by GC (PerkinElmer, Clarus 400) employing Elite Wax capillary column (column length 30 m), carrier gas: He, flow rate 0.9 ml/ min, injection temperature 220^{o}C, Flame Ionisation Detector (FID).

Table 6.6. Reaction conditions for cyclohexene oxidation with Cu^{II}-Valine catalysts : air 3.0 MPa, T=371 K, acetonitrile 35g (reactions with air and TBHP) and acetonitrile 25 g, water 10g (reactions with APB), reaction time=6h.

Cat.	Oxid.	Metal load.	Cat. (g)	Mmol of metal	Subst. (g)	Mmol of subst.	Mmol of oxid.	Subst: Metal ratio	Oxid: subst. ratio
Neat	AIR	22.4	0.008	0.027	1.29	15.7	25.1	581	1.6
Neat	TBHP	22.4	0.008	0.027	1.29	15.7	15.7	581	1
Neat	APB	22.4	0.008	0.027	1.29	15.7	15.7	581	1
MCM	AIR	9.22	0.05	0.072	1.29	15.7	25.1	218	1.6
MCM	AIR	0.42	0.03	0.002	0.26	3.16	25.1	1580	7..9
MCM	TBHP	9.22	0.05	0.072	1.29	15.7	15.7	218	1
MCM	TBHP	0.42	0.03	0.002	0.26	3.16	3.16	1580	1
MCM	APB	9.22	0.05	0.072	1.29	15.7	15.7	218	1
MCM	APB	0.42	0.03	0.002	0.26	3.16	3.16	1580	1
Polyst	AIR	8.79	0.05	0.069	1.29	15.7	25.1	228	1.6
Polyst	AIR	0.018	0.12	0.0003	0.07	0.82	25.1	2398	30.6
Polyst	TBHP	8.79	0.05	0.069	1.29	15.7	15.7	228	1
Polyst	TBHP	0.018	0.12	0.0003	0.07	0.82	0.82	2398	1
Polyst	APB	8.79	0.05	0.069	1.29	15.7	15.7	228	1
Polyst	APB	0.018	0.12	0.0003	0.07	0.82	0.82	2398	1

6.10.7. Oxidation of dimethyl sulfide with Cu^{II}-Valine, Cu^{II}-Valine -MCM-41, Cu^{II}-Valine -Polystyrene.

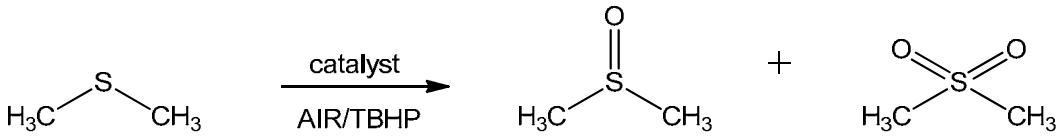

Aerobic oxidation of dimethyl sulfide was performed in a high-pressure, stainless-steel catalytic reactor (Parr 4842), air 3.0, MPa T=371K. Experiments with tert-butyl hydroxyperoxide (70% wt. in water) were carried out using a glass-lined reactor at T=371K. Blanc experiments, in absence of catalysts, were running under the same conditions. Mesitylene was used as internal standard. The contents were stirred at 1000 rpm and the reactor was heated to desired temperature. The catalyst was removed by centrifugation. The products were analysed by GC (PerkinElmer, Clarus 400) employing Elite Wax capillary column (column length 30 m), carrier gas: He, flow rate 0.9 ml/ min, injection temperature 220^{o}C, Flame Ionisation Detector (FID).

Table 6.7. Reaction conditions for dimethyl sulfide oxidation with Cu^{II}-Valine catalysts: air 3.0 MPa, T=371 K, acetonitrile 35g, reaction time=6h.

Cat.	Oxid.	Metal load.	Cat. (g)	Mmol of metal	Subst. (g)	Mmol of subst.	Mmol of oxid.	Subst: Metal ratio	Oxid: subst. ratio
Neat	AIR	22.4	0.008	0.027	0.98	15.7	25.1	581	1.6
Neat	TBHP	22.4	0.008	0.027	0.98	15.7	15.7	581	1
MCM	AIR	9.22	0.05	0.072	0.98	15.7	25.1	221	1.6
MCM	AIR	0.42	0.06	0.004	0.46	7.4	25.1	1850	3.4
MCM	TBHP	9.22	0.05	0.072	0.98	15.7	15.7	221	1
MCM	TBHP	0.42	0.06	0.004	0.46	7.4	7.4	1850	1
Polyst	AIR	8.79	0.05	0.069	0.98	15.7	25.1	227	1.6
Polyst	AIR	0.018	0.12	0.0003	0.04	0.64	25.1	2133	39.2
Polyst	TBHP	8.79	0.05	0.069	0.98	15.7	15.7	227	1
Polyst	TBHP	0.018	0.12	0.0003	0.04	0.64	0.64	2133	1

7. REFERENCES.

1. C. Copéret, M. Chabanas, R. Petroff Saint-Arroman and J.-M. Basset, *Angew. Chem., Int. Ed.*, 2003, **42**, 156-181.

2. J. M. Thomas, J. C. Hernandez-Garrido, R. Raja and R. G. Bell, *Phys. Chem. Chem. Phys.,*, 2009, **11**, 2799-2825.

3. J. M. Hawkins and T. J. N. Watson, *Angew. Chem., Int. Ed.* , 2004, **43**, 3224-3228.

4. C. Marcilly, *J. Catal.*, **216**, 47-62.

5. I. W. Davies, L. Matty, D. L. Hughes and P. J. Reider, *J. Am. Chem. Soc.* , 2001, **123**, 10139-10140.

6. N. Mizuno and M. Misono, *Chem. Rev.*, 1998, **98**, 199-218.

7. A. Corma and H. García, *Chem. Rev.*, 2003, **103**, 4307-4366.

8. C.-J. Li and B. M. Trost, *Proc. Natl. Acad. Sci.* , 2008, **105**, 13197-13202.

9. H. E. Schoemaker, D. Mink and M. G. Wubbolts, *Science*, 2003, **299**, 1694-1697.

10. B. Schulze and M. G. Wubbolts, *Curr. Opin. Biotechnol.*, 1999, **10**, 609-615.

11. O. Kirk, T. V. Borchert and C. C. Fuglsang, *Curr. Opin. Biotechnol.*, 2002, **13**, 345-351.

12. J. Thomas and R. Raja, *Top. Catal.*, 2006, **40**, 3-17.

13. J. M. Thomas, R. Raja and D. W. Lewis, *Angew. Chem., Int. Ed.* , 2005, **44**, 6456-6482.

14. G. Centi and S. Perathoner, *Catal. Today*, 2003, **77**, 287-297.

15. V. Dal Santo, F. Liguori, C. Pirovano and M. Guidotti, *Molecules*, 2010, **15**, 3829-3856.

16. R. K. Grasselli, *Top. Catal.*, 2002, **21**, 79-88.

17. D. I. Enache, J. K. Edwards, P. Landon, B. Solsona-Espriu, A. F. Carley, A. A. Herzing, M. Watanabe, C. J. Kiely, D. W. Knight and G. J. Hutchings, *Science*, 2006, **311**, 362-365.

18. U. Schuchardt, D. Cardoso, R. Sercheli, R. Pereira, R. S. da Cruz, M. C. Guerreiro, D. Mandelli, E. V. Spinacé and E. L. Pires, *Appl. Catal., A* 2001, **211**, 1-17.

19. F. Adam, J. Andas and I. A. Rahman, *Chem. Eng. J.*, 2010, **165**, 658-667.

20. G. I. Panov, *CATTECH*, 2000, **4**, 18-31.

21. E. I. Solomon, T. C. Brunold, M. I. Davis, J. N. Kemsley, S.-K. Lee, N. Lehnert, F. Neese, A. J. Skulan, Y.-S. Yang and J. Zhou, *Chem. Rev.*, 1999, **100**, 235-350.

22. H. Maid, P. Böhm, S. M. Huber, W. Bauer, W. Hummel, N. Jux and H. Gröger, *Angew. Chem., Int. Ed.*, 2011, **50**, 2397-2400.

23. K. Kerman and H.-B. Kraatz, *Angew. Chem., Int. Ed.*, 2008, **47**, 6522-6524.

24. L. Betancor and H. R. Luckarift, *Trends Biotechnol.*, 2008, **26**, 566-572.

25. I. W. C. E. Arends and R. A. Sheldon, *Appl. Catal., A*, 2001, **212**, 175-187.

26. M. L. Neidig and E. I. Solomon, *Chem. Commun.* , 2005, 5843-5863.

27. J. B. v. Beilen and E. G. Funhoff, *Curr. Opin. Biotechnol.*, 2005, **16**, 308-314.

28. J. Zhang, H. Zheng, S. L. Groce and J. D. Lipscomb, *J. Mol. Catal. A: Chem.*, 2006, **251**, 54-65.

29. T. L. Poulos, *Biochem. Biophys. Res. Commun.*, 2005, **338**, 337-345.

30. J. P. Klinman, *Chem. Rev.*, 1996, **96**, 2541-2562.

31. A. Decker and E. I. Solomon, *Curr. Opin. Chem. Biol.*, 2005, **9**, 152-163.

32. T. D. H. Bugg, *Curr. Opin. Chem. Biol.*, 2001, **5**, 550-555.

33. A. De La Lande, D. R. Salahub, J. Maddaluno, A. Scemama, J. Pilme, O. Parisel, H. Gerard, M. Caffarel and J.-P. Piquemal, *J. Comput. Chem.*, 2011, **32**, 1178-1182.

34. E. G. Kovaleva and J. D. Lipscomb, *Nat. Chem. Biol.*, 2008, **4**, 186-193.

35. M. Merkx, D. A. Kopp, M. H. Sazinsky, J. L. Blazyk, J. Müller and S. J. Lippard, *Angew. Chem. Int. Ed.*, 2001, **40**, 2782-2807.

36. S. V. Kryatov, E. V. Rybak-Akimova and S. Schindler, *J. Am. Chem. Soc.*, 2005, **105**, 2175-2226.

37. S. H. Lee, J. H. Han, H. Kwak, S. J. Lee, E. Y. Lee, H. J. Kim, J. H. Lee, C. Bae, S. N. Lee, Y. Kim and C. Kim, *Chem. Eur. J.* , 2007, **13**, 9393-9398.

38. E. I. Solomon, P. Chen, M. Metz, S.-K. Lee and A. E. Palmer, *Angew. Chem. Int. Ed.*, 2001, **40**, 4570-4590.

39. E. I. Solomon, J. W. Ginsbach, D. E. Heppner, M. T. Kieber-Emmons, C. H. Kjaergaard, P. J. Smeets, L. Tian and J. S. Woertink, *Faraday Discuss. Chem. Soc.*, 2011, **148**, 11-39.

40. S. Itoh, *Curr. Opin. Chem. Biol.*, 2006, **10**, 115-122.

41. R. H. Holm, P. Kennepohl and E. I. Solomon, *Chem. Rev.*, 1996, **96**, 2239-2314.

42. I. G. Denisov, T. M. Makris, S. G. Sligar and I. Schlichting, *Chem. Rev.*, 2005, **105**, 2253-2278.

43. D. J. Ferraro, L. Gakhar and S. Ramaswamy, *Biochem. Biophys. Res. Commun.*, 2005, **338**, 175-190.

44. C. A. Earhart, M. W. Vetting, R. Gosu, I. Michaud-Soret, L. Que Jr and D. H. Ohlendorf, *Biochem. Biophys. Res. Commun.*, 2005, **338**, 198-205.

45. D. A. Kopp and S. J. Lippard, *Curr. Opin. Chem. Biol.*, 2002, **6**, 568-576.

46. B. Meunier, S. P. de Visser and S. Shaik, *Chem. Rev.*, 2004, **104**, 3947-3980.

47. M. K. Julsing, S. Cornelissen, B. Bühler and A. Schmid, *Curr. Opin. Chem. Biol.* , 2008, **12**, 177-186.

48. H.-P. Hersleth, U. Ryde, P. Rydberg, C. H. Görbitz and K. K. Andersson, *J. Inorg. Biochem.*, 2006, **100**, 460-476.

49. F. Ogliaro, N. Harris, S. Cohen, M. Filatov, S. P. de Visser and S. Shaik, *J. Am. Chem. Soc.*, 2000, **122**, 8977-8989.

50. B. Meunier and J. Bernadou, *Top. Catal.* , 2002, **21**, 47-54.

51. W. Nam, *Acc. Chem. Res.*, 2007, **40**, 522-531.

52. W. Nam, M. H. Lim, S.-Y. Oh, J. H. Lee, H. J. Lee, S. K. Woo, C. Kim and W. Shin, *Angew. Chem., Int. Ed.* , 2000, **39**, 3646-3649.

53. K. D. Karlin, *Nature*, 2010, **463**, 168-169.

54. M. Costas, M. P. Mehn, M. P. Jensen and L. Que, *Chem. Rev.*, 2004, **104**, 939-986.

55. D. R. Tomchick, P. Phan, M. Cymborowski, W. Minor and T. R. Holman, *Biochemistry* 2001, **40**, 7509-7517.

56. M. M. Abu-Omar, A. Loaiza and N. Hontzeas, *Chem. Rev.*, 2005, **105**, 2227-2252.

57. F. H. Vaillancourt, C. J. Barbosa, T. G. Spiro, J. T. Bolin, M. W. Blades, R. F. B. Turner and L. D. Eltis, *J. Am. Chem. Soc.*, 2002, **124**, 2485-2496.

58. M. Y. Pau, J. D. Lipscomb and E. I. Solomon, *Proc. Natl. Acad. Sci.*, 2007, **104**, 18355-18362.

59. A. M. Orville, J. D. Lipscomb and D. H. Ohlendorf, *Biochemistry,* , 1997, **36**, 10052-10066.

60. N. Sato, Y. Uragami, T. Nishizaki, Y. Takahashi, G. Sazaki, K. Sugimoto, T. Nonaka, E. Masai, M. Fukuda and T. Senda, *J. Math. Biol.*, 2002, **321**, 621-636.

61. L. Westerheide, M. Pascaly and B. Krebs, *Curr. Opin. Chem. Biol.*, 2000, **4**, 235-241.

62. K. J. Walters, G. T. Gassner, S. J. Lippard and G. Wagner, *Proc. Natl. Acad. Sci.*, 1999, **96**, 7877-7882.

63. L. L. Chatwood, J. Müller, J. D. Gross, G. Wagner and S. J. Lippard, *Biochemistry*, 2004, **43**, 11983-11991.

64. P. E. M. Siegbahn and R. H. Crabtree, *J. Am. Chem. Soc.*, 1997, **119**, 3103-3113.

65. S.-K. Lee and J. D. Lipscomb, *Biochemistry*, 1999, **38**, 4423-4432.

66. L. M. Mirica, X. Ottenwaelder and T. D. P. Stack, *Chem. Rev.* , 2004, **104**, 1013-1046.

67. I. Bento, M. Carrondo and P. Lindley, *J. Biol. Inorg. Chem.*, 2006, **11**, 539-547.

68. L. Guidoni, K. Spiegel, M. Zumstein and U. Röthlisberger, *Angew. Chem. Int. Ed.*, 2004, **43**, 3286-3289.

69. S. Berry, J. Mayers and N. Zehm, *J. Biol. Inorg. Chem.*, 2009, **14**, 143-149.

70. Y. Matoba, T. Kumagai, A. Yamamoto, H. Yoshitsu and M. Sugiyama, *J. Biol. Chem.*, 2006, **281**, 8981-8990.

71. J. L. Cole, L. Avigliano, L. Morpurgo and E. I. Solomon, *J. Am. Chem. Soc.*, 1991, **113**, 9080-9089.

72. J. P. Collman, N. K. Devaraj, R. A. Decréau, Y. Yang, Y.-L. Yan, W. Ebina, T. A. Eberspacher and C. E. D. Chidsey, *Science*, 2007, **315**, 1565-1568.

73. J. A. Halfen, S. Mahapatra, E. C. Wilkinson, S. Kaderli, V. G. Young, L. Que, A. D. Zuberbühler and W. B. Tolman, *Science*, 1996, **271**, 1397-1400.

74. V. Mahadevan, R. J. M. K. Gebbink and T. D. P. Stack, *Curr. Opin. Chem. Biol.*, 2000, **4**, 228-234.

75. A. John, M. M. Shaikh and P. Ghosh, *Dalton Trans.*, 2008, 2815-2824.

76. L. Que and W. B. Tolman, *Nature*, 2008, **455**, 333-340.

77. J. W. Whittaker, *Chem. Rev.*, 2003, **103**, 2347-2364.

78. S. Torelli, C. Belle, S. Hamman, J.-L. Pierre and E. Saint-Aman, *Inorg. Chem.*, 2002, **41**, 3983-3989.

79. L. M. Mirica, M. Vance, D. J. Rudd, B. Hedman, K. O. Hodgson, E. I. Solomon and T. D. P. Stack, *Science*, 2005, **308**, 1890-1892.

80. D. E. Wilcox, A. G. Porras, Y. T. Hwang, K. Lerch, M. E. Winkler and E. I. Solomon, *J. Amer. Chem. Soc.*, 1985, **107**, 4015-4027.

81. K. Yoshizawa and Y. Shiota, *J. Am. Chem. Soc.*, 2006, **128**, 9873-9881.

82. R. L. Lieberman and A. C. Rosenzweig, *Dalton Trans.*, 2005, 3390-3396.

83. E. I. Solomon, U. M. Sundaram and T. E. Machonkin, *Chem. Rev.*, 1996, **96**, 2563-2606.

84. C. Eicken, B. Krebs and J. C. Sacchettini, *Curr. Opin. Struc. Biol.*, 1999, **9**, 677-683.

85. R. Balasubramanian and A. C. Rosenzweig, *Acc. Chem. Res.*, 2007, **40**, 573-580.

86. P. McMorn and G. J. Hutchings, *Chem. Soc. Rev.*, 2004, **33**, 108-122.

87. I. W. C. E. Arends, R. A. Sheldon, M. Wallau and U. Schuchardt, *Angew. Chem. Int. Ed.*, 1997, **36**, 1144-1163.

88. R. Hutter, T. Mallat and A. Baiker, *J. Catal.*, 1995, **153**, 177-189.

89. L. Liu, D. Ma, H. Chen, H. Zheng, M. Cheng, Y. Xu and X. Bao, *Catal. Lett.*, 2006, **108**, 25-30.

90. M. K. Song, J. S. Kim and K. T. No, *Appl. Surf. Sci.*, 2007, **253**, 5696-5700.

91. K. O. Xavier, J. Chacko and K. K. Mohammed Yusuff, *Appl. Catal., A*, 2004, **258**, 251-259.

92. I. L. V. Rosa, C. M. C. P. Manso, O. A. Serra and Y. Iamamoto, *J. Mol. Catal. A: Chem.*, 2000, **160**, 199-208.

93. J. Huang, Y. Jiang, V. R. R. Marthala, B. Thomas, E. Romanova and M. Hunger, *J. Phys. Chem. C*, 2008, **112**, 3811-3818.

94. K. Houthoofd, P. J. Grobet and P. A. Jacobs, *J. Phys. Chem. B*, 2008, **112**, 9630-9640.

95. D. E. De Vos, B. F. Sels and P. A. Jacobs, *CATTECH*, 2002, **6**, 14-29.

96. B. M. Weckhuysen, A. A. Verberckmoes, L. Fu and R. A. Schoonheydt, *J. Phys. Chem.*, 1996, **100**, 9456-9461.

97. O. Bortnovsky, Z. Sobalík and B. Wichterlová, *Microporous Mesoporous Mater.*, 2001, **46**, 265-275.

98. R. Ferreira, M. Silva, C. Freire, B. de Castro and J. L. Figueiredo, *Microporous Mesoporous Mater.*, 2000, **38**, 391-401.

99. C. R. Jacob, S. P. Varkey and P. Ratnasamy, *Appl. Catal., A*, 1998, **168**, 353-364.

100. A. A. Valente and J. Vital, *J. Mol. Catal.*, 2000, **156**, 163-172.

101. O. L. Kaliya, E. A. Lukyanets and G. N. Vorozhtsov, *J. Porphyrins Phthalocyanines*, 1999, **3**, 592-610.

102. J. Dzierzak, E. Bottinelli, G. Berlier, E. Gianotti, E. Stulz, R. M. Kowalczyk and R. Raja, *Chem. Comm.*, 2010, **46**, 2805-2807.

103. K. J. Balkus, A. G. Gabrielov, S. L. Bell, F. Bedioui, L. Roue and J. Devynck, *Inorg. Chem.*, 1994, **33**, 67-72.

104. D. J. Xuereb and R. Raja, *Catal. Sci. Technol.*, 2011, **1**, 517-534.

105. F. Bedioui, *Coord. Chem. Rev.*, 1995, **144**, 39-68.

106. M. R. Maurya, A. Kumar and J. Costa Pessoa, *Coord. Chem. Rev.*, 2011, **255**, 2315-2344.

107. R. Naik, P. Joshi and R. K. Deshpande, *Catal. Commun.*, 2004, **5**, 195-198.

108. R. A. Sheldon, I. W. C. E. Arends and H. E. B. Lempers, *Catal. Today*, 1998, **41**, 387-407.

109. R. F. Parton, I. F. J. Vankelecom, M. J. A. Casselman, C. P. Bezoukhanova, J. B. Uytterhoeven and P. A. Jacobs, *Nature*, 1994, **370**, 541-544.

110. R. F. Parton, P. E. Neys, P. A. Jacobs, R. C. Sosa and P. G. Rouxhet, *J. Catal.* , 1996, **164**, 341-346.

111. A. B. Sorokin and A. Tuel, *Catal. Today* 2000, **57**, 45-59.

112. N. Grootboom and T. Nyokong, *J. Mol. Catal. A: Chem.*, 2002, **179**, 113-123.

113. E. Armengol, A. Corma, V. Fornés, H. García and J. Primo, *Appl. Catal., A*, 1999, **181**, 305-312.

114. K. J. Balkus, M. Eissa and R. Levado, *J. Am. Chem. Soc.*, 1995, **117**, 10753-10754.

115. M. Nakamura, *Coord. Chem. Rev.*, 2006, **250**, 2271-2294.

116. B.-Z. Zhan and X.-Y. Li, *Chem. Commun.*, 1998, 349-350.

117. M. Grinstaff, M. Hill, J. Labinger and H. Gray, *Science*, 1994, **264**, 1311-1313.

118. Q. H. Xia, H. Q. Ge, C. P. Ye, Z. M. Liu and K. X. Su, *Chem. Rev.*, 2005, **105**, 1603-1662.

119. C. R. Jacob, S. P. Varkey and P. Ratnasamy, *Microporous Mesoporous Mater.*, 1998, **22**, 465-474.

120. M. J. Sabater, A. Corma, A. Domenech, V. Fornes and H. Garcia, *Chem. Commun.*, 1997, 1285-1286.

121. C. R. Jacob, S. P. Varkey and P. Ratnasamy, *Appl. Catal., A*, 1999, **182**, 91-96.

122. R. J. Corrêa, G. C. Salomão, M. H. N. Olsen, L. C. Filho, V. Drago, C. Fernandes and O. A. C. Antunes, *Appl. Catal., A*, 2008, **336**, 35-39.

123. R. Raja and P. Ratnasamy, *J. Catal.*, 1997, **170**, 244-253.

124. M. Salavati-Niasari, *Microporous Mesoporous Mater.*, 2006, **95**, 248-256.

125. R. Raja and P. Ratnasamy, *Catal. Lett.*, 1997, **48**, 1-10.

126. F. C. Skrobot, I. L. V. Rosa, A. P. A. Marques, P. R. Martins, J. Rocha, A. A. Valente and Y. Iamamoto, *J. Mol. Catal. A: Chem.*, 2005, **237**, 86-92.

127. C. Jin, W. Fan, Y. Jia, B. Fan, J. Ma and R. Li, *J. Mol. Catal. A: Chem.*, 2006, **249**, 23-30.

128. X. Yun, X. Hu, Z. Jin, J. Hu, C. Yan, J. Yao and H. Li, *J. Mol. Catal. A: Chem.*, 2010, **327**, 25-31.

129. Y. Yang, Y. Zhang, S. Hao and Q. Kan, *Chem. Eng. J.*, 2011, **171**, 1356-1366.

130. B. M. Weckhuysen, A. A. Verberckmoes, I. P. Vannijvel, J. A. Pelgrims, P. L. Buskens, P. A. Jacobs and R. A. Schoonheydt, *Angew. Chem. Int. Ed.*, 1996, **34**, 2652-2654.

131. R. Grommen, P. Manikandan, Y. Gao, T. Shane, J. J. Shane, R. A. Schoonheydt, B. M. Weckhuysen and D. Goldfarb, *J. Am. Chem. Soc.*, 2000, **122**, 11488-11496.

132. J. G. Mesu, T. Visser, F. Soulimani, E. E. van Faassen, P. de Peinder, A. M. Beale and B. M. Weckhuysen, *Inorg. Chem.*, 2006, **45**, 1960-1971.

133. J. G. Mesu, T. Visser, A. M. Beale, F. Soulimani and B. M. Weckhuysen, *Chem. Eur. J.*, 2006, **12**, 7167-7177.

134. D. Baute, D. Arieli, F. Neese, H. Zimmermann, B. M. Weckhuysen and D. Goldfarb, *J. Am. Chem. Soc.*, 2004, **126**, 11733-11745.

135. X. S. Zhao, G. Q. Lu and G. J. Millar, *Ind. Eng. Chem. Res.*, 1996, **35**, 2075-2090.

136. C. J. H. Jacobsen, C. Madsen, J. Houzvicka, I. Schmidt and A. Carlsson, *J. Am. Chem. Soc.*, 2000, **122**, 7116-7117.

137. A. Sayari and S. Hamoudi, *Chem. Mater.*, 2001, **13**, 3151-3168.

138. K. Ariga, A. Vinu, J. P. Hill and T. Mori, *Coord. Chem. Rev.*, 2007, **251**, 2562-2591.

139. M. H. Valkenberg and W. F. Hölderich, *Catal. Rev.*, 2002, **44**, 321-374.

140. J. H. Clark and D. J. Macquarrie, *Chem. Commun.*, 1998, 853-860.

141. P. M. Price, J. H. Clark and D. J. Macquarrie, *J. Chem. Soc., Dalton Trans.*, 2000, 101-110.

142. A. P. Wight and M. E. Davis, *Chem. Rev.*, 2002, **102**, 3589-3614.

143. Y. Hayashi, T. Sumiya, J. Takahashi, H. Gotoh, T. Urushima and M. Shoji, *Angew. Chem. Int. Ed.*, 2006, **45**, 958-961.

144. N. Mase, Y. Nakai, N. Ohara, H. Yoda, K. Takabe, F. Tanaka and C. F. Barbas, *J. Am. Chem. Soc.*, 2005, **128**, 734-735.

145. F. Guillier, D. Orain and M. Bradley, *Chem. Rev.*, 2000, **100**, 2091-2158.

146. F. Calderón, R. Fernández, F. Sánchez and A. Fernández-Mayoralas, 2005, **347**, 1395-1403.

147. C. R. Nakaie, E. Oliveira, E. F. Vicente, G. N. Jubilut, S. E. G. Souza, R. Marchetto and E. M. Cilli, *Bioorg. Chem.*, 2011, **39**, 101-109.

148. A. Walcarius, M. Etienne and B. Lebeau, *Chem. Mater.*, 2003, **15**, 2161-2173.

149. H. Yang, G. Zhang, X. Hong and Y. Zhu, *Microporous Mesoporous Mater.*, 2004, **68**, 119-125.

150. M. Luechinger, R. Prins and G. D. Pirngruber, *Microporous Mesoporous Mater.*, 2005, **85**, 111-118.

151. R. B. Merrifield, *J. Am. Chem. Soc.*, 1963, **85**, 2149-2154.

152. G. B. Fields and R. L. Noble, *Int. J. Pept. Protein Res.*, 1990, **35**, 161-214.

153. G. Mez'o, N. Mihala, G. Kóczán and F. Hudecz, *Tetrahedron*, 1998, **54**, 6757-6766.

154. C. G. Fields, D. H. Lloyd, R. L. Macdonald, K. M. Otteson and R. L. Noble, *Peptide Res.*, 1991, **4**, 95-101.

155. G. D. Pirngruber, L. Frunz and M. Luchinger, *Phys. Chem. Chem. Phys.*, 2009, **11**, 2928-2938.

156. L. Frunz, R. Prins and G. D. Pirngruber, *Chem. Mater.*, 2007, **19**, 4357-4366.

157. M. Luechinger, A. Kienhöfer and G. D. Pirngruber, *Chem. Mater.*, 2006, **18**, 1330-1336.

158. A. D. Baxter, *Curr. Opin. Chem. Biol.*, 1997, **1**, 79-85.

159. D. Font, C. Jimeno and M. A. Pericas, *Org. Lett.*, 2006, **8**, 4653-4655.

160. Z. P. Demko and K. B. Sharpless, *Angew. Chem. Int. Ed.*, 2002, **114**, 2214-2217.

161. V. V. Rostovtsev, L. G. Green, V. V. Fokin and K. B. Sharpless, *Angew. Chem. Int. Ed.*, 2002, **41**, 2596-2599.

162. H. C. Kolb, M. G. Finn and K. B. Sharpless, *Angew. Chem. Int. Ed.*, 2001, **40**, 2004-2021.

163. M. Gruttadauria, A. M. P. Salvo, F. Giacalone, P. Agrigento and R. Noto, *Eur. J. Org. Chem.*, 2009, **2009**, 5437-5444.

164. J. Wang, H. Li, Y. Mei, B. Lou, D. Xu, D. Xie, H. Guo and W. Wang, *J. Org. Chem.*, 2005, **70**, 5678-5687.

165. B. List, *J. Am. Chem. Soc.*, 2002, **124**, 5656-5657.

166. B. List, P. Pojarliev and C. Castello, *Org. Lett.*, 2001, **3**, 573-575.

167. V. B. Valodkar, G. L. Tembe, M. Ravindranathan and H. S. Rama, *J. Mol. Catal. A: Chem.*, 2004, **223**, 31-38.

168. V. B. Valodkar, G. L. Tembe, M. Ravindranathan, R. N. Ram and H. S. Rama, *J. Mol. Catal. A: Chem.*, 2004, **208**, 21-32.

169. J. E. Krohn and M. Tsapatsis, *Langmuir*, 2006, **22**, 9350-9356.

170. J. E. Krohn and M. Tsapatsis, *Langmuir*, 2005, **21**, 8743-8750.

171. O. Yamauchi, A. Odani and M. Takani, *J. Chem. Soc., Dalton Trans.*, 2002, 3411-3421.

172. E. Mateo Marti, S. M. Barlow, S. Haq and R. Raval, *Surf. Sci.*, 2002, **501**, 191-202.

173. A. M. Sapse, L. Mallah-Levy, S. B. Daniels and B. W. Erickson, *J. Am. Chem. Soc.*, 1987, **109**, 3526-3529.

174. S. Pandiarajan, M. Umadevi, V. Sasirekha, R. K. Rajaram and V. Ramakrishnan, *J. Raman Spectrosc.*, 2005, **36**, 950-961.

175. T. Darbre and M. Machuqueiro, *Chem. Commun.*, 2003, 1090-1091.

176. S. Bahmanyar, K. N. Houk, H. J. Martin and B. List, *J. Am. Chem. Soc.*, 2003, **125**, 2475-2479.

177. L. Hoang, S. Bahmanyar, K. N. Houk and B. List, *J. Am. Chem. Soc.*, 2002, **125**, 16-17.

178. W. Bao and Z. Wang, *Green Chem.*, 2006, **8**, 1028-1033.

179. S. Brunauer, P. H. Emmett and E. Teller, *J. Am. Chem. Soc.*, 1938, **60**, 309-319.

180. A. W. Herlinger and T. V. Long, *J. Amer. Chem. Soc.*, 1970, **92**, 6481-6486.

181. S. G. Stepanian, I. D. Reva, E. D. Radchenko and L. Adamowicz, *J. Phys. Chem. A*, 2001, **105**, 10664-10672.

182. E. Mateo Marti, S. M. Barlow, S. Haq and R. Raval, *Surf. Sci.*, 2002, **501**, 191-202.

183. S. Bordiga, R. Buzzoni, F. Geobaldo, C. Lamberti, E. Giamello, A. Zecchina, G. Leofanti, G. Petrini, G. Tozzola and G. Vlaic, *J. Catal.*, 1996, **158**, 486-501.

184. E. A. Zhilinskaya, G. Delahay, M. Mauvezin, B. Coq and A. Aboukaïs, *Langmuir*, 2003, **19**, 3596-3602.

185. N. B. Castagnola and P. K. Dutta, *J. Phys. Chem. B,*, 1998, **102**, 1696-1702.

186. J. Sebastian, S. A. Peter and R. V. Jasra, *Langmuir*, 2005, **21**, 11220-11225.

187. A. Singh, N. Torita, S. Shylesh, N. Iwasa and M. Arai, *Catal. Lett.*, 2009, **132**, 492-499.

188. G. Bellussi and C. Perego, *CATTECH*, 2000, **4**, 4-16.

189. J. J. Pignatello, E. Oliveros and A. MacKay, *Crit. Rev. Env. Sci. Technol.*, 2006, **36**, 1-84.

190. R. D. Bach and O. Dmitrenko, *J. Org. Chem.*, 2010, **75**, 3705-3714.

191. G. John T, *J. Inorg. Biochem.*, 2006, **100**, 434-447.

192. R. Gonzalez-Olmos, F. Holzer, F. D. Kopinke and A. Georgi, *Appl. Catal., A*, 2011, **398**, 44-53.

193. G. Centi, S. Perathoner, T. Torre and M. G. Verduna, *Catal. Today*, 2000, **55**, 61-69.

194. L. Que and Y. Watanabe, *Science*, 2001, **292**, 651-653.

195. X. Shan and L. Que Jr, *J. Inorg. Biochem.*, 2006, **100**, 421-433.

196. G. Roelfes, M. Lubben, R. Hage, J. L. Que and B. L. Feringa, *Chem. Eur. J.*, 2000, **6**, 2152-2159.

197. M. Sono, M. P. Roach, E. D. Coulter and J. H. Dawson, *Chem. Rev.*, 1996, **96**, 2841-2888.

198. D. H. R. Barton, V. N. Le Gloahec, H. Patin and F. Launay, *New J. Chem.*, 1998, **22**, 559-563.

199. D. H. R. Barton, V. N. Le Gloahec and H. Patin, *New J. Chem.*, 1998, **22**, 565-568.

200. J. Kim, R. G. Harrison, C. Kim and L. Que, *J. Am. Chem. Soc.*, 1996, **118**, 4373-4379.

201. A. Sorokin, A. Robert and B. Meunier, *J. Am. Chem. Soc.*, 1993, **115**, 7293-7299.

202. G.-J. t. Brink, I. W. C. E. Arends and R. A. Sheldon, *Science*, 2000, **287**, 1636-1639.

203. M. J. Schultz, R. S. Adler, W. Zierkiewicz, T. Privalov and M. S. Sigman, *J. Am. Chem. Soc.*, 2005, **127**, 8499-8507.

204. U. R. Pillai and E. Sahle-Demessie, *Appl. Catal., A*, 2003, **245**, 103-109.

205. B.-Z. Zhan and A. Thompson, *Tetrahedron*, 2004, **60**, 2917-2935.

206. T. Mallat and A. Baiker, *Chem. Rev.*, 2004, **104**, 3037-3058.

207. A. Abad, P. Concepción, A. Corma and H. García, *Angew. Chem. Int. Ed.*, 2005, **44**, 4066-4069.

208. H. Hong, L. Hu, M. Li, J. Zheng, X. Sun, X. Lu, X. Cao, J. Lu and H. Gu, *Chem. Eur. J.*, 2011, **17**, 8726-8730.

209. K. Mori, T. Hara, T. Mizugaki, K. Ebitani and K. Kaneda, *J. Am.Chem. Soc.*, 2004, **126**, 10657-10666.

210. Q. Fu, H. Saltsburg and M. Flytzani-Stephanopoulos, *Science*, 2003, **301**, 935-938.

211. D. I. Enache, D. W. Knight and G. J. Hutchings, *Catal. Lett.*, 2005, **103**, 43-52.

212. R. A. Sheldon, I. W. C. E. Arends and A. Dijksman, *Catal. Today*, 2000, **57**, 157-166.

213. T. Naota, H. Takaya and S.-I. Murahashi, *Chem. Rev.*, 1998, **98**, 2599-2660.

214. N. Koukabi, E. Kolvari, A. Khazaei, M. A. Zolfigol, B. Shirmardi-Shaghasemi and H. R. Khavasi, *Chem. Commun.*, 2011, **47**, 9230-9232.

215. F. Shi, M. K. Tse, M.-M. Pohl, A. Brückner, S. Zhang and M. Beller, *Angew. Chem. Int. Ed.*, 2007, **46**, 8866-8868.

216. R. Ganesan and B. Viswanathan, *J. Mol. Catal. A: Chem.*, 2002, **181**, 99-107.

217. S. Rani and B. R. Bhat, *Tetrahedron Lett.*, 2010, **51**, 6403-6405.

218. H. Han, S. Zhang, H. Hou, Y. Fan and Y. Zhu, *Eur. J. Inorg. Chem.*, 2006, **2006**, 1594-1600.

219. N. Y. Oh, Y. Suh, M. J. Park, M. S. Seo, J. Kim and W. Nam, *Angew. Chem. Int. Ed.*, 2005, **117**, 4307-4311.

220. O. Pestovsky and A. Bakac, *J. Am. Chem. Soc.*, 2004, **126**, 13757-13764.

221. J. H. Han, S.-K. Yoo, J. S. Seo, S. J. Hong, S. K. Kim and C. Kim, *Dalton Trans.*, 2005, 402-406.

222. M. S. Seo, T. Kamachi, T. Kouno, K. Murata, M. J. Park, K. Yoshizawa and W. Nam, *Angew. Chem. Int. Ed.*, 2007, **46**, 2291-2294.

223. R. Mas-Ballesté and L. Que, *J. Am. Chem. Soc.*, 2007, **129**, 15964-15972.

224. J. Kaizer, E. J. Klinker, N. Y. Oh, J.-U. Rohde, W. J. Song, A. Stubna, J. Kim, E. Münck, W. Nam and L. Que, . *Am. Chem. Soc.*, 2003, **126**, 472-473.

225. J. Yoon, S. A. Wilson, Y. K. Jang, M. S. Seo, K. Nehru, B. Hedman, K. O. Hodgson, E. Bill, E. I. Solomon and W. Nam, *Angew. Chem. Int. Ed.*, 2009, **48**, 1257-1260.

226. E. J. Baran, I. Viera and M. H. Torre, *Spectrochim. Acta, Part A*, 2007, **66**, 114-117.

227. S. Sugiyama, S. Yamamoto, O. Matsuoka, H. Nozoye, J. Yu, G. Zhu, S. Qiu and O. Terasaki, *Microporous Mesoporous Mater.*, 1999, **28**, 1-7.

228. V. Alfredsson, T. Ohsuna, O. Terasaki and J.-O. Bovin, *Angew. Chem. Int. Ed.*, 1993, **32**, 1210-1213.

229. X. Feng, G. E. Fryxell, L.-Q. Wang, A. Y. Kim, J. Liu and K. M. Kemner, *Science*, 1997, **276**, 923-926.

230. A. W. Herlinger, S. L. Wenhold and T. V. Long, *J. Amer. Chem. Soc.*, 1970, **92**, 6474-6481.

231. A. L. Jenkins, R. A. Larsen and T. B. Williams, *Spectrochim. Acta, Part A*, 2005, **61**, 1585-1594.

232. A. Kogelbauer, J. G. Goodwin and J. A. Lercher, *J. Phys. Chem.*, 1995, **99**, 8777-8781.

233. T. Ikeda, F. Izumi, T. Kodaira and T. Kamiyama, *Chem. Mater.*, 1998, **10**, 3996-4004.

234. J. Evans, A. B. Zaki, M. Y. El-Sheikh and S. A. El-Safty, *J. Phys. Chem. B*, 2000, **104**, 10271-10281.

235. A. Firouzi, F. Atef, A. G. Oertli, G. D. Stucky and B. F. Chmelka, *J. Am. Chem. Soc.*, 1997, **119**, 3596-3610.

236. C.-Y. Chen, S. L. Burkett, H.-X. Li and M. E. Davis, *Microporous Mater.*, 1993, **2**, 27-34.

237. D. Wei, H. Wang, X. Feng, W.-T. Chueh, P. Ravikovitch, M. Lyubovsky, C. Li, T. Takeguchi and G. L. Haller, *J. Phys. Chem. B*, 1999, **103**, 2113-2121.

238. R. Linder, M. Nispel, T. Häber and K. Kleinermanns, *Chem. Phys. Lett.*, 2005, **409**, 260-264.

239. S. Pandiarajan, M. Umadevi, R. K. Rajaram and V. Ramakrishnan, *Spectrochim. Acta, Part A*, 2005, **62**, 630-636.

240. N. Beznis, B. Weckhuysen and J. Bitter, *Catal. Lett.*, 2010, **138**, 14-22.

241. M. Jia, A. Seifert and W. R. Thiel, *Chem. Mater.*, 2003, **15**, 2174-2180.

242. I. E. Markó, A. Gautier, R. Dumeunier, K. Doda, F. Philippart, S. M. Brown and C. J. Urch, *Angew. Chem. Int. Ed.*, 2004, **43**, 1588-1591.

243. I. E. Markó, P. R. Giles, M. Tsukazaki, I. Chellé-Regnaut, A. Gautier, S. M. Brown and C. J. Urch, *J. Org. Chem.*, 1999, **64**, 2433-2439.

244. Y. Wang, J. L. DuBois, B. Hedman, K. O. Hodgson and T. D. P. Stack, *Science*, 1998, **279**, 537-540.

245. M. Zhu, B. Li, P. He, X. Wei and Y. Yuan, *Tetrahedron*, 2008, **64**, 9239-9243.

246. C. Michel, P. Belanzoni, P. Gamez, J. Reedijk and E. J. Baerends, *Inorg. Chem.*, 2009, **48**, 11909-11920.

247. J.-L. Pierre and F. Thomas, *C. R. Chimie*, 2005, **8**, 65-74.

248. P. M. Polestshuk and T. V. Magdesieva, *Inorg. Chem.*, 2010, **49**, 3370-3386.

249. R. A. Sheldon, I. W. C. E. Arends, G.-J. ten Brink and A. Dijksman, *Acc. Chem. Res.*, 2002, **35**, 774-781.

250. P. Gamez, I. W. C. E. Arends, R. A. Sheldon and J. Reedijk, *Adv. Synth. Catal.*, 2004, **346**, 805-811.

251. G. Rothenberg, L. Feldberg, H. Wiener and Y. Sasson, *J. Chem. Soc., Perkin Trans. 2*, 1998, 2429-2434.

252. K. O. Xavier, J. Chacko and K. K. Mohammed Yusuff, *J. Mol. Catal. A: Chem.*, 2002, **178**, 275-281.

253. T. Chattopadhyay, M. Kogiso, M. Asakawa, T. Shimizu and M. Aoyagi, *Catal. Commun.*, 2010, **12**, 9-13.

254. G. Centi, *Catal. Lett.*, 1993, **22**, 53-66.

255. P. Karandikar, M. Agashe, K. Vijayamohanan and A. J. Chandwadkar, *Appl. Catal., A*, 2004, **257**, 133-143.

256. G. Grigoropoulou, J. H. Clark and J. A. Elings, *Green Chem.*, 2003, **5**, 1-7.

257. B. S. Lane and K. Burgess, *Chem. Rev.*, 2003, **103**, 2457-2474.

258. M. S. Chen and M. C. White, *J. Am. Chem. Soc.*, 2004, **126**, 1346-1347.

259. J. H. Delcamp and M. C. White, *J. Am. Chem. Soc.*, 2006, **128**, 15076-15077.

260. T. Punniyamurthy and L. Rout, *Coord. Chem. Rev.*, 2008, **252**, 134-154.

261. F. V. Singh, J. M. Pena and H. A. Stefani, *Tetrahedron Lett.*, 2010, **51**, 1671-1673.

262. T. K. M. Shing, Yeung and P. L. Su, *Org. Lett.*, 2006, **8**, 3149-3151.

263. R. A. Sheldon, M. Wallau, I. W. C. E. Arends and U. Schuchardt, *Acc. Chem. Res.*, 1998, **31**, 485-493.

264. J. Dakka and H. Goris, *Catal. Lett.*, 2006, **117**, 265-270.

265. M. Ghadiri, F. Farzaneh, M. Ghandi and M. Alizadeh, *J. Mol. Catal. A: Chem.*, 2005, **233**, 127-131.

266. N. Sehlotho and T. Nyokong, *J. Mol. Catal. A: Chem.*, 2004, **209**, 51-57.

267. D. M. Boghaei, A. Bezaatpour and M. Behzad, *J. Mol. Catal. A: Chem.*, 2006, **245**, 12-16.

268. V. G. Dryuk, *Tetrahedron*, 1976, **32**, 2855-2866.

269. A. H. Hoveyda, D. A. Evans and G. C. Fu, *Chem. Rev.*, 1993, **93**, 1307-1370.

270. A. Corma, M. Domine, J. A. Gaona, J. L. Jorda, M. T. Navarro, F. Rey, J. Perez-Pariente, J. Tsuji, B. McCulloch and L. T. Nemeth, *Chem. Commun.*, 1998, 2211-2212.

271. G. A. Barf and R. A. Sheldon, *J. Mol. Catal. A: Chem.*, 1995, **102**, 23-39.

272. F. Figueras and H. Kochkar, *Catal. Lett.*, 1999, **59**, 79-81.

273. M. A. Camblor, A. Corma, P. Esteve, A. Martinez and S. Valencia, *Chem. Commun.*, 1997, 795-796.

274. R. Mbeleck, K. Ambroziak, B. Saha and D. C. Sherrington, *React. Funct. Polym.*, 2007, **67**, 1448-1457.

275. J. G. Hill, B. E. Rossiter and K. B. Sharpless, *J. Org. Chem.*, 1983, **48**, 3607-3608.

276. S. Khare and S. Shrivastava, *J. Mol. Catal. A: Chem.*, 2004, **217**, 51-58.

277. S. D.C, *Catal. Today*, 2000, **57**, 87-104.

278. D. Chatterjee and A. Mitra, *J. Mol. Catal. A: Chem.*, 1999, **144**, 363-367.

279. B. Coq and F. Figueras, *J. Mol. Catal. A: Chem.*, 2001, **173**, 117-134.

280. L. Saikia and D. Srinivas, *Catal. Today*, 2009, **141**, 66-71.

281. L. Saikia, D. Srinivas and P. Ratnasamy, *Microporous Mesoporous Mater.*, 2007, **104**, 225-235.

282. L. Chmielarz, P. Kuśtrowski, A. Rafalska-Łasocha and R. Dziembaj, *Appl. Catal., B*, 2005, **58**, 235-244.

283. G. Olason and D. C. Sherrington, *React. Funct. Polym.*, 1999, **42**, 163-172.

284. A. Bravo, H.-R. Bjorsvik, F. Fontana, L. Liguori and F. Minisci, *J. Org. Chem.*, 1997, **62**, 3849-3857.

285. E. C. McLaughlin, H. Choi, K. Wang, G. Chiou and M. P. Doyle, *J. Org. Chem.*, 2008, **74**, 730-738.

286. P. D. Bartlett and P. Günther, *J. Am. Chem. Soc.*, 1966, **88**, 3288-3294.

287. S. Miyamoto, G. R. Martinez, M. H. G. Medeiros and P. Di Mascio, *J. Am. Chem. Soc.*, 2003, **125**, 6172-6179.

288. D. W. Snelgrove, J. Lusztyk, J. T. Banks, P. Mulder and K. U. Ingold, *J. Am. Chem. Soc.*, 2000, **123**, 469-477.

289. J.-Q. Yu and E. J. Corey, *J. Am. Chem. Soc.*, 2003, **125**, 3232-3233.

290. H. Choi and M. P. Doyle, *Org. Lett.*, 2007, **9**, 5349-5352.

291. S. J. Blanksby and G. B. Ellison, *Acc. Chem. Res.*, 2003, **36**, 255-263.

292. J. W. Bozzelli and C. Sheng, *J. Phys. Chem. A*, 2002, **106**, 1113-1121.

293. A. J. Catino, R. E. Forslund and M. P. Doyle, *J. Am. Chem. Soc.*, 2004, **126**, 13622-13623.

294. W. Nam, H. J. Kim, S. H. Kim, R. Y. N. Ho and J. S. Valentine, *Inorg. Chem.*, 1996, **35**, 1045-1049.

295. J.-Q. Yu and E. J. Corey, *Org. Lett.*, 2002, **4**, 2727-2730.

296. R. Raja, J. M. Thomas, M. Greenhill-Hooper and V. Doukova, *Chem. Commun.*, 2007, 1924-1926.

297. R. Das and D. Chakraborty, *Tetrahedron Lett.*, 2010, **51**, 6255-6258.

298. M. C. Carreno, *Chem. Rev.*, 1995, **95**, 1717-1760.

299. K. Kaczorowska, Z. Kolarska, K. Mitka and P. Kowalski, *Tetrahedron*, 2005, **61**, 8315-8327.

300. R. Noyori, M. Aoki and K. Sato, *Chem. Commun.*, 2003, 1977-1986.

301. B. Karimi, M. Ghoreishi-Nezhad and J. H. Clark, *Org. Lett.*, 2005, **7**, 625-628.

302. Y. Wang, G. Lente and J. H. Espenson, *Inorg. Chem.*, 2002, **41**, 1272-1280.

303. R. S. Reddy, J. S. Reddy, R. Kumar and P. Kumar, *J. Chem. Soc., Chem. Commun.*, 1992, 84-85.

304. D. J. Robinson, L. Davies, N. McGuire, D. F. Lee, P. McMorn, D. J. Willock, G. W. Watson, P. C. Bulman Page, D. Bethell and G. J. Hutchings, *Phys. Chem. Chem. Phys.*, 2000, **2**, 1523-1529.

305. V. Hulea, P. Moreau and F. Di Renzo, *J. Mol. Catal. A: Chem.*, 1996, **111**, 325-332.

306. A. Chica, G. Gatti, B. Moden, L. Marchese and E. Iglesia, *Chem. Eur. J.*, 2006, **12**, 1960-1967.

307. R. Liu, L.-z. Wu, X.-m. Feng, Z. Zhang, Y.-z. Li and Z.-l. Wang, *Inorg. Chim. Acta*, 2007, **360**, 656-662.

308. J. E. Barker and T. Ren, *Tetrahedron Lett.*, 2004, **45**, 4681-4683.

309. A. Fuerte, M. Iglesias, F. Sánchez and A. Corma, *J. Mol. Catal. A: Chem.*, 2004, **211**, 227-235.

310. M. J. Alcón, A. Corma, M. Iglesias and F. Sánchez, *J. Mol. Catal. A: Chem.*, 2003, **194**, 137-152.

311. Y. Goto, T. Matsui, S.-i. Ozaki, Y. Watanabe and S. Fukuzumi, *J. Am. Chem. Soc.*, 1999, **121**, 9497-9502.

312. M. Taki, S. Itoh and S. Fukuzumi, *J. Am. Chem. Soc.*, 2002, **124**, 998-1002.

313. R. F. Parton, I. F. J. Vankelecom, D. Tas, K. B. M. Janssen, P.-P. Knops-Gerrits and P. A. Jacobs, *J. Mol. Catal. A: Chem.*, 1996, **113**, 283-292.

314. I. F. J. Vankelecom, R. F. Parton, M. J. A. Casselman, J. B. Uytterhoeven and P. A. Jacobs, *J. Catal.*, 1996, **163**, 457-464.

315. K. A. Vassell and J. H. Espenson, *Inorg. Chem.*, 1994, **33**, 5491-5498.

316. M. Ganesan, V. K. Sivasubramanian, S. Rajagopal and R. Ramaraj, *Tetrahedron*, 2004, **60**, 1921-1929.

317. E. Baciocchi, O. Lanzalunga and F. Marconi, *Tetrahedron Lett.*, 1994, **35**, 9771-9774.

318. Y. Yamaguchi, W. Ding, C. T. Sanderson, M. L. Borden, M. J. Morgan and C. Kutal, *Coord. Chem. Rev.*, 2007, **251**, 515-524.

319. K. Yamaguchi, K. Mori, T. Mizugaki, K. Ebitani and K. Kaneda, *J. Am. Chem. Soc.*, 2000, **122**, 7144-7145.

320. S. Mannam and G. Sekar, *Tetrahedron Lett.*, 2008, **49**, 2457-2460.

321. B. M. Weckhuysen and D. E. Keller, *Catal. Today*, 2003, **78**, 25-46.

322. N. Malumbazo and S. F. Mapolie, *J. Mol. Catal. A: Chem.*, 2009, **312**, 70-77.

323. Y. Chang, Y. Lv, F. Lu, F. Zha and Z. Lei, *J. Mol. Catal. A: Chem.*, 2010, **320**, 56-61.

324. M. Ghiaci, B. Aghabarari, A. M. Botelho do Rego, A. M. Ferraria and S. Habibollahi, *Appl. Catal., A*, 2011, **393**, 225-230.

325. S. E. Dapurkar, H. Kawanami, K. Komura, T. Yokoyama and Y. Ikushima, *Appl. Catal., A*, 2008, **346**, 112-116.

326. E. F. Murphy, T. Mallat and A. Baiker, *Catal. Today*, 2000, **57**, 115-126.

327. K. Chen, M. Costas, J. Kim, A. K. Tipton and L. Que, *J. Am. Chem. Soc.*, 2002, **124**, 3026-3035.

328. P. D. Oldenburg and J. L. Que, *Catal. Today*, 2006, **117**, 15-21.

329. A. Kumar, D. Srinivas and P. Ratnasamy, *Chem. Commun.*, 2009, 6484-6486.

330. J. Jarupatrakorn and T. D. Tilley, *J. Amer. Chem. Soc.*, 2002, **124**, 8380-8388.

331. D. Duraczynska, E. M. Serwicka, A. Drelinkiewicz and Z. Olejniczak, *Appl. Catal., A*, 2009, **371**, 166-172.

332. F. Hosseinpoor and H. Golchoubian, *Tetrahedron Lett.*, 2006, **47**, 5195-5197.

333. E. Baciocchi, M. F. Gerini and A. Lapi, *J. Org. Chem.*, 2004, **69**, 3586-3589.

334. V. K. Sivasubramanian, M. Ganesan, S. Rajagopal and R. Ramaraj, *J. Org. Chem.*, 2002, **67**, 1506-1514.

335. A. M. I. Jayaseeli and S. Rajagopal, *J. Mol. Catal. A: Chem.*, 2009, **309**, 103-110.

336. G. Li, L. Chen, J. Bao, T. Li and F. Mei, *Appl. Catal., A*, 2008, **346**, 134-139.

337. M. Müller, G. Harvey and R. Prins, *Microporous Mesoporous Mater.*, 2000, **34**, 281-290.

338. M. Kovalakova, B. H. Wouters and P. J. Grobet, *Microporous Mesoporous Mater.*, 1998, **22**, 193-201.

339. M. H. Groothaert, K. Lievens, H. Leeman, B. M. Weckhuysen and R. A. Schoonheydt, *J. Catal.*, 2003, **220**, 500-512.

340. R. Amorati, M. Lucarini, V. Mugnaini, G. F. Pedulli, F. Minisci, F. Recupero, F. Fontana, P. Astolfi and L. Greci, . *Org. Chem.*, 2003, **68**, 1747-1754.

341. M. Tada, R. Bal, T. Sasaki, Y. Uemura, Y. Inada, S. Tanaka, M. Nomura and Y. Iwasawa, *J. Phys. Chem. C*, 2007, **111**, 10095-10104.

342. A. Santos, P. Yustos, A. Quintanilla, S. Rodríguez and F. García-Ochoa, *Appl. Catal., B*, 2002, **39**, 97-113.

343. M. John R, *Appl. Catal., A*, 2001, **221**, 73-91.

344. M. Burgener, T. Tyszewski, D. Ferri, T. Mallat and A. Baiker, *Appl. Catal., A*, 2006, **299**, 66-72.

345. A. J. O'Connor, A. Hokura, J. M. Kisler, S. Shimazu, G. W. Stevens and Y. Komatsu, *Sep. Purif. Technol.*, 2006, **48**, 197-201.

346. F. Brackmann, H. Schill and A. de Meijere, *Chem. Eur. J.*, 2005, **11**, 6593-6600.

8. APPENDIX.

Table 8.1. CelRef analysis for Fe^{III}-Proline-X indexing of powder X-ray diffraction pattern.

CELREF Version 3.

Initial values : (Refinement keys on 2nd line)

Zero	Lambda	a	b	c	alpha	beta	gamma	Vol.
0	1.5406	24.345	24.345	24.345	90	90	90	14428.8
0	0	1	0	0	0	0	0	

Final values : (Standard errors on 2nd line)

Zero	Lambda	a	b	c	alpha	beta	gamma	Vol.
0	1.5406	24.5266	24.5266	24.5266	90	90	90	14754.1
0	0	0.0744	0	0	0	0	0	

H	K	L	2T(Obs)	2T-Zero	2Th(Cal)	Dif
1	1	1	6.26	6.26	6.2366	0.0234
0	2	2	10.2	10.2	10.1928	0.0072
1	1	3	11.96	11.96	11.958	0.002
3	1	3	15.74	15.74	15.7368	0.0032
3	3	3	18.78	18.78	18.7847	-0.0047
0	4	4	20.42	20.42	20.4673	-0.0473
2	0	6	22.86	22.86	22.9141	-0.0541
5	3	3	23.72	23.72	23.7699	-0.0499
4	4	4	25.06	25.06	25.1353	-0.0753
5	1	5	25.88	25.88	25.9221	-0.0421
6	2	4	27.14	27.14	27.1863	-0.0463
3	5	5	27.92	27.92	27.9194	0.0006
7	3	3	29.74	29.74	29.7931	-0.0531
0	6	6	30.84	30.84	30.9115	-0.0715
5	5	5	31.48	31.48	31.5654	-0.0854
0	4	8	32.52	32.52	32.629	-0.109
4	6	6	34.2	34.2	34.2696	-0.0696
4	6	6	34.78	34.78	34.2696	0.5104
7	3	7	37.98	37.98	37.9158	0.0642

Table 8.2. CelRef analysis for Zeolite X indexing of powder X-ray diffraction pattern.

CELREF Version 3.

Initial values : (Refinement keys on 2nd line)

Zero	Lambda	a	b	c	alpha	beta	gamma	Vol.
0	1.5406	24.345	24.345	24.345	90	90	90	14428.8
0	0	1	0	0	0	0	0	

Final values : (Standard errors on 2nd line)

Zero	Lambda	a	b	c	alpha	beta	gamma	Vol.
0	1.5406	24.5354	24.5354	24.5354	90	90	90	14770
0	0	0.1278	0	0	0	0	0	

H	K	L	2T(Obs)	2T-Zero	2Th(Cal)	Dif
1	1	1	6.26	6.26	6.2344	0.0256
0	2	2	10.22	10.22	10.1891	0.0309
1	1	3	11.94	11.94	11.9537	-0.0137
3	1	3	15.7	15.7	15.7312	-0.0312
3	3	3	18.76	18.76	18.7779	-0.0179
0	4	4	20.4	20.4	20.4599	-0.0599
2	0	6	22.88	22.88	22.9058	-0.0258
5	3	3	23.68	23.68	23.7613	-0.0813
5	1	5	25.84	25.84	25.9126	-0.0726
6	2	4	27.1	27.1	27.1764	-0.0764
3	5	5	27.84	27.84	27.9092	-0.0692
0	0	8	29.06	29.06	29.0927	-0.0327
0	6	6	30.84	30.84	30.9002	-0.0602
5	5	5	31.48	31.48	31.5538	-0.0738
0	4	8	32.52	32.52	32.617	-0.097
0	4	8	33.18	33.18	32.617	0.563
4	6	6	34.2	34.2	34.2569	-0.0569
4	6	6	34.78	34.78	34.2569	0.5231
7	3	7	37.98	37.98	37.9017	0.0783

Table 8.3. CelRef analysis for Cu^{II}-Valine LTA indexing of powder X-ray diffraction pattern.

CELREF Version 3.

Initial values : (Refinement keys on 2nd line)

Zero	Lambda	a	b	c	alpha	beta	gamma	Vol.
0	1.5406	24.61	24.61	24.61	90	90	90	14905.1
0	0	1	0	0	0	0	0	

Final values : (Standard errors on 2nd line)

Zero	Lambda	a	b	c	alpha	beta	gamma	Vol.
0	1.5406	24.4868	24.4868	24.4868	90	90	90	14682.4
0	0	0.0649	0	0	0	0	0	

H	K	L	2T(Obs)	2T-Zero	2Th(Cal)	Dif
0	0	2	7.2	7.2	7.2143	-0.0143
0	2	2	10.18	10.18	10.2094	-0.0294
2	2	2	12.48	12.48	12.5122	-0.0322
0	2	4	16.14	16.14	16.1748	-0.0348
2	2	4	17.88	17.88	17.7305	0.1495
4	0	4	20.5	20.5	20.501	-0.001
0	0	6	21.76	21.76	21.7593	0.0007
2	2	6	24.06	24.06	24.0885	-0.0285
4	0	6	26.24	26.24	26.2228	0.0172
2	4	6	27.22	27.22	27.2314	-0.0114
2	0	8	30.04	30.04	30.0698	-0.0298
2	2	8	30.96	30.96	30.9631	-0.0031
0	4	8	32.64	32.64	32.6836	-0.0436
2	4	8	33.48	33.48	33.5142	-0.0342
4	6	6	34.3	34.3	34.327	-0.027
4	4	8	35.96	35.96	35.9042	0.0558
0	0	10	36.64	36.64	36.6706	-0.0306
2	0	10	37.44	37.44	37.4235	0.0165

Table 8.4. CelRef analysis for Zeolite LTA indexing of powder X-ray diffraction pattern.

CELREF Version 3.

Initial values : (Refinement keys on 2nd line)

Zero	Lambda	a	b	c	alpha	beta	gamma	Vol.
0	1.5406	24.61	24.61	24.61	90	90	90	14905.1
0	0	1	0	0	0	0	0	

Final values : (Standard errors on 2nd line)

Zero	Lambda	a	b	c	alpha	beta	gamma	Vol.
0	1.5406	24.3555	24.3555	24.3555	90	90	90	14447.5
0	0	0.132	0	0	0	0	0	

H	K	L	2T(Obs)	2T-Zero	2Th(Cal)	Dif
0	0	2	7.44	7.44	7.2533	0.1867
0	2	2	10.44	10.44	10.2646	0.1754
2	2	2	12.72	12.72	12.58	0.14
0	2	4	16.38	16.38	16.2626	0.1174
2	2	4	17.92	17.92	17.8269	0.0931
4	0	4	20.68	20.68	20.6127	0.0673
0	0	6	21.92	21.92	21.8781	0.0419
2	0	6	23.12	23.12	23.0773	0.0427
2	2	6	24.24	24.24	24.2204	0.0196
4	0	6	26.4	26.4	26.3667	0.0333
2	4	6	27.38	27.38	27.3811	-0.0011
2	0	8	30.22	30.22	30.2358	-0.0158
2	2	8	31.12	31.12	31.1343	-0.0143
0	4	8	32.8	32.8	32.8648	-0.0648
2	4	8	33.66	33.66	33.7003	-0.0403
4	6	6	34.44	34.44	34.5179	-0.0779
4	4	8	36.02	36.02	36.1045	-0.0845
0	0	10	36.76	36.76	36.8755	-0.1155
2	2	10	38.26	38.26	38.3775	-0.1175

Table 8.5. Crystal data and structure refinement details for Cu^{II}-Valine complex.

Identification code	**2009sot1101**	
Empirical formula	$C_{10}H_{20}CuN_2O_4$	
Formula weight	295.82	
Temperature	120(2) K	
Wavelength	0.71069 Å	
Crystal system	Triclinic	
Space group	*P*1	
Unit cell dimensions	a = 4.8730(3) Å	α = 100.395(4)°
	b = 5.2030(3) Å	β = 90.326(4)°
	c = 12.1440(9) Å	γ = 100.118(4)°
Volume	297.92(3) $Å^3$	
Z	1	
Density (calculated)	1.649 Mg / m^3	

Absorption coefficient	1.838 mm^{-1}
F(000)	155
Crystal	Lath; Colourless
Crystal size	0.20 × 0.08 × 0.01 mm^3
θ range for data collection	3.41 – 27.48°
Index ranges	$-6 \le h \le 6$, $-6 \le k \le 6$, $-15 \le l \le 15$
Reflections collected	4945
Independent reflections	2475 [R_{int} = 0.0372]
Completeness to θ = 27.48°	99.3 %
Absorption correction	Semi–empirical from equivalents
Max. and min. transmission	0.9819 and 0.7100
Refinement method	Full-matrix least-squares on F^2
Data / restraints / parameters	2475 / 3 / 158
Goodness-of-fit on F^2	1.060
Final *R* indices [$F^2 > 2\sigma(F^2)$]	*R1* = 0.0353, *wR2* = 0.0791
R indices (all data)	*R1* = 0.0363, *wR2* = 0.0797
Absolute structure parameter	0.090(18)
Largest diff. peak and hole	0.406 and –0.602 e $Å^{-3}$

Table 8.6. Atomic coordinates [× 10^4], equivalent isotropic displacement parameters [$Å^2$ × 10^3] and site occupancy factors for Cu^{II}-Valine complex. U_{eq} is defined as one third of the trace of the orthogonalized U^{ij} tensor.

Atom	*x*	*y*	*z*	U_{eq}	*S.o.f.*
Cu1	7893(1)	5502(1)	9418(1)	13(1)	1
O1	985(8)	4090(8)	11029(4)	16(1)	1
O2	4541(8)	3473(8)	9921(4)	13(1)	1
O3	11275(9)	7466(8)	8943(4)	13(1)	1
O4	15009(8)	7019(8)	7940(3)	15(1)	1
N1	6813(10)	8545(10)	10492(4)	11(1)	1
N2	9152(10)	2421(10)	8482(4)	13(1)	1
C1	6140(9)	11628(7)	12753(3)	19(1)	1
C2	3966(8)	9171(7)	12249(3)	14(1)	1
C3	2759(9)	7823(8)	13203(4)	21(1)	1
C4	5329(11)	7303(10)	11395(4)	14(1)	1
C5	3424(12)	4801(12)	10747(5)	11(1)	1
C6	12641(12)	6189(11)	8201(5)	13(1)	1
C7	11085(10)	3376(10)	7657(4)	13(1)	1
C8	9612(8)	3455(7)	6546(3)	16(1)	1
C9	11656(9)	4510(8)	5713(3)	22(1)	1
C10	8081(10)	683(8)	5999(4)	25(1)	1

Table 8.7. Anisotropic displacement parameters [$Å^2 \times 10^3$] for Cu^{II}-Valine complex. The anisotropic displacement factor exponent takes the form: $-2\pi^2[h^2a^{*2}U^{11} + \cdots + 2\ h\ k\ a^*\ b^*\ U^{12}]$.

Atom	U^{11}	U^{22}	U^{33}	U^{23}	U^{13}	U^{12}
Cu1	11(1)	8(1)	17(1)	2(1)	3(1)	1(1)
O1	13(2)	17(2)	16(2)	2(2)	3(2)	−2(2)
O2	11(2)	10(2)	16(2)	4(2)	1(2)	−2(2)
O3	13(2)	6(2)	19(2)	1(2)	4(2)	2(2)
O4	12(2)	14(2)	18(2)	3(1)	5(1)	−2(2)
N1	10(2)	7(2)	14(2)	0(2)	4(2)	1(2)
N2	13(2)	11(2)	17(2)	7(2)	−2(2)	−1(2)
C1	28(2)	11(2)	19(2)	2(2)	4(2)	3(2)
C2	15(2)	13(2)	15(2)	4(1)	3(1)	3(1)
C3	22(2)	19(2)	20(2)	5(2)	6(2)	1(2)
C4	17(2)	10(2)	16(2)	6(2)	5(2)	1(2)
C5	9(2)	13(3)	11(2)	4(2)	1(2)	1(2)
C6	17(3)	5(2)	16(3)	3(2)	0(2)	4(2)
C7	15(2)	6(2)	17(2)	2(2)	6(2)	1(2)
C8	16(2)	14(2)	16(2)	1(1)	4(2)	2(1)
C9	26(2)	25(2)	14(2)	7(2)	1(2)	−1(2)
C10	34(2)	18(2)	20(2)	2(2)	−4(2)	−5(2)

Table 8.8. Hydrogen coordinates [$\times 10^4$] and isotropic displacement parameters [$Å^2 \times 10^3$] for Cu^{II}-Valine complex.

Atom	x	y	z	U_{eq}	*S.o.f.*
H901	8368	9759	10783	13	1
H902	5655	9391	10140	13	1
H903	10033	1535	8927	16	1
H904	7639	1261	8118	16	1
H1A	7699	11065	13101	29	1
H1B	5276	12791	13321	29	1
H1C	6831	12594	12159	29	1
H2	2431	9755	11863	17	1
H3A	1435	6203	12893	31	1
H3B	1796	9036	13706	31	1
H3C	4273	7366	13622	31	1
H4	6766	6674	11818	17	1
H7	12480	2169	7502	15	1
H8	8211	4654	6704	19	1
H9A	12660	6283	6050	33	1
H9B	10626	4615	5031	33	1
H9C	12993	3309	5523	33	1
H10A	7166	782	5291	38	1
H10B	6675	20	6503	38	1
H10C	9423	−527	5853	38	1

Table 8.9. Hydrogen bonds [Å and °] for Cu^{II}-Valine complex.

D–H···*A*	*d*(*D*–H)	*d*(H···*A*)	*d*(*D*···*A*)	∠(*D*H*A*)
N1–H901···O1^{i}	0.92	2.35	3.182(7)	149.8
N1–H902···O2^{ii}	0.92	2.34	3.148(7)	146.2
N1–H902···O3^{iii}	0.92	2.52	3.188(7)	129.6
N2–H903···O3^{iv}	0.92	2.31	3.079(7)	141.6
N2–H903···O2^{v}	0.92	2.46	3.057(7)	122.8
N2–H903···O1^{v}	0.92	2.65	3.139(7)	113.7
N2–H904···O4^{vi}	0.92	2.32	3.120(7)	144.9

Symmetry transformations used to generate equivalent atoms:
(i) x+1,y+1,z (ii) x,y+1,z (iii) x−1,y,z (iv) x,y−1,z
(v) x+1,y,z (vi) x−1,y−1,z